PROCEEDINGS FROM ACCM19: CELL CYCLE, DNA DAMAGE RESPONSE AND TELOMERES

EDITED BY: Andrew Burgess and Liz Caldon
PUBLISHED IN: Frontiers in Cell and Developmental Biology

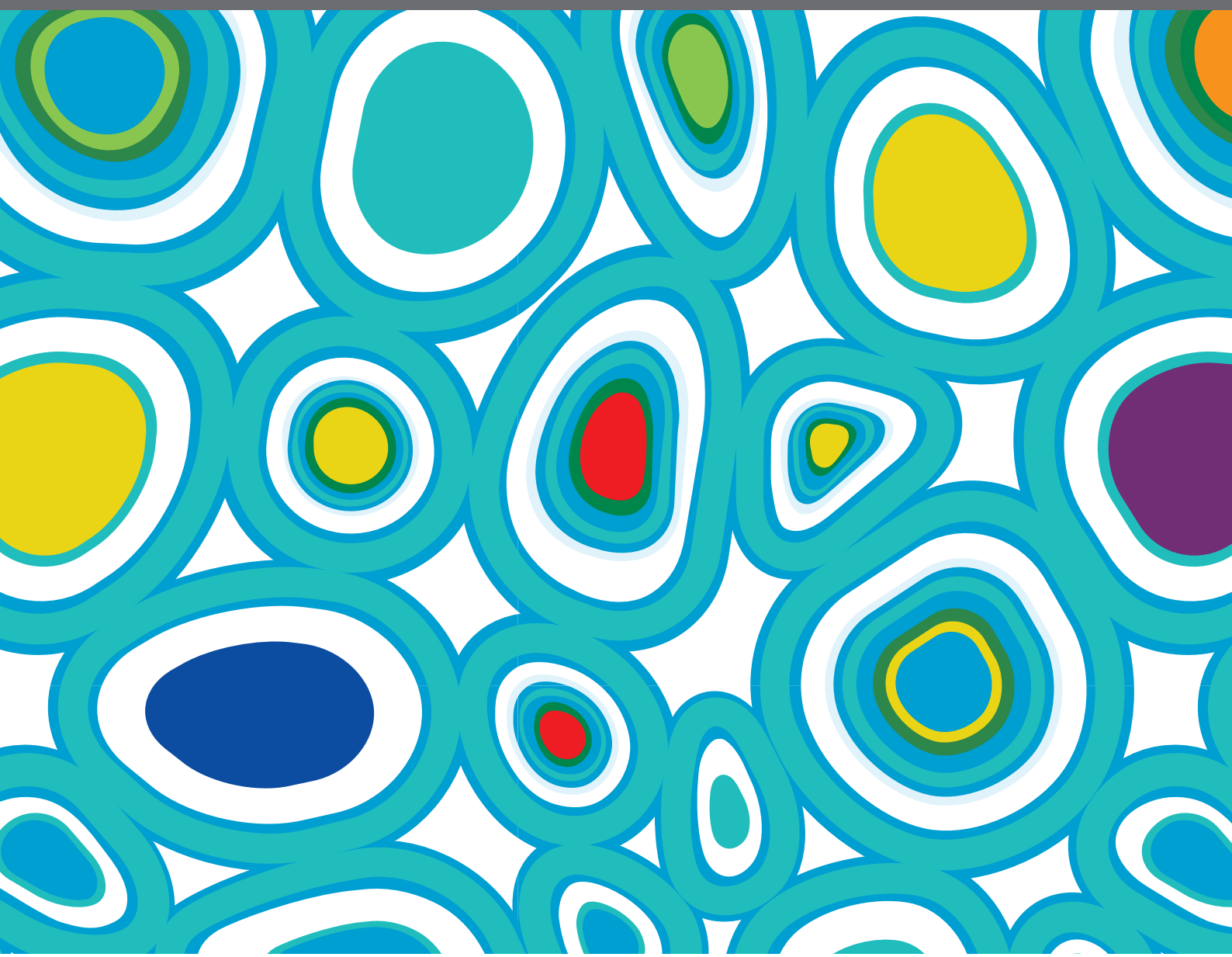

frontiers Research Topics

frontiers

ISSN 1664-8714
ISBN 978-2-88966-115-2
DOI 10.3389/978-2-88966-115-2

About Frontiers

Frontiers is more than just an open-access publisher of scholarly articles: it is a pioneering approach to the world of academia, radically improving the way scholarly research is managed. The grand vision of Frontiers is a world where all people have an equal opportunity to seek, share and generate knowledge. Frontiers provides immediate and permanent online open access to all its publications, but this alone is not enough to realize our grand goals.

Frontiers Journal Series

The Frontiers Journal Series is a multi-tier and interdisciplinary set of open-access, online journals, promising a paradigm shift from the current review, selection and dissemination processes in academic publishing. All Frontiers journals are driven by researchers for researchers; therefore, they constitute a service to the scholarly community. At the same time, the Frontiers Journal Series operates on a revolutionary invention, the tiered publishing system, initially addressing specific communities of scholars, and gradually climbing up to broader public understanding, thus serving the interests of the lay society, too.

Dedication to Quality

Each Frontiers article is a landmark of the highest quality, thanks to genuinely collaborative interactions between authors and review editors, who include some of the world's best academicians. Research must be certified by peers before entering a stream of knowledge that may eventually reach the public - and shape society; therefore, Frontiers only applies the most rigorous and unbiased reviews.
Frontiers revolutionizes research publishing by freely delivering the most outstanding research, evaluated with no bias from both the academic and social point of view. By applying the most advanced information technologies, Frontiers is catapulting scholarly publishing into a new generation.

What are Frontiers Research Topics?

Frontiers Research Topics are very popular trademarks of the Frontiers Journals Series: they are collections of at least ten articles, all centered on a particular subject. With their unique mix of varied contributions from Original Research to Review Articles, Frontiers Research Topics unify the most influential researchers, the latest key findings and historical advances in a hot research area! Find out more on how to host your own Frontiers Research Topic or contribute to one as an author by contacting the Frontiers Editorial Office: researchtopics@frontiersin.org

PROCEEDINGS FROM ACCM19: CELL CYCLE, DNA DAMAGE RESPONSE AND TELOMERES

Topic Editors:
Andrew Burgess, Anzac Research Institute, Australia
Liz Caldon, Garvan Institute of Medical Research, Australia

Citation: Burgess, A., Caldon, L., eds. (2020). Proceedings From ACCM19: Cell Cycle, DNA Damage Response and Telomeres. Lausanne: Frontiers Media SA. doi: 10.3389/978-2-88966-115-2

Table of Contents

frontiers in Cell and Developmental Biology

EDITORIAL
published: 03 September 2020
doi: 10.3389/fcell.2020.00805

Editorial: Proceedings From ACCM19: Cell Cycle, DNA Damage Response and Telomeres

Andrew Burgess[1,2*†] *and C. Elizabeth Caldon*[3,4*†]

[1] Cell Division Lab, ANZAC Research Institute, Concord Hospital, Concord, NSW, Australia, [2] Faculty of Medicine and Health, Concord Clinical School, University of Sydney, Sydney, NSW, Australia, [3] The Kinghorn Cancer Centre, Garvan Institute of Medical Research, Darlinghurst, NSW, Australia, [4] Faculty of Medicine, St. Vincent's Clinical School, UNSW Sydney, NSW, Australia

Keywords: cell cycle, telomere, DNA damage, mitosis, JNK, radiation, chemotherapy, PP2A

Editorial on the Research Topic

Proceedings From ACCM19: Cell Cycle, DNA Damage Response and Telomeres

OPEN ACCESS

Edited and reviewed by:
Philipp Kaldis,
Lund University, Sweden

***Correspondence:**
Andrew Burgess
andrew.burgess@sydney.edu.au
C. Elizabeth Caldon
l.caldon@garvan.org.au

†These authors have contributed equally to this work

Specialty section:
This article was submitted to Cell Growth and Division, a section of the journal Frontiers in Cell and Developmental Biology

Received: *27 July 2020*
Accepted: *31 July 2020*
Published: *03 September 2020*

Citation:
Burgess A and Caldon CE (2020) Editorial: Proceedings From ACCM19: Cell Cycle, DNA Damage Response and Telomeres. Front. Cell Dev. Biol. 8:805. doi: 10.3389/fcell.2020.00805

INTRODUCTION

The 19th ACCM meeting was held in Sydney, Australia, from the 17–19th of June 2019. The Australian Cell Cycle Meeting (ACCM) began in the late 1990s as a small Australian based workshop, to bring together cell cycle researchers from across the country once a year. A strong focus was placed on providing students and post-docs with the opportunity to give oral presentations of their work and establish new collaborations. It continued in this fashion for over a decade, establishing itself as a must-attend event for the local cell cycle community. In 2015, we expanded the meeting to incorporate the fields of DNA damage and telomere biology and switched to running every 2 years.

The once small local meeting has now become an internationally and respected meeting that attracts leading researchers from around the world. Our invited research leaders for 2019 were Agata Smogorzewska on genome maintenance (Rockefeller University, New York, USA), Agnel Sfeir on telomere biology (Skirball Institute of Biomolecular Medicine, New York University, Langone Medical Center, USA), Gerry Hanna on radiation oncology (Director of Radiation Oncology Peter MacCallum Institute Victoria, Australia), and Karlene Cimprich on genome stability and DNA replication (School of Medicine, Stanford University, Stanford, CA, USA). Importantly, the meeting maintained its early goal of providing a platform for students and junior scientists to present their research in a friendly and collaborative environment. The next meeting is scheduled for the end of 2021 and will return to Melbourne, where it commenced in 1999.

CELL CYCLE, DNA REPAIR, AND TELOMERES: ELEMENTS THAT UNDERPIN CANCER BIOLOGY AND TREATMENT

The 2019 ACCM meeting brought together research covering DNA repair, telomere biology, RNA transcription, early developmental biology, cell-polarity and cell-signaling, and big-data. The

exploration of these ideas in one forum provided an opportunity for in depth discussion of focused questions with cross-fertilization of ideas from closely aligned research areas.

Two excellent reviews by Sia et al. and Martin and Martin delve into Radiation therapy (RT), which is used to treat more than half of all cancers. With recent technological advancements, RT is responsible for as much as 40% of all cancer cures. The review by Sia et al., examines the types and mechanisms of cell death induced by RT in cancer. RT induces a range of death processes, from classical apoptosis and mitotic cell death through to autophagy, which is mediated by numerous intrinsic pathways in combination with the local microenvironment and radiation specific factors. In their opinion piece, Martin and Martin, contextualize the use of radiation therapy treatment by discussing the notable side effects that many radiotherapy patients face, especially accelerated aging.

This work was complemented by two reviews focused on aspects of lung cancer. Work by Johnson et al., comprehensively examined the role of the oncogene Y-Box protein 1 (YB-1) in driving lung cancer. YB-1 is a multi-function protein capable of regulating transcription, translation, and DNA repair. It is commonly over-expressed in numerous cancers, and it is implicated in driving proliferation, metastasis, and resistance to chemotherapy. In parallel, Gonzalez-Rajal et al. have identified and reviewed the recent breakthrough studies that have shed light on the underlying mechanisms of innate platinum resistance in lung cancer. Notably, platinum chemotherapy is a cornerstone and front-line treatment for many lung cancers including mesothelioma. It is essentially curative in testicular cancer but is hampered by extensive innate resistance in lung cancer, with only 30% of patients responding. In this opinion article, Gonzalez-Rajal et al. highlight how TGFβ signaling, the cell cycle and DNA repair are key central players in regulating platinum resistance in lung cancer.

Three research manuscripts provided key findings on DNA repair and telomeres with respect to cancer biology mechanisms, improved cancer biomarkers, and methodological advancement. One essential pathway that regulates platinum resistance is the Fanconi Anaemia (FA) pathway, which is responsible for removing platinum induced interstrand crosslinks (ICLs) from DNA. Exciting new research by Tan et al. examines how two crucial components of the FA pathway, FANCD2 and FANCI, are regulated by direct phosphorylation by ATR kinase. This protects the FA complex from degradation, thereby ensuring cross-linked DNA is properly repaired. Notably, cancer cells often have defective DNA repair pathways making them susceptible to novel chemotherapies. One such treatment is the RNA polymerase I (PolI) transcription inhibitor CX-5461, which causes DNA damage and is currently in phase I clinical trials for solid tumors. Work from Son et al. demonstrates the number of active rDNA repeats positively correlates with sensitivity to CX-5461 in ovarian cancer cells, and hence may be a potential clinical biomarker for this exciting new chemotherapy. Notably, telomeres protect the chromosome ends from being recognized as DNA double-strand during normal replication. Disruption of telomeres is a hallmark of cancer, and hence the ability to accurately monitor telomere length is a critical assay not only for basic research but also clinical diagnosis. In exciting new research, Kahl et al. demonstrate the Telomere length Combing Assay (TCA), which can accurately measure telomere length in cell populations by pulling DNA fibers out onto glass coverslips using a constant stretching factor.

Telomeres and DNA repair also play essential roles in early developmental biology. Kafer and Cesare provide a comprehensive review of the replication stress and HR repair factors that are essential for early mammalian embryo development covering over 347 genes. Understanding embryo development and the use of developmental systems such as *Drosophila* (Fruit flies) has been essential for discovering and new drivers of cancer. Pre-eminent among these is the c-Jun N-terminal Kinase (JNK) signaling pathway, which plays a multitude of roles from regulating cell proliferation through to survival. Here, La Marca and Richardson provide a compelling review of how the JNK pathway acts as both promoter and inhibitor of tumorigenesis in *Drosophila*. Traditionally, early developmental biology, DNA repair, and cell cycle pathways have focused on the role of kinases, however, the essential role of counterbalancing phosphatases has recently gained prominence. This is highlighted in new research by Panicker et al., where they analyse the role of the major phosphatase PP2A. PP2A is a multi-complex phosphatase, with specificity for substrates controlled by the regulatory subunit (Rogers et al., 2016). Using CRISPR/Cas9, Panicker et al., demonstrate that knocking out the B55α regulatory subunit caused embryonic lethality in mice, due to failed epidermal stratification, highlighting the importance of phosphatases.

SUMMARY

The ACCM conference and resulting special issue in Frontiers in Cell and Developmental Biology has highlighted the biological complexity that underpins cancer biology and treatment, and that major aspects of this biology are the cell cycle, DNA repair pathways, and telomere biology. A key aspect of our meeting is to bring together what are sometimes diverse fields and encourage the sharing of ideas that can accelerate knowledge gain and implementation. The studies published in this special issue cross over these fields and highlight the impact of cross-fertilization; examples include the importance of developmental biology on understanding of DNA damage pathways, and of how the basic understanding of the detection and repair of DNA lesions could alter cancer therapy.

AUTHOR CONTRIBUTIONS

All authors listed have made a substantial, direct and intellectual contribution to the work, and approved it for publication.

FUNDING

AB was supported by a NBCF Investigator Initiated Research Scheme (IIRS-18-103). CC was supported by a NBCF Career Development Fellowship (ECF17-002).

REFERENCES

Rogers, S., McCloy, R., Watkins, D. N., and Burgess, A. (2016). Mechanisms regulating phosphatase specificity and the removal of individual phosphorylation sites during mitotic exit. *Bioessays* 38, S24–S32. doi: 10.1002/bies.201670905

Conflict of Interest: The authors declare that the research was conducted in the absence of any commercial or financial relationships that could be construed as a potential conflict of interest.

frontiers in Cell and Developmental Biology

REVIEW
published: 01 October 2019
doi: 10.3389/fcell.2019.00221

Why Be One Protein When You Can Affect Many? The Multiple Roles of YB-1 in Lung Cancer and Mesothelioma

*Thomas G. Johnson[1,2,3,4], Karin Schelch[5], Sunali Mehta[6,7], Andrew Burgess[2,3] and Glen Reid[6,7]**

[1] Asbestos Diseases Research Institute, Sydney, NSW, Australia, [2] Cell Division Laboratory, The ANZAC Research Institute, Sydney, NSW, Australia, [3] School of Medicine, The University of Sydney, Sydney, NSW, Australia, [4] Sydney Catalyst Translational Cancer Research Centre, The University of Sydney, Sydney, NSW, Australia, [5] Institute of Cancer Research, Medical University of Vienna, Vienna, Austria, [6] Department of Pathology, University of Otago, Dunedin, New Zealand, [7] Maurice Wilkins Centre, University of Otago, Dunedin, New Zealand

OPEN ACCESS

Edited by:
Dominic C. Voon, Kanazawa University, Japan

Reviewed by:
Joseph William Landry, Virginia Commonwealth University, United States
Shang Li, Duke-NUS Medical School, Singapore

***Correspondence:**
Glen Reid
glen.reid@otago.ac.nz

Specialty section:
This article was submitted to Cell Growth and Division, a section of the journal Frontiers in Cell and Developmental Biology

Received: *26 July 2019*
Accepted: *18 September 2019*
Published: *01 October 2019*

Citation:
Johnson TG, Schelch K, Mehta S, Burgess A and Reid G (2019) Why Be One Protein When You Can Affect Many? The Multiple Roles of YB-1 in Lung Cancer and Mesothelioma. Front. Cell Dev. Biol. 7:221. doi: 10.3389/fcell.2019.00221

Lung cancers and malignant pleural mesothelioma (MPM) have some of the worst 5-year survival rates of all cancer types, primarily due to a lack of effective treatment options for most patients. Targeted therapies have shown some promise in thoracic cancers, although efficacy is limited only to patients harboring specific mutations or target expression. Although a number of actionable mutations have now been identified, a large population of thoracic cancer patients have no therapeutic options outside of first-line chemotherapy. It is therefore crucial to identify alternative targets that might lead to the development of new ways of treating patients diagnosed with these diseases. The multifunctional oncoprotein Y-box binding protein-1 (YB-1) could serve as one such target. Recent studies also link this protein to many inherent behaviors of thoracic cancer cells such as proliferation, invasion, metastasis and involvement in cancer stem-like cells. Here, we review the regulation of YB-1 at the transcriptional, translational, post-translational and sub-cellular levels in thoracic cancer and discuss its potential use as a biomarker and therapeutic target.

Keywords: lung cancer, mesothelioma, targeted therapy, biomarker, Y-box binding protein-1

INTRODUCTION

Lung cancers are the leading cause of cancer death worldwide (Islami et al., 2015; Kris et al., 2017), and malignant pleural mesothelioma patients continue to experience some of the worst 5-year survival rates of all malignancies (Mutti et al., 2018). Therefore, advances in therapeutic options are urgently needed and require a more thorough understanding of the underlying biology of both.

While SCLC represents ∼15–20% of all lung cancers, NSCLC represent the majority of cases (∼80–85%). NSCLC are further subtyped into adenocarcinomas (ADC; ∼40–50% of NSCLC), squamous cell carcinomas (SCC; ∼20–40%) and large cell carcinomas (LGC; ∼20%). Whilst all of these carcinomas are significantly associated with tobacco consumption, this association is much stronger in SCLC and SCC than in ADC and LGC (Khuder, 2001).

Malignant pleural mesothelioma arises from the pleural linings of the lung and is strongly linked to asbestos exposure (Tossavainen, 2004). MPM is currently subtyped as epithelioid, sarcomatoid or biphasic, which are characterized by a mixture of epithelioid and sarcomatoid cells (Marshall et al., 2015). At times, this review refers to lung cancer and mesothelioma as "thoracic cancers," although we acknowledge that this term also encompasses tumors of the trachea, esophagus and thymus.

The current clinical practice guidelines for NSCLC, SCLC, and MPM all recommend the use of platinum-based chemotherapy in combination with other agents as the standard mode of care (Vogelzang et al., 2003; Rudin et al., 2016; Bradbury et al., 2017; Kris et al., 2017; Nagasaka and Gadgeel, 2018; Szolkowska et al., 2018). Diagnosis in the early stages of NSCLC affords better survival odds, however, the majority of patients are diagnosed with advanced disease (Kris et al., 2017; Visconti et al., 2017). Such individuals face a 5-year survival rate of only 23% and treatment options are often limited to chemotherapy (Kris et al., 2017). SCLC patients face similarly poor survival odds. Patients usually respond initially to platinum-based chemotherapy but inevitably develop chemoresistant tumors (Rudin et al., 2016). Overall survival rates of SCLC patients currently sit at 10–12 months post diagnosis (Rudin et al., 2016). In MPM, the standard of care consists of a combination of cisplatin with pemetrexed, providing an overall survival rate of only 12.1 months (Vogelzang et al., 2003; Mutti et al., 2018). Epithelioid mesotheliomas present with the best prognosis, with the median overall survival being between 12 and 27 months (Yap et al., 2017). Patients with biphasic mesothelioma have median overall survival rates of 7–18 months, while sarcomatoid patients are afforded the worst prognosis of 4–12 months (Yap et al., 2017). Recent trials of immunotherapy strategies, such as the anti-PD-1 checkpoint inhibitors pembrolizumab and nivolumab, have shown promise as first-line and second-line therapies in some thoracic cancers (Visconti et al., 2017; Forde et al., 2019). However, response to immunotherapy is unpredictable due to a lack of robust biomarkers, so predicating which patients will respond is not yet possible (Ventola, 2017). Acquired resistance to these drugs also remains a significant problem (Ventola, 2017). Improved treatment options for patients suffering malignancies of the lung and mesothelial linings are therefore still desperately needed.

Abbreviations: ΔNP63α, Isoform p63α – protein isoform of p63; ADC, lung adenocarcinoma; AKT, lrotein kinase B; ALK, anaplastic lymphoma kinase; APE1, apurinic/apyrimidinic endonuclease 1; BAP1, BRCA associated protein-1; Bcl-2, B-cell lymphoma 2; BER, base-excision repair; BMP7, bone morphogenetic protein 7; BRAF, proto-oncogene B-Raf; C1QBP, complement component 1 Q subcomponent-binding protein; CAR10, CAR intergenic 10; CCND1, cyclin D1; CDC25A, M-phase inducer phosphatase 1; CDKN2A, cyclin-dependent kinase inhibitor 2A; COPD, chronic obstructive pulmonary disease; CRS, cytoplasmic retention signal; CSC, cancer stem-like cell; CSD, cold shock domain; CTD, C-terminal domain; DANCR, differentiation antagonizing non-protein coding RNA; E/M, hybrid epithelial/mesenchymal state; EGF, epidermal growth factor; EGFR, epidermal growth factor receptor; EMT, epithelial-mesenchymal transition; EPO, human erythropoietin; EZH2, enhancer of zeste homolog 2; FGFR1, fibroblast growth factor receptor 1; FOXO3a, forkhead box O3; G3BP1, Ras GTPase-activating protein-binding protein-1; GAS5, growth arrest specific 5; HACE1, HECT domain and ankyrin repeat containing E3 ubiquitin protein ligase 1; HER2, human epidermal growth factor receptor 2; HIF1α, Hypoxia-inducible factor 1-α; HMGB1, high mobility group box 1 protein; HULC, highly up-regulated in liver cancer; LGC, large cell carcinoma; LINC00312, long intergenic non-protein coding RNA 312; LMO3, LIM domain only protein 3; lncRNA, long non-coding RNA; LRP/MVP, lung resistance protein/major vault protein; MAPK/ERK, Mitogen-activated protein kinase/extracellular-signal-regulated kinase; MDCK, Madin-Darby canine kidney cell; MDR1, multi-drug resistance 1; MET, tyrosine-protein kinase Met; MIR22HG, MIR22 host gene; miRNA, microRNA; MPM, malignant pleural mesothelioma; MRP1, multidrug resistance-associated protein 1; mTOR, mammalian target of rapamycin; NANOG, homeobox protein NANOG; ncRNA, non-coding RNA; NEIL1, nei like DNA glycosylase 1; NER, nuclear excision repair; NF2, neurofibromatosis type 2; NLS, nuclear localization signal; Notch1/*NOTCH1*, notch homolog 1; Notch3, notch receptor 3; NSCLC, non-small cell lung cancer; nt, nucleotide; Oct4, octamer-binding transcription factor 4; OGT, O-linked N-acetylglucosamine transferase; PABP, Poly(A)-binding protein; PARP1, Poly(ADP-ribose) polymerase 1; PARP2, Poly(ADP-ribose) polymerase 2; PCNA, proliferating cell nuclear antigen; PIK3CA, phosphatidylinositol-4,5-bisphosphate 3-kinase, catalytic subunit α; RBBP6, retinoblastoma binding protein 6; RSK p90, ribosomal S6 kinase; SAHA, suberoylanilide hydroxamic acid; SCC, lung squamous carcinoma; SCLC,small cell lung cancer; SETD2, SET domain containing 2; SILAC, stable isotope labeling with amino acids in cell culture; siRNA, small interfering RNA; Snail, Zinc finger protein SNAI1; SOX2, sex determining region Y-box 2; SPHK1, sphingosine kinase 1; SRC3, steroid receptor co-activator 3; ssDNA, single-stranded DNA; TCGA, The Cancer Genome Atlas; TGFβ1, transforming growth factor β1; *TP53*/p53, tumor protein 53; TP53TG1, TP53 target 1; Twist1, Twist-related protein 1; XPC, xeroderma pigmentosum; YB-1, Y-box binding protein-1; YB-1/p18, 18 kDa fragment of YB-1.

Toward Personalized Therapy for Thoracic Cancer Patients

The development of next-generation sequencing has fostered a deeper understanding of the molecular drivers and mutational landscape of thoracic cancers. Multi-region whole-exome sequencing of 100 early stage NSCLC patients demonstrated that clonal alterations of oncogenes such as the growth receptor *EGFR* and the kinases *MET*, and *BRAF* were commonly found in ADC (Jamal-Hanjani et al., 2017). These were accompanied by sub-clonal modifications of the oncogene *PIK3CA* and the tumor suppressor neurofibromin 1 (Jamal-Hanjani et al., 2017). Alterations of *PIK3CA*, the transmembrane receptor *NOTCH1*, growth factor receptor *FGFR1* and transcription factor *SOX2* were also observed in early SCC (Jamal-Hanjani et al., 2017). *TP53* or p53 mutations were frequent clonal events in both subtypes, while oncogenic *ALK* translocations were not observed in any tumors (Jamal-Hanjani et al., 2017).

As for MPM, next-generation sequencing of 216 MPM patients showed that the tumor suppressors *BAP1*, *NF2*, and *SETD2* were significantly mutated through gene fusions and splicing alterations (Bueno et al., 2015). *CDKN2A*, which encodes the tumor suppressor $p16^{INK4a}$, is also frequently deleted in up to 75–90% of MPM cases (Ladanyi, 2005; Sementino et al., 2018). Data from TCGA reflects the above findings, apart from *ALK* alterations in ADC, which were present in 7% of cases (**Figures 1A–C**). An important distinction must between lung cancer and MPM is that lung cancers are generally characterized by an increase in oncogenic drivers, while MPM appears to be more commonly defined by loss of tumor suppressors (Ladanyi, 2005; Bueno et al., 2015; Jamal-Hanjani et al., 2017; **Figure 1C**). This makes identifying new therapeutic targets in MPM more challenging. Apart from bevacizumab, which targets vascular endothelial growth factor A, no targeted therapies are currently available to MPM patients (Brosseau et al., 2017).

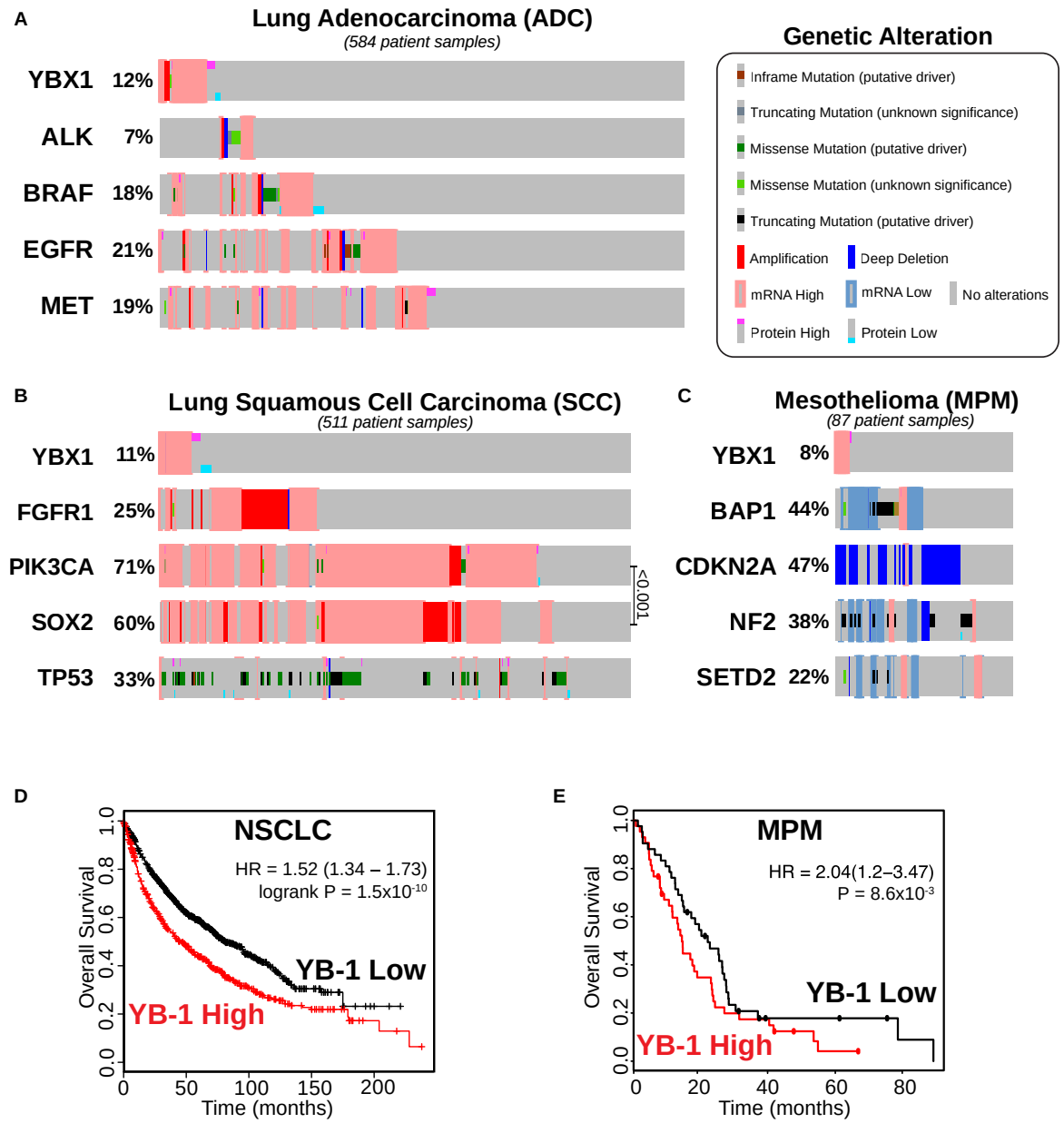

FIGURE 1 | YB-1 is altered in NSCLC (ADC and SCC) and MPM patients and high *YBX1* mRNA expression correlates with poor prognosis in both diseases. Reported alteration frequencies of *YBX1* and commonly altered genes in current TCGA Provisional datasets for all complete tumors with RNASeq V2 RSEM mRNA and RPPA protein Expression for **(A)** Lung Adenocarcinoma (ADC; $n = 584$), **(B)** Lung Squamous Cell Carcinoma (SCC; $n = 511$) and **(C)** Mesothelioma (MPM; $n = 87$). Panels **(A–C)** were adapted from the open-source platform cBioPortal for Cancer Genomics (cBioPortal.org). **(D)** High *YBX1* expression correlates with poor prognosis in NSCLC patients ($p = 1.5 \times 10^{-10}$). Kaplan-Meir plot of 1,926 NSCLC patients generated using Lung Cancer KM plotter. Univariate analysis with probe set 20862_s_at (*YBX1*) using auto-selected cutoff and excluded biased arrays. **(E)** High *YBX1* expression correlates with poor prognosis in MPM patients ($p = 8.6 \times 10^{-3}$). Kaplan-Meir plot was generated using PROGgene V2 with the TCGA mesothelioma dataset ($n = 83$) using "DEATH" as the survival measure and median as the cutoff.

The story for SCLC patients is similar with no breakthrough changes in treatment in over 25 years despite decades of research. The only exception to this is the approval of topotecan as a second-line therapy (Hirsch et al., 2017), and immunotherapy, which has shown some promise in Phase I/II trials in PD-L1 positive relapsed SCLC patients (Ott et al., 2015). Unfortunately, immunotherapy success has been limited by rapid disease progression, which can result in patient death before an effective anti-tumor response has time to occur (3–6 months), and severe immuno-related toxicities (encephalitis or myasthenia gravis) that are already highly associated with SCLC (Oronsky et al., 2017). Other drugs such as PARP inhibitors and

transcription inhibitors have shown some preclinical promise, but have yet to translate into clinical benefits for SCLC patients (Oronsky et al., 2017).

For NSCLC, targeted therapies have provided promising, albeit limited, results. The best known of these are the EGFR tyrosine kinase inhibitors such as erlotinib and osimertinib, which have proved effective for EGFR mutant ADC tumors (Hirsch et al., 2017; Winther-Larsen et al., 2019). In the ADC TCGA dataset, 21% of patients had EGFR alterations (**Figure 1A**), although the occurrence of EGFR mutations can vary between populations in ADC and NSCLC as a whole. For example, while EGFR mutation can occur in up to 40% of all NSCLC patients of Asian descent, the frequency of mutation in non-Asian NSCLC populations drops to 10–20% (Hirsch et al., 2017). Another problem is that response to EGFR inhibitors is almost always followed by the emergence of resistance (Hirsch et al., 2017). ALK inhibitors are similarly effective in patients harboring ALK translocations (Hirsch et al., 2017), present in 2% of all NSCLC patients (Hirsch et al., 2017). Alterations of ALK in ADC tumors specifically is found in up to 7% of cases, according to TCGA data (**Figure 1A**). Inhibitors targeting BRAF mutant tumors (3–5% of lung cancers), MET overexpressing tumors (3–4% of ADC cases) and tumors harboring RET fusion proteins (1–2% of NSCLC) are also currently undergoing preclinical and clinical studies (Hirsch et al., 2017). The remaining majority of patients with ADC have no known actionable targets.

Patients with SCC have even fewer options with only ∼13% of SCC tumors reported to harbor at least one currently actionable alteration (Lindquist et al., 2017). There is no subset of patients known to benefit from targeted drugs at the moment, although there is some benefit from immunotherapy (Hirsch et al., 2017; Friedlaender et al., 2019). *TP53* mutations are a common alteration in SCC patients (33%; **Figure 1B**), however, existing targeted *TP53* treatments have proven ineffective (Friedlaender et al., 2019). *PIK3CA* is also frequently altered in thoracic cancer, particularly in SCC (Friedlaender et al., 2019) (71%; **Figure 1B**), indicating that it may have significance as a therapeutic target. However, despite promising preclinical studies of PIK3CA inhibitors, the benefit of these drugs appears to be negligible in trials with NSCLC patients (Friedlaender et al., 2019). This has also been the case in other cancers where, generally, patients show limited response and many experience prohibitive toxicity (Janku et al., 2018). This pathway mediates a multitude of downstream effects, which may attest to the observed relative ineffectiveness of PIK3CA inhibitors in lung cancer. *FGFR1* amplification occurs in 20–25% of SCC cases (Friedlaender et al., 2019; **Figure 1B**), but again, targeting it in the clinic has provided limited efficacy and its potential as a viable target remains under contention (Hirsch et al., 2017; Friedlaender et al., 2019). There are a few targets that have been the focus of preclinical studies showing promising results, such as the transcription factor SOX2. SOX2 is involved in cell lineage-survival (Friedlaender et al., 2019) and is often upregulated in SCC (Karachaliou et al., 2013; Friedlaender et al., 2019) (60%; **Figure 1B**), as well as SCLC (Rudin et al., 2012; Karachaliou et al., 2013) and to a lesser degree ADC (Karachaliou et al., 2013). Finding such targets and translating them to the clinic is essential to improve outcomes for patients with SCC.

The heterogeneity of thoracic cancer biology makes finding clinically relevant therapeutic targets inherently difficult. Identifying other penetrant driver events in thoracic cancers may uncover alternative targets, which could yield more therapeutic options for patients down the line. One such potential target is YB-1. YB-1 is downstream of the commonly dysregulated PI3K-AKT-mTOR pathway, so targeting it may refine the effects of inhibiting this signal cascade. Thus, anti-YB-1 agents may provide more tumor-specific results than their upstream-targeting counterparts, such as PIK3CA inhibitors (Janku et al., 2018). Adding to this, YB-1 upregulates PIK3CA at the transcriptional level in breast cancer (Astanehe et al., 2009). This implies that YB-1 may be involved in a feed-forward loop with the PI3K-AKT pathway and that targeting it could be an effective strategy in tumors with heightened PIK3CA, such as SCC. YB-1 is also upstream of SOX2 (Jung et al., 2014) and a host of other oncogenic drivers (Lasham et al., 2013), so the downstream effects of YB-1 inhibition may still be broad enough to make it an interesting candidate. This review therefore outlines recent literature focusing on YB-1 in cancer and makes the case for its possible use as a biomarker and future therapeutic target in thoracic malignancies.

Y-Box Binding Protein-1 in Thoracic Cancers: An Overlooked Target?

Y-box binding protein-1, encoded by the *YBX1* gene, is a multifunctional oncoprotein involved in many hallmarks of cancer development including driving proliferation, invasion and metastasis, CSC biology, resistance to chemotherapy, hypoxic response, DNA repair and exosomal sorting. Despite these links YB-1 has received limited attention as a therapeutic target or biomarker in oncology (Lasham et al., 2013). Although mutations of *YBX1* are rare [∼1% in all cancers types (Cerami et al., 2012; Gao et al., 2013)], overexpression of YB-1 is found in a wide range of cancers and is often associated with poor prognosis (Lasham et al., 2013), including NSCLC and MPM. Analysis of TCGA data shows that elevated *YBX1* expression was highly prognostic in a cohort of 1,926 NSCLC patients (Győrffy et al., 2013; **Figure 1D**) and in 83 mesothelioma patients (Goswami and Nakshatri, 2014; **Figure 1E**). This supports the results of a recent meta-analysis of data from 692 NSCLC patients which found that high YB-1 protein expression significantly correlated with poorer overall survival and clinicopathological features (Jiang et al., 2017). YB-1 is overexpressed in mesothelioma compared to non-malignant mesothelial cells *in vitro* (Johnson et al., 2018) and a small study of 33 MPM patients showed a trend toward higher YB-1 expression in sarcomatoid MPM tumors, which are associated with shorter survival (Iwanami et al., 2014). Unfortunately, TCGA data is currently not available for SCLC, likely because surgically resected tissue specimens are relatively rare (Byers and Rudin, 2015) and, to our knowledge, a prognostic study on YB-1 expression in SCLC is yet to be conducted.

In the above datasets, alterations were seen in 12, 11, and 8% in ADC, SCC, and MPM, respectively, and mRNA upregulation was predominant (**Figures 1A–C**). While only PIK3CA and SOX2 were significantly co-expressed in the SCC dataset ($q < 0.001$;

Figure 1B), notably, this analysis did not show *YBX1* alteration to be significantly associated with the current targetable oncogenes *ALK*, *BRAF* or *EGFR* in ADC (**Figure 1A**), despite there being a small proportion of tumors that had elevated levels of both *YBX1* and *EGFR*. This suggests that YB-1 deregulation may represent a unique subpopulation of patients that may not have a targetable mutation. This combined with the prognostic significance of YB-1 in NSCLC and MPM, suggests that YB-1 may be a clinically relevant target worthy of further investigation.

YB-1: A MALIGNANT JACK OF ALL TRADES

A Driver of Malignant Phenotypes

Y-box binding protein-1 was first discovered as a negative transcriptional factor of major histocompatibility complex Class II where it binds to the Y-box (5′-CTGATTGG-3′) (Didier et al., 1988). Further investigation found that YB-1 stimulated the transcription of a wide variety of genes, including important oncogenes such as *EGFR* and HER2 (Lasham et al., 2013). YB-1 is a part of the cold-shock protein superfamily and contains a conserved nucleic acid binding region termed the CSD (Wolffe et al., 1992; **Figure 3**). Along with the CSD, YB-1 is comprised of two other highly disordered domains, the alanine/proline rich variable N–terminal domain and the C–terminal domain (CTD), each facilitating different biological interactions (Lyabin et al., 2014; Suresh et al., 2018). This versatility affords YB-1 a range of functions including transcriptional regulation, DNA repair and pre-mRNA splicing (Lyabin et al., 2014). YB-1 is also a major component of messenger ribonucleoprotein complexes and is integrally involved in mRNA stabilization and the translational activation or repression of many genes (Suresh et al., 2018). This assortment of functions manifest themselves in an equally broad spectrum of biological roles in cancer (Lasham et al., 2013; Lyabin et al., 2014). The general cancer-related activities of YB-1 have been previously reviewed (Lasham et al., 2013; Kosnopfel et al., 2014; Lyabin et al., 2014) and therefore we will primarily focus on recent publications on the role of YB-1 specifically in lung cancer and MPM here. The evidence supporting each phenotype driven by YB-1 and the relevant interaction partners for the following sections is summarized in **Table 1**.

A Promoter of Cell Proliferation and Cell Cycle Progression

The proliferative role of YB-1 in cancer has been demonstrated in many malignancies, driven by its regulation of highly penetrant downstream oncogenic growth promoting genes (Lasham et al., 2013). A prime example is the transcriptional activation of *EGFR* by YB-1. A study of 105 NSCLC samples showed that YB-1 and EGFR were significantly co-expressed and knockdown of YB-1 in two NSCLC cell lines resulted in reduction of EGFR (Hyogotani et al., 2012). Similar results have also been observed in basal-like breast cancer and spinal chordoma (Stratford et al., 2007; Liang et al., 2019). Notably, overexpression of EGFR in lung cancer and mesothelioma promotes cell growth, invasion and angiogenesis (Ciardiello et al., 2004; Destro et al., 2006). Several cell cycle regulators are also under YB-1 control, including the E2F family. YB-1 specifically binds to the promoter of cell cycle activators transcription factor *E2F1* and transcription factor *E2F2* and YB-1 knockdown reduced cell proliferation of a NSCLC cell line *in vitro* and *in vivo* (Lasham et al., 2011). In NSCLC cells, YB-1 transcriptionally activates *CCND1* a protein critical for progression through the G1 phase (Harada et al., 2014). YB-1 also binds to and activates the promoter of the dual specific phosphatase *CDC25A*, driving G1/S cell cycle progression (Zhao et al., 2016). These studies demonstrate the important role of YB-1 by showing that its knockdown with siRNA induces G0/G1 cell cycle arrest *in vitro* and *in vivo* (Harada et al., 2014; Zhao et al., 2016). Similarly, we have also shown that targeting YB-1 with siRNA can inhibit the growth of MPM cells *in vitro* (Johnson et al., 2018).

Y-box binding protein-1-driven proliferation may require a region within its N–terminal domain. Breast cancer cells overexpressing a YB-1 CTD fragment (from amino acid 125 onward) exhibited proliferation inhibition *in vitro* and *in vivo* (Shi et al., 2016). It is possible that the removal of Ser102, a site commonly phosphorylated and associated with growth (discussed further in section "Post-Translational Modification in the Control of YB-1 Activity and Localization"), could explain the lack of growth promotion here. However, as growth was actively inhibited in response to the upregulation of the YB-1 CTD, this could also suggest that YB-1, or certain regions of it, may inhibit proliferation under specific gene dosages or biological contexts. For example, YB-1 overexpression in Ras-MAPK activated breast cancer cells led to YB-1-mediated translational repression of growth-promoting genes, lowering proliferation rates. This was accompanied by the induction of EMT-like changes which promoted migration, invasion and allowed cells to survive in anchorage-independent conditions (Evdokimova et al., 2009b). This suggests that YB-1 expression levels determine its function, driving either a proliferative or invasive phenotype.

YB-1 Is a Central Player in EMT, Invasion and Metastasis

Invasion and metastasis are key behaviors of lung cancer and mesothelioma cells that contribute to patient death and the poor prognosis observed with these tumors. YB-1 is known to play a role in the migration of thoracic cancer cells. Stable overexpression of YB-1 in lung ADC cells induced E-cadherin downregulation, N-cadherin upregulation, accelerated TGFβ1-induced EMT and cell migration (Ha et al., 2015). In support, silencing YB-1 inhibited the invasion and metastasis of lung cancer cells *in vitro* and *in vivo* (Guo et al., 2017). YB-1 overexpression also significantly increased the invasive capacity of these cells *in vitro* (Guo et al., 2017). Similarly, knockdown of YB-1 inhibited lung cancer migration (Zhao et al., 2016) and MPM migration and invasion (Johnson et al., 2018) *in vitro*. YB-1 has also been implicated in the migration and invasion of breast cancer (Lim et al., 2017), melanoma (Jia et al., 2017), nasopharyngeal cancer (Zhou et al., 2017b), skin squamous

TABLE 1 | Roles and interaction partners of YB-1 related to thoracic cancer biology.

Phenotype	Role in thoracic cancer behavior	Targets or interactions	Other cancers/evidence
Proliferation and cell cycle progression	Knockdown induces growth inhibition of NSCLC (Harada et al., 2014; Zhao et al., 2016) and MPM (Johnson et al., 2018)	Transcriptional regulation of *EGFR* (Hyogotani et al., 2012), E2F family members (Lasham et al., 2011), *CCND1* (Harada et al., 2014) and *CDC25A* (Zhao et al., 2016)	Basal-like breast cancer (Stratford et al., 2007) spinal chordoma (Liang et al., 2019)
Migration, EMT, invasion and metastasis	Overexpression in lung ADC promotes E- to N-cadherin shift, EMT and migration (Ha et al., 2015) Knockdown inhibits invasion and metastasis of lung cancer cells (Zhao et al., 2016; Guo et al., 2017) Knockdown inhibits migration and invasion of MPM cells (Johnson et al., 2018)	Translational activation of *SNAI1* (Evdokimova et al., 2009a,b) Involvement in E/M related Wnt signaling – β-catenin (Chao et al., 2017)	Breast cancer (Lim et al., 2017), melanoma (Jia et al., 2017), nasopharyngeal cancer (Zhou et al., 2017b), skin squamous cell carcinoma (Wang W. et al., 2017) spinal chordoma (Liang et al., 2019) Overexpression induces E/M phenotype (Gopal et al., 2015)
Cancer stem-like cells	Drives metastatic CSC-like properties in lung cancer (Guo et al., 2017)	Transcriptional regulation of *SOX2* (Jung et al., 2014; Bledzka et al., 2017), *NANOG* (Bledzka et al., 2017; Chao et al., 2017; Guo et al., 2017) and *Oct4* (Bledzka et al., 2017; Chao et al., 2017)	Hepatocellular carcinoma (Chao et al., 2017), brain (Mantwill et al., 2013), osteosarcoma (Xu et al., 2015), and breast (Davies et al., 2015) CSCs
Hypoxic response	*Requires further investigation*	Translational regulation of *HIF1α*(El-Naggar et al., 2015) and *FOXO3a* (Emerling et al., 2008; Chou et al., 2015) Transcriptional repression of *EPO* (Rauen et al., 2016)	Translocation to nucleus under hypoxic stress (Rauen et al., 2016)
LRP downregulation after YB-1 knockdown and correlation with LRP (Hyogotani et al., 2012) response	LRP downregulation after YB-1 knockdown and correlation with LRP (Hyogotani et al., 2012)	Transcriptional regulation of *LRP* (Stein et al., 2005) and *MRP1* (Stein et al., 2001; Mantwill et al., 2006)	Neuroblastoma (Wang H. et al., 2017), esophageal SCC (Xu and Hu, 2016), bladder cancer (Shiota et al., 2011), melanoma (Schittek et al., 2007), ovarian cancer (Yahata et al., 2002)
DNA repair	Involved in cigarette-smoke induced guanine oxidization prevention and correlations in COPD patients (Deslee et al., 2010)	Complex with PCNA at cisplatin-modified DNA (Ise et al., 1999; Gaudreault et al., 2004) PARP1 poly(ADP-ribosyl)ation of YB-1 (Alemasova et al., 2015) Scaffold for BER proteins (Dutta et al., 2015; Alemasova et al., 2016) Scaffolds for XPC (NER protein) (Fomina et al., 2015)	Preferential binding to cisplatin-modified DNA (Ise et al., 1999)
Exosomes	*Requires further investigation*	ncRNA (Shurtleff et al., 2017; Suresh et al., 2018)	Presence in non-malignant and malignant exosomes (Shurtleff et al., 2017; Suresh et al., 2018) Role in exosomal ncRNA sorting (Shurtleff et al., 2017; Suresh et al., 2018)

cell carcinoma (Wang W. et al., 2004) and spinal chordoma (Liang et al., 2019).

Epithelial-mesenchymal transition is thought to be a primary mechanism facilitating cancer cell invasion and metastasis through inducing phenotypic plasticity (Brabletz, 2012). Current evidence suggests that EMT is a progressive, transient and reversible process and that cells in a hybrid E/M state - partial EMT – exhibit significantly higher tumorigenic potential compared to exclusively epithelial or mesenchymal cells (Pastushenko et al., 2018; Kröger et al., 2019).

Hybrid epithelial/mesenchymal state hybrids can be promoted by Zinc finger protein SNAI1 (Snail, gene *SNAI1*) transcription factor activity, the expression of which is specific to E/M populations of basal breast cancer cells (Kröger et al., 2019). Snail protein was found to be 5-fold higher in such cells compared to mesenchymal populations, while epithelial cells displayed undetectable levels (Kröger et al., 2019). However, this was only accompanied by a 1.5-fold increase in *SNAI1* transcript expression, implying that translational activation is more important in Snail overexpression than transcriptional regulation (Kröger et al., 2019). YB-1 translationally upregulates Snail expression (Evdokimova et al., 2009a,b), suggesting that YB-1 could also be a key promoter the E/M state. In support, stable YB-1 overexpressing epithelial Madin-Darby canine kidney ($MDCK^{YB-1}$) cells exhibited a partial EMT-like phenotype and establish viable tumor xenografts in mice, while parental MDCK

cells did not (Gopal et al., 2015). This increased tumorigenicity was also accompanied by elevated secretion of angiogenic factors (Gopal et al., 2015). Treatment of endothelial cells with concentrated conditioned medium from MDCK^{YB-1} cells also stimulated cell migration (Gopal et al., 2015).

Wnt signaling is also a primary driver of partial and complete EMT. β-catenin-dependent canonical Wnt signaling is thought to be preferentially active in E/M populations (Reya and Clevers, 2005; Kröger et al., 2019), while β-catenin-independent non-canonical signaling is more associated with a mesenchymal state, migration and invasion (Weeraratna et al., 2002; Gujral et al., 2014). Knockdown of YB-1 in hepatocellular carcinoma cells disrupted stemness and suppressed β-catenin protein expression and nuclear translocation, which was rescued by overexpression of the active form of β-catenin (Chao et al., 2017). This regulation of β-catenin-dependent Wnt signaling further supports a potential role for YB-1 in driving a partial EMT state. Interestingly, populations in the partial EMT state are also enriched with CSCs (Kröger et al., 2019), suggesting that YB-1 may also play are role in regulating these important cancer progenitors.

Involvement in Cancer Stem-Like Cells

Cancer stem-like cells are becoming recognized as important drivers of disease progression and are thought to be a major contributing factor toward metastasis, the development of drug resistance and recurrence of most cancers, including those of the thorax (Leon et al., 2016; MacDonagh et al., 2016; Makena et al., 2018). CSCs are a heterogeneous, slow growing population of cells within a tumor. They have self-renewal ability but one subpopulation, termed metastatic CSCs, can disseminate through blood vessels and initiate metastasis (Dalerba and Clarke, 2007). This was clearly demonstrated in pancreatic cancer, where eradicating the metastatic CSC population dramatically reduced metastatic but not tumorigenic potential, implying that a subgroup of CSCs are responsible for metastasis (Hermann et al., 2007).

One recent study has shown that YB-1 enforces lung cancer metastatic CSC-like properties *in vitro* and *in vivo* through transcriptional upregulation of *NANOG*, a marker of CSCs required for the invasion and sphere formation of ADC cells *in vitro* (Guo et al., 2017). Supporting this, knockdown of YB-1 in hepatocellular carcinoma cells reduced *NANOG* and *Oct4*, as well as α-fetoprotein transcript expression (Chao et al., 2017). This follows findings showing NANOG and Oct4 are upregulated in ADC, which induce sphere formation, drug resistance and EMT (Chiou et al., 2010). YB-1 also regulates SOX2 in breast CSCs, maintaining stem-like properties and tumorigenic potential (Jung et al., 2014). Given the probable importance and frequent upregulation of SOX2 in lung cancer (Rudin et al., 2012; Karachaliou et al., 2013; Friedlaender et al., 2019; **Figure 1B**), a study investigating the relationship between YB-1 and SOX2 in thoracic cancer may further implicate YB-1 in the biology of these diseases.

Y-box binding protein-1 has been shown to be important in other cancer CSCs as well. Brain CSCs were shown to have high expression of YB-1 which was utilized in a YB-1-based virotherapy *in vitro* (Mantwill et al., 2013). The re-expression of the microRNA miR-382 in osteosarcoma cells significantly decreased the CSC population resulting in reduced relapse after doxorubicin treatment, EMT and metastasis both *in vitro* and *in vivo* (Xu et al., 2015). The authors attributed these tumor suppressive functions of miR-382 to targeting and downregulating YB-1 (Xu et al., 2015). This microRNA is downregulated in NSCLC and exogenous miR-382 expression inhibits NSCLC growth, migration and invasion via the suppression of *SETD2* (Chen T. et al., 2017) and *LMO3* (Chen et al., 2019). In breast cancer, inhibition of p90 RSK, a major kinase involved in YB-1 phosphorylation; see section "Post-Translational Modification in the Control of YB-1 Activity and Localization") using the small molecule LJI308 eradicated the population of breast CSCs and induced apoptosis in breast cancer cells (Davies et al., 2015). RSK is thought to have potential as a therapeutic target as it is involved in the proliferation of lung cancer (Poomakkoth et al., 2016). Furthermore, knockdown of WAVE3, a protein required for nuclear translocation of YB-1, prevented YB-1 mediated transcriptional activation *NANOG*, *SOX2* and *Oct4* in breast CSCs (Bledzka et al., 2017). WAVE3 expression was also correlated with that of YB-1 and more aggressive phenotypes of breast cancer (Bledzka et al., 2017).

YB-1 Is Involved in Hypoxic Response

The maintenance of CSCs is intertwined with the effects of hypoxia (Li and Rich, 2010). Supporting its role in thoracic CSC biology, hypoxia promotes an aggressive phenotype in MPM and upregulates Oct4, a marker of CSCs (Kim et al., 2018). Oct4 is also important in gefitinib-resistant lung CSCs and cisplatin-induced stemness in NSCLC has been linked to hypoxia-inducible factors (Kobayashi et al., 2016). Hypoxia occurs in most solid tumors and has been linked to CSC maintenance and behavior (Li and Rich, 2010; Bao et al., 2012), as well as disorganized tumor vascularization, EMT and metastasis (Muz et al., 2015). Factors such as HIF1α drive hypoxia-mediated transcription, influencing cell immortalization, metastasis and vascularization (Semenza, 2014). YB-1 translationally regulates HIF1α (El-Naggar et al., 2015) and acts as a transcriptional repressor for the HIF1α inhibitor *FOXO3a* via competition for p300 during vascular development (Emerling et al., 2008; Chou et al., 2015). Under hypoxic conditions YB-1 translocates to the nucleus where it binds to hypoxia response elements within the 3′ enhancer of the *EPO* gene and blocks its expression (Rauen et al., 2016). Hypoxia plays an important role in driving malignant cellular behavior, including resistance to chemotherapy (Rohwer and Cramer, 2011). While YB-1-driven response to hypoxia may contribute toward chemoresistance, its activity as a transcription factor may also play a role in drug inefficacy.

A Possible Role for YB-1 in Resistance to Platinum-Based Chemotherapy

Although the role of YB-1 has not yet been studied in lung cancer or MPM, it has been shown to be involved in the

chemoresistance of many cancers including that of platinum-based chemotherapies (To et al., 2010; Kang et al., 2013; Lasham et al., 2013; Shiota et al., 2014; Yamashita et al., 2017). Silencing YB-1 induces cisplatin sensitization in neuroblastoma (Wang H. et al., 2017), esophageal SCC (Xu and Hu, 2016), bladder cancer (Shiota et al., 2011) and melanoma (Schittek et al., 2007). Treatment with cisplatin also stimulates YB-1 production in bladder cancer (Shiota et al., 2010), while ovarian cancer cells with acquired cisplatin resistance show an increase in nuclear YB-1 expression (Yahata et al., 2002), suggesting that cancer cells may increase YB-1 production as a protective measure. The reasons why YB-1 may provide protection are still unclear. However, YB-1 does transcriptionally upregulate *LRP*, aka *MVP* (Stein et al., 2005), the principal component of vaults in human cells. Vaults are highly conserved ribonucleoproteins which have been suggested to play a role in the resistance of cancer cells to cisplatin, among other chemotherapies, by sequestering drugs away from their intended targets (Wang W. et al., 2004; Lara et al., 2011). YB-1 knockdown in lung cancer cell lines resulted in LRP downregulation and nuclear staining of YB-1 correlated with LRP expression in 105 NSCLC samples, conferring significantly lower overall survival (Hyogotani et al., 2012). However, this study did not investigate the effect of this knockdown on the chemoresistance of any drug.

Y-box binding protein-1 has also been linked to *MRP1* gene activation (Stein et al., 2001; Mantwill et al., 2006), an efflux ATP-binding cassette transporter which is thought to contribute toward multidrug resistance (Stefan and Wiese, 2019). High levels of LRP and MRP1 correlated with lower response to cisplatin chemotherapy, poorer progression free survival and overall survival in advanced NSCLC patients receiving cisplatin-based chemotherapy (Li J. et al., 2009; Li X.Q. et al., 2009). Treatment with cisplatin also induces heightened LRP expression in ADC and SCC cell lines (Xu et al., 2017a) and *LRP* gene expression was significantly increased compared to control pleura samples in a study of MPM patients (Singhal et al., 2003). *MDR1* gene (encoding P-glycoprotein 1), which is dependent on the nuclease and base excision repair enzyme APE1 expression, has also been implicated in YB-1-driven cisplatin resistance (Ohga et al., 1998; Chattopadhyay et al., 2008). However, the evidence supporting a clear role for P-glycoprotein 1 as an integral player in the chemoresistance of lung cancer and mesothelioma remains contentious, implying that other targets may be more important (Soini et al., 2001; Wangari-Talbot and Hopper-Borge, 2013).

An Agent of DNA Repair in Response to Cisplatin and Oxidative Stress

Y-box binding protein-1 may drive chemoresistance through the upregulation of the above targets and through driving a hypoxic response. However, some of its other functions may also contribute, such as its role as part of the DNA repair machinery. Oxidative stress and resulting chronic inflammation has long been implicated as a primary driver of cigarette smoking-related diseases, including lung cancer (Park et al., 2009; Sears, 2019). Altered DNA repair pathways have been implicated in the carcinogenesis of lung cancer in response to cigarette smoke-related DNA damage, particularly the NER and BER pathways (Sears, 2019). There is also a body of evidence supporting the suggestion that COPD leads to the development of lung cancer, or at least that the two are correlated (Sears, 2019). Chronic inflammation caused by asbestos-related oxidative stress is a major driver of MPM carcinogenesis (Benedetti et al., 2015; Chew and Toyokuni, 2015), implying that aberrations in DNA repair machinery in response to oxidization play a role in the progression of many thoracic cancers.

Y-box binding protein-1 has been suggested to be part of the DNA repair machinery as it binds to enzymes involved in BER, mismatch repair and DNA double-stranded break repair, previously reviewed (Alemasova and Lavrik, 2017). YB-1 binds preferentially to cisplatin-damaged DNA complexed with PCNA, where it works to separate cisplatin-damaged DNA strands, recruit DNA repair proteins and displays weak endonucleolytic and exonucleolytic function (Ise et al., 1999; Gaudreault et al., 2004). PARP1 has also been shown to catalyze the poly(ADP-ribosyl)ation of YB-1 in the presence of DNA damage, further supporting a role for YB-1 in DNA repair (Alemasova et al., 2015).

Y-box binding protein-1 is also involved in NER and BER in response to oxidative stress. DNA damage-related stress stimulates YB-1 nuclear translocation (Cohen et al., 2010) (discussed further in section "Control of YB-1 Subcellular Localization") where it can bind to oxidized DNA lesions, structurally altering DNA to allow access to the damaged site while recruiting and scaffolding proteins involved in BER including PARP1, PARP2, NEIL1, and PCNA, among others (Dutta et al., 2015; Alemasova et al., 2016). In ssDNA, YB-1 suppresses NEIL1-mediated apurinic/apyrimidinic site cleavage, and it has been suggested that the role of YB-1 in DNA repair can prevent ssDNA breaks and induce oxidative nucleotide repair in double-stranded DNA (Dutta et al., 2015). YB-1 has also been linked to NER. Cross-talk between YB-1 and XPC (an important player in NER which has significance in lung cancer carcinogenesis and is affected by germline mutation in MPM), results in their assembly at DNA damage sites (Jin et al., 2014; Fomina et al., 2015; Betti et al., 2017; Sears, 2019).

Y-box binding protein-1 was found to be involved in mitigating cigarette smoke-induced guanine oxidization in lung fibroblasts and mice chronically exposed to cigarette smoke, and that lung samples of late-stage COPD patients exhibited significantly lower YB-1 levels compared to early mid stage patients or patients without COPD (Deslee et al., 2010). The role YB-1 plays in DNA repair (particularly from oxidization) and the fact that it is secreted under oxidizing conditions (see section "YB-1 is Secreted Into the Extracellular Space Under Cellular Stress") implies that YB-1 may promote the oxidation-related carcinogenesis of lung cancer and MPM. Cigarette-induced oxidative stress has additionally been suggested to induce the release of exosomes (Ryu et al., 2018), the sorting of which are also mediated in part by YB-1.

YB-1 and Exosomal RNA Sorting

Extracellular vesicles such as exosomes are used by cells for intercellular communication to both their immediate and distant surroundings (Mashouri et al., 2019). Exosomes carry factors such as proteins, mRNA and miRNA to mediate processes including embryonic development, injury response and homeostasis (Mashouri et al., 2019). Exosomes also play versatile and key roles in cancer cell behavior and remodeling of the tumor microenvironment (Mashouri et al., 2019). A malignant role for exosomes in lung cancer is well documented, where exosomes can induce proliferation, angiogenesis, EMT changes and metastasis (Vanni et al., 2017; Zhou et al., 2017a; Ryu et al., 2018). Exposure to cigarette smoke is also thought to induce the release of extracellular vesicles, such as exosomes, which has been linked to the development of COPD and possibly the development of lung cancers (Ryu et al., 2018). Asbestos exposure also alters the exosomal cargo of lung epithelial cells *in vitro* and exposing non-malignant mesothelial cells to these exosomes induces gene expression changes related to EMT and other cancer related pathways (Munson et al., 2018). This indicates that exosomes may play an integral role in the carcinogenesis of mesothelioma. MPM cell lines also secrete higher levels of exosome-associated proteins linked to stress response and proliferation compared to their non-malignant counterparts (Creaney et al., 2017). Supporting this, exosomes from MPM cells have a distinct oncogenic signature and stimulate the migration of fibroblasts and endothelial cells (Greening et al., 2016).

Y-box binding protein-1 is known to be involved in exosomal RNA-sorting, reviewed previously (Suresh et al., 2018), which may indicate it is involved in altering malignant exosomal expression profiles. Briefly, the presence of YB-1 in exosomes has been shown in both malignant and non-malignant cells alike where it helps to define the levels of several RNA species, including miRNA and tRNA (Shurtleff et al., 2017; Suresh et al., 2018). However, to our knowledge no study has investigated YB-1 in lung cancer and mesothelioma exosomal sorting. Future studies following this line may shed further light into the underlying mechanisms of exosomes and their role in thoracic cancer biology.

A Role in Immune Evasion?

Evidence in other tumor types suggests that the upregulation of YB-1 could drive immune evasion. For example, in doxorubicin-resistant hepatocellular carcinoma cells, YB-1 is overexpressed, which in turn transcriptionally upregulates the expression of PD-L1 and decreases the secretion of the chemokines IL1β, IL10, and TGFβ *in vitro* (Tao et al., 2019). High YB-1 was also associated with resistance to cisplatin, gemcitabine, docetaxel, dasatinib and gefitinib in this study (Tao et al., 2019). This suggests that resistance to these drugs may also result in heightened PD-L1 and subsequent immunosuppression via YB-1 upregulation, at least in hepatocellular carcinoma. In light of these results, investigating the potential of a similar role in thoracic cancers would be of great interest.

YB-1 Regulation: A Complex Network of Transcriptional, Translational and Post-translational Control

The wide-ranging roles of YB-1 in cell biology imply that its expression, localization and function must be tightly regulated in normal physiology. As YB-1 is frequently overexpressed in cancer, dysregulation of these controlling systems may play a role in malignant transformation. The expression and localization of YB-1 is controlled by a complex network of transcriptional, translational and autoregulatory signals discussed below.

Transcriptional Control

Several transcription factors have been found to promote YB-1 transcription by binding to motifs in the *YBX1* promoter. For example, *YBX1* transcription has been shown to be promoted by GATA transcription factors, although recent evidence suggests the GATA family is less important for promoting *YBX1* expression in ADC (Yokoyama et al., 2003; Murugesan et al., 2018). Possibly more important are the six E-boxes located in the promoter of *YBX1* (Makino et al., 1996). The first is located at 48–53 nucleotide residues away from the promoter, the second at 353–358, the third at 458–463, the fourth at 531–536, the fifth at 1147–1152, and the sixth at 1201–1206 (Makino et al., 1996). The E-box binding transcription factor Twist1 also stimulates *YBX1* transcription, driving cell growth and EMT (Shiota et al., 2008; He et al., 2015; **Figure 2**). A recent meta-analysis of 572 NSCLC patients showed that high Twist1 expression significantly correlated with poorer patient prognosis, recurrence-free survival and lymph node or other metastasis (Li et al., 2018). A small retrospective study of mesothelioma samples also showed that Twist1 expression was significantly higher in sarcomatoid tumors (expressed in 7/7 of samples) compared to biphasic (6/10) and epithelioid tumors (7/17) (Iwanami et al., 2014). Although the percentage of samples positive for YB-1 was almost identical to that of Twist1 in this study (6/7 in sarcomatoid, 6/10 in biphasic and 7/17 in epithelioid), whether YB-1 and Twist1 were co-expressed in the same samples was not determined (Iwanami et al., 2014).

An E-box within the YB-1 promoter is also trans-activated by Myc and p73 to drive the transcription of *YBX1* (Uramoto et al., 2002; **Figure 2**). The ability of Myc to transcriptionally activate *YBX1* is interesting, not only as Myc drives malignant behavior and is often associated with poor prognosis in thoracic cancers (Jiang et al., 1992; Volm and Koomagi, 2000; Riquelme et al., 2014), but because YB-1 can itself initiate *Myc* translation by acting as a specific internal ribosome entry segment-trans-activating factor (Cobbold et al., 2010). YB-1 was also shown to regulate *Myc* at the transcriptional level in bladder cancer, with implications on aerobic glycolysis (Warburg effect) (Xu et al., 2017b). This feed forward loop was first described in multiple myeloma (Bommert et al., 2013), however, it is quite possible that a similar feed forward loop accounts for both YB-1 and Myc overexpression in thoracic cancers, driving malignant progression and aggressiveness.

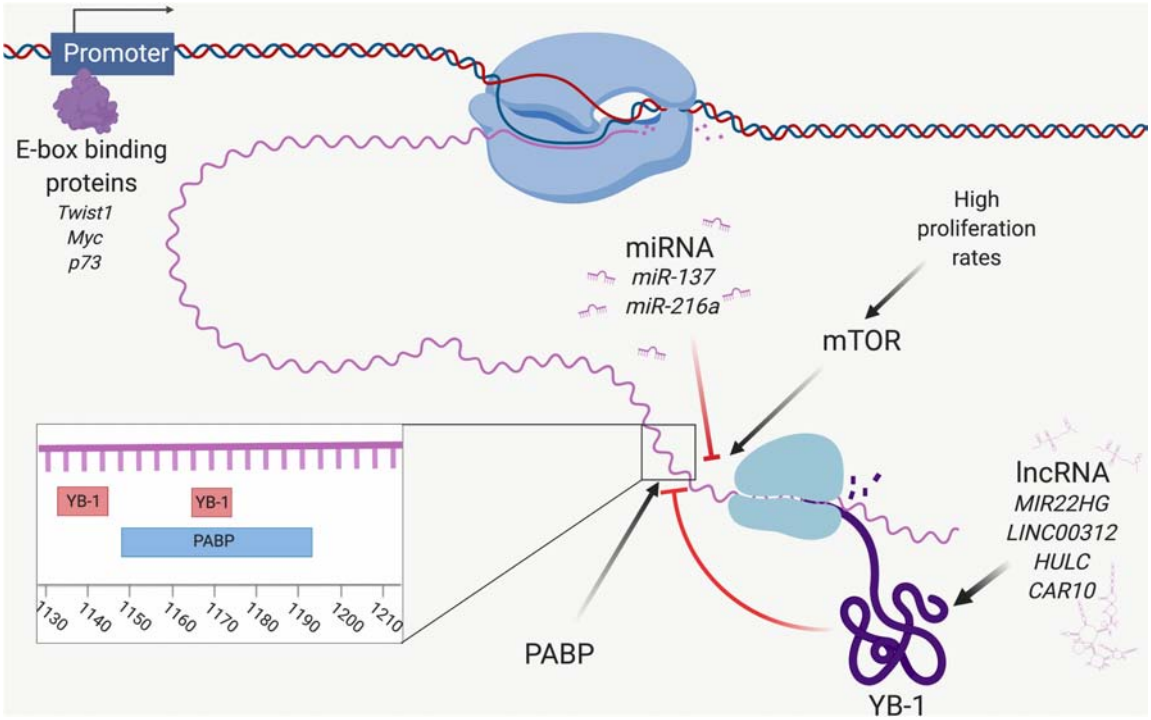

FIGURE 2 | Control of YB-1 expression. A network of factors controls *YBX1* expression at the transcriptional and translational levels. The E-box binding proteins Twist1, Myc and p73 interact with the promoter of *YBX1* and initiate transcription of *YBX1* mRNA. *YBX1* mRNA expression is downregulated by targeting miRNA, including miR-137 and miR-216a. *YBX1* translation is stimulated by mTOR, which itself is influenced by proliferation rate. YB-1 protein function and expression are modulated by lncRNA, including MIR22HG and LINC00312. YB-1 is involved in an autoregulatory feedback loop and binds to *YBX1* mRNA at two sites (nucleotides 1133–1145 and 1165–1172), inhibiting its own translation. PABP stimulates *YBX1* translation by binding to a site located at 1149–1196, overlapping the second YB-1 binding site. Poly(A)-binding protein (PABP) and YB-1 compete for this site and hence regulate the level of YB-1 protein expression. Created with Biorender.com.

Translational Regulation of YB-1

Y-box binding protein-1 expression is also regulated at the translational level, most notably via signaling through the mTOR pathway (**Figure 2**), which regulates cell growth, motility, survival, transcription and protein synthesis via the integration of signals from hormone and growth factor stimulation, availability of nutrients, and stress (Zarogoulidis et al., 2014). mTOR signaling promotes the translation of *YBX1* and increases the phosphorylation of RSK, a serine/threonine kinase which phosphorylates and thereby activates YB-1 (Mendoza et al., 2011; Lyabin et al., 2012). RSK has been implicated in lung cancer proliferation and has itself been suggested as a target with therapeutic significance (Poomakkoth et al., 2016).

The division rate of eukaryotic cells affects *YBX1* translation via mTOR regulation. Slow dividing and serum-starved cell populations exhibit attenuated mTOR signaling, which in turn inhibits *YBX1* translation (Lyabin et al., 2012). This pathway is frequently activated in lung cancer and antagonizing mTOR in such cells has proven to be a potential therapeutic avenue (Zarogoulidis et al., 2014). The PI3K/mTOR pathway is also highly activated in mesothelioma, but not in non-malignant mesothelial cells (Zhou et al., 2014) or adjacent tissue (Hoda et al., 2011), and phospho-mTOR was significantly associated with poorer overall survival in a cohort of 107 mesothelioma patients (Bitanihirwe et al., 2014). Dactolisib (BEZ235) treatment inhibited mesothelioma cell growth by targeting mTOR (Zhou et al., 2014) and similarly, treatment with the mTOR inhibitor temsirolimus stopped MPM cell proliferation and was synergistic with cisplatin treatment *in vitro* and *in vivo* (Hoda et al., 2011). It stands to reason that YB-1 overexpression is likely to be, at least in part, linked to the prominent role mTOR signaling plays in thoracic cancers.

Autoregulation of YB-1 – An Unsolved Piece of the Puzzle

Y-box binding protein-1 is controlled by an autoregulatory feedback loop in which YB-1 binds its own mRNA at two 8 nucleotide motifs at (nt) 1133–1145 and nt 1165–1172, inhibiting translation prior to 40S ribosomal subunit binding (Skabkina et al., 2005; **Figure 2**). PABP competes with YB-1 at one of these overlapping sites (nt 1149–1196), and stimulates *YBX1* translation (Skabkina et al., 2003, 2005). Considering YB-1 overexpression is frequently observed in cancer, this feedback system may be dysregulated before or during malignant progression. It is possible that PABP upregulation could cause a bias for PABP translational activation of *YBX1*, although PABP itself is controlled by a similar autoregulatory loop (Ma et al., 2006). Nonetheless, recent expression and interactome analysis

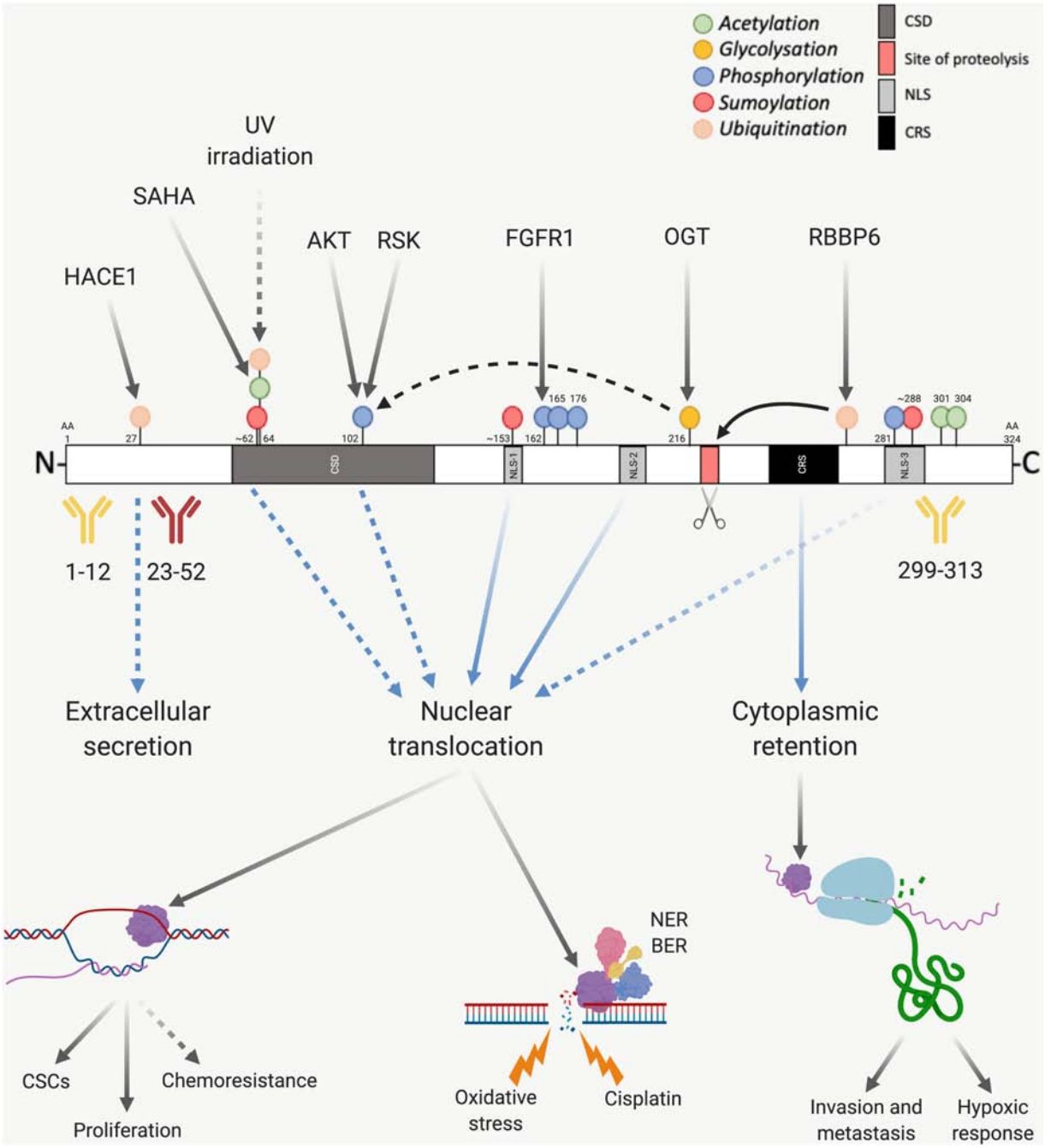

FIGURE 3 | Post-translational modification of YB-1. The presence of various sites before or after proteasomal cleavage of YB-1 modulates its function and localization, which has implications on antibody use. YB-1 is comprised of a CSD shown in dark gray, an N-terminal domain in white and a CTD, also in white. Within the CTD there are three nuclear localization signals (NLS-1 from amino acid (aa) 149–156, NLS-2 from aa 185 to 194 and NLS-3 from aa 276 to 292), shown in light gray, and one cytoplasmic retention signal (CRS from aa 247 to 267), shown in black. YB-1 is proteolytically cleaved at Glu216 and Glu219 (shown in red and highlighted with a scissors icon), which is thought to stimulate YB-1 translocation. Three commonly used antibodies targeting YB-1 are also shown, two of which have been validated using mass spectrometry (in yellow) and one which is known to cross react with hnRNP1A (in red). If the proteolytic theory of YB-1 translocation is correct, this would also have implications on the use of antibodies. Various post-translational modifications also effect the downstream function and nuclear localization of YB-1. Green dots indicate acetylation, yellow glycosylation, blue phosphorylation, red sumoylation and orange ubiquitination. Solid black arrows indicate a post-translational modification that is produced by a known upstream regulator, or a known function of YB-1. Dotted black arrows indicate a post-translational modification or function that is yet to be fully proven. Blue and dotted blue arrows indicate the movement or supposed movement of YB-1 throughout cellular compartments, respectively. Created with BioRender.com.

of YB-1 showed that PABP significantly correlated with YB-1 expression in ADC, implying it plays a central role in YB-1 upregulation and highlighting the need for further investigation into the PABP/YB-1 loop (Murugesan et al., 2018).

Non-coding RNA Modulate YB-1 Expression

Various families of ncRNAs also play a role in regulating YB-1 levels (**Figure 2**). One such family are miRNAs – a conserved class of short, ncRNAs that regulate gene expression by binding to and initiating RNA-induced silencing complex-mediated degradation of target mRNA (Jonas and Izaurralde, 2015). The inhibition of *YBX1* by several miRNAs has been shown in other cancers, although to our knowledge such interactions have not been investigated in thoracic cancers. We recently demonstrated regulation of *YBX1* by miR-137 in MPM cells, inhibiting growth, migration and invasion (Johnson et al., 2018). This miRNA is also known to act as a tumor suppressor in lung cancer by targeting SRC3 (Chen R. et al., 2017) and BMP7 (Yang et al., 2015). Another miRNA known to target *YBX1* is miR-216a, which suppresses YB-1-mediated metastasis in pancreatic cancer (Lu et al., 2017). MiR-216a acts as an tumor suppressor in SCLC by targeting and downregulating the anti-apoptotic protein B-cell lymphoma 2 (Bcl-2) (Wang et al., 2018), although it is likely that these effects are also, in part, due to *YBX1* downregulation.

The lncRNA DANCR has been implicated in reducing the levels of this miRNA through its complimentary miR-216a binding site, sequestering it away from miR-216a targets (Zhen et al., 2018). DANCR is associated with advanced tumor grade and poor prognosis in lung cancer and promotes ADC cell growth *in vitro* and *in vivo* (Zhen et al., 2018). Dysregulation of DANCR and subsequent lowering of miR-216a could represent one mechanism of YB-1 overexpression in thoracic cancer, representing an area which requires further investigation.

In addition to DANCR, other lncRNAs as well as transfer RNA-derived fragments can also play a role in regulating YB-1 expression, reviewed previously (Suresh et al., 2018). One example is the lncRNA GAS5, which interacts with YB-1 protein and activates *YBX1* translation, upregulating p21 and initiating G1 cell cycle arrest in stomach cancer (Liu et al., 2015). Interestingly, GAS5 knockdown did not affect *YBX1* mRNA expression, something the authors attribute to possible interactions with other proteins (Liu et al., 2015). GAS5 is a known competing endogenous RNA for miR-137, which targets *YBX1* in thoracic cancers (see above in this section) (Chen et al., 2018), so it is possible that this may contribute toward *YBX1* translational upregulation. However, GAS5 knockdown does not affect *YBX1* mRNA expression (Liu et al., 2015), as would be expected by an increase in miR-137 availability, so this does not fully explain this relationship. Further inquiry into the GAS5/YB-1 and possibly miR-137 relationship is required. GAS5 acts as a tumor suppressor and is lost in lung cancer and mesothelioma (Renganathan et al., 2014; Shi et al., 2015), which is consistent with findings in other cancer types (Gutschner et al., 2018). The apparent discrepancy between the tumor suppressive function of GAS5 and GAS5-mediated translational upregulation of the oncogene *YBX1* remains unanswered and also warrants further study.

More recently, the lncRNA *MIR22HG* was shown to prevent proteasomal degradation of YB-1 in lung cancer cells, which might contribute to YB-1 overexpression (Su et al., 2018). LINC00312 also interacts with YB-1 driving invasion, migration and vascular mimicry of ADC cells, and LINC00312 is associated with metastasis in ADC patients (Peng et al., 2018). HULC is another lncRNA that binds to YB-1 in hepatocellular carcinoma cells, promoting Ser102 phosphorylation, the significance of which is further described in section "Post-Translational Modification in the Control of YB-1 Activity and Localization" (Li et al., 2017). HULC is overexpressed in NSCLC and can promote proliferation via SPHK1 upregulation, which is upstream of the PI3K/AKT pathway (Liu L. et al., 2018). This implies that HULC may also be involved in PI3K-mediated YB-1 activation. TP53TG1, yet another lncRNA, can also bind to YB-1 and inhibit its nuclear translocation, stopping it from transcriptionally activating its oncogenic targets (Diaz-Lagares et al., 2016). TP53TG1 is downregulated in NSCLC and its upregulation sensitized cisplatin resistant NSCLC cells to cisplatin (Xiao et al., 2018). This was attributed to the downregulation of miR-18 (Xiao et al., 2018), however, considering the likely role of YB-1 transcriptional regulation in cisplatin resistance (see section "A Possible Role for YB-1 in Resistance to Platinum-Based Chemotherapy"), it is possible that cytoplasmic retention of YB-1 also played a part in the cisplatin sensitivity seen here. Finally, CAR10 binds to and stabilizes YB-1, leading to the upregulation of EGFR in lung cancer and promoting proliferation (Wei et al., 2016). ncRNA therefore play an integral role in the expression and activity of YB-1, and dysregulation of these families is likely to contribute to YB-1 overexpression in cancer.

Post-translational Modification in the Control of YB-1 Activity and Localization

The activity of YB-1 is modulated through various post-translational modifications (**Figure 3**), with phosphorylation being the best studied. Ser102 (located in the CSD of YB-1) is currently the most comprehensively studied phosphorylation site. This site is a target of AKT and RSK, making it downstream of both the MAPK/ERK and PI3K/AKT pathways (Sutherland et al., 2005; Stratford et al., 2008; Mendoza et al., 2011). Several additional phosphorylation sites on YB-1 have been identified including Tyr281, which is located within a NLS toward the C-terminal of YB-1 and correlates with the nuclear localization of either a YB-1 C-terminal fragment or full length YB-1 (van Roeyen et al., 2013) (refer to next section for more detail). Tyr162 on YB-1 is also reportedly phosphorylated by FGFR1 (Kasyapa et al., 2009), an important oncogenic driver in lung cancer (Jamal-Hanjani et al., 2017; Friedlaender et al., 2019) and mesothelioma (Schelch et al., 2014; Quispel-Janssen et al., 2018), however, to our knowledge the significance of this modification has not yet been established. Ser165 and Ser176 on YB-1 are also phosphorylated, each promoting distinct groups of nuclear factor-κB target gene expression. This pathway is commonly

dysregulated in thoracic cancers and drives cell survival, chemo- and radiotherapy resistance (Chen et al., 2011; Nishikawa et al., 2014; Prabhu et al., 2015; Martin et al., 2017).

In the case of Ser102, it seems that phosphorylation is linked to the hexosamine biosynthetic pathway, in which OGT and O-linked N-acetylglucosamine add or remove N-acetylglucosamine groups to serine or threonine residues, respectively. OGT-mediated O-linked glycosylation of YB-1 at Thr216 aids in the phosphorylation of Ser102 and subsequent transcriptional activity of YB-1 in hepatocellular carcinoma (Liu et al., 2016; **Figure 3**).

Sumoylation, acetylation and ubiquitination are also prominent post-translational modifications that can contribute toward regulating YB-1 activity and localization. In addition, the nuclear localization of YB-1 has been linked to three NLS, mapped to amino acid residues 149–156 (NLS-1), residues 185–194 (NLS-2) and residues 276–292 (NLS-3) (van Roeyen et al., 2013).

Y-box binding protein-1 is sumoylated at three distinct sites in response to circadian rhythm in zebra fish cells, which has implications on its nuclear shuttling (Pagano et al., 2017). One of these sites is a canonical inverted sumoylation site (at amino acids 287–290 within NLS-3), while the other two are non-canonical sites (at 60–63 which is within the CSD and at 151–154, within NLS-1; **Figure 3**) (Pagano et al., 2017). Circadian disruption has been correlated with an increased risk of cancer development (Hansen, 2017; Liu W. et al., 2018) and many processes integral to tumorigenesis follow circadian rhythms (cell cycle regulation and DNA repair, for example). Although one study failed to find a link between night shift work and lung cancer among a cohort of female textile workers in Shanghai, China (Kwon et al., 2015), preclinical data indicates that disturbance of the circadian clock can promote lung tumor growth *in vivo* (Papagiannakopoulos et al., 2016). Modulation of YB-1 localization in response to light may represent one contributing factor in the observed correlation between circadian rhythm and cancer and warrants further investigation.

Acetylation of YB-1 has been reported to occur in lung cancer cells, however, the significance of this remains unclear. YB-1 was one of 542 proteins acetylated by the histone deacetylase inhibitor SAHA in SILAC experiments in a NSCLC cell line (Wu et al., 2015). Here, YB-1 was acetylated at Lys64 (**Figure 3**). Lys301/304 of YB-1 can also be acetylated and the amount of acetylated YB-1 is significantly increased in monocytes of hemodialysis patients (Ewert et al., 2018).

Ubiquitination may also play an important role in YB-1 expression and subcellular localization. RBBP6 initiates proteasomal degradation of YB-1 by binding to and ubiquitinating it within a 62-residue fragment of the YB-1 CTD (Chibi et al., 2008). The protein isoform of p63 ΔNp63α counteracts this by preventing proteolysis of full-length YB-1 and stimulating accumulation of poly-ubiquitinated YB-1 in the nucleus (di Martino et al., 2016), possibly supporting the role of proteolytic cleavage-dependent YB-1 nuclear shuttling (discussed further in section "Control of YB-1 Subcellular Localization"; **Figures 3**, **4**). Further supporting this theory, UV irradiated DNA damage stimulates YB-1 ubiquitination at Lys64 (Boeing et al., 2016) (the same lysine residue that is acetylated, above in this section; **Figure 3**). Considering the DNA repair function of YB-1 and the aforementioned ubiquitination-driven proteasomal cleavage of YB-1, this possibly induces a similar nuclear translocation of YB-1. This is further supported by results showing that YB-1 is shuttled to the nucleus upon UV irradiation (Koike et al., 1997).

Ubiquitination is also important in the secretion of YB-1 via the multi-vesicular body pathway. The E3 ligase activity of HACE1 polyubiquitinates YB-1 at K27, facilitating tumor susceptibility gene 101 binding, which initiates YB-1 secretion (Palicharla and Maddika, 2015). In summary, post-translational modification influences the levels, activity and localization of YB-1, which in turn impacts the downstream effects of YB-1.

Control of YB-1 Subcellular Localization

In non-malignant cells, YB-1 is primarily located in the cytoplasm and functions as a major component of free messenger ribonucleoprotein complexes, where it can inhibit or stimulate cap-dependent translation depending on the ratio of YB-1 to mRNA (Suresh et al., 2018). Under certain stresses such as cisplatin treatment (Yahata et al., 2002), hypoxia (Rauen et al., 2016), UV radiation (Koike et al., 1997), and hyperthermia (Stein et al., 2001), YB-1 translocates to the nucleus, however, the underlying mechanism of this remains unclear. As above, YB-1 has three NLS sites which have been mapped to amino acid residues 149–156, residues 185–194 and residues 276–292 (van Roeyen et al., 2013), which are recognized by transportin-1 (Mordovkina et al., 2016) and WAVE3 (Bledzka et al., 2017). In addition YB-1 also contains a CRS at residues 247–267 (Woolley et al., 2011; **Figure 3**). The locations of these sites are postulated to regulate YB-1 nuclear-cytoplasmic translocation.

One line of evidence suggests that nuclear translocation is preceded by a specific proteolytic cleavage by the 20S proteasome of YB-1 at Glu216 and Glu219 under cellular stress (Sorokin et al., 2005; Kim et al., 2013; **Figures 3**, **4**). This results in loss of a 105-amino acid sequence from the C-terminus, including the CRS, and accumulation of the remaining N–terminal fragment in the nucleus (Sorokin et al., 2005; Kim et al., 2013). The presence of an NLS in the CTD suggests that a C–terminal fragment may also be shuttled to the nucleus, presumably if the nearby CRS has been cleaved off (van Roeyen et al., 2013; **Figures 3**, **4**). Supporting this, breast cancer cells preincubated with the proteasome inhibitor MG-132 before treatment with doxorubicin displayed reduced nuclear and enhanced cytoplasmic levels of YB-1 (visualized with a C-terminal-targeting antibody; **Figure 3**), compared to cells treated with doxorubicin alone (van Roeyen et al., 2013). However, this does not rule out whether full-length YB-1 translocation occurs by some other mechanism.

Countering the proteasomal theory is one study that suggests the YB-1 N-terminal fragment has been misidentified as another protein, hnRNP1A, and that only full-length YB-1 is found in the nucleus (Cohen et al., 2010). Full-length YB-1 nuclear translocation could be facilitated by its phosphorylation. For example, there is evidence showing that YB-1 is phosphorylated at Ser102 by the serine/threonine kinase AKT before being shuttled to the nucleus (Sutherland et al., 2005; **Figures 3**, **5**).

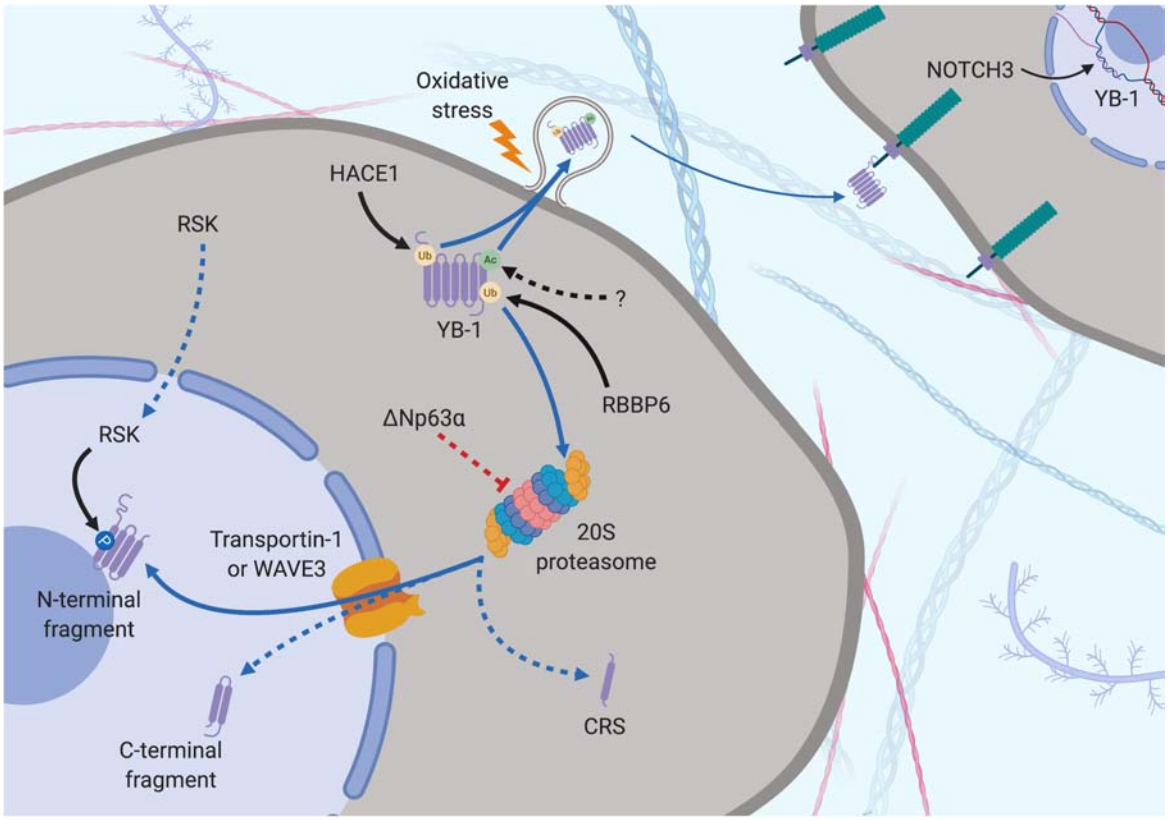

FIGURE 4 | Subcellular localization of YB-1 – the proteolytic theory of nuclear localization. YB-1 can be found in the nucleus, cytoplasm and extracellular space and its localization is mediated by various factors. Secretion can be preceded by Ubiquitination (orange dot) by HACE1 and acetylation (green dot) by a currently unknown protein. Oxidative stress stimulates stress-granule localization and eventual section of YB-1, where it can bind to the transmembrane protein Notch3 on other cells. YB-1 is cleaved by the proteasome prior to nuclear translocation. Ubiquitination by RBBP6 initiates YB-1 proteolytic cleavage. ΔNp63α prevents full length proteolysis by partially inhibiting YB-1 degradation, resulting in the removal of the CRS. Transportin-1 or WAVE3 bind to NLS of YB-1 and translocate it to the nucleus. RSK can cross into the nucleus, phosphorylating nuclear YB-1 fragments. Solid black arrows indicate a post-translational modification that is produced by a described or known mechanism. Dotted black arrows indicate a post-translational modification whose significance is yet to be realized. Blue and dotted blue arrows indicate the movement or supposed movement of YB-1 throughout cellular compartments, respectively. Created with BioRender.com.

This may cause a conformational change which could block the CRS of YB-1, stimulating its nuclear shuttling. However, a recent study found that while ionizing radiation, EGF stimulation and overexpression of the KRAS G12V mutant induced Ser102 phosphorylation of YB-1 in both the nucleus and the cytoplasm, there was no increase in YB-1 expression in nuclear fractions (Tiwari et al., 2018). The authors attribute this to nuclear translocation of RSK, phosphorylating pre-existing nuclear YB-1 – not the shuttling of YB-1 itself (**Figure 4**). It may be that the translocation of either YB-1, RSK or both is dependent on the type of cellular stress applied. As mentioned in section "Post-Translational Modification in the Control of YB-1 Activity and Localization," phosphorylation of Thr281 within the NLS 276–292 of YB-1 also correlates with its nuclear translocation (van Roeyen et al., 2013), however, it is not yet clear whether this modification is actively involved in YB-1 shuttling.

The localization of YB-1 also appears to be dependent on its ability to bind RNA and other proteins in the cytoplasm as YB-1 nuclear localization is hampered by higher cytoplasmic mRNA levels (Tanaka et al., 2018). This group also found that p53 (along with 4 other nucleocytoplasmic-shuttling proteins) binds to a YB-1 NLS and co-accumulates with YB-1 in the nucleus in response to actinomycin D treatment (Tanaka et al., 2016). This implies that YB-1 nuclear localization is a p53-mediated response to DNA stress. Another factor, C1QBP inhibits nuclear localization by binding to and blocking an NLS region (Matsumoto et al., 2018). C1QBP binding also moderately attenuated YB-1-mediated mRNA stabilization (Matsumoto et al., 2018). It is likely that the balance of this cytoplasmic interactome determines where YB-1 is localized under different conditions and that a disruption of this balance may lead to malignant progression.

YB-1 Is Secreted Into the Extracellular Space Under Cellular Stress

Stress-related secretion of factors found in the nucleus and cytoplasm have been found to be biologically relevant in thoracic cancer biology and may serve as potential non-invasive biomarkers. Secretion of the nuclear protein HMGB1 in response

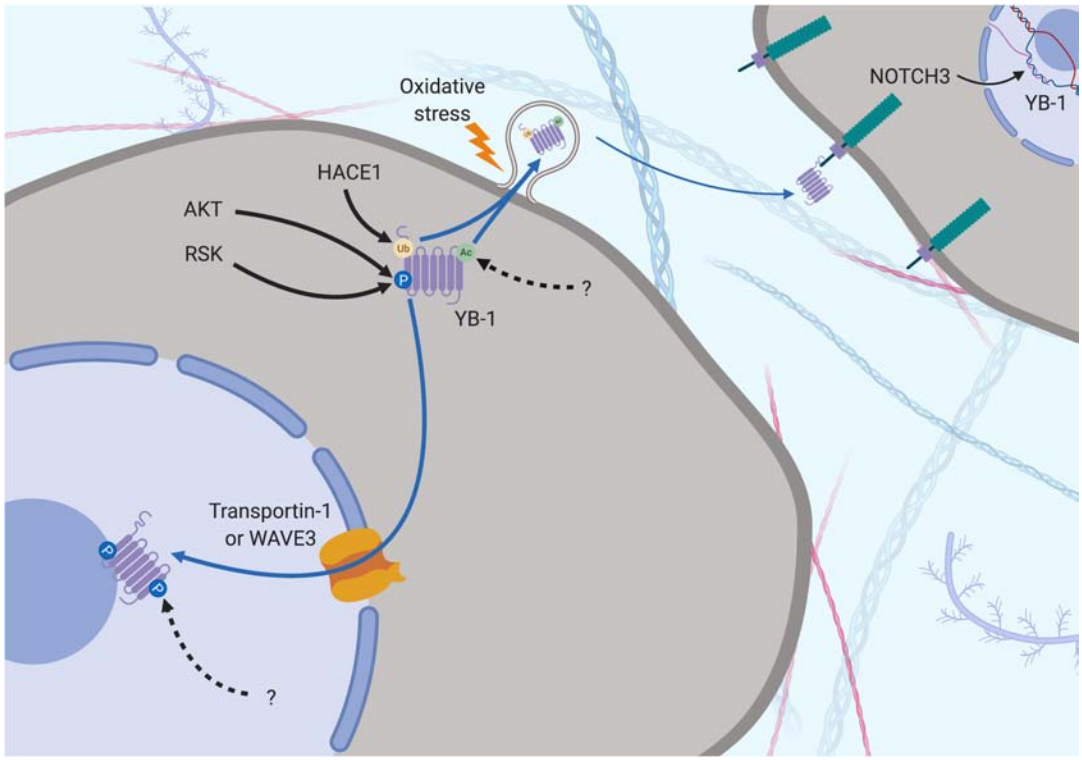

FIGURE 5 | Subcellular localization of YB-1 – the phosphorylation theory of nuclear localization. YB-1 can be found in the nucleus, cytoplasm and extracellular space and its localization is mediated by various factors. Secretion can be preceded by Ubiquitination (orange dot) by HACE1 and acetylation (green dot) by a currently unknown protein. Oxidative stress stimulates stress-granule localization and eventual section of YB-1, where it can bind to the transmembrane protein Notch3 on other cells. Phosphorylation is required before nuclear shuttling can take place. Ser102 is phosphorylated by upstream kinases, changing the configuration of YB-1 to block the CRS and allow nuclear shuttling via Transportin-1 or WAVE3. Phosphorylation of Tyr281 by a currently unknown upstream regulator may play a role here too. Solid black arrows indicate a post-translational modification that is produced by a described or known mechanism. Dotted black arrows indicate a post-translational modification whose significance is yet to be realized. Blue and dotted blue arrows indicate the movement or supposed movement of YB-1 throughout cellular compartments, respectively. Created with BioRender.com.

to asbestos-related necrosis in MPM cells, which acts as an alarmin to stimulate inflammation is one example (Yang et al., 2010). Serum HMGB1 has shown prognostic relevance as a possible biomarker in MPM (Tabata et al., 2013).

Y-box binding protein-1 is related on an evolutionary level to HMGB1 and is also secreted under certain cellular stresses. This was first evident in monocytes stimulated with bacterial lipopolysaccharide through an active, non-classical pathway and appears to require the same two lysine residues (Lys301/304) that are the site of acetylation in hemodialysis patients (Frye et al., 2009; Ewert et al., 2018; **Figures 3–5**). Secreted YB-1 stimulated DNA synthesis, cell proliferation and migration of kidney cells (Frye et al., 2009). More pertinent to thoracic cancer, YB-1 is also secreted under oxidative stress. YB-1 translationally upregulates *G3BP1* under oxidative stress and localizes to cytoplasmic stress granules where it is involved in pro-survival mRNA reprogramming (Somasekharan et al., 2015). G3BP1 also promotes the invasion and metastasis of sarcoma cells *in vivo* (Somasekharan et al., 2015). In support, YB-1 enrichment in stress granules is also linked to its secretion to the extracellular space under oxidizing conditions (Guarino et al., 2018; **Figures 4**, **5**). Secretion of YB-1 resulted in depletion of cytoplasmic YB-1, leaving nuclear expression intact (presumably to allow for YB-1-mediated DNA repair), while secreted YB-1 inhibited the growth of neighboring keratinocytes (Guarino et al., 2018).

Extracellular YB-1 acts as a ligand for Notch3, binding to epidermal growth factor-like repeats 17–24 on Notch3 and subsequently promoting *YBX1* translation in a feed-forward, autoregulatory fashion (Rauen et al., 2009; Raffetseder et al., 2011; Gera and Dighe, 2018; **Figures 4**, **5**). Notch3 is frequently overexpressed in NSCLC where high levels correlate with poor prognosis, making it a candidate target for therapeutic intervention (Zong et al., 2016). Considering the prevalence of oxidative stress and Notch3 in thoracic cancers, the secretion of YB-1 may be biologically important, although more studies are required to fully understand this process.

YB-1 IN THORACIC CANCERS: CLINICAL RELEVANCE

YB-1 as a Prognostic Biomarker

There is evidence supporting the use of YB-1 as a prognostic biomarker in thoracic cancers, and subcellular localization is

important in this regard. Analysis of TCGA data demonstrate that high levels of *YBX1* mRNA correlate significantly with poor prognosis in NSCLC and MPM patients (**Figures 1D,E**). YB-1 protein has been correlated with poor prognosis previously (Shibahara et al., 2001; Gessner et al., 2004), supported by a recent meta-analysis of six studies covering data on 692 NSCLC patients, where YB-1 was associated with worse overall survival, tumor stage and depth of invasion (Jiang et al., 2017). A study in MPM patients also supports the TCGA data (albeit tentatively due to the low number of patients in the cohort) (Iwanami et al., 2014). Here, YB-1 levels were shown to be higher in sarcomatoid MPM tumors, which confer the worst prognosis (Iwanami et al., 2014).

There has been some contention surrounding the use of particular YB-1 antibodies in prognostic studies across cancer types. One N-terminal targeting YB-1 antibody that binds to residues 23–52 has been used in prognostic studies in the past (**Figure 3**). However, this antibody has been shown to cross reacts with the ubiquitously expressed hnRNPA1 protein via mass spectrometry making it unsuitable for such application (Woolley et al., 2011). Antibodies targeting the extreme N-'terminus of YB-1 (residues 1–12) or residues 299–313 in the CTD (C-terminal) have been shown to be specific for YB-1, again by mass spectrometry (Woolley et al., 2011; **Figure 3**). However, the N–terminal antibody has been suggested as more suitable for prognostic applications as this region does not interact with other proteins, so this epitope may be more accessible (Woolley et al., 2011). Notably, all prognostic studies cited in this review utilize the C-terminal targeting antibody. Regardless, a universal standardization of one reliable antibody would significantly enhance the prognostic potential of YB-1 for diagnosis using traditional pathological tissue staining.

Secreted YB-1 may also have prognostic significance in cancer. One study of 44 breast cancer patients with bone metastases found that serum YB-1 was present in 50% of patients and associated with extra-bone metastases and faster bone disease progression (Ferreira et al., 2017). There was a trend toward poorer overall survival in high-YB-1 patients, although a bigger cohort is needed to provide a more definitive answer (Ferreira et al., 2017). Another group found an YB-1/p18 in the plasma of patients with various diseases (including 32/38 lung cancers) but not in healthy controls via Western Blot using a monoclonal YB-1 antibody (Tacke et al., 2014). This study found no prognostic significance of YB-1/p18 in any of the cancers tested, but they assert that YB-1/p18 may have diagnostic significance (Tacke et al., 2014). The small sample number in this study should be noted before the prognostic applicability of secreted YB-1 is ruled out. Investigating the prognostic significance of secreted full-length or other fragments of YB-1, not just YB-1/p18, may also be of interest. The potential of YB-1 as a circulating biomarker is intriguing as a non-invasive method of prognosis and diagnosis, although more studies with larger cohorts are required.

Targeting YB-1: An Achievable Feat?

In the past YB-1 has been overlooked as a therapeutic target because of its role as a transcription and translation factor, which have been traditionally hard to target with small molecule inhibitors. However, recent advancements in the delivery of RNA-based drugs has opened up new potential avenues of targeting oncoproteins such as YB-1 (Seton-Rogers, 2012; Afonin et al., 2014). We and others have shown that miRNA or siRNA can be used to target *YBX1* in thoracic cancer cells in preclinical studies (Xu et al., 2015; Johnson et al., 2018). The delivery of miRNA mimics in the clinic is now thought to be a viable anti-cancer strategy. For example, MRX34 (a liposomal miR-34a mimic) showed evidence of efficacy and safety in a phase I trial in patients with various solid tumors including 1 NSCLC patient (Beg et al., 2017). More pertinently, a phase 1 clinical trial delivering miR-16-based mimics using bacterial minicells (EnGeneIC Dream Vectors) in mesothelioma and advanced NSCLC patients demonstrated the safety and efficacy of miRNA-based therapy (van Zandwijk et al., 2017), evidencing the potential for miRNA replacement therapy in patients with thoracic cancer.

There are a number of systems which pose as attractive options to deliver RNA-based drug payloads in thoracic cancer such as lipid, RNA, inorganic and polymer-based nanoparticles, all with their respective advantages and drawbacks (Shu et al., 2014). The delivery of siRNA or miRNA using nanoparticles in lung cancers, and to a lesser extent MPM, has been achieved *in vitro* and *in vivo*, evidencing the potential of these delivery systems (Lee et al., 2016). The *in vivo* transport of siRNA to large cell lung carcinoma tumors using lipoprotein nanoparticles (Tagalakis et al., 2018) and ADC tumors using polyethylene glycol nanoparticles (Wen et al., 2017) has demonstrated the applicability of nanoparticle delivery systems for targeted therapy. However, these studies treated subcutaneously grown tumors, which do not reflect the orthotopic context of thoracic cancer and the problems with delivery that come with it. Recently though, an siRNA targeting anti-*EZH2* was successfully delivered to orthotopically grown NSCLC tumors in mice using modified polyethyleneimine nanoparticles (Yuan et al., 2017), and delivery and retention of amiloride-sensitive epithelial sodium channel-specific siRNA into the lungs of normal mice was achieved (Tagalakis et al., 2018). The successful delivery of miR-215-5p miRNA mimics complexed in an atelocollagen vehicle was also recently achieved in an orthotopic MPM mouse model, which significantly suppressed tumor growth (Singh et al., 2019). The advances in RNA-based drug delivery in preclinical and clinical studies mean that siRNA or miRNA delivery is an appealing YB-1 targeting strategy in thoracic cancers. However, other potential strategies may also be of interest, although these are yet to be investigated in humans.

Inhibiting YB-1 activation may be one such viable targeting strategy. Fisetin (3,7,3′,4′-tetrahydroxy flavone) is a flavanol that binds to the CSD of YB-1, inhibiting its phosphorylation at Ser102 and blocking EMT in prostate cancer cells *in vitro* (Khan et al., 2014). Targeting YB-1 using fisetin also attenuated the growth of melanoma cells *in vitro* and *in vivo* (Sechi et al., 2018). Fisetin was also found to inhibit mTOR and PI3K/Akt signaling in NSCLC cells, both of which are important in both thoracic cancer biology and YB-1 regulation (see section "Translational Regulation of YB-1") (Khan et al., 2012). Another possible method for targeting YB-1 was demonstrated by using an interference cell permeable peptide that prevented YB-1 Ser102

phosphorylation. This led to an inhibition of EGFR expression and reduced growth of prostate and breast cancer cells, but not of non-malignant mammary epithelial cells (Law et al., 2010). Upstream inhibitors such as those targeting mTOR may also be an option (Hoda et al., 2011; Zhou et al., 2014), but would not be specific. A recent study showed that 2,4-dihydroxy-5-pyrimidinyl imidothiocarbomate antagonizes YB-1, inhibits YB-1 nuclear translocation and increases doxorubicin accumulation in breast cancer cells (Gunasekaran et al., 2018).

The use of oncolytic viruses that require YB-1 for replication is another potential therapeutic approach. XVir-N-31-mediated lysis of brain CSCs and virus production was significantly reduced in non-malignant astrocyte cells that expressed significantly less YB-1 compared to CSC cells (Mantwill et al., 2013). XVir-N-31 also repressed the growth of bladder cancer cells with strong YB-1 expression *in vitro* and intra-tumor delivery significantly repressed tumor volume *in vivo* (Lichtenegger et al., 2018). Consequently, virotherapy may prove to be an interesting avenue for targeting YB-1 overexpressing lung cancer and MPM.

Preclinical evidence in other tumors suggests that targeting YB-1 could also benefit immunotherapy in some cases. YB-1 knockdown increased the efficacy of IFN-α in renal cell carcinoma cells *in vitro* and *in vivo* (Takeuchi et al., 2013). IFN-α in combination with cisplatin provided a partial response in five out of ten patients in an open-label non-comparative phase II study of NSCLC patients (Chao et al., 1995). A phase II randomized study in SCLC patients with limited disease also showed a survival benefit of IFN-α in combination with a chemotherapy regime of carboplatin, ifosfamide and etoposide (Zarogoulidis et al., 2013). Based on these results, further investigating whether targeting YB-1 could increase the modest efficacy of IFN-α in thoracic cancer is warranted.

The use of YB-1 as a tumor-associated antigen in therapeutic vaccination has also shown promise in other cancers. YB-1 was identified as a tumor-associated antigen in neuroblastoma by serological expression of cDNA expression libraries (Zheng et al., 2009). In the context of regulatory T-cell depletion, YB-1 immunization enhanced $CD8^+$ response against neuroblastoma cells and conferred significantly higher mouse survival compared to control groups (Zheng et al., 2012). Adoptive T-cell therapy from immunized mice into neuroblastoma tumor-bearing mice also conferred a significant survival benefit and reduced tumor growth (Zheng et al., 2012). Again, further study in the context of thoracic cancer is warranted.

It must be noted that as with all current targeted therapies, it is likely that a YB-1-based approach to thoracic cancer management would benefit only a sub-population of patients. YB-1 overexpression, rather than mutation, would probably be the best predictive marker as mutations of YB-1 are very rare

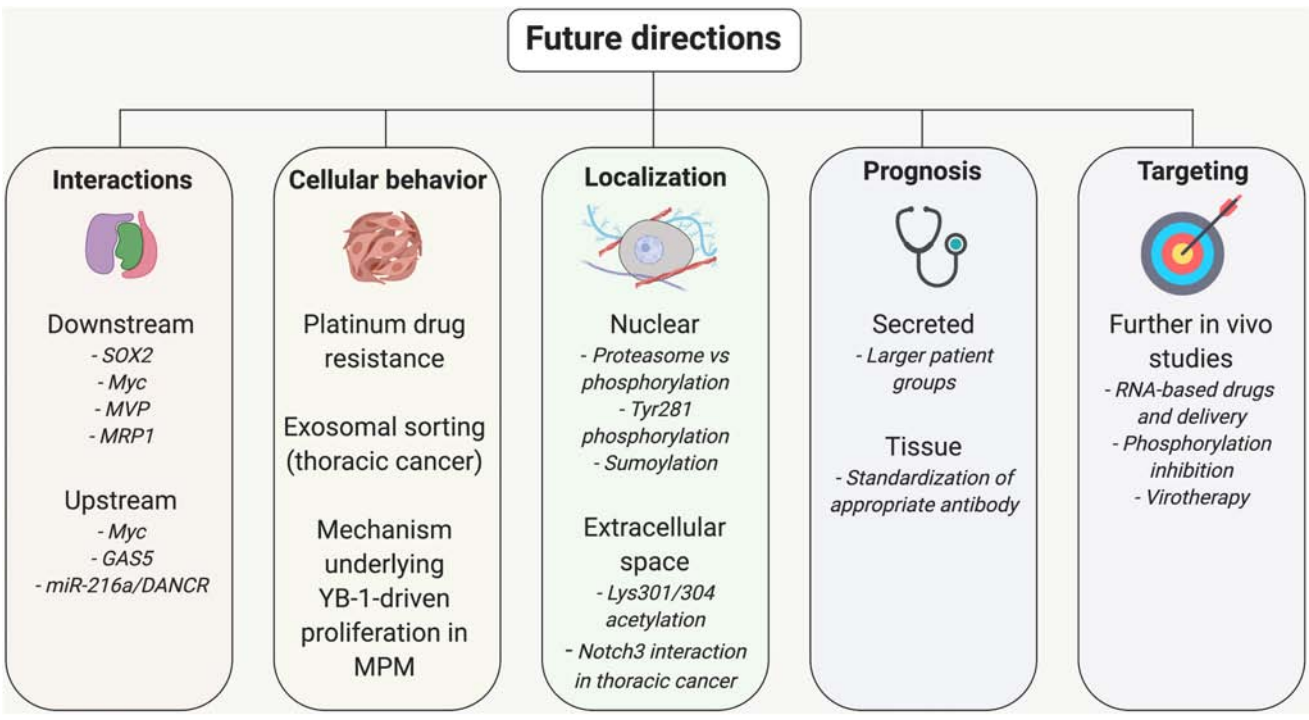

FIGURE 6 | Further study required to understand the role of YB-1 and use it in the treatment and management of thoracic cancer patients. Various upstream and downstream regulatory loops and the role of YB-1 in platinum drug resistance, exosomal sorting and proliferation need further study to fully understand the biology of YB-1 in lung cancer and MPM. The mechanism of YB-1 nuclear localization is also under contention and the occurrence and significance of secreted YB-1 is yet to be determined. Standardization of a suitable YB-1 antibody for prognostic application would also be a step forward. Finally, evaluating the current strategies of YB-1 inhibition *in vivo* further would build a stronger case for translation into humans. Created with BioRender.com.

(Cerami et al., 2012; Gao et al., 2013). TCGA data (**Figure 1**) suggests that ∼10% of thoracic cancer patients would benefit, making it comparable to ALK inhibitors in ADC according to these datasets.

FUTURE DIRECTIONS AND AREAS REQUIRING FURTHER STUDY

Throughout this review we have highlighted some avenues for potential future research that currently require further consideration, summarized briefly below. The YB-1/SOX2 axis needs to be further investigated in lung cancer, particularly in SCC and SCLC where the development of new therapeutic strategies is most urgent. The feed-forward loop of YB-1 and Myc also requires further investigation in the context of thoracic cancer. The roles of certain ncRNA in the dysregulation of YB-1 are also still unclear, namely the relationship between GAS5, miR-137 and YB-1 and the potential DANCR/miR-216a/YB-1 loop. Also, the apparent tumor suppressor function of GAS5 does not fit with its role in promoting YB-1 translation, which is another area requiring further attention.

While there is strong evidence supporting YB-1-driven resistance to platinum chemotherapy in other cancers, a study looking at the effect of YB-1 knockdown on cisplatin or other platinum drug sensitivity in lung cancer or MPM cells is still required. Also, while YB-1 has been shown to upregulate LRP and MRP1, the effect of these interactions on cisplatin resistance are yet to be determined. Determining the involvement of YB-1 in thoracic cancer exosomes would also be of interest. And while the mechanism underlying YB-1-driven growth in lung cancer has been studied well, similar studies in MPM cells are yet to be conducted.

Perhaps the most contentious area warranting further study relates to the regulation of YB-1 localization. Determining whether the proteolytic theory, phosphorylation theory or both is correct remains an important determination to be made. While these theories represent the most studied lines of evidence covering YB-1 nuclear localization, other post-translational modifications could also play a role and deserve further attention, including the phosphorylation of Tyr281. However, what upstream regulator phosphorylates YB-1 here and whether this post-translational modification actually plays an important role is not yet known. Determining whether sumoylation and circadian-related YB-1 translocation occurs and is important in lung cancer and MPM patients would also be of interest.

The secretion of YB-1 into the extracellular space in response to oxidative stress has been reported in other cell types but is yet to be studied in thoracic cancers. If secretion does occur in these contexts, it would be interesting to determine whether acetylation of Lys301/304 is required, as in immune cells. Evaluating the potential interaction between secreted YB-1 and Notch3 here would also be interesting. It is also possible that secreted YB-1 could be used as a biomarker down the line, however, studies with larger patient numbers are required to determine this. Regardless, the evidence supports utilizing YB-1 as a prognostic tissue biomarker, however, universal standardization of an appropriate YB-1 antibody is would be favorable.

Finally, YB-1 remains an interesting target in thoracic cancer, but further *in vivo* studies delivering YB-1-targeting drugs need to be done before translation into humans can occur. This section is summarized in **Figure 6**.

CONCLUSION

In summary, this review covers recent advances in the understanding of YB-1 in cancer biology with a focus on thoracic cancers. YB-1 plays an important role in the malignant behaviors of lung cancer and MPM including proliferation, invasion and metastasis. It also has been shown to be involved in the maintenance and behavioral regulation of CSCs. The demonstrated prognostic significance of YB-1 and developments in the delivery of RNA-based drugs mean that utilizing this multifunctional oncoprotein in the management of thoracic cancer may soon become a reality.

AUTHOR CONTRIBUTIONS

This review was drafted by TJ and critically revised by KS, SM, AB, and GR.

FUNDING

TJ was supported by a Ph.D. Scholarship from the Asbestos Diseases Foundation of Australia and a Top-Up Ph.D. Scholarship from the Sydney Catalyst Translational Cancer Research Centre, Australia (scholarship ID 470119385). KD was supported by a Firnberg Program Grant from the FWF (Austrian Science Fund, project number T 1062 Firnberg Program). AB was supported by a NBCF Investigator Initiated Research Scheme (IIRS-18-103). We would also like to thank the Asbestos Diseases Research Institute and Sydney Catalyst for funding the publication costs associated with this review.

ACKNOWLEDGMENTS

We would like to acknowledge the contributions of and thank Dr. Yuen Yee Cheng and Prof. Ken Takahashi from the Asbestos Diseases Research Institute, Prof. Fiona Blyth from the University of Sydney and Prof. Monica Robotin from the University of Notre Dame for their helpful suggestions and additions to this work.

REFERENCES

Afonin, K. A., Viard, M., Kagiampakis, I., Case, C. L., Dobrovolskaia, M. A., Hofmann, J., et al. (2014). Triggering of RNA Interference with RNA–RNA, RNA–DNA, and DNA–RNA Nanoparticles. *ACS Nano* 9, 251–259. doi: 10.1021/nn504508s

Alemasova, E., and Lavrik, O. (2017). At the interface of three nucleic acids: the role of RNA-binding proteins and poly (ADP-ribose) in DNA repair. *Acta Naturae* 9, 4–16. doi: 10.32607/20758251-2017-9-2-4-16

Alemasova, E. E., Moor, N. A., Naumenko, K. N., Kutuzov, M. M., Sukhanova, M. V., Pestryakov, P. E., et al. (2016). Y-box-binding protein 1 as a non-canonical factor of base excision repair. *Biochim. Biophys. Acta Proteins Proteom.* 1864, 1631–1640. doi: 10.1016/j.bbapap.2016.08.012

Alemasova, E. E., Pestryakov, P. E., Sukhanova, M. V., Kretov, D. A., Moor, N. A., Curmi, P. A., et al. (2015). Poly (ADP-ribosyl) ation as a new posttranslational modification of YB-1. *Biochimie* 119, 36–44. doi: 10.1016/j.biochi.2015.10.008

Astanehe, A., Finkbeiner, M., Hojabrpour, P., To, K., Fotovati, A., Shadeo, A., et al. (2009). The transcriptional induction of PIK3CA in tumor cells is dependent on the oncoprotein Y-box binding protein-1. *Oncogene* 28:2406. doi: 10.1038/onc.2009.81

Bao, B., Azmi, A. S., Ali, S., Ahmad, A., Li, Y., Banerjee, S., et al. (2012). The biological kinship of hypoxia with CSC and EMT and their relationship with deregulated expression of miRNAs and tumor aggressiveness. *Biochim. Biophys. Acta Rev. Cancer* 1826, 272–296. doi: 10.1016/j.bbcan.2012.04.008

Beg, M. S., Brenner, A. J., Sachdev, J., Borad, M., Kang, Y.-K., Stoudemire, J., et al. (2017). Phase I study of MRX34, a liposomal miR-34a mimic, administered twice weekly in patients with advanced solid tumors. *Invest. New Drugs* 35, 180–188. doi: 10.1007/s10637-016-0407-y

Benedetti, S., Nuvoli, B., Catalani, S., and Galati, R. (2015). Reactive oxygen species a double-edged sword for mesothelioma. *Oncotarget* 6:16848.

Betti, M., Casalone, E., Ferrante, D., Aspesi, A., Morleo, G., Biasi, A., et al. (2017). Germline mutations in DNA repair genes predispose asbestos-exposed patients to malignant pleural mesothelioma. *Cancer Lett.* 405, 38–45. doi: 10.1016/j.canlet.2017.06.028

Bitanihirwe, B. K., Meerang, M., Friess, M., Soltermann, A., Frischknecht, L., Thies, S., et al. (2014). PI3K/mTOR signaling in mesothelioma patients treated with induction chemotherapy followed by extrapleural pneumonectomy. *J. Thorac. Oncol.* 9, 239–247. doi: 10.1097/JTO.0000000000000055

Bledzka, K., Schiemann, B., Schiemann, W. P., Fox, P., Plow, E. F., and Sossey-Alaoui, K. (2017). The WAVE3-YB1 interaction regulates cancer stem cells activity in breast cancer. *Oncotarget* 8:104072. doi: 10.18632/oncotarget.22009

Boeing, S., Williamson, L., Encheva, V., Gori, I., Saunders, R. E., Instrell, R., et al. (2016). Multiomic analysis of the UV-induced DNA damage response. *Cell Rep.* 15, 1597–1610. doi: 10.1016/j.celrep.2016.04.047

Bommert, K., Effenberger, M., Leich, E., Küspert, M., Murphy, D., Langer, C., et al. (2013). The feed-forward loop between YB-1 and MYC is essential for multiple myeloma cell survival. *Leukemia* 27, 441–450. doi: 10.1038/leu.2012.185

Brabletz, T. (2012). To differentiate or not—routes towards metastasis. *Nat. Rev. Cancer* 12, 425–436. doi: 10.1038/nrc3265

Bradbury, P., Sivajohanathan, D., Chan, A., Kulkarni, S., Ung, Y., and Ellis, P. M. (2017). Postoperative adjuvant systemic therapy in completely resected non–small-cell lung cancer: a systematic review. *Clin. Lung Cancer* 18, 259.e8–273.e8. doi: 10.1016/j.cllc.2016.07.002

Brosseau, S., Assoun, S., Naltet, C., Steinmetz, C., Gounant, V., and Zalcman, G. (2017). A review of bevacizumab in the treatment of malignant pleural mesothelioma. *Future Oncol.* 13, 2537–2546. doi: 10.2217/fon-2017-0307

Bueno, R., Stawiski, E. W., Goldstein, L. D., Durinck, S., De Rienzo, A., Modrusan, Z., et al. (2015). Comprehensive genomic analysis of malignant pleural mesothelioma identifies recurrent mutations, gene fusions and splicing alterations. *Nat. Genet.* 47, 407–416. doi: 10.1038/ng.3520

Byers, L. A., and Rudin, C. M. (2015). Small cell lung cancer: where do we go from here? *Cancer* 121, 664–672. doi: 10.1002/cncr.29098

Cerami, E., Gao, J., Dogrusoz, U., Gross, B. E., Sumer, S. O., Aksoy, B. A., et al. (2012). The cBio cancer genomics portal: an open platform for exploring multidimensional cancer genomics data. *Cancer Discov.* 2, 401–404. doi: 10.1158/2159-8290.CD-12-0095

Chao, H.-M., Huang, H.-X., Chang, P.-H., Tseng, K.-C., Miyajima, A., and Chern, E. (2017). Y-box binding protein-1 promotes hepatocellular carcinoma-initiating cell progression and tumorigenesis via Wnt/β-catenin pathway. *Oncotarget* 8:2604. doi: 10.18632/oncotarget.13733

Chao, T., Hwang, W., Yang, M., Chang, J.-Y., Wang, C., Hseuh, E., et al. (1995). Combination chemoimmunotherapy with interferon-alpha and cisplatin in patients with advanced non-small cell lung cancer. *Zhonghua yi xue za zhi* 56, 232–238.

Chattopadhyay, R., Das, S., Maiti, A. K., Boldogh, I., Xie, J., Hazra, T. K., et al. (2008). Regulatory role of human AP-endonuclease (APE1/Ref-1) in YB-1-mediated activation of the multidrug resistance gene MDR1. *Mol. Cell. Biol.* 28, 7066–7080. doi: 10.1128/MCB.00244-08

Chen, D., Zhang, Y., Lin, Y., Shen, F., Zhang, Z., and Zhou, J. (2019). MicroRNA-382 inhibits cancer cell growth and metastasis in NSCLC via targeting LMO3. *Exp. Ther. Med.* 17, 2417–2424. doi: 10.3892/etm.2019.7271

Chen, F., Zhang, L., Wang, E., Zhang, C., and Li, X. (2018). LncRNA GAS5 regulates ischemic stroke as a competing endogenous RNA for miR-137 to regulate the Notch1 signaling pathway. *Biochem. Biophys. Res. Commun.* 496, 184–190. doi: 10.1016/j.bbrc.2018.01.022

Chen, R., Zhang, Y., Zhang, C., Wu, H., and Yang, S. (2017). miR-137 inhibits the proliferation of human non-small cell lung cancer cells by targeting SRC3. *Oncol. Lett.* 13, 3905–3911. doi: 10.3892/ol.2017.5904

Chen, T., Ren, H., Thakur, A., Yang, T., Li, Y., Zhang, S., et al. (2017). miR-382 inhibits tumor progression by targeting SETD8 in non-small cell lung cancer. *Biomed. Pharmacother.* 86, 248–253. doi: 10.1016/j.biopha.2016.12.007

Chen, W., Li, Z., Bai, L., and Lin, Y. (2011). NF-kappaB in lung cancer, a carcinogenesis mediator and a prevention and therapy target. *Front. Biosci.* 16:1172–1185.

Chew, S. H., and Toyokuni, S. (2015). Malignant mesothelioma as an oxidative stress-induced cancer: an update. *Free Radic. Biol. Med.* 86, 166–178. doi: 10.1016/j.freeradbiomed.2015.05.002

Chibi, M., Meyer, M., Skepu, A., Rees, D. J. G., Moolman-Smook, J. C., and Pugh, D. J. (2008). RBBP6 interacts with multifunctional protein YB-1 through its RING finger domain, leading to ubiquitination and proteosomal degradation of YB-1. *J. Mol. Biol.* 384, 908–916. doi: 10.1016/j.jmb.2008.09.060

Chiou, S.-H., Wang, M.-L., Chou, Y.-T., Chen, C.-J., Hong, C.-F., Hsieh, W.-J., et al. (2010). Coexpression of Oct4 and Nanog enhances malignancy in lung adenocarcinoma by inducing cancer stem cell–like properties and epithelial–mesenchymal transdifferentiation. *Cancer Res.* 70, 10433–10444. doi: 10.1158/0008-5472.can-10-2638

Chou, C.-C., Chuang, H.-C., Salunke, S. B., Kulp, S. K., and Chen, C.-S. (2015). A novel HIF-1α-integrin-linked kinase regulatory loop that facilitates hypoxia-induced HIF-1α expression and epithelial-mesenchymal transition in cancer cells. *Oncotarget* 6:8271.

Ciardiello, F., De Vita, F., Orditura, M., and Tortora, G. (2004). The role of EGFR inhibitors in nonsmall cell lung cancer. *Curr. Opin. Oncol.* 16, 130–135. doi: 10.1097/00001622-200403000-00008

Cobbold, L., Wilson, L., Sawicka, K., King, H., Kondrashov, A., Spriggs, K., et al. (2010). Upregulated c-myc expression in multiple myeloma by internal ribosome entry results from increased interactions with and expression of PTB-1 and YB-1. *Oncogene* 29:2884. doi: 10.1038/onc.2010.31

Cohen, S., Ma, W., Valova, V., Algie, M., Harfoot, R., Woolley, A., et al. (2010). Genotoxic stress-induced nuclear localization of oncoprotein YB-1 in the absence of proteolytic processing. *Oncogene* 29, 403–410. doi: 10.1038/onc.2009.321

Creaney, J., Dick, I. M., Leon, J. S., and Robinson, B. W. (2017). A proteomic analysis of the malignant mesothelioma secretome using iTRAQ. *Cancer Genomics Proteom.* 14, 103–117.

Dalerba, P., and Clarke, M. F. (2007). Cancer stem cells and tumor metastasis: first steps into uncharted territory. *Cell Stem Cell* 1, 241–242. doi: 10.1016/j.stem.2007.08.012

Davies, A. H., Reipas, K., Hu, K., Berns, R., Firmino, N., Stratford, A. L., et al. (2015). Inhibition of RSK with the novel small-molecule inhibitor LJI308 overcomes chemoresistance by eliminating cancer stem cells. *Oncotarget* 6:20570.

Deslee, G., Adair-Kirk, T. L., Betsuyaku, T., Woods, J. C., Moore, C. H., Gierada, D. S., et al. (2010). Cigarette smoke induces nucleic-acid oxidation in lung

fibroblasts. *Am. J. Respir. Cell Mol. Biol.* 43, 576–584. doi: 10.1165/rcmb.2009-0221OC

Destro, A., Ceresoli, G., Falleni, M., Zucali, P., Morenghi, E., Bianchi, P., et al. (2006). EGFR overexpression in malignant pleural mesothelioma: an immunohistochemical and molecular study with clinico-pathological correlations. *Lung Cancer* 51, 207–215.

di Martino, O., Troiano, A., Guarino, A. M., Pollice, A., Vivo, M., La Mantia, G., et al. (2016). ΔNp63α controls YB-1 protein stability: evidence on YB-1 as a new player in keratinocyte differentiation. *Genes Cells* 21, 648–660. doi: 10.1111/gtc.12373

Diaz-Lagares, A., Crujeiras, A. B., Lopez-Serra, P., Soler, M., Setien, F., Goyal, A., et al. (2016). Epigenetic inactivation of the p53-induced long noncoding RNA TP53 target 1 in human cancer. *Proc. Natl. Acad. Sci. U.S.A.* 113, E7535–E7544.

Didier, D. K., Schiffenbauer, J., Woulfe, S. L., Zacheis, M., and Schwartz, B. D. (1988). Characterization of the cDNA encoding a protein binding to the major histocompatibility complex class II Y box. *Proc. Natl. Acad. Sci. U.S.A.* 85, 7322–7326. doi: 10.1073/pnas.85.19.7322

Dutta, A., Yang, C., Sengupta, S., Mitra, S., and Hegde, M. L. (2015). New paradigms in the repair of oxidative damage in human genome: mechanisms ensuring repair of mutagenic base lesions during replication and involvement of accessory proteins. *Cell. Mol. Life Sci.* 72, 1679–1698. doi: 10.1007/s00018-014-1820-z

El-Naggar, A. M., Veinotte, C. J., Cheng, H., Grunewald, T. G., Negri, G. L., Somasekharan, S. P., et al. (2015). Translational activation of HIF1α by YB-1 promotes sarcoma metastasis. *Cancer Cell* 27, 682–697. doi: 10.1016/j.ccell.2015.04.003

Emerling, B. M., Weinberg, F., Liu, J.-L., Mak, T. W., and Chandel, N. S. (2008). PTEN regulates p300-dependent hypoxia-inducible factor 1 transcriptional activity through Forkhead transcription factor 3a (FOXO3a). *Proc. Natl. Acad. Sci. U.S.A.* 105, 2622–2627. doi: 10.1073/pnas.0706790105

Evdokimova, V., Tognon, C., Ng, T., Ruzanov, P., Melnyk, N., Fink, D., et al. (2009a). Translational activation of snail1 and other developmentally regulated transcription factors by YB-1 promotes an epithelial-mesenchymal transition. *Cancer Cell* 15, 402–415. doi: 10.1016/j.ccr.2009.03.017

Evdokimova, V., Tognon, C., Ng, T., and Sorensen, P. H. (2009b). Reduced proliferation and enhanced migration: two sides of the same coin? Molecular mechanisms of metastatic progression by YB-1. *Cell Cycle* 8, 2901–2906. doi: 10.4161/cc.8.18.9537

Ewert, L., Fischer, A., Brandt, S., Scurt, F. G., Philipsen, L., Müller, A. J., et al. (2018). Cold shock Y-box binding protein-1 acetylation status in monocytes is associated with systemic inflammation and vascular damage. *Atherosclerosis* 278, 156–165. doi: 10.1016/j.atherosclerosis.2018.09.020

Ferreira, A., Bettencourt, M., Alho, I., Costa, A., Sousa, A., Mansinho, A., et al. (2017). Serum YB-1 (Y-box binding protein 1) as a biomarker of bone disease progression in patients with breast cancer and bone metastases. *J. Bone Oncol.* 6, 16–21. doi: 10.1016/j.jbo.2017.01.002

Fomina, E., Pestryakov, P., Maltseva, E., Petruseva, I., Kretov, D., Ovchinnikov, L., et al. (2015). Y-box binding protein 1 (YB-1) promotes detection of DNA bulky lesions by XPC-HR23B factor. *Biochemistry* 80, 219–227. doi: 10.1134/S000629791502008X

Forde, P. M., Scherpereel, A., and Tsao, A. S. (2019). Use of immune checkpoint inhibitors in mesothelioma. *Curr. Treat. Options Oncol.* 20:18. doi: 10.1007/s11864-019-0613-x

Friedlaender, A., Banna, G., Malapelle, U., Pisapia, P., and Addeo, A. (2019). Next generation sequencing and genetic alterations in squamous cell lung carcinoma: where are we today? *Front. Oncol.* 9:166. doi: 10.3389/fonc.2019.00166

Frye, B. C., Halfter, S., Djudjaj, S., Muehlenberg, P., Weber, S., Raffetseder, U., et al. (2009). Y-box protein-1 is actively secreted through a non-classical pathway and acts as an extracellular mitogen. *EMBO Rep.* 10, 783–789. doi: 10.1038/embor.2009.81

Gao, J., Aksoy, B. A., Dogrusoz, U., Dresdner, G., Gross, B., Sumer, S. O., et al. (2013). Integrative analysis of complex cancer genomics and clinical profiles using the cBioPortal. *Sci. Signal.* 6:l1. doi: 10.1126/scisignal.2004088

Gaudreault, I., Guay, D., and Lebel, M. (2004). YB-1 promotes strand separation in vitro of duplex DNA containing either mispaired bases or cisplatin modifications, exhibits endonucleolytic activities and binds several DNA repair proteins. *Nucleic Acids Res.* 32, 316–327. doi: 10.1093/nar/gkh170

Gera, S., and Dighe, R. R. (2018). The soluble ligand Ybox-1 activates Notch3 receptor by binding to epidermal growth factor like repeats 20-23. *Arch. Biochem. Biophys.* 660, 129–136. doi: 10.1016/j.abb.2018.10.009

Gessner, C., Woischwill, C., Schumacher, A., Liebers, U., Kuhn, H., Stiehl, P., et al. (2004). Nuclear YB-1 expression as a negative prognostic marker in nonsmall cell lung cancer. *Eur. Respir. J.* 23, 14–19. doi: 10.1183/09031936.03.00033203

Gopal, S. K., Greening, D. W., Mathias, R. A., Ji, H., Rai, A., Chen, M., et al. (2015). YBX1/YB-1 induces partial EMT and tumourigenicity through secretion of angiogenic factors into the extracellular microenvironment. *Oncotarget* 6:13718.

Goswami, C. P., and Nakshatri, H. (2014). PROGgeneV2: enhancements on the existing database. *BMC Cancer* 14:970. doi: 10.1186/1471-2407-14-970

Greening, D. W., Ji, H., Chen, M., Robinson, B. W., Dick, I. M., Creaney, J., et al. (2016). Secreted primary human malignant mesothelioma exosome signature reflects oncogenic cargo. *Sci. Rep.* 6:32643. doi: 10.1038/srep32643

Guarino, A., Troiano, A., Pizzo, E., Bosso, A., Vivo, M., Pinto, G., et al. (2018). Oxidative stress causes enhanced secretion of YB-1 Protein that restrains proliferation of receiving cells. *Genes.* 9:E513. doi: 10.3390/genes9100513

Gujral, T. S., Chan, M., Peshkin, L., Sorger, P. K., Kirschner, M. W., and MacBeath, G. (2014). A noncanonical Frizzled2 pathway regulates epithelial-mesenchymal transition and metastasis. *Cell* 159, 844–856. doi: 10.1016/j.cell.2014.10.032

Gunasekaran, V. P., Nishi, K., Sivakumar, D., Sivaraman, T., and Mathan, G. (2018). Identification of 2, 4-dihydroxy-5-pyrimidinyl imidothiocarbomate as a novel inhibitor to Y box binding protein-1 (YB-1) and its therapeutic actions against breast cancer. *Eur. J. Pharm. Sci.* 116, 2–14. doi: 10.1016/j.ejps.2017.09.019

Guo, T., Kong, J., Liu, Y., Li, Z., Xia, J., Zhang, Y., et al. (2017). Transcriptional activation of NANOG by YBX1 promotes lung cancer stem-like properties and metastasis. *Biochem. Biophys. Res. Commun.* 487, 153–159. doi: 10.1016/j.bbrc.2017.04.033

Gutschner, T., Richtig, G., Haemmerle, M., and Pichler, M. (2018). From biomarkers to therapeutic targets—the promises and perils of long non-coding RNAs in cancer. *Cancer Metastasis Rev.* 37, 83–105. doi: 10.1007/s10555-017-9718-5

Győrffy, B., Surowiak, P., Budczies, J., and Lánczky, A. (2013). Online survival analysis software to assess the prognostic value of biomarkers using transcriptomic data in non-small-cell lung cancer. *PLoS One* 8:e82241. doi: 10.1371/journal.pone.0082241

Ha, B., Lee, E. B., Cui, J., Kim, Y., and Jang, H. H. (2015). YB-1 overexpression promotes a TGF-β1-induced epithelial–mesenchymal transition via Akt activation. *Biochem. Biophys. Res. Commun.* 458, 347–351. doi: 10.1016/j.bbrc.2015.01.114

Hansen, J. (2017). Night shift work and risk of breast cancer. *Curr. Environ. Health Rep.* 4, 325–339. doi: 10.1007/s40572-017-0155-y

Harada, M., Kotake, Y., Ohhata, T., Kitagawa, K., Niida, H., Matsuura, S., et al. (2014). YB-1 promotes transcription of cyclin D1 in human non-small-cell lung cancers. *Genes Cells* 19, 504–516. doi: 10.1111/gtc.12150

He, L., Che, M., Hu, J., Li, S., Jia, Z., Lou, W., et al. (2015). Twist contributes to proliferation and epithelial-to-mesenchymal transition–induced fibrosis by regulating YB-1 in human peritoneal mesothelial cells. *Am. J. Pathol.* 185, 2181–2193. doi: 10.1016/j.ajpath.2015.04.008

Hermann, P. C., Huber, S. L., Herrler, T., Aicher, A., Ellwart, J. W., Guba, M., et al. (2007). Distinct populations of cancer stem cells determine tumor growth and metastatic activity in human pancreatic cancer. *Cell Stem Cell* 1, 313–323. doi: 10.1016/j.stem.2007.06.002

Hirsch, F. R., Scagliotti, G. V., Mulshine, J. L., Kwon, R., Curran , W. J. Jr., Wu, Y.-L., et al. (2017). Lung cancer: current therapies and new targeted treatments. *Lancet* 389, 299–311. doi: 10.1016/s0140-6736(16)30958-8

Hoda, M. A., Mohamed, A., Ghanim, B., Filipits, M., Hegedus, B., Tamura, M., et al. (2011). Temsirolimus inhibits malignant pleural mesothelioma growth in vitro and in vivo: synergism with chemotherapy. *J. Thorac. Oncol.* 6, 852–863. doi: 10.1097/JTO.0b013e31820e1a25

Hyogotani, A., Ito, K.-I., Yoshida, K., Izumi, H., Kohno, K., and Amano, J. (2012). Association of nuclear YB-1 localization with lung resistance-related protein and epidermal growth factor receptor expression in lung cancer. *Clin. Lung Cancer* 13, 375–384. doi: 10.1016/j.cllc.2011.11.006

Ise, T., Nagatani, G., Imamura, T., Kato, K., Takano, H., Nomoto, M., et al. (1999). Transcription factor Y-box binding protein 1 binds preferentially to cisplatin-modified DNA and interacts with proliferating cell nuclear antigen. *Cancer Res.* 59, 342–346.

Islami, F., Torre, L. A., and Jemal, A. (2015). Global trends of lung cancer mortality and smoking prevalence. *Transl. Lung Cancer Res.* 4, 327–338. doi: 10.3978/j.issn.2218-6751.2015.08.04

Iwanami, T., Uramoto, H., Nakagawa, M., Shimokawa, H., Yamada, S., Kohno, K., et al. (2014). Clinical significance of epithelial-mesenchymal transition-associated markers in malignant pleural mesothelioma. *Oncology* 86, 109–116. doi: 10.1159/000356874

Jamal-Hanjani, M., Wilson, G. A., McGranahan, N., Birkbak, N. J., Watkins, T. B., Veeriah, S., et al. (2017). Tracking the evolution of non–small-cell lung cancer. *N. Engl. J. Med.* 376, 2109–2121.

Janku, F., Yap, T. A., and Meric-Bernstam, F. (2018). Targeting the PI3K pathway in cancer: are we making headway? *Nat. Rev. Clin. Oncol.* 15, 273–291. doi: 10.1038/nrclinonc.2018.28

Jia, J., Zheng, Y., Wang, W., Shao, Y., Li, Z., Wang, Q., et al. (2017). Antimicrobial peptide LL-37 promotes YB-1 expression, and the viability, migration and invasion of malignant melanoma cells. *Mol. Med. Rep.* 15, 240–248. doi: 10.3892/mmr.2016.5978

Jiang, L., Yuan, G.-L., Liang, Q.-L., Zhang, H.-J., Huang, J., Cheng, S.-A., et al. (2017). Positive expression of Y-box binding protein 1 and prognosis in non-small cell lung cancer: a meta-analysis. *Oncotarget* 8:55613. doi: 10.18632/oncotarget.14732

Jiang, W., Kahn, S. M., Tomita, N., Zhang, Y.-J., Lu, S.-H., and Weinstein, I. B. (1992). Amplification and expression of the human cyclin D gene in esophageal cancer. *Cancer Res.* 52, 2980–2983.

Jin, B., Dong, Y., Zhang, X., Wang, H., and Han, B. (2014). Association of XPC polymorphisms and lung cancer risk: a meta-analysis. *PLoS One* 9:e93937. doi: 10.1371/journal.pone.0093937

Johnson, T. G., Schelch, K., Cheng, Y. Y., Williams, M., Sarun, K. H., Kirschner, M. B., et al. (2018). Dysregulated expression of the MicroRNA miR-137 and its target YBX1 contribute to the invasive characteristics of malignant pleural mesothelioma. *J. Thorac. Oncol.* 13, 258–272. doi: 10.1016/j.jtho.2017.10.016

Jonas, S., and Izaurralde, E. (2015). Towards a molecular understanding of microRNA-mediated gene silencing. *Nat. Rev. Genet.* 16, 421–433. doi: 10.1038/nrg3965

Jung, K., Wu, F., Wang, P., Ye, X., Abdulkarim, B. S., and Lai, R. (2014). YB-1 regulates Sox2 to coordinately sustain stemness and tumorigenic properties in a phenotypically distinct subset of breast cancer cells. *BMC Cancer* 14:328. doi: 10.1186/1471-2407-14-328

Kang, Y., Hu, W., Ivan, C., Dalton, H. J., Miyake, T., Pecot, C. V., et al. (2013). Role of focal adhesion kinase in regulating YB–1–mediated paclitaxel resistance in ovarian cancer. *J. Natl. Cancer Inst.* 105, 1485–1495. doi: 10.1093/jnci/djt210

Karachaliou, N., Rosell, R., and Viteri, S. (2013). The role of SOX2 in small cell lung cancer, lung adenocarcinoma and squamous cell carcinoma of the lung. *Transl. Lung Cancer Res.* 2, 172–179. doi: 10.3978/j.issn.2218-6751.2013.01.01

Kasyapa, C., Gu, T. L., Natarajan, L., Polakiewicz, R., and Cowell, J. K. (2009). Phosphorylation of the SSBP2 and ABL proteins by the ZNF198-FGFR1 fusion kinase seen in atypical myeloproliferative disorders as revealed by phosphopeptide-specific MS. *Proteomics* 9, 3979–3988. doi: 10.1002/pmic.200800852

Khan, M. I., Adhami, V. M., Lall, R. K., Sechi, M., Joshi, D. C., Haidar, O. M., et al. (2014). YB-1 expression promotes epithelial-to-mesenchymal transition in prostate cancer that is inhibited by a small molecule fisetin. *Oncotarget* 5, 2462–2474.

Khan, N., Afaq, F., Khusro, F. H., Adhami, V. M., Suh, Y., and Mukhtar, H. (2012). Dual inhibition of phosphatidylinositol 3-kinase/Akt and mammalian target of rapamycin signaling in human nonsmall cell lung cancer cells by a dietary flavonoid fisetin. *Int. J. Cancer* 130, 1695–1705. doi: 10.1002/ijc.26178

Khuder, S. A. (2001). Effect of cigarette smoking on major histological types of lung cancer: a meta-analysis. *Lung Cancer* 31, 139–148. doi: 10.1016/s0169-5002(00)00181-1

Kim, E. R., Selyutina, A. A., Buldakov, I. A., Evdokimova, V., Ovchinnikov, L. P., and Sorokin, A. V. (2013). The proteolytic YB-1 fragment interacts with DNA repair machinery and enhances survival during DNA damaging stress. *Cell Cycle* 12, 3791–3803. doi: 10.4161/cc.26670

Kim, M.-C., Hwang, S.-H., Kim, N.-Y., Lee, H.-S., Ji, S., Yang, Y., et al. (2018). Hypoxia promotes acquisition of aggressive phenotypes in human malignant mesothelioma. *BMC Cancer* 18:819. doi: 10.1186/s12885-018-4720-z

Kobayashi, I., Takahashi, F., Nurwidya, F., Nara, T., Hashimoto, M., Murakami, A., et al. (2016). Oct4 plays a crucial role in the maintenance of gefitinib-resistant lung cancer stem cells. *Biochem. Biophys. Res. Commun.* 473, 125–132. doi: 10.1016/j.bbrc.2016.03.064

Koike, K., Uchiumi, T., Ohga, T., Toh, S., Wada, M., Kohno, K., et al. (1997). Nuclear translocation of the Y-box binding protein by ultraviolet irradiation. *FEBS Lett.* 417, 390–394. doi: 10.1016/s0014-5793(97)01296-9

Kosnopfel, C., Sinnberg, T., and Schittek, B. (2014). Y-box binding protein 1–a prognostic marker and target in tumour therapy. *Eur. J. Cell Biol.* 93, 61–70. doi: 10.1016/j.ejcb.2013.11.007

Kris, M. G., Gaspar, L. E., Chaft, J. E., Kennedy, E. B., Azzoli, C. G., Ellis, P. M., et al. (2017). Adjuvant systemic therapy and adjuvant radiation therapy for stage I to IIIA completely resected non-small-cell lung cancers: American Society of Clinical Oncology/Cancer Care Ontario clinical practice guideline update. *J. Clin. Oncol.* 35, 2960–2974. doi: 10.1200/JCO.2017.72.4401

Kröger, C., Afeyan, A., Mraz, J., Eaton, E. N., Reinhardt, F., Khodor, Y. L., et al. (2019). Acquisition of a hybrid E/M state is essential for tumorigenicity of basal breast cancer cells. *Proc. Natl. Acad. Sci.* 116, 7353–7362. doi: 10.1073/pnas.1812876116

Kwon, P., Lundin, J., Li, W., Ray, R., Littell, C., Gao, D., et al. (2015). Night shift work and lung cancer risk among female textile workers in shanghai, china. *J. Occup. Environ. Hyg.* 12, 334–341. doi: 10.1080/15459624.2014.993472

Ladanyi, M. (2005). Implications of P16/CDKN2A deletion in pleural mesotheliomas. *Lung Cancer* 49, S95–S98.

Lara, P. C., Pruschy, M., Zimmermann, M., and Henríquez-Hernández, L. A. (2011). MVP and vaults: a role in the radiation response. *Radiat. Oncol.* 6:148. doi: 10.1186/1748-717X-6-148

Lasham, A., Samuel, W., Cao, H., Patel, R., Mehta, R., Stern, J. L., et al. (2011). YB-1, the E2F pathway, and regulation of tumor cell growth. *J. Natl. Cancer Inst.* 104, 133–146. doi: 10.1093/jnci/djr512

Lasham, A., Woolley, A. G., Dunn, S. E., and Braithwaite, A. W. (2013). YB-1: oncoprotein, prognostic marker and therapeutic target? *Biochem. J.* 449, 11–23. doi: 10.1042/bj20121323

Law, J. H., Li, Y., To, K., Wang, M., Astanehe, A., Lambie, K., et al. (2010). Molecular decoy to the Y-box binding protein-1 suppresses the growth of breast and prostate cancer cells whilst sparing normal cell viability. *PLoS One* 5:e12661. doi: 10.1371/journal.pone.0012661

Lee, H.-Y., Mohammed, K. A., and Nasreen, N. (2016). Nanoparticle-based targeted gene therapy for lung cancer. *Am. J. Cancer Res.* 6, 1118–1134.

Leon, G., MacDonagh, L., Finn, S. P., Cuffe, S., and Barr, M. P. (2016). Cancer stem cells in drug resistant lung cancer: targeting cell surface markers and signaling pathways. *Pharmacol. Ther.* 158, 71–90. doi: 10.1016/j.pharmthera.2015.12.001

Li, D., Liu, X., Zhou, J., Hu, J., Zhang, D., Liu, J., et al. (2017). Long noncoding RNA HULC modulates the phosphorylation of YB-1 through serving as a scaffold of extracellular signal–regulated kinase and YB-1 to enhance hepatocarcinogenesis. *Hepatology* 65, 1612–1627. doi: 10.1002/hep.29010

Li, J., Li, Z.-N., Du, Y.-J., Li, X.-Q., Bao, Q.-L., and Chen, P. (2009). Expression of MRP1, BCRP, LRP, and ERCC1 in advanced non–small-cell lung cancer: correlation with response to chemotherapy and survival. *Clin. Lung Cancer* 10, 414–421. doi: 10.3816/CLC.2009.n.078

Li, M., Zhang, X., Xu, X., Wu, J., Hu, K., Guo, X., et al. (2018). Clinicopathological and prognostic significance of Twist overexpression in NSCLC. *Oncotarget* 9, 14642–14651. doi: 10.18632/oncotarget.24489

Li, X.-Q., Li, J., Shi, S.-B., Chen, P., Yu, L.-C., and Bao, Q.-L. (2009). Expression of MRP1, BCRP, LRP and ERCC1 as prognostic factors in non-small cell lung cancer patients receiving postoperative cisplatin-based chemotherapy. *Int. J. Biol. Mark.* 24, 230–237. doi: 10.5301/jbm.2009.5437

Li, Z., and Rich, J. N. (2010). Hypoxia and hypoxia inducible factors in cancer stem cell maintenance. *Curr. Top. Microbiol. Immunol.* 345, 21–30. doi: 10.1007/82_2010_75

Liang, C., Ma, Y., Yong, L., Yang, C., Wang, P., Liu, X., et al. (2019). Y-box binding protein-1 promotes tumorigenesis and progression via the epidermal growth factor receptor/AKT pathway in spinal chordoma. *Cancer Sci.* 110:166. doi: 10.1111/cas.13875

Lichtenegger, E., Koll, F., Haas, H., Mantwill, K., Janssen, K.-P., Laschinger, M., et al. (2018). The oncolytic adenovirus XVir-N-31 as a novel therapy in muscle-invasive bladder cancer. *Hum. Gene Ther.* 30, 44–56. doi: 10.1089/hum.2018.026

Lim, J. P., Shyamasundar, S., Gunaratne, J., Scully, O. J., Matsumoto, K., and Bay, B. H. (2017). YBX1 gene silencing inhibits migratory and invasive potential via CORO1C in breast cancer in vitro. *BMC Cancer* 17:201. doi: 10.1186/s12885-017-3187-7

Lindquist, K. E., Karlsson, A., Levéen, P., Brunnström, H., Reuterswärd, C., Holm, K., et al. (2017). Clinical framework for next generation sequencing based analysis of treatment predictive mutations and multiplexed gene fusion detection in non-small cell lung cancer. *Oncotarget* 8, 34796–34810. doi: 10.18632/oncotarget.16276

Liu, L., Zhou, X., Zhang, J., Wang, G., He, J., Chen, Y., et al. (2018). LncRNA HULC promotes non-small cell lung cancer cell proliferation and inhibits the apoptosis by up-regulating sphingosine kinase 1 (SPHK1) and its downstream PI3K/Akt pathway. *Eur. Rev. Med. Pharmacol. Sci.* 22, 8722–8730. doi: 10.26355/eurrev_201812_16637

Liu, Q., Tao, T., Liu, F., Ni, R., Lu, C., and Shen, A. (2016). Hyper-O-GlcNAcylation of YB-1 affects Ser102 phosphorylation and promotes cell proliferation in hepatocellular carcinoma. *Exp. Cell Res.* 349, 230–238. doi: 10.1016/j.yexcr.2016.10.011

Liu, W., Zhou, Z., Dong, D., Sun, L., and Zhang, G. (2018). Sex differences in the association between night shift work and the risk of cancers: a meta-analysis of 57 articles. *Dis. Mark.* 2018:7925219. doi: 10.1155/2018/7925219

Liu, Y., Zhao, J., Zhang, W., Gan, J., Hu, C., Huang, G., et al. (2015). lncRNA GAS5 enhances G1 cell cycle arrest via binding to YBX1 to regulate p21 expression in stomach cancer. *Sci. Rep.* 5:10159. doi: 10.1038/srep10159

Lu, J., Li, X., Wang, F., Guo, Y., Huang, Y., Zhu, H., et al. (2017). YB-1 expression promotes pancreatic cancer metastasis that is inhibited by microRNA-216a. *Exp. Cell Res.* 359, 319–326. doi: 10.1016/j.yexcr.2017.07.039

Lyabin, D. N., Eliseeva, I. A., and Ovchinnikov, L. P. (2012). YB-1 synthesis is regulated by mTOR signaling pathway. *PLoS One* 7:e52527. doi: 10.1371/journal.pone.0052527

Lyabin, D. N., Eliseeva, I. A., and Ovchinnikov, L. P. (2014). YB-1 protein: functions and regulation. *Wiley Interdiscipl. Rev. RNA* 5, 95–110. doi: 10.1002/wrna.1200

Ma, S., Musa, T., and Bag, J. (2006). Reduced stability of mitogen-activated protein kinase kinase-2 mRNA and phosphorylation of poly (A)-binding protein (PABP) in cells overexpressing PABP. *J. Biol. Chem.* 281, 3145–3156. doi: 10.1074/jbc.m508937200

MacDonagh, L., Gray, S. G., Breen, E., Cuffe, S., Finn, S. P., O'Byrne, K. J., et al. (2016). Lung cancer stem cells: the root of resistance. *Cancer Lett.* 372, 147–156. doi: 10.1016/j.canlet.2016.01.012

Makena, M. R., Ranjan, A., Thirumala, V., and Reddy, A. (2018). Cancer stem cells: road to therapeutic resistance and strategies to overcome resistance. *Biochim. Biophys. Acta Mol. Basis Dis.* doi: 10.1016/j.bbadis.2018.11.015 [Epub ahead of print].

Makino, Y., Ohga, T., Toh, S., Koike, K., Okumura, K., Wada, M., et al. (1996). Structural and functional analysis of the human Y-box binding protein (YB-1) gene promoter. *Nucleic Acids Res.* 24, 1873–1878. doi: 10.1093/nar/24.10.1873

Mantwill, K., Köhler-Vargas, N., Bernshausen, A., Bieler, A., Lage, H., Kaszubiak, A., et al. (2006). Inhibition of the multidrug-resistant phenotype by targeting YB-1 with a conditionally oncolytic adenovirus: implications for combinatorial treatment regimen with chemotherapeutic agents. *Cancer Res.* 66, 7195–7202. doi: 10.1158/0008-5472.can-05-2339

Mantwill, K., Naumann, U., Seznec, J., Girbinger, V., Lage, H., Surowiak, P., et al. (2013). YB-1 dependent oncolytic adenovirus efficiently inhibits tumor growth of glioma cancer stem like cells. *J. Transl. Med.* 11:216. doi: 10.1186/1479-5876-11-216

Marshall, A., Bayes, H., Bardgett, J., Wedderburn, S., Kerr, K., and Currie, G. (2015). Survival from malignant mesothelioma: where are we now? *J. R. Coll. Phys. Edinburgh* 45, 123–126. doi: 10.4997/JRCPE.2015.207

Martin, M., Hua, L., Wang, B., Wei, H., Prabhu, L., Hartley, A.-V., et al. (2017). Novel Serine 176 phosphorylation of YBX1 activates NF-κB in colon cancer. *J. Biol. Chem.* 292, 3433–3444. doi: 10.1074/jbc.M116.740258

Mashouri, L., Yousefi, H., Aref, A. R., Mohammad Ahadi, A., Molaei, F., and Alahari, S. K. (2019). Exosomes: composition, biogenesis, and mechanisms in cancer metastasis and drug resistance. *Mol. Cancer* 18:75.

Matsumoto, K., Kose, S., Kuwahara, I., Yoshimura, M., Imamoto, N., and Yoshida, M. (2018). Y-box protein-associated acidic protein (YBAP1/C1QBP) affects the localization and cytoplasmic functions of YB-1. *Sci. Rep.* 8:6198. doi: 10.1038/s41598-018-24401-3

Mendoza, M. C., Er, E. E., and Blenis, J. (2011). The Ras-ERK and PI3K-mTOR pathways: cross-talk and compensation. *Trends Biochem. Sci.* 36, 320–328. doi: 10.1016/j.tibs.2011.03.006

Mordovkina, D. A., Kim, E. R., Buldakov, I. A., Sorokin, A. V., Eliseeva, I. A., Lyabin, D. N., et al. (2016). Transportin-1-dependent YB-1 nuclear import. *Biochem. Biophys. Res. Commun.* 480, 629–634. doi: 10.1016/j.bbrc.2016.10.107

Munson, P., Lam, Y.-W., Dragon, J., MacPherson, M., and Shukla, A. (2018). Exosomes from asbestos-exposed cells modulate gene expression in mesothelial cells. *FASEB J.* 32, 4328–4342. doi: 10.1096/fj.201701291RR

Murugesan, S. N., Yadav, B. S., Maurya, P. K., Chaudhary, A., Singh, S., and Mani, A. (2018). Expression and network analysis of YBX1 interactors for identification of new drug targets in lung adenocarcinoma. *J. Genomics* 6, 103–112. doi: 10.7150/jgen.20581

Mutti, L., Peikert, T., Robinson, B. W., Scherpereel, A., Tsao, A. S., de Perrot, M., et al. (2018). Scientific advances and new frontiers in mesothelioma therapeutics. *J. Thorac. Oncol.* 13, 1269–1283. doi: 10.1016/j.jtho.2018.06.011

Muz, B., de la Puente, P., Azab, F., and Azab, A. K. (2015). The role of hypoxia in cancer progression, angiogenesis, metastasis, and resistance to therapy. *Hypoxia* 3, 83–92.

Nagasaka, M., and Gadgeel, S. M. (2018). Role of chemotherapy and targeted therapy in early-stage non-small cell lung cancer. *Expert Rev. Anticancer Ther.* 18, 63–70. doi: 10.1080/14737140.2018.1409624

Nishikawa, S., Tanaka, A., Matsuda, A., Oida, K., Jang, H., Jung, K., et al. (2014). A molecular targeting against nuclear factor-κB, as a chemotherapeutic approach for human malignant mesothelioma. *Cancer Med.* 3, 416–425. doi: 10.1002/cam4.202

Ohga, T., Uchiumi, T., Makino, Y., Koike, K., Wada, M., Kuwano, M., et al. (1998). Direct involvement of the Y-box binding protein YB-1 in genotoxic stress-induced activation of the human multidrug resistance 1 gene. *J. Biol. Chem.* 273, 5997–6000. doi: 10.1074/jbc.273.11.5997

Oronsky, B., Reid, T. R., Oronsky, A., and Carter, C. A. (2017). What's new in SCLC? a review. *Neoplasia* 19, 842–847. doi: 10.1016/j.neo.2017.07.007

Ott, P. A., Fernandez, M. E. E., Hiret, S., Kim, D.-W., Moss, R. A., Winser, T., et al. (2015). Pembrolizumab (MK-3475) in patients (pts) with extensive-stage small cell lung cancer (SCLC): preliminary safety and efficacy results from KEYNOTE-028. *J. Clin. Oncol.* 33(Suppl. 15), 7502–7502. doi: 10.1200/jco.2015.33.15_suppl.7502

Pagano, C., di Martino, O., Ruggiero, G., Guarino, A. M., Mueller, N., Siauciunaite, R., et al. (2017). The tumor-associated YB-1 protein: new player in the circadian control of cell proliferation. *Oncotarget* 8, 6193–6205. doi: 10.18632/oncotarget.14051

Palicharla, V. R., and Maddika, S. (2015). HACE1 mediated K27 ubiquitin linkage leads to YB-1 protein secretion. *Cell Signal.* 27, 2355–2362. doi: 10.1016/j.cellsig.2015.09.001

Papagiannakopoulos, T., Bauer, M. R., Davidson, S. M., Heimann, M., Subbaraj, L., Bhutkar, A., et al. (2016). Circadian rhythm disruption promotes lung tumorigenesis. *Cell Metab.* 24, 324–331. doi: 10.1016/j.cmet.2016.07.001

Park, H. S., Kim, S. R., and Lee, Y. C. (2009). Impact of oxidative stress on lung diseases. *Respirology* 14, 27–38. doi: 10.1111/j.1440-1843.2008.01447.x

Pastushenko, I., Brisebarre, A., Sifrim, A., Fioramonti, M., Revenco, T., Boumahdi, S., et al. (2018). Identification of the tumour transition states occurring during EMT. *Nature* 556, 463–468. doi: 10.1038/s41586-018-0040-3

Peng, Z., Wang, J., Shan, B., Li, B., Peng, W., Dong, Y., et al. (2018). The long noncoding RNA LINC00312 induces lung adenocarcinoma migration and vasculogenic mimicry through directly binding YBX1. *Mol. Cancer* 17:167. doi: 10.1186/s12943-018-0920-z

Poomakkoth, N., Issa, A., Abdulrahman, N., Abdelaziz, S. G., and Mraiche, F. (2016). p90 ribosomal S6 kinase: a potential therapeutic target in lung cancer. *J. Transl. Med.* 14:14. doi: 10.1186/s12967-016-0768-1

Prabhu, L., Mundade, R., Wang, B., Wei, H., Hartley, A.-V., Martin, M., et al. (2015). Critical role of phosphorylation of serine 165 of YBX1 on the activation of NF-κB in colon cancer. *Oncotarget* 6, 29396–29412. doi: 10.18632/oncotarget.5120

Quispel-Janssen, J. M., Badhai, J., Schunselaar, L., Price, S., Brammeld, J., Iorio, F., et al. (2018). Comprehensive pharmacogenomic profiling of malignant pleural mesothelioma identifies a subgroup sensitive to FGFR inhibition. *Clin. Cancer Res.* 24, 84–94. doi: 10.1158/1078-0432.CCR-17-1172

Raffetseder, U., Rauen, T., Boor, P., Ostendorf, T., Hanssen, L., Floege, J., et al. (2011). Extracellular YB-1 blockade in experimental nephritis upregulates Notch-3 receptor expression and signaling. *Nephron Exp. Nephrol.* 118, e100–e108. doi: 10.1159/000324209

Rauen, T., Frye, B. C., Wang, J., Raffetseder, U., Alidousty, C., En-Nia, A., et al. (2016). Cold shock protein YB-1 is involved in hypoxia-dependent gene transcription. *Biochem. Biophys. Res. Commun.* 478, 982–987. doi: 10.1016/j.bbrc.2016.08.064

Rauen, T., Raffetseder, U., Frye, B. C., Djudjaj, S., Mühlenberg, P. J., Eitner, F., et al. (2009). YB-1 acts as ligand for Notch-3 receptors and modulates receptor activation. *J. Biol. Chem.* 284, 26928–26940. doi: 10.1074/jbc.M109.046599

Renganathan, A., Kresoja-Rakic, J., Echeverry, N., Ziltener, G., Vrugt, B., Opitz, I., et al. (2014). GAS5 long non-coding RNA in malignant pleural mesothelioma. *Mol. Cancer* 13:119. doi: 10.1186/1476-4598-13-119

Reya, T., and Clevers, H. (2005). Wnt signalling in stem cells and cancer. *Nature* 434, 843–850. doi: 10.1038/nature03319

Riquelme, E., Suraokar, M. B., Rodriguez, J., Mino, B., Lin, H. Y., Rice, D. C., et al. (2014). Frequent coamplification and cooperation between C-MYC and PVT1 oncogenes promote malignant pleural mesothelioma. *J. Thorac. Oncol.* 9, 998–1007. doi: 10.1097/JTO.0000000000000202

Rohwer, N., and Cramer, T. (2011). Hypoxia-mediated drug resistance: novel insights on the functional interaction of HIFs and cell death pathways. *Drug Resist. Updat.* 14, 191–201. doi: 10.1016/j.drup.2011.03.001

Rudin, C. M., Durinck, S., Stawiski, E. W., Poirier, J. T., Modrusan, Z., Shames, D. S., et al. (2012). Comprehensive genomic analysis identifies SOX2 as a frequently amplified gene in small-cell lung cancer. *Nat. Genet.* 44, 1111–1116. doi: 10.1038/ng.2405

Rudin, C. M., Giaccone, G., and Ismaila, N. (2016). Treatment of small-cell lung cancer: American Society of Clinical Oncology endorsement of the American College of Chest Physicians guideline. *J. Oncol. Pract.* 12, 83–86. doi: 10.1200/jop.2015.008201

Ryu, A., Kim, D. H., Kim, E., and Lee, M. Y. (2018). The potential roles of extracellular vesicles in cigarette smoke-associated diseases. *Oxidat. Med. Cell. Longev.* 2018:4692081. doi: 10.1155/2018/4692081

Schelch, K., Hoda, M. A., Klikovits, T., Münzker, J., Ghanim, B., Wagner, C., et al. (2014). Fibroblast growth factor receptor inhibition is active against mesothelioma and synergizes with radio-and chemotherapy. *Am. J. Respir. Crit. Care Med.* 190, 763–772. doi: 10.1164/rccm.201404-0658OC

Schittek, B., Psenner, K., Sauer, B., Meier, F., Iftner, T., and Garbe, C. (2007). The increased expression of Y box-binding protein 1 in melanoma stimulates proliferation and tumor invasion, antagonizes apoptosis and enhances chemoresistance. *Int. J. Cancer* 120, 2110–2118. doi: 10.1002/ijc.22512

Sears, C. R. (2019). DNA repair as an emerging target for COPD-lung cancer overlap. *Respir. Investig.* 57, 111–121. doi: 10.1016/j.resinv.2018.11.005

Sechi, M., Lall, R. K., Afolabi, S. O., Singh, A., Joshi, D. C., Chiu, S.-Y., et al. (2018). Fisetin targets YB-1/RSK axis independent of its effect on ERK signaling: insights from in vitro and in vivo melanoma models. *Sci. Rep.* 8:15726. doi: 10.1038/s41598-018-33879-w

Sementino, E., Menges, C. W., Kadariya, Y., Peri, S., Xu, J., Liu, Z., et al. (2018). Inactivation of Tp53 and Pten drives rapid development of pleural and peritoneal malignant mesotheliomas. *J. Cell. Physiol.* 233, 8952–8961. doi: 10.1002/jcp.26830

Semenza, G. L. (2014). Oxygen sensing, hypoxia-inducible factors, and disease pathophysiology. *Annu. Rev. Pathol. Mech. Dis.* 9, 47–71. doi: 10.1146/annurev-pathol-012513-104720

Seton-Rogers, S. (2012). Therapeutics: siRNAs jump the hurdle. *Nat. Rev. Cancer* 12, 376–377. doi: 10.1038/nrc3281

Shi, J. H., Cui, N. P., Wang, S., Zhao, M. Z., Wang, B., Wang, Y. N., et al. (2016). Overexpression of YB 1 C-terminal domain inhibits proliferation, angiogenesis and tumorigenicity in a SK-BR-3 breast cancer xenograft mouse model. *FEBS Open Bio.* 6, 33–42. doi: 10.1002/2211-5463.12004

Shi, X., Sun, M., Liu, H., Yao, Y., Kong, R., Chen, F., et al. (2015). A critical role for the long non-coding RNA GAS5 in proliferation and apoptosis in non-small-cell lung cancer. *Mol. Carcinog.* 54, E1–E12. doi: 10.1002/mc.22120

Shibahara, K., Sugio, K., Osaki, T., Uchiumi, T., Maehara, Y., Kohno, K., et al. (2001). Nuclear expression of the Y-box binding protein, YB-1, as a novel marker of disease progression in non-small cell lung cancer. *Clin. Cancer Res.* 7, 3151–3155.

Shiota, M., Itsumi, M., Yokomizo, A., Takeuchi, A., Imada, K., Kashiwagi, E., et al. (2014). Targeting ribosomal S6 kinases/Y-box binding protein-1 signaling improves cellular sensitivity to taxane in prostate cancer. *Prostate* 74, 829–838. doi: 10.1002/pros.22799

Shiota, M., Izumi, H., Onitsuka, T., Miyamoto, N., Kashiwagi, E., Kidani, A., et al. (2008). Twist promotes tumor cell growth through YB-1 expression. *Cancer Res.* 68, 98–105. doi: 10.1158/0008-5472.CAN-07-2981

Shiota, M., Yokomizo, A., Itsumi, M., Uchiumi, T., Tada, Y., Song, Y., et al. (2011). Twist1 and Y-box-binding protein-1 promote malignant potential in bladder cancer cells. *BJU Int.* 108, E142–E149. doi: 10.1111/j.1464-410X.2010.09810.x

Shiota, M., Yokomizo, A., Tada, Y., Uchiumi, T., Inokuchi, J., Tatsugami, K., et al. (2010). P300/CBP-associated factor regulates Y-box binding protein-1 expression and promotes cancer cell growth, cancer invasion and drug resistance. *Cancer Sci.* 101, 1797–1806. doi: 10.1111/j.1349-7006.2010.01598.x

Shu, Y., Pi, F., Sharma, A., Rajabi, M., Haque, F., Shu, D., et al. (2014). Stable RNA nanoparticles as potential new generation drugs for cancer therapy. *Adv. Drug Deliv. Rev.* 66, 74–89. doi: 10.1016/j.addr.2013.11.006

Shurtleff, M. J., Yao, J., Qin, Y., Nottingham, R. M., Temoche-Diaz, M. M., Schekman, R., et al. (2017). Broad role for YBX1 in defining the small noncoding RNA composition of exosomes. *Proc. Natl. Acad. Sci. U.S.A.* 114, E8987–E8995. doi: 10.1073/pnas.1712108114

Singh, A., Bhattacharyya, N., Srivastava, A., Pruett, N., Ripley, R. T., Schrump, D. S., et al. (2019). microRNA-215-5p treatment suppresses mesothelioma progression via the MDM2-p53 signaling axis. *Mol. Ther.* 27, 1665–1680. doi: 10.1016/j.ymthe.2019.05.020

Singhal, S., Wiewrodt, R., Malden, L. D., Amin, K. M., Matzie, K., Friedberg, J., et al. (2003). Gene expression profiling of malignant mesothelioma. *Clin. Cancer Res.* 9, 3080–3097.

Skabkina, O. V., Lyabin, D. N., Skabkin, M. A., and Ovchinnikov, L. P. (2005). YB-1 autoregulates translation of its own mRNA at or prior to the step of 40S ribosomal subunit joining. *Mol. Cell. Biol.* 25, 3317–3323. doi: 10.1128/mcb.25.8.3317-3323.2005

Skabkina, O. V., Skabkin, M. A., Popova, N. V., Lyabin, D. N., Penalva, L. O., and Ovchinnikov, L. P. (2003). Poly (A)-binding protein positively affects YB-1 mRNA translation through specific interaction with YB-1 mRNA. *J. Biol. Chem.* 278, 18191–18198. doi: 10.1074/jbc.m209073200

Soini, Y., Järvinen, K., Kaarteenaho-Wiik, R., and Kinnula, V. (2001). The expression of P-glycoprotein and multidrug resistance proteins 1 and 2 (MRP1 and MRP2) in human malignant mesothelioma. *Ann. Oncol.* 12, 1239–1245. doi: 10.1023/a:1012292230480

Somasekharan, S. P., El-Naggar, A., Leprivier, G., Cheng, H., Hajee, S., Grunewald, T. G., et al. (2015). YB-1 regulates stress granule formation and tumor progression by translationally activating G3BP1. *J. Cell Biol.* 208, 913–929. doi: 10.1083/jcb.201411047

Sorokin, A. V., Selyutina, A. A., Skabkin, M. A., Guryanov, S. G., Nazimov, I. V., Richard, C., et al. (2005). Proteasome-mediated cleavage of the Y-box-binding protein 1 is linked to DNA-damage stress response. *EMBO J.* 24, 3602–3612. doi: 10.1038/sj.emboj.7600830

Stefan, S. M., and Wiese, M. (2019). Small-molecule inhibitors of multidrug resistance-associated protein 1 and related processes: a historic approach and recent advances. *Med. Res. Rev.* 39, 176–264. doi: 10.1002/med.21510

Stein, U., Bergmann, S., Scheffer, G. L., Scheper, R. J., Royer, H.-D., Schlag, P. M., et al. (2005). YB-1 facilitates basal and 5-fluorouracil-inducible expression of the human major vault protein (MVP) gene. *Oncogene* 24, 3606–3618. doi: 10.1038/sj.onc.1208386

Stein, U., Jürchott, K., Walther, W., Bergmann, S., Schlag, P. M., and Royer, H.-D. (2001). Hyperthermia-induced nuclear translocation of transcription factor YB-1 leads to enhanced expression of multidrug resistance-related ABC transporters. *J. Biol. Chem.* 276, 28562–28569. doi: 10.1074/jbc.m100311200

Stratford, A. L., Fry, C. J., Desilets, C., Davies, A. H., Cho, Y. Y., Li, Y., et al. (2008). Y-box binding protein-1 serine 102 is a downstream target of p90 ribosomal S6 kinase in basal-like breast cancer cells. *Breast Cancer Res.* 10:R99. doi: 10.1186/bcr2202

Stratford, A. L., Habibi, G., Astanehe, A., Jiang, H., Hu, K., Park, E., et al. (2007). Epidermal growth factor receptor (EGFR) is transcriptionally induced by the Y-box binding protein-1 (YB-1) and can be inhibited with Iressa in basal-like breast cancer, providing a potential target for therapy. *Breast Cancer Res.* 9:R61.

Su, W., Feng, S., Chen, X., Yang, X., Mao, R., Guo, C., et al. (2018). Silencing of long non-coding RNA MIR22HG triggers cell survival/death signaling via oncogenes YBX1, MET, and p21 in lung cancer. *Cancer Res.* 78, 3207–3219. doi: 10.1158/0008-5472.CAN-18-0222

Suresh, P. S., Tsutsumi, R., and Venkatesh, T. (2018). YBX1 at the crossroads of non-coding transcriptome, exosomal, and cytoplasmic granular signaling. *Eur. J. Cell Biol.* 97, 163–167. doi: 10.1016/j.ejcb.2018.02.003

Sutherland, B. W., Kucab, J., Wu, J., Lee, C., Cheang, M. C., Yorida, E., et al. (2005). Akt phosphorylates the Y-box binding protein 1 at Ser102 located in the cold shock domain and affects the anchorage-independent growth of breast cancer cells. *Oncogene* 24, 4281–4292. doi: 10.1038/sj.onc.1208590

Szolkowska, M., Blasinska-Przerwa, K., Knetki-Wroblewska, M., Rudzinski, P., and Langfort, R. (2018). Malignant pleural mesothelioma: main topics of American Society of Clinical Oncology clinical practice guidelines for diagnosis and treatment. *J. Thorac. Dis.* 10(Suppl. 17), S1966–S1970.

Tabata, C., Shibata, E., Tabata, R., Kanemura, S., Mikami, K., Nogi, Y., et al. (2013). Serum HMGB1 as a prognostic marker for malignant pleural mesothelioma. *BMC Cancer* 13:205. doi: 10.1186/1471-2407-13-205

Tacke, F., Galm, O., Kanig, N., Yagmur, E., Brandt, S., Lindquist, J. A., et al. (2014). High prevalence of Y-box protein-1/p18 fragment in plasma of patients with malignancies of different origin. *BMC Cancer* 14:33. doi: 10.1186/1471-2407-14-33

Tagalakis, A. D., Munye, M. M., Ivanova, R., Chen, H., Smith, C. M., Aldossary, A. M., et al. (2018). Effective silencing of ENaC by siRNA delivered with epithelial-targeted nanocomplexes in human cystic fibrosis cells and in mouse lung. *Thorax* 73, 847–856. doi: 10.1136/thoraxjnl-2017-210670

Takeuchi, A., Shiota, M., Tatsugami, K., Yokomizo, A., Kuroiwa, K., Dejima, T., et al. (2013). YB-1 suppression induces STAT3 proteolysis and sensitizes renal cancer to interferon-α. *Cancer Immunol. Immunother.* 62, 517–527. doi: 10.1007/s00262-012-1356-8

Tanaka, T., Kasai, M., and Kobayashi, S. (2018). Mechanism responsible for inhibitory effect of indirubin 3'-oxime on anticancer agent-induced YB-1 nuclear translocation in HepG2 human hepatocellular carcinoma cells. *Exp. Cell Res.* 370, 454–460. doi: 10.1016/j.yexcr.2018.07.009

Tanaka, T., Ohashi, S., and Kobayashi, S. (2016). Four nucleocytoplasmic-shuttling proteins and p53 interact specifically with the YB-NLS and are involved in anticancer reagent-induced nuclear localization of YB-1. *Biochem. Biophys. Res. Commun.* 478, 1363–1369. doi: 10.1016/j.bbrc.2016.08.129

Tao, Z., Ruan, H., Sun, L., Kuang, D., Song, Y., Wang, Q., et al. (2019). Targeting the YB-1/PD-L1 axis to enhance chemotherapy and antitumor immunity. *Cancer Immunol. Res.* 7, 1135–1147. doi: 10.1158/2326-6066.CIR-18-0648

Tiwari, A., Rebholz, S., Maier, E., Dehghan Harati, M., Zips, D., Sers, C., et al. (2018). Stress-induced phosphorylation of nuclear YB-1 depends on nuclear trafficking of p90 Ribosomal S6 Kinase. *Int. J. Mol. Sci.* 19:2441. doi: 10.3390/ijms19082441

To, K., Fotovati, A., Reipas, K. M., Law, J. H., Hu, K., Wang, J., et al. (2010). Y-box binding protein-1 induces the expression of CD44 and CD49f leading to enhanced self-renewal, mammosphere growth, and drug resistance. *Cancer Res.* 70, 2840–2851. doi: 10.1158/0008-5472.can-09-3155

Tossavainen, A. (2004). Global use of asbestos and the incidence of mesothelioma. *Int. J. Occup. Environ. Health* 10, 22–25. doi: 10.1179/oeh.2004.10.1.22

Uramoto, H., Izumi, H., Ise, T., Tada, M., Uchiumi, T., Kuwano, M., et al. (2002). p73 Interacts with c-Myc to regulate Y-box-binding protein-1 expression. *J. Biol. Chem.* 277, 31694–31702. doi: 10.1074/jbc.m200266200

van Roeyen, C. R., Scurt, F. G., Brandt, S., Kuhl, V. A., Martinkus, S., Djudjaj, S., et al. (2013). Cold shock Y-box protein-1 proteolysis autoregulates its transcriptional activities. *Cell Commun. Signal.* 11:63. doi: 10.1186/1478-811X-11-63

van Zandwijk, N., Pavlakis, N., Kao, S. C., Linton, A., Boyer, M. J., Clarke, S., et al. (2017). Safety and activity of microRNA-loaded minicells in patients with recurrent malignant pleural mesothelioma: a first-in-man, phase 1, open-label, dose-escalation study. *Lancet Oncol.* 18, 1386–1396. doi: 10.1016/S1470-2045(17)30621-6

Vanni, I., Alama, A., Grossi, F., Dal Bello, M. G., and Coco, S. (2017). Exosomes: a new horizon in lung cancer. *Drug Discov. Today* 22, 927–936. doi: 10.1016/j.drudis.2017.03.004

Ventola, C. L. (2017). Cancer immunotherapy, part 3: challenges and future trends. *Pharm. Ther.* 42, 514–521.

Visconti, R., Morra, F., Guggino, G., and Celetti, A. (2017). The between now and then of lung cancer chemotherapy and immunotherapy. *Int. J. Mol. Sci.* 18:E1374.

Vogelzang, N. J., Rusthoven, J. J., Symanowski, J., Denham, C., Kaukel, E., Ruffie, P., et al. (2003). Phase III study of pemetrexed in combination with cisplatin versus cisplatin alone in patients with malignant pleural mesothelioma. *J. Clin. Oncol.* 21, 2636–2644. doi: 10.1200/jco.2003.11.136

Volm, M., and Koomagi, R. (2000). Prognostic relevance of c-Myc and caspase-3 for patients with non-small cell lung cancer. *Oncol. Rep.* 7, 95–103.

Wang, H., Sun, R., Chi, Z., Li, S., and Hao, L. (2017). Silencing of Y-box binding protein-1 by RNA interference inhibits proliferation, invasion, and metastasis, and enhances sensitivity to cisplatin through NF-κB signaling pathway in human neuroblastoma SH-SY5Y cells. *Mol. Cell. Biochem.* 433, 1–12. doi: 10.1007/s11010-017-3011-3

Wang, W., Ke, S., Chen, G., Gao, Q., Wu, S., Wang, S., et al. (2004). Effect of lung resistance-related protein on the resistance to cisplatin in human ovarian cancer cell lines. *Oncol. Rep.* 12, 1365–1370.

Wang, W., Zheng, Y., Jia, J., Li, C., Duan, Q., Li, R., et al. (2017). Antimicrobial peptide LL-37 promotes the viability and invasion of skin squamous cell carcinoma by upregulating YB-1. *Exp. Ther. Med.* 14, 499–506. doi: 10.3892/etm.2017.4546

Wang, Y., Wu, J., Yang, Y., Wei, Y., Peng, X., Chen, R., et al. (2018). miR-216a-5p inhibits malignant progression in small cell lung cancer: involvement of the Bcl-2 family proteins. *Cancer Manag. Res.* 10, 4735–4745. doi: 10.2147/CMAR.S178380

Wangari-Talbot, J., and Hopper-Borge, E. (2013). Drug resistance mechanisms in non-small cell lung carcinoma. *J. Cancer Res. Updates* 2, 265–282.

Weeraratna, A. T., Jiang, Y., Hostetter, G., Rosenblatt, K., Duray, P., Bittner, M., et al. (2002). Wnt5a signaling directly affects cell motility and invasion of metastatic melanoma. *Cancer Cell* 1, 279–288. doi: 10.1016/s1535-6108(02)00045-4

Wei, M.-M., Zhou, Y.-C., Wen, Z.-S., Zhou, B., Huang, Y.-C., Wang, G.-Z., et al. (2016). Long non-coding RNA stabilizes the Y-box-binding protein 1 and regulates the epidermal growth factor receptor to promote lung carcinogenesis. *Oncotarget* 7, 59556–59571. doi: 10.18632/oncotarget.10006

Wen, Z.-M., Jie, J., Zhang, Y., Liu, H., and Peng, L.-P. (2017). A self-assembled polyjuglanin nanoparticle loaded with doxorubicin and anti-Kras siRNA for attenuating multidrug resistance in human lung cancer. *Biochem. Biophys. Res. Commun.* 493, 1430–1437. doi: 10.1016/j.bbrc.2017.09.132

Winther-Larsen, A., Fynboe Ebert, E. B., Meldgaard, P., and Sorensen, B. S. (2019). EGFR gene polymorphism predicts improved outcome in patients With EGFR mutation-positive non-small cell lung cancer treated with erlotinib. *Clin. Lung Cancer* 20, 161.e1–166.e1. doi: 10.1016/j.cllc.2019.02.011

Wolffe, A., Tafuri, S., Ranjan, M., and Familari, M. (1992). The Y-box factors: a family of nucleic acid binding proteins conserved from *Escherichia coli* to man. *New Biol.* 4, 290–298.

Woolley, A. G., Algie, M., Samuel, W., Harfoot, R., Wiles, A., Hung, N. A., et al. (2011). Prognostic association of YB-1 expression in breast cancers: a matter of antibody. *PLoS One* 6:e20603. doi: 10.1371/journal.pone.0020603

Wu, Q., Cheng, Z., Zhu, J., Xu, W., Peng, X., Chen, C., et al. (2015). Suberoylanilide hydroxamic acid treatment reveals crosstalks among proteome, ubiquitylome and acetylome in non-small cell lung cancer A549 cell line. *Sci. Rep.* 5:9520. doi: 10.1038/srep09520

Xiao, H., Liu, Y., Liang, P., Wang, B., Tan, H., Zhang, Y., et al. (2018). TP53TG1 enhances cisplatin sensitivity of non-small cell lung cancer cells through regulating miR-18a/PTEN axis. *Cell Biosci.* 8:23. doi: 10.1186/s13578-018-0221-7

Xu, J., and Hu, Z. (2016). Y-box-binding protein 1 promotes tumor progression and inhibits cisplatin chemosensitivity in esophageal squamous cell carcinoma. *Biomed. Pharmacother.* 79, 17–22. doi: 10.1016/j.biopha.2016.01.037

Xu, L., Fu, Y., Li, Y., and Han, X. (2017a). Cisplatin induces expression of drug resistance-related genes through c-jun N-terminal kinase pathway in human

lung cancer cells. *Cancer Chemother. Pharmacol.* 80, 235–242. doi: 10.1007/s00280-017-3355-0

Xu, L., Li, H., Wu, L., and Huang, S. (2017b). YBX1 promotes tumor growth by elevating glycolysis in human bladder cancer. *Oncotarget* 8, 65946–65956. doi: 10.18632/oncotarget.19583

Xu, M., Jin, H., Xu, C.-X., Sun, B., Song, Z.-G., Bi, W.-Z., et al. (2015). miR-382 inhibits osteosarcoma metastasis and relapse by targeting Y box-binding protein 1. *Mol. Ther.* 23, 89–98. doi: 10.1038/mt.2014.197

Yahata, H., Kobayashi, H., Kamura, T., Amada, S., Hirakawa, T., Kohno, K., et al. (2002). Increased nuclear localization of transcription factor YB-1 in acquired cisplatin-resistant ovarian cancer. *J. Cancer Res. Clin. Oncol.* 128, 621–626. doi: 10.1007/s00432-002-0386-6

Yamashita, T., Higashi, M., Momose, S., Morozumi, M., and Tamaru, J.-I. (2017). Nuclear expression of Y box binding-1 is important for resistance to chemotherapy including gemcitabine in TP53-mutated bladder cancer. *Int. J. Oncol.* 51, 579–586. doi: 10.3892/ijo.2017.4031

Yang, H., Rivera, Z., Jube, S., Nasu, M., Bertino, P., Goparaju, C., et al. (2010). Programmed necrosis induced by asbestos in human mesothelial cells causes high-mobility group box 1 protein release and resultant inflammation. *Proc. Natl. Acad. Sci. U.S.A.* 107, 12611–12616. doi: 10.1073/pnas.1006542107

Yang, Y.-R., Li, Y.-X., Gao, X.-Y., Zhao, S.-S., Zang, S.-Z., and Zhang, Z.-Q. (2015). MicroRNA-137 inhibits cell migration and invasion by targeting bone morphogenetic protein-7 (BMP7) in non-small cell lung cancer cells. *Int. J. Clin. Exp. Pathol.* 8, 10847–10853.

Yap, T. A., Aerts, J. G., Popat, S., and Fennell, D. A. (2017). Novel insights into mesothelioma biology and implications for therapy. *Nat. Rev. Cancer* 17, 475–488. doi: 10.1038/nrc.2017.42

Yokoyama, H., Harigae, H., Takahashi, S., Takahashi, S., Furuyama, K., Kaku, M., et al. (2003). Regulation of YB-1 gene expression by GATA transcription factors. *Biochem. Biophys. Res. Commun.* 303, 140–145. doi: 10.1016/s0006-291x(03)00296-1

Yuan, Z.-Q., Chen, W.-L., You, B.-G., Liu, Y., Li, J.-Z., Zhu, W.-J., et al. (2017). Multifunctional nanoparticles co-delivering EZH2 siRNA and etoposide for synergistic therapy of orthotopic non-small-cell lung tumor. *J. Control. Release* 268, 198–211. doi: 10.1016/j.jconrel.2017.10.025

Zarogoulidis, K., Ziogas, E., Boutsikou, E., Zarogoulidis, P., Darwiche, K., Kontakiotis, T., et al. (2013). Immunomodifiers in combination with conventional chemotherapy in small cell lung cancer: a phase II, randomized study. *Drug Design Dev. Ther.* 7, 611–617. doi: 10.2147/DDDT.S43184

Zarogoulidis, P., Lampaki, S., Turner, J., Huang, H., Kakolyris, S., and Syrigos, K. (2014). mTOR pathway: a current, up-to-date mini-review (Review). *Oncol. Lett.* 8, 2367–2370. doi: 10.3892/ol.2014.2608

Zhao, S., Wang, Y., Guo, T., Yu, W., Li, J., Tang, Z., et al. (2016). YBX1 regulates tumor growth via CDC25a pathway in human lung adenocarcinoma. *Oncotarget* 7, 82139–82157. doi: 10.18632/oncotarget.10080

Zhen, Q., Gao, L.-N., Wang, R.-F., Chu, W.-W., Zhang, Y.-X., Zhao, X.-J., et al. (2018). LncRNA DANCR promotes lung cancer by sequestering miR-216a. *Cancer Control* 25:1073274818769849. doi: 10.1177/1073274818769849

Zheng, J., Jing, W., and Orentas, R. J. (2009). Discovery of YB-1 as a new immunological target in neuroblastoma by vaccination in the context of regulatory T cell blockade. *Acta Biochim. Biophys. Sin.* 41, 980–990. doi: 10.1093/abbs/gmp092

Zheng, J., Liu, P., and Yang, X. (2012). YB-1 immunization combined with regulatory T-cell depletion induces specific T-cell responses that protect against neuroblastoma in the early stage. *Acta Biochim. Biophys. Sin.* 44, 1006–1014. doi: 10.1093/abbs/gms089

Zhou, L., Lv, T., Zhang, Q., Zhu, Q., Zhan, P., Zhu, S., et al. (2017a). The biology, function and clinical implications of exosomes in lung cancer. *Cancer Lett.* 407, 84–92. doi: 10.1016/j.canlet.2017.08.003

Zhou, L.-L., Ni, J., Feng, W.-T., Yao, R., Yue, S., Zhu, Y.-N., et al. (2017b). High YBX1 expression indicates poor prognosis and promotes cell migration and invasion in nasopharyngeal carcinoma. *Exp. Cell Res.* 361, 126–134. doi: 10.1016/j.yexcr.2017.10.009

Zhou, S., Liu, L., Li, H., Eilers, G., Kuang, Y., Shi, S., et al. (2014). Multipoint targeting of the PI3K/mTOR pathway in mesothelioma. *Br. J. Cancer* 110, 2479–2488. doi: 10.1038/bjc.2014.220

Zong, D., Ouyang, R., Li, J., Chen, Y., and Chen, P. (2016). Notch signaling in lung diseases: focus on Notch1 and Notch3. *Ther. Adv. Respir. Dis.* 10, 468–484. doi: 10.1177/1753465816654873

Conflict of Interest: GR has an issued patent, US 9,006,200, covering use of microRNAs for cancer therapy.

The remaining authors declare that the research was conducted in the absence of any commercial or financial relationships that could be construed as a potential conflict of interest.

frontiers in Cell and Developmental Biology

CORRECTION
published: 22 November 2019
doi: 10.3389/fcell.2019.00293

Corrigendum: Why Be One Protein When You Can Affect Many? The Multiple Roles of YB-1 in Lung Cancer and Mesothelioma

Thomas G. Johnson[1,2,3,4], *Karin Schelch*[5], *Sunali Mehta*[6,7], *Andrew Burgess*[2,3] and *Glen Reid*[6,7]*

[1] Asbestos Diseases Research Institute, Sydney, NSW, Australia, [2] Cell Division Laboratory, The ANZAC Research Institute, Sydney, NSW, Australia, [3] School of Medicine, The University of Sydney, Sydney, NSW, Australia, [4] Sydney Catalyst Translational Cancer Research Centre, The University of Sydney, Sydney, NSW, Australia, [5] Institute of Cancer Research, Medical University of Vienna, Vienna, Austria, [6] Department of Pathology, University of Otago, Dunedin, New Zealand, [7] Maurice Wilkins Centre, University of Otago, Dunedin, New Zealand

Keywords: lung cancer, mesothelioma, targeted therapy, biomarker, Y-box binding protein-1

A Corrigendum on

Why Be One Protein When You Can Affect Many? The Multiple Roles of YB-1 in Lung Cancer and Mesothelioma

by Johnson, T. G., Schelch, K., Mehta, S., Burgess, A., and Reid, G. (2019). Front. Cell Dev. Biol. 7:221. doi: 10.3389/fcell.2019.00221

In the original article, there was an error. The authors wrote "adenylation" instead of "acetylation".

A correction has been made to the **YB-1: a malignant jack of all trades** section, subsection **YB-1 is secreted into the extracellular space under cellular stress**, paragraph two:

"Y-box binding protein-1 is related on an evolutionary level to HMGB1 and is also secreted under certain cellular stresses. This was first evident in monocytes stimulated with bacterial lipopolysaccharide through an active, non-classical pathway and appears to require the same two lysine residues (Lys301/304) that are the site of acetylation in hemodialysis patients (Frye et al., 2009; Ewert et al., 2018; Figures 3–5). Secreted YB-1 stimulated DNA synthesis, cell proliferation and migration of kidney cells (Frye et al., 2009). More pertinent to thoracic cancer, YB-1 is also secreted under oxidative stress. YB-1 translationally upregulates *G3BP1* under oxidative stress and localizes to cytoplasmic stress granules where it is involved in pro-survival mRNA reprogramming (Somasekharan et al., 2015). G3BP1 also promotes the invasion and metastasis of sarcoma cells *in vivo* (Somasekharan et al., 2015). In support, YB-1 enrichment in stress granules is also linked to its secretion to the extracellular space under oxidizing conditions (Guarino et al., 2018; Figures 4, 5). Secretion of YB-1 resulted in depletion of cytoplasmic YB-1, leaving nuclear expression intact (presumably to allow for YB-1-mediated DNA repair), while secreted YB-1 inhibited the growth of neighboring keratinocytes (Guarino et al., 2018)."

The authors apologize for this error and state that this does not change the scientific conclusions of the article in any way. The original article has been updated.

OPEN ACCESS

Edited and reviewed by:
Dominic C. Voon, Kanazawa University, Japan

***Correspondence:**
Glen Reid
glen.reid@otago.ac.nz

Specialty section:
This article was submitted to Cell Growth and Division, a section of the journal Frontiers in Cell and Developmental Biology

Received: *22 October 2019*
Accepted: *06 November 2019*
Published: *22 November 2019*

Citation:
Johnson TG, Schelch K, Mehta S, Burgess A and Reid G (2019) Corrigendum: Why Be One Protein When You Can Affect Many? The Multiple Roles of YB-1 in Lung Cancer and Mesothelioma. Front. Cell Dev. Biol. 7:293. doi: 10.3389/fcell.2019.00293

REFERENCES

Ewert, L., Fischer, A., Brandt, S., Scurt, F. G., Philipsen, L., Müller, A. J., et al. (2018). Cold shock Y-box binding protein-1 acetylation status in monocytes is associated with systemic inflammation and vascular damage. *Atherosclerosis* 278, 156–165. doi: 10.1016/j.atherosclerosis.2018.09.020

Frye, B. C., Halfter, S., Djudjaj, S., Muehlenberg, P., Weber, S., Raffetseder, U., et al. (2009). Y-box protein-1 is actively secreted through a non-classical pathway and acts as an extracellular mitogen. *EMBO Rep.* 10, 783–789. doi: 10.1038/embor.2009.81

Guarino, A., Troiano, A., Pizzo, E., Bosso, A., Vivo, M., Pinto, G., et al. (2018). Oxidative stress causes enhanced secretion of YB-1 Protein that restrains proliferation of receiving cells. *Genes.* 9:E513. doi: 10.3390/genes9100513

Somasekharan, S. P., El-Naggar, A., Leprivier, G., Cheng, H., Hajee, S., Grunewald, T. G., et al. (2015). YB-1 regulates stress granule formation and tumor progression by translationally activating G3BP1. *J. Cell Biol.* 208, 913–929. doi: 10.1083/jcb.201411047

frontiers in Cell and Developmental Biology

BRIEF RESEARCH REPORT
published: 04 February 2020
doi: 10.3389/fcell.2020.00002

ATR-Mediated FANCI Phosphorylation Regulates Both Ubiquitination and Deubiquitination of FANCD2

*Winnie Tan[1,2], Sylvie van Twest[1], Vincent J. Murphy[1] and Andrew J. Deans[1,2]**

[1] Genome Stability Unit, St Vincent's Institute of Medical Research, Fitzroy, VIC, Australia, [2] Department of Medicine (St Vincent's Hospital), The University of Melbourne, Melbourne, VIC, Australia

DNA interstrand crosslinks (ICLs) are a physical barrier to replication and therefore toxic to cell viability. An important mechanism for the removal of ICLs is the Fanconi Anemia DNA repair pathway, which is initiated by mono-ubiquitination of FANCD2 and its partner protein FANCI. Here, we show that maintenance of FANCD2 and FANCI proteins in a monoubiquitinated form is regulated by the ATR-kinase. Using recombinant proteins in biochemical reconstitution experiments we show that ATR directly phosphorylates FANCI on serine 556, 559, and 565 to stabilize its association with DNA and FANCD2. This increased association with DNA stimulates the conjugation of ubiquitin to both FANCI and FANCD2, but also inhibits ubiquitin deconjugation. Using phosphomimetic and phosphodead mutants of FANCI we show that S559 and S565 are particularly important for protecting the complex from the activity of the deubiquitinating enzyme USP1:UAF1. Our results reveal a major mechanism by which ATR kinase maintains the activation of the FA pathway, by promoting the accumulation of FANCD2 in the ubiquitinated form active in DNA repair.

Keywords: FANCI, phosphorylation, FANCD2, ubiquitination, deubiquitination

OPEN ACCESS

Edited by:
Andrew Burgess,
Anzac Research Institute, Australia

Reviewed by:
Indrajit Chaudhury,
University of Minnesota, Morris, United States
Angelos Constantinou,
Centre National de la Recherche Scientifique (CNRS), France
Michael G. Kemp,
Wright State University, United States

***Correspondence:**
Andrew J. Deans
adeans@svi.edu.au

Specialty section:
This article was submitted to Cell Growth and Division, a section of the journal Frontiers in Cell and Developmental Biology

Received: *22 November 2019*
Accepted: *03 January 2020*
Published: *04 February 2020*

Citation:
Tan W, van Twest S, Murphy VJ and Deans AJ (2020) ATR-Mediated FANCI Phosphorylation Regulates Both Ubiquitination and Deubiquitination of FANCD2. Front. Cell Dev. Biol. 8:2. doi: 10.3389/fcell.2020.00002

INTRODUCTION

Many chemotherapeutic drugs kill cancer cells by inducing toxic DNA interstrand crosslinks (ICLs). ICLs prevent DNA strand separation and therefore stall DNA transcription and replication complexes (Deans and West, 2011). A critical step in the repair of replication forks stalled by ICLs is the biochemical modification of FANCD2 protein by mono-ubiquitination. Genetic deficiency in this pathway leads to Fanconi anemia (FA), characterized by hypersensitivity to DNA crosslinking agents, bone marrow failure, infertility, and cancer predisposition (Garaycoechea and Patel, 2014; Tsui and Crismani, 2019).

FANCD2 monoubiquitination is temporally and spatially controlled at stalled forks by the FA core complex (a RING E3 ligase), USP1:UAF1 (a deubiquitinating enzyme) and ATR kinase (Ishiai et al., 2017). FANCI is the heterodimeric partner of FANCD2 and plays an essential role in this regulation. In particular, FANCI itself is a target for monoubiquitination by the FA core complex (Smogorzewska et al., 2007), is a substrate of ATR kinase (Chen et al., 2015) and contains a USP1:UAF1 binding site necessary for deubiquitination of FANCD2 (Cohn et al., 2009). FANCD2 associates with FANCI as a heterodimer during ICL repair to signal DNA repair proteins that contain ubiquitin binding motifs, to promote DNA repair via homologous recombination or translesion synthesis (Smogorzewska et al., 2010; Klein Douwel et al., 2014).

A crystal structure of FANCI:FANCD2 complex revealed that the lysine residues targeted for monoubiquitination in FANCI (K522 in mouse corresponding to K523 in human) and FANCD2 (K559 in mouse corresponding to K561 in human) are embedded in the dimer interface (Joo et al., 2011). This raised questions regarding the accessibility of ubiquitin and E3 enzyme into the dimer during the conjugation reaction. In contrast, several validated ATR kinase sites of FANCI (S556, 559, and 565) within an ST/Q cluster (Chen et al., 2015; Cheung et al., 2017) were found to be exposed on the FANCI surface adjacent to the heterodimer interface (Joo et al., 2011). As ATR kinase activity is required for optimal FANCD2 monoubiquitination (Shigechi et al., 2012), it was proposed that ATR phosphorylation of FANCI occurs prior to FANCI:FANCD2 ubiquitination to promote a partial opening of the FANCI:FANCD2 complex, and access to the ubiquitin ligase complex. Support for this comes from the observation that FANCI phosphorylation at serine sites 559 and 565 occurs predominantly on the monoubiquitinated form (Cheung et al., 2017). The UAF1-binding SIM domain of FANCI is next to serines 559 and 565, so an alternative explanation is that ATR acts on these sites post-monoubiquitination, to prevent USP1:UAF1 binding. In this manner, phosphorylation would prevent deubiquitination by USP1. Indeed, phosphomimetic FANCI-S559D/S565D promotes partial cellular resistance to the USP1 inhibitor ML323 (Cheung et al., 2017), but the complication in living cells is that inhibition of deubiquitination actually prevents the correct localization of FANCD2 to new DNA breaks (Castella et al., 2015). The complex intersection of phosphorylation, monoubiquitination, and deubiquitination in regulation of the FA pathway requires investigation using a defined biochemical system.

We previously reconstituted the *in vitro* monoubiquitination and de-ubiquitination of FANCI:FANCD2 using purified proteins. Maximal monoubiquitination required the FANCB-FANCL-FAAP100 (BL100 enzyme module) and FANCC-FANCE-FANCF (CEF substrate adaptor module) components of the FA core complex (Swuec et al., 2017; van Twest et al., 2017). Deubiquitination was more nuanced – USP1:UAF1 could efficiently remove ubiquitin from FANCD2-^{Ub}-FANCI but not FANCD2-^{Ub}-FANCI-^{Ub}. However if FANCD2-^{Ub}-FANCI-^{Ub} is dissociated from DNA, it then becomes a USP1:UAF1 substrate (van Twest et al., 2017). In this way, USP1:UAF1 drives FANCI:FANCD2 complex toward a uniformly di-ubiquitinated state, that can only be de-ubiquitinated post-repair. We have now used this robust reconstituted system to determine if FANCI phosphorylation regulates monoubiquitination and/or deubiquitination of the complex.

MATERIALS AND METHODS

Protein Purification

Table 1 outlines the plasmids and bacmids used in this study and their derivation. Plasmids were propagated using NEB-10-beta competent cells and purified using Monarch miniprep kits (NEB). Bacmids were generated using the Multibac system (Berger et al., 2004) and purified using alkaline lysis method followed by isopropanol precipitation and resuspension in TE.

Human FANCI:FANCD2 complex and Avi-ubiquitin was purified as described in Tan et al. (2020). *Xenopus laevis* (frog) FANCI:FANCD2, human FANCB:FANCL:FAAP100, FANCC:FANCE:FANCF and UBE2T were expressed and purified as described in van Twest et al. (2017). USP1:UAF1, HA-ubiquitin and UBE1 were purchased from Boston Biochem. ATR-ATRIP was purchased from Eurofins DiscoverX. Lambda phosphatase was purchased from New England Biolabs.

FANCI Phosphomutants

Xenopus laevis StrepII-FANCD2, Flag-FANCI and human Flag-FANCI were cloned into pFastBac1 plasmid (Thermo Fisher). Expression plasmids for StrepII-FANCD2, Flag-FANCI, FANCI phosphomimic mutant (S6D) and phosphodead mutant (S6A) were previously described (Knipscheer et al., 2009; Sareen et al., 2012; van Twest et al., 2017). *Xenopus* FANCI with six codons encoding for serine (S) residues S557, S560, S566, S597, S618, and S630 (corresponding to serine residues S556, S559, S565, S595, S617, and S629 in human FANCI) mutated to encode either for aspartic acid (D) residues (FANCI6S➔D) or alanine residues (FANCI6➔A) were kindly provided by Alexandra Sobeck lab (Sareen et al., 2012). Different permutations of FANCI phosphomimic (➔D) or phosphodead (➔A) in the S3 clusters were generated as indicated in **Figure 2A**. Recombinant baculoviruses were generated by standard protocols (Berger et al., 2004). *Trichoplusia ni* (Hi5) insect cells were co-infected with *Xenopus* FANCI and FANCD2 viruses or infected only with human or *Xenopus* FANCI (Flag-tagged) or FANCD2 (StrepII-tagged) (MOI = 2) and harvested after 72 h. Cell pellets were washed in 1X PBS and resuspended in 9 mL Flag Lysis buffer (50 mM Tris-HCI pH 8.0, 100 mM NaCl, 1 mM EDTA, 1X mammalian protease inhibitor (Sigma-Aldrich), 10% glycerol) or Strep Lysis buffer (50 mM Tris-HCl pH 8.0, 100 mM NaCl, 1 mM EDTA, 1X mammalian protease inhibitor (Sigma-Aldrich), 10% glycerol, 20 μg/mL avidin, 1 mM DTT). Lysates were briefly sonicated and cleared by centrifugation for 45 min at 16,000 × *g*, 4°C. 1 mL M2 Flag resin (Sigma-Aldrich) or 1 mL StrepTactin Sepharose resin (VWR International) was washed with 5 CVs each of water, followed by 0.1M glycine pH 3.5 or 0.5M NaOH, and equilibrated with 10 CVs buffer A (20 mM Tris-HCl pH 8.0, 100 mM NaCl, 10% glycerol). Lysate was added to the Flag or Streptactin resin, and incubated with gentle mixing at 4°C for 2 h. Resin was washed with 10 CVs of buffer A and eluted in 1 CV buffer A with 5 μg/mL Flag peptide (Assay Matrix) or 100 μg/mL D-desthiobiotin (Sigma-Aldrich). Flag fractions containing FANCI:FANCD2 complex were pooled, and loaded onto a MiniQ anion purification column (GE) and equilibrated with buffer A. Using a gradient between buffer A and buffer B (20 mM Tris-HCl pH 8.0, 1M NaCl, 10% glycerol), FANCI:FANCD2 complex were eluted between 250 and 350 mM NaCl. The peak fractions were pooled, and assessed by SDS-PAGE. Protein concentration was determined by Nanodrop (Absorbance at 280 nm and calculated extinction coefficients).

TABLE 1 | Plasmids and Bacmids used in this study.

Plasmid	Protein	Selection	Affinity tag	Use
FASTBAC1-FLAG-xFANCI	xFANCI	Ampicilin	Flag	Bacmid generation
pFASTBAC1-STREPII-xFANCD2	xFANCD2	Ampicilin	StrepII	Bacmid generation
pFASTBAC1-FLAG-hFANCD2	hFANCD2	Ampicilin	Flag	Bacmid generation
pFL-EGFP-HIS-hFANCI	hFANCI	Ampicilin	His	Bacmid generation
pFL-EGFP-FLAG-FANCB-pSPL-FAAP100-FANCL	BL100	Ampicilin, Spectinomycin	Flag	Bacmid generation
pFL-MBP-FANCC-FANCE-FANCF	CEF	Ampicilin	MBP	Bacmid generation
pGEX-KG-GST-UBE2T	UBE2T	Ampicilin	GST	*E. coli* expression

In vitro Kinase and Phosphatase Assays

Ten μg of recombinant FANCI:FANCD2, FANCI, or FANCD2 were incubated in 60 μL 20 mM Tris-HCl pH 7.4, 10 mM MgAc, 0.5 mM DTT, 0.05% Tween-20, 100 mM KCl and 0.2 mM ATP in the presence of 0.1 μg of ATR:ATRIP for 30 min at 30°C. For phosphatase experiments, 600 units of lambda phosphatase was added to reactions together with 1 mM $MnCl_2$ and incubated for 30 min at 30°C prior to establishment of ubiquitination reaction.

In vitro Ubiquitination and Deubiquitination Assays

Standard ubiquitination reactions contained 10 μM recombinant human AviTag-biotin-ubiquitin, 50 nM human recombinant UBE1, 100 nM UBE2T, 100 nM pUC19 plasmid or dsDNA oligonucleotide substrate, 2 mM ATP, 100 nM FANCI:FANCD2 complex wild type (WT) or ubiquitination-deficient (KR), in reaction buffer (50 mM Tris-HCl pH 7.4, 2.5 mM $MgCl_2$, 150 mM NaCl, 0.01% Triton X-100). The dsDNA substrates were generated using oligonucleotide 1 (5′-ACGC TGCCGAATTCTACCAGTGCCTTGCTAGGACATCTTTGCC CACCTGCAGGTTCACCC-3′) and oligonucleotide 2 (5′-GG GTGAACCTGCAGGTGGGCAAAGATGTCCTAGCAAGGCA CTGGTAGAATTCGGCAGCGT-3′). 20 μL reactions were set up on ice and incubated at 25°C for 90 min. To perform deubiquitination assays, FANCI:FANCD2 monoubiquitination was arrested using apyrase (NEB) and 100 nM recombinant USP1:UAF1 (Boston Biochem) were added for 30 min at room temperature. Reactions were stopped by adding 10 μL NuPage LDS sample buffer and heated at 80°C for 5 min. Reactions were loaded onto 4–12% SDS PAGE and run using NuPAGE® MOPS buffer and assessed by western blot analysis using Flag (Jomar Life Research) or StrepII (Abcam) antibody.

In gel Proteolytic Digestion and Mass Spectrometry Analysis of FANCI Proteins

Proteins were separated by SDS-PAGE, and the band excised for manual digestion to maximize sensitivity and efficiency. Protein bands were destained and dehydrated with 500 μL acetonitrile (ACN). Subsequently, proteins were reduced with 500 μL 10 mM dithiothreitol (DTT) in 25 mM ammonium bicarbonate (NH_4HCO_3) at 55°C for 1 h and alkylated with 50 μL 55 mM iodoacetamide in 25 mM NH_4HCO_3 at room temperature for 45 min in the dark. Samples were incubated overnight with 20 μL trypsin (125 ng, 37°C). The resulted proteolytic peptides were subjected to sonication with 50 μL of 50% ACN, 5% formic acid and analyzed by mass spectrometry after concentration under vacuum to a 10–15 μL final volume. Mass spectra of digested protein gel bands were obtained on ESI-quadropole-time-of-flight mass spectrometer coupled to reverse-phase HPLC-MS/MS. The analysis program MASCOT was used to identify phosphorylation sites on FANCI.

Biolayer Inferometry (BLItz) Kinetic Analysis

Kinetic titration series were performed in buffer F (20 mM Tris-HCl pH 8.0, 150 mM NaCl). 100 μg/ml FANCD2 or FANCI was diluted in buffer F and further diluted three times with a dilution factor of two. To measure the interaction between FANCD2 and FANCI, the association and dissociation times were 180 and 300 s, respectively, for every analyte concentration. In total, four Streptavidin sensors (ForteBio) were used to measure four different analyte concentrations in parallel, while one sensor was used to measure the buffer reference. All steps were performed at 25°C with an agitation speed of 1000 rpm. Sensorgrams were measured on a ForteBio BLItz instrument and referenced against the buffer reference signal using the Data Analysis software 7.1.0.36 (ForteBio). The sensorgrams obtained with the concentrations: 334.7, 167.3, 83.7, and 41.8 nM were fitted with the BiaEvaluation software 4.1 from Biacore using a 1:1 binding model.

Electromobility Shift Assay (EMSA)

Sixty bp fluorescently labeled dsDNA substrates were prepared as described in van Twest et al. (2017) by annealing oligonucleotide XOm1 5′-labeled with IRDye-700 (IDTDNA) and oligonucleotide XOm1.com. 25 nM dsDNA were incubated with the indicated amounts of protein for 30 min at room temperature in a 15 μL reaction containing 6 mM Tris pH 7.5, 0.1 mM EDTA, 1 mM DTT, 6% glycerol. The reaction was resolved by electrophoresis through a 6% non-denaturing polyacrylamide gel in 1X TBE (100 mM Tris, 90 mM boric acid, 1 mM EDTA) buffer and visualized by Licor Odyssey system.

Pull-Down Assays

Two μg of purified Flag-FANCI proteins were incubated with 2 μg of His-USP1:UAF1 (Boston Biochem) for 30 min at 25°C in 40 μL of pull-down buffer (20 mM Tris-HCl pH 8.0, 100 mM

NaCl and 5% glycerol). 10 μL of TALON metal affinity resin (Takara Bio) were added to the reaction mixtures and were gently mixed for 30 min at 25°C. The resin were then washed three times with 1 mL pull-down buffer. The proteins bound to the resin were separated by SDS-PAGE and stained with Coomassie blue. The band intensities of FANCI were quantitated and visualized by Licor Odyssey system.

RESULTS

Dephosphorylation of Recombinant FANCI:FANCD2 Complex Inhibits Its *in vitro* Monoubiquitination

We determined that a percentage of recombinant FANCI purified from baculovirus infected insect cells is phosphorylated within a previously described S/TQ cluster domain (Ishiai et al., 2008 and **Supplementary Figure 1**). Tandem mass spectrometry (MS/MS) analysis of the purified protein revealed FANCI phosphorylation of multiple serine residues (**Supplementary Figures 1B–D**), including residues previously reported S557, S560, and S566 (Cheung et al., 2017). These correspond to exposed surface residues that are conserved during evolution (**Figure 1A**), but differ in their structure between the unbound and FANCD2-bound FANCI (**Figure 1B**). ATR is the kinase predicted to phosphorylate S557, S560, and S566 in FANCI.

To determine the contribution of the identified phosphorylation sites to FANCD2:FANCI monoubiquitination, we performed an extended phosphatase treatment and then performed *in vitro* ubiquitination reactions using recombinant FA core complex. In both human (**Figure 1C**) and *Xenopus* FANCI:FANCD2 (**Figure 1D**), treatment with λ-phosphatase almost completely eliminated the monoubiquitination of FANCI, and significantly reduced the monoubiquitination rate of FANCD2. We show that addition of recombinant ATR-ATRIP kinase can restore the mono-ubiquitination levels in these preparations. As such, we observed the reappearance of positive bands when using phosphospecific antibodies raised against these three residues, only in ATR-ATRIP treated human FANCI:FANCD2 samples (**Figure 1E**). Together using phospho-specific antibodies and mass spectrometry analysis (**Supplementary Figure 1**), we show that three FANCI serine residues are the substrates of ATR kinase, and are required for optimal monoubiquitination of FANCI and FANCD2.

Free hFANCI, and to some extent hFANCD2, can also be substrates for monoubiquitination by the FA core complex (Longerich et al., 2009; Hodson et al., 2014). We therefore tested the requirement for ATR-phosphorylation in mediating the monoubiquitination of each subunit in isolation. Surprisingly, we found that human FANCI is monoubiquitinated faster in a free state, than when it is in complex with FANCD2, while free FANCD2 remains unubiquitinated (**Figure 1F**). Furthermore, free FANCI is ubiquitinated at the same fast rate as ATR:ATRIP treated FANCI, but is very slow when dephosphorylated (**Figure 1G**). This result suggests phosphorylation of FANCI specifically mediates its effects on FANCI even when it is not bound to FANCD2.

FANCI S6D Phosphomimic Mutant Binds to FANCD2 With Reduced Affinity

Three S/TQ residues, in additional to those described above, were also predicted to be conserved ATR sites in human (Ishiai et al., 2008) and *Xenopus* FANCI (Sareen et al., 2012). However, these predictions were made prior to the derivation of the FANCI:FANCD2 crystal structure. The residues, S597, S618, and S630 turned out to be completely buried in the solenoid structure of FANCI and unlikely to be accessible to any kinase without complete unfolding of the protein structure. None-the-less, the xFANCI-S6D (6 serines changed to aspartate "phosphomimic") and xFANCI-S6A (6 serines changed to alanine "phosphodead") mutants were subsequently used to hypothesize that FANCI phosphorylation leads to the dissociation of FANCD2 and FANCI (Sareen et al., 2012). In our *in vitro* studies, ATR phosphorylation of FANCI did not cause dissociation of the FANCD2:FANCI heterodimer. This led us to suspect that phosphomutant S6A and phosphomimic S6D amino acid substitutions at these residues could be affecting the integrity of the FANCI structure and/or heterodimer formation. We examined xFANCI-S6D (where all 6 serines in the SQ cluster are changed to phosphomimic aspartate residues, **Figure 2A**) and confirmed that it has reduced co-purification with xFANCD2 (**Figure 2B** and **Supplementary Figure 2**). This was a result of an order of magnitude decrease in the affinity of xFANCI-S6D compared to WT, as measured by biolayer inferometry (**Figures 2C,D,F**). xFANCI-S6A, showed normal co-purification with xFANCD2 and a similar affinity to FANCD2 as WT (**Figures 2B,E**).

We never observed S597, S618, and S630 to be phosphorylated in our mass spectrometry studies of recombinant ATR-ATRIP phosphorylated xFANCI or hFANCI protein, and a recent publication failed to identify phosphorylation of these sites in endogenous human FANCI (Cheung et al., 2017). We therefore conclude that the S557/S560/S566 (the 3SQ cluster) is likely to be the functional ATR-phosphorylation cassette in FANCI. So, we repeated the co-purification experiments using phospho-mimic/dead mutants of the 3SQ cluster in various permutations to determine if affinity changes were also observed when these sites only are altered. Unlike for xFANCI-S6D, each of the xFANCI 3SQ mutants bound to xFANCD2 in a 1:1 ratio (**Figure 2B** and **Supplementary Figure 2**). We conclude that ATR-regulation of FANCI on the surface 3SQ cluster does not lead to dissociation of the heterodimer, and likely plays some other role in regulation of FANCD2 and/or FANCI monoubiquitination.

Phosphorylation of FANCI in the S3Q Cluster Promotes FANCI:D2 Monoubiquitination by Increasing Its Retention on DNA

To test if phospho-mimic or phospho-dead mutants within the xFANCI 3SQ cluster affect FANCI:FANCD2 ubiquitination, we performed *in vitro* ubiquitination assays of FANCI:FANCD2

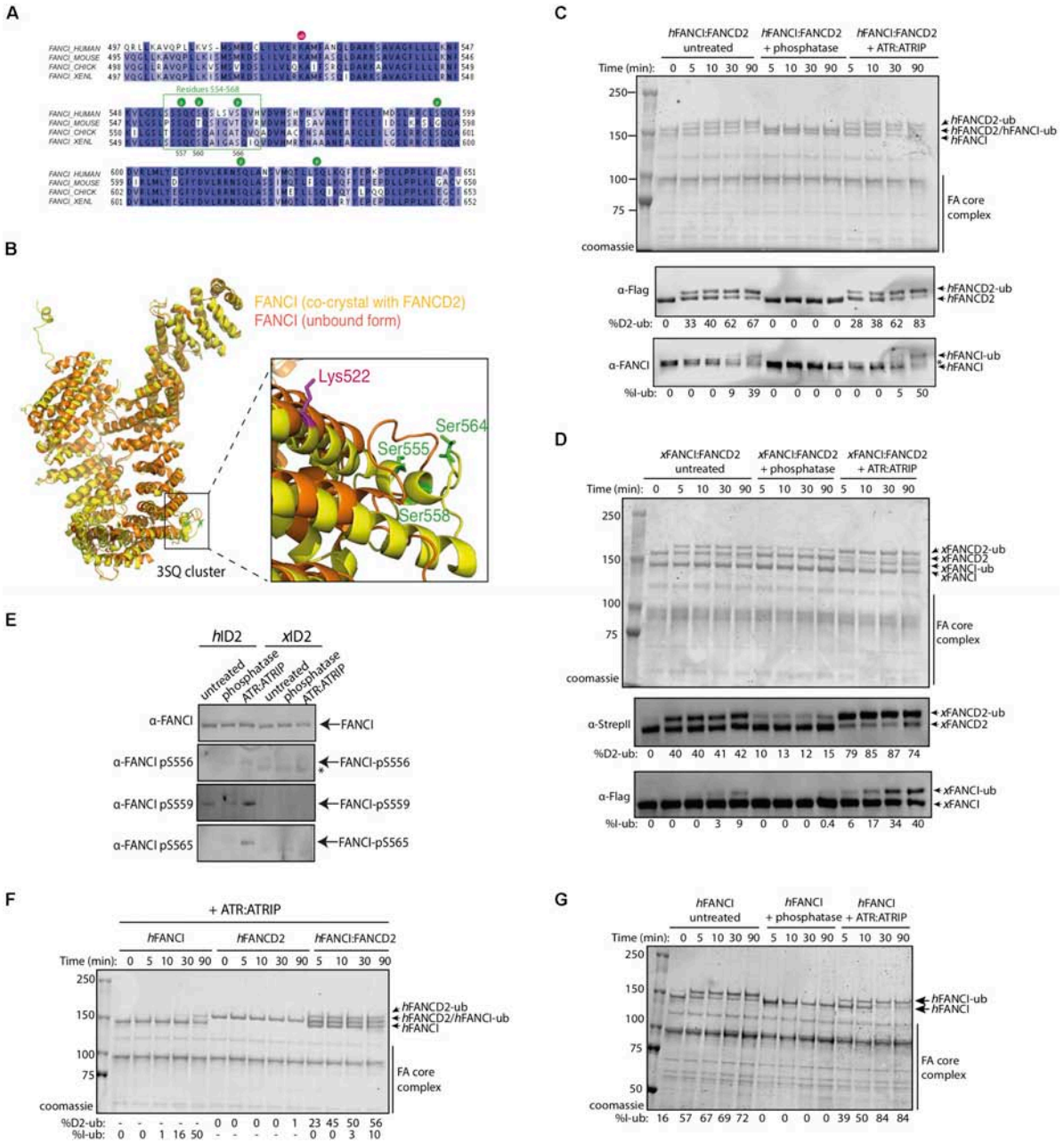

FIGURE 1 | FANCI phosphorylation at serines 557, 560, and 566 are required for FANCI:FANCD2 monoubiquitination. **(A)** Sequence alignment of the FANCI SQ/TQ loop across different species including human, mouse, chicken and *Xenopus laevis* (frog). Phosphorylation sites are indicated and residues 554–569 accounting for FANCI SQ/TQ loop are boxed in green. **(B)** Superposition of FANCI unbound (orange, PDB ID 3Z51) and FANCD2-bound (yellow, PDB ID 3S4W) structures revealed little conformational differences except in the clustered SQ/TQ sites near FANCI monoubiquitination site, Lysine 522. **(C)** Coomassie stained SDS-PAGE gel showing *in vitro* ubiquitination assays of untreated, Lambda phosphatase or ATR-ATRIP kinase treated human FANCI:FANCD2 (hID2) and **(D)** Coomassie stained SDS-PAGE gel showing *in vitro* ubiquitination assays of untreated, Lambda phosphatase or ATR-ATRIP kinase treated *Xenopus* FANCI:FANCD2 (xID2) complex. **(E)** Western blot showing that human FANCI phosphosites 556, 559, and 565 are phosphorylated in ATR-ATRIP treated ID2. **(F)** Coomassie stained SDS-PAGE gel showing the ubiquitination time course of ATR:ATRIP treated isolated human FANCI, FANCD2, or FANCI:FANCD2 complex. **(G)** Coomassie stained SDS-PAGE gel showing the ubiquitination time course of untreated, phosphatase or ATR:ATRIP treated human FANCI. All data are representative of three experiments.

WT and each of the FANCI-3SQ-mutants using recombinant FA core complex proteins. Four of the xFANCI phosphomimic mutants (ADD, ADA, DAD, and DDD) showed faster monoubiquitination rates than for WT xFANCI:FANCD2 complex. In particular, the FANCI-ADD and -DDD variants stimulated the highest rate of xFANCD2 monoubiquitination. Conversely, two of the FANCI-3SQ mutants (AAD and AAA) and both of the FANCI-6SQ mutants (S6D and S6A) showed

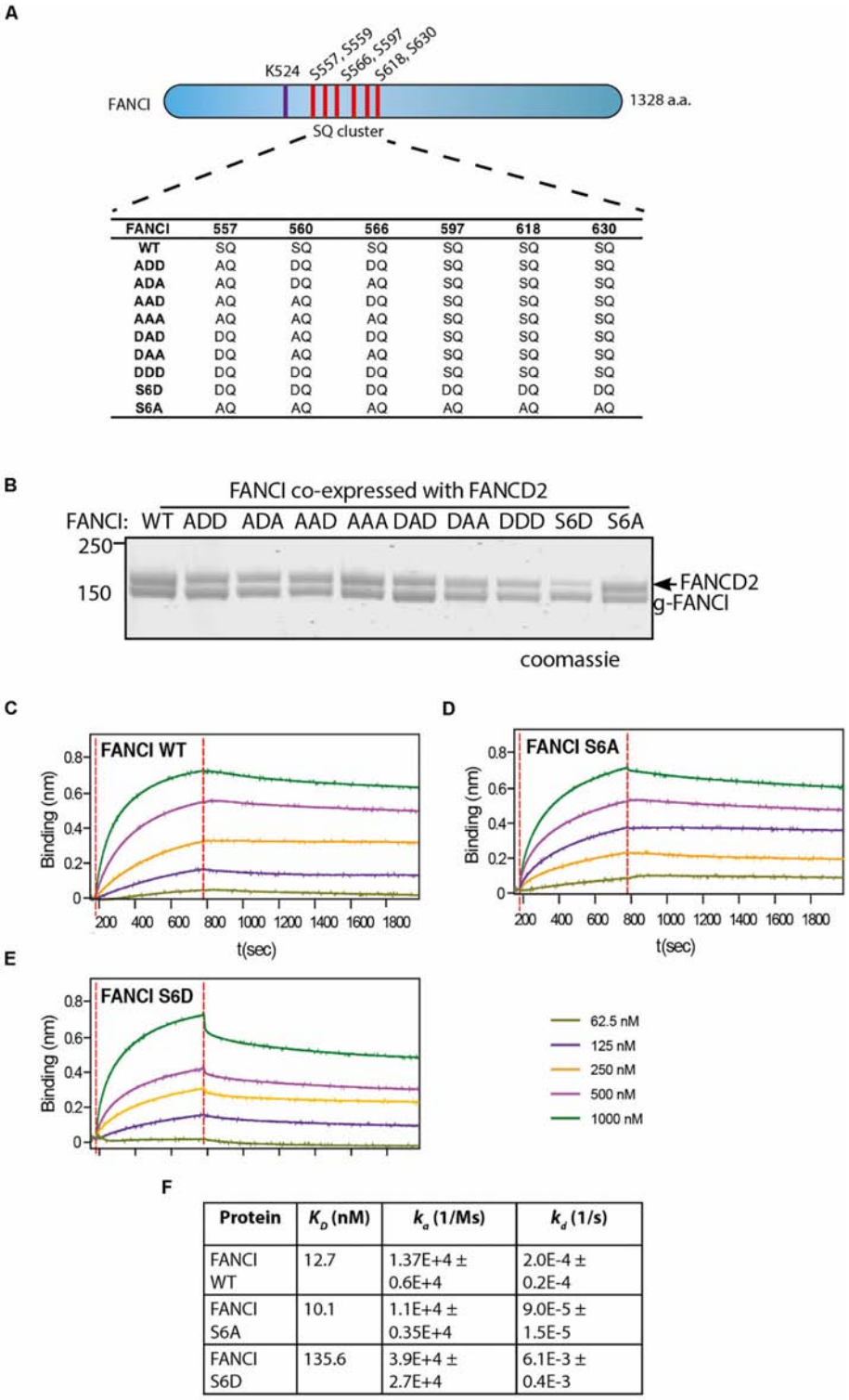

FANCI	557	560	566	597	618	630
WT	SQ	SQ	SQ	SQ	SQ	SQ
ADD	AQ	DQ	DQ	SQ	SQ	SQ
ADA	AQ	DQ	AQ	SQ	SQ	SQ
AAD	AQ	AQ	DQ	SQ	SQ	SQ
AAA	AQ	AQ	AQ	SQ	SQ	SQ
DAD	DQ	AQ	DQ	SQ	SQ	SQ
DAA	DQ	AQ	AQ	SQ	SQ	SQ
DDD	DQ	DQ	DQ	SQ	SQ	SQ
S6D	DQ	DQ	DQ	DQ	DQ	DQ
S6A	AQ	AQ	AQ	AQ	AQ	AQ

F

Protein	K_D (nM)	k_a (1/Ms)	k_d (1/s)
FANCI WT	12.7	1.37E+4 ± 0.6E+4	2.0E-4 ± 0.2E-4
FANCI S6A	10.1	1.1E+4 ± 0.35E+4	9.0E-5 ± 1.5E-5
FANCI S6D	135.6	3.9E+4 ± 2.7E+4	6.1E-3 ± 0.4E-3

FIGURE 2 | FANCI phosphomimic mutant at six serine sites but not three serine sites dissociates ID2 complex. **(A)** Schematic of *Xenopus* FANCI, indicating the six phosphorylation sites within the SQ cluster region. The phosphorylation sites serine 557, 560, 566, 597, 618, and 630 were replaced either by aspartate (DQ) or alanine (AQ). The FANCI mono-ubiquitination site lysine 524 is also shown. **(B)** Coomassie stained SDS-PAGE of Flag-ID2 complex with StrepII-FANCD2 co-expressed with various flag-FANCI phosphomutants. **(C–E)** Biolayer inferometry (BLItz) sensorgrams obtained using StrepII-FANCD2-loaded biosensors in 20 ng/mL solution, with red dotted lines indicating the start of binding (left) and dissociation (right) phases. Biosensors loaded with StrepII-FANCD2 were incubated with different concentrations of FANCI wild type (WT), S6A or S6d mutants, as indicated to generate a series of sensorgrams. **(F)** Summary of dissociation constant (K_D), association (K_a), dissociation (K_d) rate constants obtained from the sensorgrams. Data are representative of four experiments.

lower xFANCD2 monoubiquitination than WT (**Figure 3A**). These results demonstrate that phosphomimic mutations in S560 together with S565 are sufficient to maximally stimulate monoubiquitination of FANCI:FANCD2 complex by the FA core complex (**Figure 3B**).

Previous studies have shown that optimal FANCI:FANCD2 monoubiquitination requires the association of the complex with DNA (Sato et al., 2012; Longerich et al., 2014; van Twest et al., 2017) leading us to speculate that phosphorylation may increase the affinity of FANCI:FANC2 complex to DNA. To examine this hypothesis, we performed electromobility shift assays (EMSAs). Remarkably, the DNA binding measured by EMSA shift was greatly reduced in lambda-phosphatase treated FANCI:FANCD2 complex or FANCI AAA mutant compared to control (**Figure 3C**). DNA binding was not only restored after phosphorylation by ATR and in the FANCI DDD mutant, but occurred at significantly lower FANCI:FANCD2 concentration (i.e., higher affinity). We further tested the association of isolated FANCI with DNA and found that phosphatase treatment also caused a reduction in DNA binding that was restored by ATR-kinase treatment (**Figure 3D**). These results are consistent with ATR-phosphorylation creating a higher affinity of FANCI (and associated FANCD2) for DNA binding, leading to a greater stimulation of monoubiquitination of FANCD2 by the FA core complex.

FANCI Phosphorylation or Phosphomimics Also Protect FANCD2 From Deubiquitination

Published evidence from cell-based studies suggests phosphorylation of FANCI by ATR could also regulate FANCD2 deubiquitination (Cheung et al., 2017). To examine whether FANCI deubiquitination activity by USP1:UAF1 is regulated by the 3SQ cluster, we performed *in vitro* deubiquitination reactions where xFANCI^{Ub}:xFANCD2^{Ub} was treated with lambda phosphatase after ubiquitination. Most of the xFANCI^{Ub} was resistant to deubiquitination in the native state, but dephosphorylation accelerated the deubiquitination. xFANCD2^{Ub} was also significantly faster. Re-phosphorylation of the xFANCI^{Ub}:xFANCD2^{Ub} restored the slower rate of USP1:UAF1-mediated deubiquitination (**Figure 4A**). This was due to a direct effect of ATR phosphorylation on FANCI because xFANCD2 and FANCI-(AAA)^{Ub} was also deubiquitinated significantly faster than xFANCI^{Ub} or xFANCI-(ADD)^{Ub}. Overall, the rate of FANCD2 deubiquitination when bound to FANCI-ADD or WT-FANCI is fourfold slower than for FANCI-AAA (**Figures 4B,C**).

Taken together, our results suggest that ATR-mediated FANCI phosphorylation both promotes monoubiquitination and inhibits deubiquitination of FANCD2.

DISCUSSION

In humans, ATR kinase strongly influences the activation of the Fanconi Anemia DNA repair pathway (Andreassen et al., 2004). In particular, FANCI phosphorylation by ATR kinase was proposed to be an "on switch" for FANCD2 monoubiquitination (Ishiai et al., 2008; Cheung et al., 2017). The present work uncovers additional evidence that it is the direct phosphorylation of FANCI by ATR that influences the biochemical rate of FANCD2 ubiquitination *and* deubiquitination to reveal fundamental insights into how FANCD2-monoubiquitination is maintained at sites of DNA damage.

We found that three sites on the surface of FANCI, serines 557, 560 and 565, are the main targets of recombinant ATR kinase *in vitro*. Phosphomimic mutations at these sites, create a charge effect similar to true phosphorylation, and stimulated the *in vitro* monoubiquitination of FANCD2. However, we did not see this effect when we used a mutant called S6D. We propose that the additional three serines (S597, S618, and S630) mutated in this variant may cause structural malformation of FANCI, given their location within α-helices of the solenoid structure of the protein. As such, FANCI-S6D only binds weakly to FANCD2 and does not stimulate its mono-ubiquitination. This finding supports the *in vivo* cell-based studies of Cheung et al. (2017) where only these three phospho-serines were identified in mass-spectrometry based analysis, but does not support the concept of FANCI dissociation from FANCD2 after phosphorylation or monoubiquitination (Sareen et al., 2012). The actions of ATR kinase on the FANCI:FANCD2 complex are therefore likely to be restricted to these sites associated with DNA damage response.

We previously showed that DNA-PKcs, a kinase related to ATR, could phosphorylate FANCI but could not stimulate FANCD2 monoubiquitination (van Twest et al., 2017). This indicates that DNA-PKcs is a poor substitute for ATR, or that it cannot catalyze the correct combination of FANCI phosphorylation events necessary for activation. However, it's possible that other kinases could further modulate the temporal and/or spatial localization of FANCD2 and FANCI monoubiquitination *in vitro* or in cells. For example, Casein Kinase 2 phosphorylation of FANCD2 at a cluster of serines between residues 882–898 inhibits its DNA association and subsequent monoubiquitination (Lopez-Martinez et al., 2019), while ATM phosphorylates many residues in FANCD2 independent of monoubiquitination, but only during S-phase and after ionizing radiation (Taniguchi et al., 2002b; Ho et al., 2006). Other kinases with an important role in DNA replication and DNA damage response have yet to be explored, although several such as Chk1 and CDK also phosphorylate subunits in the FA core complex (Deans et al., 2006; Wang et al., 2007). Kinases may also regulate enigmatic dimerization and monoubiquitination-independent functions of FANCI and FANCD2, that appear to be necessary only after certain types DNA damage (Sareen et al., 2012; Chaudhury et al., 2013; Chen et al., 2016). A thorough biochemical investigation of the complex interplay of known and unknown kinases in the FA pathway is likely to be fruitful.

Deubiquitination of FANCD2 and FANCI appears to be as important as ubiquitination, in the regulation of the Fanconi Anemia pathway. There are at least two reasons for this: (1) it prevents the retention of FANCD2 at spurious, non-repair sites in the nucleus and (2) it allows completion of DNA repair (Cohn et al., 2009; Tan and Deans, 2017). A major function

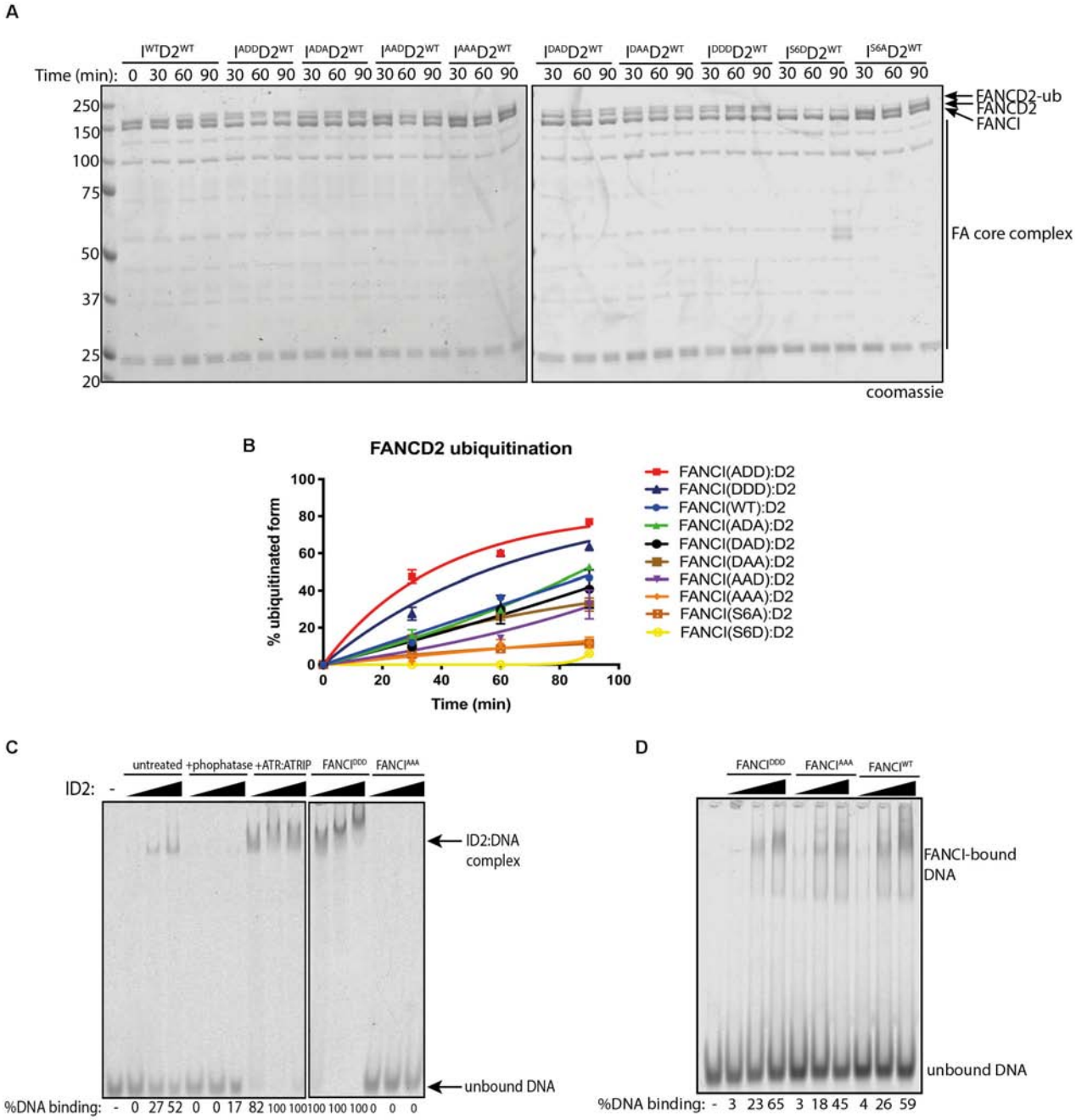

FIGURE 3 | FANCI phosphorylation in the S3Q cluster regulates FANCD2 ubiquitination by increasing its retention on DNA. **(A)** *In vitro* ubiquitination assays of various FANCI-phosphomutant:FANCD2 complexes showing that phosphomimic mutants present higher ubiquitination rate than phosphodead mutant. **(B)** Quantification showing the percentage of FANCD2 monoubiquitination using various FANCI phosphomutants. Data are representative of three experiments. **(C)** Electro mobility shift assay (EMSA) gels showing 100. 200 and 400 nM of untreated, phosphatase or ATR: ATRIP treated ID2 (WT. DDD or AAA) complexes and **(D)** isolated FANCI (WT. DDD or AAA) proteins in the presence of 25 nM IRDye-700 dsDNA. The percentage of protein binding to DNA was calculated and shown under native PAGE gels. Data are representative of three experiments.

of $FANCI^{Ub}$ appears to be the prevention of $FANCD2^{Ub}$ deubiquitination, but only while it is DNA associated. Our data show that a phosphomimic mutant of FANCI is further protective to $FANCD2^{Ub}$ deubiquitination. Supporting our results, Cheung et al. (2017) showed that FANCI phosphomimic mutant at serine 560 and 566 prevents deubiquitination of FANCD2 *in vivo* (Cheung et al., 2017). Together, these results suggest that FANCI dephosphorylation might be required for efficient FANCI:FANCD2 deubiquitination. Additional studies will be required to understand the dephosphorylation of FANCI

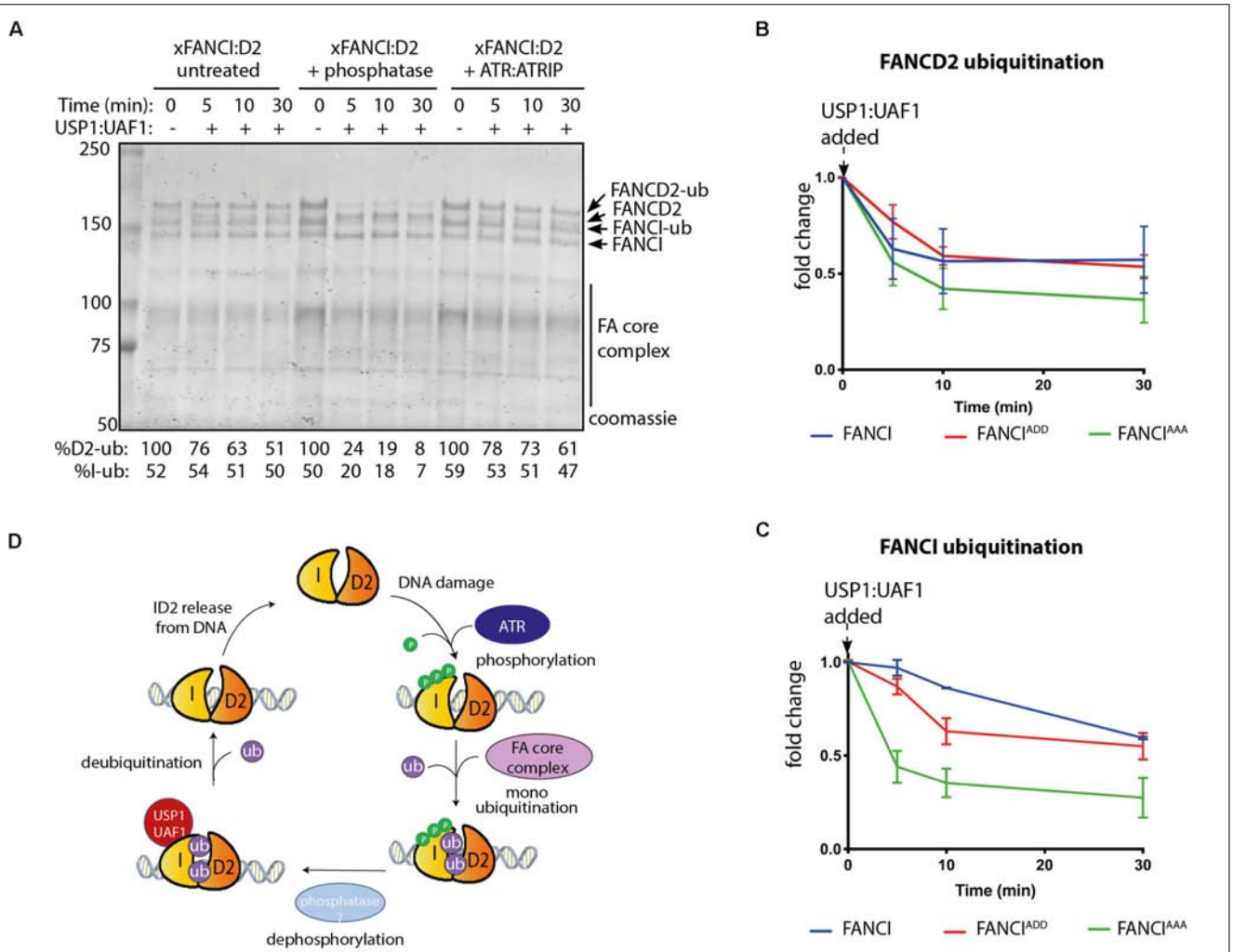

FIGURE 4 | FANCI dephosphorylation as a switch to turn off FANCLFANCD2 deubiquitination. **(A)** Coomassie stained SDS-PAGE showing the deubiquitination time course of untreated, phosphatase and ATR-ATRIP treated *Xenopus* FANCLFANCD2 complexes. **(B)** Graphical representation of FANCD2 or **(C)** FANCI ubiquitination fold change after USP1:UAF1 is added within the FANCI^{WT}:FANCD2, FANCI^{ADD}:FANCD2 and FANCI^{AAA}:FANCD2 complexes (representative experiment of $n = 3$). **(D)** Model of the role of FANCI phosphorylation in regulating FANCL:FANCD2 monoubiquitination and deubiquitination.

and whether it alters FANCD2 ubiquitination in cells. CTDP1 and PTEN are phosphatases known to act in the FA pathway, although neither have been demonstrated to act directly on FANCI (Vuono et al., 2016; Hu et al., 2019). Our *in vitro* reconstitution system will be useful for answering mechanistic questions regarding FANCI dephosphorylation and for identifying potential phosphatases that regulate the FA pathway.

FANCD2 monoubiquitination by FA core complex and deubiquitination by USP1:UAF occurs at steady state levels associated with ongoing replication (Taniguchi et al., 2002a; Liang et al., 2016). We propose that upon replication fork stalling, ATR kinase is activated, with locally high concentrations of active ATR promoted by the activity of FANCM:FAAP24:hCLK2 complex (Collis et al., 2008). ATR phosphorylates the FANCI-3SQ cluster. From structural models, phosphorylation of these residues are predicted to increase the surface area of interaction between FANCD2 and FANCI by at least twenty-five percent (Joo et al., 2011), which likely explains the increased affinity of the complex on DNA. This would stabilize the complex at damage sites, leading to its increased monoubiquitination by the FA core complex, which is also localized by FANCM (Deans and West, 2009). We also predict that a conformational change induced by phosphorylation of the S3Q cluster alters the association of the adjacent SLIM domain of FANCI with USP1:UAF1, as a mechanism for the observed reduction in USP1:UAF1 binding in S3Q phosphomimic proteins. Therefore, deubiquitination is prevented until repair is completed and the ATR kinase is deactivated (**Figure 4D**).

Given the critical importance of FANCI as an ATR target, the phosphorylation state of the FANCI-3SQ cluster may be an appropriate biomarker of the effectiveness of several classes of ATR kinase inhibitor currently in clinical trial for the treatment of cancer (Lecona and Fernandez-Capetillo, 2018). Our work also suggests that direct modulation of FANCI phosphorylation

plays a twofold role in stabilizing FANCD2 monoubiquitination, with relevance to understanding and treating both Fanconi anemia and cancer.

DATA AVAILABILITY STATEMENT

The datasets generated for this study are available on request to the corresponding author.

AUTHOR CONTRIBUTIONS

WT performed protein purification, biolayer inferometry, ubiquitination, deubiquitination, and DNA binding assays. ST performed deubiquitination assays. VM generated FANCI phosphomutants and assisted with protein purifications. WT and AD wrote the manuscript and designed experiments for this article.

FUNDING

This work was supported by grants from the Fanconi Anemia Research Fund, the National Health and Medical Research Council (GNT1123100 and GNT1181110 to AD), and the Victoria government IOS program. WT was supported by an Australian Government Research Training Scheme postgraduate scholarship. AD was a Victorian Cancer Agency mid-career fellow.

ACKNOWLEDGMENTS

We would like to thank Dr. Alexandra Sobeck (University of Minnesota) for providing xFANCI WT, monoubiquitination-dead (KR), phosphomimic (S6A) and phosphodead (S6D) mutant constructs. We thank Robert Cheung for antibodies against FANCI serine 556, 559, and 565. We thank Genome Stability lab members for thoughtful contributions.

SUPPLEMENTARY MATERIAL

The Supplementary Material for this article can be found online at: https://www.frontiersin.org/articles/10.3389/fcell.2020.00002/full#supplementary-material

REFERENCES

Andreassen, P. R., D'Andrea, A. D., and Taniguchi, T. (2004). ATR couples FANCD2 monoubiquitination to the DNA-damage response. *Genes Dev.* 18, 1958–1963. doi: 10.1101/gad.1196104

Berger, I., Fitzgerald, D. J., and Richmond, T. J. (2004). Baculovirus expression system for heterologous multiprotein complexes. *Nat. Biotechnol.* 22, 1583–1587. doi: 10.1038/nbt1036

Castella, M., Jacquemont, C., Thompson, E. L., Yeo, J. E., Cheung, R. S., Huang, J.-W., et al. (2015). FANCI regulates recruitment of the FA core complex at sites of DNA damage independently of FANCD2. *PLoS Genet.* 11:e1005563. doi: 10.1371/journal.pgen.1005563

Chaudhury, I., Sareen, A., Raghunandan, M., and Sobeck, A. (2013). FANCD2 regulates BLM complex functions independently of FANCI to promote replication fork recovery. *Nucleic Acids Res.* 41, 6444–6459. doi: 10.1093/nar/gkt348

Chen, X., Bosques, L., Sung, P., and Kupfer, G. M. (2016). A novel role for non-ubiquitinated FANCD2 in response to hydroxyurea-induced DNA damage. *Oncogene* 35, 22–34. doi: 10.1038/onc.2015.68

Chen, Y.-H., Jones, M. J. K., Yin, Y., Crist, S. B., Colnaghi, L., Sims, R. J., et al. (2015). ATR-mediated phosphorylation of FANCI regulates dormant origin firing in response to replication stress. *Mol. Cell* 58, 323–338. doi: 10.1016/j.molcel.2015.02.031

Cheung, R. S., Castella, M., Abeyta, A., Gafken, P. R., Tucker, N., and Taniguchi, T. (2017). Ubiquitination-linked phosphorylation of the FANCI S/TQ cluster contributes to activation of the fanconi anemia I/D2 complex. *Cell Rep.* 19, 2432–2440. doi: 10.1016/j.celrep.2017.05.081

Cohn, M. A., Kee, Y., Haas, W., Gygi, S. P., and D'Andrea, A. D. (2009). UAF1 is a subunit of multiple deubiquitinating enzyme complexes. *J. Biol. Chem.* 284, 5343–5351. doi: 10.1074/jbc.M808430200

Collis, S. J., Ciccia, A., Deans, A. J., Horejsí, Z., Martin, J. S., Maslen, S. L., et al. (2008). FANCM and FAAP24 function in ATR-mediated checkpoint signaling independently of the Fanconi anemia core complex. *Mol. Cell.* 32, 313–324. doi: 10.1016/j.molcel.2008.10.014

Deans, A. J., Khanna, K. K., McNees, C. J., Mercurio, C., Heierhorst, J., and McArthur, G. A. (2006). Cyclin-dependent kinase 2 functions in normal DNA repair and is a therapeutic target in BRCA1-deficient cancers. *Cancer Res.* 66, 8219–8226. doi: 10.1158/0008-5472.CAN-05-3945

Deans, A. J., and West, S. C. (2009). FANCM connects the genome instability disorders Bloom's syndrome and Fanconi anemia. *Mol. Cell.* 36, 943–953. doi: 10.1016/j.molcel.2009.12.006

Deans, A. J., and West, S. C. (2011). DNA interstrand crosslink repair and cancer. *Nat. Rev. Cancer* 11, 467–480. doi: 10.1038/nrc3088

Garaycoechea, J. I., and Patel, K. J. (2014). Why does the bone marrow fail in Fanconi anemia? *Blood* 123, 26–34. doi: 10.1182/blood-2013-09-427740

Ho, G. P., Margossian, S., Taniguchi, T., and D'Andrea, A. D. (2006). Phosphorylation of FANCD2 on two novel sites is required for mitomycin C resistance. *Mol. Cell Biol.* 26, 7005–7015. doi: 10.1128/mcb.02018-2015

Hodson, C., Purkiss, A., Miles, J. A., and Walden, H. (2014). Structure of the human FANCL RING-Ube2T complex reveals determinants of cognate E3-E2 selection. *Structure* 22, 337–344. doi: 10.1016/j.str.2013.12.004

Hu, W. F., Krieger, K. L., Lagundzin, D., Li, X., Cheung, R. S., Taniguchi, T., et al. (2019). CTDP1 regulates breast cancer survival and DNA repair through BRCT-specific interactions with FANCI. *Cell Death Discov.* 5:105. doi: 10.1038/s41420-019-0185-183

Ishiai, M., Kitao, H., Smogorzewska, A., Tomida, J., Kinomura, A., Uchida, E., et al. (2008). FANCI phosphorylation functions as a molecular switch to turn on the Fanconi anemia pathway. *Nat. Struct. Mol. Biol.* 15, 1138–1146. doi: 10.1038/nsmb.1504

Ishiai, M., Sato, K., Tomida, J., Kitao, H., Kurumizaka, H., and Takata, M. (2017). Activation of the FA pathway mediated by phosphorylation and ubiquitination. *Mutat. Res.* 80, 89–95. doi: 10.1016/j.mrfmmm.2017.05.003

Joo, W., Xu, G., Persky, N. S., Smogorzewska, A., Rudge, D. G., Buzovetsky, O., et al. (2011). Structure of the FANCI-FANCD2 complex: insights into the Fanconi anemia DNA repair pathway. *Science* 333, 312–316. doi: 10.1126/science.1205805

Klein Douwel, D., Boonen Rick, A. C. M., Long, David, T., Szypowska, Anna, A., et al. (2014). XPF-ERCC1 Acts in unhooking DNA interstrand crosslinks in cooperation with FANCD2 and FANCP/SLX4. *Mol. Cell* 54, 460–471. doi: 10.1016/j.molcel.2014.03.015

Knipscheer, P., Räschle, M., Smogorzewska, A., Enoiu, M., Ho, T. V., Schärer, O. D., et al. (2009). The Fanconi anemia pathway promotes replication-dependent DNA interstrand crosslink repair. *Science* 326, 1698–1701. doi: 10.1126/science.1182372

Lecona, E., and Fernandez-Capetillo, O. (2018). Targeting ATR in cancer. *Nat. Rev. Cancer* 18, 586–595. doi: 10.1038/s41568-018-0034-33

Liang, C. C., Li, Z., Lopez-Martinez, D., Nicholson, W. V., Venien-Bryan, C., and Cohn, M. A. (2016). The FANCD2-FANCI complex is recruited to DNA interstrand crosslinks before monoubiquitination of FANCD2. *Nat. Commun.* 7:12124. doi: 10.1038/ncomms12124

Longerich, S., Kwon, Y., Tsai, M. S., Hlaing, A. S., Kupfer, G. M., and Sung, P. (2014). Regulation of FANCD2 and FANCI monoubiquitination by their interaction and by DNA. *Nucleic Acids Res.* 42, 5657–5670. doi: 10.1093/nar/gku198

Longerich, S., San Filippo, J., Liu, D., and Sung, P. (2009). Fanci binds branched DNA and is mono-ubiquitinated by UBE2T-FANCL. *J. Biol. Chem.* 284, 23182–23186. doi: 10.1074/jbc.C109.038075

Lopez-Martinez, D., Kupculak, M., Yang, D., Yoshikawa, Y., Liang, C.-C., Wu, R., et al. (2019). Phosphorylation of FANCD2 inhibits the FANCD2/FANCI complex and suppresses the Fanconi anemia pathway in the absence of DNA damage. *Cell Rep.* 27, 2990.e5–3005.e5. doi: 10.1016/j.celrep.2019.05.003

Sareen, A., Chaudhury, I., Adams, N., and Sobeck, A. (2012). Fanconi anemia proteins FANCD2 and FANCI exhibit different DNA damage responses during S-phase. *Nucleic Acids Res.* 40, 8425–8439. doi: 10.1093/nar/gks638

Sato, K., Toda, K., Ishiai, M., Takata, M., and Kurumizaka, H. (2012). DNA robustly stimulates FANCD2 monoubiquitylation in the complex with FANCI. *Nucleic Acids Res.* 40, 4553–4561. doi: 10.1093/nar/gks053

Shigechi, T., Tomida, J., Sato, K., Kobayashi, M., Eykelenboom, J. K., Pessina, F., et al. (2012). ATR–ATRIP kinase complex triggers activation of the Fanconi anemia DNA repair pathway. *Cancer Res.* 72, 1149–1156. doi: 10.1158/0008-5472.can-11-2904

Smogorzewska, A., Desetty, R., Saito, T. T., Schlabach, M., Lach, F. P., Sowa, M. E., et al. (2010). A genetic screen identifies FAN1, a Fanconi anemia-associated nuclease necessary for DNA interstrand crosslink repair. *Mol. Cell* 39, 36–47. doi: 10.1016/j.molcel.2010.06.023

Smogorzewska, A., Matsuoka, S., Vinciguerra, P., McDonald, E. R., Hurov, K. E., Luo, J., et al. (2007). Identification of the FANCI Protein, a monoubiquitinated FANCD2 paralog required for DNA repair. *Cell* 129, 289–301. doi: 10.1016/j.cell.2007.03.009

Swuec, P., Renault, L., Borg, A., Shah, F., Murphy, V. J., van Twest, S., et al. (2017). The FA core complex contains a homo-dimeric catalytic module for the symmetric mono-ubiquitination of FANCI-FANCD2. *Cell Rep.* 18, 611–623. doi: 10.1016/j.celrep.2016.11.013

Tan, W., and Deans, A. J. (2017). A defined role for multiple Fanconi anemia gene products in DNA-damage-associated ubiquitination. *Exp. Hematol.* 50, 27–32. doi: 10.1016/j.exphem.2017.03.001

Tan, W., Murphy, V. J., Charron, A., van Twest, S., Sharp, M., Bythell-Douglas, R., et al. (2020). Preparation and purification of mono-ubiquitinated proteins using Avi-tagged ubiquitin. *PLoS One* (in press).

Taniguchi, T., Garcia-Higuera, I., Andreassen, P. R., Gregory, R. C., Grompe, M., and D'Andrea, A. D. (2002a). S-phase-specific interaction of the Fanconi anemia protein, FANCD2, with BRCA1 and RAD51. *Blood* 100, 2414–2420. doi: 10.1182/blood-2002-01-0278

Taniguchi, T., Garcia-Higuera, I., Xu, B., Andreassen, P. R., Gregory, R. C., Kim, S. T., et al. (2002b). Convergence of the Fanconi anemia and ataxia telangiectasia signaling pathways. *Cell* 109, 459–472. doi: 10.1016/s0092-8674(02)00747-x

Tsui, V., and Crismani, W. (2019). The fanconi anemia pathway and fertility. *Trends Genet.* 35, 199–214. doi: 10.1016/j.tig.2018.12.007

van Twest, S., Murphy, V. J., Hodson, C., Tan, W., Swuec, P., O'Rourke, J. J., et al. (2017). Mechanism of ubiquitination and deubiquitination in the Fanconi anemia pathway. *Mol. Cell* 65, 247–259. doi: 10.1016/j.molcel.2016.11.005

Vuono, E. A., Mukherjee, A., Vierra, D. A., Adroved, M. M., Hodson, C., Deans, A. J., et al. (2016). The PTEN phosphatase functions cooperatively with the Fanconi anemia proteins in DNA crosslink repair. *Sci. Rep.* 6:36439. doi: 10.1038/srep36439

Wang, X., Kennedy, R. D., Ray, K., Stuckert, P., Ellenberger, T., and D'Andrea, A. D. (2007). Chk1-mediated phosphorylation of FANCE is required for the Fanconi anemia/BRCA pathway. *Mol. Cell Biol.* 27, 3098–3108. doi: 10.1128/MCB.02357-2356

Conflict of Interest: The authors declare that the research was conducted in the absence of any commercial or financial relationships that could be construed as a potential conflict of interest.

frontiers in Cell and Developmental Biology

REVIEW
published: 05 February 2020
doi: 10.3389/fcell.2020.00042

Two-Faced: Roles of JNK Signalling During Tumourigenesis in the *Drosophila* Model

John E. La Marca and Helena E. Richardson*

Richardson Laboratory, Department of Biochemistry and Genetics, La Trobe Institute for Molecular Science, La Trobe University, Melbourne, VIC, Australia

The highly conserved c-Jun N-terminal Kinase (JNK) signalling pathway has many functions, regulating a diversity of processes: from cell movement during embryogenesis to the stress response of cells after environmental insults. Studies modelling cancer using the vinegar fly, *Drosophila melanogaster*, have identified both pro- and anti-tumourigenic roles for JNK signalling, depending on context. As a tumour suppressor, JNK signalling commonly is activated by conserved Tumour Necrosis Factor (TNF) signalling, which promotes the caspase-mediated death of tumourigenic cells. JNK pathway activation can also occur via actin cytoskeleton alterations, and after cellular damage inflicted by reactive oxygen species (ROS). Additionally, JNK signalling frequently acts in concert with Salvador-Warts-Hippo (SWH) signalling – either upstream of or parallel to this potent growth-suppressing pathway. As a tumour promoter, JNK signalling is co-opted by cells expressing activated Ras-MAPK signalling (among other pathways), and used to drive cell morphological changes, induce invasive behaviours, block differentiation, and enable persistent cell proliferation. Furthermore, JNK is capable of non-autonomous influences within tumour microenvironments by effecting the transcription of various cell growth- and proliferation-promoting molecules. In this review, we discuss these aspects of JNK signalling in *Drosophila* tumourigenesis models, and highlight recent publications that have expanded our knowledge of this important and versatile pathway.

Keywords: JNK, *Drosophila*, tumourigenesis, *scrib*, Ras, apoptosis

OPEN ACCESS

Edited by:
Liz Caldon,
Garvan Institute of Medical Research, Australia

Reviewed by:
Jormay Lim,
National Taiwan University, Taiwan
Rajprasad Loganathan,
Johns Hopkins University, United States

****Correspondence:***
John E. La Marca
e.lamarca@latrobe.edu.au

Specialty section:
This article was submitted to Cell Growth and Division, a section of the journal Frontiers in Cell and Developmental Biology

Received: *12 November 2019*
Accepted: *17 January 2020*
Published: *05 February 2020*

Citation:
La Marca JE and Richardson HE (2020) Two-Faced: Roles of JNK Signalling During Tumourigenesis in the Drosophila Model. Front. Cell Dev. Biol. 8:42. doi: 10.3389/fcell.2020.00042

INTRODUCTION

Jun N-terminal kinase signalling is a conserved Mitogen-Activated Protein Kinase (MAPK, N.B. for a glossary of abbreviated terms refer to **Supplementary Table 1**) signalling pathway which, through a conserved kinase cascade, acts to influence gene transcription, and hence the cellular response to various stimuli. In *Drosophila*, the sole JNK is Basket (Bsk; orthologue of human JNK1, JNK2, and JNK3, also known as MAPK8, MAPK9, and MAPK10, respectively), which acts to phosphorylate and activate a number of transcription factors (TFs). The best known JNK-activated TFs are Jun-related antigen (Jra) and Kayak (Kay; whose closest human orthologues are JUN (Jun proto-oncogene, AP-1 TF subunit) and FOS (Fos proto-oncogene, AP-1 TF subunit), respectively) (**Figure 1**), which together make up the heterodimeric Activator Protein-1 (AP-1) complex. While other Bsk targets also exist, upstream of Bsk the signalling network is much more complex. In order to activate JNK/Bsk there are at least two JNK kinases (JNKKs) – Hemipterous (Hep) and MAP kinase kinase 4 (Mkk4; orthologues of human MAP2K7 and MAP2K4, respectively) – and at least four JNKK kinases (JNKKKs) – Slipper (Slpr, human orthologues MAP3K9, MAP3K10,

MAP3K11, and MAP3K21), Wallenda (Wnd, human orthologues MAP3K13 and MAP3K12), TGFβ-associated kinase 1 (Tak1, human orthologue MAP3K7), and Apoptotic signal-regulating kinase 1 (Ask1, human orthologues MAP3K15 and MAP3K5) (**Figure 1**). These kinases follow an ever-growing multitude of signalling pathways, molecules, and stimuli that feed into the activation of JNK. Despite this complexity, the kinase core of Hep-Bsk is generally considered to be the canonical and main effector of JNK signalling.

Originally identified in the Heidelberg genetic screens as a mutant that had improper dorsal closure during embryogenesis (Nüsslein-Volhard et al., 1984), it was not until a decade later that *bsk* was determined to be the orthologue of the mammalian JNK genes (Riesgo-Escovar et al., 1996; Sluss et al., 1996), a discovery that followed closely on the heels of the identification of *hep* as a JNKK (Glise et al., 1995). Since then, astonishingly large bodies of work have identified JNK signalling as being critical in a multitude of biological processes, such as regulating cell morphology and migration behaviours (via inducing the expression of genes like the actin cross-linker *cheerio* (*cher*) (Pastor-Pareja et al., 2004; Külshammer and Uhlirova, 2013), or by upregulating targets like the integrin-associated scaffolding protein Paxillin (Huang et al., 2003; Llense and Martín-Blanco, 2008; Leong et al., 2009)), regulating organ size (Willsey et al., 2016), and promoting cell death by upregulating genes like *head involution defective* (*hid*) and *reaper* (*rpr*) (Moreno et al., 2002; Luo et al., 2007).

With such diverse functionality, it is perhaps no surprise that JNK signalling has also emerged as a key player in tumourigenesis in *Drosophila*, something it shares with its mammalian orthologue (reviewed in Wagner and Nebreda, 2009; Wu et al., 2019). Almost all human orthologues of the core JNK signalling hierarchy have been implicated in multiple cancers, though their roles are often not well understood, and are often context dependent. We have summarised some of the recent literature concerning the links between JNK signalling and human cancer in our **Supplementary Material** (**Supplementary Table 2**). The role of JNK in tumourigenesis in flies is relatively better understood, but still exceedingly complex, with the pathway fulfilling different, seemingly opposing roles depending on the context. Simply put, JNK signalling is capable of both eliminating pre-tumourigenic cells via apoptosis, but also can cooperate with various genetic insults to promote tumourigenesis. In this review, we will examine these pro- and anti-tumourigenic roles of JNK signalling, non-autonomous roles of the pathway during tumourigenesis, and the various activation modes of the pathway in these contexts.

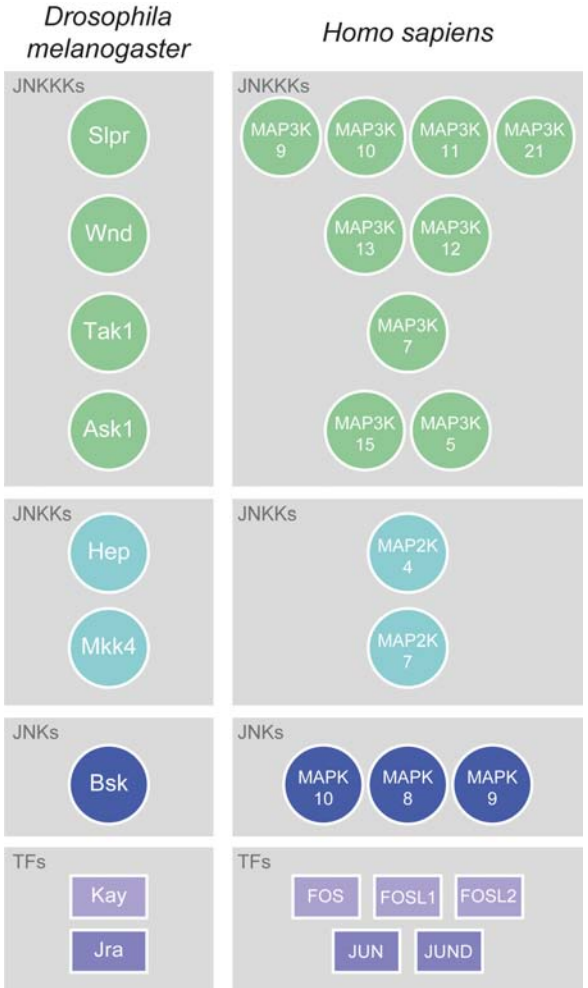

FIGURE 1 | Conservation of JNK signalling core. The kinase core of JNK signalling is well-conserved between flies and mammals. In *Drosophila*, there are at least four JNKKKs: Slpr (Slipper), Wnd (Wallenda), Tak1 (TGFβ-associated kinase 1), and Ask1 (Apoptotic signal-regulating kinase 1). All have multiple human orthologues, which are Mitogen-activated protein kinase kinase kinases (MAP3Ks), with the most highly conserved being shown here. Slpr is most closely related to MAP3K9, MAP3K10, MAP3K11, and MAP3K21, Wnd to MAP3K13 and MAP3K12, Tak1 to MAP3K7, and Ask1 to MAP3K15 and MAP3K5. The *Drosophila* JNKKs are Hep (Hemipterous) and Mkk4 (MAP kinase kinase 4), which have human orthologues amongst the Mitogen-activated protein kinase kinases (MAP2Ks). Hep is most closely related to MAP2K4, and Mkk4 to MAP2K7. While *Drosophila* has only one JNK, Basket (Bsk), there are three conserved Mitogen-activated protein kinase (MAPK) orthologues to Bsk in humans: MAPK10, MAPK8, and MAPK9. JNKs upregulate the activity of various TFs, the best known of which are those that form the heterodimeric AP-1 complex. In *Drosophila*, those TFs are Kay (Kayak) and Jra (Jun-related antigen). In humans, the orthologues of Kay are FOS (Fos proto-oncogene, AP-1 transcription factor subunit), FOSL1 (FOS like 1, AP-1 transcription factor subunit), and FOSL2 (FOS like 2, AP-1 transcription factor subunit), while the orthologues of Jra are JUN (Jun proto-oncogene, AP-1 transcription factor subunit) and JUND (JunD proto-oncogene, AP-1 transcription factor subunit).

ANTI-TUMOURIGENIC JNK SIGNALLING

The anti-tumourigenic effect of JNK signalling ultimately induces cell death due to the upregulation of apoptosis-inducing genes like *hid* and *rpr*, and the activation of caspases (Moreno et al., 2002; Luo et al., 2007; Shlevkov and Morata, 2012; Li et al., 2019). One scenario where this role is well documented is upon the clonal disruption of cell polarity. Cell polarity is the asymmetric distribution of proteins within a cell, and the disruption of polarity is considered one of the hallmarks of cancer (Hanahan and Weinberg, 2011).

In *Drosophila*, apico-basal polarity is critical to the proper formation of larval epithelial tissues, such as the wing and eye-antennal imaginal discs, and is controlled predominantly by the mutually antagonistic behaviours of three polarity protein modules: Scribble/Discs large 1/Lethal (2) giant larvae (Scrib/Dlg1/L(2)gl), Crumbs/Stardust/Patj (Crb/Sdt/Patj), and Bazooka/Par-6/atypical protein kinase C (Baz/Par-6/aPKC) (reviewed in Tepass, 2012). The largest body of work has examined Scrib/Dlg1/L(2)gl, where animals wholly mutant for any of these components produce neoplastic tumours, in which tissues overproliferate and show aberrant differentiation alongside a disorganised morphology – *scrib*, *dlg1*, and *l(2)gl* are therefore referred to as neoplastic tumour suppressor genes (nTSGs) (Bilder, 2004). However, while these wholly mutant tissues overgrow, clonal patches of epithelial tissue mutant for these genes are eliminated via a process termed cell competition. Cell competition is a surveillance mechanism that leads to the active elimination of cells that are "less fit" by their "more fit" neighbouring cells (reviewed in Fahey-Lozano et al., 2019; Ohsawa, 2019). Clones mutant for *scrib* ($scrib^{-/-}$) are eliminated by apoptosis in *Drosophila* imaginal tissues, and this process is dependent on JNK signalling activity, as blocking JNK enables the cells to survive (**Figure 2**; Brumby and Richardson, 2003). These polarity mutant clones are therefore thought of as pre-tumourigenic, since if they are not removed tumours will develop. Furthermore, while $scrib^{-/-}$ cells have enhanced proliferative capacity via JNK-independent upregulation of the cell cycle regulator, *Cyclin E* (*CycE*) (Brumby and Richardson, 2003; Leong et al., 2009), JNK signalling promotes their apoptosis, and the balance between these opposing phenotypes can be pushed in either direction by enhancing or disrupting JNK (Uhlirova and Bohmann, 2006).

Jun N-terminal kinase signalling was found to be primarily upregulated in cells at the borders of $scrib^{-/-}$ clones and *wildtype* tissue, suggesting that its upregulation was not a direct consequence of *scrib* mutation (Leong et al., 2009). What, then, was the source? It was determined that JNK signalling, and the elimination of *scrib* or *dlg1* mutant clones, was dependent on activation of the pathway by TNF signalling – the *Drosophila* TNF, Eiger (Egr), binds to the TNF Receptors (TNFRs) Wengen (Wgn) and/or Grindelwald (Grnd), and eventually triggers activation of the kinase core of the JNK signalling pathway (**Figure 2**; Igaki et al., 2009; Andersen et al., 2015). Mislocalisation of Egr to endosomes within the $scrib^{-/-}$ cells, rather than its upregulation, was determined to be the cause of the ectopic JNK signalling, with endocytosis increased in the clones – though, notably, endocytosis was only increased when *wildtype* tissue was adjacent to the $scrib^{-/-}$ cells (Igaki et al., 2009). Although Egr was detectable in all the epithelial cells in the $scrib^{-/-}$ mosaic tissue, genetic analyses showed that it acts in an autocrine manner within the $scrib^{-/-}$ cells (Igaki et al., 2009), but this is unlikely to be the whole story – Egr was later shown to also be produced by haemocytes, circulating macrophage-like cells within the *Drosophila* haemolymph, and that its presence in these cells was sufficient for the activation of JNK in $scrib^{-/-}$ cells (**Figure 2**; Vidal, 2010). While not investigated in $scrib^{-/-}$ cells specifically, haemocyte attraction was shown to depend on JNK-mediated secretion of a cleaved form of the protein Tyrosyl-tRNA synthetase (Casas-Tintó et al., 2015). Additionally, *egr* is necessary for the elimination of *dlg1*-knockdown cells in wing imaginal discs, and for apoptosis within wholly *scrib* (or *dlg1*) mutant animals (Cordero et al., 2010). Regardless of the source of Egr, JNK signalling has a key role in eliminating $scrib^{-/-}$ cells during cell competition by promoting apoptosis – however, blocking apoptosis in these $scrib^{-/-}$ clones is not, in fact, as effective at preventing their elimination (and thus promoting tumourigenesis) as simply blocking JNK signalling, suggesting other removal mechanisms are at play (Brumby and Richardson, 2003). To wit, JNK signalling has been demonstrated to upregulate the genes *slit*, *roundabout 2* (*robo2*), and *enabled* (*ena*), which together act to promote $scrib^{-/-}$ cell extrusion from the tissue – Sli-Robo2-Ena signalling disrupts Shotgun (shg, a.k.a. E-cadherin), and also forms a positive feedback loop with JNK signalling by promoting F-actin accumulation (**Figure 2**; Vaughen and Igaki, 2016).

Jun N-terminal kinase signalling is not exclusively active within polarity-impaired cells during cell competition. The pathway has also been shown to be active within their *wildtype* neighbours – Egr-dependent JNK activation in the *wildtype* cells promotes signalling via PDGF- and VEGF-receptor related (Pvr), which in turn activates Ced-12 and Myoblast city (Mbc) to promote engulfment and removal of the mutant cells by their healthy neighbours (**Figure 2**; Ohsawa et al., 2011). Furthermore, mechanisms have been identified that are involved in the recognition of polarity-impaired cells. Protein tyrosine phosphatase 10D (Ptp10D) is expressed on the surface of $scrib^{-/-}$ cells, and is bound and activated by the ligand Stranded at second (Sas) expressed on the surface of their *wildtype* neighbours (Yamamoto et al., 2017). Activated Ptp10D suppresses epidermal growth factor receptor (Egfr) activity, allowing JNK signalling to act in its anti-tumourigenic capacity (Yamamoto et al., 2017). If Egfr activity were permitted due to *sas* or *Ptp10D* downregulation, activated Ras-MAPK signalling would occur alongside JNK signalling, the consequences of which we will discuss in a later section ("Pro-tumourigenic JNK signalling").

Interestingly, *l(2)gl* mutant ($l(2)gl^{-/-}$) clones and tissues behave somewhat differently to $scrib^{-/-}$ cells, though they also upregulate JNK signalling, and are eliminated by JNK-dependent apoptosis (Froldi et al., 2010; Grzeschik et al., 2010; Menéndez et al., 2010; Tamori et al., 2010). Autocrine Egr is dispensable in $l(2)gl^{-/-}$ clones, as they still upregulate JNK signalling even when *egr* is knocked down in these cells; however, it is thought that $l(2)gl^{-/-}$ tissue growth and survival is more dependent on levels of the oncogenic TF Myc than on JNK signalling (Froldi et al., 2010).

As mentioned, $scrib^{-/-}$ clones exhibit ectopic proliferation, but their potential to overgrow is modulated by JNK signalling-induced apoptosis. Inhibiting JNK allows these clones to overgrow, but where does this capability come from? One important growth regulating pathway is the SWH signalling pathway, which is a conserved inhibitor of tissue growth, which functions by phosphorylating and thus cytoplasmically sequestering the TF coactivator, Yorkie (Yki). This prevents Yki from interacting with and activating the TF Scalloped

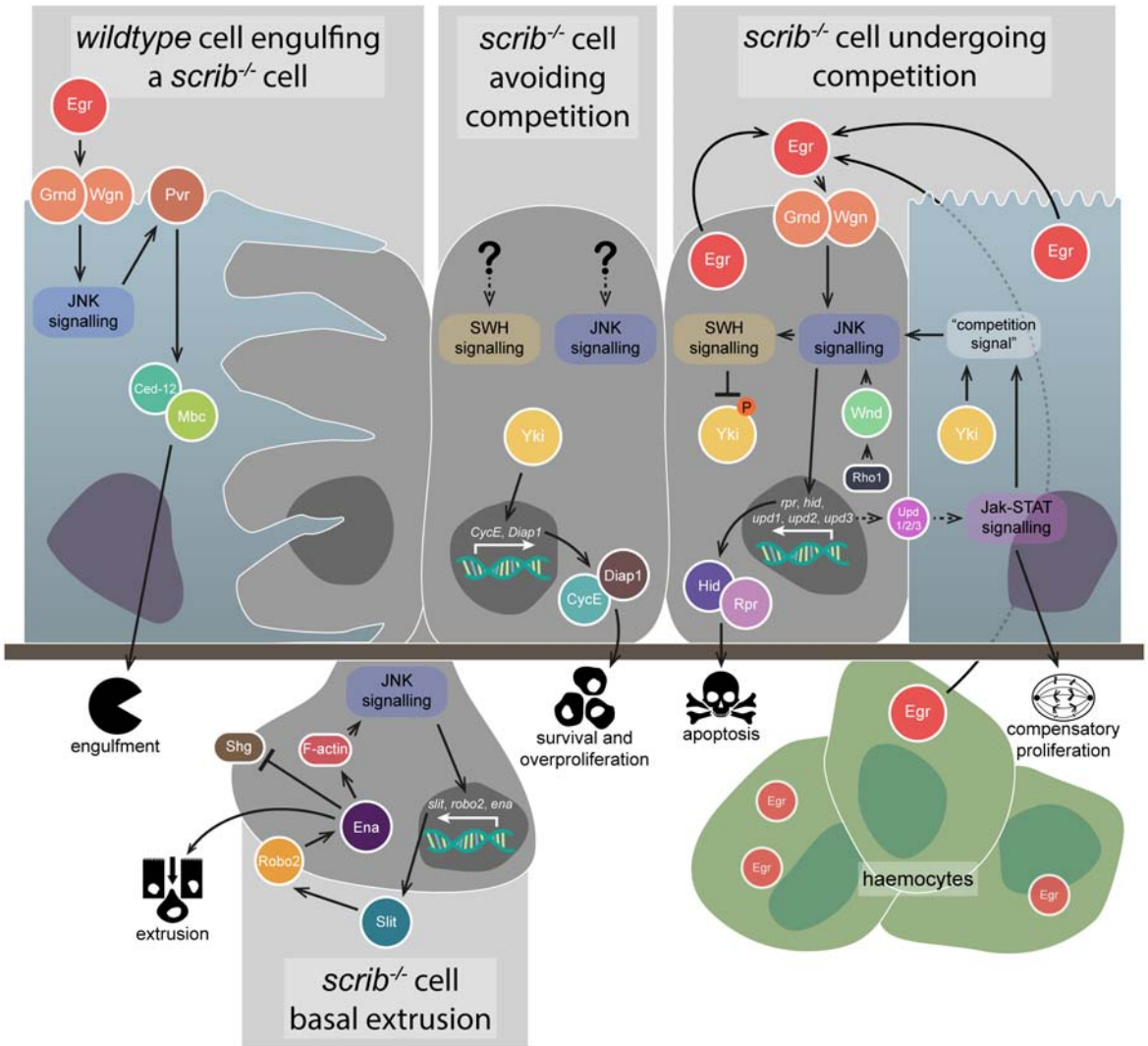

FIGURE 2 | Anti-tumourigenic JNK signalling. JNK signalling has several different anti-tumourigenic roles, which are best understood in the context of *scrib*$^{-/-}$ clone elimination from epithelial tissues. During cell competition, *scrib*$^{-/-}$ cell elimination depends on JNK signalling (rightmost image) – the pathway is activated by both autocrine and paracrine Egr and promotes apoptosis via Hid and Rpr, as well as SWH signalling-mediated Yki downregulation. JNK signalling is also activated by Rho1 signalling through Wnd, and partly depends on an unknown "competition signal" from the *wildtype* neighbours, which itself depends on Yki and Jak-STAT signalling. Jak-STAT signalling is activated in *wildtype* neighbour cells by JNK-mediated Upd family ligand expression in the *scrib*$^{-/-}$ cells, and contributes to their compensatory proliferation. Autocrine JNK signalling also promotes *scrib*$^{-/-}$ cell extrusion from the epithelial layer (lower image) – upregulation of the Slit-Robo2-Ena pathway downregulates Shg (E-cadherin) and promotes detachment from the tissue, while also upregulating JNK via an F-actin-mediated feedback loop. The *wildtype* neighbour cells are also capable of actively eliminating the *scrib*$^{-/-}$ cells (leftmost image) – JNK signalling activated by Egr promotes engulfment behaviours by the *wildtype* cells, activated via Pvr, Ced-12, and Mbc. However, if *scrib*$^{-/-}$ cells can evade competition, JNK signalling and SWH signalling (if they occur) are not capable of downregulating Yki activity to a sufficient degree that the cells can be eliminated (central image) – instead, Yki promotes cell survival and overproliferation by upregulating targets such as CycE and Diap1. Gene and protein name abbreviations used in the diagram are as follows: Eiger (Egr), Grindelwald (Grnd), Wengen (Wgn), PDGF- and VEGF-receptor related (Pvr), Myoblast city (Mbc), Yorkie (Yki), *Cyclin E* (*CycE*), *Death-associated inhibitor of apoptosis 1* (*Diap1*), Wallenda (Wnd), *reaper* (*rpr*), *head involution defective* (*hid*), *unpaired 1* (*upd1*), *unpaired 2* (*upd2*), *unpaired 3* (*upd3*), *roundabout 2* (*robo2*), *enabled* (*ena*), Shotgun (Shg).

(Sd, a TEAD family TF) and its target genes, which include the cell cycle regulator *CycE* and the apoptosis inhibitor *Death-associated inhibitor of apoptosis 1* (*Diap1*) (reviewed in Misra and Irvine, 2018). Many reports have indicated that both the JNK and SWH signalling pathways are interwoven but elucidating exactly how they interact in polarity-impaired tumours has been difficult. Initial experiments in eye-antennal imaginal disc *scrib*$^{-/-}$ clones indicated that reporters for certain Yki target genes were highly expressed (though variable), suggesting some level of SWH inhibition may be in effect and, indeed, *scrib*$^{-/-}$ cell overproliferation was found to depend on Yki and Sd activity – however, blocking JNK signalling resulted in SWH inhibition, as revealed by the upregulation of Yki targets (Doggett et al., 2011). More light was shed on these results in a later study, which more closely examined SWH signalling in *scrib*$^{-/-}$ clones in both eye-antennal and wing imaginal discs and found that Yki

activity was specifically dependent on whether cell competition was occurring (Chen et al., 2012). Specifically, *scrib*$^{-/-}$ clones not facing cell competition (by artificially lowering the fitness of their neighbours, or in wholly *scrib*$^{-/-}$ tissue) showed elevated Yki activity and the cells overgrew, but in *scrib*$^{-/-}$ cells undergoing competition Yki activity was downregulated, and this downregulation was mediated by JNK signalling (though other mechanisms are likely to contribute) (**Figure 2**; Chen et al., 2012). Notably, Yki activation is also required in the *wildtype* neighbours for their compensatory proliferation, where it is thought to act parallel to Janus kinase-Signal Transduction and Activator of Transcription (Jak-STAT) signalling to promote the elimination of the *scrib*$^{-/-}$ cells (**Figure 2**; Chen et al., 2012; Schroeder et al., 2013).

Somewhat incongruous with these results is data from wing imaginal disc regions (not clones), where the induction of apoptosis in regions of disc tissue induced Yki activation in adjacent cells to promote compensatory proliferation (Sun and Irvine, 2011). Here, Yki activation was dependent on JNK signalling and, indeed, JNK signalling initiation was sufficient to induce Yki activity (Sun and Irvine, 2011). Interestingly, initiating neoplastic growth via the knockdown of *dlg1*/*l(2)gl* in large tissue regions also upregulated Yki activity and, in these instances, Yki upregulation was again dependent on JNK activity – possibly this is similar to the aforementioned *scrib*$^{-/-}$ clones when dodging cell competition (Sun and Irvine, 2011). JNK signalling in these contexts may mediate Yki activation via downregulation of SWH signalling at the level of the Warts (Wts) protein kinase – JNK activity phosphorylates Ajuba LIM protein (Jub), which in turn binds and inactivates Wts (Sun and Irvine, 2013).

Interactions between JNK signalling and SWH/Yki in the context of JNK acting in an anti-tumourigenic role are not limited to the context of disrupted cell polarity. Inducing cytokinesis failure in wing imaginal disc cells promotes aneuploidy, which can lead to tumourigenesis, but JNK signalling is also upregulated in these cells and acts to downregulate Diap1 and a cell cycle regulator, String (Stg, orthologue of the human CDC25 proteins), thus promoting cell death and suppressing cell proliferation (Gerlach et al., 2018). However, SWH inhibition or Yki activation can bypass this JNK-mediated tumourigenesis prevention by facilitating Diap1 and Stg upregulation (Gerlach et al., 2018).

Overall, JNK signalling, primarily in its capacity as a pro-apoptotic regulator, plays a fundamental role as an anti-tumourigenic signal. This is particularly apparent (and best studied) in the context of polarity-deficient pre-tumourigenic cells, where it acts both autonomously and non-autonomously in facilitating their elimination. Furthermore, JNK signalling has a complex relationship with the SWH signalling pathway, where its interactions vary depending on context – in polarity-impaired, pre-tumourigenic cells, activated JNK signalling suppresses Yki activity (Doggett et al., 2011; Chen et al., 2012), whereas in regenerating wing imaginal disc tissue JNK signalling suppresses SWH signalling, and hence promotes Yki activity (Sun and Irvine, 2011). This role in promoting Yki activity is a hint at the two-faced nature of JNK signalling – depending on context, it can also be pro-tumourigenic.

PRO-TUMOURIGENIC JNK SIGNALLING

Pro-tumourigenic JNK signalling in *Drosophila* was discovered during the study of cooperative tumourigenesis. Cancer is a multi-step process, and cooperative tumourigenesis is the phenomenon by which different genetic lesions in a cell, or in different cells, can cooperate to drive the initiation and progression of cancer. In *Drosophila*, cooperative tumourigenesis was discovered by one group of researchers looking at the consequences of introducing oncogenic mutations into *scrib*$^{-/-}$ clones (Brumby and Richardson, 2003), and simultaneously by another group of researchers screening for mutations that cooperate with oncogenic mutations to produce metastatic tumours (Pagliarini and Xu, 2003). Coming from opposite directions, both groups identified that expressing an activated form of *Ras oncogene at 85D* (*Ras85D* – the most commonly used activated form is often referred to as *Ras*^{V12}, but hereafter is referred to as *Ras85D*^{V12}) cooperated with mutations in cell polarity regulator genes such as *scrib* to produce overgrown and invasive tumours in eye-antennal imaginal discs (**Figure 3**; Brumby and Richardson, 2003; Pagliarini and Xu, 2003). Ras85D is a GTPase, and canonically acts via the "Ras-MAPK" signalling pathway to effect gene transcription.

These initial studies did not determine a role for JNK signalling in *Ras85D*^{V12}/*scrib*$^{-/-}$ tumours, but it was clear that JNK-mediated apoptosis must be blocked in some way (Brumby and Richardson, 2005). Surprisingly, the JNK signalling pathway was in fact strongly upregulated in *Ras85D*^{V12}/*scrib*$^{-/-}$ tumours (and was not upregulated in the benign tumours formed after expression of *Ras85D*^{V12} in isolation) (Igaki et al., 2006; Uhlirova and Bohmann, 2006). Indeed, JNK signalling was necessary (and sufficient when induced via activated Hep, but insufficient when induced via Egr overexpression) for *Ras85D*^{V12}/*scrib*$^{-/-}$ tumour invasiveness, which was further demonstrated to be due to the JNK-induced transcription of *Matrix metalloproteinase 1* (*Mmp1*) (**Figure 3**; Igaki et al., 2006; Uhlirova and Bohmann, 2006). Mmp1 is from a family of genes strongly linked to cell motility, and is necessary for basement membrane degradation and invasive behaviours by *Ras85D*^{V12}/*scrib*$^{-/-}$ tumours (Srivastava et al., 2007). Other JNK signalling targets that are thought to contribute to invasive behaviours include the actin cross-linker *cher* (Pastor-Pareja et al., 2004; Külshammer and Uhlirova, 2013) and the integrin-associated scaffolding protein Paxillin (Huang et al., 2003; Llense and Martín-Blanco, 2008; Leong et al., 2009).

It was therefore thought that JNK signalling was switched from pro-apoptotic to pro-growth/proliferation in the face of *Ras85D*^{V12}, a role that was known from experiments in undead cells – when apoptosis is triggered, but caspase activity is prevented via expression of the effector caspase inhibitor p35, cells are referred to as "undead" and undergo behaviours associated with cell death, but remain in the tissue and can induce non-autonomous effects (see also section "Non-autonomous effects of JNK signalling") (reviewed in Martín et al., 2009). In *Drosophila* wing imaginal disc cells, undead cells induce JNK-dependent overproliferation in their *wildtype* neighbours, which reflects this observed role reversal (Pérez-Garijo et al., 2004;

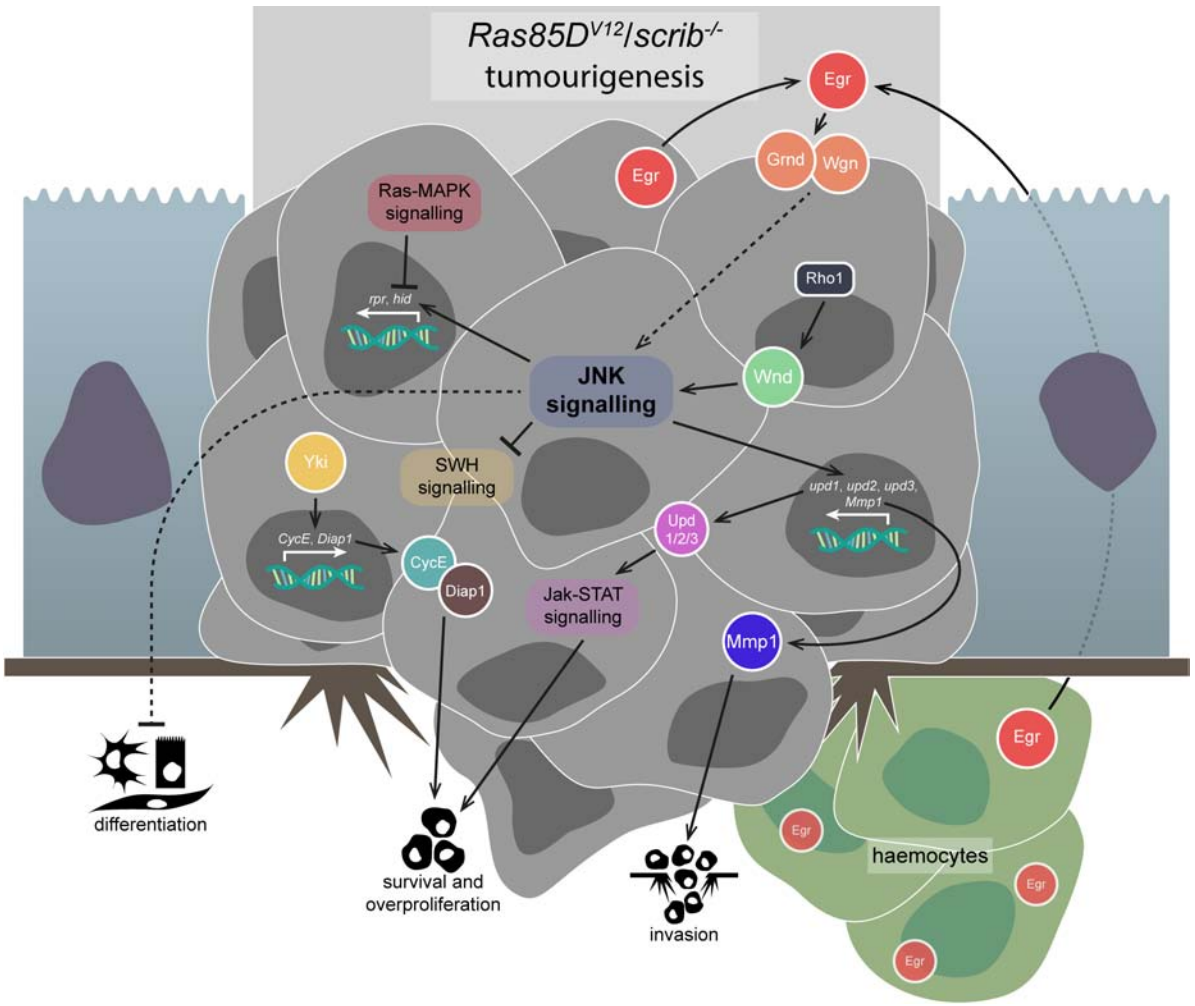

FIGURE 3 | Pro-tumourigenic JNK signalling. JNK signalling in the face of apoptosis-suppressing signals, like that which occur via Ras-MAPK signalling in *Ras85D*^{V12}*/scrib*$^{-/-}$ tumours, is co-opted to promote several tumourigenic behaviours. JNK signalling in these tumours is activated via some combination of Egr-mediated TNFR activation and Rho1-Wnd signalling – the proportions of each are not fully understood, but TNF signalling has been shown to be dispensable. JNK signalling suppresses differentiation in *Ras85D*^{V12}*/scrib*$^{-/-}$ tumours, but the precise mechanism of this interaction is unclear. JNK signalling also appears to suppress SWH signalling, allowing Yki to promote the survival and overproliferation of the tumourous cells. Jak-STAT signalling, initiated by the Upd-family ligands whose expression is promoted by JNK signalling, also contributes to tumourigenic survival and overproliferation. Lastly, JNK signalling promotes invasiveness of the tumour cells and basement membrane degradation by upregulating proteins such as Mmp1. Gene and protein name abbreviations used in the diagram are as follows: Eiger (Egr), Grindelwald (Grnd), Wengen (Wgn), Wallenda (Wnd), *unpaired 1* (*upd1*), *unpaired 2* (*upd2*), *unpaired 3* (*upd3*), *Matrix metalloproteinase 1* (*Mmp1*), Yorkie (Yki), *Cyclin E* (*CycE*), *Death-associated inhibitor of apoptosis 1* (*Diap1*), *reaper* (*rpr*), *head involution defective* (*hid*).

Ryoo et al., 2004). Similarly, JNK signalling resulting from non-apoptotic levels of caspase activation in undead cells also autonomously promotes invasiveness via *Mmp1* upregulation (Rudrapatna et al., 2013).

The aforementioned studies demonstrate that the malignancy of *Ras85D*^{V12}*/scrib*$^{-/-}$ tumours depends on JNK signalling, and the downstream effectors of that JNK signal have recently been identified. Three key TFs act downstream of JNK signalling in *Ras85D*^{V12}*/scrib*$^{-/-}$ tumours – Kay (a.k.a. Fos), Ftz TF 1 (Ftz-f1), and Ets at 21C (Ets21C) (Külshammer et al., 2015). Similarly, another study demonstrated that a majority of the phenotypes seen in *Ras85D*^{V12}*/scrib*$^{-/-}$ tumours can be traced back to a network of around 10 interconnected TFs that act downstream of JNK, SWH, and Jak-STAT signalling (Atkins et al., 2016), with Jak-STAT signalling being a key contributor to *Ras85D*^{V12}*/scrib*$^{-/-}$ tumour overgrowth (**Figure 3**; Wu et al., 2010; Atkins et al., 2016). Regardless, it was shown that Kay was solely responsible for JNK-related differentiation defects and *Mmp1* upregulation, but both Kay and Ftz-f1 are necessary for tumour invasiveness, and Ets21C overexpression can cooperate with Ras85D^{V12} to produce invasive (but non-overgrowing) clones (Külshammer et al., 2015).

Jun N-terminal kinase signalling inhibits differentiation of *Ras85D*^{V12}*/scrib*$^{-/-}$ tumour cells via an unclear mechanism (**Figure 3**), but it can be observed in the eye imaginal disc tissue due to decreased expression of embryonic lethal abnormal

vision (Elav), a marker of photoreceptor cell differentiation, which is restored upon JNK signalling inhibition (Leong et al., 2009). When cooperative tumourigenesis between $Ras85D^{V12}$ and $scrib^{-/-}$ was first identified, it was also demonstrated that an activated form of Notch (N – the activated form is commonly and hereafter referred to as N^{ACT}) also cooperated with $scrib^{-/-}$ to induce tumourigenesis (Brumby and Richardson, 2003). While invasiveness of $N^{ACT}/scrib^{-/-}$ tumours is driven by JNK signalling, differentiation suppression is not, as blocking JNK did not rescue differentiation as indicated by Elav expression (Leong et al., 2009). However, blocking aPKC and JNK simultaneously was able to completely rescue the differentiation defects in, and the overgrowth and invasion phenotypes of, $N^{ACT}/scrib^{-/-}$ tumours (Leong et al., 2009). Interestingly, it was recently found that N^{ACT} can also cooperate with *l(2)gl* mutation to produce tumours, which also have their invasiveness driven by JNK-induced Mmp1 activity (Paul et al., 2018). Similarly, ectopic JNK signalling also contributes to tumourigenesis driven by $Ras85D^{V12}$ expression and *l(2)gl* mutation – $Ras85D^{V12}/l(2)gl^{-/-}$ tumours upregulate JNK signalling, which is thought to proceed via Src oncogene at 42A (Src42A), Ubiquitin-conjugating enzyme variant 1A (Uev1A), and the E2 ubiquitin ligase, Bendless (Ben) (Ma et al., 2013a,b). Uev1A and Ben play a highly conserved role in regulating the DNA damage response in cells via their role in K63-linked polyubiquitination, but whether such activity is required in JNK signalling remains to be determined (Bai et al., 2018). Activation of the Wingless (Wg, orthologue of the human *WNT* family) signalling pathway by JNK signalling is also thought to drive invasiveness via upregulation of *Mmp1* expression and activity in $Ras85D^{V12}/l(2)gl^{-/-}$ tumours (Zhang et al., 2019). Indeed, direct activation of JNK signalling together with $Ras85D^{V12}$ expression is sufficient for neoplastic tumourigenesis (Brumby et al., 2011).

While there are clearly differences between $Ras85D^{V12}/scrib^{-/-}$ and $N^{ACT}/scrib^{-/-}$ tumours, research has also uncovered many genetic similarities between them. Microarray data from $Ras85D^{V12}/scrib^{-/-}$ and $N^{ACT}/scrib^{-/-}$ tumours has identified just over 500 genes that were similarly misregulated between the two tumours, as well as 103 genes that were specifically responsive to JNK signalling shared between them (Doggett et al., 2015). Four of those genes were BTB-zinc finger TFs, and one of those was *chronologically inappropriate morphogenesis* (*chinmo*), which was shown to be capable of cooperating with both $Ras85D^{V12}$ and N^{ACT} to drive tumourigenesis, even if JNK signalling was blocked (Doggett et al., 2015). A similar role was identified for the BTB-zinc finger TF *fruitless*, while another BTB-zinc finger TF, *abrupt*, was able to compensate for *chinmo* removal in driving tumourigenesis of $scrib^{-/-}$ $/Ras85D^{V12}$ clones (Doggett et al., 2015). This indicates that these BTB-zinc finger TFs are important transcriptional targets of JNK signalling in cooperative tumourigenesis.

As with JNK in its anti-tumourigenic role, questions exist regarding the source of pro-tumourigenic JNK signalling. Egr is suspected, and haemocytes appear to be attracted to tumourous tissue just as they are attracted to pre-tumourigenic tissue (**Figure 3**), though not necessarily by the same mechanism – $Ras85D^{V12}/scrib^{-/-}$ tumours, in their undead-like state, have been shown to co-opt the activity of caspases to generate reactive oxygen species (ROS), which can attract haemocytes, which then activate JNK signalling and caspases in the tumourigenic cells, forming a feedback loop (Pérez et al., 2017). It is also thought that the increased JNK signalling in $Ras85D^{V12}/scrib^{-/-}$ tumours may increase haemocyte proliferation via JNK-dependent upregulation of the *unpaired* (*upd1*, *upd2*, and *upd3*) family of genes (behaviourally similar to mammalian IL-6), which act as ligands for the proliferation-promoting Jak-STAT signalling pathway (Pastor-Pareja et al., 2008; Cordero et al., 2010; Wu et al., 2010; Bunker et al., 2015). Regardless, haemocytes produce Egr when associated with pre-tumourigenic and tumourigenic tissue, but while Egr activates apoptosis promoting TNF-JNK signalling in pre-tumourigenic tissue, it is thought to promote tumour growth in $Ras85D^{V12}/scrib^{-/-}$ tumourigenic tissue, as well as invasive capacity via TNF-JNK-mediated *Mmp1* upregulation (Cordero et al., 2010). However, there is debate regarding the importance of Egr in JNK activation in polarity-impaired tumourigenesis. It has recently been shown that, in two different JNK-driven tumourigenesis models in the eye-antennal imaginal discs – tumourigenesis induced via polarity-impairment ($Ras85D^{V12}/scrib^{-/-}$) or via chromosomal instability (CIN) – JNK signalling initiation primarily derives from the tumourous epithelia itself, rather than recruited haemocytes or mesenchymal myoblasts (Muzzopappa et al., 2017). Furthermore, it was found that *egr* and *grnd* were dispensable in the process – instead, JNK signalling derived from signalling through the JNKKKs Wnd and Ask1 in polarity-impairment- and CIN-induced tumourigenesis, respectively (**Figure 3**; Muzzopappa et al., 2017). The authors reasoned this was due to CIN-induced tumourigenesis producing ROS, to which Ask1 is sensitive (Sekine et al., 2012), while Wnd mediates JNK signalling in response to polarity-impairment (see also section "Upstream regulation of JNK signalling") (Ma et al., 2016; Muzzopappa et al., 2017).

We have highlighted how anti-tumourigenic JNK signalling is thought to be partly responsible for blocking Yki activation in pre-tumourigenic $scrib^{-/-}$ clones (Doggett et al., 2011; Chen et al., 2012). However, it is currently unclear whether co-opting JNK signalling into being pro-tumourigenic in $Ras85D^{V12}/scrib^{-/-}$ tumours alters its effect on SWH signalling. In $Ras85D^{V12}/scrib^{-/-}$ tumourigenesis, SWH signalling is impaired, and Yki is active and contributes to the observed neoplastic overgrowth, but not invasion (**Figure 3**; Doggett et al., 2011). Conversely, it has been demonstrated that Yki-driven overgrowth in wing and eye-antennal imaginal discs is suppressed via JNK-mediated Wts activity (Enomoto et al., 2015). However, when $Ras85D^{V12}$ is coupled with active JNK signalling (via *egr* overexpression) tumourigenesis occurs similar to that driven by $Ras85D^{V12}/scrib^{-/-}$, and the combination of Ras-MAPK and JNK signalling leads to Yki activation via the accumulation of F-actin, dependent on the actin regulators Jub, Diaphanous (Dia), and Rac1, as well as inactivation of Wts (Enomoto et al., 2015). These data suggest SWH signalling modulation and Yki upregulation contribute to $Ras85D^{V12}/scrib^{-/-}$ tumourigenesis, but more research is needed to understand how JNK signalling interacts with SWH signalling and Yki during the process.

As briefly discussed, tumourigenesis can be modelled in *Drosophila* by more mechanisms than just oncogene activation coupled with polarity-impairment (as per $Ras85D^{V12}/scrib^{-/-}$), and many of these alternative mechanisms are also reliant on JNK signalling. However, while activated Ras85D is known to block apoptosis (Bergmann et al., 1998; Kurada and White, 1998) and thus co-opt JNK signalling into promoting tissue growth (**Figure 3**), in other cases of cooperative tumourigenesis it is not clear how the apoptosis promoting role of JNK is halted. Examples of both such JNK-driven tumour types have recently been described elsewhere (reviewed in Richardson and Portela, 2018). We list some newly identified examples of JNK-driven tumourigenesis in various *Drosophila* tissues below.

(1) Aneuploid cells formed via CIN undergo tumourigenesis via JNK signalling activation, with the delamination and invasive behaviour of the cells driven by JNK targets promoting misregulation of the actin-myosin cytoskeleton (Benhra et al., 2018).
(2) *Src oncogene at 64B* (*Src64B*) and *Src42A* are capable of inducing tumourigenesis in eye-antennal imaginal discs when overexpressed by cooperating with $Ras85D^{V12}$ – JNK signalling in these tumours is necessary for their neoplastic overgrowth and invasion, and the Raf-MAPK and Phosphoinositide 3-kinase (PI3K) signalling pathways act downstream of $Ras85D^{V12}$ to facilitate this cooperation (Poon et al., 2018). These findings are consistent with a previous study that demonstrated the upregulation of Src family genes alone is capable of activating JNK signalling in the wing imaginal disc, and promotes invasion via actin cytoskeleton remodelling (Rudrapatna et al., 2014).
(3) A *Drosophila* glioblastoma, complete with tumour cell-interconnecting microtubules (TMs), is driven by constitutively active EGFR and PI3K signalling in glial cells (Read et al., 2009; Portela et al., 2019). Wg signalling is activated in the glioma cell TMs due to "vampirisation" of the ligand from the surrounding *wildtype* neurons and drives tumour progression (Portela et al., 2019). Furthermore, TNF-JNK-Mmp1/2 signalling, acting via Grnd, is also upregulated in the TMs, is necessary for the "vampirisation" process, and forms a positive feedback loop with Wg signalling by promoting TM formation (Portela et al., 2019).
(4) Epigenetic silencers of the Polycomb Group (PcG) can cause tumourigenesis to occur if mutated (Beira et al., 2018). One PcG family member is *polyhomeotic*, the clonal mutants of which upregulate JNK signalling via Egr and Grnd (as well as Notch and Jak-STAT signalling), and promote neoplastic overgrowth, invasion, and polarity loss (Beira et al., 2018).
(5) Genes involved with the endocytic process, such as *Rab5*, *Syntaxin 7* (*Syx7*, a.k.a *avalanche*), *Tumour susceptibility gene 101* (*TSG101*, a.k.a. *erupted*), and various Vacuolar protein sorting family genes, represent another relatively well-studied class of nTSGs. In tissues predominantly mutant for these genes, JNK signalling is upregulated, and shares tumourigenesis-promoting roles with Jak-STAT signalling (Woodfield et al., 2013). Similar phenomena are observed upon overexpression of Vacuolar H+ ATPase 44kD subunit (Vha44), the C-subunit of V-ATPase, which is involved in the acidification of endosomes, and also leads to JNK-dependent tumourigenesis (Petzoldt et al., 2013). More recently, it has been shown that endocytic nTSG clones generated in eye-antennal imaginal discs also have some degree of polyploidy due to JNK and Yki coactivation, with JNK signalling downregulating the G2-M phase cell cycle regulator *Cyclin B* (*CycB*) and Yki upregulating *Diap1* to promote polyploidy-inducing endoreplication (Cong et al., 2018). Interestingly, it was shown that polyploid cells also form in $Ras85D^{V12}/scrib^{-/-}$ tumours due to *CycB* downregulation, and blocking their formation inhibits the invasive behaviours of these tumours (Cong et al., 2018).
(6) Jun N-terminal kinase signalling can be important in tumourigenesis at transition zones – where different epithelial cell populations meet, which are often hotspots for tumourigenesis (reviewed in Tamori and Deng, 2017). One such zone occurs in the *Drosophila* larvae at a site where polyploid salivary gland cells meet the diploid imaginal ring cells, where tumourigenesis occurs after transient whole animal N^{ACT} expression due to upregulation of TNF-JNK and Jak-STAT signalling (Yang et al., 2019).
(7) Overexpression of Canoe (Cno, an adherens junction scaffold protein) in the *patched* (*ptc*) expression domain in wing imaginal discs conversely promotes both overproliferation and ectopic cell death, as well as cell migration/invasion (Ma et al., 2019). While JNK signalling was upregulated in the Cno-expressing cells, moderate inhibition of JNK signalling was able to block cell death and promote massive tissue overgrowth, while strong JNK inhibition led to only partial overgrowth (Ma et al., 2019), indicating JNK signalling levels are balancing pro- and anti-tumourigenic roles in this model.

In summary, the second face of JNK signalling is as a powerful driver of tumourigenesis. Pro-proliferation and survival functionalities are co-opted by apoptosis suppression signals such as Ras-MAPK signalling, and JNKs regulation of cell movement and migration is converted into promoting invasion and metastasis. Modulation of SWH signalling is thought to be involved with the pro-tumourigenic roles of JNK, but more research is needed to fully clarify this signalling cross-talk. JNK signalling in *Drosophila* is therefore a powerful pro-tumourigenic force, but context is key.

NON-AUTONOMOUS EFFECTS OF JNK SIGNALLING

Most of our previous discussions regarding the effects of JNK signalling dealt with autonomous induction and action of the pathway, however, non-autonomous effects of JNK signalling have been identified. One of the earliest explorations of non-autonomous JNK signalling effects came from examinations

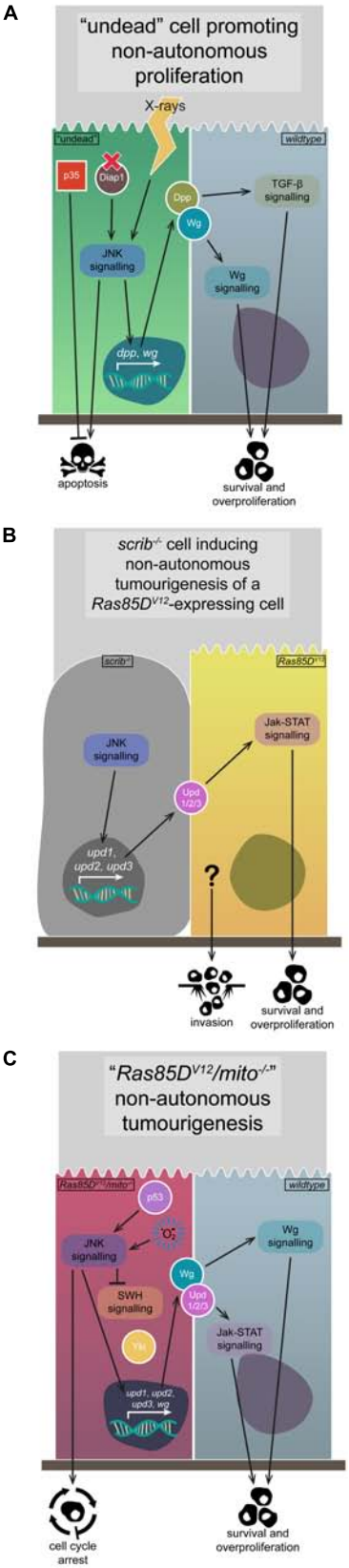

FIGURE 4 | Continued

FIGURE 4 | Non-autonomous JNK signalling. The activation of JNK signalling in one group of cells can have non-autonomous effects on the growth and proliferation of their neighbours, due to the upregulation of various signalling pathway initiators. **(A)** The generation of "undead" cells via the upregulation of p35 while simultaneously inducing apoptosis via *Diap1* mutation or X-ray application leads to JNK signalling activation, the expression and secretion of Wg and Dpp ligands, and the survival and overproliferation of neighbouring cells due to Wg and TGF-β signalling pathway activation. **(B)** The upregulation of JNK signalling that occurs in *scrib*$^{-/-}$ cells leads to expression and secretion of the Upd-family ligands, which can activate Jak-STAT signalling in neighbouring *Ras85D*^{V12}-expressing tumourigenic cells, leading to their survival and overproliferation, and possibly their invasiveness. **(C)** Cells expressing *Ras85D*^{V12} coupled with mitochondrial gene mutations upregulate JNK signalling, due to p53 and ROS activity. Said JNK signalling downregulates SWH signalling, derepressing Yki, and also upregulates expression and secretion of Wg and the Upd-family ligands, activating Jak-STAT and Wg signalling in neighbouring cells and promoting their survival and overproliferation. Gene and protein name abbreviations used in the diagram are as follows: Death-associated inhibitor of apoptosis 1 (Diap1), *decapentaplegic* (*dpp*), *wingless* (*wg*), *unpaired 1* (*upd1*), *unpaired 2* (*upd2*), *unpaired 3* (*upd3*), Yorkie (Yki).

of cooperative tumours generated via *scrib* mutation and *Raf oncogene* (*Raf*) activation (using a *Raf* gain-of-function allele (*Raf*^{GOF})) (Uhlirova et al., 2005). These *Raf*^{GOF}/*scrib*$^{-/-}$ tumours are indistinguishable from *Ras85D*^{V12}/*scrib*$^{-/-}$ tumours. Upregulating JNK signalling in *Raf*^{GOF}/*scrib*$^{-/-}$ tumours via *hep*^{ACT} expression led to a reduction in the size of eye-antennal imaginal discs, but adult eyes increased in size, and in both cases the GFP-positive cells (where the different transgenes were clonally expressed) were eliminated, suggesting a non-autonomous effect on the growth of the surrounding *wildtype* tissue (Uhlirova et al., 2005). The researchers suggested that the addition of *hep*^{ACT} overcomes the apoptosis inhibition of *Raf*^{GOF}, and prompts compensatory proliferation from the *wildtype* cells, but the secretion of cytokines by the *Raf*^{GOF}/*scrib*$^{-/-}$/*hep*^{ACT} cells leads to the malformation observed (Uhlirova et al., 2005).

Compensatory proliferation is one of the key mechanisms through which non-autonomous JNK signalling is realised, and it is usually effected via secretable JNK targets that induce proliferation, such as Wg or the Upd family ligands (Uhlirova et al., 2005; Pastor-Pareja et al., 2008; Sun and Irvine, 2011). While a healthy level of compensatory proliferation maintains tissue homeostasis in the face of wounding or cell competition, the process can be corrupted if apoptosis is induced (e.g., by *Diap1* mutation or X-ray exposure) but the pathway is blocked by *p35* expression – these undead cells upregulate JNK signalling, which promotes the expression and secretion of Wg and Decapentaplegic (Dpp), ligands that then promote the non-autonomous overproliferation and overgrowth of neighbouring cells (**Figure 4A**; Pérez-Garijo et al., 2004; Ryoo et al., 2004). Interestingly, TNF-JNK signalling in undead cells can also, conversely, trigger non-autonomous apoptosis, with cell death being induced in different wing imaginal disc compartments, a process the researchers termed "apoptosis-induced apoptosis" (Pérez-Garijo et al., 2013).

Perhaps unsurprisingly, non-autonomous effects of JNK signalling can be tumourigenic, such as the phenomenon of interclonal cooperation, where *scrib*$^{-/-}$ (or *l(2)gl*$^{-/-}$) clones

adjacent to $Ras85D^{V12}$-expressing clones ($Ras85D^{V12}$//$scrib^{-/-}$) cooperate to induce tumourigenesis of the $Ras85D^{V12}$ cells – these tumours appear functionally identical to those where *scrib* is mutated and $Ras85D^{V12}$ is expressed in the same cells ($Ras85D^{V12}$/$scrib^{-/-}$) (**Figure 4B**; Wu et al., 2010). Researchers found that the interclonal cooperation was due to the secretion of the Upd family ligands, which activate Jak-STAT signalling and are targets of JNK-mediated transcription in $scrib^{-/-}$ cells (**Figure 4B**; Wu et al., 2010; Bunker et al., 2015). Indeed, co-expression of *upd1*, *upd2*, or *upd3* and $Ras85D^{V12}$ replicated the interclonal cooperation phenotype, and inhibiting JNK signalling rescued $Ras85D^{V12}$//$scrib^{-/-}$ tumourigenesis, but not $Ras85D^{V12}$/*upd1/2/3* tumourigenesis (**Figure 4B**; Wu et al., 2010). In this example of interclonal cooperation, the $scrib^{-/-}$ cells upregulate JNK signalling and, while they are eventually eliminated, the JNK signal non-autonomously allows for the tumourigenic overgrowth of the $Ras85D^{V12}$-expressing cells (Wu et al., 2010).

Another example of non-autonomous JNK signalling activity is the case of $Ras85D^{V12}$ cooperation with mutated genes from the mitochondrial respiratory system, including *NADH dehydrogenase (ubiquinone) PDSW subunit*, *mitochondrial ribosomal protein L4*, and *Cytochrome c oxidase subunit 5A* – their cooperation induces overgrowth in *wildtype* neighbours, but not in the mutated cells (Ohsawa et al., 2012). ROS production in the $Ras85D^{V12}$/mitochondrial gene mutant clones ($Ras85D^{V12}$/$mito^{-/-}$) promotes ectopic JNK signalling, which contributes to SWH downregulation, Yki upregulation, and the transcription of *wg* and *upd1*/*upd2*/*upd3* (Ohsawa et al., 2012). The expression and secretion of Wg and Upd1/Upd2/Upd3 acts on the surrounding *wildtype* cells to promote their proliferation (**Figure 4C**), but if the surrounding cells overexpress $Ras85D^{V12}$, they develop into neoplastic invasive tumours (Ohsawa et al., 2012). Whether tumourigenic or not, the Upd gene family being a transcriptional target of JNK signalling is a common theme in how non-autonomous JNK signalling is effected – this is also seen in clones mutant for the early endosomal regulatory gene *Rab5*, where the concomitant disruptions to endocytic processes lead to upregulated TNF-JNK and Ras-MAPK signalling, Yki activation, and Upd ligand expression and secretion to drive overgrowth of surrounding tissue (Takino et al., 2014). Research using the same model system ($Ras85D^{V12}$/$mito^{-/-}$ clones) further dissected how JNK signalling was regulated and acted. It was shown that $Ras85D^{V12}$/$mito^{-/-}$ clones displayed phenotypes associated with cellular senescence – their cell cycle was arrested in G1, they upregulated various senescence-associated markers, the individual cells were overgrown, and they displayed a senescence-associated secretory phenotype (SASP) (**Figure 4C**; Nakamura et al., 2014). In these cells, ROS production and p53 upregulation contribute to the activation of JNK signalling, which then induces Upd1/Upd2/Upd3 expression and secretion, leading to non-autonomous tissue growth effects (**Figure 4C**; Nakamura et al., 2014). A somewhat related role for JNK signalling was recently observed for cells upon wounding in wing imaginal discs – wounding induced JNK signalling, and cells became transiently "stalled" in the cell cycle at G2 phase (or near-permanently "arrested" in G2 phase after JNK induction via *egr* overexpression in the *rotund* expression domain) (Cosolo et al., 2019). Researchers found that JNK signalling induces G2 phase stalling/arrest via downregulating the activity of Stg (an inducer of mitosis) and, furthermore, that cells with this G2 profile were protected from JNK-mediated apoptosis (Cosolo et al., 2019). It was also shown that the G2-biased profile of clones mutant for *wts* or *dlg1* was due to JNK signalling (Cosolo et al., 2019). Interestingly, the *wildtype* tissue adjacent to these mutant clones overgrows, and was suggested by researchers to be another example of JNK-induced non-autonomous tissue growth (Cosolo et al., 2019). Similar cell cycle arrest has also been observed in wholly $scrib^{-/-}$ wing imaginal disc tumours – strong JNK signalling in periphery cells early in tumourigenesis induces G2/M phase arrest, but JNK signalling decreases over time in these cells and, together with a concomitant increase in Ras-MAPK signalling, the cell cycle arrest ceases and the tumours overgrow (Ji et al., 2019).

One final example of JNK signalling-induced non-autonomous effects concerns imaginal disc clones overexpressing *Src64B* that are eliminated via cell competition, but cause the overgrowth of their *wildtype* neighbours (Enomoto and Igaki, 2013). Clonal *Src64B*-overexpression activates JNK signalling, in part via the induction of F-actin accumulation (Enomoto and Igaki, 2013) – further links have been drawn between the actin cytoskeleton and JNK signalling activation, as Src genes have also been shown to promote JNK signalling via Rho1-induced actin remodelling (Rudrapatna et al., 2014). Regardless, the F-actin accumulation also promotes Yki activation in the *Src64B*-overexpressing clones – though their overgrowth is opposed by the upregulated JNK signal, the Yki signal propagates to the *wildtype* neighbours in a JNK-dependent manner, and there upregulates Yki and promotes non-autonomous overgrowth (Enomoto and Igaki, 2013). Interestingly, however, if JNK signalling is inhibited in the *Src64B*-overexpressing clones, Yki activity promotes the tumourigenic overgrowth of those cells instead (Enomoto and Igaki, 2013).

Non-autonomous JNK signalling is necessary for the maintenance of tissue homeostasis, regulating as it does the process of compensatory proliferation after cell competition or wounding events. However, the above examples also show that JNK signalling is two-faced, and can be co-opted to effect non-autonomous tumourigenesis, inducing or enhancing the overgrowth and invasion of otherwise benign cells.

UPSTREAM REGULATION OF JNK SIGNALLING

The activation of JNK signalling is complex. While the kinase core remains largely the same, upstream activation contexts can vary wildly. Most of the cases discussed so far (where it has been examined) are thought to have utilised the TNF-JNK signalling pathway in various ways, but clearly this is not the only way JNK can be activated. In this section, we will discuss some of the more unique ways in which JNK

signalling can be activated when acting in a pro- or anti-tumourigenic fashion.

Regulating JNK Signalling in Development and Tissue Homeostasis

Besides acting as a pro-apoptotic signal, JNK signalling is arguably best understood as a regulator of cell morphology and migration in a variety of developmental contexts (reviewed in Harden, 2002; Ríos-Barrera and Riesgo-Escovar, 2013). During *Drosophila* embryogenesis, JNK signalling plays a critical role during the epithelial sheet migration process of dorsal closure, and similarly in thoracic closure during pupariation (**Figure 5**). Activation of JNK signalling during thoracic closure is mediated by Pvr signalling via Crk oncogene (Crk), Ced-12, Mbc, and Rac1 (Ishimaru et al., 2004). As an aside, constitutively activated Pvr signalling is oncogenic, and in wing imaginal discs activates JNK signalling (alongside Ras-MAPK and PI3K signalling) to effect metabolic reprogramming of the tumour cells (Wang et al., 2016). Another process in which both Pvr and JNK signalling are involved is border cell migration (BCM), a process during oogenesis involving the movement of a cluster of "border cells" from the apical end of the egg chamber to the surface of the oocyte itself, and which is an established model of cell migration and invasion in *Drosophila* (reviewed in Montell et al., 2012). During BCM, JNK signalling regulates clustering and migratory behaviours of the border cells, and is thought to be activated by the GTPases Rho1 and Cdc42 (Mathieu et al., 2007; Llense and Martín-Blanco, 2008; Melani et al., 2008). It is further thought that JNK signalling contributes to the Pvr signalling-mediated guidance of the border cells, but this interaction is not fully understood (Llense and Martín-Blanco, 2008).

Returning to dorsal and thoracic closure, in both processes Rac1 is thought to activate JNK signalling via the JNKKK Slpr (Garlena et al., 2010), whereas in thoracic closure the JNKKK Wnd has been shown to be dispensable (Ma et al., 2015b). JNK signalling via Slpr during dorsal closure is believed to be initiated by the activity of the Src family proteins (and/or Btk family kinase at 29A (Btk29A)) and their downstream targets, SH2 ankyrin repeat kinase (Shark) and Downstream of kinase (Dok), and that Rac1 may act downstream of these molecules (reviewed in Ríos-Barrera and Riesgo-Escovar, 2013) – however, the upstream regulation of JNK signalling in these developmental contexts is not fully understood (**Figure 5**). The role of JNK signalling during dorsal closure has also been shown to rely on additional signalling pathways. Transforming growth factor-β (TGF-β) signalling, activated by Dpp, has been demonstrated as acting to suppress the pro-apoptotic activity of the JNK signalling pathway – while the JNK-induced AP-1 TF complex promotes *rpr* expression and apoptosis, the TGF-β-induced TF Schnurri (Shn) suppresses *rpr* expression (Beira et al., 2014). This is an elegant example of how JNK signals can be co-opted during developmental events, like in tumourigenesis, via the mechanism of apoptosis suppression.

It is believed that JNK signalling-mediated cell death during development generally proceeds via input from the TNF signalling pathway. However, research in this vein has largely examined how TNF-JNK signalling proceeds after induction, rather than how endogenous TNF-JNK signalling is regulated or initiated. In the *Drosophila* eye, JNK-mediated cell death induced by Egr expression acts predominantly via Tak1, though Wnd plays a small role, whereas JNK-mediated cell death induced by Rac1 expression acts predominantly via Wnd, but Tak1 is dispensable (Ma et al., 2015b). Furthermore, cell death (and invasion) within the *Drosophila* wing imaginal disc can be induced via *scrib* knockdown in the *ptc* expression domain – this was also suppressed by *wnd* knockdown, which appears to act via both Hep and Mkk4 in this context (Ma et al., 2015b). This study demonstrates the complex nature of JNK signalling regulation. Research suggests Rho1, like Rac1, can activate JNK signalling, but does not do so identically. As mentioned, it has been shown that Rho1 is likely responsible for JNK signalling upregulation in response to polarity-impairment in $Ras85D^{V12}/scrib^{-/-}$ tumours (Muzzopappa et al., 2017). Furthermore, it has been shown that knockdown of *Rho1* (and *wnd*) suppressed *scrib* knockdown-induced cell death and invasion in the *ptc* expression domain in wing imaginal discs (**Figure 5**; Ma et al., 2016). Overexpression of *wnd* or *Rho1* in the *ptc* expression domain were found to promote epithelial to mesenchymal transition (EMT)-like invasive phenotypes and *Mmp1* upregulation (**Figure 5**; Ma et al., 2016). Knocking down *wnd* while overexpressing *grnd* (and *vice versa*) led to a rescue of the invasion phenotypes (though actin remodelling was not dependent on JNK signalling), suggesting some kind of feedback loop may occur (Ma et al., 2016). Furthermore, while *Rac1* overexpression in the *ptc* expression domain also led to JNK-dependent invasive behaviours, it was shown that *wnd* was dispensable (in contrast to the aforementioned necessity of *wnd* in Rac1-induced JNK-mediated cell death in the eye (Ma et al., 2015b)) and, curiously, that both *Rho1* and *Rac1* overexpression-induced phenotypes were rescued upon simultaneous disruption of Tak1 and Slpr (Ma et al., 2016).

Overexpression of *wnd* has also been shown to cooperate with $Ras85D^{V12}$ to generate tumours where, similar to what is seen in $Ras85D^{V12}/scrib^{-/-}$ tumours, it induces JNK signalling to promote upregulation of the Wg signalling pathway, promoting cell proliferation (Ma et al., 2016). Various cell morphology regulators have also been identified as interacting with $Ras85D^{V12}$ to promote both tumourigenesis and JNK signalling. These include the aforementioned Rho-family GTPases *Rho1* and *Rac1*, as well as their partner *Rho guanine nucleotide exchange factor 2* (*RhoGEF2*), which cooperate with $Ras85D^{V12}$ to enhance adult eye overgrowth phenotypes when overexpressed, due to their role as positive regulators of JNK signalling (Brumby et al., 2011). Moreover, clonally, *Rac1*, *RhoGEF2*, or activated *Rho1* expression in isolation led to clones that were eliminated, but cooperated when expressed alongside $Ras85D^{V12}$ to induce the formation of invasive tumours via activation of JNK signalling (Brumby et al., 2011). Specifically, RhoGEF2 and Rho1 act upstream of Rho kinase (Rok) and Spaghetti squash (Sqh, a.k.a Myosin II Regulatory Light Chain) to activate JNK signalling and cooperate with $Ras85D^{V12}$ in tumourigenesis, but they also promote actin/myosin contractility

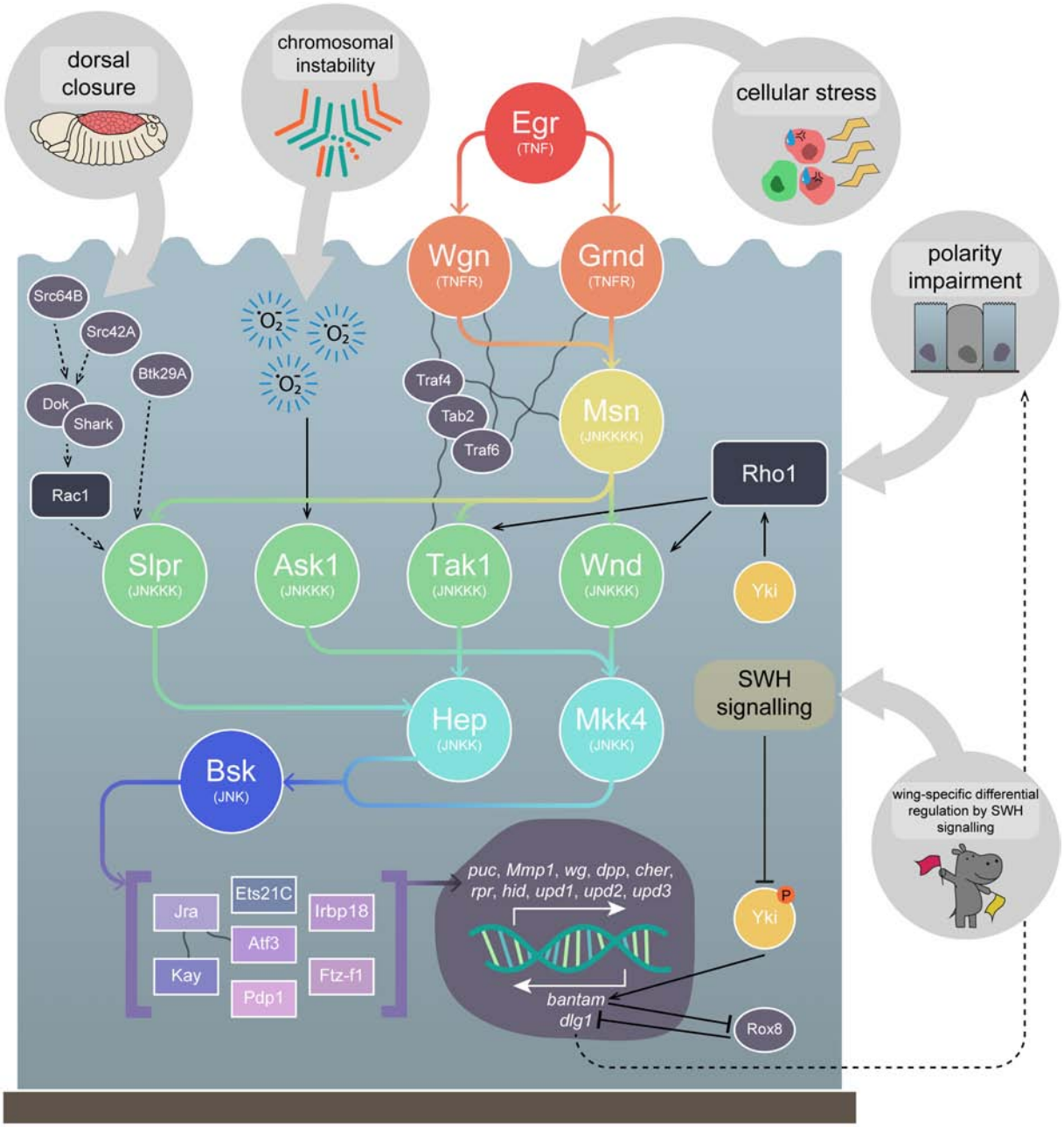

FIGURE 5 | Upstream regulation of JNK signalling. JNK signalling can be activated by a variety of different upstream mechanisms. JNK signalling mediates cell morphology changes, such as those during embryonic dorsal closure, where it is thought to act via Src42A and Src64B (and/or Btk29A) to activate the kinase Shark and its adapter, Dok. This signalling may in turn activate Rac1 and promote JNK signalling via Slpr. In cells with chromosomal instability, accumulated ROS promote Ask1 signalling, stimulating the JNK signalling pathway to promote apoptosis. Arguably, the best understood pathway is the TNF-JNK signalling pathway, which is generally considered to be activated as a response to cellular stresses. Egr, the *Drosophila* TNF, binds to Grnd or Wgn (TNFRs), which activate Msn (JNKKKK) and Tak1 (JNKKK), via the adapter proteins Traf4, Tab2, and Traf6. JNK signalling is activated in polarity-impaired cells, which is thought to occur via the stimulation of Wnd by the actin cytoskeleton regulator Rho1, although TNF signalling contributes to amplify JNK activity. Lastly, in *Drosophila* wing imaginal discs, differential JNK signalling regulation by the SWH signalling pathway has been observed. While non-active SWH signalling allows Yki to promote JNK activation via Rho1, activated SWH signalling suppresses Yki activity, preventing *bantam* transcription, a miRNA that suppresses Rox8, which acts as a positive regulator of JNK signalling, possibly by downregulating *dlg1*. Msn is thought to be capable of activating Tak1, Wnd, and Slpr, but has not yet been shown to activate Ask1. Tak1, Wnd, and Ask1 are then thought to be capable of activating both the JNKKs, Hep and Mkk4, while Slpr has only yet been shown to act via Hep. Both Hep and Mkk4 can activate the sole *Drosophila* JNK, Bsk, which positively regulates a number of TFs, including the well known Jra and Kay. These TFs promote transcription of a number of important genes, including the apoptosis promoters *hid* and *rpr*, the Jak-STAT ligands *upd1*, *upd2*, and *upd3*, the invasion promoter *Mmp1*, and the negative JNK regulator *puc*. Dotted lines represent uncertain interactions. Wavy lines represent known physical interactions between core pathway members and

(Continued)

FIGURE 5 | Continued
their adapters. Gene and protein name abbreviations used in the diagram are as follows: Src oncogene at 64B (Src64B), Src oncogene at 42A (Src42A), Btk family kinase at 29A (Btk29A), Downstream of kinase (Dok), SH2 ankyrin repeat kinase (Shark), Eiger (Egr), Grindelwald (Grnd), Wengen (Wgn), Misshapen (Msn), TNF-receptor-associated factor 4 (Traf4), TAK1-associated binding protein 2 (Tab2), TNF-receptor-associated factor 6 (Traf6), Slipper (Slpr), Wallenda (Wnd), TGF-β activated kinase 1 (Tak1), Apoptotic signal-regulating kinase 1 (Ask1), Hemipterous (Hep), MAP kinase kinase 4 (Mkk4), Basket (Bsk), Jun-related antigen (Jra), Kayak (Kay), Ets at 21C (Ets21C), Activating transcription factor 3 (Atf3), PAR-domain protein 1 (Pdp1), Inverted repeat binding protein 18 kDa (Irbp18), Ftz transcription factor 1 (Ftz-f1), puckered (puc), *Matrix metalloproteinase 1* (*Mmp1*), *wingless* (*wg*), *decapentaplegic* (*dpp*), *cheerio* (*cher*), *reaper* (*rpr*), *head involution defective* (*hid*), *unpaired 1* (*upd1*), *unpaired 2* (*upd2*), *unpaired 3* (*upd3*), Yorkie (Yki), *discs large 1* (*dlg1*).

and cell shape changes independently of JNK signalling (Khoo et al., 2013).

TNF-JNK Signalling

TNF-JNK signalling has already been discussed in earlier sections, but a more detailed exploration is pertinent, as it is one of the best understood activation contexts of the JNK pathway. The TNF ligand of the pathway, Egr, was identified in 2002 as an orthologue of multiple members of the mammalian TNF gene family (Igaki et al., 2002; Moreno et al., 2002). Identification of the first *Drosophila* TNFR orthologue, Wgn, quickly followed (Kanda et al., 2002). It is thought that TNF-JNK signalling occurs primarily via interactions between activated TNFRs, the JNKKK kinase (JNKKKK) Misshapen (Msn), and the JNKKK Tak1, which are mediated by the adapter proteins TNF-receptor-associated factor 4 (Traf4), TNF-receptor-associated factor 6 (Traf6), and TAK1-associated binding protein 2 (Tab2) (**Figure 5**; reviewed in Igaki and Miura, 2014). The pathway then drives transcription via the canonical kinase core of Hep and Bsk, and TFs including the AP-1 complex members Kay and Jra – these effectors are, as we have discussed, primarily involved in mediating apoptosis as a response to cellular stresses, such as polarity-impairment, but can be co-opted into a role in tumourigenesis.

Recently, another *Drosophila* TNFR-encoding gene, *grnd*, was identified, and found to also play a role in the apoptosis of polarity-impaired cells, as well as in cooperative tumourigenesis (**Figure 5**; Andersen et al., 2015). It was found in a screen for genes necessary for neoplastic growth induced by knockdown of the endocytic gene *Syx7*, where most genes found to rescue tumourigenesis when disrupted were JNK pathway components (Andersen et al., 2015). Overexpression of *egr* in the adult eye results in cell death, which was rescued upon knockdown of *grnd*, but not of *wgn* (Andersen et al., 2015). It is thought that Grnd binds Egr, prevents its diffusion, and hence controls the autonomy of cell death – it was shown that wing imaginal disc clones overexpressing *egr* were eliminated via apoptosis, and co-expressing RNAi against *Tak1* prevented that autonomous cell death, but co-expressing RNAi against *grnd* prevented autonomous cell death while also promoting non-autonomous cell death (Andersen et al., 2015). Interestingly, proper identification of a classic *Drosophila* tumour suppressor gene, *lethal(2)tumorous imaginal discs*, as *ALG3, alpha-1,3- mannosyltransferase* (*Alg3*), has shed light on how Grnd might be regulated – *Alg3* mutants fail to glycosylate (and thus inactivate) Grnd, enabling persistent TNF-JNK signalling activation via Egr secreted by the fat body, which promotes JNK-mediated tissue overgrowth via SWH signalling inhibition and Yki activation (de Vreede et al., 2018). Furthermore, Grnd is likely to be involved in both polarity-impairment-induced cell competition and cooperative tumourigenesis – clones with *scrib* knockdown die, while those with knockdown of both *scrib* and *grnd* survive, and the invasiveness of $Ras85D^{V12}/scrib^{-/-}$ tumours is blocked via *grnd* knockdown, as is their overexpression of the JNK target, *Mmp1* (Andersen et al., 2015).

As we have discussed, there is some debate over how JNK signalling is activated in polarity-impaired cells – some studies implicate Egr as the key effector of the pathway (Igaki et al., 2009; Vidal, 2010), but others have suggested JNK signalling is initiated by direct activation of JNKKKs by molecules involved in cytoskeletal regulation, such as Rho1 (Ma et al., 2016; Muzzopappa et al., 2017). In this vein, one recent study has demonstrated a new method by which Egr can regulate polarity-impaired cell elimination. Knocking down *scrib* via RNAi in wing imaginal discs, within the *spalt major* expression domain, leads to large areas of polarity-impaired cells upregulating JNK signalling (Poernbacher and Vincent, 2018). Disrupting *egr* in those same cells was shown to only partially rescue the ectopic JNK signalling, while disrupting *grnd* or *adenosine receptor* (*AdoR*) completely rescued the ectopic JNK signalling (Poernbacher and Vincent, 2018). *AdoR* positively regulates JNK signalling when *scrib* is knocked down in various expression domains, and also in wholly $scrib^{-/-}$ imaginal discs (Poernbacher and Vincent, 2018). Researchers found that the activation of JNK signalling was likely due to an increase in extracellular adenosine secreted by the polarity-impaired cells stimulating AdoR activity, which was then also necessary for *egr* transcript upregulation (Poernbacher and Vincent, 2018).

Feedback Loops and ROS

An assortment of feedback loops involving JNK signalling have been identified in various contexts, allowing for persistent activation of the pathway. One of the key positive feedback loops identified occurs during apoptosis in response to stress, where death regulator Nedd2-like caspase (Dronc), an initiator caspase, is activated by and activates JNK signalling (Shlevkov and Morata, 2012; Rudrapatna et al., 2013). Other examples of positive feedback loops include when JNK signalling is activated due to signalling from the Src family members (Rudrapatna et al., 2014), and during $Ras85D^{V12}/scrib^{-/-}$ tumourigenesis when haemocyte recruitment and ROS production promote JNK signalling (Pérez et al., 2017). Another feedback loop was recently identified that stresses the importance of JNK signalling

activation in tumourigenesis progression, and also illustrates the stepwise process by which cooperative tumourigenesis can occur. Transient initiation of JNK signalling (via irradiation, *p53* expression, or activated *hep* (hep^{ACT}) expression) in cells where apoptosis was functional led to activity of the pathway gradually ceasing (Pinal et al., 2018). Conversely, where apoptosis was blocked (via $Ras85D^{V12}$ expression or apoptotic pathway component mutation) JNK signalling persisted, leading to overgrowth when $Ras85D^{V12}$ was expressed and upregulation of growth-promoting JNK targets such as the Wg and Jak-STAT signalling pathway ligands (Pinal et al., 2018). Researchers identified that the transient JNK signalling-induced ROS production, and the sustained JNK signalling in apoptosis-deficient cells was dependent on ROS production and the ROS-producing gene *moladietz*, itself a JNK signalling target, and hence a feedback loop was formed (Khan et al., 2017; Pinal et al., 2018). As we have mentioned, ROS production can also occur during CIN-induced tumourigenesis, where it is thought to activate JNK signalling via Ask1 activity (**Figure 5**; Muzzopappa et al., 2017).

SWH Signalling

We have discussed how JNK signalling can differentially regulate the SWH signalling pathway – upregulating Yki during compensatory proliferation and tumourigenesis (Doggett et al., 2011; Ohsawa et al., 2011; Sun and Irvine, 2011, 2013; Enomoto et al., 2015), and downregulating Yki during cell competition and tissue growth regulation (Doggett et al., 2011; Chen et al., 2012). However, it has also been recently shown that the opposite is possible – SWH signalling is capable of regulating JNK signalling. Yki/Sd activity was shown to promote tissue overgrowth, as well as *Rho1* transcription which, as we have discussed, is capable of then promoting JNK signalling – specifically, researchers found that Rho1 activated JNK signalling via Tak1 and Hep (**Figure 5**; Ma et al., 2015a). Interestingly, this interaction was only observed in the wing, and not eye-antennal, imaginal discs, suggesting it is context dependent (Ma et al., 2015a). Furthermore, Yki-mediated overgrowth was rescued by blocking JNK signalling, and was phenocopied via coupling Rho1 and p35 expression (promoting JNK signalling and blocking apoptosis) (Ma et al., 2015a). Conversely, it has also been demonstrated that activating SWH signalling, and hence blocking Yki, can lead to invasive behaviour, which is primarily governed by JNK signalling – indeed, JNK signalling was upregulated and responsible for the invasiveness (Ma et al., 2017). Mechanistically, researchers showed that the Yki target, *bantam* (a microRNA), suppresses *Rox8*, which acts as a positive regulator of JNK signalling, possibly via its role in downregulating *dlg1* (**Figure 5**; Ma et al., 2017). Therefore, an interesting regulatory situation occurs in the wing epithelium: SWH signalling inactivation promotes tissue growth via Yki-mediated activation of JNK signalling (Ma et al., 2015a), while SWH signalling activation promotes JNK-mediated invasiveness (Ma et al., 2017). Another interesting example of interaction between Yki and JNK signalling occurs during wound healing, a process JNK is well known to be involved in via its capacity as a regulator of cell movement and morphology (Lesch et al., 2010). Researchers found that Yki was required (alongside Sd) for wound closure in larval epidermal tissue not via its canonical roles in proliferation, but rather by regulating actin polymerisation (Tsai et al., 2017). Furthermore, they found that Yki activity during wound closure occurred independently of Pvr signalling, but likely acts parallel to or downstream of JNK signalling (Tsai et al., 2017).

Other Regulators

Lastly, while these previous examples highlight how JNK signalling can be activated due to certain signalling pathways, or as a result of different biological phenotypes, the pathway can also be induced or repressed by simple genetic lesions. As such, these mutations can potentially contribute significantly to tumourigenesis, and so we feel it is important to call attention to some of the more recently identified examples. JNK signalling can be activated by mutations in genes such as *jumeau* (*jumu*, a Fork head family TF) (Wang et al., 2019) or *pontin* (*pont*, member of the ATPases Associated with various cellular Activities (AAA+) family) (Wang et al., 2018), or by overexpression of genes such as *growth arrest and DNA damage-inducible 45* (*Gadd45*, orthologue of human *GADD45G*) (Camilleri-Robles et al., 2019). Other negative regulators of JNK signalling include the Striatin interacting phosphatase and kinase (STRIPAK) complex members, Connector of kinase to AP-1 (Cka) and Striatin interacting protein (Strip) – when JNK signalling is activated via Immune Deficiency (IMD) signalling, part of the *Drosophila* innate immune system (reviewed in Hoffmann, 2003; Kaneko and Silverman, 2005), these molecules act to suppress JNK pathway activity (Bond and Foley, 2009; Ashton-Beaucage et al., 2014). However, it has also been shown that mutating or knocking down *Cka* or *Strip* during *Drosophila* larval spermatogenesis induces JNK signalling via Egr, independently of IMD signalling, suggesting Cka and Strip may act more universally (La Marca et al., 2019). Conversely, JNK signalling can be inhibited by mutations in genes such as *deltex* (*dx*, a positive regulator of Notch signalling) (Dutta et al., 2018), *Glycine N-acyltransferase* (*Glyat*, orthologue of human GLYATL3) (Ren et al., 2017), and various members of the Toll (a.k.a. NF-κB) signalling pathway (Wu et al., 2015). Interestingly, while Toll signalling is necessary for JNK-mediated cell death (Wu et al., 2015), it is repressed in $scrib^{-/-}$ cell competition where, if activated, Toll signalling in $scrib^{-/-}$ cells then occurs alongside simultaneous activation of JNK signalling and accumulation of F-actin, which promotes Yki activity and tumourigenesis (Katsukawa et al., 2018). Some more unusual examples are genes that promote JNK signalling when overexpressed, but inhibit it when mutated, such as *licorne* (*lic*, orthologue of human *MAP2K6*) (Sun et al., 2019) or *tankyrase* (*Tnks*, encodes NAD(+) ADP-ribosyltransferase) (Feng et al., 2018).

In summary, a wide variety of activation contexts exist for JNK signalling, each of which seem to drive markedly different cellular behaviours and outcomes. Direct regulation of the

JNKKKs appears to be a key method for inducing different roles for the pathway, and occurs through mechanisms as diverse as actin cytoskeleton regulation and ROS production. The Rho-family GTPases are, in particular, granted a key role in these non-canonical activations, and the pathway is also capable of activating itself via a number of different feedback loops. Many more JNK-activating signals are doubtless waiting to be discovered.

CONCLUSION AND PERSPECTIVES

Jun N-terminal kinase signalling is a complex process. An intricate array of upstream signalling molecules feed into the activation of the single titular JNK in *Drosophila*, Bsk, which then activates an equally vast and detailed collection of downstream TFs and target genes. However, this highly conserved pathway is significantly more complex in mammals and, hence, the relative simplicity of JNK signalling in *Drosophila*, coupled with the powerful genetic techniques available to researchers using this model organism, means *Drosophila* has been (and will doubtless continue to be) an indispensable tool in uncovering the molecular basis for the two-faced nature of JNK: being both pro- and anti-tumourigenic. There has been a massive increase in our understanding of these processes over the last decade, which we have attempted to capture in this review. This final section will look at some of the future directions the field may take, as informed by a number of recent and unique explorations of JNK signalling.

While the upstream complexity of JNK signalling contributes to the power of the pathway to drive such varied outcomes, it is also an obstacle to obtaining a comprehensive understanding of its biological contributions. Further complications arise due to the possibility that components of the pathway are effecting roles unrelated to the central JNK signalling cascade. One such example has been shown for Egr – in tumourigenic tissue wholly mutant for *dlg1*, Egr secreted by attracted haemocytes sensitises the cells of the tumour to activity of the antimicrobial peptide Defensin, which promotes tumour cell death (Parvy et al., 2019). Though a role for JNK signalling in the process was not explicitly ruled out, the possibility of more JNK-unrelated roles for JNK pathway members lends itself to potential new avenues of research.

Alongside the various upstream actuators of JNK signalling, there is considerable potential to explore how the intensity of the JNK signal affects its pro- and anti-tumourigenic properties. As discussed, one recent study found that Cno overexpression led to JNK-mediated tissue overgrowth, but slightly modulating JNK signalling then led to massive overgrowth (Ma et al., 2019). The researchers determined that Cno overexpression upregulated both JNK and Ras-MAPK signalling, each of which downregulated SWH signalling to promote Yki-dependent tissue growth, and suggested that subsequent modulation of JNK signalling inhibited its anti-tumourigenic role in promoting apoptosis, while leaving its pro-tumourigenic role as a SWH pathway inhibitor intact (Ma et al., 2019). In a similar vein another recent study examined JNK signalling levels in response to tissue damage. It was shown that high levels of ROS produced in damaged tissue phosphorylated and activated Ask1 and, therefore, strong JNK signalling and apoptosis (Santabárbara-Ruiz et al., 2019). However, it was found that the ROS signal propagated to undamaged neighbouring tissue, and Ask1 was then phosphorylated by both the ROS signal and Akt1, a downstream protein kinase of the PI3K signalling pathway (Santabárbara-Ruiz et al., 2019). This altered activation context for Ask1 led to a lower level of JNK signal, which promoted cell proliferation and survival rather than apoptosis (Santabárbara-Ruiz et al., 2019). Both these studies are examples of the potential for altering JNK signalling levels to profoundly alter the outcome of the pathway, and are exemplars of an exciting new avenue of research regarding pro- and anti-tumourigenic JNK signalling.

The importance of subcellular localisation of JNK signalling components is also an area that is ripe for exploration. A critical role for endocytosis in JNK signalling has been demonstrated, with increased endocytosis thought to be key in upregulating the TNF-JNK signalling observed in *scrib*$^{-/-}$ clones (Igaki et al., 2009). Furthermore, another study has shown Rho1 specifically localised to the cell membrane can activate apoptosis-inducing JNK signalling that acts primarily via Slpr and Tak1 and, indeed, regulates the subcellular localisation of Slpr via physical interaction (Neisch et al., 2010).

The relationship between JNK and SWH signalling is, as yet, unresolved. There is clearly complex interplay between the pathways, highly dependent on cellular context, but its elucidation is critical for obtaining a more complete understanding of pro- and anti-tumourigenic JNK signalling. While recent research discussed in this review has undoubtedly advanced our knowledge greatly (Doggett et al., 2011; Sun and Irvine, 2011; Chen et al., 2012; Enomoto et al., 2015; Ma et al., 2015a, 2017; Gerlach et al., 2018), there is still much to be discovered, particularly with regard to how the pathways interact during cooperative tumourigenesis. This relationship between JNK and SWH signalling is undoubtedly one that will be examined closely in coming years.

There is a preponderance of different model systems used in the study of JNK signalling within *Drosophila* (e.g., different tissues and tissue regions, different mutant clones, different models of cooperative tumourigenesis). While this is certainly a great strength of the organism as a model, it is also a complicating factor, making it difficult to generate a cogent, unified model for JNK signalling (if this indeed exists). While the exploration of JNK signalling in a wide variety of contexts is undoubtedly beneficial, and should be encouraged and highlighted, we believe that a discussion regarding standardised systems in which observations regarding JNK signalling might be examined and replicated is worthwhile.

Finally, it is worth reiterating the relevance of *Drosophila* studies to explorations of mammalian genetics and disease. We have touched upon how JNK signalling has two faces in humans, as it does in flies – it can be both

pro- and anti-tumourigenic (or pro- and anti-survival), depending on the context (reviewed in Wagner and Nebreda, 2009; Wu et al., 2019). The inherently increased complexity of human JNK signalling makes the pathway difficult to work with, however, and this leaves *Drosophila* research at an advantage, able to use parallels between the highly conserved systems to position itself as a foundational body of knowledge for the field – conclusions drawn in flies can be adapted and extended into mammalian research. For example, we have discussed how Rho-family GTPases have emerged as key activators of JNK signalling in *Drosophila* (Garlena et al., 2010; Brumby et al., 2011; Khoo et al., 2013; Rudrapatna et al., 2014; Ma et al., 2016), and similar conclusions have been reached in mammals – *RAC1* gain-of-function mutations are common in *BRAF* and *NRAS*-driven melanomas, and said mutations can drive RAC1 binding to and activation of targets like PAK1 (p21 (RAC1) activated kinase 1) and MAP3K11 (mitogen-activated protein kinase kinase kinase 11, a.k.a. MLK3) (Krauthammer et al., 2012). Both PAK1 (Qing et al., 2012) and MAP3K11 (reviewed in Gallo and Johnson, 2002) have been shown to be activators of JNK signalling in mammals. Interestingly, while the *Drosophila* PAK1 orthologue, p21-activated kinase (Pak), is not known to act via JNK signalling (Conder et al., 2004), the orthologue of MAP3K11 is Slpr, thought to be the key JNKKK in cell morphological changes and embryogenesis processes like dorsal closure (reviewed in Ríos-Barrera and Riesgo-Escovar, 2013). Another study examining *BRAF*-driven melanoma found that ectopic JNK signalling via JUN was likely partly responsible for the invasiveness of the tumour cells (Ramsdale et al., 2015). As discussed, JUN is one half of the AP-1 TF complex, alongside FOS, which is conserved in *Drosophila*. Furthermore, pharmacologically inhibiting both BRAF and JNK signalling proved an effective way of suppressing invasiveness and increasing tumour cell death (Ramsdale et al., 2015). This example is clearly reminiscent of the invasive tumourigenesis seen when overactive Ras-MAPK and JNK signalling are coupled in *Drosophila*, as discussed throughout this review.

While a direct connection has not yet been made between JNK signalling research in *Drosophila* and the development of human cancer therapeutics, the JNK signalling pathway is clearly two-faced during tumourigenesis in both flies and humans (**Supplementary Table 2**), and therefore the extensive research generated in the fly model may serve to inform which types of human cancer types are likely to be JNK-dependent, in order to triage these patients for treatment with JNK pathway inhibitors. For example, genetic analyses of the *Drosophila* Ret oncogene (Ret) protein tyrosine kinase pathway revealed that the JNK pathway was anti-tumourigenic, which was paralleled in cases of the human Ret-driven cancer, multiple endocrine neoplasia type 2 (Read et al., 2005), thereby implying that targeting the JNK pathway in these cancers would not be beneficial. There has been considerable interest in developing drugs that target JNK signalling for use in the treatment of cancers (and other diseases), and some success has been obtained, but the pathway is so context dependent, with such a diverse array of targets and effectors, that determining how best to exploit the pathway pharmacologically can be difficult (reviewed in Messoussi et al., 2014; Cicenas, 2015; Cicenas et al., 2017). Nonetheless, research into *Drosophila* JNK signalling has, does, and will continue to support our understanding of JNK signalling in humans but, as it relates to cancer progression, more research is clearly needed. With the advent of transgenic RNAi (reviewed in Perrimon et al., 2010) and, more recently, CRISPR/Cas9 technology in *Drosophila* (reviewed in Housden and Perrimon, 2016; Bier et al., 2018), the generation of more sophisticated models of human cancer in flies has been possible, which can be used for chemical screening for anti-cancer compounds (Richardson et al., 2015; Sonoshita and Cagan, 2017; Cagan et al., 2019), a process already achieving promising results (Bangi et al., 2016, 2019). Similar methodologies using *Drosophila* as avatars for specific human cancers could be applied specifically to investigate whether the JNK pathway is pro- or anti-tumourigenic in particular contexts, and how it might be targeted to be beneficial therapeutically. Moreover, *Drosophila* JNK-dependent cancer models can be used in the development of JNK pathway inhibitors that are more bioavailable, and which have greater efficacy and lower toxicity, as has been achieved using a *Drosophila* model of Ret-driven cancer (Dar et al., 2012; Sonoshita et al., 2018; Ung et al., 2019). With the adoption of these new technologies, the *Drosophila* model still has much to offer toward the understanding and targeting of the JNK pathway in human cancers.

AUTHOR CONTRIBUTIONS

JL wrote the manuscript and prepared the figures. HR provided intellectual direction and editorial advice.

FUNDING

JL is supported by Australian Research Council (DP170102549) awarded to HR, who is supported by funding from the School of Molecular Sciences, La Trobe University.

ACKNOWLEDGMENTS

Apologies to all authors whose work we were unable to include in this review. Thanks to Sarah T. Diepstraten for assistance with figure preparation, as well as manuscript proofreading and suggestions. Thanks also to Natasha Fahey-Lozano and Marta Portela for manuscript proofreading and suggestions.

SUPPLEMENTARY MATERIAL

The Supplementary Material for this article can be found online at: https://www.frontiersin.org/articles/10.3389/fcell.2020.00042/full#supplementary-material

REFERENCES

Andersen, D. S., Colombani, J., Palmerini, V., Chakrabandhu, K., Boone, E., Röthlisberger, M., et al. (2015). The *Drosophila* TNF receptor Grindelwald couples loss of cell polarity and neoplastic growth. *Nature* 522, 482–486. doi: 10.1038/nature14298

Ashton-Beaucage, D., Udell, C. M., Gendron, P., Sahmi, M., Lefrançois, M., Baril, C., et al. (2014). A functional screen reveals an extensive layer of transcriptional and splicing control underlying RAS/MAPK signaling in *Drosophila*. *PLoS Biol.* 12:e1001809. doi: 10.1371/journal.pbio.1001809

Atkins, M., Potier, D., Romanelli, L., Jacobs, J., Mach, J., Hamaratoglu, F., et al. (2016). An ectopic network of transcription factors regulated by Hippo signaling drives growth and invasion of a malignant tumor model. *Curr. Biol.* 26, 2101–2113. doi: 10.1016/j.cub.2016.06.035

Bai, Z., Li, Z., and Xiao, W. (2018). *Drosophila* bendless catalyzes K63-linked polyubiquitination and is involved in the response to DNA damage. *Mutat. Res.* 808, 39–47. doi: 10.1016/j.mrfmmm.2018.02.003

Bangi, E., Ang, C., Smibert, P., Uzilov, A. V., Teague, A. G., Antipin, Y., et al. (2019). A personalized platform identifies trametinib plus zoledronate for a patient with KRAS-mutant metastatic colorectal cancer. *Sci. Adv.* 5:eaav6528. doi: 10.1126/sciadv.aav6528

Bangi, E., Murgia, C., Teague, A. G. S., Sansom, O. J., and Cagan, R. L. (2016). Functional exploration of colorectal cancer genomes using *Drosophila*. *Nat. Commun.* 7:13615. doi: 10.1038/ncomms13615

Beira, J. V., Springhorn, A., Gunther, S., Hufnagel, L., Pyrowolakis, G., and Vincent, J.-P. (2014). The Dpp/TGFβ-dependent corepressor Schnurri protects epithelial Cells from JNK-induced apoptosis in *Drosophila* embryos. *Dev. Cell* 31, 240–247. doi: 10.1016/j.devcel.2014.08.015

Beira, J. V., Torres, J., and Paro, R. (2018). Signalling crosstalk during early tumorigenesis in the absence of Polycomb silencing. *PLoS Genet.* 14:e1007187. doi: 10.1371/journal.pgen.1007187

Benhra, N., Barrio, L., Muzzopappa, M., and Milán, M. (2018). Chromosomal instability induces cellular invasion in epithelial tissues. *Dev. Cell* 47, 161–174. doi: 10.1016/j.devcel.2018.08.021

Bergmann, A., Agapite, J., McCall, K., and Steller, H. (1998). The *Drosophila* gene hid is a direct molecular target of Ras-dependent survival signaling. *Cell* 95, 331–341. doi: 10.1016/s0092-8674(00)81765-1

Bier, E., Harrison, M. M., O'Connor-Giles, K. M., and Wildonger, J. (2018). Advances in engineering the Fly genome with the CRISPR-Cas system. *Genetics* 208, 1–18. doi: 10.1534/genetics.117.1113

Bilder, D. (2004). Epithelial polarity and proliferation control: links from the *Drosophila* neoplastic tumor suppressors. *Genes Dev.* 18, 1909–1925. doi: 10.1101/gad.1211604

Bond, D., and Foley, E. (2009). A quantitative RNAi screen for JNK modifiers identifies Pvr as a novel regulator of *Drosophila* immune signaling. *PLoS Pathog.* 5:e1000655. doi: 10.1371/journal.ppat.1000655

Brumby, A. M., Goulding, K. R., Schlosser, T., Loi, S., Galea, R., Khoo, P., et al. (2011). Identification of novel Ras-Cooperating oncogenes in *Drosophila melanogaster*: a RhoGEF/Rho-family/JNK pathway is a central driver of tumorigenesis. *Genetics* 188, 105–125. doi: 10.1534/genetics.111.127910

Brumby, A. M., and Richardson, H. E. (2003). Scribble mutants cooperate with oncogenic Ras or Notch to cause neoplastic overgrowth in *Drosophila*. *EMBO J.* 22, 5769–5779. doi: 10.1093/emboj/cdg548

Brumby, A. M., and Richardson, H. E. (2005). Using *Drosophila melanogaster* to map human cancer pathways. *Nat. Rev. Cancer* 5, 626–639. doi: 10.1038/nrc1671

Bunker, B. D., Nellimoottil, T. T., Boileau, R. M., Classen, A. K., and Bilder, D. (2015). The transcriptional response to tumorigenic polarity loss in *Drosophila*. *eLife* 4:e03189. doi: 10.7554/eLife.03189

Cagan, R. L., Zon, L. I., and White, R. M. (2019). Modeling cancer with flies and fish. *Dev. Cell* 49, 317–324. doi: 10.1016/j.devcel.2019.04.013

Camilleri-Robles, C., Serras, F., and Corominas, M. (2019). Role of D-GADD45 in JNK-dependent apoptosis and regeneration in *Drosophila*. *Genes* 10, 378. doi: 10.3390/genes10050378

Casas-Tintó, S., Lolo, F.-N., and Moreno, E. (2015). Active JNK-dependent secretion of *Drosophila* Tyrosyl-tRNA synthetase by loser cells recruits haemocytes during cell competition. *Nat. Commun.* 6:10022. doi: 10.1038/ncomms10022

Chen, C.-L., Schroeder, M. C., Kango-Singh, M., Tao, C., and Halder, G. (2012). Tumor suppression by cell competition through regulation of the Hippo pathway. *Proc. Natl. Acad. Sci. U.S.A.* 109, 484–489. doi: 10.1073/pnas.1113882109

Cicenas, J. (2015). JNK inhibitors: is there a future? *MAP Kinase* 4:5700. doi: 10.4081/mk.2015.5700

Cicenas, J., Zalyte, E., Rimkus, A., Dapkus, D., Noreika, R., and Urbonavicius, S. (2017). JNK, p38, ERK, and SGK1 inhibitors in cancer. *Cancers* 10:E1. doi: 10.3390/cancers10010001

Conder, R., Yu, H., Ricos, M., Hing, H., Chia, W., Lim, L., et al. (2004). dPak is required for integrity of the leading edge cytoskeleton during *Drosophila* dorsal closure but does not signal through the JNK cascade. *Dev. Biol.* 276, 378–390. doi: 10.1016/j.ydbio.2004.08.044

Cong, B., Ohsawa, S., and Igaki, T. (2018). JNK and Yorkie drive tumor progression by generating polyploid giant cells in *Drosophila*. *Oncogene* 37, 3088–3097. doi: 10.1038/s41388-018-0201-8

Cordero, J. B., Macagno, J. P., Stefanatos, R. K., Strathdee, K. E., Cagan, R. L., and Vidal, M. (2010). Oncogenic Ras diverts a Host TNF tumor suppressor activity into tumor promoter. *Dev. Cell* 18, 999–1011. doi: 10.1016/j.devcel.2010.05.014

Cosolo, A., Jaiswal, J., Csordás, G., Grass, I., Uhlirova, M., and Classen, A.-K. (2019). JNK-dependent cell cycle stalling in G2 promotes survival and senescence-like phenotypes in tissue stress. *eLife* 8:e41036. doi: 10.7554/eLife.41036

Dar, A. C., Das, T. K., Shokat, K. M., and Cagan, R. L. (2012). Chemical genetic discovery of targets and anti-targets for cancer polypharmacology. *Nature* 486, 80–84. doi: 10.1038/nature11127

de Vreede, G., Morrison, H. A., Houser, A. M., Boileau, R. M., Andersen, D. S., Colombani, J., et al. (2018). A *Drosophila* tumor suppressor gene prevents tonic TNF signaling through receptor N-glycosylation. *Dev. Cell* 45, 595–605. doi: 10.1016/j.devcel.2018.05.012

Doggett, K., Grusche, F. A., Richardson, H. E., and Brumby, A. M. (2011). Loss of the *Drosophila* cell polarity regulator Scribbled promotes epithelial tissue overgrowth and cooperation with oncogenic Ras-Raf through impaired Hippo pathway signaling. *BMC Dev. Biol* 11:57. doi: 10.1186/1471-213X-11-57

Doggett, K., Turkel, N., Willoughby, L. F., Ellul, J., Murray, M. J., Richardson, H. E., et al. (2015). BTB-Zinc finger oncogenes are required for Ras and Notch-Driven tumorigenesis in *Drosophila*. *PLoS One* 10:e0132987. doi: 10.1371/journal.pone.0132987

Dutta, D., Singh, A., Paul, M. S., Sharma, V., Mutsuddi, M., and Mukherjee, A. (2018). Deltex interacts with Eiger and consequently influences the cell death in *Drosophila melanogaster*. *Cell. Signal.* 49, 17–29. doi: 10.1016/j.cellsig.2018.05.003

Enomoto, M., and Igaki, T. (2013). Src controls tumorigenesis via JNK-dependent regulation of the Hippo pathway in *Drosophila*. *EMBO Rep.* 14, 65–72. doi: 10.1038/embor.2012.185

Enomoto, M., Kizawa, D., Ohsawa, S., and Igaki, T. (2015). JNK signaling is converted from anti- to pro-tumor pathway by Ras-mediated switch of Warts activity. *Dev. Biol.* 403, 162–171. doi: 10.1016/j.ydbio.2015.05.001

Fahey-Lozano, N., La Marca, J. E., Portela, M., and Richardson, H. E. (2019). "Drosophila models of cell polarity and cell competition in tumourigenesis," in *Advances in Experimental Medicine and Biology – The Drosophila Model in Cancer*, ed. W.-M. Deng, (Cham: Springer Nature), 37–64.

Feng, Y., Li, Z., Lv, L., Du, A., Lin, Z., Ye, X., et al. (2018). Tankyrase regulates apoptosis by activating JNK signaling in *Drosophila*. *Biochem. Biophys. Res. Commun.* 503, 2234–2239. doi: 10.1016/j.bbrc.2018.06.143

Froldi, F., Ziosi, M., Garoia, F., Pession, A., Grzeschik, N. A., and Bellosta, P. (2010). The lethal giant larvae tumour suppressor mutation requires dMyc oncoprotein to promote clonal malignancy. *BMC Biol.* 8:33. doi: 10.1186/1741-7007-8-33

Gallo, K. A., and Johnson, G. L. (2002). Mixed-lineage kinase control of JNK and p38 MAPK pathways. *Nat. Rev. Mol. Cell Biol.* 3, 663–672. doi: 10.1038/nrm906

Garlena, R. A., Gonda, R. L., Green, A. B., Pileggi, R. M., and Stronach, B. (2010). Regulation of mixed-lineage kinase activation in JNK-dependent morphogenesis. *J. Cell Sci.* 123, 3177–3188. doi: 10.1242/jcs.063313

Gerlach, S. U., Eichenlaub, T., and Herranz, H. (2018). Yorkie and JNK control tumorigenesis in *Drosophila* Cells with cytokinesis failure. *Cell Rep.* 23, 1491–1503. doi: 10.1016/j.celrep.2018.04.006

Glise, B., Bourbon, H., and Noselli, S. (1995). Hemipterous encodes a novel *Drosophila* MAP kinase kinase, required for epithelial cell sheet movement. *Cell* 83, 451–461. doi: 10.1016/0092-8674(95)90123-X

Grzeschik, N. A., Parsons, L. M., and Richardson, H. E. (2010). Lgl, the SWH pathway and tumorigenesis: it's a matter of context and competition. *Cell Cycle* 9, 3222–3232. doi: 10.4161/cc.9.16.12633

Hanahan, D., and Weinberg, R. A. (2011). Hallmarks of cancer: the next generation. *Cell* 144, 646–674. doi: 10.1016/j.cell.2011.02.013

Harden, N. (2002). Signaling pathways directing the movement and fusion of epithelial sheets: lessons from dorsal closure in *Drosophila*. *Differentiation* 70, 181–203. doi: 10.1046/j.1432-0436.2002.700408.x

Hoffmann, J. A. (2003). The immune response of *Drosophila*. *Nature* 426, 33–38. doi: 10.1038/nature02021

Housden, B. E., and Perrimon, N. (2016). Cas9-Mediated genome engineering in *Drosophila melanogaster*. *Cold Spring Harb. Protoc.* 2016, 747–750. doi: 10.1101/pdb.top086843

Huang, C., Rajfur, Z., Borchers, C., Schaller, M. D., and Jacobson, K. (2003). JNK phosphorylates paxillin and regulates cell migration. *Nature* 424, 219–223. doi: 10.1038/nature01745

Igaki, T., Kanda, H., Yamamoto-Goto, Y., Kanuka, H., Kuranaga, E., Aigaki, T., et al. (2002). Eiger, a TNF superfamily ligand that triggers the *Drosophila* JNK pathway. *EMBO J.* 21, 3009–3018. doi: 10.1093/emboj/cdf306

Igaki, T., and Miura, M. (2014). The *Drosophila* TNF ortholog eiger: emerging physiological roles and evolution of the TNF system. *Semin. Immunol.* 26, 267–274. doi: 10.1016/j.smim.2014.05.003

Igaki, T., Pagliarini, R. A., and Xu, T. (2006). Loss of cell polarity drives tumor Growth and invasion through JNK activation in *Drosophila*. *Curr. Biol.* 16, 1139–1146. doi: 10.1016/j.cub.2006.04.042

Igaki, T., Pastor-Pareja, J. C., Aonuma, H., Miura, M., and Xu, T. (2009). Intrinsic tumor suppression and epithelial maintenance by endocytic activation of eiger/TNF signaling in *Drosophila*. *Dev. Cell* 16, 458–465. doi: 10.1016/j.devcel.2009.01.002

Ishimaru, S., Ueda, R., Hinohara, Y., Ohtani, M., and Hanafusa, H. (2004). PVR plays a critical role via JNK activation in thorax closure during *Drosophila metamorphosis*. *EMBO J.* 23, 3984–3994. doi: 10.1038/sj.emboj.7600417

Ji, T., Zhang, L., Deng, M., Huang, S., Wang, Y., and Pham, T. T. (2019). Dynamic MAPK signaling activity underlies a transition from growth arrest to proliferation in *Drosophila* scribble mutant tumors. *Dis. Mod. Mech.* 12:040147. doi: 10.1242/dmm.040147

Kanda, H., Igaki, T., Kanuka, H., Yagi, T., and Miura, M. (2002). Wengen, a member of the *Drosophila* tumor necrosis factor receptor superfamily, is required for eiger signaling. *J. Biol. Chem.* 277, 28372–28375. doi: 10.1074/jbc.C200324200

Kaneko, T., and Silverman, N. (2005). Bacterial recognition and signalling by the *Drosophila* IMD pathway. *Cell. Microbiol.* 7, 461–469. doi: 10.1111/j.1462-5822.2005.00504.x

Katsukawa, M., Ohsawa, S., Zhang, L., Yan, Y., and Igaki, T. (2018). Serpin facilitates tumor-suppressive cell competition by blocking toll-mediated Yki activation in *Drosophila*. *Curr. Biol.* 28, 1756–1767. doi: 10.1016/j.cub.2018.04.022

Khan, S. J., Abidi, S. N. F., Skinner, A., Tian, Y., and Smith-Bolton, R. K. (2017). The *Drosophila* Duox maturation factor is a key component of a positive feedback loop that sustains regeneration signaling. *PLoS Genet.* 13:e1006937. doi: 10.1371/journal.pgen.1006937

Khoo, P., Allan, K., Willoughby, L., Brumby, A. M., and Richardson, H. E. (2013). In *Drosophila*, RhoGEF2 cooperates with activated Ras in tumorigenesis through a pathway involving Rho1-Rok-Myosin-II and JNK signalling. *Dis. Mod. Mech.* 6, 661–678. doi: 10.1242/dmm.010066

Krauthammer, M., Kong, Y., Ha, B. H., Evans, P., Bacchiocchi, A., and McCusker, J. P. (2012). Exome sequencing identifies recurrent somatic RAC1 mutations in melanoma. *Nat. Genet.* 44, 1006–1014. doi: 10.1038/ng.2359

Külshammer, E., Mundorf, J., Kilinc, M., Frommolt, P., Wagle, P., and Uhlirova, M. (2015). Interplay among *Drosophila* transcription factors Ets21c, Fos and Ftz-F1 drives JNK-mediated tumor malignancy. *Dis. Mod. Mech.* 8, 1279–1293. doi: 10.1242/dmm.020719

Külshammer, E., and Uhlirova, M. (2013). The actin cross-linker Filamin/Cheerio mediates tumor malignancy downstream of JNK signaling. *J. Cell Sci.* 126, 927–938. doi: 10.1242/jcs.114462

Kurada, P., and White, K. (1998). Ras promotes cell survival in *Drosophila* by downregulating hid expression. *Cell* 95, 319–329. doi: 10.1016/s0092-8674(00)81764-x

La Marca, J. E., Diepstraten, S. T., Hodge, A. L., Wang, H., Hart, A. H., Richardson, H. E., et al. (2019). Strip and Cka negatively regulate JNK signalling during *Drosophila* spermatogenesis. *Development* 146:dev174292. doi: 10.1242/dev.174292

Leong, G. R., Goulding, K. R., Amin, N., Richardson, H. E., and Brumby, A. M. (2009). Scribble mutants promote aPKC and JNK-dependent epithelial neoplasia independently of Crumbs. *BMC Biol.* 7:62. doi: 10.1186/1741-7007-7-62

Lesch, C., Jo, J., Wu, Y., Fish, G. S., and Galko, M. J. (2010). A Targeted UAS-RNAi screen in *Drosophila* larvae identifies wound closure genes regulating distinct cellular processes. *Genetics* 186, 943–957. doi: 10.1534/genetics.110.121822

Li, M., Sun, S., Priest, J., Bi, X., and Fan, Y. (2019). Characterization of TNF-induced cell death in *Drosophila* reveals caspase- and JNK-dependent necrosis and its role in tumor suppression. *Cell Death Dis.* 10:613. doi: 10.1038/s41419-019-1862-0

Llense, F., and Martín-Blanco, E. (2008). JNK signaling controls border cell cluster integrity and collective cell migration. *Curr. Biol.* 18, 538–544. doi: 10.1016/j.cub.2008.03.029

Luo, X., Puig, O., Hyun, J., Bohmann, D., and Jasper, H. (2007). Foxo and Fos regulate the decision between cell death and survival in response to UV irradiation. *EMBO J.* 26, 380–390. doi: 10.1038/sj.emboj.7601484

Ma, X., Chen, Y., Xu, W., Wu, N., Li, M., Cao, Y., et al. (2015a). Impaired Hippo signaling promotes Rho1–JNK-dependent growth. *Proc. Natl. Acad. Sci. U.S.A.* 112, 1065–1070. doi: 10.1073/pnas.1415020112

Ma, X., Chen, Y., Zhang, S., Xu, W., Shao, Y., Yang, Y., et al. (2016). Rho1–Wnd signaling regulates loss-of-cell polarity-induced cell invasion in *Drosophila*. *Oncogene* 35, 846–855. doi: 10.1038/onc.2015.137

Ma, X., Shao, Y., Zheng, H., Li, M., Li, W., and Xue, L. (2013a). Src42A modulates tumor invasion and cell death via Ben/dUev1a-mediated JNK activation in *Drosophila*. *Cell Death Dis.* 4:e864. doi: 10.1038/cddis.2013.392

Ma, X., Xu, W., Zhang, D., Yang, Y., Li, W., and Xue, L. (2015b). Wallenda regulates JNK-mediated cell death in *Drosophila*. *Cell Death Dis.* 6:e1737. doi: 10.1038/cddis.2015.111

Ma, X., Yang, L., Yang, Y., Li, M., Li, W., and Xue, L. (2013b). dUev1a modulates TNF-JNK mediated tumor progression and cell death in *Drosophila*. *Dev. Biol.* 380, 211–221. doi: 10.1016/j.ydbio.2013.05.013

Ma, X., Wang, H., Ji, J., Xu, W., Sun, Y., Li, W., et al. (2017). Hippo signaling promotes JNK-dependent cell migration. *Proc. Natl. Acad. Sci. U.S.A.* 114, 1934–1939. doi: 10.1073/pnas.1621359114

Ma, Z., Li, P., Hu, X., and Song, H. (2019). Polarity protein Canoe mediates overproliferation via modulation of JNK, Ras-MAPK and Hippo signalling. *Cell Prolif.* 52:e12529. doi: 10.1111/cpr.12529

Martín, F. A., Pérez-Garijo, A., and Morata, G. (2009). Apoptosis in *Drosophila*: compensatory proliferation and undead cells. *Int. J. Dev. Biol.* 53, 1341–1347. doi: 10.1387/ijdb.072447fm

Mathieu, J., Sung, H.-H., Pugieux, C., Soetaert, J., and Rorth, P. (2007). A sensitized piggybac-based screen for regulators of border cell migration in *Drosophila*. *Genetics* 176, 1579–1590. doi: 10.1534/genetics.107.071282

Melani, M., Simpson, K. J., Brugge, J. S., and Montell, D. (2008). Regulation of cell adhesion and collective cell migration by hindsight and its human homolog RREB1. *Curr. Biol.* 18, 532–537. doi: 10.1016/j.cub.2008.03.024

Menéndez, J., Pérez-Garijo, A., Calleja, M., and Morata, G. (2010). A tumor-suppressing mechanism in *Drosophila* involving cell competition and the Hippo pathway. *Proc. Natl. Acad. Sci. U.S.A.* 107, 14651–14656. doi: 10.1073/pnas.1009376107

Messoussi, A., Feneyrolles, C., Bros, A., Deroide, A., Daydé-Cazals, B., Chevé, G., et al. (2014). Recent progress in the design, study, and development of c-Jun N-terminal kinase inhibitors as anticancer agents. *Chem. Biol.* 21, 1433–1443. doi: 10.1016/j.chembiol.2014.09.007

Misra, J. R., and Irvine, K. D. (2018). The Hippo signaling network and Its biological functions. *Annu. Rev. Genet.* 52, 65–87. doi: 10.1146/annurev-genet-120417-031621

Montell, D. J., Yoon, W. H., and Starz-Gaiano, M. (2012). Group choreography: mechanisms orchestrating the collective movement of border cells. *Nat. Rev. Mol. Cell Biol.* 13, 631–645. doi: 10.1038/nrm3433

Moreno, E., Yan, M., and Basler, K. (2002). Evolution of TNF signaling mechanisms: JNK-dependent apoptosis triggered by eiger, the *Drosophila* homolog of the TNF superfamily. *Curr. Biol.* 12, 1263–1268. doi: 10.1016/S0960-9822(02)00954-5

Muzzopappa, M., Murcia, L., and Milán, M. (2017). Feedback amplification loop drives malignant growth in epithelial tissues. *Proc. Natl. Acad. Sci. U.S.A.* 114, 7291–7300. doi: 10.1073/pnas.1701791114

Nakamura, M., Ohsawa, S., and Igaki, T. (2014). Mitochondrial defects trigger proliferation of neighbouring cells via a senescence-associated secretory phenotype in *Drosophila*. *Nat. Commun.* 5:5264. doi: 10.1038/ncomms6264

Neisch, A. L., Speck, O., Stronach, B., and Fehon, R. G. (2010). Rho1 regulates apoptosis via activation of the JNK signaling pathway at the plasma membrane. *J. Cell Biol.* 189, 311–323. doi: 10.1083/jcb.200912010

Nüsslein-Volhard, C., Wieschaus, E., and Kluding, H. (1984). Mutations affecting the pattern of the larval cuticle in *Drosophila melanogaster*. *Roux. Arch. Dev. Biol.* 193, 267–282. doi: 10.1007/BF00848156

Ohsawa, S. (2019). Elimination of oncogenic cells that regulate epithelial homeostasis in *Drosophila*. *Dev. Growth Differ.* 61, 337–342. doi: 10.1111/dgd.12604

Ohsawa, S., Sato, Y., Enomoto, M., Nakamura, M., Betsumiya, A., and Igaki, T. (2012). Mitochondrial defect drives non-autonomous tumour progression through Hippo signalling in *Drosophila*. *Nature* 490, 547–551. doi: 10.1038/nature11452

Ohsawa, S., Sugimura, K., Takino, K., Xu, T., Miyawaki, A., and Igaki, T. (2011). Elimination of oncogenic neighbors by JNK-mediated engulfment in *Drosophila*. *Dev. Cell* 20, 315–328. doi: 10.1016/j.devcel.2011.02.007

Pagliarini, R. A., and Xu, T. (2003). A genetic screen in *Drosophila* for metastatic behavior. *Science* 302, 1227–1231. doi: 10.1126/science.1088474

Parvy, J.-P., Yu, Y., Dostalova, A., Kondo, S., Kurjan, A., and Bulet, P. (2019). The antimicrobial peptide defensin cooperates with tumour necrosis factor to drive tumour cell death in *Drosophila*. *eLife* 8:e45061. doi: 10.7554/eLife.45061

Pastor-Pareja, J. C., Grawe, F., Martìn-Blanco, E., and Garcìa-Bellido, A. (2004). Invasive cell behavior during *Drosophila* imaginal disc eversion is mediated by the JNK signaling cascade. *Dev. Cell* 7, 387–399. doi: 10.1016/j.devcel.2004.07.022

Pastor-Pareja, J. C., Wu, M., and Xu, T. (2008). An innate immune response of blood cells to tumors and tissue damage in *Drosophila*. *Dis. Mod. Mech.* 1, 144–154. doi: 10.1242/dmm.000950

Paul, M. S., Singh, A., Dutta, D., Mutsuddi, M., and Mukherjee, A. (2018). Notch signals modulate lgl mediated tumorigenesis by the activation of JNK signaling. *BMC Res. Notes* 11:247. doi: 10.1186/s13104-018-3350-5

Pérez, E., Lindblad, J. L., and Bergmann, A. (2017). Tumor-promoting function of apoptotic caspases by an amplification loop involving ROS, macrophages and JNK in *Drosophila*. *eLife* 6:e26747. doi: 10.7554/eLife.26747

Pérez-Garijo, A., Fuchs, Y., and Steller, H. (2013). Apoptotic cells can induce non-autonomous apoptosis through the TNF pathway. *eLife* 2:e01004. doi: 10.7554/eLife.01004

Pérez-Garijo, A., Martín, F. A., and Morata, G. (2004). Caspase inhibition during apoptosis causes abnormal signalling and developmental aberrations in *Drosophila*. *Development* 131, 5591–5598. doi: 10.1242/dev.01432

Perrimon, N., Ni, J.-Q., and Perkins, L. (2010). In vivo RNAi: today and tomorrow. *Cold Spring Harb. Perspect. Biol.* 2:a003640. doi: 10.1101/cshperspect.a003640

Petzoldt, A. G., Gleixner, E. M., Fumagalli, A., Vaccari, T., and Simons, M. (2013). Elevated expression of the V-ATPase C subunit triggers JNK-dependent cell invasion and overgrowth in a *Drosophila* epithelium. *Dis. Mod. Mech.* 6, 689–700. doi: 10.1242/dmm.010660

Pinal, N., Martín, M., Medina, I., and Morata, G. (2018). Short-term activation of the Jun N-terminal kinase pathway in apoptosis-deficient cells of *Drosophila* induces tumorigenesis. *Nat. Commun.* 9:1541. doi: 10.1038/s41467-018-04000-6

Poernbacher, I., and Vincent, J.-P. (2018). Epithelial cells release adenosine to promote local TNF production in response to polarity disruption. *Nat. Commun.* 9:4675. doi: 10.1038/s41467-018-07114-z

Poon, C. L. C., Brumby, A. M., and Richardson, H. E. (2018). Src cooperates with oncogenic Ras in tumourigenesis via the JNK and PI3K pathways in *Drosophila* epithelial tissue. *Int. J. Mol. Sci.* 19:1585. doi: 10.3390/ijms19061585

Portela, M., Venkataramani, V., Fahey-Lozano, N., Seco, E., Losada-Perez, M., Winkler, F., et al. (2019). Glioblastoma cells vampirize WNT from neurons and trigger a JNK/MMP signaling loop that enhances glioblastoma progression and neurodegeneration. *PLoS Biol.* 17:e3000545. doi: 10.1371/journal.pbio.3000545

Qing, H., Gong, W., Che, Y., Wang, X., Peng, L., and Liang, Y. (2012). PAK1-dependent MAPK pathway activation is required for colorectal cancer cell proliferation. *Tumor Biol.* 33, 985–994. doi: 10.1007/s13277-012-0327-1

Ramsdale, R., Jorissen, R. N., Li, F. Z., Al-Obaidi, S., Ward, T., Sheppard, K. E., et al. (2015). The transcription cofactor c-JUN mediates phenotype switching and BRAF inhibitor resistance in melanoma. *Sci. Signal.* 8:ra82. doi: 10.1126/scisignal.aab1111

Read, R. D., Cavenee, W. K., Furnari, F. B., and Thomas, J. B. (2009). A *Drosophila* model for EGFR-Ras and PI3K-dependent human glioma. *PLoS Genet.* 5:e1000374. doi: 10.1371/journal.pgen.1000374

Read, R. D., Goodfellow, P. J., Mardis, E. R., Novak, N., Armstrong, J. R., and Cagan, R. L. (2005). A *Drosophila* model of multiple endocrine neoplasia type 2. *Genetics* 171, 1057–1081. doi: 10.1534/genetics.104.038018

Ren, P., Li, W., and Xue, L. (2017). GLYAT regulates JNK-mediated cell death in *Drosophila*. *Sci. Rep.* 7:5183. doi: 10.1038/s41598-017-05482-y

Richardson, H. E., and Portela, M. (2018). Modelling cooperative tumorigenesis in *Drosophila*. *BioMed Res. Int.* 2018:4258387. doi: 10.1155/2018/4258387

Richardson, H. E., Willoughby, L., and Humbert, P. O. (2015). "Screening for anti-cancer drugs in *Drosophila*," in *Encyclopedia of Life Sciences*. Chichester: John Wiley & Sons, Ltd.

Riesgo-Escovar, J. R., Jenni, M., Fritz, A., and Hafen, E. (1996). The *Drosophila* Jun-N-terminal kinase is required for cell morphogenesis but not for DJun-dependent cell fate specification in the eye. *Genes Dev.* 10, 2759–2768. doi: 10.1101/gad.10.21.2759

Ríos-Barrera, L. D., and Riesgo-Escovar, J. R. (2013). Regulating cell morphogenesis: the *Drosophila* Jun N-terminal kinase pathway. *Genesis* 51, 147–162. doi: 10.1002/dvg.22354

Rudrapatna, V. A., Bangi, E., and Cagan, R. L. (2013). Caspase signalling in the absence of apoptosis drives Jnk-dependent invasion. *EMBO Rep.* 14, 172–177. doi: 10.1038/embor.2012.217

Rudrapatna, V. A., Bangi, E., and Cagan, R. L. (2014). A Jnk-Rho-Actin remodeling positive feedback network directs Src-driven invasion. *Oncogene* 33, 2801–2806. doi: 10.1038/onc.2013.232

Ryoo, H. D., Gorenc, T., and Steller, H. (2004). Apoptotic cells can induce compensatory cell proliferation through the JNK and the wingless signaling pathways. *Dev. Cell* 7, 491–501. doi: 10.1016/j.devcel.2004.08.019

Santabárbara-Ruiz, P., Esteban-Collado, J., Pérez, L., Viola, G., Abril, J. F., Milán, M., et al. (2019). Ask1 and Akt act synergistically to promote ROS-dependent regeneration in *Drosophila*. *PLoS Genet.* 15:e1007926. doi: 10.1371/journal.pgen.1007926

Schroeder, M. C., Chen, C.-L., Gajewski, K., and Halder, G. (2013). A non-cell-autonomous tumor suppressor role for Stat in eliminating oncogenic scribble cells. *Oncogene* 32, 4471–4479. doi: 10.1038/onc.2012.476

Sekine, Y., Hatanaka, R., Watanabe, T., Sono, N., Iemura, S., Natsume, T., et al. (2012). The kelch repeat protein KLHDC10 regulates oxidative stress-induced ASK1 activation by suppressing PP5. *Mol. Cell* 48, 692–704. doi: 10.1016/j.molcel.2012.09.018

Shlevkov, E., and Morata, G. (2012). A dp53/JNK-dependant feedback amplification loop is essential for the apoptotic response to stress in *Drosophila*. *Cell Death Differ.* 19, 451–460. doi: 10.1038/cdd.2011.113

Sluss, H. K., Han, Z., Barrett, T., Davis, R. J., and Ip, Y. T. (1996). A JNK signal transduction pathway that mediates morphogenesis and an immune response in *Drosophila*. *Genes Dev.* 10, 2745–2758. doi: 10.1101/gad.10.21.2745

Sonoshita, M., and Cagan, R. L. (2017). "Modeling human cancers in *Drosophila*," in *Current Topics in Developmental Biology*, ed. L. Pick, (Cambridge, MA: Academic Press), 287–309.

Sonoshita, M., Scopton, A. P., Ung, P. M. U., Murray, M. A., Silber, L., Maldonado, A. Y., et al. (2018). A whole-animal platform to advance a clinical kinase inhibitor into new disease space. *Nat. Chem. Biol.* 14, 291–298. doi: 10.1038/nchembio.2556

Srivastava, A., Pastor-Pareja, J. C., Igaki, T., Pagliarini, R. A., and Xu, T. (2007). Basement membrane remodeling is essential for *Drosophila* disc eversion and

tumor invasion. *Proc. Natl. Acad. Sci. U.S.A.* 104, 2721–2726. doi: 10.1073/pnas.0611666104

Sun, G., and Irvine, K. D. (2011). Regulation of Hippo signaling by Jun kinase signaling during compensatory cell proliferation and regeneration, and in neoplastic tumors. *Dev. Biol.* 350, 139–151. doi: 10.1016/j.ydbio.2010.11.036

Sun, G., and Irvine, K. D. (2013). Ajuba family proteins Link JNK to Hippo signaling. *Sci. Signal.* 6:ra81. doi: 10.1126/scisignal.2004324

Sun, Y., Zhang, D., Li, C., Huang, J., Li, W., Qiu, Y., et al. (2019). Lic regulates JNK-mediated cell death in *Drosophila*. *Cell Prolif.* 52:e12593. doi: 10.1111/cpr.12593

Takino, K., Ohsawa, S., and Igaki, T. (2014). Loss of Rab5 drives non-autonomous cell proliferation through TNF and Ras signaling in *Drosophila*. *Dev. Biol.* 395, 19–28. doi: 10.1016/j.ydbio.2014.09.003

Tamori, Y., Bialucha, C. U., Tian, A.-G., Kajita, M., Huang, Y.-C., Norman, M., et al. (2010). Involvement of Lgl and mahjong/VprBP in cell competition. *PLoS Biol.* 8:e1000422. doi: 10.1371/journal.pbio.1000422

Tamori, Y., and Deng, W.-M. (2017). Tissue-intrinsic tumor hotspots: terroir for tumorigenesis. *Trends Cancer* 3, 259–268. doi: 10.1016/j.trecan.2017.03.003

Tepass, U. (2012). The apical polarity protein network in *Drosophila* epithelial cells: regulation of polarity, junctions, morphogenesis, cell growth, and survival. *Annu. Rev. Cell Dev. Biol.* 28, 655–685. doi: 10.1146/annurev-cellbio-092910-154033

Tsai, C.-R., Anderson, A. E., Burra, S., Jo, J., and Galko, M. J. (2017). Yorkie regulates epidermal wound healing in *Drosophila* larvae independently of cell proliferation and apoptosis. *Dev. Biol.* 427, 61–71. doi: 10.1016/j.ydbio.2017.05.006

Uhlirova, M., and Bohmann, D. (2006). JNK- and Fos-regulated Mmp1 expression cooperates with Ras to induce invasive tumors in *Drosophila*. *EMBO J.* 25, 5294–5304. doi: 10.1038/sj.emboj.7601401

Uhlirova, M., Jasper, H., and Bohmann, D. (2005). Non-cell-autonomous induction of tissue overgrowth by JNK/Ras cooperation in a *Drosophila* tumor model. *Proc. Natl. Acad. Sci. U.S.A.* 102, 13123–13128. doi: 10.1073/pnas.0504170102

Ung, P. M. U., Sonoshita, M., Scopton, A. P., Dar, A. C., Cagan, R. L., and Schlessinger, A. (2019). Integrated computational and *Drosophila* cancer model platform captures previously unappreciated chemicals perturbing a kinase network. *PLoS Comput. Biol.* 15:e1006878. doi: 10.1371/journal.pcbi.1006878

Vaughen, J., and Igaki, T. (2016). Slit-Robo repulsive signaling extrudes tumorigenic cells from epithelia. *Dev. Cell* 39, 683–695. doi: 10.1016/j.devcel.2016.11.015

Vidal, M. (2010). The dark side of fly TNF. *Cell Cycle* 9, 3851–3856. doi: 10.4161/cc.9.19.13280

Wagner, E. F., and Nebreda, ÁR. (2009). Signal integration by JNK and p38 MAPK pathways in cancer development. *Nat. Rev. Cancer* 9, 537–549. doi: 10.1038/nrc2694

Wang, C.-W., Purkayastha, A., Jones, K. T., Thaker, S. K., and Banerjee, U. (2016). In vivo genetic dissection of tumor growth and the Warburg effect. *eLife* 5:e18126. doi: 10.7554/eLife.18126

Wang, X., Huang, X., Wu, C., and Xue, L. (2018). Pontin/Tip49 negatively regulates JNK-mediated cell death in *Drosophila*. *Cell Death Dis.* 4:74. doi: 10.1038/s41420-018-0074-1

Wang, X. C., Liu, Z., and Jin, L. H. (2019). *Drosophila* jumu modulates apoptosis via a JNK-dependent pathway and is required for other processes in wing development. *Apoptosis* 24, 465–477. doi: 10.1007/s10495-019-01527-x

Willsey, H. R., Zheng, X., Pastor-Pareja, J. C., Willsey, A. J., Beachy, P. A., and Xu, T. (2016). Localized JNK signaling regulates organ size during development. *eLife* 5:e11491. doi: 10.7554/eLife.11491

Woodfield, S. E., Graves, H. K., Hernandez, J. A., and Bergmann, A. (2013). De-regulation of JNK and JAK/STAT signaling in ESCRT-II mutant tissues cooperatively contributes to neoplastic tumorigenesis. *PLoS One* 8:e56021. doi: 10.1371/journal.pone.0056021

Wu, C., Chen, C., Dai, J., Zhang, F., Chen, Y., and Li, W. (2015). Toll pathway modulates TNF-induced JNK-dependent cell death in *Drosophila*. *Open Biol.* 5:140171. doi: 10.1098/rsob.140171

Wu, M., Pastor-Pareja, J. C., and Xu, T. (2010). Interaction between RasV12 and scribbled clones induces tumour growth and invasion. *Nature* 463, 545–548. doi: 10.1038/nature08702

Wu, Q., Wu, W., Fu, B., Shi, L., Wang, X., and Kuca, K. (2019). JNK signaling in cancer cell survival. *Med. Res. Rev.* 39, 2082–2104. doi: 10.1002/med.21574

Yamamoto, M., Ohsawa, S., Kunimasa, K., and Igaki, T. (2017). The ligand Sas and its receptor PTP10D drive tumour-suppressive cell competition. *Nature* 542, 246–250. doi: 10.1038/nature21033

Yang, S.-A., Portilla, J.-M., Mihailovic, S., Huang, Y.-C., and Deng, W.-M. (2019). Oncogenic notch triggers neoplastic tumorigenesis in a transition-zone-like tissue microenvironment. *Dev. Cell* 49, 461–472. doi: 10.1016/j.devcel.2019.03.015

Zhang, S., Guo, X., Wu, H., Sun, Y., Ma, X., Li, J., et al. (2019). Wingless modulates activator protein-1-mediated tumor invasion. *Oncogene* 38, 3871–3885. doi: 10.1038/s41388-018-0629-x

Conflict of Interest: The authors declare that the research was conducted in the absence of any commercial or financial relationships that could be construed as a potential conflict of interest.

frontiers in Cell and Developmental Biology

MINI REVIEW
published: 13 February 2020
doi: 10.3389/fcell.2020.00041

Molecular Mechanisms of Radiation-Induced Cancer Cell Death: A Primer

Joseph Sia[1,2,3], *Radoslaw Szmyd*[4,6], *Eric Hau*[5,6] *and Harriet E. Gee*[5,6]*

[1] Department of Radiation Oncology, Peter MacCallum Cancer Centre, Melbourne, VIC, Australia, [2] Division of Cancer Research, Peter MacCallum Cancer Centre, Melbourne, VIC, Australia, [3] Sir Peter MacCallum Department of Oncology, The University of Melbourne, Melbourne, VIC, Australia, [4] Children's Medical Research Institute, Sydney, NSW, Australia, [5] The University of Sydney, Sydney, NSW, Australia, [6] Sydney West Radiation Oncology Network, Sydney, NSW, Australia

Radiation therapy (RT) is responsible for at least 40% of cancer cures, however treatment resistance remains a clinical problem. There have been recent advances in understanding the molecular mechanisms of radiation-induced cell death. The type of cell death after radiation depends on a number of factors including cell type, radiation dose and quality, oxygen tension, *TP53* status, DNA repair capacity, cell cycle phase at time of radiation exposure, and the microenvironment. Mitotic catastrophe (a pathway preceding cell death that happens in mitosis or as a consequence of aberrant mitotic progression) is the primary context of radiation-induced cell death in solid cancers, although in a small subset of cancers such as haematopoietic malignancies, radiation results in immediate interphase apoptosis, occurring within hours after exposure. There is intense therapeutic interest in using stereotactic ablative body radiotherapy (SABR), a precise, high-dose form of RT given in a small number of fractions, to prime the immune system for cancer cell killing, but the optimal radiation dose and fractionation remain unclear. Additionally, promising novel radiosensitisers targeting the cell cycle and DNA repair pathways are being trialled. In the context of the increasing use of SABR and such novel agents in the clinic, we provide an updated primer on the major types of radiation-induced cell death, focussing on their molecular mechanisms, factors affecting their initiation, and their implications on immunogenicity.

Keywords: radiotherapy, radiation therapy, stereotactic ablative radiotherapy, cell death, immunogenic cell death, abscopal effect

OPEN ACCESS

Edited by:
Andrew Burgess,
Anzac Research Institute, Australia

Reviewed by:
Brian Gabrielli,
The University of Queensland, Australia
Suneil Jain,
Queen's University Belfast, United Kingdom

***Correspondence:**
Harriet E. Gee
harriet.gee@sydney.edu.au;
Harriet.Gee@health.nsw.gov.au

Specialty section:
This article was submitted to Cell Growth and Division, a section of the journal Frontiers in Cell and Developmental Biology

Received: *14 November 2019*
Accepted: *17 January 2020*
Published: *13 February 2020*

Citation:
Sia J, Szmyd R, Hau E and Gee HE (2020) Molecular Mechanisms of Radiation-Induced Cancer Cell Death: A Primer. Front. Cell Dev. Biol. 8:41. doi: 10.3389/fcell.2020.00041

INTRODUCTION

Radiation therapy (RT) is a major cancer treatment modality and is responsible for at least 40% of cancer cures (Ringborg et al., 2003), yet treatment resistance remains a clinical problem. A primary reason for this is the capacity for cancer cells to evade radiation-induced cell death. Treatment paradigms have traditionally viewed cancer as a cell-autonomous problem of dysregulated proliferation while side-lining host-tumour interactions, but this dogma has undergone a remarkable revolution in the last few decades, with increasing appreciation of the tumour stroma and immune milieu in shaping tumour evolution. Trials of novel radiosensitisers targeting not only key cell death pathways but also the stromal and immune microenvironment, particularly together with stereotactic ablative body radiotherapy (SABR), have gained intense interest.

Here, we provide an updated primer on the major types of radiation-induced cell death, focussing on their molecular mechanisms, factors affecting their initiation, and their implications

on immunogenicity. We conclude with discussing these aspects in the context of the increasing use of SABR and novel agents in the clinic. We point readers interested in further detail to the excellent referenced reviews.

THE CELL CYCLE AND TYPES OF RADIATION-INDUCED CELL DEATH

The cell cycle is a highly regulated process occurring in two major phases: interphase (consisting of the G1, S, and G2 phases) and mitosis (cell division). During interphase, the cell grows its organelle counts (G1 phase), copies its DNA (S phase), and reorganises contents in preparation for division (G2 phase). Radiation-induced DNA damage is sensed by the kinases ataxia-telangiectasia mutated (ATM) and ataxia-telangiectasia and Rad3-related protein (ATR), which activate downstream proteins to initiate the DNA damage response (reviewed in Maier et al., 2016). This places the cell into cell cycle arrest, during which DNA double-strand breaks (DSBs) are repaired mainly by two pathways: non-homologous end joining (NHEJ) and homologous recombination (HR). NHEJ is error-prone but active throughout the cell cycle, while HR is error-free but requires an undamaged sister chromatid as the repair template, and therefore is only available in the late S and G2 phases. If damage is too significant for repair, cell death will occur via one of the types described below, at varying time points after the initial irradiation event (interphase or mitotic). In classical radiobiology, cell death is defined by loss of replicative capacity (i.e., replicative or reproductive death) and is determined by clonogenic assays. While this has undoubtedly served the field tremendously, it ignores the types and effects of cell death, discussed in this review.

Mitotic Catastrophe and Mitotic Death

Mitotic catastrophe is a mechanism for the control of cells unable to complete mitosis, by the triggering of mitotic arrest and ultimately regulated cell death (RCD) or senescence. Mitotic death refers to RCD (usually intrinsic apoptosis) that is driven by mitotic catastrophe (Galluzzi et al., 2018). Because cells in mitotic catastrophe are almost always incapable of further replication, mitotic catastrophe is often confused as a bona fide cell death type. However, these cells eventually trigger one of the 'other' cell death pathways, or less commonly escape from this state (Gascoigne and Taylor, 2008; Vakifahmetoglu et al., 2008). Dysfunctional cell cycle checkpoints, a common hallmark of cancer cells, allow radiation-damaged cells to enter mitosis prematurely with misrepaired DNA, leading to mitotic catastrophe. The exact mechanisms for the initiation of mitotic catastrophe and the deciding of final cell fate are unclear. Several attempted divisions can occur before sufficient genetic damage is accumulated to trigger mitotic death, underlining why solid tumours often demonstrate delayed responses to RT.

Apoptosis

Apoptosis is a highly regulated form of cell death with characteristic morphological and molecular features. The intrinsic (mitochondrial) apoptotic pathway is activated when the DNA damage repair machinery, with p53 as a central player, disrupts the balance between pro- and anti-apoptotic factors, resulting in the release of cytochrome c from the mitochondria into the cytoplasm to activate the intrinsic pathway-specific caspase 9 (Eriksson and Stigbrand, 2010). The extrinsic pathway, in contrast, is initiated by external signalling via binding of the tumour necrosis factor (TNF) family of ligands to plasma membrane death receptors, eventually causing downstream activation of the extrinsic pathway-specific caspase 8. Irradiated cells can upregulate death receptors, making them susceptible to death through this pathway (Wu et al., 1997; Chakraborty et al., 2003; Sheard et al., 2003). The third pathway, the ceramide pathway, is triggered by radiation-induced activation of acid sphingomyelinase in the plasma membrane, producing ceramide via hydrolysis of sphingomyelin. Radiation-induced DNA damage can also activate mitochondrial ceramide synthase for *de novo* synthesis of ceramide. Ceramide acts as a second messenger in initiating the apoptotic programme, but its signalling targets are complex (Pettus et al., 2002; Kolesnick and Fuks, 2003). The intrinsic, extrinsic and ceramide pathways converge in the activation of caspase 3 and 7, which sets off a cascade of controlled degradation of cellular components.

Necrosis

Necrosis is an unregulated, chaotic form of cell death, triggered by unfavourable conditions such as extreme changes in pH, energy loss, and ion imbalance within the cell and its microenvironment after irradiation (Kroemer et al., 2009). Traditionally identified in histological specimens, it is a diagnosis of exclusion and based on morphology, characterised by a gain in cellular volume, plasma membrane rupture and spill of intracellular contents.

Senescence

Senescence refers to permanent cell cycle arrest. Radiation-induced senescence is triggered by DNA damage and the induction of the p53 and pRb pathways causing cell cycle block, but other factors including oxidative stress may also be relevant triggers in the irradiation context (Sabin and Anderson, 2011; Li et al., 2018). Importantly, senescent cells while "dead" in terms of clonogenicity continue to be viable and metabolically active, over time developing a specific expression pattern of immunomodulatory factors. This senescence-associated secretory phenotype is a result of the extrusion of cytoplasmic chromatin fragments in senescent cells, which act on the DNA sensing and effector cGAS-STING pathway to drive expression of interferon and NF-kB elements (Dou et al., 2017; Gluck et al., 2017).

Autophagy

Autophagy describes the process of sequestrating damaged or old cytoplasmic organelles within vesicles for lysosomal degradation in response to cellular stress. It is usually a cytoprotective process, but autophagic cell death occurs when the autophagic response is excessive (Kroemer and Levine, 2008). The autophagic machinery is a highly regulated pathway involving the ATG genes and is known to be triggered by irradiation, likely via

the endoplasmic stress module and mTOR pathway, although the exact mechanisms are unclear (Tam et al., 2017). Autophagy observed after irradiation may be a mechanism of treatment resistance or of cell death, being likely context-dependent (Levy et al., 2017; Dikic and Elazar, 2018).

Other Types of Cell Death

More recently, forms of RCD have been identified in response to irradiation, including necroptosis and ferroptosis, although the extent to which these occur *in vivo* are uncertain (Gong et al., 2019; Lang et al., 2019; Lei et al., 2019). Necroptosis has similar morphological appearances to necrosis, but is regulated. It can be activated by death receptors, but signalling is transduced via caspase-independent pathways converging on RIPK3 and MLKL. Ferroptosis is a type of cell death triggered by the accumulation of lipid peroxides as the lethal event due to decreased degradation by glutathione peroxidase (GPX4). With irradiation, this is shown to happen via ATM, which represses the cystene-glutamate antiporter system xc-, resulting in decreased glutathione, a co-factor for GPX4 (Lang et al., 2019).

FACTORS AFFECTING TYPE OF CELL DEATH

Cell-Intrinsic Factors

The type of cell death after irradiation depends on a number of factors, with many remaining uncertainties. Cell type is a key determinant. In a subset of tumours such as haematopoietic malignancies (Radford et al., 1994; Jonathan et al., 1999), radiation results in immediate interphase apoptosis. In the majority of solid tumours however, mitotic catastrophe is the most frequent context of radiation-induced cell death (Eriksson and Stigbrand, 2010), whereas normal tissues commonly undergo senescence after irradiation (Nguyen et al., 2018).

The importance of cell type could be related to the cellular status and function of p53 and ATM. p53 is a key regulator of apoptosis and senescence. Intact p53 is required for interphase apoptosis (Fridman and Lowe, 2003), while disruptive TP53 mutations are associated with increased radioresistance via the inhibition of senescence (Skinner et al., 2012). As most tumour cells have lost normal p53 function or inactivated its downstream pathways, the G1/S checkpoint is impaired and DNA damage repair is consequently dependent on ATR/Chk1-mediated intra-S and G2/M arrest (Soussi and Beroud, 2001; Brady et al., 2011; Dillon et al., 2014). Thus, irradiated cells with inactivated p53 will enter mitosis with unrepaired DNA damage, resulting in mitotic catastrophe rather than immediate apoptosis or senescence (Ianzini et al., 2006). While manipulation of p21 or p53 levels may dramatically alter the kinetics of cell death after irradiation, it may not always correlate with the overall loss of replicative capacity (Wouters et al., 1997; Brown and Wouters, 1999). Similarly, ATM impacts cell death by regulating apoptosis, autophagy, and possibly necroptosis (Liang et al., 2013; Tripathi et al., 2013; Chen et al., 2015) (reviewed in Wu et al., 2017), but it is not clear yet how ATM may affect the decision between these types of cell death.

The phase of the cell cycle in which irradiation occurs also influences timing and type of cell death. Studies have demonstrated cells irradiated in G1 phase divide more times and survive longer before undergoing apoptosis compared to cells irradiated in G2 phase, while cells irradiated in mid-to-late S phase died without undergoing mitosis. Post-mitotic apoptosis however appeared to be stochastic and variable between cell lines (Forrester et al., 1999; Endlich et al., 2000).

Radiation Factors

It may be tempting to speculate that ablative doses incline cells to a different type of cell death compared to conventional doses per fraction, but whether this occurs as a direct effect of irradiation is uncertain. The complexities of establishing this link surround dissecting the effect of dose per fraction from biological effective dose (BED), and accounting for temporal confounding by repopulation and cell death dynamics. Worth noting here is that the induction of sufficient damage to non-nuclear cellular components to evoke upfront necrosis may require clinically-irrelevant high doses (Warters et al., 1978). Nonetheless, the rate of apoptotic events after irradiation can be proportional to the number of fractions given, in line with the reassortment principle (cells cycling inter-fraction into states predisposed for interphase apoptosis) (Verheij and Bartelink, 2000).

Radiation quality may also affect mode of cell death. High linear energy transfer (LET) radiation such as alpha particles has been shown to result in enhanced chromosome rearrangements and reproductive death (Franken et al., 2011), due to both the complexity and absolute number of DNA damage clusters (Pinto et al., 2005; Obe et al., 2010).

Microenvironment Factors

The above factors are strongly influenced by the cellular microenvironment. In brief, oxygen tension modulates cell death after irradiation, with a reduction in chromosomal aberrations and reproductive capacity of cells irradiated under hypoxic conditions. This is presumed due to kinetic competition between the oxygen 'fixation' of DNA damage and chemical repair processes (reviewed in Stewart et al., 2011). Under the hypoxic, nutrient-deprived conditions *in vivo*, cell death will be influenced both by the chemical properties of oxygen fixation and indirect effects of hypoxia on cellular processes including cell metabolism, DNA repair, and hypoxia inducible factor (HIF)-related survival mechanisms (Harris, 2002). An acidic microenvironment and serum deprivation also suppress the progression of cells to apoptosis and the formation of micronuclei after irradiation (Paglin et al., 1997; Park et al., 2000).

RADIATION-INDUCED IMMUNOGENIC CELL DEATH

The observation that an intact host immune system improves the tumour control probability of RT, first made in 1979 (Stone et al., 1979), suggests that the anti-tumour effects of RT must extend beyond its direct effects on cancer cells. Over the last decade, the concept of immunogenic cell death (ICD) has emerged to

redefine cancer cell death from an immune-functional aspect, whereby the dying cell through peri-mortem processes is able to evoke anti-tumour adaptive immune responses (Ma et al., 2010; Kepp et al., 2014).

Defining ICD

Historically, necrosis has been traditionally thought to be immunogenic (Scaffidi et al., 2002; Sancho et al., 2009), while apoptosis has been viewed as immunologically silent or even tolerogenic (Voll et al., 1997; Krysko and Vandenabeele, 2010). This relationship is an oversimplification. Apoptosis (Casares et al., 2005; Obeid et al., 2007b), necrosis (Scaffidi et al., 2002; Sancho et al., 2009), and autophagy (Michaud et al., 2011; Ko et al., 2014), have all been demonstrated to be capable of inducing immunogenic responses, while necrosis can in fact contribute to a chronic inflammatory microenvironment that is protumourigenic and immunosuppressive (Vakkila and Lotze, 2004).

The current framework for understanding ICD disengages from the traditional forms of cell death and requires two components: the exposure of danger signals, termed damage-associated molecular patterns (DAMPs), from the dying cell to alert antigen presenting cells (APCs), which include dendritic cells (DCs); and an antigenic epitope to be cross-presented by APCs for training of T cells (Galluzzi et al., 2017).

Observations That RT Can Induce ICD

Bona fide ICD induced by RT has been directly demonstrated with *in vivo* vaccination assays in mouse models (Apetoh et al., 2007a; Obeid et al., 2007a; Gorin et al., 2014). A strong body of work now corroborate these landmark findings across different murine and human cell lines using surrogate measures (Deng et al., 2014; Gameiro et al., 2014; Golden et al., 2014; Ko et al., 2014; Lim et al., 2014). Radiation-induced ICD can also be implied from a growing number of pre-clinical and clinical studies combining RT with immunotherapy showing improved systemic tumour responses (reviewed in Deloch et al., 2016; Grassberger et al., 2019). Although the link is indirect, the release of DAMPs and antigenic determinants to evoke cancer-specific immunity in these studies are thought to be at least partially mediated through radiation-induced ICD. Other important trials testing RT for this role have yielded negative results for yet-uncertain reasons (Kwon et al., 2014; Voorwerk et al., 2019), suggesting that while the phenomenon of radiation-induced ICD is real, its desired clinical impact is a highly selective event.

Mechanisms of Radiation-Induced ICD

Our understanding of the molecular mechanisms of radiation-induced ICD and the determinants for their efficient triggering are in its nascency. Calreticulin, HMGB1, and ATP, the classically described DAMPs, act on CD91, TLR4, and purinergic receptors on DCs respectively, to attract, activate, and promote phagocytosis of cellular corpses by DCs (Ma et al., 2010). Calreticulin, an endoplasmic reticulum chaperone, is translocated to the cell surface as part of the unfolded protein response in stressed cells as a pre-apoptotic event (Obeid et al., 2007b). HMGB1 is a nuclear chromatin-binding protein that is released on necrosis (Scaffidi et al., 2002; Apetoh et al., 2007b). Unlike HMGB1 where passive release can occur, optimal secretion of ATP in radiation-induced ICD is active and dependent on intact pre-mortem autophagic machinery for the accumulation of ATP within autolysosomes (Michaud et al., 2011; Ko et al., 2014). A host of other DAMPs have since been identified, including cytosolic double stranded DNA (dsDNA), the heat shock proteins 70 kDa (HSP70) and 90 kDa (HSP90), F-actin, and interleukin-33 (reviewed in Krysko et al., 2012; Galluzzi et al., 2017).

Cytosolic dsDNA and the cGAS-STING axis have recently emerged as subjects of intense therapeutic interest. dsDNA is released from either the mitochondria and/or nucleus of irradiated cells into the cytoplasm and binds to its sensor cGAS, producing the cyclic dinucleotide cGAMP. Micronuclei that accumulate when irradiated cells progress through mitosis with radiation-induced DSBs also constitute a source of dsDNA (Harding et al., 2017). cGAMP ligates with the adaptor protein STING to ultimately upregulate the expression of type I interferon, an important immunomodulatory cytokine (Burdette and Vance, 2013; Paludan and Bowie, 2013). Importantly, dsDNA does not need to activate STING in a cell-intrinsic fashion, but dsDNA or cGAMP can be released upon ICD and taken up by myeloid cells, including DCs, to activate STING within those cells (Deng et al., 2014; Diamond et al., 2018; Schadt et al., 2019). This axis can be shut down by ablative radiation doses due to the simultaneous induction of the exonuclease TREX1, which degrades cytosolic dsDNA (Vanpouille-Box et al., 2017). While this mechanism explains the negative impact of ablative radiation doses on abscopal responses in a murine mammary carcinoma model (Dewan et al., 2009), the observation is not consistently held up in non-abscopal readouts of tumour immunity, suggesting that other factors may be involved in this regulation (Burnette et al., 2011; Deng et al., 2014; Schadt et al., 2019). On the other hand, generation of DAMPs such as ATP and HMGB1 appears to be proportional to radiation doses of up to 100 Gy *in vitro* (Gameiro et al., 2014), but whether this translates to increased immunogenicity *in vivo* is unknown.

On the antigenicity side, RT increases the processing and MHC-I-restricted presentation of surface antigens in a cell-autonomous manner, at least partially via the mTOR pathway (Santin et al., 1997; Verbrugge et al., 2014). More provocatively, as a result of altered transcriptional activity and antigen processing, irradiated tumour cells *in vitro* demonstrate a diversification of epitope repertoire presented on MHC-I (Reits et al., 2006). A recent clinical trial combining RT with immune checkpoint blockade reported a patient case with expansion of T cell clones against a radiation-induced neoantigen, serving as the first in-human proof of this concept (Formenti et al., 2018).

DISCUSSION AND CLINICAL RELEVANCE

Increasingly, our appreciation of the anti-tumour effects of RT extends beyond a DNA and cancer cell-centric perspective

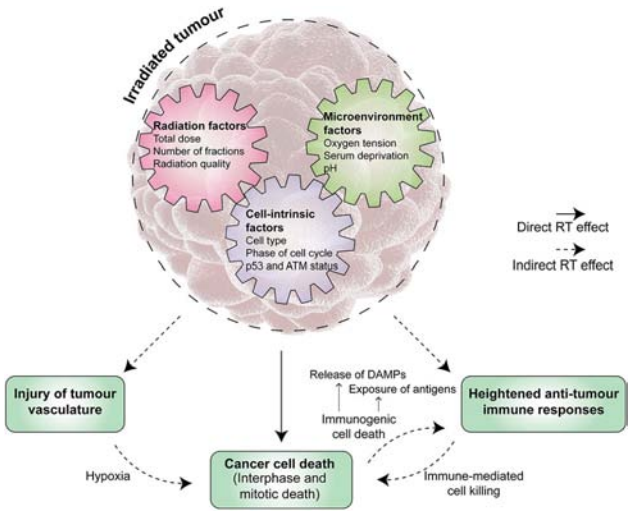

FIGURE 1 | The anti-tumour activity of radiation therapy (RT) is multi-faceted. Tumour irradiation induces both direct and indirect effects in controlling the tumour. Direct effects are the result of significant radiation-induced DNA damage in cancer cells leading to their death, which may occur at various time points after the initial irradiation event. Radiation therapy (RT) also exerts anti-tumour activity via indirect effects, which include, but are not limited to, injury of tumour vasculature and priming of host anti-tumour immune responses. A range of factors influence the triggering and magnitude of these effects, broadly falling into cell-intrinsic, radiation, and microenvironment factors. A deeper knowledge of the underpinning mechanisms and their interplay will reveal opportunities for enhancing the overall anti-tumour activity of RT. ATM, ataxia-telangiectasia mutated. DAMP, danger associated-molecular pattern.

DEFINITIONS

Radiation therapy terms:

Fraction – single treatment session into which the overall radiation therapy course is broken down.

Stereotactic ablative body radiotherapy/stereotactic body radiation therapy (SABR/SBRT) – precise, high-dose radiation therapy given in a small number of fractions.

Abscopal effect – regression of a tumour lesion distant to the radiation field.

Oligometastatic – Stage IV (distant spread) but with a limited number of metastases (usually less than five).

Linear energy transfer (LET) – measure of radiation quality, describing the pattern of energy deposition by the radiation.

Biological effective dose (BED) – an expression of total dose for comparison of biological effects between radiation dose-fractionation regimens.

Reassortment – the redistribution of cells previously in radioresistant phases into more radiosensitive phases after each radiation fraction.

Oxygen fixation – the making permanent of DNA damage induced by radiation, via the formation of irreparable peroxyl radicals.

(**Figure 1**). The need to better understand the molecular pathways of radiation-induced cell death is even more important in light of recent technological advances in the safe delivery of RT and the increasing use of novel agents in clinic. SABR is progressively adopted into routine clinical practice with a growing number of studies backing its remarkable efficacy, greater than predicted by a simple extrapolation from lower doses per fraction. For example, it has been shown to double median survival for oligometastatic disease (Palma et al., 2019) and more than double the response rate to immunotherapy (Formenti et al., 2018; Theelen et al., 2019), leading to the hypothesis that the biology of tumour response to irradiation is different when given high dose per fraction. Theoretically, SABR would induce DNA damage that was more difficult to repair and decrease tumour cell repopulation due to reduced overall treatment time, albeit with a cost from decreased inter-fraction cellular reassortment and reoxygenation. There is currently insufficient data to confidently propose a model by which SABR achieves such high efficacy (Moding et al., 2016; Song et al., 2019). Indeed, some authors argue that the improved local control seen with SABR purely results from a higher dose (Brown et al., 2013, 2014).

Others posit that SABR has additional indirect effects on cancer cells. Significant tumour vascular injury has been shown to result from SABR, leading to hypoxic cancer cell death several days after irradiation (Song et al., 2019). Interestingly, the ceramide apoptotic pathway in the tumour vascular endothelium, activated with ablative radiation doses, is thought to be especially important (Garcia-Barros et al., 2003; Rao et al., 2014). These results, however, have been directly challenged in other models (Moding et al., 2015), while others contend that hypoxia induced by SABR in fact inhibits its efficacy (Carlson et al., 2011).

The other reason measurements of radiation-induced cancer cell death *in vitro* fail to represent the extent of clinically observed responses is due to host immune responses (Golden et al., 2012; Haikerwal et al., 2015). For example, inhibition of the pro-survival autophagy machinery radiosensitises cell kill *in vitro*, but in fact impairs radiation tumour control in immunocompetent mice due to loss of autophagy-dependent ATP release as an immune adjuvant (Ko et al., 2014). As such, a pressing question is the impact of radiation dose-fractionation on cell death pathways, especially those related to ICD. Studying fractionated regimens in the pre-clinical setting is complicated because of the physiologically artificial context and logistical difficulties of irradiating animals *in vivo* over an extended number of fractions. Pre-clinical studies therefore typically employ moderately hypofractionated or ablative regimens (Demaria and Formenti, 2012; Deloch et al., 2016), potentially biassing the commonly-held hypothesis that such regimens are better inducers of ICD.

Finally, greater understanding of the mechanisms of cell death will enable the application of novel radiosensitisers (Moding et al., 2016). For example, the dependence of many cancer cells specifically on the G2/M checkpoint has led to the development of agents that target this checkpoint, particularly Chk1, Wee1, ATM, and ATR (Dillon et al., 2014). Hypoxia-modifying therapy might prevent HIF-mediated revascularisation, recurrence, and metastasis (Moding et al., 2016). Additionally, targeting previously under-appreciated cell death types such as ferroptosis may support the combination of RT

and immunotherapy (Lang et al., 2019). Alongside these developments, biomarker driven studies must not be neglected to help guide patient selection.

CONCLUSION

Cancer cells undergo a range of interphase and mitotic death after irradiation via direct and indirect effects of RT. An increased understanding of the molecular mechanisms of radiation-induced cell death will reveal novel opportunities for improving the overall anti-tumour efficacy of RT.

AUTHOR CONTRIBUTIONS

JS, RS, EH, and HG conceived and designed the study, revised the manuscript, and read and approved the submitted version. JS wrote the first draft of the manuscript. HG wrote sections of the manuscript.

REFERENCES

Apetoh, L., Ghiringhelli, F., Tesniere, A., Criollo, A., Ortiz, C., Lidereau, R., et al. (2007a). The interaction between HMGB1 and TLR4 dictates the outcome of anticancer chemotherapy and radiotherapy. *Immunol. Rev.* 220, 47–59. doi: 10.1111/j.1600-065X.2007.00573.x

Apetoh, L., Ghiringhelli, F., Tesniere, A., Obeid, M., Ortiz, C., Criollo, A., et al. (2007b). Toll-like receptor 4-dependent contribution of the immune system to anticancer chemotherapy and radiotherapy. *Nat. Med.* 13, 1050–1059. doi: 10.1038/nm1622

Brady, C. A., Jiang, D., Mello, S. S., Johnson, T. M., Jarvis, L. A., Kozak, M. M., et al. (2011). Distinct p53 transcriptional programs dictate acute DNA-damage responses and tumor suppression. *Cell* 145, 571–583. doi: 10.1016/j.cell.2011.03.035

Brown, J. M., Brenner, D. J., and Carlson, D. J. (2013). Dose escalation, not "new biology," can account for the efficacy of stereotactic body radiation therapy with non-small cell lung cancer. *Int. J. Radiat. Oncol. Biol. Phys.* 85, 1159–1160. doi: 10.1016/j.ijrobp.2012.11.003

Brown, J. M., Carlson, D. J., and Brenner, D. J. (2014). The tumor radiobiology of SRS and SBRT: are more than the 5 Rs involved? *Int. J. Radiat. Oncol. Biol. Phys.* 88, 254–262. doi: 10.1016/j.ijrobp.2013.07.022

Brown, J. M., and Wouters, B. G. (1999). Apoptosis, p53, and tumor cell sensitivity to anticancer agents. *Cancer Res.* 59, 1391–1399.

Burdette, D. L., and Vance, R. E. (2013). STING and the innate immune response to nucleic acids in the cytosol. *Nat. Immunol.* 14, 19–26. doi: 10.1038/ni.2491

Burnette, B. C., Liang, H., Lee, Y., Chlewicki, L., Khodarev, N. N., Weichselbaum, R. R., et al. (2011). The efficacy of radiotherapy relies upon induction of type i interferon-dependent innate and adaptive immunity. *Cancer Res.* 71, 2488–2496. doi: 10.1158/0008-5472.CAN-10-2820

Carlson, D. J., Keall, P. J., Loo, B. W. Jr., Chen, Z. J., and Brown, J. M. (2011). Hypofractionation results in reduced tumor cell kill compared to conventional fractionation for tumors with regions of hypoxia. *Int. J. Radiat. Oncol. Biol. Phys.* 79, 1188–1195. doi: 10.1016/j.ijrobp.2010.10.007

Casares, N., Pequignot, M. O., Tesniere, A., Ghiringhelli, F., Roux, S., Chaput, N., et al. (2005). Caspase-dependent immunogenicity of doxorubicin-induced tumor cell death. *J. Exp. Med.* 202, 1691–1701. doi: 10.1084/jem.20050915

Chakraborty, M., Abrams, S. I., Camphausen, K., Liu, K., Scott, T., Coleman, C. N., et al. (2003). Irradiation of tumor cells up-regulates Fas and enhances CTL lytic activity and CTL adoptive immunotherapy. *J. Immunol.* 170, 6338–6347. doi: 10.4049/jimmunol.170.12.6338

Chen, J. H., Zhang, P., Chen, W. D., Li, D. D., Wu, X. Q., Deng, R., et al. (2015). ATM-mediated PTEN phosphorylation promotes PTEN nuclear translocation and autophagy in response to DNA-damaging agents in cancer cells. *Autophagy* 11, 239–252. doi: 10.1080/15548627.2015.1009767

Deloch, L., Derer, A., Hartmann, J., Frey, B., Fietkau, R., and Gaipl, U. S. (2016). Modern radiotherapy concepts and the impact of radiation on immune activation. *Front. Oncol.* 6:141. doi: 10.3389/fonc.2016.00141

Demaria, S., and Formenti, S. C. (2012). Radiation as an immunological adjuvant: current evidence on dose and fractionation. *Front. Oncol.* 2:153. doi: 10.3389/fonc.2012.00153

Deng, L., Liang, H., Xu, M., Yang, X., Burnette, B., Arina, A., et al. (2014). STING-Dependent Cytosolic DNA sensing promotes radiation-induced Type I interferon-dependent antitumor immunity in immunogenic tumors. *Immunity* 41, 843–852. doi: 10.1016/j.immuni.2014.10.019

Dewan, M. Z., Galloway, A. E., Kawashima, N., Dewyngaert, J. K., Babb, J. S., Formenti, S. C., et al. (2009). Fractionated but not single-dose radiotherapy induces an immune-mediated abscopal effect when combined with anti-CTLA-4 antibody. *Clin. Cancer Res.* 15, 5379–5388. doi: 10.1158/1078-0432.ccr-09-0265

Diamond, J. M., Vanpouille-Box, C., Spada, S., Rudqvist, N. P., Chapman, J. R., Ueberheide, B. M., et al. (2018). Exosomes shuttle TREX1-Sensitive IFN-Stimulatory dsDNA from irradiated cancer cells to DCs. *Cancer Immunol. Res.* 6, 910–920. doi: 10.1158/2326-6066.CIR-17-0581

Dikic, I., and Elazar, Z. (2018). Mechanism and medical implications of mammalian autophagy. *Nat. Rev. Mol. Cell Biol.* 19, 349–364. doi: 10.1038/s41580-018-0003-4

Dillon, M. T., Good, J. S., and Harrington, K. J. (2014). Selective targeting of the G2/M cell cycle checkpoint to improve the therapeutic index of radiotherapy. *Clin. Oncol.* 26, 257–265. doi: 10.1016/j.clon.2014.01.009

Dou, Z., Ghosh, K., Vizioli, M. G., Zhu, J., Sen, P., Wangensteen, K. J., et al. (2017). Cytoplasmic chromatin triggers inflammation in senescence and cancer. *Nature* 550, 402–406. doi: 10.1038/nature24050

Endlich, B., Radford, I. R., Forrester, H. B., and Dewey, W. C. (2000). Computerized video time-lapse microscopy studies of ionizing radiation-induced rapid-interphase and mitosis-related apoptosis in lymphoid cells. *Radiat. Res.* 153, 36–48. doi: 10.1667/0033-7587(2000)153%5B0036:cvtlms%5D2.0.co;2

Eriksson, D., and Stigbrand, T. (2010). Radiation-induced cell death mechanisms. *Tumour. Biol.* 31, 363–372. doi: 10.1007/s13277-010-0042-8

Formenti, S. C., Rudqvist, N. P., Golden, E., Cooper, B., Wennerberg, E., Lhuillier, C., et al. (2018). Radiotherapy induces responses of lung cancer to CTLA-4 blockade. *Nat. Med.* 24, 1845–1851. doi: 10.1038/s41591-018-0232-2

Forrester, H. B., Vidair, C. A., Albright, N., Ling, C. C., and Dewey, W. C. (1999). Using computerized video time lapse for quantifying cell death of X-irradiated rat embryo cells transfected with c-myc or c-Ha-ras. *Cancer Res.* 59, 931–939.

Franken, N. A., ten Cate, R., Krawczyk, P. M., Stap, J., Haveman, J., Aten, J., et al. (2011). Comparison of RBE values of high-LET alpha-particles for the induction of DNA-DSBs, chromosome aberrations and cell reproductive death. *Radiat. Oncol.* 6:64. doi: 10.1186/1748-717X-6-64

Fridman, J. S., and Lowe, S. W. (2003). Control of apoptosis by p53. *Oncogene* 22, 9030–9040. doi: 10.1038/sj.onc.1207116

Galluzzi, L., Buque, A., Kepp, O., Zitvogel, L., and Kroemer, G. (2017). Immunogenic cell death in cancer and infectious disease. *Nat. Re.v Immunol.* 17, 97–111. doi: 10.1038/nri.2016.107

Galluzzi, L., Vitale, I., Aaronson, S. A., Abrams, J. M., Adam, D., Agostinis, P., et al. (2018). Molecular mechanisms of cell death: recommendations of the nomenclature committee on Cell Death 2018. *Cell Death Differ.* 25, 486–541. doi: 10.1038/s41418-017-0012-4

Gameiro, S. R., Jammeh, M. L., Wattenberg, M. M., Tsang, K. Y., Ferrone, S., and Hodge, J. W. (2014). Radiation-induced immunogenic modulation of tumor enhances antigen processing and calreticulin exposure, resulting in enhanced T-cell killing. *Oncotarget* 5, 403–416. doi: 10.18632/oncotarget.1719

Garcia-Barros, M., Paris, F., Cordon-Cardo, C., Lyden, D., Rafii, S., Haimovitz-Friedman, A., et al. (2003). Tumor response to radiotherapy regulated by endothelial cell apoptosis. *Science* 300, 1155–1159. doi: 10.1126/science.1082504

Gascoigne, K. E., and Taylor, S. S. (2008). Cancer cells display profound intra- and interline variation following prolonged exposure to antimitotic drugs. *Cancer Cell* 14, 111–122. doi: 10.1016/j.ccr.2008.07.002

Gluck, S., Guey, B., Gulen, M. F., Wolter, K., Kang, T. W., Schmacke, N. A., et al. (2017). Innate immune sensing of cytosolic chromatin fragments through cGAS promotes senescence. *Nat Cell Biol.* 19, 1061–1070. doi: 10.1038/ncb3586

Golden, E. B., Frances, D., Pellicciotta, I., Demaria, S., Helen Barcellos-Hoff, M., and Formenti, S. C. (2014). Radiation fosters dose-dependent and chemotherapy-induced immunogenic cell death. *Oncoimmunology* 3:e28518. doi: 10.4161/onci.28518

Golden, E. B., Pellicciotta, I., Demaria, S., Barcellos-Hoff, M. H., and Formenti, S. C. (2012). The convergence of radiation and immunogenic cell death signaling pathways. *Front. Oncol.* 2:88. doi: 10.3389/fonc.2012.00088

Gong, Y., Fan, Z., Luo, G., Yang, C., Huang, Q., Fan, K., et al. (2019). The role of necroptosis in cancer biology and therapy. *Mol. Cancer* 18:100. doi: 10.1186/s12943-019-1029-8

Gorin, J. B., Menager, J., Gouard, S., Maurel, C., Guilloux, Y., Faivre-Chauvet, A., et al. (2014). Antitumor immunity induced after alpha irradiation. *Neoplasia* 16, 319–328. doi: 10.1016/j.neo.2014.04.002

Grassberger, C., Ellsworth, S. G., Wilks, M. Q., Keane, F. K., and Loeffler, J. S. (2019). Assessing the interactions between radiotherapy and antitumour immunity. *Nat. Rev. Clin. Oncol.* 16, 729–745. doi: 10.1038/s41571-019-0238-9

Haikerwal, S. J., Hagekyriakou, J., MacManus, M., Martin, O. A., and Haynes, N. M. (2015). Building immunity to cancer with radiation therapy. *Cancer Lett.* 368, 198–208. doi: 10.1016/j.canlet.2015.01.009

Harding, S. M., Benci, J. L., Irianto, J., Discher, D. E., Minn, A. J., and Greenberg, R. A. (2017). Mitotic progression following DNA damage enables pattern recognition within micronuclei. *Nature* 548, 466–470. doi: 10.1038/nature23470

Harris, A. (2002). Hypoxia–a key regulatory factor in tumour growth. *Nat. Rev. Cancer* 2, 38–47. doi: 10.1038/nrc704

Ianzini, F., Bertoldo, A., Kosmacek, E. A., Phillips, S. L., and Mackey, M. A. (2006). Lack of p53 function promotes radiation-induced mitotic catastrophe in mouse embryonic fibroblast cells. *Cancer Cell Int.* 6:11. doi: 10.1186/1475-2867-6-11

Jonathan, E. C., Bernhard, E. J., and McKenna, W. G. (1999). How does radiation kill cells? *Curr. Opin. Chem. Biol.* 3, 77–83. doi: 10.1016/s1367-5931(99)80014-3

Kepp, O., Senovilla, L., Vitale, I., Vacchelli, E., Adjemian, S., Agostinis, P., et al. (2014). Consensus guidelines for the detection of immunogenic cell death. *Oncoimmunology* 3:e955691. doi: 10.4161/21624011.2014.955691

Ko, A., Kanehisa, A., Martins, I., Senovilla, L., Chargari, C., Dugue, D., et al. (2014). Autophagy inhibition radiosensitizes in vitro, yet reduces radioresponses in vivo due to deficient immunogenic signalling. *Cell Death Differ.* 21, 92–99. doi: 10.1038/cdd.2013.124

Kolesnick, R., and Fuks, Z. (2003). Radiation and ceramide-induced apoptosis. *Oncogene* 22, 5897–5906. doi: 10.1038/sj.onc.1206702

Kroemer, G., Galluzzi, L., Vandenabeele, P., Abrams, J., Alnemri, E. S., Baehrecke, E. H., et al. (2009). Classification of cell death: recommendations of the nomenclature committee on cell death 2009. *Cell Death Differ.* 16, 3–11. doi: 10.1038/cdd.2008.150

Kroemer, G., and Levine, B. (2008). Autophagic cell death: the story of a misnomer. *Nat. Rev. Mol. Cell Biol.* 9, 1004–1010. doi: 10.1038/nrm2529

Krysko, D. V., Garg, A. D., Kaczmarek, A., Krysko, O., Agostinis, P., and Vandenabeele, P. (2012). Immunogenic cell death and DAMPs in cancer therapy. *Nat. Rev. Cancer* 12, 860–875. doi: 10.1038/nrc3380

Krysko, D. V., and Vandenabeele, P. (2010). Clearance of dead cells: mechanisms, immune responses and implication in the development of diseases. *Apoptosis* 15, 995–997. doi: 10.1007/s10495-010-0524-6

Kwon, E. D., Drake, C. G., Scher, H. I., Fizazi, K., Bossi, A., van den Eertwegh, A. J., et al. (2014). Ipilimumab versus placebo after radiotherapy in patients with metastatic castration-resistant prostate cancer that had progressed after docetaxel chemotherapy (CA184-043): a multicentre, randomised, double-blind, phase 3 trial. *Lancet Oncol.* 15, 700–712. doi: 10.1016/S1470-2045(14)70189-5

Lang, X., Green, M. D., Wang, W., Yu, J., Choi, J. E., Jiang, L., et al. (2019). Radiotherapy and immunotherapy promote tumoral lipid oxidation and ferroptosis via synergistic repression of SLC7A11. *Cancer Discov.* 9, 1673–1685. doi: 10.1158/2159-8290.CD-19-0338

Lei, P., Bai, T., and Sun, Y. (2019). Mechanisms of ferroptosis and relations with regulated cell death: a review. *Front. Physiol.* 10:139. doi: 10.3389/fphys.2019.00139

Levy, J. M. M., Towers, C. G., and Thorburn, A. (2017). Targeting autophagy in cancer. *Nat. Rev. Cancer* 17, 528–542. doi: 10.1038/nrc.2017.53

Li, M., You, L., Xue, J., and Lu, Y. (2018). Ionizing radiation-induced cellular senescence in normal, non-transformed cells and the involved DNA damage response: a mini review. *Front. Pharmacol.* 9:522. doi: 10.3389/fphar.2018.00522

Liang, N., Jia, L., Liu, Y., Liang, B., Kong, D., Yan, M., et al. (2013). ATM pathway is essential for ionizing radiation-induced autophagy. *Cell Signal.* 25, 2530–2539. doi: 10.1016/j.cellsig.2013.08.010

Lim, J. Y., Gerber, S. A., Murphy, S. P., and Lord, E. M. (2014). Type I interferons induced by radiation therapy mediate recruitment and effector function of CD8(+) T cells. *Cancer Immunol. Immunother.* 63, 259–271. doi: 10.1007/s00262-013-1506-7

Ma, Y., Kepp, O., Ghiringhelli, F., Apetoh, L., Aymeric, L., Locher, C., et al. (2010). Chemotherapy and radiotherapy: cryptic anticancer vaccines. *Semin. Immunol.* 22, 113–124. doi: 10.1016/j.smim.2010.03.001

Maier, P., Hartmann, L., Wenz, F., and Herskind, C. (2016). Cellular pathways in response to ionizing radiation and their targetability for tumor radiosensitization. *Int. J. Mol. Sci.* 17:E102. doi: 10.3390/ijms17010102

Michaud, M., Martins, I., Sukkurwala, A. Q., Adjemian, S., Ma, Y., Pellegatti, P., et al. (2011). Autophagy-dependent anticancer immune responses induced by chemotherapeutic agents in mice. *Science* 334, 1573–1577. doi: 10.1126/science.1208347

Moding, E. J., Castle, K. D., Perez, B. A., Oh, P., Min, H. D., Norris, H., et al. (2015). Tumor cells, but not endothelial cells, mediate eradication of primary sarcomas by stereotactic body radiation therapy. *Sci. Transl. Med.* 7:278ra234. doi: 10.1126/scitranslmed.aaa4214

Moding, E. J., Mowery, Y. M., and Kirsch, D. G. (2016). Opportunities for radiosensitization in the stereotactic body radiation therapy (SBRT) Era. *Cancer J.* 22, 267–273. doi: 10.1097/PPO.0000000000000203

Nguyen, H. Q., To, N. H., Zadigue, P., Kerbrat, S., De La Taille, A., Le Gouvello, S., et al. (2018). Ionizing radiation-induced cellular senescence promotes tissue fibrosis after radiotherapy. A review. *Crit. Rev. Oncol. Hematol.* 129, 13–26. doi: 10.1016/j.critrevonc.2018.06.012

Obe, G., Johannes, C., and Ritter, S. (2010). The number and not the molecular structure of DNA double-strand breaks is more important for the formation of chromosomal aberrations: a hypothesis. *Mutat. Res.* 701, 3–11. doi: 10.1016/j.mrgentox.2010.05.010

Obeid, M., Panaretakis, T., Joza, N., Tufi, R., Tesniere, A., van Endert, P., et al. (2007a). Calreticulin exposure is required for the immunogenicity of gamma-irradiation and UVC light-induced apoptosis. *Cell Death Differ.* 14, 1848–1850. doi: 10.1038/sj.cdd.4402201

Obeid, M., Tesniere, A., Ghiringhelli, F., Fimia, G. M., Apetoh, L., Perfettini, J. L., et al. (2007b). Calreticulin exposure dictates the immunogenicity of cancer cell death. *Nat. Med.* 13, 54–61. doi: 10.1038/nm1523

Paglin, S., Delohery, T., Erlandson, R., and Yahalom, J. (1997). Radiation-induced micronuclei formation in human breast cancer cells: dependence on serum and cell cycle distribution. *Biochem. Biophys. Res. Commun.* 237, 678–684. doi: 10.1006/bbrc.1997.7117

Palma, D. A., Olson, R., Harrow, S., Gaede, S., Louie, A. V., Haasbeek, C., et al. (2019). Stereotactic ablative radiotherapy versus standard of care palliative treatment in patients with oligometastatic cancers (SABR-COMET): a randomised, phase 2, open-label trial. *Lancet* 393, 2051–2058. doi: 10.1016/S0140-6736(18)32487-5

Paludan, S. R., and Bowie, A. G. (2013). Immune sensing of DNA. *Immunity* 38, 870–880. doi: 10.1016/j.immuni.2013.05.004

Park, H. J., Lyons, J. C., Ohtsubo, T., and Song, C. W. (2000). Cell cycle progression and apoptosis after irradiation in an acidic environment. *Cell Death Differ.* 7, 729–738. doi: 10.1038/sj.cdd.4400702

Pettus, B. J., Chalfant, C. E., and Hannun, Y. A. (2002). Ceramide in apoptosis: an overview and current perspectives. *Biochim. Biophys. Acta* 1585, 114–125. doi: 10.1016/s1388-1981(02)00331-1

Pinto, M., Prise, K. M., and Michael, B. D. (2005). Evidence for complexity at the nanometer scale of radiation-induced DNA DSBs as a determinant of rejoining kinetics. *Radiat. Res.* 164, 73–85. doi: 10.1667/rr3394

Radford, I. R., Murphy, T. K., Radley, J. M., and Ellis, S. L. (1994). Radiation response of mouse lymphoid and myeloid cell lines. Part II. Apoptotic death

is shown by all lines examined. *Int. J. Radiat. Biol.* 65, 217–227. doi: 10.1080/09553009414550251

Rao, S. S., Thompson, C., Cheng, J., Haimovitz-Friedman, A., Powell, S. N., Fuks, Z., et al. (2014). Axitinib sensitization of high Single Dose Radiotherapy. *Radiother. Oncol.* 111, 88–93. doi: 10.1016/j.radonc.2014.02.010

Reits, E. A., Hodge, J. W., Herberts, C. A., Groothuis, T. A., Chakraborty, M., Wansley, E. K., et al. (2006). Radiation modulates the peptide repertoire, enhances MHC class I expression, and induces successful antitumor immunotherapy. *J. Exp. Med.* 203, 1259–1271. doi: 10.1084/jem.20052494

Ringborg, U., Bergqvist, D., Brorsson, B., Cavallin-Stahl, E., Ceberg, J., Einhorn, N., et al. (2003). The swedish council on technology assessment in health care (SBU) systematic overview of radiotherapy for cancer including a prospective survey of radiotherapy practice in Sweden 2001–summary and conclusions. *Acta Oncol.* 42, 357–365. doi: 10.1080/02841860310010826

Sabin, R. J., and Anderson, R. M. (2011). Cellular Senescence - its role in cancer and the response to ionizing radiation. *Genome Integr.* 2:7. doi: 10.1186/2041-9414-2-7

Sancho, D., Joffre, O. P., Keller, A. M., Rogers, N. C., Martinez, D., Hernanz-Falcon, P., et al. (2009). Identification of a dendritic cell receptor that couples sensing of necrosis to immunity. *Nature* 458, 899–903. doi: 10.1038/nature07750

Santin, A. D., Hermonat, P. L., Hiserodt, J. C., Chiriva-Internati, M., Woodliff, J., Theus, J. W., et al. (1997). Effects of irradiation on the expression of major histocompatibility complex class I antigen and adhesion costimulation molecules ICAM-1 in human cervical cancer. *Int. J. Radiat. Oncol. Biol. Phys.* 39, 737–742. doi: 10.1016/s0360-3016(97)00372-6

Scaffidi, P., Misteli, T., and Bianchi, M. E. (2002). Release of chromatin protein HMGB1 by necrotic cells triggers inflammation. *Nature* 418, 191–195. doi: 10.1038/nature00858

Schadt, L., Sparano, C., Schweiger, N. A., Silina, K., Cecconi, V., Lucchiari, G., et al. (2019). Cancer-Cell-Intrinsic cGAS expression mediates tumor immunogenicity. *Cell Rep* 29, 1236.e7–1248.e7. doi: 10.1016/j.celrep.2019.09.065

Sheard, M. A., Uldrijan, S., and Vojtesek, B. (2003). Role of p53 in regulating constitutive and X-radiation-inducible CD95 expression and function in carcinoma cells. *Cancer Res.* 63, 7176–7184.

Skinner, H. D., Sandulache, V. C., Ow, T. J., Meyn, R. E., Yordy, J. S., Beadle, B. M., et al. (2012). TP53 disruptive mutations lead to head and neck cancer treatment failure through inhibition of radiation-induced senescence. *Clin. Cancer Res.* 18, 290–300. doi: 10.1158/1078-0432.CCR-11-2260

Song, C. W., Glatstein, E., Marks, L. B., Emami, B., Grimm, J., Sperduto, P. W., et al. (2019). Biological principles of stereotactic body radiation therapy (SBRT) and stereotactic radiation surgery (SRS): indirect cell death. *Int. J. Radiat. Oncol. Biol. Phys.* S0360-3016, 30291–30293. doi: 10.1016/j.ijrobp.2019.02.047

Soussi, T., and Beroud, C. (2001). Assessing TP53 status in human tumours to evaluate clinical outcome. *Nat. Rev. Cancer* 1, 233–240. doi: 10.1038/35106009

Stewart, R. D., Yu, V. K., Georgakilas, A. G., Koumenis, C., Park, J. H., and Carlson, D. J. (2011). Effects of radiation quality and oxygen on clustered DNA lesions and cell death. *Radiat. Res.* 176, 587–602. doi: 10.1667/rr2663.1

Stone, H. B., Peters, L. J., and Milas, L. (1979). Effect of host immune capability on radiocurability and subsequent transplantability of a murine fibrosarcoma. *J. Natl. Cancer Inst.* 63, 1229–1235.

Tam, S. Y., Wu, V. W., and Law, H. K. (2017). Influence of autophagy on the efficacy of radiotherapy. *Radiat. Oncol.* 12, 57. doi: 10.1186/s13014-017-0795-y

Theelen, W., Peulen, H. M. U., Lalezari, F., van der Noort, V., de Vries, J. F., Aerts, J., et al. (2019). Effect of pembrolizumab after stereotactic body radiotherapy vs pembrolizumab alone on tumor response in patients with advanced non-small cell lung cancer: results of the PEMBRO-RT Phase 2 randomized clinical trial. *JAMA Oncol.* doi: 10.1001/jamaoncol.2019.1478 [Epub ahead of print].,

Tripathi, D. N., Chowdhury, R., Trudel, L. J., Tee, A. R., Slack, R. S., Walker, C. L., et al. (2013). Reactive nitrogen species regulate autophagy through ATM-AMPK-TSC2-mediated suppression of mTORC1. *Proc. Natl. Acad. Sci. U.S.A.* 110, E2950–E2957. doi: 10.1073/pnas.1307736110

Vakifahmetoglu, H., Olsson, M., and Zhivotovsky, B. (2008). Death through a tragedy: mitotic catastrophe. *Cell Death Differ.* 15, 1153–1162. doi: 10.1038/cdd.2008.47

Vakkila, J., and Lotze, M. T. (2004). Inflammation and necrosis promote tumour growth. *Nat. Rev. Immunol.* 4, 641–648. doi: 10.1038/nri1415

Vanpouille-Box, C., Formenti, S. C., and Demaria, S. (2017). TREX1 dictates the immune fate of irradiated cancer cells. *Oncoimmunology* 6, e1339857. doi: 10.1080/2162402X.2017.1339857

Verbrugge, I., Gasparini, A., Haynes, N. M., Hagekyriakou, J., Galli, M., Stewart, T. J., et al. (2014). The curative outcome of radioimmunotherapy in a mouse breast cancer model relies on mTOR signaling. *Radiat. Res.* 182, 219–229. doi: 10.1667/RR13511.1

Verheij, M., and Bartelink, H. (2000). Radiation-induced apoptosis. *Cell Tissue Res.* 301, 133–142. doi: 10.1007/s004410000188

Voll, R. E., Herrmann, M., Roth, E. A., Stach, C., Kalden, J. R., and Girkontaite, I. (1997). Immunosuppressive effects of apoptotic cells. *Nature* 390, 350–351. doi: 10.1038/37022

Voorwerk, L., Slagter, M., Horlings, H. M., Sikorska, K., van de Vijver, K. K., de Maaker, M., et al. (2019). Immune induction strategies in metastatic triple-negative breast cancer to enhance the sensitivity to PD-1 blockade: the TONIC trial. *Nat. Med.* 25, 920–928. doi: 10.1038/s41591-019-0432-4

Warters, R. L., Hofer, K. G., Harris, C. R., and Smith, J. M. (1978). Radionuclide toxicity in cultured mammalian cells: elucidation of the primary site of radiation damage. *Curr. Top. Radiat. Res. Q.* 12, 389–407.

Wouters, B. G., Giaccia, A. J., Denko, N. C., and Brown, J. M. (1997). Loss of p21Waf1/Cip1 sensitizes tumors to radiation by an apoptosis-independent mechanism. *Cancer Res.* 57, 4703–4706.

Wu, G. S., Burns, T. F., McDonald, E. R. III, Jiang, W., Meng, R., Krantz, I. D., et al. (1997). KILLER/DR5 is a DNA damage-inducible p53-regulated death receptor gene. *Nat. Genet.* 17, 141–143. doi: 10.1038/ng1097-141

Wu, Q., Allouch, A., Martins, I., Brenner, C., Modjtahedi, N., Deutsch, E., et al. (2017). Modulating both tumor cell death and innate immunity is essential for improving radiation therapy effectiveness. *Front. Immunol.* 8:613. doi: 10.3389/fimmu.2017.00613

Conflict of Interest: The authors declare that the research was conducted in the absence of any commercial or financial relationships that could be construed as a potential conflict of interest.

frontiers in Cell and Developmental Biology

OPINION
published: 24 April 2020
doi: 10.3389/fcell.2020.00261

Cancer Radiotherapy: Understanding the Price of Tumor Eradication

Olga A. Martin[1]* *and Roger F. Martin*[2]

[1] Sir Peter MacCallum Department of Oncology, The University of Melbourne, Melbourne, VIC, Australia, [2] School of Chemistry, The University of Melbourne, Melbourne, VIC, Australia

Keywords: cancer radiotherapy, quality of life, normal tissue toxicity, aging, systemic effects, DNA damage, DNA repair, radioprotectors

Cancer radiotherapy (RT) is involved in the treatment of more than a half of all cancer patients, because it is highly effective; 40% of cancer cures can be attributed to RT (Baskar et al., 2012). Moreover, the efficacy of RT is steadily improving, largely due to the striking progress in technology, aimed at maximizing the radiation dose to the tumor and minimizing the dose to normal tissues. This continual improvement contributes to the increasing numbers of cancer survivors. In Australia, the 5-years relative survival from all cancers (excluding skin cancer) increased from 48% in 1984–1988 to 68% in 2009–2013[1]. In 2012, 410,530 ex-cancer patients were alive 5 years after treatment; 1.8% of the population. In the USA, there are now 14M cancer survivors; ∼4% of the population (Travis, 2006; Travis et al., 2013). Accordingly, increasing attention is now directed to the quality of life (QoL) of cancer survivors, particularly to treatment-related toxicities (Stone et al., 2003; De Ruysscher et al., 2019), as highlighted in a recent report from the National Cancer Research Institute in the UK[2].

Normal tissue toxicity from RT can be attributed to three different etiologies. The most obvious of these can be defined as "targeted", due to relatively high radiation doses to normal tissues in the vicinity of a tumor. Ironically, the technological improvements in dose delivery that have diminished this problem, have contributed to the second category of normal tissue toxicity. Modern RT techniques (e.g., Intensity-Modulated RT, IMRT) use multiple moving beams that sculpt a volume of high dose encompassing the tumor, so quite large volumes of normal tissues are 'bathed' in low doses, within and between beams (Kry et al., 2005; Harrison, 2017). This category also includes scattered radiation that spreads out in different directions from each radiation beam. The third category can be considered as "systemic," reflecting the radiation-induced abscopal ("out-of-field") effect (RIAE). This is attributed to the localized stress in the irradiated volume, that triggers a systemic biological response that is propagated to sites distant from the irradiated volume, and is largely mediated by the immune system (Reynders et al., 2015; Siva et al., 2015). In a sense, the RIAE can be considered as the systemic counterpart of the cellular radiation-induced bystander effect (RIBE), although the historical understanding of the phenomena was quite different. The recognition of the RIBE (Nagasawa and Little, 1992; Prise and O'Sullivan, 2009) is much more recent, compared to early observations the RIAE by radiation oncologists, that manifest both as out-of-field tumor responses and out-of-field RT-associated toxicities (Mole, 1953; Siva et al., 2015).

The best-known RT-induced normal tissue toxicities are targeted effects (tissue responses in the higher dose volume), the subject of many classical and contemporary radiobiological studies (Stewart and Dorr, 2009). They can be acute (appear within weeks of irradiation), late (months to years after RT), or both. For targeted effects, there is a wide spectrum of individual radiosensitivity (RS) manifested as normal tissue toxicity (Barnett et al., 2009). Low dose- and RIAE-generated "silent" toxicities, e.g., chronic inflammatory responses and mutagenesis in radiosensitive tissues,

[1] Cancer in Australia Australian Association of Cancer Registries, 2017.
[2] https://www.ncri.org.uk/lwbc/

OPEN ACCESS

Edited by:
Liz Caldon,
Garvan Institute of Medical Research, Australia

Reviewed by:
Alexandros G. Georgakilas,
National Technical University of Athens, Greece
Michael Jackson,
University of New South Wales, Australia

***Correspondence:**
Olga A. Martin
olga.martin@petermac.org

Specialty section:
This article was submitted to Cell Growth and Division, a section of the journal Frontiers in Cell and Developmental Biology

Received: *13 December 2019*
Accepted: *27 March 2020*
Published: *24 April 2020*

Citation:
Martin OA and Martin RF (2020) Cancer Radiotherapy: Understanding the Price of Tumor Eradication. Front. Cell Dev. Biol. 8:261. doi: 10.3389/fcell.2020.00261

can also lead to long-term tissue dysfunction, even for future generations (Dubrova, 2003). Just as it is well-established for targeted effects, one can expect that there will be a spectrum of individual RS for low dose and systemic effects.

Epidemiological findings in long-term cancer survivors treated with RT indicate the increased incidence of degenerative pathological conditions normally associated with aging, or age-related diseases (e.g., cardio- and cerebrovascular disorders, neurodegeneration including dementia, hormonal disturbances, cataracts, bone marrow insufficiency, immune system dysfunction, second cancers, and overall life shortening) (Cupit-Link et al., 2017). Evidence is accumulating for similar consequences of low dose IR exposure (Majer et al., 2014; Harrison, 2017). Therefore, aging may be the common link between the diverse late morbidities and RT. By amplifying the mechanisms that are responsible for cellular aging (Sabatier et al., 1995; Dubrova et al., 2002; Dubrova, 2003; Miller et al., 2008; Paulino et al., 2010; Azzam et al., 2012; Sabatino et al., 2012; Merrifield and Kovalchuk, 2013; Ungvari et al., 2013; Sprung et al., 2015; Shimura et al., 2016; Yin et al., 2018), RT may induce a premature aging manifested as an accelerated onset of chronic degenerative disorders in some patients. **Figure 1** highlights the similarities between the response to IR and aging, but there are some differences, e.g., differences in the spectra and severity of DNA lesions (Nikitaki et al., 2015). Premature cellular senescence (Nakamura et al., 2008) is also an important common feature of the two pathologies. It is important to note that the idea of RT-induced accelerated aging is not a new one (Richardson, 2009), but given the growing aging population, it has increasingly important consequences for the cost of community health care. Moreover, the availability of improved biomarkers provides a means of monitoring both the need for intervention, and the efficacy of proposed interventions.

Therefore, to fully understand the role of RT in accelerating the aging process, research aimed at the following objectives is required: (1) Development of a "signature" profile of systemic markers to identify RT cancer patients susceptible to development of premature aging; (2) Improving mechanistic understanding of systemic propagation of genotoxic events and the associated aging phenotype following local exposure to IR; (3) Development of strategies for prevention, protection and mitigation of RT-related systemic genotoxic events.

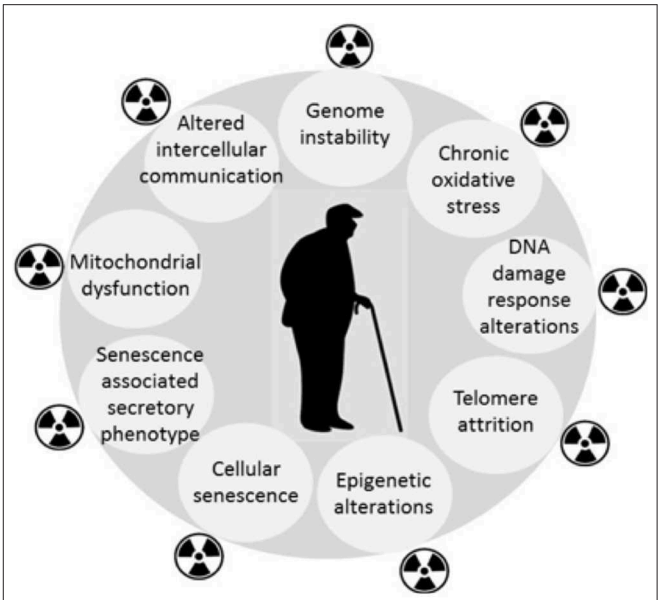

FIGURE 1 | RT amplifies processes reminiscent the biological hallmarks of aging.

IDENTIFICATION OF A SIGNATURE OF SYSTEMIC MARKERS FOR PREMATURE AGING IN RT CANCER PATIENTS

The kinetics of aging biomarkers could be monitored in blood of RT-treated cancer patients and compared with the pre-treatment values. Suitable patients, scheduled for treatment with RT, would be <50–60 years of age, and without evidence of non-cancer morbidities at the time of work-up. Examples of a suitable cohort would be breast or head & neck cancer patients, with an anticipated 5-years survival >90%.

Studies indicate that accumulated unrepaired systemic DNA damage underlies RT-induced pathologies (De Ruysscher et al., 2019). The DNA damage response (DDR) varies in young, mature and old mice, slow down with age, making old mice the most vulnerable to radiation effects (Kovalchuk et al., 2014). DDR declines in senescent cells and during normal and premature human aging (Sedelnikova et al., 2008), and individual RS continuously rises with age (Schuster et al., 2018). Novel functional assays of radiation-induced DNA damage recognition and repair efficiency in *ex-vivo* irradiated primary human fibroblasts and peripheral blood mononuclear cells (PBMC) have been recently developed. The tests are based on post-irradiation formation of nuclear repair foci at the sites of DNA double-strand breaks (DSBs) for two DNA damage markers, phosphorylated ATM kinase ("ATM nucleo-shuttling") (Bodgi and Foray, 2016; Pereira et al., 2018) and histone H2AX (γ-H2AX) (Martin et al., 2013; Lobachevsky et al., 2015a, 2016). Both assays efficiently separated radiosensitive individuals with impaired DDR from those with normal RS. In our retrospective study, ex-RT patients who had documented to have severe RT-induced toxicity (and matched controls who responded normally) were recalled for blood sampling. A novel statistical algorithm was developed by Lobachevsky et al. (2016), based on non-linear regression analysis of the kinetics of repair of γ-H2AX foci, following *ex-vivo* irradiation of the PBMC. Subsequently the same dataset was analyzed by Bayesian modeling (Herschtal et al., 2018). Both methods of analysis distinguished the radiosensitive patients from controls, but the Bayesian statistics also outlined the importance of assessment of both the initial radiation-induced DNA damage and DNA damage repair. In a later study, the *ex-vivo* γ-H2AX response was assayed in PBMC collected before and during RT, and this showed that RT itself can affect individual RS, as reflected by changes in DSB repair efficiency in PBMC

(Yin et al., 2018), adding a further dimension to the challenge of implementation.

Also, the number of endogenous γ-H2AX foci per cell in PBMC of normal individuals increases with age in a linear fashion (Sedelnikova et al., 2008; Schurman et al., 2012). The outliers identified in the linear regression analysis (Schurman et al., 2012) included elevated γ-H2AX foci/cell in patients with clinical morbidities. Interestingly, DDR has been linked with the immune response for normal and tumor tissues, as evidenced by cumulative bioinformatics studies (Georgakilas et al., 2015).

Therefore, the numbers of γ-H2AX foci/cell and efficiency of DDR in PBMC could provide a basis for identification of RT patients susceptible to RT-induced premature aging. However, it is more likely that a combination of markers will be required to constitute an effective "signature" to identify patients requiring added attention. Candidates for such auxiliary biomarkers include those reflecting immune and epigenetic alterations, increased immune cell senescence, oxidative stress, and mitochondrial dysfunction.

IMPROVING THE MECHANISTIC UNDERSTANDING OF SYSTEMIC PROPAGATION OF GENOTOXIC EVENTS AND THE ASSOCIATED AGING PHENOTYPE FOLLOWING LOCAL EXPOSURE TO IR

Conventional RT triggers systemic biological effects in animal models (Koturbash et al., 2006, 2008; Mancuso et al., 2008), but due to significant scatter, RIAEs are difficult to interpret. The scatter problem associated with conventional radiation sources is much reduced with Synchrotron radiation, providing a useful tool to study RIAE. The defined geometry and coherence of the synchrotron beam delivers IR to small volumes with lower scatter, and the high dose rate (up to >1,000 Gy/sec) minimizes motion artifacts, but also introduces the "FLASH" effect (Durante et al., 2018). Ventura et al. (2017) reported that that various synchrotron settings (IR dose, volume, beam modality) trigger similar systemic effects in normal mouse tissues of wild-type C57BL/6 mice. Depending on the level of scatter radiation (Lobachevsky et al., 2015b), these effects were attributed to either true abscopal signaling, or to direct low-dose scatter radiation. RIAE was abrogated in mice with immune deficiencies, e.g., in mice with non-functional macrophages (Lobachevsky et al., 2019). Possible extensions of these studies using synchrotron irradiation include comparison of targeted and out-of-field effects of IR in young and old mice of wild-type and immune-deficient strains, as well as verification of salient features using a model with conventional radiation beams. The objective would be to understand the pathways by which IR modulates the aging processes in various organs crucial for the development of IR-related late pathologies (e.g., spleen, bone marrow, heart, vasculature, gonads, brain). These experimental models could also be used to evaluate potential therapeutic targets that emerge from the clinical studies described in the previous section.

DEVELOPMENT OF STRATEGIES FOR PREVENTION, PROTECTION AND MITIGATION OF RT-RELATED SYSTEMIC GENOTOXIC EVENTS

Targeted radiation effects and RIAE are both associated with elevated DNA damage and genome instability mediated by reactive oxygen species (ROS), so it is critical that any strategy aimed at reducing systemic genotoxic events does not compromise the cancer therapy, mediated by targeted radiation effects. Similarly, whilst normal tissue toxicities associated RIAE are mediated by the immune response, the tumor response to RT also involves the immune response (Haikerwal et al., 2015; Xing et al., 2019). However, kinetic studies on the impact with immunomodulators on the response of targeted tumors, out-of-field metastases and RIAE in normal tissues may reveal differences in response kinetics enabling selective suppression of RIAE in normal tissues. Such kinetic differences enabled scatter effects to be distinguished from the systemic RIAE (Ventura et al., 2017).

Our mouse studies revealed that molecules that block cytokines/cytokine receptors and macrophages can be expected to mitigate abscopal genotoxic events in normal tissues (Ventura et al., 2017; Lobachevsky et al., 2019). Our extensive review of potential strategies for prevention of RT-induced second cancers (Martin et al., 2016) illustrates the range of approaches that can be considered for all toxicities mediated by RIAE. A review on radiation-induced cardiotoxicity (Stewart et al., 2013), which noted the role of systemic effects, also discussed strategies for prevention. Another report extensively reviewed strategies for amelioration of radiation effects on the eye (Kleiman et al., 2017), some of which could be applicable to RT. In this context, a relatively new family of radioprotectors developed by one of the authors (RFM) is of interest. The first example, methylproamine (Martin et al., 2004), is a potent radioprotector *in vitro*; a dose modification factor of 2.0 at a concentration of 10 uM (Lobachevsky et al., 2011) and improved analogs, including *in vivo* activity, have been reported in the patent literature (Martin et al., 2011). Such radioprotectors have the potential to take advantage of the slow kinetics observed for the RIAE, illustrated by the report of the delayed appearance of DNA damage in eyebrow hair follicles after RT of lung cancer patients; 24 h after the first fraction (Siva et al., 2015). A delayed DDR is well-established for the cellular RIBE (Sedelnikova et al., 2007). Interestingly, methylproamine protects bystander cells in the *in vitro* RIBE setting, e.g., if present with recipient cells at the time of transfer of media irradiated cells (Burdak-Rothkamm et al., 2015). By contrast, in the context of targeted radiation effects, methylproamine must be present before and during irradiation to endow radioprotection of cultured cells (Lobachevsky et al., 2011), consistent with the mechanism (DNA-binding antioxidant) of radioprotection (Martin and Anderson, 1998). Thus, one can envisage an RT scenario in which such radioprotectors could be administered after irradiation, and thus not compromise response of the tumor, but nevertheless mitigate the subsequent RIAE mediated toxicity in normal tissues.

Whilst scheduling that avoids the possibility of compromising the tumor response might be challenging in the setting of conventional fractionation, this would be less problematical for hypofractionation modalities.

CONCLUSIONS

RT has an established role in cancer therapy and is unlikely to be superseded in the foreseeable future. In addition to pursuing better treatments, it is time now for more focus on the QoL of cancer RT survivors. The priorities include the need to understand the biological basis of treatment side-effects and their management, and, in particular, the mechanisms responsible for RT-induced aging phenotype and associated pathologies. This new knowledge is expected to enable development of systemic markers to identify patients most susceptible to accelerated aging, and the early stages of that process, as well as novel interventions for prevention and mitigation. Thus, the overall objective is early diagnosis, monitoring and management of RT-related morbidities, and identification of those cancer patients at most risk of these morbidities so their treatments can be modified accordingly.

AUTHOR CONTRIBUTIONS

OM and RM contributed ideas and wrote the manuscript.

ACKNOWLEDGMENTS

The authors acknowledge continuous support and advice of clinical colleagues from the Department of Radiation Oncology, Peter MacCallum Cancer Center. OM's membership in the Multidisciplinary European Low-Dose Initiative (MELODI) contributed to her awareness of ionizing radiation-induced premature aging.

REFERENCES

Azzam, E. I., Jay-Gerin, J. P., and Pain, D. (2012). Ionizing radiation-induced metabolic oxidative stress and prolonged cell injury. *Cancer Lett*. 327, 48–60. doi: 10.1016/j.canlet.2011.12.012

Barnett, G. C., West, C. M., Dunning, A. M., Elliott, R. M., Coles, C. E., Pharoah, P. D., et al. (2009). Normal tissue reactions to radiotherapy: towards tailoring treatment dose by genotype. *Nat. Rev. Cancer*. 9, 134–142. doi: 10.1038/nrc2587

Baskar, R., Lee, K. A., Yeo, R., and Yeoh, K. W. (2012). Cancer and radiation therapy: current advances and future directions. *Int. J. Med. Sci*. 9, 193–199. doi: 10.7150/ijms.3635

Bodgi, L., and Foray, N. (2016). The nucleo-shuttling of the ATM protein as a basis for a novel theory of radiation response: resolution of the linear-quadratic model. *Int. J. Radiat. Biol*. 92, 117–131. doi: 10.3109/09553002.2016.1135260

Burdak-Rothkamm, S., Smith, A., Lobachevsky, P., Martin, R., and Prise, K. M. (2015). Radioprotection of targeted and bystander cells by methylproamine. *Strahl. Onkol*. 191, 248–255. doi: 10.1007/s00066-014-0751-9

Cupit-Link, M. C., Kirkland, J. L., Ness, K. K., Armstrong, G. T., Tchkonia, T., LeBrasseur, N. K., et al. (2017). Biology of premature ageing in survivors of cancer. *ESMO Open*. 2:e000250. doi: 10.1136/esmoopen-2017-000250

De Ruysscher, D., Niedermann, G., Burnet, N. G., Siva, S., Lee, A. W. M., and Hegi-Johnson, F. (2019). Radiotherapy toxicity. *Nat. Rev. Dis. Primers*. 5:13. doi: 10.1038/s41572-019-0064-5

Dubrova, Y. E. (2003). Radiation-induced transgenerational instability. *Oncogene* 22, 7087–7093. doi: 10.1038/sj.onc.1206993

Dubrova, Y. E., Grant, G., Chumak, A. A., Stezhka, V. A., and Karakasian, A. N. (2002). Elevated minisatellite mutation rate in the post-chernobyl families from ukraine. *Am. J. Hum. Genet*. 71, 801–809. doi: 10.1086/342729

Durante, M., Brauer-Krisch, E., and Hill, M. (2018). Faster and safer? FLASH ultra-high dose rate in radiotherapy. *Br. J. Radiol*. 91:20170628. doi: 10.1259/bjr.20170628

Georgakilas, A. G., Pavlopoulou, A., Louka, M., Nikitaki, Z., Vorgias, C. E., Bagos, P. G., et al. (2015). Emerging molecular networks common in ionizing radiation, immune and inflammatory responses by employing bioinformatics approaches. *Cancer Lett*. 368, 164–172. doi: 10.1016/j.canlet.2015.03.021

Haikerwal, S. J., Hagekyriakou, J., MacManus, M., Martin, O. A., and Haynes, N. M. (2015). Building immunity to cancer with radiation therapy. *Cancer Lett*. 368, 198–208. doi: 10.1016/j.canlet.2015.01.009

Harrison, R. (2017). Out-of-field doses in radiotherapy: Input to epidemiological studies and dose-risk models. *Phys. Med*. 42:239–246. doi: 10.1016/j.ejmp.2017.02.001

Herschtal, A., Martin, R. F., Leong, T., Lobachevsky, P., and Martin, O. A. (2018). A bayesian approach for prediction of patient radiosensitivity. *Int. J. Radiat. Oncol. Biol. Phys*. 102, 627–634. doi: 10.1016/j.ijrobp.2018.06.033

Kleiman, N. J., Stewart, F. A., and Hall, E. J. (2017). Modifiers of radiation effects in the eye. *Life Sci. Space Res.* 15, 43–54. doi: 10.1016/j.lssr.2017.07.005

Koturbash, I., Loree, J., Kutanzi, K., Koganow, C., Pogribny, I., and Kovalchuk, O. (2008). In vivo bystander effect: cranial X-irradiation leads to elevated DNA damage, altered cellular proliferation and apoptosis, and increased p53 levels in shielded spleen. *Int. J. Radiat. Oncol. Biol. Phys*. 70, 554–562. doi: 10.1016/j.ijrobp.2007.09.039

Koturbash, I., Rugo, R. E., Hendricks, C. A., Loree, J., Thibault, B., Kutanzi, K., et al. (2006). Irradiation induces DNA damage and modulates epigenetic effectors in distant bystander tissue *in vivo*. *Oncogene* 25, 4267–4275. doi: 10.1038/sj.onc.1209467

Kovalchuk, I. P., Golubov, A., Koturbash, I. V., Kutanzi, K., Martin, O. A., and Kovalchuk, O. (2014). Age-dependent changes in DNA repair in radiation-exposed mice. *Radiat. Res*. 182, 683–694. doi: 10.1667/RR13697.1

Kry, S. F., Salehpour, M., Followill, D. S., Stovall, M., Kuban, D. A., White, R. A., et al. (2005). The calculated risk of fatal secondary malignancies from intensity-modulated radiation therapy. *Int. J. Radiat. Oncol. Biol. Phys*. 62, 1195–1203. doi: 10.1016/j.ijrobp.2005.03.053

Lobachevsky, P., Ivashkevich, A., Forrester, H. B., Stevenson, A. W., Hall, C. J., Sprung, C. N., et al. (2015b). Assessment and implications of scattered microbeam and broadbeam synchrotron radiation for bystander effect studies. *Radiat. Res*. 184, 650–659. doi: 10.1667/RR13720.1

Lobachevsky, P., Leong, T., Daly, P., Smith, J., Best, N., Tomaszewski, J., et al. (2016). Compromized DNA repair as a basis for identification of cancer radiotherapy patients with extreme radiosensitivity. *Cancer Lett*. 383, 212–219. doi: 10.1016/j.canlet.2016.09.010

Lobachevsky, P., Woodbine, L., Hsiao, K. C., Choo, S., Fraser, C., Gray, P., et al. (2015a). Evaluation of severe combined immunodeficiency and combined immunodeficiency pediatric patients on the basis of cellular radiosensitivity. *J. Mol. Diagnost.* 17, 560–575. doi: 10.1016/j.jmoldx.2015.05.004

Lobachevsky, P. N., Vasireddy, R. S., Broadhurst, S., Sprung, C. N., Karagiannis, T. C., Smith, A. J., et al. (2011). Protection by methylproamine of irradiated human keratinocytes correlates with reduction of DNA damage. *Int. J. Radiat. Biol*. 87, 274–283. doi: 10.3109/09553002.2011.530333

Lobachevsky, P. N., Ventura, J., Giannakandropoulou, L., Forrester, H., Palazzolo, J. S., Haynes, N. M., et al. (2019). A functional immune system is required for the systemic genotoxic effects of localized irradiation. *Int. J. Radiat. Oncol. Biol. Phys*. 103, 1184–1193. doi: 10.1016/j.ijrobp.2018.11.066

Majer, M., Knezevic, Z., and Saveta, M. (2014). Current trends in estimating risk of cancer from exposure to low doses of ionising radiation. *Arh. Hig. Rada Toksikol*. 65, 251–257. doi: 10.2478/10004-1254-65-2014-2425

Mancuso, M., Pasquali, E., Leonardi, S., Tanori, M., Rebessi, S., Di Majo, V., et al. (2008). Oncogenic bystander radiation effects in Patched heterozygous

mouse cerebellum. *Proc. Natl. Acad. Sci. U.S.A.* 105, 12445–12450. doi: 10.1073/pnas.0804186105

Martin, O. A., Ivashkevich, A., Choo, S., Woodbine, L., Jeggo, P. A., Martin, R. F., et al. (2013). Statistical analysis of kinetics, distribution and co-localisation of DNA repair foci in irradiated cells: cell cycle effect and implications for prediction of radiosensitivity. *DNA Repair*. 12, 844–855. doi: 10.1016/j.dnarep.2013.07.002

Martin, O. A., Yin, X., Forrester, H. B., Sprung, C. N., and Martin, R. F. (2016). Potential strategies to ameliorate risk of radiotherapy-induced second malignant neoplasms. *Semin. Cancer Biol.* 37–38, 65–76. doi: 10.1016/j.semcancer.2015.12.003

Martin, R., Francis, W.hite J., Lobachevsky, P., Winkler, D., Skene, C., and Marcuccio, S. (2011). *Radioprotector Compounds and Methods*. Patent WO/2011/123890. Melbourne, Australia.

Martin, R. F., and Anderson, R. F. (1998). Pulse radiolysis studies indicate that electron transfer is involved in radioprotection by Hoechst 33342 and methylproamine. *Int. J. Radiat. Oncol. Biol. Phys.* 42, 827–831. doi: 10.1016/S0360-3016(98)00316-2

Martin, R. F., Broadhurst, S., Reum, M. E., Squire, C. J., Clark, G. R., Lobachevsky, P. N., et al. (2004). *In vitro* studies with methylproamine: a potent new radioprotector. *Cancer Res.* 64, 1067–1070. doi: 10.1158/0008-5472.CAN-03-2423

Merrifield, M., and Kovalchuk, O. (2013). Epigenetics in radiation biology: a new research frontier. *Front. Genet.* 4:40. doi: 10.3389/fgene.2013.00040

Miller, J. H., Jin, S., Morgan, W. F., Yang, A., Wan, Y., Aypar, U., et al. (2008). Profiling mitochondrial proteins in radiation-induced genome-unstable cell lines with persistent oxidative stress by mass spectrometry. *Radiat. Res.* 169, 700–706. doi: 10.1667/RR1186.1

Mole, R. H. (1953). Whole body irradiation; radiobiology or medicine? *Br. J. Radiol.* 26, 234–241. doi: 10.1259/0007-1285-26-305-234

Nagasawa, H., and Little, J. B. (1992). Induction of sister chromatid exchanges by extremely low doses of alpha-particles. *Cancer Res.* 52, 6394–6396.

Nakamura, A. J., Chiang, Y. J., Hathcock, K. S., Horikawa, I., Sedelnikova, O. A., Hodes, R. J., et al. (2008). Both telomeric and non-telomeric DNA damage are determinants of mammalian cellular senescence. *Epigenetics Chromatin*. 1:6. doi: 10.1186/1756-8935-1-6

Nikitaki, Z., Hellweg, C. E., Georgakilas, A. G., and Ravanat, J. L. (2015). Stress-induced DNA damage biomarkers: applications and limitations. *Front Chem.* 3:35. doi: 10.3389/fchem.2015.00035

Paulino, A. C., Constine, L. S., Rubin, P., and Williams, J. P. (2010). Normal tissue development, homeostasis, senescence, and the sensitivity to radiation injury across the age spectrum. *Semin. Radiat. Oncol.* 20, 12–20. doi: 10.1016/j.semradonc.2009.08.003

Pereira, S., Bodgi, L., Duclos, M., Canet, A., Ferlazzo, M. L., Devic, C., et al. (2018). Fast and binary assay for predicting radiosensitivity based on the theory of ATM nucleo-shuttling: development, validation, and performance. *Int. J. Radiat. Oncol. Biol. Phys.* 100, 353–360. doi: 10.1016/j.ijrobp.2017.10.029

Prise, K. M., and O'Sullivan, J. M. (2009). Radiation-induced bystander signalling in cancer therapy. *Nat. Rev. Cancer*. 9, 351–360. doi: 10.1038/nrc2603

Reynders, K., Illidge, T., Siva, S., Chang, J. Y., and De Ruysscher, D. (2015). The abscopal effect of local radiotherapy: using immunotherapy to make a rare event clinically relevant. *Cancer Treat. Rev.* 41, 503–510. doi: 10.1016/j.ctrv.2015.03.011

Richardson, R. B. (2009). Ionizing radiation and aging: rejuvenating an old idea. *Aging* 1, 887–902. doi: 10.18632/aging.100081

Sabatier, L., Lebeau, J., and Dutrillaux, B. (1995). Radiation-induced carcinogenesis: individual sensitivity and genomic instability. *Radiat. Environ. Biophys.* 34, 229–232. doi: 10.1007/BF01209747

Sabatino, L., Picano, E., and Andreassi, M. G. (2012). Telomere shortening and ionizing radiation: a possible role in vascular dysfunction? *Int. J. Radiat. Biol.* 88, 830–839. doi: 10.3109/09553002.2012.709307

Schurman, S. H., Dunn, C. A., Greaves, R., Yu, B., Ferrucci, L., Croteau, D. L., et al. (2012). Age-related disease association of endogenous gamma-H2AX foci in mononuclear cells derived from leukapheresis. *PLoS ONE*. 7:e45728. doi: 10.1371/journal.pone.0045728

Schuster, B., Ellmann, A., Mayo, T., Auer, J., Haas, M., Hecht, M., et al. (2018). Rate of individuals with clearly increased radiosensitivity rise with age both in healthy individuals and in cancer patients. *BMC Geriatr.* 18:105. doi: 10.1186/s12877-018-0799-y

Sedelnikova, O. A., Horikawa, I., Redon, C., Nakamura, A., Zimonjic, D. B., Popescu, N. C., et al. (2008). Delayed kinetics of DNA double-strand break processing in normal and pathological aging. *Aging Cell.* 7, 89–100. doi: 10.1111/j.1474-9726.2007.00354.x

Sedelnikova, O. A., Nakamura, A., Kovalchuk, O., Koturbash, I., Mitchell, S. A., Marino, S. A., et al. (2007). DNA double-strand breaks form in bystander cells after microbeam irradiation of three-dimensional human tissue models. *Cancer Res.* 67, 4295–4302. doi: 10.1158/0008-5472.CAN-06-4442

Shimura, T., Kobayashi, J., Komatsu, K., and Kunugita, N. (2016). Severe mitochondrial damage associated with low-dose radiation sensitivity in ATM- and NBS1-deficient cells. *Cell Cycle*. 15, 1099–1107. doi: 10.1080/15384101.2016.1156276

Siva, S., MacManus, M. P., Martin, R. F., and Martin, O. A. (2015). Abscopal effects of radiation therapy: a clinical review for the radiobiologist. *Cancer Lett.* 356, 82–90. doi: 10.1016/j.canlet.2013.09.018

Sprung, C. N., Ivashkevich, A., Forrester, H. B., Redon, C. E., Georgakilas, A., and Martin, O. A. (2015). Oxidative DNA damage caused by inflammation may link to stress-induced non-targeted effects. *Cancer Lett.* 356, 72–81. doi: 10.1016/j.canlet.2013.09.008

Stewart, F. A., and Dorr, W. (2009). Milestones in normal tissue radiation biology over the past 50 years: from clonogenic cell survival to cytokine networks and back to stem cell recovery. *Int. J. Radiat. Biol.* 85, 574–586. doi: 10.1080/09553000902985136

Stewart, F. A., Seemann, I., Hoving, S., and Russell, N. S. (2013). Understanding radiation-induced cardiovascular damage and strategies for intervention. *Clin. Oncol.* 25, 617–624. doi: 10.1016/j.clon.2013.06.012

Stone, H. B., Coleman, C. N., Anscher, M. S., and McBride, W. H. (2003). Effects of radiation on normal tissue: consequences and mechanisms. *Lancet Oncol.* 4, 529–536. doi: 10.1016/S1470-2045(03)01191-4

Travis, L. B. (2006). The epidemiology of second primary cancers. *Cancer Epidemiol. Biomarkers Prev.* 15, 2020–2026. doi: 10.1158/1055-9965.EPI-06-0414

Travis, L. B., Demark Wahnefried, W., Allan, J. M., Wood, M. E., and Ng, A. K. (2013). Aetiology, genetics and prevention of secondary neoplasms in adult cancer survivors. *Nat. Rev. Clin. Oncol.* 10, 289–301. doi: 10.1038/nrclinonc.2013.41

Ungvari, Z., Podlutsky, A., Sosnowska, D., Tucsek, Z., Toth, P., Deak, F., et al. (2013). Ionizing radiation promotes the acquisition of a senescence-associated secretory phenotype and impairs angiogenic capacity in cerebromicrovascular endothelial cells: role of increased DNA damage and decreased DNA repair capacity in microvascular radiosensitivity. *J. Gerontol. Series A Biol. Sci. Med. Sci.* 68, 1443–1457. doi: 10.1093/gerona/glt057

Ventura, J., Lobachevsky, P. N., Palazzolo, J. S., Forrester, H., Haynes, N. M., Ivashkevich, A., et al. (2017). Localized synchrotron irradiation of mouse skin induces persistent systemic genotoxic and immune responses. *Cancer Res.* 77, 6389–6399. doi: 10.1158/0008-5472.CAN-17-1066

Xing, D., Siva, S., and Hanna, G. G. (2019). The abscopal effect of stereotactic radiotherapy and immunotherapy: fool's gold or El dorado? *Clin. Oncol.* 31, 432–443. doi: 10.1016/j.clon.2019.04.006

Yin, X., Mason, J., Lobachevsky, P. N., Munforte, L., Selbie, L., Ball, D. L., et al. (2018). Radiotherapy modulates DNA repair efficiency in peripheral blood mononuclear cells of patients with non-small cell lung cancer. *Int. J. Rad. Oncol. Biol. Phys.* 103, 521–531. doi: 10.1016/j.ijrobp.2018.10.001

Conflict of Interest: RM has a commercial interest associated with his intellectual property on DNA-binding radioprotectors.

The remaining author declares that the research was conducted in the absence of any commercial or financial relationships that could be construed as a potential conflict of interest.

frontiers in Cell and Developmental Biology

OPINION
published: 08 May 2020
doi: 10.3389/fcell.2020.00305

Breathing New Life into the Mechanisms of Platinum Resistance in Lung Adenocarcinoma

Alvaro Gonzalez-Rajal[1], *Jordan F. Hastings*[2], *D. Neil Watkins*[3,4], *David R. Croucher*[2,5] *and Andrew Burgess*[1,6]*

[1] ANZAC Research Institute, Concord, NSW, Australia, [2] The Kinghorn Cancer Centre, Garvan Institute of Medical Research, Sydney, NSW, Australia, [3] Research Institute in Oncology and Hematology, Cancer Care Manitoba, Winnipeg, MB, Canada, [4] Department of Internal Medicine, Rady Faculty of Health Sciences, University of Manitoba, Winnipeg, MB, Canada, [5] St Vincent's Hospital Clinical School, University of New South Wales, Sydney, NSW, Australia, [6] The University of Sydney Concord Clinical School, Faculty of Medicine and Health, Sydney, NSW, Australia

Keywords: cisplatin, TGF-β, DNA damage, DNA repair, follistatin, cell cycle, p21, p53

INTRODUCTION

Lung cancer accounts for approximately 11% of all cancer cases, however the 5-year survival rate is often below 20%. Consequently, lung cancer is the leading cause of cancer related mortality worldwide (Bray et al., 2018). There are two major types of lung cancer; small cell lung cancer (SCLC), which accounts for ∼15% of cases and non-small cell lung cancer (NSCLC), which accounts for ∼85% (Herbst et al., 2018). NSCLC is further separated into lung adenocarcinoma (LUAD, ∼50%), squamous cell carcinoma (∼30%) and multiple smaller subtypes (∼20%). Notably, up to 75% of NSCLC patients are diagnosed with advanced stage III/IV lung cancer (Walters et al., 2013), limiting surgical intervention.

While smoking is strongly associated with all lung cancer types, at least 20% of LUAD cases are from non–or never smokers (Herbst et al., 2018). Furthermore, while LUAD is characterized by a high somatic mutation rate, with deletion or mutation of TP53 occurring in up to 46% of cases, <20% of patients carry targetable mutations such as those within EGFR, ALK, or BRAF or NTRK (Arbour and Riely, 2019). Consequently, the overwhelming majority of LUAD patients receive platinum-based chemotherapy as standard of care.

Unfortunately, response rates to platinum in LUAD are below 30%, due to innate/acquired resistance and rate-limiting side-effects such as nephrotoxicity (Marini et al., 2018). Importantly, potential synergy between platinum chemotherapy and immunotherapy has emerged as a therapeutic opportunity in LUAD (Mathew et al., 2018). Therefore, improving platinum efficacy and identifying mechanism of resistance could significantly improve patient outcomes. In this opinion article, we cover several of the latest landmark publications that shed new light on the mechanisms of platinum resistance in LUAD.

OVERVIEW OF PLATINUM CHEMOTHERAPY

The anti-tumor abilities of cisplatin were identified over 50 years ago (Rosenberg et al., 1969). Since then platinum has become one of the most successful chemotherapeutics developed. It is essentially curative in testicular cancer, with survival rates >90% (Koster et al., 2013). It is also used with varying degrees of success to treat ovarian, head and neck, bladder and cervical cancer. Second and third generation cisplatin analogs have now been developed with the aim of lessening nephrotoxicity, neurotoxicity, ototoxicity, or providing better bioavailability and overcoming tumor resistance. Of these, carboplatin and oxiplatin are the most well-known, however nedaplatin, heptaplatin, lobaplatin and satraplatin are also used clinically (Wang and Lippard, 2005).

OPEN ACCESS

Edited by:
Weimin Li,
Washington State University, United States

Reviewed by:
Joseph William Landry,
Virginia Commonwealth University, United States

***Correspondence:**
Andrew Burgess
andrew.burgess@sydney.edu.au

Specialty section:
This article was submitted to Cell Growth and Division, a section of the journal Frontiers in Cell and Developmental Biology

Received: *17 December 2019*
Accepted: *07 April 2020*
Published: *08 May 2020*

Citation:
Gonzalez-Rajal A, Hastings JF, Watkins DN, Croucher DR and Burgess A (2020) Breathing New Life into the Mechanisms of Platinum Resistance in Lung Adenocarcinoma. Front. Cell Dev. Biol. 8:305. doi: 10.3389/fcell.2020.00305

Cisplatin and its derivates rely on their platinum group to exert killing. Platinum compounds can bind to many biological targets including DNA, RNA, and proteins (Stordal and Davey, 2007). The binding of cisplatin to DNA forms platinum-DNA adducts (**Figure 1**), which must be repaired by the cell. Approximately 90% of cisplatin-induced adducts are intra-strand crosslinks that are rapidly repaired mostly by the base-excision and nucleotide excision repair (BER, NER) pathways during G1 phase (Slyskova et al., 2018). In contrast, inter-strand crosslinks (ICL) represent <5% of cisplatin-induced adducts but are far more difficult for cells to remove as they are "hidden" within the DNA helix. ICLs prevent the unzipping of the double helix, creating a physical barrier to efficient DNA replication. The removal, largely by the Fanconi anemia (FA) pathway (Michl et al., 2016; Niraj et al., 2019; Smogorzewska, 2019), results in the formation of single and double strand breaks (SSBs and DSBs). The damaged DNA is then repaired by either the high-fidelity homologous recombination (HR) pathway during S/G2-phase (Karanam et al., 2012) or by the error-prone non-homologous end joining (NHEJ) pathway in G1 phase (Enoiu et al., 2012). The extent of, or failure to repair the DNA damage caused by cisplatin can result in cell death, accounting for the cytotoxic mode of action for most platinum agents. The exception is oxiplatin, which kill cells through increasing ribosome biogenesis stress (Bruno et al., 2017). For simplicity, here we will only focus on the mechanisms of cisplatin resistance in LUAD.

Screening for Platinum Sensitisers

To date over 147 mechanisms of platinum resistance have been proposed (Stewart, 2007), yet there remains a lack of viable clinical options to improve response rates. To overcome this, several recent publications (Cheng et al., 2016; Jhuraney et al., 2016; Jin et al., 2018; Marini et al., 2018; Ding et al., 2019; Hsu C.-H et al., 2019), have looked at potential mechanisms of resistance in LUAD using unbiased screens, and detailed preclinical models. Based on these new data, it is clear that the main points of resistance arise from alterations to DNA repair, TGF-β signaling, cell cycle and apoptosis (**Figure 1**). Put simply, the ability of cisplatin to kill cells requires actively cycling cells that generate sufficient DNA damage and a functional apoptotic pathway to induce death. Consequently, disruption at any point along these pathways can prevent cell death, thereby reducing sensitivity to platinum mediated killing. Conversely, synergising therapies in general either block inhibitory cell death pathways, thereby lowering the threshold required to trigger death or increase the amount of damage induced by platinum.

DNA Repair and Resistance to Platinum

The DNA Damage response (DDR), has been extensively reviewed (Jackson and Bartek, 2009; O'Connor, 2015; Pearl et al., 2015; Matt and Hofmann, 2016), as has its role in LUAD (O'Grady et al., 2014). Briefly, the DDR comprises of several functional layers including sensors (e.g., MRN complex, RPA, ATRIP), signaling kinases (e.g., ATM, ATR), damage mediators (e.g., 53BP1, BRCA1/2, H2AX), downstream kinases (e.g., CHK1/2), and cell cycle checkpoint effectors (e.g., p53, p21, WEE1). Unsurprisingly, defects at each level have been reported to regulate sensitivity to cisplatin in a variety of cancers including LUAD. Perhaps the best example of this is the well-reported link between BRCA1/2 mutations and sensitivity to cisplatin in breast cancer (Tutt et al., 2018). Similarly, the BRACness phenotype, which is defined as any defect that impacts HR repair and phenocopies the mutation or loss BRCA1/2 (Byrum et al., 2019b), is also strongly linked with sensitivity to platinum and PARP inhibitors (Ding et al., 2019), especially in ovarian (Pillay et al., 2019) and breast cancer (Tung and Garber, 2018). The links with BRCA1/2 mutations, BRACness and cisplatin sensitivity are less clear in LUAD. Although recent reports indicate that DNA methyltransferase inhibitors can induce a BRACness phenotype in NSCLC cells, sensitizing them to PARP inhibitors (Abbotts et al., 2019), and hence may extend to other DNA damage chemotherapies such as cisplatin (**Figure 1**). Early preclinical studies showed significant promise for directly inhibiting ATR kinase activity (Hall et al., 2014; Vendetti et al., 2015) to enhance cisplatin killing of LUAD cells. Interestingly, inhibition of ATM does not appear to synergise with cisplatin (Schmitt et al., 2017), although it may reduce the metastatic potential of cisplatin resistant LUAD cells (Shen et al., 2019). Furthermore, co-depletion of ATM and MCL-1 can re-sensitize cells to cisplatin (Zhang et al., 2017). While phase 1/2 trials of the CHK1 inhibitor LY2603618 in combination with cisplatin showed promising anti-tumor activity, but also caused significant thromboembolic side-effects (Wehler et al., 2017), indicating that despite promising results in SCLC (Sen et al., 2017; Hsu W.-H. et al., 2019; Nagel et al., 2019), Chk1 inhibitors may not translate to LUAD. Indirectly targeting the DDR has also shown some promise, with inhibition of the JMJD2 histone demethylase family re-sensitizing resistant LUAD to cisplatin by preventing ATR association to sites of DNA damage, thereby weakening the DDR (Duan et al., 2019). Similarly, targeting specific forms of the PP2A phosphatase complex (PPP2R2A2), which are responsible for dephosphorylating and inactivating ATM and ATR, enhanced sensitivity to PARP inhibition in LUAD by maintaining the DDR response (Kalev et al., 2012). What is becoming clear is that there are a number of non-canonical DDR pathways, many of which become upregulated during oncogenesis and can increase replication fork stability and counterbalance BRACness and BRCA mutations (Chaudhuri et al., 2016). A surprising recent example is the discovery that the mitotic kinase Aurora A and its targeting factor TPX2 can regulate 53BP1 and HR repair in a pathway parallel to BRCA1 (Byrum et al., 2019a), possibly explaining why shRNA knockdown of Aurora A sensitized LUAD cells to cisplatin (Cheng et al., 2016). These results highlight the need for additional research that maps all of the pathways regulating the DDR in LUAD.

TGF-β Signaling, EMT and Resistance

The sensing and repair of cisplatin adducts does not happen in isolation from the rest of the cell or its local environment. The DDR signaling pathway is intimately integrated into multiple signaling networks, with a prime example being the transforming growth factor β (TGF-β) pathway. TGF-β regulates a multitude of cellular pathways including the DDR, cellular proliferation and the epithelial-mesenchymal transition (EMT). It plays

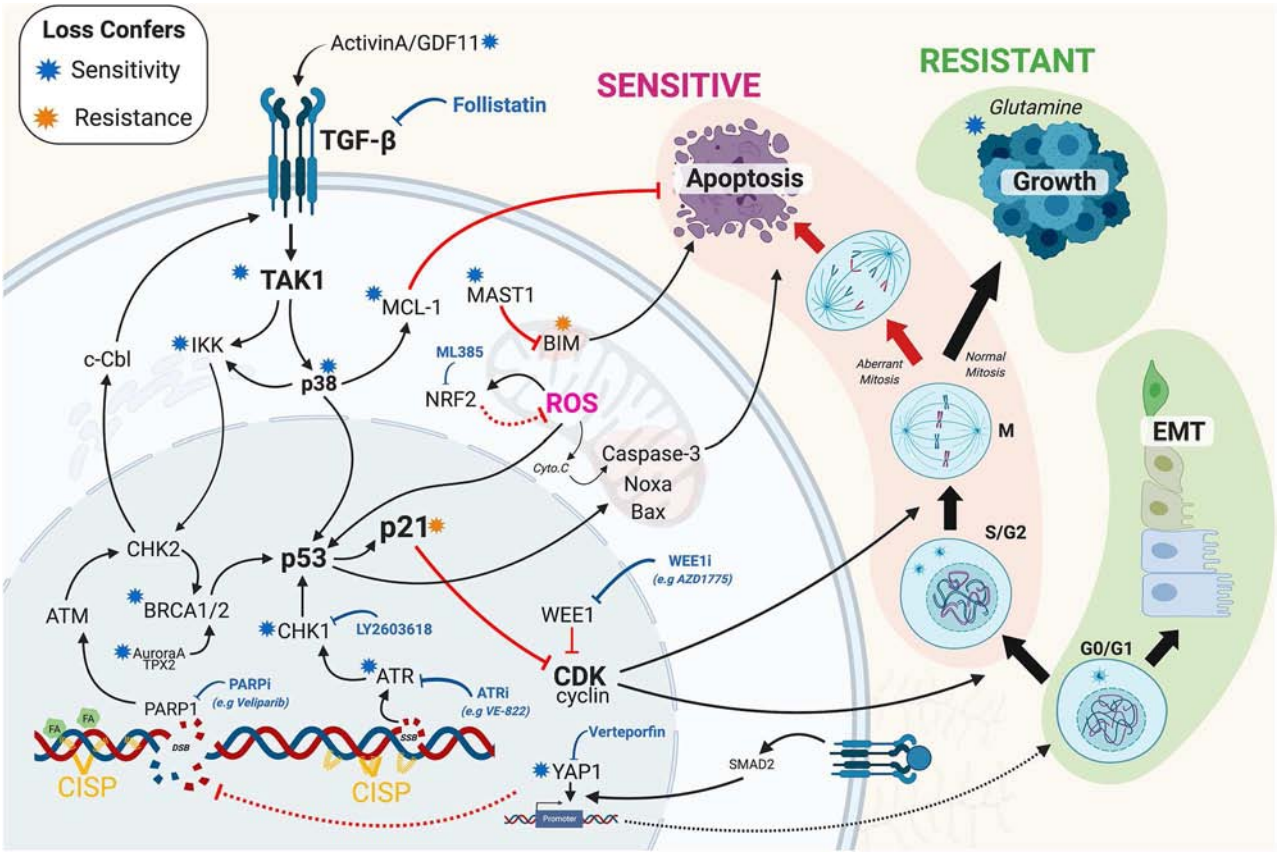

FIGURE 1 | Overview of the recent mechanisms of resistance identified in lung adenocarcinoma. Briefly, mechanism of resistance work to increase repair of DNA damage and or prevent the triggering of cell death through inhibition of apoptotic signaling. Black solid arrows indicated activation. Red arrows indicate inhibition. Solid and dashed lines indicate direct and indirect mechanisms. Blue and orange stars indicate that loss (e.g., by RNAi, CRISPR, or chemical inhibition) confers sensitivity and resistance to cisplatin, respectively. Blue block arrow indicates potential therapeutic cisplatin synergistic treatment options. CISP, cisplatin; EMT, epithelial-mesenchymal transition; SSB/DSB, single/double strand breaks; FA, Fanconi Anemia pathway; ROS, reactive oxygen species; Cyto.C, Cytochrome C. The Figure created with BioRender.com.

both positive and negative roles in cancer development and progression. In established tumors, high TGF-β expression can drive metastasis, tumor heterogeneity and chemoresistance (Li J. et al., 2019). We recently demonstrated that members of the TGF-β pathway, including ACVR1B, TGFBR1, TAK1 and GDF11, mediated innate cisplatin resistance in LUAD (**Figure 1**), a possible consequence of epithelial airway cell lineage (Kretser et al., 2011). Critically, inhibition of activin receptor signaling reversed the resistance, as did blockage of activin A and GDF11 by the endogenous protein Follistatin (Marini et al., 2018). The mechanisms for TGF-β resistance are multifaceted, likely acting to suppress cell proliferation, apoptosis, and the DDR. In support, the antiapoptotic protein MCL-1 decreased upon chemical inhibition of the TGF-β pathway in cisplatin treated cells (Marini et al., 2018). TAK1 has also recently been shown to phosphorylate p38 MAPK and IKKα after DNA damage (Colomer et al., 2019), promoting ATM phosphorylation and increasing DNA repair, leading to chemoresistance. In turn, ATM can feedback into the TGF-β pathway, phosphorylating c-Cbl, stabilizing TβRII receptor and activating TFG-β signaling (Li Y. et al., 2019), creating a positive feedback loop (**Figure 1**). TGF-β can also drive EMT (Hao et al., 2019) and chemoresistance (Fischer et al., 2015), in part due increased YAP1 mediated transcription of TGF-β target genes (Pefani et al., 2016). Consequently, TGFBR1 and YAP1 inhibitors have been shown to be synergistic in GATA4 deficient (Hao et al., 2019) and EGFR-mutant (Cheng et al., 2016) lung cancers, respectively (Gao et al., 2019), offering another potential therapeutic approach to enhancing cisplatin selectivity.

Cell Cycle and Apoptosis

In general, non-cycling cells are more resistant to cytotoxic chemotherapies such as cisplatin, however, proliferating cells that increase repair or reduce death signaling are more resistant, and often more deadly. Once a proliferating cell encounters DNA damage it must halt cell cycle progression so that repair can occur. If the damage is deemed too great, then apoptosis will be initiated, thereby preventing the damage being passed on to subsequent generations. The key central regulator of this decision pathway is $p21^{waf1/kip}$, which inhibits G1 and G2 cell cycle progression (Burgess et al., 2019) and blocks

caspase 3 dependent apoptosis (Suzuki et al., 2000). Interestingly, intermediate "goldilocks" levels of p21 strongly correlate with continued cell proliferation post cisplatin exposure, while low or high levels result in damaged cells undergoing senescence (Hsu C.-H et al., 2019). Similarly, over-riding the protective cell cycle checkpoints in S and G2 phase through WEE1 inhibition has also shown promise, especially in p53 null and mutant cell lines (Jhuraney et al., 2016; Richer et al., 2017). Interestingly, some resistant cycling cells become highly dependent on glutamine for a multitude of metabolic reactions. Consequently, removal of glutamine makes resistant cells highly sensitive to cisplatin, and lowers the threshold required to trigger apoptosis (Guidi and Longo, 2018). Similarly, metformin, which blocks glucose uptake and ATP production, has also been linked with increasing sensitivity to cisplatin (Liu et al., 2017; Riaz et al., 2019). While, inhibition of NRF2, which protects against hypoxia and reactive oxygen species (ROS), synergises with cisplatin by enhancing DNA damage (Singh et al., 2016; Shi et al., 2019). Notably, NRF2 is commonly upregulated in LUAD by KRAS (Tao et al., 2014) and mutant p53 (Tung et al., 2015). Disrupting apoptosis is another common mechanism, with upregulation of MAST1 in LUAD cells resulting in a rewiring of downstream MEK signaling and a reduction in pro-apoptotic protein Bim (**Figure 1**), thereby increasing the threshold required to trigger apoptosis (Jin et al., 2018). Likewise, mutations in SET containing 2 (SETD2), a histone methyltransferase, confers cisplatin resistance in LUAD by altering ERK signaling and inhibiting apoptosis (Kim et al., 2019). While, as mention, TAK1-p38 signaling results in an increase in anti-apoptotic MCL1 levels, raising the threshold required to trigger apoptosis (Marini et al., 2018).

DISCUSSION AND CONCLUSION

A more complete understanding of the signaling, repair and apoptotic networks that are re-wired in LUAD will be key to improving platinum efficacy in LUAD. In addition, better temporal information on the dynamic nature of the signaling responses will greatly aid in the identification and prediction of resistance mechanisms. Any models will need to take into account cell cycle status, repair pathway and apoptotic thresholds in order to identify suitable synergising treatments. Finally, better preclinical models that more accurately model the dosing of platinum will be essential. Currently, the majority of studies rely on prolonged exposure, often >10-fold higher than what is achievable in patients (Urien and Lokiec, 2004; Jacobs et al., 2005). Screening of synergistic treatments using this extreme exposure may have increased the rate of false positives and failure of some preclinical studies to translate clinically. This is further cofounded by the disparate effect that platinum has on various organs (Yimit et al., 2019), especially the kidneys. Consequently, treatments such as Follistatin (Marini et al., 2018), which not only protect these vital organs but also enhance tumor selective killing, may have significant clinical potential. In summary, the advent of large-scale screens combined with detailed preclinical studies has given a greater understanding of the mechanisms of cisplatin resistance in LUAD, breathing new life into this stalwart of chemotherapy.

AUTHOR CONTRIBUTIONS

AG-R and JH co-wrote the initial draft. DW and DC co-wrote and edited the manuscript. AB conceived and wrote the article.

FUNDING

AB was supported by a NBCF Investigator Initiated Research Scheme (IIRS-18-103). DC is also supported by NBCF Investigator Initiated Research Schemes (IIRS-18-121 and IIRS-20-032).

REFERENCES

Abbotts, R., Topper, M. J., Biondi, C., Fontaine, D., Goswami, R., Stojanovic, L., et al. (2019). DNA methyltransferase inhibitors induce a BRCAness phenotype that sensitizes NSCLC to PARP inhibitor and ionizing radiation. *Proc. Natl. Acad. Sci. U.S.A.* 116, 22609–22618. doi: 10.1073/pnas.1903765116

Arbour, K. C., and Riely, G. J. (2019). Systemic therapy for locally advanced and metastatic non-small cell lung cancer. *JAMA* 322, 764–774. doi: 10.1001/jama.2019.11058

Bray, F., Ferlay, J., Soerjomataram, I., Siegel, R. L., Torre, L. A., and Jemal, A. (2018). Global cancer statistics 2018: GLOBOCAN estimates of incidence and mortality worldwide for 36 cancers in 185 countries. *CA Cancer J. Clin.* 68, 394–424. doi: 10.3322/caac.21492

Bruno, P. M., Liu, Y., Park, G. Y., Murai, J., Koch, C. E., Eisen, T. J., et al. (2017). A subset of platinum-containing chemotherapeutic agents kills cells by inducing ribosome biogenesis stress. *Nat. Med.* 23, 4614471. doi: 10.1038/nm.4291

Burgess, A., Vuong, J., Marzec, K. A., Lichtenberg, U. N., de O'Donoghue, S. I., and Jensen, L. J. (2019). SnapShot: S-phase entry and exit. *Cell* 179, 802–802.e1. doi: 10.1016/j.cell.2019.09.031

Byrum, A. K., Carvajal-Maldonado, D., Mudge, M. C., Valle-Garcia, D., Majid, M. C., Patel, R., et al. (2019a). Mitotic regulators TPX2 and aurora A protect DNA forks during replication stress by counteracting 53BP1 function. *J. Cell Biol.* 218, 422–432. doi: 10.1083/jcb.201803003

Byrum, A. K., Vindigni, A., and Mosammaparast, N. (2019b). Defining and modulating 'BRCAness.' *Trends. Cell. Biol* 29, 740–751. doi: 10.1016/j.tcb.2019.06.005

Chaudhuri, A. R., Callen, E., Ding, X., Gogola, E., Duarte, A. A., Lee, J.-E., et al. (2016). Replication fork stability confers chemoresistance in BRCA-deficient cells. *Nature* 535: 3823387. doi: 10.1038/nature19826

Cheng, H., Zhang, Z., Rodriguez-Barrueco, R., Borczuk, A., Liu, H., Yu, J., et al. (2016). Functional genomics screen identifies YAP1 as a key determinant to enhance treatment sensitivity in lung cancer cells. *Oncotarget* 7, 28976–28988. doi: 10.18632/oncotarget.6721

Colomer, C., Margalef, P., Villanueva, A., Vert, A., Pecharroman, I., Solé, L., et al. (2019). IKKα kinase regulates the DNA damage response and drives chemo-resistance in cancer. *Mol. Cell* 75, 669-682.e5. doi: 10.1016/j.molcel.2019.05.036

Ding, H., Zhao, J., Zhang, Y., Yu, J., Liu, M., Li, X., et al. (2019). Systematic analysis of drug vulnerabilities conferred by tumor suppressor loss. *Cell Reports* 27, 3331–3344.e6. doi: 10.1016/j.celrep.2019.05.043

Duan, L., Perez, R. E., Chastain, P. D., Mathew, M. T., Bijukumar, D. R., and Maki, C. G. (2019). JMJD2 promotes acquired cisplatin resistance in non-small cell lung carcinoma cells. *Oncogene* 38, 5643–5657. doi: 10.1038/s41388-019-0814-6

Enoiu, M., Jiricny, J., and Schärer, O. D. (2012). Repair of cisplatin-induced DNA interstrand crosslinks by a replication-independent pathway involving transcription-coupled repair and translesion synthesis. *Nucleic Acids Res.* 40, 8953–8964. doi: 10.1093/nar/gks670

Fischer, K. R., Durrans, A., Lee, S., Sheng, J., Li, F., Wong, S. T. C., et al. (2015). Epithelial-to-mesenchymal transition is not required for lung metastasis but contributes to chemoresistance. *Nature* 527:472. doi: 10.1038/nature15748

Gao, L., Hu, Y., Tian, Y., Fan, Z., Wang, K., Li, H., et al. (2019). Lung cancer deficient in the tumor suppressor GATA4 is sensitive to TGFBR1 inhibition. *Nat. Commun*. 10:1665. doi: 10.1038/s41467-019-09295-7

Guidi, N., and Longo, V. D. (2018). Periodic fasting starves cisplatin-resistant cancers to death. *EMBO J*. 37:e99815. doi: 10.15252/embj.201899815

Hall, A. B., Newsome, D., Wang, Y., Boucher, D. M., Eustace, B., Gu, Y., et al. (2014). Potentiation of tumor responses to DNA damaging therapy by the selective ATR inhibitor VX-970. *Oncotarget* 5, 5674–5685. doi: 10.18632/oncotarget.2158

Hao, Y., Baker, D., and Dijke, P., ten (2019). TGF-β-Mediated Epithelial-Mesenchymal Transition and Cancer Metastasis. *Int. J. Mol. Sci*. 20: 2767. doi: 10.3390/ijms20112767

Herbst, R. S., Morgensztern, D., and Boshoff, C. (2018). The biology and management of non-small cell lung cancer. *Nature* 553, 446–454. doi: 10.1038/nature25183

Hsu, C.-H., Altschuler, S. J., and Wu, L. F. (2019). Patterns of early p21 dynamics determine proliferation-senescence cell fate after chemotherapy. *Cell* 178, 361–373. doi: 10.1016/j.cell.2019.05.041

Hsu, W.-H., Zhao, X., Zhu, J., Kim, I.-K., Rao, G., McCutcheon, J., et al. (2019). Chk1 inhibition enhances cisplatin cytotoxicity and overcomes cisplatin resistance in small cell lung cancer by promoting mitotic cell death. *J. Thorac. Oncol.* 14, 1032–1045. doi: 10.1016/j.jtho.2019.01.028

Jackson, S. P., and Bartek, J. (2009). The DNA-damage response in human biology and disease. *Nature* 461, 1071–1078. doi: 10.1038/nature08467

Jacobs, S. S., Fox, E., Dennie, C., Morgan, L. B., McCully, C. L., and Balis, F. M. (2005). Plasma and cerebrospinal fluid pharmacokinetics of intravenous oxaliplatin, cisplatin, and carboplatin in nonhuman primates. *Clin. Cancer Res.* 11:166911674. doi: 10.1158/1078-0432.CCR-04-1807

Jhuraney, A., Woods, N. T., Wright, G., Rix, L., Kinose, F., Kroeger, J. L., et al. (2016). PAXIP1 potentiates the combination of WEE1 Inhibitor AZD1775 and platinum agents in lung cancer. *Mol. Cancer Ther*. 15, 1669–1681. doi: 10.1158/1535-7163.MCT-15-0182

Jin, L., Chun, J., Pan, C., Li, D., Lin, R., Alesi, G. N., et al. (2018). MAST1 drives cisplatin resistance in human cancers by rewiring cRaf-independent MEK activation. *Cancer Cell* 34, 315–330.e7. doi: 10.1016/j.ccell.2018.06.012

Kalev, P., Simicek, M., Vazquez, I., Munck, S., Chen, L., Soin, T., et al. (2012). Loss of PPP2R2A inhibits homologous recombination DNA repair and predicts tumor sensitivity to PARP inhibition. *Cancer Res*. 72, 6414–6424. doi: 10.1158/0008-5472.CAN-12-1667

Karanam, K., Kafri, R., Loewer, A., and Lahav, G. (2012). Quantitative live cell imaging reveals a gradual shift between DNA repair mechanisms and a maximal use of HR in mid S phase. *Mol. Cell* 47, 320–329. doi: 10.1016/j.molcel.2012.05.052

Kim, I.-K., McCutcheon, J. N., Rao, G., Liu, S. V., Pommier, Y., Skrzypski, M., et al. (2019). Acquired SETD2 mutation and impaired CREB1 activation confer cisplatin resistance in metastatic non-small cell lung cancer. *Oncogene* 38, 180–193. doi: 10.1038/s41388-018-0429-3

Koster, R., van Vugt, M. A., Timmer-Bosscha, H., Gietema, J. A., and de Jong, S. (2013). Unravelling mechanisms of cisplatin sensitivity and resistance in testicular cancer. *Expert Rev. Mol. Med*. 15:e12. doi: 10.1017/erm.2013.13

Kretser, D. M., de O'Hehir, R. E., Hardy, C. L., and Hedger, M. P. (2011). The roles of activin A and its binding protein, follistatin, in inflammation and tissue repair. *Mol. Cell Endocrinol*. 359, 101–106. doi: 10.1016/j.mce.2011.10.009

Li, J., Shen, C., Wang, X., Lai, Y., Zhou, K., Li, P., et al. (2019). Prognostic value of TGF-β in lung cancer: systematic review and meta-analysis. *Bmc Cancer* 19:691. doi: 10.1186/s12885-019-5917-5

Li, Y., Liu, Y., Chiang, Y. J., Huang, F., Li, Y., Li, X., et al. (2019). DNA daimage activates TGF-β signaling via ATM-c-Cbl-mediated stabilization of the Type II receptor TβRII. *Cell Reports* 28, 735–745.e4. doi: 10.1016/j.celrep.2019.06.045

Liu, Y., He, C., and Huang, X. (2017). Metformin partially reverses the carboplatin-resistance in NSCLC by inhibiting glucose metabolism. *Oncotarget* 8:75206775216. doi: 10.18632/oncotarget.20663

Marini, K. D., Croucher, D. R., McCloy, R. A., Vaghjiani, V., Gonzalez-Rajal, A., Hastings, J. F., et al. (2018). Inhibition of activin signaling in lung adenocarcinoma increases the therapeutic index of platinum chemotherapy. *Sci. Transl. Med*. 10:eaat3504. doi: 10.1126/scitranslmed.aat3504

Mathew, M., Enzler, T., Shu, C. A., and Rizvi, N. A. (2018). Combining chemotherapy with PD-1 blockade in NSCLC. *Pharmacol. Therapeut*. 186, 130–137. doi: 10.1016/j.pharmthera, 2018.01.003

Matt, S., and Hofmann, T. G. (2016). The DNA damage-induced cell death response: a roadmap to kill cancer cells. *Cell Mol. Life Sci*. 73, 2829–2850. doi: 10.1007/s00018-016-2130-4

Michl, J., Zimmer, J., and Tarsounas, M. (2016). Interplay between Fanconi anemia and homologous recombination pathways in genome integrity. *Embo J*. 35, 909–923. doi: 10.15252/embj.201693860

Nagel, R., Avelar, A. T., Aben, N., Proost, N., van de Ven, M., van der Vliet, J., et al. (2019). Inhibition of the replication stress response is a synthetic vulnerability in SCLC that acts synergistically in combination with cisplatin. *Mol. Cancer Ther*. 18, 762–770. doi: 10.1158/1535-7163.MCT-18-0972

Niraj, J., Färkkilä, A., and D'Andrea, A. D. (2019). The fanconi anemia pathway in cancer. *Annu. Rev. Cancer Biol.* 3, 457–478. doi: 10.1146/annurev-cancerbio-030617-050422

O'Connor, M. J. (2015). Targeting the DNA damage response in cancer. *Mol. Cell* 60, 547–560. doi: 10.1016/j.molcel.2015.10.040

O'Grady, S., Finn, S. P., Cuffe, S., Richard, D. J., O'Byrne, K. J., and Barr, M. P. (2014). The role of DNA repair pathways in cisplatin resistant lung cancer. *Cancer Treatment Rev*. 40, 116111170. doi: 10.1016/j.ctrv.2014.10.003

Pearl, L. H., Schierz, A. C., Ward, S. E., Al-Lazikani, B., and Pearl, F. M. G. (2015). Therapeutic opportunities within the DNA damage response. *Nat. Rev. Cancer* 15, 166–180. doi: 10.1038/nrc3891

Pefani, D.-E., Pankova, D., Abraham, A. G., Grawenda, A. M., Vlahov, N., Scrace, S., et al. (2016). TGF-β targets the hippo pathway scaffold RASSF1A to facilitate YAP/SMAD2 nuclear translocation. *Mol. Cell* 63, 156–166. doi: 10.1016/j.molcel.2016.05.012

Pillay, N., Tighe, A., Nelson, L., Littler, S., Coulson-Gilmer, C., Bah, N., et al. (2019). DNA replication vulnerabilities render ovarian cancer cells sensitive to poly(ADP-Ribose) glycohydrolase inhibitors. *Cancer Cell* 35, 519–533.e8. doi: 10.1016/j.ccell.2019.02.004

Riaz, M. A., Sak, A., Erol, Y. B., Groneberg, M., Thomale, J., and Stuschke, M. (2019). Metformin enhances the radiosensitizing effect of cisplatin in non-small cell lung cancer cell lines with different cisplatin sensitivities. *Sci Rep-uk* 9:1282. doi: 10.1038/s41598-018-38004-5

Richer, A. L., Cala, J. M., O'Brien, K., Carson, V. M., Inge, L. J., and Whitsett, T. G. (2017). WEE1 kinase inhibitor AZD1775 has preclinical efficacy in LKB1-deficient non-small cell lung cancer. *Cancer Res* 77, 4663–4672. doi: 10.1158/0008-5472.CAN-16-3565

Rosenberg, B., Vancamp, L., Trosko, J. E., and and, Mansour, V. H. (1969). Platinum compounds: a new class of potent antitumour agents. *Nature* 222, 385–386. doi: 10.1038/222385a0

Schmitt, A., Knittel, G., Welcker, D., Yang, T.-P., George, J., Nowak, M., et al. (2017). ATM deficiency is associated with sensitivity to PARP1- and ATR inhibitors in lung adenocarcinoma. *Cancer Res* 77, 3040–3056. doi: 10.1158/0008-5472.CAN-16-3398

Sen, T., Tong, P., Stewart, C. A., Cristea, S., Valliani, A., Shames, D. S., et al. (2017). CHK1 inhibition in small-cell lung cancer produces single-agent activity in biomarker-defined disease subsets and combination activity with cisplatin or olaparib. *Cancer Res*. 77, 3870–3884. doi: 10.1158/0008-5472.CAN-16-3409

Shen, M., Xu, Z., Xu, W., Jiang, K., Zhang, F., Ding, Q., et al. (2019). Inhibition of ATM reverses EMT and decreases metastatic potential of cisplatin-resistant lung cancer cells through JAK/STAT3/PD-L1 pathway. *J. Exp. Clin. Canc. Res.* 38:149. doi: 10.1186/s13046-019-1161-8

Shi, Y., Fan, S., Wu, M., Zuo, Z., Li, X., Jiang, L., et al. (2019). YTHDF1 links hypoxia adaptation and non-small cell lung cancer progression. *Nat. Commun*. 10:4892. doi: 10.1038/s41467-019-12801-6

Singh, A., Venkannagari, S., Oh, K. H., Zhang, Y.-Q., Rohde, J. M., Liu, L., et al. (2016). Small molecule inhibitor of NRF2 Selectively intervenes therapeutic

resistance in KEAP1-deficient NSCLC tumors. *Acs Chem. Biol*. 11, 3214–3225. doi: 10.1021/acschembio.6b00651

Slyskova, J., Sabatella, M., Ribeiro-Silva, C., Stok, C., Theil, A. F., Vermeulen, W., et al. (2018). Base and nucleotide excision repair facilitate resolution of platinum drugs-induced transcription blockage. *Nucleic Acids Res*. 46, 9537–9549. doi: 10.1093/nar/gky764

Smogorzewska, A. (2019). Fanconi anemia: a paradigm for understanding DNA repair during replication. *Blood* 134, SCI-32-SCI-32. doi: 10.1182/blood-2019-121229

Stewart, D. J. (2007). Mechanisms of resistance to cisplatin and carboplatin. *Crit. Rev. Oncol. Hemat*. 63, 12–31. doi: 10.1016/j.critrevonc.2007.02.001

Stordal, B., and Davey, M. (2007). Understanding cisplatin resistance using cellular models. *IUBMB Life* 59:6966699. doi: 10.1080/15216540701636287

Suzuki, A., Kawano, H., Hayashida, M., Hayasaki, Y., Tsutomi, Y., and Akahane, K. (2000). Procaspase 3/p21 complex formation to resist Fas-mediated cell death is initiated as a result of the phosphorylation of p21 by protein kinase A. *Cell Death Differ*. 7, 721–728. doi: 10.1038/sj.cdd.4400706

Tao, S., Wang, S., Moghaddam, S. J., Ooi, A., Chapman, E., Wong, P. K., et al. (2014). Oncogenic KRAS confers chemoresistance by upregulating NRF2. *Cancer Res*. 74, 7430–7441. doi: 10.1158/0008-5472.CAN-14-1439

Tung, M.-C., Lin, P.-L., Wang, Y.-C., He, T.-Y., Lee, M.-C., Yeh, S. D., et al. (2015). Mutant p53 confers chemoresistance in non-small cell lung cancer by upregulating Nrf2. *Oncotarget* 6, 41692–41705. doi: 10.18632/oncotarget.6150

Tung, N. M., and Garber, J. E. (2018). BRCA1/2 testing: therapeutic implications for breast cancer management. *Brit. J. Cancer* 119, 141–152. doi: 10.1038/s41416-018-0127-5

Tutt, A., Tovey, H., Cheang, M. C. U., Kernaghan, S., Kilburn, L., Gazinska, P., et al. (2018). Carboplatin in BRCA1/2-mutated and triple-negative breast cancer BRCAness subgroups: the TNT Trial. *Nat. Med.* 24, 628–637. doi: 10.1038/s41591-018-0009-7

Urien, S., and Lokiec, F. (2004). Population pharmacokinetics of total and unbound plasma cisplatin in adult patients. *British J. Clin. Pharmacol.* 57:7567763. doi: 10.1111/j.1365-2125.2004.02082.x

Vendetti, F. P., Lau, A., Schamus, S., Conrads, T. P., O'Connor, M. J., and Bakkenist, C. J. (2015). The orally active and bioavailable ATR kinase inhibitor AZD6738 potentiates the anti-tumor effects of cisplatin to resolve ATM-deficient non-small cell lung cancer *in vivo*. *Oncotarget* 6, 44289–44305. doi: 10.18632/oncotarget.6247

Walters, S., Maringe, C., Coleman, M. P., Peake, M. D., Butler, J., Young, N., et al. (2013). Lung cancer survival and stage at diagnosis in Australia, Canada, Denmark, Norway, Sweden and the UK: a population-based study, 2004-2007. *Thorax* 68, 551–564. doi: 10.1136/thoraxjnl-2012-202297

Wang, D., and Lippard, S. J. (2005). Cellular processing of platinum anticancer drugs. *Nat Rev Drug Discov* 4, 307–320. doi: 10.1038/nrd1691

Wehler, T., Thomas, M., Schumann, C., Bosch-Barrera, J., Segarra, N. V., Dickgreber, N. J., et al. (2017). A randomized, phase 2 evaluation of the CHK1 inhibitor, LY2603618, administered in combination with pemetrexed and cisplatin in patients with advanced nonsquamous non-small cell lung cancer. *Lung Cancer* 108, 212–216. doi: 10.1016/j.lungcan.2017.03.001

Yimit, A., Adebali, O., Sancar, A., and Jiang, Y. (2019). Differential damage and repair of DNA-adducts induced by anti-cancer drug cisplatin across mouse organs. *Nat. Commun*. 10:309. doi: 10.1038/s41467-019-08290-2

Zhang, F., Shen, M., Yang, L., Yang, X., Tsai, Y., Keng, P. C., et al. (2017). Simultaneous targeting of ATM and Mcl-1 increases cisplatin sensitivity of cisplatin-resistant non-small cell lung cancer. *Cancer Biol. Ther*. 18, 606–615. doi: 10.1080/15384047.2017.1345391

Conflict of Interest: DW is a coinventor on a patent application relating to components of this work (U.S. 20180125936-A1).

The remaining authors declare that the research was conducted in the absence of any commercial or financial relationships that could be construed as a potential conflict of interest.

frontiers in Cell and Developmental Biology

REVIEW
published: 29 May 2020
doi: 10.3389/fcell.2020.00416

A Survey of Essential Genome Stability Genes Reveals That Replication Stress Mitigation Is Critical for Peri-Implantation Embryogenesis

*Georgia R. Kafer and Anthony J. Cesare**

Genome Integrity Unit, Children's Medical Research Institute, The University of Sydney, Westmead, NSW, Australia

Murine development demands that pluripotent epiblast stem cells in the peri-implantation embryo increase from approximately 120 to 14,000 cells between embryonic days (E) 4.5 and E7.5. This is possible because epiblast stem cells can complete cell cycles in under 3 h *in vivo*. To ensure conceptus fitness, epiblast cells must undertake this proliferative feat while maintaining genome integrity. How epiblast cells maintain genome health under such an immense proliferation demand remains unclear. To illuminate the contribution of genome stability pathways to early mammalian development we systematically reviewed knockout mouse data from 347 DDR and repair associated genes. Cumulatively, the data indicate that while many DNA repair functions are dispensable in embryogenesis, genes encoding replication stress response and homology directed repair factors are essential specifically during the peri-implantation stage of early development. We discuss the significance of these findings in the context of the unique proliferative demands placed on pluripotent epiblast stem cells.

Keywords: early development, embryology, pluripotency, DNA damage response, DNA repair, DNA replication, replication stress response

OPEN ACCESS

Edited by:
Liz Caldon,
Garvan Institute of Medical Research, Australia

Reviewed by:
Fumiko Esashi,
University of Oxford, United Kingdom
Yibo Luo,
The University of Toledo, United States

***Correspondence:**
Anthony J. Cesare
tcesare@cmri.org.au

Specialty section:
This article was submitted to Cell Growth and Division, a section of the journal Frontiers in Cell and Developmental Biology

Received: *10 February 2020*
Accepted: *05 May 2020*
Published: *29 May 2020*

Citation:
Kafer GR and Cesare AJ (2020) A Survey of Essential Genome Stability Genes Reveals That Replication Stress Mitigation Is Critical for Peri-Implantation Embryogenesis. Front. Cell Dev. Biol. 8:416. doi: 10.3389/fcell.2020.00416

INTRODUCTION

Overview

Pluripotent cells in early mammalian embryos proliferate at a phenomenal rate. This is necessary to maintain embryo growth and reach critical developmental milestones within defined temporal windows. Because all somatic tissues are derived from these early pluripotent precursors, it is critical that genome integrity is maintained during early development. Embryonic pluripotent stem cells are thus subjected to unique challenges to maintain their DNA health. To elucidate which genome stability pathways are essential for early development we probed the Mouse Genome Informatics Gene Ontology Project (MGI-GO) database (Bult et al., 2019). Within MGI-GO we identified 347 genes grouped within the ontologies of major DNA repair pathways (MGI-GO designations: DNA damage checkpoint, nucleotide excision repair, mismatch repair, base excision repair, homologous recombination, and non-homologous end joining). Of these genes, we identified 297 with a validated mouse knockout. From these 297 murine models, only 108 gene knockouts were lethal during embryonic development (**Supplementary Table S1**). Within the grouping of 108 embryonic

lethal genes, 10 knockouts were lethal during preimplantation development prior to E4.5 (**Table 1**), and 36 knockouts were lethal during somite stages from E8.5 (**Supplementary Table S1**). Notably, most of the targeted genes that conferred embryonic lethality, 62 genes, did so specifically during the period of rapid cell proliferation occurring with peri-implantation development (E4.5 to E8.5) (**Table 2**). Below we briefly review pre- and peri-implantation murine development before considering the function of essential genome stability factors across the early stages of embryonic development. Finally, we discuss why the unique cells of the peri-implantation embryo appear to specifically require replication stress response factors for cell viability.

Early Murine Development

Embryonic development consists of a series of events occurring in chronological progression. Murine development takes 19 to 20 days depending on mouse strain (**Figure 1**; Murray et al., 2010). Preimplantation development occurs between fertilization (E0) and the initiation of embryo implantation in the uterine wall (around E4.0). Following fertilization, embryonic cells are uniformly totipotent and identical until formation of the morula at E2.5 (Condic, 2014) (see **Box 1** for a detailed explanation of cell potency). Within the morula cells undergo polarization and compaction (Humięcka et al., 2017). By E3.0 the embryo forms a blastocyst structure containing two distinct cell populations; an outer layer of multipotent trophectoderm cells that eventually derive the placental tissues, and an inner group of pluripotent inner cell mass (ICM) cells which primarily serve as precursors for the embryo proper (Morris et al., 2010).

Peri-implantation is the developmental period from implantation to organogenesis (E4.0 to E8.5). Implantation begins at E4.0 when the free-floating embryo contains 64 cells (Behringer et al., 2014). At this point, the embryo loses its glycoprotein zona pellucida shell and the outer trophoblast attaches to the uterine wall. Single cell transcriptomics demonstrate that at E4.0 the ICM has differentiated into two pluripotent cell types: the primitive endoderm (PrE, sometimes referred to as the hypoblast) and the epiblast (Mohammed et al., 2017). Peri-implantation development is associated with exceptionally rapid cell proliferation during "gastrulation," which begins at E5.5 as the embryo elongates and a luminal pro-amniotic cavity opens in the center of the epiblast cell mass (Snow, 1976). At E6.5 the primitive streak emerges from the epiblast, and from the epiblast all three dermal lineages of the conceptus will arise (Tam et al., 1993). These are the ectoderm

BOX 1 | Potency states. Totipotent cells are present in the embryo between fertilization and morula formation. They can give rise to any cell type from any stage of the animal's life, including germ and placental cells. Pluripotent cells exist in the inner cell mass (ICM) and epiblast region of the developing embryo from the blastocyst stage to immediately prior to organogenesis. Pluripotent cells can give rise to any cell of dermal lineage (mesoderm, endoderm or ectoderm) but not placental or germ cells. Multipotent cells exist in newly formed tissues or organs and can develop into a limited number of cell types within their original dermal lineage.

TABLE 1 | Genome stability factors essential for preimplantation development.

Targeted gene	Lethal at	Phenotype details	Gene Function	References
Ercc2 (Xpd)	E1.5	Mutant embryos do not implant. *In vitro* culture indicates embryo failure at the 2-cell stage.	NER*	de Boer et al., 1998
Dtl	E2.5	Embryos develop to the morula stage but do not form blastocysts.	CC, DDR	Liu et al., 2007
Pcna	E2.5	Embryos do not survive to the blastocyst stage.	Rep, BER, NER, MMR	Roa et al., 2008
Rpa1	E2.5	Morula form but do not progress to blastocysts.	Rep, HDR, NER, BER, MMR	Wang et al., 2005
Wee1	E2.5	Morula form but do not progress to blastocysts.	CC, DDR	Tominaga et al., 2006
Nop53 (Pict1)	Before E3.5	Mutant embryos develop morphologically typical morula, but do not form well-structured blastocysts.	CC, DDR*	Sasaki et al., 2011
Cdk1	Before E3.5	Morula form but do not progress to blastocysts.	CC, DDR	Diril et al., 2012
Plk1	E3.5	Mutant embryos develop to the morula stage but do not form viable blastocysts *in vitro*.	CC, DDR	Lu et al., 2008
Xab2	E3.5	Mutant embryos form morula and show some signs of compaction, but do not form blastocysts.	NER*	Yonemasu et al., 2005
Pot1a	After E3.5	Morula are recovered and can be cultured but do not form blastocysts.	Telomere	Hockemeyer et al., 2006

*Key: (E) = Embryonic day; DDR = DNA damage response/damage sensing; CC = cell cycle control; Rep = DNA replication and/or replication stress; HDR = Homologous directed repair; EJ = End joining pathways; BER = Base excision repair; NER = Nucleotide excision repair; MMR = Mismatch repair; Telomere = telomere protein. Gene functions are cross-referenced with the literature and may diverge from the MGI-GO categorization. Factors labeled with * indicate when the gene encodes a protein with additional functions outside genome stability that likely contribute to embryonic lethality.*

TABLE 2 | Genome stability factors essential for peri-implantation development.

Targeted gene	Lethal at	Phenotype details	Gene function	References
Zfp830 (Omcg1)	E3.5	Knockouts blastocysts form but fail to outgrow and do not induce an implantation response *in vivo*.	CC, Rep, DDR*	Artus et al., 2005
Actr2	After E3.5	Lethal after blastocyst stage.	HDR*	Zhang et al., 2007
Cdc7	After E3.5	Blastocysts form and can hatch. Outgrowth assays demonstrate with *in vitro* culture knockout embryos have a small ICM population by E5.5.	CC, Rep, DDR	Kim et al., 2002
Chek1	After E3.5	Blastocysts form *in vivo* but are resorbed following implantation. *In vitro* cultured blastocysts have elevated apoptosis in ICM populations.	Rep, DDR	Takai et al., 2000 Zaugg et al., 2007
Atr	E4.5	Blastocysts form, hatch, and show evidence of initiating implantation *in utero*. ICM outgrowth assays are consistent with wildtype embryos, but ICM populations succumb to apoptosis with continued culture.	CC, Rep, DDR, HDR	de Klein et al., 2000 Brown and Baltimore, 2000 Murga et al., 2009
Cdc25A	E4.5	Blastocysts form but suffer from impaired hatching ability.	CC, Rep	Ray et al., 2007
Ctip (Rbbp8)	E4.5	Embryos form blastocysts but fail to form an egg cylinder. Cells appear to suffer from reduced DNA synthesis.	Rep, HDR	Chen et al., 2005
Recql4	From E4.5	Outcomes are dependent on the genetic manipulation. Deletion of exons 5–8 are lethal during gastrulation, deletion of exon 13 results in lethality just after birth.	Rep, HDR	Hoki et al., 2003
Rint1	From E4.5	Null embryos implant *in vivo* but are severely developmentally delayed and resorbed from E6.5. The ICM and trophoblasts initially outgrow *in vitro*, but proliferation fails after 6 days.	HDR*	Lin et al., 2013
Thoc1	From E4.5	Embryos form a blastocyst, hatch, and attach in *in vitro*, but suffer from reduced proliferation of the ICM after several days in culture. No embryos are recovered *in vivo* before E8.5, but decidua are present, suggesting the embryos die during gastrulation.	CC, HDR, DDR*	Wang et al., 2006
Apex1	After E4.5	Blastocysts form and attach but die soon after.	Rep, BER	Xanthoudakis et al., 1996
Cdc45	After E4.5	Blastocysts form and can hatch. Blastocyst outgrowth assays demonstrate that after several days of culture the ICM mass is smaller or not present.	CC, Rep	Yoshida et al., 2001
Cdk7 (Cdks)	After E4.5	Decidual resorption at peri-implantation stages *in vivo. In vitro* cultured embryos demonstrate increased apoptosis in the blastocyst and severely reduced ICM proliferation.	CC, Rep	Ganuza et al., 2012
Fen1	After E4.5	Blastocysts form and hatch but are compromised during peri-implantation.	Rep, EJ, BER,	Larsen et al., 2003
Gins4 (Sld5)	After E4.5	Embryos form blastocysts that hatch and implant. Development is compromised after implantation as embryos do not form egg cylinders. Embryos attach in outgrowth assays, but after 2 days of culture the ICM becomes compromised.	Rep	Mohri et al., 2013
Hinfp	After E4.5	Knockout blastocysts can form, hatch, and attach, but embryos do not survive past E6.5.	CC, Rep*	Xie et al., 2009
Mdm2	After E4.5	Embryos can implant but are quickly resorbed.	DDR	Jones et al., 1995
Mnat1	After E4.5	Blastocysts form that are indistinguishable from wildtype littermates, but no embryos are found after gastrulation.	CC, Rep*	Rossi et al., 2001

(Continued)

TABLE 2 | Continued

Targeted gene	Lethal at	Phenotype details	Gene function	References
Pold3	After E4.5	Blastocysts form, hatch, and attach *in vitro* but show reduced outgrowth compared to wildtype embryos. *In vivo*, no embryos are recovered at E7.5 consistent with embryo failure during gastrulation.	Rep, NER, TLS	Zhou et al., 2018
Prpf19	After E4.5	Same as above.	CC, Rep, DDR, HDR	Fortschegger et al., 2007
Ptpn11	After E4.5	Same as above.	CC*	Yang et al., 2006
Topbp1	After E4.5	Blastocysts form and hatch but are unable to attach to the tissue culture dish *in vitro*.	CC, Rep, DDR, HDR	Jeon et al., 2011
Yy1	From E5.0	Knockout blastocysts, form, hatch, and outgrow normally *in vitro.* However, *in vivo*, embryos fail to form and egg cylinder and die during gastrulation.	DDR, HDR*	Affar El et al., 2006
Rad51	Before E5.5	Blastocysts appear normal, but post-implantation embryos fail to properly develop an amniotic cavity, display no discernible mesoderm, have a reduced proliferation rate, and elevated apoptosis.	Rep, HDR	Lim and Hasty, 1996 Tsuzuki et al., 1996
Thoc5	Before E5.5	Embryos are not recovered from the uterus from E5.5 suggestive of death during preimplantation or gastrulation.	CC, HDR, DDR*	Mancini et al., 2010
Timeless	From E5.5	Embryos display severe cellular disorganization during gastrulation.	Rep	Gotter et al., 2000
Brca1	E5.5	Growth arrest and impaired proliferation resulting in resorption.	Rep, HDR	Hakem et al., 1996 Ludwig et al., 1997
Mre11A	E5.5	Embryos compromised during gastrulation.	Rep, HDR, DDR, EJ	Xiao and Weaver, 1997 Theunissen et al., 2003 Buis et al., 2008
Nbn (Nbs1)	E5.5	Blastocysts form and hatch, but embryos are smaller after implantation and are resorbed around gastrulation.	Rep, DDR, HDR, EJ	Zhu et al., 2001
Ube2N	E5.5	Embryos are never recovered, and timed mating suggests that embryos die during gastrulation.	HDR	Fukushima et al., 2007
Rad50	Before E6.0	Embryos are abnormal from gastrulation onset and are resorbed.	Rep, DDR, HDR, EJ	Luo et al., 1999
Fh1	E6.0	Embryos do not appear to grow past the early egg cylinder stage.	NHEJ*	Pollard et al., 2007
Blm	E6.5	Reduced embryo size, epiblast population and mesoderm population. The primitive streak forms but there is increased apoptosis throughout the embryo.	HDR, Rep	Chester et al., 1998
Cops5	E6.5	Gastrulating embryos are smaller and cannot develop all germ layers. Embryos display elevated apoptosis.	CC, DDR*	Tomoda et al., 2004
Kdm1A	E6.5	Blastocysts form, hatch, and attach *in vitro*, but are developmentally stunted from E6.5.	DDR, HDR*	Foster et al., 2010
Usp7	E6.5	Embryos die during gastrulation due to reduced proliferation.	Rep, NER	Kon et al., 2010
Xrcc1	E6.5	Epiblast cell numbers are reduced in early gastrulating embryos due to apoptosis and slow proliferation, which impacts lineage specification.	EJ, BER	Tebbs et al., 1999
Pold1	Before E7.5	Knockout embryos form blastocysts at E4.5 but no embryos are retrieved at E7.5.	Rep, BER, NER, MMR	Uchimura et al., 2009
Cul4A	Before E7.5	Embryos form blastocysts *in vitro* that hatch from the zona pellucida with no ICM or trophoblast compromise. No characterization of lethality presented.	CC, Rep, DDR, NER	Li et al., 2002
Dna2	Before E7.5	No embryos retrieved after E7.5. The cause of lethality was not investigated further.	Rep, HDR, BER	Lin et al., 2013
Rif1	From E7.5	Null embryos are lethal from gastrulation in some genetic backgrounds but are viable in different mouse strains. Dimorphism in embryo survivability observed where male knockouts survive but female knockouts do not.	Rep, HDR	Chapman et al., 2013

(Continued)

TABLE 2 | Continued

Targeted gene	Lethal at	Phenotype details	Gene function	References
Bard1	E7.5	Embryos do not develop past egg cylinder stage.	Rep, HDR	McCarthy et al., 2003 Shakya et al., 2008
Brca2	E7.5	Reduced embryo size and persisting Oct4 positive egg cylinder indicates retarded dermal commitment of epiblast cells.	Rep, HDR	Sharan et al., 1997
Hus1	E7.5	Gastrulating embryos appear normal but are smaller than wildtype littermates. Development becomes severely delayed from mid-gastrulation.	Rep, DDR, BER, NER	Weiss et al., 2000
Ino80	E7.5	Knockout embryos implant as deciduas are found at E7.5, but embryos are resorbed during organogenesis.	Rep, DDR, HDR*	Min et al., 2013
Lig3	E7.5	Embryos are smaller from gastrulation onset and do not develop past mid-gastrulation.	Rep, EJ, BER, NER	Puebla-Osorio et al., 2006
Ptip	E7.5	Gastrulating embryos display increased apoptosis. Embryos can be recovered in the early stages of organogenesis but are poorly formed.	Rep, DDR, EJ, HDR	Cho et al., 2003
Rad51B (Rec2)	E7.5	Knockout embryos implant, but do not develop pro-amniotic cavities and are resorbed by E7.5.	HDR	Shu et al., 1999
Uvrag	E7.5	Knockout mice die by E7.5 but no additional data is provided as to the cause of the lethality.	EJ*	Afzal et al., 2015
Wdr48 (Uaf1)	E7.5	Knockout mice die during gastrulation.	Rep, HDR	Park et al., 2013
Ercc3 (Xpb)	Before E8.5	No healthy embryos are recovered by early organogenesis. Embryos may be compromised earlier but no additional details are provided.	NER*	Andressoo et al., 2009
Ddb1	Before E8.5	Same as above.	CC, Rep, DDR, NER	Cang et al., 2006
Palb2	E8.5	Embryos are developmentally retarded after gastrulation and die during organogenesis.	Rep, HDR	Bowman-Colin et al., 2013
Rad51C	E8.5	Knockout embryos implant but are developmentally delayed, resulting in impaired gastrulation and resorption from E8.5.	Rep, HDR	Kuznetsov et al., 2009
Rev3L	After E8.5	Blastocysts form but do not thrive *in vitro*. Embryos are smaller than wildtype littermates during gastrulation.	HDR, TLS	Bemark et al., 2000
Pnkp	After E9.0	Embryos are not recovered from the onset of organogenesis. No further details are provided as to the cause of lethality.	EJ, BER	Shimada et al., 2015
Nipbl (Scc2)	Before E9.5	No knockout mice are recovered from the onset of organogenesis, but no additional data is provided.	Rep, DDR, HDR, EJ	Smith et al., 2014
Srpq	Before E9.5	Knockouts cannot be recovered from the start of organogenesis, implying that embryos die during gastrulation.	HDR*	Takeuchi et al., 2018
Ppp4C	Before E9.5	Same as above.	HDR	Shui et al., 2007
Rnaseh2B	From E9.5	Knockouts are smaller than littermates at gastrulation conclusion and die early in organogenesis.	Rep, DDR	Hiller et al., 2012
Syf2	E9.5	Knockouts do not survive organogenesis. Embryos can implant but gastrulation does not proceed normally.	CC, Rep	Chen et al., 2012
Nsmce2	Before E10.5	Knockout mice are not recovered from the uterus by E10.5. Embryos recovered at E2.5 appear normal but do not thrive *in vitro*. The cause of embryonic failure is not reported.	HDR	Jacome et al., 2015

*Key: (E) = Embryonic day; DDR = DNA damage response/damage sensing; CC = cell cycle control; Rep = DNA replication and/or replication stress; HDR = Homologous directed repair; EJ = End joining pathways; BER = Base excision repair; NER = Nucleotide excision repair; MMR = Mismatch repair; Telomere = telomere protein; TLS = Translesion synthesis. Gene functions are cross-referenced with the literature and may diverge from the MGI-GO categorization. Factors labeled with * indicate when the gene encodes a protein with additional functions outside genome stability that likely contribute to embryonic lethality.*

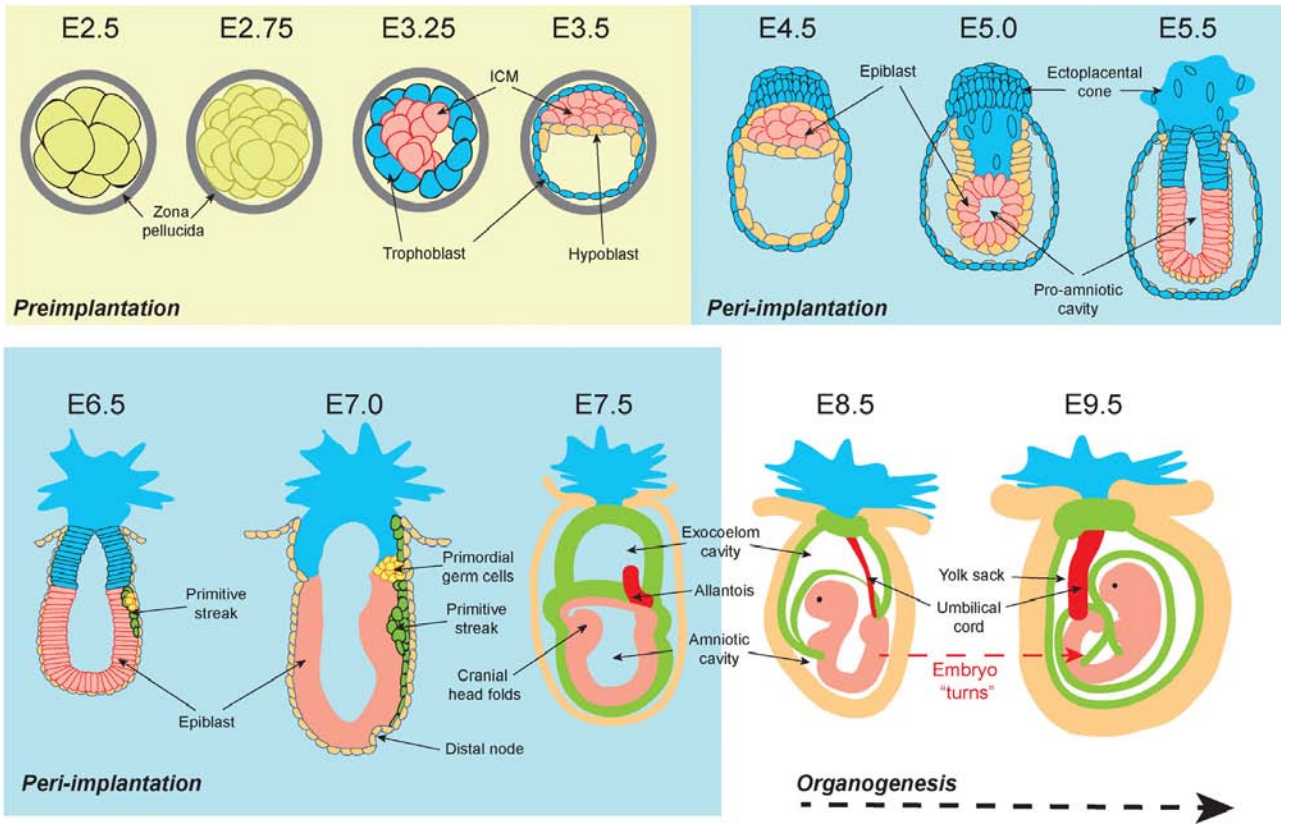

FIGURE 1 | Graphical representation of the early stages of murine development. At embryonic day 2.5 (E2.5) totipotent cells within the preimplantation morula are encased within a protective zona pellucida shell. From E3.25 the blastocoel cavity opens, and the embryonic cells differentiate into the inner cell mass (ICM) (pink) and the outer trophoblast (blue). By E3.5 the hypoblast (orange) has developed. During peri-implantation the zona pellucida shell is lost by E4.5 and the ICM are now termed "epiblast cells" (pink). The outer trophoblast cell layer continues to encapsulate the embryo and expands to form the ecto-placental cone that is the precursor for placental tissues. From E5.0 a pro-amniotic cavity opens and elongates. By E6.5 the embryo has implanted, the primitive streak (green) emerges, and the primordial germ cell populations form (yellow). The primitive streak continues to elongate and is accompanied by the formation of the distal node at E7.0. At E7.5 the primitive streak derived mesoderm extends around the embryo and divides the pro-amniotic cavity into the exocoelom cavity and the amniotic cavity. At E8.5 the exocoelom becomes the yolk sack. Between E8.5 and E9.5 the embryo turns, resulting in complete envelopment of the embryo within the supporting extraembryonic tissues. Embryo depictions are not to scale.

(nervous system and skin precursor), endoderm (gut precursor), and mesoderm (precursor for all other tissues) (Watson and Tam, 2001). Because continued gastrulation requires a critical mass of 1000 cells, delays in epiblast proliferation at E6.5 may result in the embryo forming a small primitive streak but developing no further (Snow and Tam, 1979; Tam, 1989; Power and Tam, 1993).

Between E6.5 and E7.5 the rate of epiblast proliferation is exceptionally pronounced, with some cell cycles completed in 2.2 h (Snow, 1977). Elongation of the primitive streak between E6.5 and E7.0 is associated with the first evidence of epithelial to mesenchymal transition (EMT) (Carver et al., 2001). EMT mobilizes epiblast cells to form the endoderm and mesoderm lineages, while cells that do not undergo EMT become the ectoderm (Acloque et al., 2009). At E7.5 the mouse embryo contains over 14,000 cells derived from epiblast progenitors. Proliferation slows at this point resulting in an increased average cell cycle duration of 8.1 h (Snow, 1977). There is evidence to suggest a that a specialized "proliferative zone" with sub 4-h cell cycles is maintained within the primitive streak after E7.5, however, definitive evidence remains to be substantiated (Tam et al., 2013).

Genome Instability Differentially Impacts Cell Viability in Pre- and Peri-Implantation Embryos

Embryonic lethality implies that one or more cell populations are compromised during development at the time of embryo failure. This may arise through DNA damage or genome instability, with multiple lines of evidence indicating that preimplantation embryos are more resistant to genome perturbations than peri-implantation embryos. For example, gamma irradiation-induced DNA damage at E6.5 or E7.5 confers apoptosis specifically within the epiblast (Heyer et al., 2000). Conversely, apoptosis levels are low in preimplantation embryos irradiated between E3.5 and E5.5, or during organogenesis from E8.5. It is therefore the epiblast that is particularly sensitive to these types of DNA lesions. Similarly, despite tetraploidy driving additional

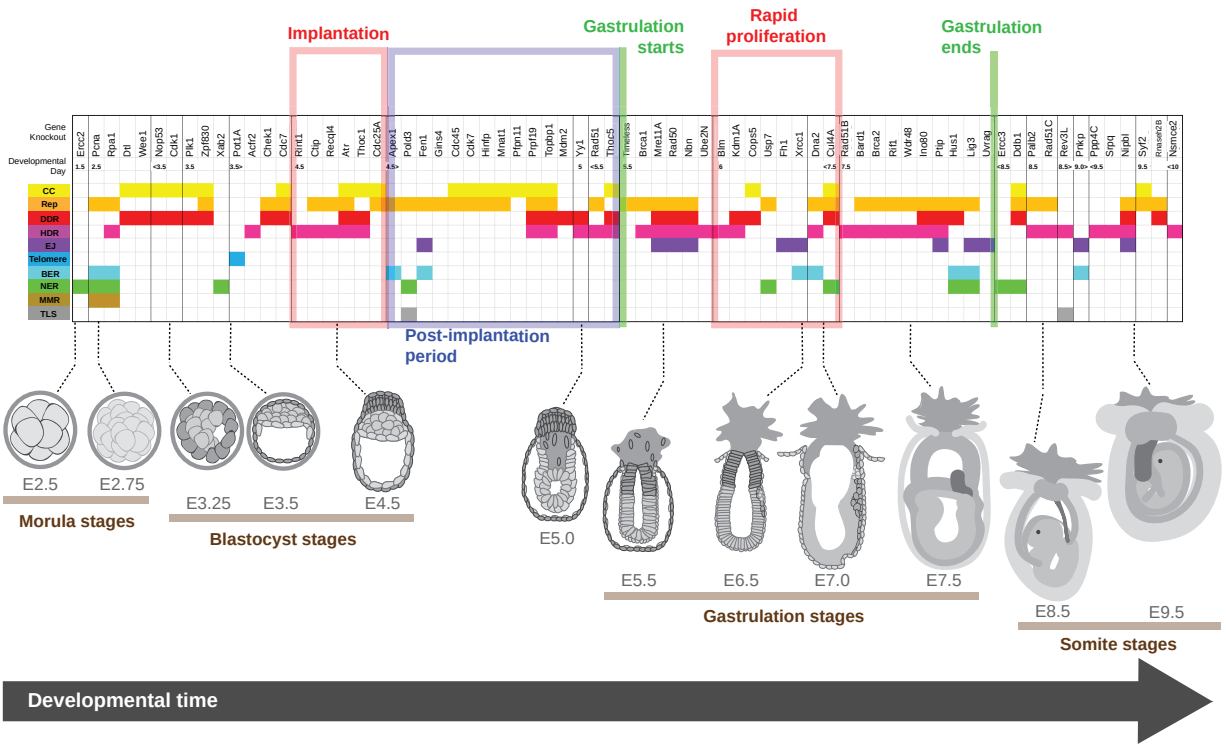

FIGURE 2 | Lethality onset in embryos deleted for genome stability factors relative to developmental stage. Spatiotemporal heat map illustrating the timing of lethality for embryos lacking genome stability factors essential for early development. Genes are listed above and organized temporally relative to the reported timing of embryo compromise. Graphical depiction of normal embryo structure at the time of lethality is shown below and key developmental periods are highlighted. Gene functions according to the literature are color coded as follows: cell cycle regulation (CC, yellow); DNA replication and/or the replication stress response (Rep, orange); DNA damage response (DDR, red); Homology directed repair (HDR, pink); canonical and alternative non-homologous end joining (EJ, purple); telomere biology (Telomere, blue); base excision repair (BER, cyan); nucleotide excision repair (NER, green); mismatch repair (MMR, brown) and translesion synthesis (TLS, gray). Embryo depictions are not to scale.

chromosomal instability in preimplantation cells (Paim and FitzHarris, 2019) chimeric mouse embryos with a mixture of diploid and tetraploid cells will develop through preimplantation before dying during peri-implantation (Horii et al., 2015). Notably, tetraploid sensitivity *in vivo* appears to be specific to the epiblast as embryos with tetraploid trophoblast cells and diploid epiblast cells can generate live pups (Wen et al., 2017). Mouse embryos containing a mixture of diploid and aneuploid cells will also develop to peri-implantation before the aneuploid cells are specifically depleted in the epiblast through apoptosis (Bolton et al., 2016).

As with somatic tissues, the tumor suppressor *TP53* (p53) plays a central role regulating stem cell outcomes following genomic insult. p53 orchestrates growth arrest or apoptosis following activation of the DNA damage response (Mello and Attardi, 2018). Concordantly, inhibiting p53-dependant signaling pathways enables chimeric embryos made from tetraploid preimplantation murine embryonic stem cells (mESCs) to survive until birth (Horii et al., 2015). Deleting *TP53* also reduced apoptosis levels in irradiated E6.5 embryos (Heyer et al., 2000) and extended the survival of embryos co-deleted for essential DNA repair factors (Jones et al., 1995; Haupt et al., 1997; Ludwig et al., 1997; Kim et al., 2002; McCarthy et al., 2003; Cang et al., 2006; Reinhardt and Schumacher, 2012). Not surprisingly, *TP53* was identified as a critical mediator of apoptosis in the gastrulating epiblast (Laurent and Blasi, 2015). However, when activated in pluripotent stem cells, p53 also influences the expression of pluripotency factors to regulate differentiation (Lin et al., 2005; Li et al., 2012; Akdemir et al., 2014; Jain et al., 2016). p53 therefore functions through canonical and unique pathways in early development to regulate cellular outcomes. This highlights that our classic understanding of genome stability pathways may not strictly apply to early development or certain pluripotent cell types (Zaveri and Dhawan, 2018).

DNA DAMAGE RESPONSE AND REPAIR PATHWAYS

Replication Stress Response

Somatic mammalian cells prepare for DNA replication in G1 phase by licensing replication origins and loading inactive Cdc45-MCM-GINS replicative helicase complexes (Bleichert, 2019; Miller et al., 2019). Cyclin dependent kinase activity promotes E2F transactivation to initiate replication

at the G1/S transition (Kent and Leone, 2019). Replication then proceeds throughout the S-phase with origins firing in temporal coordination and DNA synthesis occurring across the entirety of the genome (Burgers and Kunkel, 2017; Limas and Cook, 2019). Intrinsic and extrinsic factors may disrupt replication fork processivity: a phenomenon known as "replication stress" (Zeman and Cimprich, 2014). Replication stress is sensed through the accumulation of RPA binding to its single strand DNA (ssDNA) substrate (Bhat and Cortez, 2018). When replication stress stalls DNA synthesis the replicative helicase continues to unwind its substrate exposing ssDNA for RPA coating (Byun et al., 2005). ATR kinase is the master regulator of the replication stress response (Saldivar et al., 2017). RPA coated ssDNA recruits ATR and its associated protein ATRIP (Cortez et al., 2001) to stalled replication forks through parallel pathways mediated by TopBP1 and ETAA1 (Kumagai et al., 2006; Bass et al., 2016; Haahr et al., 2016). Once localized to the stalled fork, ATR is activated and propagates a signaling cascade resulting in engagement of the replication stress response. This includes activation of the downstream effector CHK1 kinase to arrest S phase until replication stress is resolved (Zhang and Hunter, 2014). During the replication stress response, stalled replication forks are often remodeled into a four-way structure and protected before engaging one of many diverse repair mechanisms dependent upon the underlying stress the fork encountered (Quinet et al., 2017; Cortez, 2019).

If replicative stress is unresolved, arrested replication forks may collapse into one-ended double strand breaks (DSBs) (Ait Saada et al., 2018). Additionally, persistent replication stress can result in under-replicated DNA persisting through S-phase, the second growth (G2) phase, and into the mitotic (M) phase of the cell cycle (Mankouri et al., 2013). Specialized repair mechanisms address replication defects carried into mitosis (Minocherhomji et al., 2015), during which time the canonical DSB repair pathways are inhibited (Orthwein et al., 2014). Replication defects passed into mitosis can confer chromosome segregation errors resulting in aneuploidy (Burrell et al., 2013; Wilhelm et al., 2019), or if severe mitotic death (Masamsetti et al., 2019). If a replication stressed cell escapes mitosis this is often evident in the daughter cells where the under-replicated DNA is present as a scar in the first growth phase (G1) that is repaired in the subsequent S phase (Lukas et al., 2011; Spies et al., 2019).

Double Strand Break Repair

DSBs are a major threat to genome stability because a failure in repair may result in loss of an entire chromosome arm (Scully et al., 2019). Additionally, chromosome segregation errors resulting from inadequate DSB repair are rife with implications for genome instability, including chromothripsis and kataegis (Maciejowski et al., 2015; Ly and Cleveland, 2017). DSBs are sensed by Ku70/80 (Gottlieb and Jackson, 1993; Ochi et al., 2015), PARP1 (Ali et al., 2012; Liu C. et al., 2017), and the MRN (MRE11, RAD50 and NBS1) complex (Lee and Paull, 2005; Stracker and Petrini, 2011). MRN facilitates recruitment of the ATM kinase to DSBs (Uziel et al., 2003) while Ku70/80 recruits a related kinase DNA-PKcs (Hnizda and Blundell, 2019). Once recruited to the break, ATM is activated and engages downstream DDR pathways (Dupre et al., 2006; Maréchal and Zou, 2013). This includes phosphorylation of the histone variant H2AX (termed γ-H2AX when phosphorylated) within the break adjacent chromatin and assembly of factors at the break locus to facilitate repair (Rogakou et al., 1998). ATM activation also results in growth arrest, including activation of the p53 pathway (Banin et al., 1998). Subsequent repair of DNA breaks is then orchestrated by homology directed repair (HDR) or end-joining (EJ) pathways.

Homology directed repair utilizes the homologous sister chromatid as a template for repair and is thus limited to the S and G2 cell cycle phases (Hustedt and Durocher, 2016). HDR initiates with resection at the broken DNA end to provide a 3′ ssDNA overhang for insertion into homologous regions of the sister chromatid (Symington, 2016). Once resection occurs at a canonical two-ended DSB, a series of enzymatic steps facilitate strand-invasion of the broken end into the sister chromatid, formation of a displacement-loop, template copying from the invaded DNA end, potential formation of a "Holliday Junction," and resolution of strand invasion (Scully et al., 2019). HDR factors also function within the replication stress response though diverse mechanisms including the remodeling and stabilization of stressed replication forks into four-way structures prior to repair (Neelsen and Lopes, 2015). Additionally, HDR factors participate in resolving one-ended DSBs that arise from collapsed replication forks to restart replication (Ait Saada et al., 2018). HDR is thus intrinsically linked to the replication stress response.

Conversely, EJ involves the covalent ligation of broken DNA ends to repair DSBs and thus does not require an additional chromatid template. End-joining mechanisms function in S and G2, but notably are the only DSB repair pathway available in G1 (Chang et al., 2017). Classical non-homologous end joining (c-NHEJ) directly ligates DNA ends, and if unregulated can also drive chromosome translocations (Ghezraoui et al., 2014) or telomere fusions (Celli et al., 2006; Van Ly et al., 2018). Cells can also engage alternative non-homologous end joining (alt-NHEJ), where DNA resection creates 3′ overhangs to align the DNA ends for repair through microhomology (Sfeir and Symington, 2015). This often requires a fill-in reaction by the error prone polymerase Pol θ which can introduce errors into the repaired sequence (Mateos-Gomez et al., 2015; Mateos-Gomez et al., 2017).

Nucleotide and Base Damage

In addition to DNA breaks, cells must also contend with damage to nucleotide bases, base mismatches, and bulky DNA lesions that distort the DNA double helix. Base excision repair (BER) mends small non-distorting DNA lesions such as oxidized DNA bases (Wallace, 2014), while nucleotide excision repair (NER) corrects bulky lesions such UV-induced pyrimidine dimers (Schärer, 2013). BER is mediated by DNA

glycosylases that cleave and remove the damaged bases at the lesion. A correct base is then inserted by specialized DNA polymerases (Wallace, 2014). In NER, a 25–30 nucleotide patch of ssDNA containing the bulky lesion is excised from the double strand helix before specialized DNA polymerases fill in the ssDNA gap (Schärer, 2013). Mismatch repair (MMR) proofreads the newly replicated DNA to identify misincorporated bases (Liu D. et al., 2017). When a mismatch is identified, the newly synthesized strand is nicked and resected creating a patch of exposed ssDNA for fill in by a high-fidelity DNA polymerase.

Essentiality of DNA Repair During Embryogenesis

Not all DNA repair activities are essential for early development (**Supplementary Table S1**). The most striking example is the dichotomy between the major DSB repair pathways. While many HDR factors are essential, the core c-NHEJ factors are either dispensable for development [*Ku70* (Ouyang et al., 1997), *Ku80* (Nussenzweig et al., 1996; Gu et al., 1997), *Prkdc* (DNA-PKcs) (Kurimasa et al., 1999), *Nhej1* (XLF) (Li et al., 2008)] or only required for organogenesis [*Lig4* (Frank et al., 1998), *Xrcc4* (Dickinson et al., 2016)]. Some alt-NHEJ components are required for early development. Alt-NHEJ is promoted by the polymerase Pol θ which primes the DNA ends for repair by removing RPA from exposed ssDNA regions (Kent et al., 2015; Mateos-Gomez et al., 2017). Alt-NHEJ is also dependent on PARP-1, XRCC1 and LIG3 (Audebert et al., 2004), with PARP-1 having a critical role in synapsis, and XRCC1 and LIG3 mediating DNA ligation (Audebert et al., 2004). While *Lig3* and *Xrcc1* knockout embryos die during gastrulation (Tebbs et al., 1999; Puebla-Osorio et al., 2006), both genes encode factors that have functions in other DNA metabolic activities outside EJ (Wallace, 2014). Conversely *Pol* θ knockout mice are viable (Shima et al., 2004; Masuda et al., 2005), as are *Parp1* knockouts (Wang et al., 1995), suggesting that alt-NHEJ is not essential for embryogenesis.

Preference for HDR over NHEJ is further evident in mechanistic studies of DDR engagement within embryonic stem cells (Tichy et al., 2010). Following DSB induction, ATM-dependent γ-H2AX phosphorylation at the break locus recruits the scaffolding protein MDC1 (Stewart et al., 2003). MDC1 subsequently recruits the ubiquitin ligases RNF8 and RNF168 that signal downstream recruitment of 53BP1 (Jackson and Durocher, 2013). 53BP1 then establishes a physical domain at the repair locus in coordination with RIF1 to inhibit end resection and HDR in favor of c-NHEJ (Chapman et al., 2013; Zimmermann et al., 2013; Lou et al., 2019; Ochs et al., 2019). Notably, many factors that promote c-NHEJ are dispensable for embryonic development, including *Atm* (Barlow et al., 1996; Xu et al., 1996), *H2ax* (Celeste et al., 2002), *Mdc1* (Lou et al., 2006), *Rnf8* (Valnegri et al., 2017), *Rfn168* (Zong et al., 2019), and *Trp53bp1* (53BP1) (Ward et al., 2003). Additionally, multiple reports demonstrate that 53BP1 does not localize to DSB foci in the ICM of preimplantation embryos or mESCs grown in culture (Ziegler-Birling et al., 2009; Kafer et al., 2016). *In vivo*, 53BP1 localizes to damage in E5.5 embryos, but only in the epiblast cells and not the endoderm or trophoblast cells (Laurent and Blasi, 2015). While *Trp53bp1* expression is unchanged in early development, *Rnf168* expression is limited prior to the epiblast stage which may explain differential engagement of DDR pathways in pre- and peri-implantation cells (Laurent and Blasi, 2015).

GENES ESSENTIAL FOR PREIMPLANTATION DEVELOPMENT

Consistent with a greater tolerance of genome instability in preimplantation cells, only 10 knockouts of genome stability factors that we reviewed were lethal during preimplantation (**Table 1** and **Supplementary Table S1**). Factors encoded by many of these preimplantation essential genes also possessed critical functions outside DDR or repair. Additionally, preimplantation embryos commonly survive to the morula stage even if a targeted gene is essential for viability. This is because embryonic genomes are not immediately active following fertilization while the inherited maternal mRNA guides protein translation (Jukam et al., 2017).

Multifunctional Factors Essential for Preimplantation Development

Of the 10 genome stability factors required for preimplantation development, only *Ercc2* deletion did not permit morula generation. $Ercc2^{-/-}$ embryos fail to develop past the 2-cell stage *in vitro* and there is no evidence of embryo implantation *in vivo* (de Boer et al., 1998). *Ercc2* encodes the XPD helicase that functions both in NER and as a core component of the general transcription factor IIH (TFIIH) complex. TFIIH opens DNA and anchors the cdk-activating kinase (CAK) complex to facilitate transcription (Egly, 2001). Given that *Ercc2* knockouts are compromised during embryonic genome activation (EGA), a reasonable conclusion is that preimplantation lethality is associated with a loss of XPD transcriptional activity. Likewise, *Xab2* is a TFIIH and NER component and *Xab2* deletion is lethal prior to the blastocyst stage (Yonemasu et al., 2005). However, *Xab2* null embryos survive past the 2-cell stage suggesting *Xab2* is not required for EGA.

Pcna and *Rpa1* both function in multiple genome maintenance pathways and deleting either gene confers preimplantation lethality (Wang et al., 2005; Roa et al., 2008). PCNA (proliferating cell nuclear antigen) forms a homotrimeric sliding clamp that encircles DNA. The protein clamp travels with the replication fork to promote replicative polymerase processivity and mediate diverse functions in DNA replication and the replication stress response (Mailand et al., 2013). PCNA also functions in NER and MMR (Strzalka and Ziemienowicz, 2011). *Rpa1* (Replication Protein A 1) codes

for the 70 kDa subunit of the heterotrimeric RPA ssDNA binding complex that participates in replication, but which also functions in ATR activation, replication fork repair, HDR and NER (Bhat and Cortez, 2018). Analysis of *Pcna* mRNA showed a significant reduction of maternal transcripts from the zygote to the 2-cell stage consistent with the observed early embryonic lethality (Hamatani et al., 2004; Roa et al., 2008; Bult et al., 2019). *Rpa1* null embryos form blastocysts at E3.5 that are smaller than their heterozygous littermates and which fail in blastocyst outgrowth assays, indicating *Rpa1* is required for trophectoderm and ICM growth (Wang et al., 2005). While both *Rpa1* and *Pcna* function in diverse aspects of genome maintenance, both genes are also required for DNA replication. Preimplantation failure of *Pcna* or *Rpa1* null embryos likely stems from an inability to polymerize nascent DNA coupled with simultaneous attenuation of multiple DNA repair pathways.

Two additional genes classified as DNA repair factors in the MGI-GO database are also essential during preimplantation. *Nop53* encodes a nucleolar protein with suggested roles regulating p53, DNA repair, and the cellular response to mitochondrial stress (Lee et al., 2012; Yoon et al., 2014). *Nop53* null embryos fail to develop past the blastocyst stage, while *Nop53*$^{-/-}$ mESCs are viable, suggesting that *Nop53* functions in morula to blastocyst maturation (Sasaki et al., 2011). In somatic cells, *Pot1a* encodes a telomere specific ssDNA binding protein that suppresses ATR and p53 activation by the chromosome end (Hockemeyer et al., 2005, 2006; Denchi and de Lange, 2007). Loss of *Pot1a* likely confers robust ATR activation which explains the failure of *Pot1a*$^{-/-}$ embryos to form an ICM (Hockemeyer et al., 2006).

Cell Cycle and Checkpoint Factors Essential for Preimplantation Viability

In the event of replication stress or DSBs, checkpoints slow the cell cycle to provide time for DNA repair. Deletion of several genes that encode checkpoint regulatory factors confer preimplantation embryo failure at the morula stage. These include *Wee1* (Tominaga et al., 2006), *Cdk1* (Diril et al., 2012), and *Plk1* (Lu et al., 2008; Wachowicz et al., 2016). CDK1 promotes the G2/M transition through interaction with cyclin B, and CDK1-cyclin B activity is regulated by WEE1 (Harvey et al., 2005; Gavet and Pines, 2010). ATR and CHK1 activate the G2/M checkpoint by stimulating WEE1 to inhibit CDK1 (O'Connell et al., 1997; Nigg, 2001). Polo-like kinase 1 (PLK1) controls numerous mitotic activities, participates in the G2/M transition, may function in DNA replication, and is implicated in HDR through phosphorylation of RAD51 (Watanabe et al., 2004; Mandal and Strebhardt, 2013; Yata et al., 2014; Pintard and Archambault, 2018). *Dtl* is also required for preimplantation development (Liu et al., 2007). *Dtl* encodes a component of the CUL4A-DDB1 E3-ubiquitin ligase complex that degrades the replication licensing factor CDT1 to stimulate replication and S phase progression (Nishitani et al., 2001; Li and Blow, 2005). Because these essential cell cycle genes function in DDR-regulated checkpoints and normal cell cycle transitions, the mechanism of embryonic lethality following their deletion likely involves deregulation of both the DDR and normal cell cycles.

GENES ESSENTIAL FOR PERI-IMPLANTATION DEVELOPMENT

Peri-implantation is the period of embryonic development most associated with lethality following deletion of genome stability factors. Within the MGI-GO derived gene list, it stands out that 54 of the 62 genes essential for peri-implantation development have direct or indirect functions in DNA replication, the replication stress response, and/or HDR (**Table 2** and **Supplementary Table S1**). Below we focus specifically on these pathways.

Genes Regulating Replication Initiation, DNA Polymerization, and the Replication Stress Response Are Essential for Peri-Implantation Development

Because of the rate of cell proliferation in peri-implantation embryos, it is perhaps unsurprising that factors which regulate the G1/S transition and initiate DNA replication are essential for peri-implantation development. This includes *Cdc7* (Kim et al., 2002), *Cdc45* (Yoshida et al., 2001), *Cdk7* (Ganuza et al., 2012), *Mnat1* (Rossi et al., 2001), *Gins4* (Mohri et al., 2013), *Cul4A* (Li et al., 2002), and *Ddb1* (Cang et al., 2006). Additionally, the *Pold3* subunit of the replicative polymerase *Pol*δ is required for peri-implantation development (Uchimura et al., 2009; Zhou et al., 2018), as is *Fen1*, which plays a central role in processing Okazaki fragments on the lagging strand of DNA synthesis (Larsen et al., 2003). Lethality following deletion of most of these genes occurs on or near E4.5 and is associated with proliferative failure within the ICM after blastocyst formation but prior to gastrulation. A likely explanation is that peri-implantation development is rapidly compromised when fundamental functions necessary for cellular proliferation and/or DNA replication are dysregulated.

Even in the absence of exogenous threats to replication, the exceptionally fast cell cycles within the developing epiblast are expected to confer intrinsic replication stress. For example, blastocyst derived mESCs display replication stress in unperturbed cultures *in vitro* (Ahuja et al., 2016). mESCs appear to manage this replication stress by effectively coupling replication and repair activities to facilitate near continuous DNA synthesis punctuated by brief G1 and M phases (Ahuja et al., 2016). Epiblast cell cycles *in vivo* are more rapid than cell cycles in cultured mESCs (Snow, 1977; Mohammed et al., 2017) suggesting that a similar reliance on efficient coupling of DNA replication and the repair activity is required to manage replication stress in peri-implantation embryos.

The replication stress response begins when ATR/ATRIP localizes to RPA-coated ssDNA, and ATR is activated through

TOPBP1 and the RAD9-RAD1-HUS1 (9-1-1) protein complex (Kumagai et al., 2006; Navadgi-Patil and Burgers, 2009; Choi et al., 2010). 9-1-1 is a sliding clamp loaded onto DNA (Bermudez et al., 2003). TOPBP1 bridges ATR/ATRIP and 9-1-1, thereby stabilizing ATR at the fork. Once stabilized at the site of replication stress, ATR regulates downstream replication stress repair and cell cycle arrest via CHK1 kinase and CDC25A (Liu et al., 2000; Xiao et al., 2003; Delacroix et al., 2007). TIMELESS, a component of the replication fork protection complex (Kemp et al., 2010; Couch et al., 2013; Buisson et al., 2017), and the ubiquitin ligase PRP19 (*Prpf19*) (Maréchal et al., 2014), also function in ATR and CHK1 activation. Embryos null for *Atr* (Brown and Baltimore, 2000; de Klein et al., 2000; Murga et al., 2009), *Topbp1* (Jeon et al., 2011), *Hus1* (Weiss et al., 2000), *Chek1* (CHK1) (Takai et al., 2000; Zaugg et al., 2007), *Cdc25A* (Ray et al., 2007), *Timeless* (Gotter et al., 2000), and *Prpf19* (Fortschegger et al., 2007) are all compromised during peri-implantation.

In somatic tissues, ATR or CHK1 inhibition coupled with replication stress induces replication catastrophe and S-phase apoptosis (Myers et al., 2009; Toledo et al., 2013; van Harten et al., 2019). Similarly, *Atr* null embryos form blastocysts that *in vitro* display widespread apoptosis within the ICM but not in the trophoblast, and which are eventually compromised by day three of culture (Brown and Baltimore, 2000; de Klein et al., 2000; Murga et al., 2009). ATR activity is therefore essential in the pluripotent and rapidly proliferating epiblast cells that will become the embryo proper, but not in the multipotent placental precursors. *Chek1* null embryos also form blastocysts, but unlike *Atr* null embryos, are unable to attach to the culture vessels in outgrowth experiments (Takai et al., 2000). The more severe embryonic response to a loss of CHK1 activity compared to ATR inhibition is consistent with observations in somatic cells (Buisson et al., 2015).

HDR Genes Are Essential for Peri-Implantation Development

Common HDR factors manipulate DNA substrates at two-ended DNA breaks and stressed replication forks (Ait Saada et al., 2018). During replication stress, this entails regressing and protecting stalled forks in 4-way DNA structures to facilitate repair (Quinet et al., 2017). HDR factors essential for peri-implantation that function in canonical DSB repair and replication fork protection include: *Brca1* (Hakem et al., 1996; Ludwig et al., 1997; Taglialatela et al., 2017), *Brca2* (Sharan et al., 1997; Lemaçon et al., 2017; Mijic et al., 2017), *Rad51* (Lim and Hasty, 1996; Tsuzuki et al., 1996; Zellweger et al., 2015), *Bard1* (McCarthy et al., 2003; Shakya et al., 2008; Daza-Martin et al., 2019), *Palb2* (Bowman-Colin et al., 2013), and *Rad51C* (Kuznetsov et al., 2009; Somyajit et al., 2015). Similarly, common factors promote resection during HDR repair of canonical two-ended DSBs and at stalled replication forks (Ait Saada et al., 2018). This includes the essential peri-implantation genes: *Ctip* (Chen et al., 2005; Przetocka et al., 2018); *Ptip* (Cho et al., 2003; Ray Chaudhuri et al., 2016); *Dna2* (Lin et al., 2013; Thangavel et al., 2015), and the MRN complex [*Mre11*, *Rad50*, and *Nbs1* (Xiao and Weaver, 1997; Luo et al., 1999; Zhu et al., 2001; Theunissen et al., 2003; Buis et al., 2008; Schlacher et al., 2011).

Homology directed repair activity in replication fork remodeling and protection is an emerging topic in the DNA repair field, and it remains unclear which HDR functions are essential for cell viability. However, lethality in *Brca2* null mESCs is rescued when fork protection is facilitated by inhibiting PARP activity to protect replication forks from MRE11 nuclease (Ding et al., 2016). For BRCA2, fork protection may be the essential function. *In vivo*, deleting factors that participate in both canonical HDR-dependent DSB repair and fork remodeling or resection, typically confers reduced cell proliferation and embryo failure during gastrulation. For example, *Brca1*$^{-/-}$ embryos are severely malformed with an underdeveloped pro-amniotic cavity and mesoderm (Hakem et al., 1996; Ludwig et al., 1997). Concordantly, *Brca1* null embryos display a significant reduction of DNA synthesis by E6.5, increased p21 [a factor induced by p53 transactivation to mediate cell cycle arrest (Georgakilas et al., 2017)], and a high incidence of G1 arrested cells (Hakem et al., 1996). Similarly, *Rad51* null embryos suffer from reduced proliferation and begin to degenerate during gastrulation by E7.5, but development can be extended to E9.5 in *TP53/Rad51* double knockouts (Lim and Hasty, 1996). Loss of HDR factors therefore appears to primarily confer proliferative failure through p53-induced growth arrest and subsequently through accumulated genome instability if p53 function is compromised.

Additional Peri-Implantation Genes Linked to HDR or Replication

Peri-implantation development additionally requires several genes that are functionally linked to HDR or replication stress mitigation. Such genes include *Apex1* (Xanthoudakis et al., 1996), *Rnaseh2B* (Hiller et al., 2012), *Rif1* (Chapman et al., 2013), *Blm* (Chester et al., 1998), *Rev3L* (Bemark et al., 2000), *Usp7* (Kon et al., 2010), and *Ino80* (Min et al., 2013). *Apex1* does not directly function in replication, but is critical for the repair of abasic DNA sites that if left unresolved confer replication stress (Boiteux and Guillet, 2004). Similarly, *Rnaseh2B* resolves RNA within RNA-DNA hybrids, including mis-incorporated ribonucleotides, which if not resolved can impede replication (Pizzi et al., 2015). In addition to functioning in DSB repair pathway choice, *Rif1* also coordinates replication timing (Yamazaki et al., 2012; Foti et al., 2016). *Blm* encodes a helicase that functions in homologous recombination, the replication stress response (Davies et al., 2007; Machwe et al., 2011), promotes replication at telomeres (Barefield and Karlseder, 2012), and participates in a specialized form of break induced replication at chromosome ends (Sobinoff et al., 2017). *Rev3L* encodes the catalytic subunit of POL ζ which facilitates translesion synthesis to enable replication forks to negotiate lesions within DNA without stalling (Bhat et al., 2013).

Usp7 is a deubiquitylating enzyme that promotes efficient DNA replication (Lecona et al., 2016) and *Ino80* encodes a chromatin remodeling factor that functions in both replication and HDR (Poli et al., 2017).

MAINTAINING GENOME STABILITY DURING PERI-IMPLANTATION DEVELOPMENT

While HDR and replication associated genes are not the only genome stability factors required for peri-implantation development, their predominance on the list of genes essential for this developmental window is compelling. Conditions enabling *in vitro* culture of peri-implantation murine epiblast stem cells are now established (Brons et al., 2007; Tesar et al., 2007). However, there are no published studies focusing on genome maintenance in isolated epiblast cells. It is thus necessary to extrapolate from studies of other rapidly dividing cells why HDR and replication factors may be essential during peri-implantation development.

Replication Stress in Peri-Implantation Cells

The fastest cell cycles in the lifetime of a mouse are likely during the brief window of epiblast development. Outside of the embryo, rapid proliferation contributes to replication stress in hematopoietic and cancerous tissues by robbing cells of the time to properly execute DNA polymerization (Pilzecker et al., 2017). For example, during a somatic G1-phase replication is facilitated by increasing the abundance of MCM proteins and loading these factors at replication origins in preparation for S-phase (Boos et al., 2012). Late G1 cells also upregulate dNTP production for the oncoming burst of DNA synthesis (Hirschi et al., 2010; Dick and Rubin, 2013). When origins are not established properly, or dNTP production is dysregulated, cancer and aging hematopoietic cells are susceptible to replication stress (Flach et al., 2014; Aird and Zhang, 2015; Alvarez et al., 2015; Garzon et al., 2017).

Pluripotent cells in the early embryo display almost non-existent G1 phases and appear to use unique mechanisms to ensure S-phase progression is not impeded. For example, human ESCs counter G1 brevity by loading MCM proteins faster than cultured non-pluripotent cells (Matson et al., 2017). Retinoblastoma protein is also constitutively hyperphosphorylated in mouse and human ESCs (Conklin et al., 2012; Ter Huurne et al., 2017), which maintains high E2F transactivation to promote unperturbed dNTP synthesis (Hirschi et al., 2010; Dick and Rubin, 2013). To ensure rapid S-phase progression, mouse ESCs also license more dormant origins than non-embryonic progenitor cells (Ge et al., 2015). This increases the ability of ESCs to complete replication during a short S phase (Courtot et al., 2018). ESCs also demonstrate an increased ability to restart stalled replication forks (Ahuja et al., 2016; Zhao et al., 2018). Human induced pluripotent stem cells (iPSC) also license replication origins rapidly in their abbreviated G1 phase (Matson et al., 2017), and dormant origins are critical to maintain rapid proliferation in hematopoietic stem cell pools (Alvarez et al., 2015). Although not yet directly tested, we anticipate that epiblast cells employ similar countermeasures to expedite DNA synthesis.

Despite these efforts, human and mouse ESCs display endogenous replication stress in unperturbed cultures (Ahuja et al., 2016; Lamm et al., 2016). It is not clear why replication is stressed in pluripotent cells, however in proliferating cancer cells transcription commonly drives replication stress through collisions between RNA and DNA polymerases, or persistent RNA/DNA hybrid molecules termed R-loops (Crossley et al., 2019). Primary somatic cells mitigate transcription and R-loop interference by temporally coordinating transcription and replication during S-phase (Meryet-Figuiere et al., 2014). It is probable that peri-implantation epiblast cells facilitate rapid genome duplication by simultaneously engaging large numbers of origins. Such activity could increase the probability of replisome and transcriptome collisions and/or R-loop induced replication stress.

Under-replication due to endogenous stress is described in mESCs and human iPSCs (Ahuja et al., 2016; Vallabhaneni et al., 2018). Lengthening the G1 phase reduces replication defects in mESCs consistent with the notion that replication stress is driven by rushed cell cycles (Ahuja et al., 2016). Pluripotent cells are reported to have enhanced DNA repair capacities and it is possible this translates to highly effectively management of inefficient replication in embryos (Maynard et al., 2008; Luo et al., 2012). Alternatively, pluripotent blastocyst cells persist for a limited number of cell divisions *in vivo*, and it is feasible that pre-implantation embryos simply tolerate under-replication for this brief period. Tolerance of replication defects is consistent with observations that preimplantation embryonic cells are more resistant to genomic insult than peri-implantation cells. Compromising the replication stress response should confer similar DDR activation, chromosomal segregation errors, and aneuploidy in both pre- and peri-implantation cells. However, cells with supernumerary chromosomes persist in the blastocyst before elimination during peri-implantation (Bolton et al., 2016). This may explain why many genome stability factors become essential specifically during peri-implantation development. *In vivo,* activating p53 through deletion of its negative regulator *Mdm2* leads to lethality during peri-implantation (Jones et al., 1995). This suggests that p53 signaling during peri-implantation is a conduit to remove genomically unstable cells *in vivo*.

Additionally, it is important to recognize that genome stability factors may possesses cryptic essential functions during early development. For example, PARP1 is DDR factor involved in multiple aspects of genome integrity (Ray Chaudhuri and Nussenzweig, 2017). However, in mESCs, *Parp1* has roles preventing the *trans*-differentiation of extraembryonic trophoblast cells (Nozaki et al., 1999; Hemberger et al., 2003). This pluripotency-specific function is linked to the DNA binding ability of PARP1 which confers an epigenetic-like regulation of pluripotency (Roper et al., 2014). Additionally, pluripotency-specific repair factors may provide essential

functions in early development. The Filia-Floped protein complex is abundantly expressed in pluripotent but not somatic cells, and is suggested to increase the abundance of essential repair factors including BLM and promote ATR activation to encourage fork restart (Zhao et al., 2015; Zhao et al., 2018; Zheng, 2020).

Essential Roles for HDR Factors During Peri-Implantation

It is possible the canonical G1-phase c-NHEJ DSB repair pathway is dispensable during peri-implantation because cells rapidly transition through their brief G1 phase and engage alt-NHEJ or HDR in S-phase. Conversely, c- and alt-NHEJ remain active in HDR-deficient embryos, and in principle EJ functions could provide redundant DSB repair activity. An explanation why c- or alt-NHEJ cannot rescue HDR during peri-implantation may stem from the diversity of substrates repaired by HDR. While two-ended DSBs are readily repaired by EJ, collapsed replication forks present as one-ended DNA breaks which c- or alt-NHEJ cannot process (Feng and Jasin, 2017; Scully et al., 2019). One-ended breaks, however, can be repaired through a specialized HDR mechanism termed break-induced replication (BIR). During BIR, the exposed DNA end is resected, and following strand-invasion to form a displacement loop on the sister chromatid, DNA is polymerized from the invaded strand in a conservative manner (Kramara et al., 2018). While BIR is commonly studied in yeast, the analogous mechanism in vertebrates remains poorly defined. Notwithstanding, *Blm* promotes BIR at chromosome ends in human cancer cells that maintain telomere length through the alternative lengthening of telomeres mechanism suggesting that *Blm* may promote BIR elsewhere in the genome following replication stress (Sobinoff et al., 2017). Additionally, *Pold3* is also implicated in vertebrate BIR (Costantino et al., 2014). Conversely, the non-essential gene *Rad52* also functions in vertebrate BIR casting doubt on the requirement for BIR in early development and indicating the need for future studies (Sotiriou et al., 2016).

Multiple HDR factors essential for peri-implantation also play central roles in replication stress management. This includes HDR factors that regress, stabilize, or resect stalled replication forks including *Brca1/2, Bard1, Rad51* and *Rad51C*, *Ctip, Ptip, Dna2*, and genes encoding the MRN complex. Interestingly, the helicases and translocases that promote fork regression, including *Smarcal1*, are not essential for peri-implantation (Baradaran-Heravi et al., 2012). This may reflect redundancy in the mechanisms that drive formation of 4-strand structures at stalled replication forks (Quinet et al., 2017). Given the essentiality of the replication stress response for epiblast development, it stands to reason that replication fork remodeling and protective functions encoded by HDR factors play a role in the viability of peri-implantation embryos. Failure to facilitate these activities would confer genome instability, chromosome segregation errors, and molecular outcomes consistent with unrepaired replication stress. As described above, this would activate p53 surveillance systems during peri-implantation. In the future it will be interesting to determine which specific HDR functions are essential for embryogenesis.

CONCLUSION AND FUTURE DIRECTIONS

While most DDR and repair factors are non-essential, this does not exclude non-essential genome stability pathways from playing an important role in healthy development. Deletion of non-essential DDR and repair genes commonly results in the birth of live pups exhibiting a wide array of deleterious phenotypes (**Supplementary Table S1**). Additionally, cancer predisposition and a reduced lifespan are common in mice lacking non-essential genome stability factors (**Supplementary Table S1**). The difference between essential and non-essential genome stability genes is likely derived from the necessity of the targeted repair pathway to resolve lethal genome instability that arises during a specific window of development.

The critical genome stability pathways required for cell survival are determined by the type of genomic lesions the cell encounters and when in the cell cycle those lesions arise. Early embryonic development is largely protected from exogenous influence. Preimplantation embryos are wholly contained, and maternal blood supply begins at E9.5 (Behringer et al., 2014). The critical early stages of development likely benefit from sequestration from external threats to genome stability. We suggest the imminent threat to genome stability in early development stems from the need to mitigate endogenous replication stress within the epiblast to sustain rapid cell cycles. If left unresolved, replication stress drives genome instability, chromosome segregation errors, growth arrest and/or cell death. Dwindling cell numbers of epiblast cells that fail to effectively replicate their genome will progressively lead to embryo compromise. This premise is supported by the timing of embryo failure associated with deletion of essential DDR and repair genes. Consistent with systemic proliferative failure, deletion of factors required for basal DNA replication, or up-stream signaling in the replication stress response, typically induce an early embryonic demise (E5.0 or before). Whereas deleting HDR factors induces death at a subsequent time (E5.5 or later), potentially as the additive outcome of progressive genome instability.

Another caveat of reports reviewed here is that many were pioneering studies that utilized the newly developed technology of gene targeting in mice. In the intervening decades, our understanding of early development and experimental capability has blossomed. Development of new stem cell culture technologies now enables mechanistic study of peri-implantation development within three-dimensional gastrula structures *in vitro*. Co-culture of ICM derived ESCs, trophectoderm derived trophoblast stem cells, and extraembryonic endoderm stem cells results in the spontaneous self-assembly of a structure remarkably like the gastrulating embryo. These structures, termed "ETX embryos" will enable directed gene deletion within specific embryonic cell types (Sozen et al., 2018). Coupled with precise mechanistic investigations, ETX embryo models will reveal new insights on the mechanisms of cell compromise

during embryogenesis. It will be exciting to learn in the coming years why a limited number of DDR and repair pathways are essential for development, and the underlying reasons for their importance within the peri-implantation embryo.

DATA AVAILABILITY STATEMENT

MGI-GO designations discussed in this review can be found at the following. DNA damage checkpoint: http://www.informatics.jax.org/go/term/GO:0000077; nucleotide excision repair: http://www.informatics.jax.org/go/term/GO:0006289; mismatch repair: http://www.informatics.jax.org/go/term/GO:0006298; base excision repair: http://www.informatics.jax.org/go/term/GO:0006284; DSB repair via homologous recombination: http://www.informatics.jax.org/go/term/GO:0000724; DSB repair via non-homologous end joining: http://www.informatics.jax.org/go/term/GO:0006303.

AUTHOR CONTRIBUTIONS

GK and AC conceived of the review manuscript. GK compiled the information presented in **Tables 1**, **2** and **Supplementary Table S1** from the MGI-GO database as indicated. GK made the figures. GK and AC composed the manuscript.

FUNDING

The Cesare laboratory is supported by grants from the Australian National Health and Medical Research Council (1162886 and 1185870) and The Neil and Norma Hill Foundation.

ACKNOWLEDGMENTS

The authors thank members of the Cesare and Tam laboratories at the Children's Medical Research Institute for their helpful discussion.

SUPPLEMENTARY MATERIAL

The Supplementary Material for this article can be found online at: https://www.frontiersin.org/articles/10.3389/fcell.2020.00416/full#supplementary-material

REFERENCES

Acloque, H., Adams, M. S., Fishwick, K., Bronner-Fraser, M., and Nieto, M. A. (2009). Epithelial-mesenchymal transitions: the importance of changing cell state in development and disease. *J. Clin. Invest.* 119, 1438–1449. doi: 10.1172/JCI38019

Affar El, B., Gay, F., Shi, Y., Liu, H., Huarte, M., Wu, S., et al. (2006). Essential dosage-dependent functions of the transcription factor yin yang 1 in late embryonic development and cell cycle progression. *Mol. Cell. Biol.* 26, 3565–3581. doi: 10.1128/MCB.26.9.3565-3581.2006

Afzal, S., Hao, Z., Itsumi, M., Abouelkheer, Y., Brenner, D., Gao, Y., et al. (2015). Autophagy-independent functions of UVRAG are essential for peripheral naive T-cell homeostasis. *Proc. Natl. Acad. Sci. U.S.A.* 112, 1119–1124. doi: 10.1073/pnas.1423588112

Ahuja, A. K., Jodkowska, K., Teloni, F., Bizard, A. H., Zellweger, R., Herrador, R., et al. (2016). A short G1 phase imposes constitutive replication stress and fork remodelling in mouse embryonic stem cells. *Nat. Commun.* 7:10660. doi: 10.1038/ncomms10660

Aird, K. M., and Zhang, R. (2015). Nucleotide metabolism, oncogene-induced senescence and cancer. *Cancer Lett.* 356, 204–210. doi: 10.1016/j.canlet.2014.01.017

Ait Saada, A., Lambert, S. A. E., and Carr, A. M. (2018). Preserving replication fork integrity and competence via the homologous recombination pathway. *DNA Repair* 71, 135–147. doi: 10.1016/j.dnarep.2018.08.017

Akdemir, K. C., Jain, A. K., Allton, K., Aronow, B., Xu, X., Cooney, A. J., et al. (2014). Genome-wide profiling reveals stimulus-specific functions of p53 during differentiation and DNA damage of human embryonic stem cells. *Nucleic Acids Res.* 42, 205–223. doi: 10.1093/nar/gkt866

Ali, A. A. E., Timinszky, G., Arribas-Bosacoma, R., Kozlowski, M., Hassa, P. O., Hassler, M., et al. (2012). The zinc-finger domains of PARP1 cooperate to recognize DNA strand breaks. *Nat. Struct. Mol. Biol.* 19, 685–692. doi: 10.1038/nsmb.2335

Alvarez, S., Diaz, M., Flach, J., Rodriguez-Acebes, S., Lopez-Contreras, A. J., Martinez, D., et al. (2015). Replication stress caused by low MCM expression limits fetal erythropoiesis and hematopoietic stem cell functionality. *Nat. Commun.* 6:8548. doi: 10.1038/ncomms9548

Andressoo, J. O., Weeda, G., De Wit, J., Mitchell, J. R., Beems, R. B., Van Steeg, H., et al. (2009). An Xpb mouse model for combined xeroderma pigmentosum and cockayne syndrome reveals progeroid features upon further attenuation of DNA repair. *Mol. Cell. Biol.* 29, 1276–1290. doi: 10.1128/MCB.01229-08

Artus, J., Vandormael-Pournin, S., Frodin, M., Nacerddine, K., Babinet, C., and Cohen-Tannoudji, M. (2005). Impaired mitotic progression and preimplantation lethality in mice lacking OMCG1, a new evolutionarily conserved nuclear protein. *Mol. Cell. Biol.* 25, 6289–6302. doi: 10.1128/MCB.25.14.6289-6302.2005

Audebert, M., Salles, B., and Calsou, P. (2004). Involvement of poly(ADP-ribose) polymerase-1 and XRCC1/DNA ligase III in an alternative route for DNA double-strand breaks rejoining. *J. Biol. Chem.* 279, 55117–55126. doi: 10.1074/jbc.M404524200

Banin, S., Moyal, L., Shieh, S., Taya, Y., Anderson, C. W., Chessa, L., et al. (1998). Enhanced phosphorylation of p53 by ATM in response to DNA damage. *Science* 281, 1674–1677. doi: 10.1126/science.281.5383.1674

Baradaran-Heravi, A., Cho, K. S., Tolhuis, B., Sanyal, M., Morozova, O., Morimoto, M., et al. (2012). Penetrance of biallelic SMARCAL1 mutations is associated with environmental and genetic disturbances of gene expression. *Hum. Mol. Genet.* 21, 2572–2587. doi: 10.1093/hmg/dds083

Barefield, C., and Karlseder, J. (2012). The BLM helicase contributes to telomere maintenance through processing of late-replicating intermediate structures. *Nucleic Acids Res.* 40, 7358–7367. doi: 10.1093/nar/gks407

Barlow, C., Hirotsune, S., Paylor, R., Liyanage, M., Eckhaus, M., Collins, F., et al. (1996). Atm-deficient mice: a paradigm of ataxia telangiectasia. *Cell* 86, 159–171. doi: 10.1016/s0092-8674(00)80086-0

Bass, T. E., Luzwick, J. W., Kavanaugh, G., Carroll, C., Dungrawala, H., Glick, G. G., et al. (2016). ETAA1 acts at stalled replication forks to maintain genome integrity. *Nat. Cell Biol.* 18, 1185–1195. doi: 10.1038/ncb3415

Behringer, R., Gertsenstein, M., Nagy, K. V., and Nagy, A. (2014). *Manipulating the Mouse Embryo*. Cold Spring Harbor, NY: Cold Spring Harbor Laboratory Press.

Bemark, M., Khamlichi, A. A., Davies, S. L., and Neuberger, M. S. (2000). Disruption of mouse polymerase zeta (Rev3) leads to embryonic lethality and impairs blastocyst development in vitro. *Curr. Biol.* 10, 1213–1216. doi: 10.1016/s0960-9822(00)00724-7

Bermudez, V. P., Lindsey-Boltz, L. A., Cesare, A. J., Maniwa, Y., Griffith, J. D., Hurwitz, J., et al. (2003). Loading of the human 9-1-1 checkpoint complex onto DNA by the checkpoint clamp loader hRad17-replication factor C complex

in vitro. *Proc. Natl. Acad. Sci. U.S.A.* 100, 1633–1638. doi: 10.1073/pnas.0437927100

Bhat, A., Andersen, P. L., Qin, Z., and Xiao, W. (2013). Rev3, the catalytic subunit of Polzeta, is required for maintaining fragile site stability in human cells. *Nucleic Acids Res.* 41, 2328–2339. doi: 10.1093/nar/gks1442

Bhat, K. P., and Cortez, D. (2018). RPA and RAD51: fork reversal, fork protection, and genome stability. *Nat. Struct. Mol. Biol.* 25, 1–8. doi: 10.1038/s41594-018-0075-z

Bleichert, F. (2019). Mechanisms of replication origin licensing: a structural perspective. *Curr. Opin. Struct. Biol.* 59, 195–204. doi: 10.1016/j.sbi.2019.08.007

Boiteux, S., and Guillet, M. (2004). Abasic sites in DNA: repair and biological consequences in Saccharomyces cerevisiae. *DNA Repair.* 3, 1–12. doi: 10.1016/j.dnarep.2003.10.002

Bolton, H., Graham, S. J. L., Van Der Aa, N., Kumar, P., Theunis, K., Fernandez Gallardo, E., et al. (2016). Mouse model of chromosome mosaicism reveals lineage-specific depletion of aneuploid cells and normal developmental potential. *Nat. Commun.* 7:11165. doi: 10.1038/ncomms11165

Boos, D., Frigola, J., and Diffley, J. F. (2012). Activation of the replicative DNA helicase: breaking up is hard to do. *Curr. Opin. Cell Biol.* 24, 423–430. doi: 10.1016/j.ceb.2012.01.011

Bowman-Colin, C., Xia, B., Bunting, S., Klijn, C., Drost, R., Bouwman, P., et al. (2013). Palb2 synergizes with Trp53 to suppress mammary tumor formation in a model of inherited breast cancer. *Proc. Natl. Acad. Sci. U.S.A.* 110, 8632–8637. doi: 10.1073/pnas.1305362110

Brons, I. G., Smithers, L. E., Trotter, M. W., Rugg-Gunn, P., Sun, B., Chuva De Sousa Lopes, S. M., et al. (2007). Derivation of pluripotent epiblast stem cells from mammalian embryos. *Nature* 448, 191–195. doi: 10.1038/nature05950

Brown, E. J., and Baltimore, D. (2000). ATR disruption leads to chromosomal fragmentation and early embryonic lethality. *Genes Dev.* 14, 397–402.

Buis, J., Wu, Y., Deng, Y., Leddon, J., Westfield, G., Eckersdorff, M., et al. (2008). Mre11 nuclease activity has essential roles in DNA repair and genomic stability distinct from ATM activation. *Cell* 135, 85–96. doi: 10.1016/j.cell.2008.08.015

Buisson, R., Boisvert, J. L., Benes, C. H., and Zou, L. (2015). Distinct but concerted roles of ATR, DNA-PK, and Chk1 in countering replication stress during S Phase. *Mol. Cell* 59, 1011–1024. doi: 10.1016/j.molcel.2015.07.029

Buisson, R., Niraj, J., Rodrigue, A., Ho, C. K., Kreuzer, J., Foo, T. K., et al. (2017). Coupling of Homologous Recombination and the Checkpoint by ATR. *Mol. Cell* 65, 336–346. doi: 10.1016/j.molcel.2016.12.007

Bult, C. J., Blake, J. A., Smith, C. L., Kadin, J. A., Richardson, J. E., and Mouse Genome Database, G. (2019). Mouse Genome Database (MGD) 2019. *Nucleic Acids Res.* 47, D801–D806. doi: 10.1093/nar/gky1056

Burgers, P. M. J., and Kunkel, T. A. (2017). Eukaryotic DNA Replication Fork. *Annu. Rev. Biochem.* 86, 417–438. doi: 10.1146/annurev-biochem-061516-044709

Burrell, R. A., Mcclelland, S. E., Endesfelder, D., Groth, P., Weller, M. C., Shaikh, N., et al. (2013). Replication stress links structural and numerical cancer chromosomal instability. *Nature* 494, 492–496. doi: 10.1038/nature11935

Byun, T. S., Pacek, M., Yee, M.-C., Walter, J. C., and Cimprich, K. A. (2005). Functional uncoupling of MCM helicase and DNA polymerase activities activates the ATR-dependent checkpoint. *Genes Dev.* 19, 1040–1052. doi: 10.1101/gad.1301205

Cang, Y., Zhang, J., Nicholas, S. A., Bastien, J., Li, B., Zhou, P., et al. (2006). Deletion of DDB1 in mouse brain and lens leads to p53-dependent elimination of proliferating cells. *Cell* 127, 929–940. doi: 10.1016/j.cell.2006.09.045

Carver, E. A., Jiang, R., Lan, Y., Oram, K. F., and Gridley, T. (2001). The mouse snail gene encodes a key regulator of the epithelial-mesenchymal transition. *Mol. Cell. Biol.* 21, 8184–8188. doi: 10.1128/MCB.21.23.8184-8188.2001

Celeste, A., Petersen, S., Romanienko, P. J., Fernandez-Capetillo, O., Chen, H. T., Sedelnikova, O. A., et al. (2002). Genomic instability in mice lacking histone H2AX. *Science* 296, 922–927. doi: 10.1126/science.1069398

Celli, G. B., Denchi, E. L., and De Lange, T. (2006). Ku70 stimulates fusion of dysfunctional telomeres yet protects chromosome ends from homologous recombination. *Nat. Cell Biol.* 8, 885–890. doi: 10.1038/ncb1444

Chang, H. H. Y., Pannunzio, N. R., Adachi, N., and Lieber, M. R. (2017). Non-homologous DNA end joining and alternative pathways to double-strand break repair. *Nat. Rev. Mol. Cell Biol.* 18, 495–506. doi: 10.1038/nrm.2017.48

Chapman, J. R., Barral, P., Vannier, J. B., Borel, V., Steger, M., Tomas-Loba, A., et al. (2013). RIF1 is essential for 53BP1-dependent nonhomologous end joining and suppression of DNA double-strand break resection. *Mol. Cell* 49, 858–871. doi: 10.1016/j.molcel.2013.01.002

Chen, C. H., Chu, P. C., Lee, L., Lien, H. W., Lin, T. L., Fan, C. C., et al. (2012). Disruption of murine mp29/Syf2/Ntc31 gene results in embryonic lethality with aberrant checkpoint response. *PLoS One* 7:e33538. doi: 10.1371/journal.pone.0033538

Chen, P.-L., Liu, F., Cai, S., Lin, X., Li, A., Chen, Y., et al. (2005). Inactivation of CtIP leads to early embryonic lethality mediated by G1 restraint and to tumorigenesis by haploid insufficiency. *Mol. Cell. Biol.* 25, 3535–3542. doi: 10.1128/MCB.25.9.3535-3542.2005

Chester, N., Kuo, F., Kozak, C., O'hara, C. D., and Leder, P. (1998). Stage-specific apoptosis, developmental delay, and embryonic lethality in mice homozygous for a targeted disruption in the murine Bloom's syndrome gene. *Genes Dev.* 12, 3382–3393. doi: 10.1101/gad.12.21.3382

Cho, E. A., Prindle, M. J., and Dressler, G. R. (2003). BRCT domain-containing protein PTIP is essential for progression through mitosis. *Mol. Cell. Biol.* 23, 1666–1673. doi: 10.1128/mcb.23.5.1666-1673.2003

Choi, J.-H., Lindsey-Boltz, L. A., Kemp, M., Mason, A. C., Wold, M. S., and Sancar, A. (2010). Reconstitution of RPA-covered single-stranded DNA-activated ATR-Chk1 signaling. *Proc. Natl. Acad. Sci. U.S.A.* 107, 13660–13665. doi: 10.1073/pnas.1007856107

Condic, M. L. (2014). Totipotency: what it is and what it is not. *Stem Cells Dev.* 23, 796–812. doi: 10.1089/scd.2013.0364

Conklin, J. F., Baker, J., and Sage, J. (2012). The RB family is required for the self-renewal and survival of human embryonic stem cells. *Nat. Commun.* 3:1244. doi: 10.1038/ncomms2254

Cortez, D. (2019). Replication-Coupled DNA Repair. *Mol. Cell* 74, 866–876. doi: 10.1016/j.molcel.2019.04.027

Cortez, D., Guntuku, S., Qin, J., and Elledge, S. J. (2001). ATR and ATRIP: partners in checkpoint signaling. *Science* 294, 1713–1716. doi: 10.1126/science.1065521

Costantino, L., Sotiriou, S. K., Rantala, J. K., Magin, S., Mladenov, E., Helleday, T., et al. (2014). Break-induced replication repair of damaged forks induces genomic duplications in human cells. *Science* 343, 88–91. doi: 10.1126/science.1243211

Couch, F. B., Bansbach, C. E., Driscoll, R., Luzwick, J. W., Glick, G. G., Betous, R., et al. (2013). ATR phosphorylates SMARCAL1 to prevent replication fork collapse. *Genes Dev.* 27, 1610–1623. doi: 10.1101/gad.214080.113

Courtot, L., Hoffmann, J. S., and Bergoglio, V. (2018). The protective role of dormant origins in response to replicative stress. *Int. J. Mol. Sci.* 19:E3569. doi: 10.3390/ijms19113569

Crossley, M. P., Bocek, M., and Cimprich, K. A. (2019). R-Loops as Cellular Regulators and Genomic Threats. *Mol. Cell* 73, 398–411. doi: 10.1016/j.molcel.2019.01.024

Davies, S. L., North, P. S., and Hickson, I. D. (2007). Role for BLM in replication-fork restart and suppression of origin firing after replicative stress. *Nat. Struct. Mol. Biol.* 14, 677–679. doi: 10.1038/nsmb1267

Daza-Martin, M., Starowicz, K., Jamshad, M., Tye, S., Ronson, G. E., Mackay, H. L., et al. (2019). Isomerization of BRCA1-BARD1 promotes replication fork protection. *Nature* 571, 521–527. doi: 10.1038/s41586-019-1363-4

de Boer, J., Donker, I., De Wit, J., Hoeijmakers, J. H., and Weeda, G. (1998). Disruption of the mouse xeroderma pigmentosum group D DNA repair/basal transcription gene results in preimplantation lethality. *Cancer Res.* 58, 89–94.

de Klein, A., Muijtjens, M., Van Os, R., Verhoeven, Y., Smit, B., Carr, A. M., et al. (2000). Targeted disruption of the cell-cycle checkpoint gene ATR leads to early embryonic lethality in mice. *Curr. Biol.* 10, 479–482. doi: 10.1016/s0960-9822(00)00447-4

Delacroix, S., Wagner, J. M., Kobayashi, M., Yamamoto, K., and Karnitz, L. M. (2007). The Rad9-Hus1-Rad1 (9-1-1) clamp activates checkpoint signaling via TopBP1. *Genes Dev.* 21, 1472–1477. doi: 10.1101/gad.1547007

Denchi, E. L., and de Lange, T. (2007). Protection of telomeres through independent control of ATM and ATR by TRF2 and POT1. *Nature* 448, 1068–1071. doi: 10.1038/nature06065

Dick, F. A., and Rubin, S. M. (2013). Molecular mechanisms underlying RB protein function. *Nat. Rev. Mol. Cell Biol.* 14, 297–306. doi: 10.1038/nrm3567

Dickinson, M. E., Flenniken, A. M., Ji, X., Teboul, L., Wong, M. D., White, J. K., et al. (2016). High-throughput discovery of novel developmental phenotypes. *Nature* 537, 508–514. doi: 10.1038/nature19356

Ding, X., Ray Chaudhuri, A., Callen, E., Pang, Y., Biswas, K., Klarmann, K. D., et al. (2016). Synthetic viability by BRCA2 and PARP1/ARTD1 deficiencies. *Nat. Commun.* 7:12425. doi: 10.1038/ncomms12425

Diril, M. K., Ratnacaram, C. K., Padmakumar, V. C., Du, T., Wasser, M., Coppola, V., et al. (2012). Cyclin-dependent kinase 1 (Cdk1) is essential for cell division and suppression of DNA re-replication but not for liver regeneration. *Proc. Natl. Acad. Sci. U S.A.* 109, 3826–3831. doi: 10.1073/pnas.1115201109

Dupre, A., Boyer-Chatenet, L., and Gautier, J. (2006). Two-step activation of ATM by DNA and the Mre11-Rad50-Nbs1 complex. *Nat. Struct. Mol. Biol.* 13, 451–457. doi: 10.1038/nsmb1090

Egly, J. M. (2001). The 14th Datta Lecture. TFIIH: from transcription to clinic. *FEBS Lett.* 498, 124–128. doi: 10.1016/s0014-5793(01)02458-9

Feng, W., and Jasin, M. (2017). BRCA2 suppresses replication stress-induced mitotic and G1 abnormalities through homologous recombination. *Nat. Commun.* 8:525. doi: 10.1038/s41467-017-00634-0

Flach, J., Bakker, S. T., Mohrin, M., Conroy, P. C., Pietras, E. M., Reynaud, D., et al. (2014). Replication stress is a potent driver of functional decline in ageing haematopoietic stem cells. *Nature* 512, 198–202. doi: 10.1038/nature13619

Fortschegger, K., Wagner, B., Voglauer, R., Katinger, H., Sibilia, M., and Grillari, J. (2007). Early embryonic lethality of mice lacking the essential protein SNEV. *Mol. Cell. Biol.* 27, 3123–3130. doi: 10.1128/MCB.01188-06

Foster, C. T., Dovey, O. M., Lezina, L., Luo, J. L., Gant, T. W., Barlev, N., et al. (2010). Lysine-specific demethylase 1 regulates the embryonic transcriptome and CoREST stability. *Mol. Cell. Biol.* 30, 4851–4863. doi: 10.1128/MCB.00521-10

Foti, R., Gnan, S., Cornacchia, D., Dileep, V., Bulut-Karslioglu, A., Diehl, S., et al. (2016). Nuclear Architecture Organized by Rif1 Underpins the Replication-Timing Program. *Mol. Cell* 61, 260–273. doi: 10.1016/j.molcel.2015.12.001

Frank, K. M., Sekiguchi, J. M., Seidl, K. J., Swat, W., Rathbun, G. A., Cheng, H. L., et al. (1998). Late embryonic lethality and impaired V(D)J recombination in mice lacking DNA ligase IV. *Nature* 396, 173–177. doi: 10.1038/24172

Fukushima, T., Matsuzawa, S., Kress, C. L., Bruey, J. M., Krajewska, M., Lefebvre, S., et al. (2007). Ubiquitin-conjugating enzyme Ubc13 is a critical component of TNF receptor-associated factor (TRAF)-mediated inflammatory responses. *Proc. Natl. Acad. Sci. U.S.A.* 104, 6371–6376. doi: 10.1073/pnas.0700548104

Ganuza, M., Sáiz-Ladera, C., Cañamero, M., Gómez, G., Schneider, R., Blasco, M. A., et al. (2012). Genetic inactivation of Cdk7 leads to cell cycle arrest and induces premature aging due to adult stem cell exhaustion. *EMBO J.* 31, 2498–2510. doi: 10.1038/emboj.2012.94

Garzon, J., Rodriguez, R., Kong, Z., Chabes, A., Rodriguez-Acebes, S., Mendez, J., et al. (2017). Shortage of dNTPs underlies altered replication dynamics and DNA breakage in the absence of the APC/C cofactor Cdh1. *Oncogene* 36, 5808–5818. doi: 10.1038/onc.2017.186

Gavet, O., and Pines, J. (2010). Progressive activation of CyclinB1-Cdk1 coordinates entry to mitosis. *Dev. Cell* 18, 533–543. doi: 10.1016/j.devcel.2010.02.013

Ge, X. Q., Han, J., Cheng, E. C., Yamaguchi, S., Shima, N., Thomas, J. L., et al. (2015). Embryonic Stem Cells License a High Level of Dormant Origins to Protect the Genome against Replication Stress. *Stem Cell Rep.* 5, 185–194. doi: 10.1016/j.stemcr.2015.06.002

Georgakilas, A. G., Martin, O. A., and Bonner, W. M. (2017). p21: a two-faced genome guardian. *Trends Mol. Med.* 23, 310–319. doi: 10.1016/j.molmed.2017.02.001

Ghezraoui, H., Piganeau, M., Renouf, B., Renaud, J.-B., Sallmyr, A., Ruis, B., et al. (2014). Chromosomal translocations in human cells are generated by canonical nonhomologous end-joining. *Mol. Cell* 55, 829–842. doi: 10.1016/j.molcel.2014.08.002

Gotter, A. L., Manganaro, T., Weaver, D. R., Kolakowski, LF Jr, Possidente, B., Sriram, S., et al. (2000). A time-less function for mouse timeless. *Nat. Neurosci.* 3, 755–756.

Gottlieb, T. M., and Jackson, S. P. (1993). The DNA-dependent protein kinase: requirement for DNA ends and association with Ku antigen. *Cell* 72, 131–142. doi: 10.1016/0092-8674(93)90057-w

Gu, Y., Seidl, K. J., Rathbun, G. A., Zhu, C., Manis, J. P., Van Der Stoep, N., et al. (1997). Growth retardation and leaky SCID phenotype of Ku70-deficient mice. *Immunity* 7, 653–665. doi: 10.1016/s1074-7613(00)80386-6

Haahr, P., Hoffmann, S., Tollenaere, M. A., Ho, T., Toledo, L. I., Mann, M., et al. (2016). Activation of the ATR kinase by the RPA-binding protein ETAA1. *Nat. Cell Biol.* 18, 1196–1207. doi: 10.1038/ncb3422

Hakem, R., De La Pompa, J. L., Sirard, C., Mo, R., Woo, M., Hakem, A., et al. (1996). The tumor suppressor gene Brca1 is required for embryonic cellular proliferation in the mouse. *Cell* 85, 1009–1023. doi: 10.1016/s0092-8674(00)81302-1

Hamatani, T., Carter, M. G., Sharov, A. A., and Ko, M. S. H. (2004). Dynamics of global gene expression changes during mouse preimplantation development. *Dev. Cell* 6, 117–131. doi: 10.1016/s1534-5807(03)00373-3

Harvey, S. L., Charlet, A., Haas, W., Gygi, S. P., and Kellogg, D. R. (2005). Cdk1-dependent regulation of the mitotic inhibitor Wee1. *Cell* 122, 407–420. doi: 10.1016/j.cell.2005.05.029

Haupt, Y., Maya, R., Kazaz, A., and Oren, M. (1997). Mdm2 promotes the rapid degradation of p53. *Nature* 387, 296–299. doi: 10.1038/387296a0

Hemberger, M., Nozaki, T., Winterhager, E., Yamamoto, H., Nakagama, H., Kamada, N., et al. (2003). Parp1-deficiency induces differentiation of ES cells into trophoblast derivatives. *Dev. Biol.* 257, 371–381. doi: 10.1016/s0012-1606(03)00097-6

Heyer, B. S., Macauley, A., Behrendtsen, O., and Werb, Z. (2000). Hypersensitivity to DNA damage leads to increased apoptosis during early mouse development. *Genes Dev.* 14, 2072–2084.

Hiller, B., Achleitner, M., Glage, S., Naumann, R., Behrendt, R., and Roers, A. (2012). Mammalian RNase H2 removes ribonucleotides from DNA to maintain genome integrity. *J. Exp. Med.* 209, 1419–1426. doi: 10.1084/jem.20120876

Hirschi, A., Cecchini, M., Steinhardt, R. C., Schamber, M. R., Dick, F. A., and Rubin, S. M. (2010). An overlapping kinase and phosphatase docking site regulates activity of the retinoblastoma protein. *Nat. Struct. Mol. Biol.* 17, 1051–1057. doi: 10.1038/nsmb.1868

Hnizda, A., and Blundell, T. L. (2019). Multicomponent assemblies in DNA-double-strand break repair by NHEJ. *Curr. Opin. Struct. Biol.* 55, 154–160. doi: 10.1016/j.sbi.2019.03.026

Hockemeyer, D., Daniels, J.-P., Takai, H., and De Lange, T. (2006). Recent expansion of the telomeric complex in rodents: Two distinct POT1 proteins protect mouse telomeres. *Cell* 126, 63–77. doi: 10.1016/j.cell.2006.04.044

Hockemeyer, D., Sfeir, A. J., Shay, J. W., Wright, W. E., and De Lange, T. (2005). POT1 protects telomeres from a transient DNA damage response and determines how human chromosomes end. *EMBO J.* 24, 2667–2678. doi: 10.1038/sj.emboj.7600733

Hoki, Y., Araki, R., Fujimori, A., Ohhata, T., Koseki, H., Fukumura, R., et al. (2003). Growth retardation and skin abnormalities of the Recql4-deficient mouse. *Hum. Mol. Genet.* 12, 2293–2299. doi: 10.1093/hmg/ddg254

Horii, T., Yamamoto, M., Morita, S., Kimura, M., Nagao, Y., and Hatada, I. (2015). p53 suppresses tetraploid development in mice. *Sci. Rep.* 5:8907. doi: 10.1038/srep08907

Humięcka, M., Szpila, M., Kłoś, P., Maleszewski, M., and Szczepańska, K. (2017). Mouse blastomeres acquire ability to divide asymmetrically before compaction. *PLoS One* 12:e0175032. doi: 10.1371/journal.pone.0175032

Hustedt, N., and Durocher, D. (2016). The control of DNA repair by the cell cycle. *Nat. Cell Biol.* 19, 1–9. doi: 10.1038/ncb3452

Jackson, S. P., and Durocher, D. (2013). Regulation of DNA damage responses by ubiquitin and SUMO. *Mol. Cell* 49, 795–807. doi: 10.1016/j.molcel.2013.01.017

Jacome, A., Gutierrez-Martinez, P., Schiavoni, F., Tenaglia, E., Martinez, P., Rodriguez-Acebes, S., et al. (2015). NSMCE2 suppresses cancer and aging in mice independently of its SUMO ligase activity. *EMBO J.* 34, 2604–2619. doi: 10.15252/embj.201591829

Jain, A. K., Xi, Y., Mccarthy, R., Allton, K., Akdemir, K. C., Patel, L. R., et al. (2016). LncPRESS1 is a p53-Regulated LncRNA that safeguards pluripotency by disrupting SIRT6-mediated de-acetylation of histone H3K56. *Mol. Cell* 64, 967–981. doi: 10.1016/j.molcel.2016.10.039

Jeon, Y., Ko, E., Lee, K. Y., Ko, M. J., Park, S. Y., Kang, J., et al. (2011). TopBP1 deficiency causes an early embryonic lethality and induces cellular senescence in primary cells. *J. Biol. Chem.* 286, 5414–5422. doi: 10.1074/jbc.M110.189704

Jones, S. N., Roe, A. E., Donehower, L. A., and Bradley, A. (1995). Rescue of embryonic lethality in Mdm2-deficient mice by absence of p53. *Nature* 378, 206–208. doi: 10.1038/378206a0

Jukam, D., Shariati, S. A. M., and Skotheim, J. M. (2017). Zygotic genome activation in vertebrates. *Dev. Cell* 42, 316–332.

Kafer, G. R., Li, X., Horii, T., Suetake, I., Tajima, S., Hatada, I., et al. (2016). 5-Hydroxymethylcytosine Marks Sites of DNA Damage and Promotes Genome Stability. *Cell Rep.* 14, 1283–1292. doi: 10.1016/j.celrep.2016.01.035

Kemp, M. G., Akan, Z., Yilmaz, S., Grillo, M., Smith-Roe, S. L., Kang, T. H., et al. (2010). Tipin-replication protein A interaction mediates Chk1 phosphorylation by ATR in response to genotoxic stress. *J. Biol. Chem.* 285, 16562–16571. doi: 10.1074/jbc.M110.110304

Kent, L. N., and Leone, G. (2019). The broken cycle: E2F dysfunction in cancer. *Nat. Rev. Cancer* 19, 326–338. doi: 10.1038/s41568-019-0143-7

Kent, T., Chandramouly, G., Mcdevitt, S. M., Ozdemir, A. Y., and Pomerantz, R. T. (2015). Mechanism of microhomology-mediated end-joining promoted by human DNA polymerase θ. *Nat. Struct. Mol. Biol.* 22, 230–237. doi: 10.1038/nsmb.2961

Kim, J. M., Nakao, K., Nakamura, K., Saito, I., Katsuki, M., Arai, K.-I., et al. (2002). Inactivation of Cdc7 kinase in mouse ES cells results in S-phase arrest and p53-dependent cell death. *EMBO J.* 21, 2168–2179. doi: 10.1093/emboj/21.9.2168

Kon, N., Kobayashi, Y., Li, M., Brooks, C. L., Ludwig, T., and Gu, W. (2010). Inactivation of HAUSP in vivo modulates p53 function. *Oncogene* 29, 1270–1279. doi: 10.1038/onc.2009.427

Kramara, J., Osia, B., and Malkova, A. (2018). Break-induced replication: the Where. The Why, and The How. *Trends Genet.* 34, 518–531. doi: 10.1016/j.tig.2018.04.002

Kumagai, A., Lee, J., Yoo, H. Y., and Dunphy, W. G. (2006). TopBP1 activates the ATR-ATRIP complex. *Cell* 124, 943–955.

Kurimasa, A., Ouyang, H., Dong, L. J., Wang, S., Li, X., Cordon-Cardo, C., et al. (1999). Catalytic subunit of DNA-dependent protein kinase: impact on lymphocyte development and tumorigenesis. *Proc. Natl. Acad. Sci. U.S.A.* 96, 1403–1408. doi: 10.1073/pnas.96.4.1403

Kuznetsov, S. G., Haines, D. C., Martin, B. K., and Sharan, S. K. (2009). Loss of Rad51c leads to embryonic lethality and modulation of Trp53-dependent tumorigenesis in mice. *Cancer Res.* 69, 863–872. doi: 10.1158/0008-5472.CAN-08-3057

Lamm, N., Ben-David, U., Golan-Lev, T., Storchova, Z., Benvenisty, N., and Kerem, B. (2016). Genomic instability in human pluripotent stem cells arises from replicative stress and chromosome condensation defects. *Cell Stem Cell* 18, 253–261. doi: 10.1016/j.stem.2015.11.003

Larsen, E., Gran, C., Saether, B. E., Seeberg, E., and Klungland, A. (2003). Proliferation failure and gamma radiation sensitivity of Fen1 null mutant mice at the blastocyst stage. *Mol. Cell. Biol.* 23, 5346–5353. doi: 10.1128/mcb.23.15.5346-5353.2003

Laurent, A., and Blasi, F. (2015). Differential DNA damage signalling and apoptotic threshold correlate with mouse epiblast-specific hypersensitivity to radiation. *Development* 142, 3675–3685. doi: 10.1242/dev.125708

Lecona, E., Rodriguez-Acebes, S., Specks, J., Lopez-Contreras, A. J., Ruppen, I., Murga, M., et al. (2016). USP7 is a SUMO deubiquitinase essential for DNA replication. *Nat. Struct. Mol. Biol.* 23, 270–277. doi: 10.1038/nsmb.3185

Lee, J. H., and Paull, T. T. (2005). ATM activation by DNA double-strand breaks through the Mre11-Rad50-Nbs1 complex. *Science* 308, 551–554. doi: 10.1126/science.1108297

Lee, S., Kim, J. Y., Kim, Y. J., Seok, K. O., Kim, J. H., Chang, Y. J., et al. (2012). Nucleolar protein GLTSCR2 stabilizes p53 in response to ribosomal stresses. *Cell Death Differ.* 19, 1613–1622. doi: 10.1038/cdd.2012.40

Lemaçon, D., Jackson, J., Quinet, A., Brickner, J. R., Li, S., Yazinski, S., et al. (2017). MRE11 and EXO1 nucleases degrade reversed forks and elicit MUS81-dependent fork rescue in BRCA2-deficient cells. *Nat. Commun.* 8:860. doi: 10.1038/s41467-017-01180-5

Li, A., and Blow, J. J. (2005). Cdt1 downregulation by proteolysis and geminin inhibition prevents DNA re-replication in Xenopus. *EMBO J.* 24, 395–404. doi: 10.1038/sj.emboj.7600520

Li, B., Ruiz, J. C., and Chun, K. T. (2002). CUL-4A is critical for early embryonic development. *Mol. Cell. Biol.* 22, 4997–5005. doi: 10.1128/mcb.22.14.4997-5005.2002

Li, G., Alt, F. W., Cheng, H. L., Brush, J. W., Goff, P. H., Murphy, M. M., et al. (2008). Lymphocyte-specific compensation for XLF/cernunnos end-joining functions in V(D)J recombination. *Mol. Cell* 31, 631–640. doi: 10.1016/j.molcel.2008.07.017

Li, M., He, Y., Dubois, W., Wu, X., Shi, J., and Huang, J. (2012). Distinct regulatory mechanisms and functions for p53-activated and p53-repressed DNA damage response genes in embryonic stem cells. *Mol. Cell* 46, 30–42. doi: 10.1016/j.molcel.2012.01.020

Lim, D. S., and Hasty, P. (1996). A mutation in mouse rad51 results in an early embryonic lethal that is suppressed by a mutation in p53. *Mol. Cell. Biol.* 16, 7133–7143. doi: 10.1128/mcb.16.12.7133

Limas, J. C., and Cook, J. G. (2019). Preparation for DNA replication: the key to a successful S phase. *FEBS Lett.* 593, 2853–2867. doi: 10.1002/1873-3468.13619

Lin, T., Chao, C., Saito, S., Mazur, S. J., Murphy, M. E., Appella, E., et al. (2005). p53 induces differentiation of mouse embryonic stem cells by suppressing Nanog expression. *Nat. Cell Biol.* 7, 165–171. doi: 10.1038/ncb1211

Lin, W., Sampathi, S., Dai, H., Liu, C., Zhou, M., Hu, J., et al. (2013). Mammalian DNA2 helicase/nuclease cleaves G-quadruplex DNA and is required for telomere integrity. *EMBO J.* 32, 1425–1439. doi: 10.1038/emboj.2013.88

Liu, C., Vyas, A., Kassab, M. A., Singh, A. K., and Yu, X. (2017). The role of poly ADP-ribosylation in the first wave of DNA damage response. *Nucleic Acids Res.* 45, 8129–8141. doi: 10.1093/nar/gkx565

Liu, C.-L., Yu, I. S., Pan, H.-W., Lin, S.-W., and Hsu, H.-C. (2007). L2dtl is essential for cell survival and nuclear division in early mouse embryonic development. *J. Biol. Chem.* 282, 1109–1118. doi: 10.1074/jbc.M606535200

Liu, D., Keijzers, G., and Rasmussen, L. J. (2017). DNA mismatch repair and its many roles in eukaryotic cells. *Mutat. Res.* 773, 174–187. doi: 10.1016/j.mrrev.2017.07.001

Liu, Q., Guntuku, S., Cui, X. S., Matsuoka, S., Cortez, D., Tamai, K., et al. (2000). Chk1 is an essential kinase that is regulated by Atr and required for the G(2)/M DNA damage checkpoint. *Genes Dev.* 14, 1448–1459.

Lou, J., Scipioni, L., Wright, B. K., Bartolec, T. K., Zhang, J., Masamsetti, V. P., et al. (2019). Phasor histone FLIM-FRET microscopy quantifies spatiotemporal rearrangement of chromatin architecture during the DNA damage response. *Proc. Natl. Acad. Sci. U.S.A.* 116, 7323–7332. doi: 10.1073/pnas.1814965116

Lou, Z., Minter-Dykhouse, K., Franco, S., Gostissa, M., Rivera, M. A., Celeste, A., et al. (2006). MDC1 maintains genomic stability by participating in the amplification of ATM-dependent DNA damage signals. *Mol. Cell* 21, 187–200. doi: 10.1016/j.molcel.2005.11.025

Lu, L. Y., Wood, J. L., Minter-Dykhouse, K., Ye, L., Saunders, T. L., Yu, X., et al. (2008). Polo-like kinase 1 is essential for early embryonic development and tumor suppression. *Mol. Cell. Biol.* 28, 6870–6876. doi: 10.1128/MCB.00392-08

Ludwig, T., Chapman, D. L., Papaioannou, V. E., and Efstratiadis, A. (1997). Targeted mutations of breast cancer susceptibility gene homologs in mice: lethal phenotypes of Brca1, Brca2, Brca1/Brca2, Brca1/p53, and Brca2/p53 nullizygous embryos. *Genes Dev.* 11, 1226–1241. doi: 10.1101/gad.11.10.1226

Lukas, C., Savic, V., Bekker-Jensen, S., Doil, C., Neumann, B., Pedersen, R. S., et al. (2011). 53BP1 nuclear bodies form around DNA lesions generated by mitotic transmission of chromosomes under replication stress. *Nat. Cell Biol.* 13, 243–253. doi: 10.1038/ncb2201

Luo, G., Yao, M. S., Bender, C. F., Mills, M., Bladl, A. R., Bradley, A., et al. (1999). Disruption of mRad50 causes embryonic stem cell lethality, abnormal embryonic development, and sensitivity to ionizing radiation. *Proc. Natl. Acad. Sci. U.S.A.* 96, 7376–7381. doi: 10.1073/pnas.96.13.7376

Luo, L. Z., Gopalakrishna-Pillai, S., Nay, S. L., Park, S. W., Bates, S. E., Zeng, X., et al. (2012). DNA repair in human pluripotent stem cells is distinct from that in non-pluripotent human cells. *PLoS One* 7:e30541. doi: 10.1371/journal.pone.0030541

Ly, P., and Cleveland, D. W. (2017). Rebuilding chromosomes after catastrophe: emerging mechanisms of chromothripsis. *Trends Cell Biol.* 27, 917–930. doi: 10.1016/j.tcb.2017.08.005

Machwe, A., Karale, R., Xu, X., Liu, Y., and Orren, D. K. (2011). The Werner and Bloom syndrome proteins help resolve replication blockage by converting (regressed) holliday junctions to functional replication forks. *Biochemistry* 50, 6774–6788. doi: 10.1021/bi2001054

Maciejowski, J., Li, Y., Bosco, N., Campbell, P. J., and De Lange, T. (2015). Chromothripsis and Kataegis Induced by Telomere Crisis. *Cell* 163, 1641–1654. doi: 10.1016/j.cell.2015.11.054

Mailand, N., Gibbs-Seymour, I., and Bekker-Jensen, S. (2013). Regulation of PCNA-protein interactions for genome stability. *Nat. Rev. Mol. Cell Biol.* 14, 269–282. doi: 10.1038/nrm3562

Mancini, A., Niemann-Seyde, S. C., Pankow, R., El Bounkari, O., Klebba-Farber, S., Koch, A., et al. (2010). THOC5/FMIP, an mRNA export TREX complex protein, is essential for hematopoietic primitive cell survival in vivo. *BMC Biol* 8:1. doi: 10.1186/1741-7007-8-1

Mandal, R., and Strebhardt, K. (2013). Plk1: unexpected roles in DNA replication. *Cell Res.* 23, 1251–1253. doi: 10.1038/cr.2013.130

Mankouri, H. W., Huttner, D., and Hickson, I. D. (2013). How unfinished business from S-phase affects mitosis and beyond. *EMBO J.* 32, 2661–2671. doi: 10.1038/emboj.2013.211

Maréchal, A., Li, J.-M., Ji, X. Y., Wu, C.-S., Yazinski, S. A., Nguyen, H. D., et al. (2014). PRP19 transforms into a sensor of RPA-ssDNA after DNA damage and drives ATR activation via a ubiquitin-mediated circuitry. *Mol. Cell* 53, 235–246. doi: 10.1016/j.molcel.2013.11.002

Maréchal, A., and Zou, L. (2013). DNA damage sensing by the ATM and ATR kinases. *Cold Spring Harb. Perspect. Biol.* 5:a012716. doi: 10.1101/cshperspect.a012716

Masamsetti, V. P., Low, R. R. J., Mak, K. S., O'connor, A., Riffkin, C. D., Lamm, N., et al. (2019). Replication stress induces mitotic death through parallel pathways regulated by WAPL and telomere deprotection. *Nat. Commun.* 10:4224. doi: 10.1038/s41467-019-12255-w

Masuda, K., Ouchida, R., Takeuchi, A., Saito, T., Koseki, H., Kawamura, K., et al. (2005). DNA polymerase theta contributes to the generation of C/G mutations during somatic hypermutation of Ig genes. *Proc. Natl. Acad. Sci. U.S.A.* 102, 13986–13991. doi: 10.1073/pnas.0505636102

Mateos-Gomez, P. A., Gong, F., Nair, N., Miller, K. M., Lazzerini-Denchi, E., and Sfeir, A. (2015). Mammalian polymerase θ promotes alternative NHEJ and suppresses recombination. *Nature* 518, 254–257. doi: 10.1038/nature14157

Mateos-Gomez, P. A., Kent, T., Deng, S. K., Mcdevitt, S., Kashkina, E., Hoang, T. M., et al. (2017). The helicase domain of Polθ counteracts RPA to promote alt-NHEJ. *Nat. Struct. Mol. Biol.* 24, 1116–1123. doi: 10.1038/nsmb.3494

Matson, J. P., Dumitru, R., Coryell, P., Baxley, R. M., Chen, W., Twaroski, K., et al. (2017). Rapid DNA replication origin licensing protects stem cell pluripotency. *eLife* 6:e30473.

Maynard, S., Swistowska, A. M., Lee, J. W., Liu, Y., Liu, S. T., Da Cruz, A. B., et al. (2008). Human embryonic stem cells have enhanced repair of multiple forms of DNA damage. *Stem Cells* 26, 2266–2274. doi: 10.1634/stemcells.2007-1041

McCarthy, E. E., Celebi, J. T., Baer, R., and Ludwig, T. (2003). Loss of Bard1, the heterodimeric partner of the Brca1 tumor suppressor, results in early embryonic lethality and chromosomal instability. *Mol. Cell. Biol.* 23, 5056–5063. doi: 10.1128/mcb.23.14.5056-5063.2003

Mello, S. S., and Attardi, L. D. (2018). Deciphering p53 signaling in tumor suppression. *Curr. Opin. Cell Biol.* 51, 65–72. doi: 10.1016/j.ceb.2017.11.005

Meryet-Figuiere, M., Alaei-Mahabadi, B., Ali, M. M., Mitra, S., Subhash, S., Pandey, G. K., et al. (2014). Temporal separation of replication and transcription during S-phase progression. *Cell Cycle* 13, 3241–3248. doi: 10.4161/15384101.2014.953876

Mijic, S., Zellweger, R., Chappidi, N., Berti, M., Jacobs, K., Mutreja, K., et al. (2017). Replication fork reversal triggers fork degradation in BRCA2-defective cells. *Nat. Commun.* 8:859. doi: 10.1038/s41467-017-01164-5

Miller, T. C. R., Locke, J., Greiwe, J. F., Diffley, J. F. X., and Costa, A. (2019). Mechanism of head-to-head MCM double-hexamer formation revealed by cryo-EM. *Nature* 575, 704–710. doi: 10.1038/s41586-019-1768-0

Min, J.-N., Tian, Y., Xiao, Y., Wu, L., Li, L., and Chang, S. (2013). The mINO80 chromatin remodeling complex is required for efficient telomere replication and maintenance of genome stability. *Cell Res.* 23, 1396–1413. doi: 10.1038/cr.2013.113

Minocherhomji, S., Ying, S., Bjerregaard, V. A., Bursomanno, S., Aleliunaite, A., Wu, W., et al. (2015). Replication stress activates DNA repair synthesis in mitosis. *Nature* 528, 286–290. doi: 10.1038/nature16139

Mohammed, H., Hernando-Herraez, I., Savino, A., Scialdone, A., Macaulay, I., Mulas, C., et al. (2017). Single-cell landscape of transcriptional heterogeneity and cell fate decisions during mouse early gastrulation. *Cell Rep.* 20, 1215–1228. doi: 10.1016/j.celrep.2017.07.009

Mohri, T., Ueno, M., Nagahama, Y., Gong, Z.-Y., Asano, M., Oshima, H., et al. (2013). Requirement of SLD5 for early embryogenesis. *PLoS One* 8:e78961. doi: 10.1371/journal.pone.0078961

Morris, S. A., Teo, R. T., Li, H., Robson, P., Glover, D. M., and Zernicka-Goetz, M. (2010). Origin and formation of the first two distinct cell types of the inner cell mass in the mouse embryo. *Proc. Natl. Acad. Sci. U.S.A.* 107, 6364–6369. doi: 10.1073/pnas.0915063107

Murga, M., Bunting, S., Montaña, M. F., Soria, R., Mulero, F., Cañamero, M., et al. (2009). A mouse model of ATR-Seckel shows embryonic replicative stress and accelerated aging. *Nat. Genet.* 41, 891–898. doi: 10.1038/ng.420

Murray, S. A., Morgan, J. L., Kane, C., Sharma, Y., Heffner, C. S., Lake, J., et al. (2010). Mouse gestation length is genetically determined. *PLoS One* 5:e12418. doi: 10.1371/journal.pone.0012418

Myers, K., Gagou, M. E., Zuazua-Villar, P., Rodriguez, R., and Meuth, M. (2009). ATR and Chk1 suppress a caspase-3-dependent apoptotic response following DNA replication stress. *PLoS Genet.* 5:e1000324. doi: 10.1371/journal.pgen.1000324

Navadgi-Patil, V. M., and Burgers, P. M. (2009). A tale of two tails: activation of DNA damage checkpoint kinase Mec1/ATR by the 9-1-1 clamp and by Dpb11/TopBP1. *DNA Repair* 8, 996–1003. doi: 10.1016/j.dnarep.2009.03.011

Neelsen, K. J., and Lopes, M. (2015). Replication fork reversal in eukaryotes: from dead end to dynamic response. *Nat. Rev. Mol. Cell Biol.* 16, 207–220. doi: 10.1038/nrm3935

Nigg, E. A. (2001). Mitotic kinases as regulators of cell division and its checkpoints. *Nat. Rev. Mol. Cell Biol.* 2, 21–32. doi: 10.1038/35048096

Nishitani, H., Taraviras, S., Lygerou, Z., and Nishimoto, T. (2001). The human licensing factor for DNA replication Cdt1 accumulates in G1 and is destabilized after initiation of S-phase. *J. Biol. Chem.* 276, 44905–44911. doi: 10.1074/jbc.M105406200

Nozaki, T., Masutani, M., Watanabe, M., Ochiya, T., Hasegawa, F., Nakagama, H., et al. (1999). Syncytiotrophoblastic giant cells in teratocarcinoma-like tumors derived from Parp-disrupted mouse embryonic stem cells. *Proc. Natl. Acad. Sci. U.S.A.* 96, 13345–13350. doi: 10.1073/pnas.96.23.13345

Nussenzweig, A., Chen, C., Da Costa Soares, V., Sanchez, M., Sokol, K., Nussenzweig, M. C., et al. (1996). Requirement for Ku80 in growth and immunoglobulin V(D)J recombination. *Nature* 382, 551–555. doi: 10.1038/382551a0

Ochi, T., Blackford, A. N., Coates, J., Jhujh, S., Mehmood, S., Tamura, N., et al. (2015). DNA repair. *PAXX, a paralog of XRCC4* and XLF, interacts with Ku to promote DNA double-strand break repair. *Science* 347, 185–188. doi: 10.1126/science.1261971

Ochs, F., Karemore, G., Miron, E., Brown, J., Sedlackova, H., Rask, M. B., et al. (2019). Stabilization of chromatin topology safeguards genome integrity. *Nature* 574, 571–574. doi: 10.1038/s41586-019-1659-4

O'Connell, M. J., Raleigh, J. M., Verkade, H. M., and Nurse, P. (1997). Chk1 is a wee1 kinase in the G2 DNA damage checkpoint inhibiting cdc2 by Y15 phosphorylation. *EMBO J.* 16, 545–554. doi: 10.1093/emboj/16.3.545

Orthwein, A., Fradet-Turcotte, A., Noordermeer, S. M., Canny, M. D., Brun, C. M., Strecker, J., et al. (2014). Mitosis inhibits DNA double-strand break repair to guard against telomere fusions. *Science* 344, 189–193. doi: 10.1126/science.1248024

Ouyang, H., Nussenzweig, A., Kurimasa, A., Soares, V. C., Li, X., Cordon-Cardo, C., et al. (1997). Ku70 is required for DNA repair but not for T cell antigen receptor gene recombination *in vivo*. *J. Exp. Med.* 186, 921–929. doi: 10.1084/jem.186.6.921

Paim, L. M. G., and FitzHarris, G. (2019). Tetraploidy causes chromosomal instability in acentriolar mouse embryos. *Nat. Commun.* 10:4834. doi: 10.1038/s41467-019-12772-8

Park, E., Kim, J. M., Primack, B., Weinstock, D. M., Moreau, L. A., Parmar, K., et al. (2013). Inactivation of Uaf1 causes defective homologous recombination and early embryonic lethality in mice. *Mol. Cell. Biol.* 33, 4360–4370. doi: 10.1128/MCB.00870-13

Pilzecker, B., Buoninfante, O. A., Van Den Berk, P., Lancini, C., Song, J. Y., Citterio, E., et al. (2017). DNA damage tolerance in hematopoietic stem and progenitor cells in mice. *Proc. Natl. Acad. Sci. U.S.A.* 114, E6875–E6883. doi: 10.1073/pnas.1706508114

Pintard, L., and Archambault, V. (2018). A unified view of spatio-temporal control of mitotic entry: Polo kinase as the key. *Open Biol.* 8:180114. doi: 10.1098/rsob.180114

Pizzi, S., Sertic, S., Orcesi, S., Cereda, C., Bianchi, M., Jackson, A. P., et al. (2015). Reduction of hRNase H2 activity in Aicardi-Goutieres syndrome cells leads to replication stress and genome instability. *Hum. Mol. Genet.* 24, 649–658. doi: 10.1093/hmg/ddu485

Poli, J., Gasser, S. M., and Papamichos-Chronakis, M. (2017). The INO80 remodeller in transcription, replication and repair. *Philos. Trans. R. Soc. Lond. B Biol. Sci.* 372:20160290. doi: 10.1098/rstb.2016.0290

Pollard, P. J., Spencer-Dene, B., Shukla, D., Howarth, K., Nye, E., El-Bahrawy, M., et al. (2007). Targeted inactivation of fh1 causes proliferative renal cyst development and activation of the hypoxia pathway. *Cancer Cell* 11, 311–319. doi: 10.1016/j.ccr.2007.02.005

Power, M. A., and Tam, P. P. (1993). Onset of gastrulation, morphogenesis and somitogenesis in mouse embryos displaying compensatory growth. *Anat. Embryol.* 187, 493–504. doi: 10.1007/BF00174425

Przetocka, S., Porro, A., Bolck, H. A., Walker, C., Lezaja, A., Trenner, A., et al. (2018). CtIP-mediated fork protection synergizes with BRCA1 to suppress genomic instability upon DNA replication stress. *Mol. Cell* 72, doi: 10.1016/j.molcel.2018.09.014

Puebla-Osorio, N., Lacey, D. B., Alt, F. W., and Zhu, C. (2006). Early embryonic lethality due to targeted inactivation of DNA ligase III. *Mol. Cell. Biol.* 26, 3935–3941. doi: 10.1128/MCB.26.10.3935-3941.2006

Quinet, A., Lemaçon, D., and Vindigni, A. (2017). Replication fork reversal: players and guardians. *Mol. Cell* 68, 830–833. doi: 10.1016/j.molcel.2017.11.022

Ray, D., Terao, Y., Nimbalkar, D., Hirai, H., Osmundson, E. C., Zou, X., et al. (2007). Hemizygous disruption of Cdc25A inhibits cellular transformation and mammary tumorigenesis in mice. *Cancer Res.* 67, 6605–6611. doi: 10.1158/0008-5472.CAN-06-4815

Ray Chaudhuri, A., Callen, E., Ding, X., Gogola, E., Duarte, A. A., Lee, J. E., et al. (2016). Replication fork stability confers chemoresistance in BRCA-deficient cells. *Nature* 535, 382–387. doi: 10.1038/nature18325

Ray Chaudhuri, A., and Nussenzweig, A. (2017). The multifaceted roles of PARP1 in DNA repair and chromatin remodelling. *Nat. Rev. Mol. Cell Biol.* 18, 610–621. doi: 10.1038/nrm.2017.53

Reinhardt, H. C., and Schumacher, B. (2012). The p53 network: cellular and systemic DNA damage responses in aging and cancer. *Trends Genet.* 28, 128–136. doi: 10.1016/j.tig.2011.12.002

Roa, S., Avdievich, E., Peled, J. U., Maccarthy, T., Werling, U., Kuang, F. L., et al. (2008). Ubiquitylated PCNA plays a role in somatic hypermutation and class-switch recombination and is required for meiotic progression. *Proc. Natl. Acad. Sci. U.S.A.* 105, 16248–16253. doi: 10.1073/pnas.0808182105

Rogakou, E. P., Pilch, D. R., Orr, A. H., Ivanova, V. S., and Bonner, W. M. (1998). DNA double-stranded breaks induce histone H2AX phosphorylation on serine 139. *J. Biol. Chem.* 273, 5858–5868. doi: 10.1074/jbc.273.10.5858

Roper, S. J., Chrysanthou, S., Senner, C. E., Sienerth, A., Gnan, S., Murray, A., et al. (2014). ADP-ribosyltransferases Parp1 and Parp7 safeguard pluripotency of ES cells. *Nucleic Acids Res.* 42, 8914–8927. doi: 10.1093/nar/gku591

Rossi, D. J., Londesborough, A., Korsisaari, N., Pihlak, A., Lehtonen, E., Henkemeyer, M., et al. (2001). Inability to enter S phase and defective RNA polymerase II CTD phosphorylation in mice lacking Mat1. *EMBO J.* 20, 2844–2856. doi: 10.1093/emboj/20.11.2844

Saldivar, J. C., Cortez, D., and Cimprich, K. A. (2017). The essential kinase ATR: ensuring faithful duplication of a challenging genome. *Nat. Rev. Mol. Cell Biol.* 18, 622–636. doi: 10.1038/nrm.2017.67

Sasaki, M., Kawahara, K., Nishio, M., Mimori, K., Kogo, R., Hamada, K., et al. (2011). Regulation of the MDM2-P53 pathway and tumor growth by PICT1 via nucleolar RPL11. *Nat. Med.* 17, 944–951. doi: 10.1038/nm.2392

Schärer, O. D. (2013). Nucleotide excision repair in eukaryotes. *Cold Spring Harb. Perspect. Biol.* 5:a012609. doi: 10.1101/cshperspect.a012609

Schlacher, K., Christ, N., Siaud, N., Egashira, A., Wu, H., and Jasin, M. (2011). Double-strand break repair-independent role for BRCA2 in blocking stalled replication fork degradation by MRE11. *Cell* 145, 529–542. doi: 10.1016/j.cell.2011.03.041

Scully, R., Panday, A., Elango, R., and Willis, N. A. (2019). DNA double-strand break repair-pathway choice in somatic mammalian cells. *Nat. Rev. Mol. Cell Biol.* 20, 698–714. doi: 10.1038/s41580-019-0152-0

Sfeir, A., and Symington, L. S. (2015). Microhomology-mediated end joining: a back-up survival mechanism or dedicated pathway? *Trends Biochem. Sci.* 40, 701–714. doi: 10.1016/j.tibs.2015.08.006

Shakya, R., Szabolcs, M., Mccarthy, E., Ospina, E., Basso, K., Nandula, S., et al. (2008). The basal-like mammary carcinomas induced by Brca1 or Bard1 inactivation implicate the BRCA1/BARD1 heterodimer in tumor suppression. *Proc. Natl. Acad. Sci. U.S.A.* 105, 7040–7045. doi: 10.1073/pnas.0711032105

Sharan, S. K., Morimatsu, M., Albrecht, U., Lim, D. S., Regel, E., Dinh, C., et al. (1997). Embryonic lethality and radiation hypersensitivity mediated by Rad51 in mice lacking Brca2. *Nature* 386, 804–810. doi: 10.1038/386804a0

Shima, N., Munroe, R. J., and Schimenti, J. C. (2004). The mouse genomic instability mutation chaos1 is an allele of Polq that exhibits genetic interaction with Atm. *Mol. Cell. Biol.* 24, 10381–10389. doi: 10.1128/MCB.24.23.10381-10389.2004

Shimada, M., Dumitrache, L. C., Russell, H. R., and Mckinnon, P. J. (2015). Polynucleotide kinase-phosphatase enables neurogenesis via multiple DNA repair pathways to maintain genome stability. *EMBO J.* 34, 2465–2480. doi: 10.15252/embj.201591363

Shu, Z., Smith, S., Wang, L., Rice, M. C., and Kmiec, E. B. (1999). Disruption of muREC2/RAD51L1 in mice results in early embryonic lethality which can Be partially rescued in a p53(-/-) background. *Mol. Cell. Biol.* 19, 8686–8693. doi: 10.1128/mcb.19.12.8686

Shui, J. W., Hu, M. C., and Tan, T. H. (2007). Conditional knockout mice reveal an essential role of protein phosphatase 4 in thymocyte development and pre-T-cell receptor signaling. *Mol. Cell. Biol.* 27, 79–91. doi: 10.1128/MCB.00799-06

Smith, T. G., Laval, S., Chen, F., Rock, M. J., Strachan, T., and Peters, H. (2014). Neural crest cell-specific inactivation of Nipbl or Mau2 during mouse development results in a late onset of craniofacial defects. *Genesis* 52, 687–694. doi: 10.1002/dvg.22780

Snow, M. H., and Tam, P. P. (1979). Is compensatory growth a complicating factor in mouse teratology? *Nature* 279, 555–557. doi: 10.1038/279555a0

Snow, M. H. L. (1976). "Embryo Growth during the Immediate Postimplantation Period," in *Embryogenesis in Mammals: Ciba Foundation Symposium 40 - Embryogenesis in Mammals*, eds K. Elliott, and M. O'Connor (Amsterdam: Elsevier), 53–70.

Snow, M. H. L. (1977). Gastrulation in the mouse: growth and regionalization of the epiblast. *Development* 42, 293–303. doi: 10.1111/dgd.12568

Sobinoff, A. P., Allen, J. A., Neumann, A. A., Yang, S. F., Walsh, M. E., Henson, J. D., et al. (2017). BLM and SLX4 play opposing roles in recombination-dependent replication at human telomeres. *EMBO J.* 36, 2907–2919. doi: 10.15252/embj.201796889

Somyajit, K., Saxena, S., Babu, S., Mishra, A., and Nagaraju, G. (2015). Mammalian RAD51 paralogs protect nascent DNA at stalled forks and mediate replication restart. *Nucleic Acids Res.* 43, 9835–9855. doi: 10.1093/nar/gkv880

Sotiriou, S. K., Kamileri, I., Lugli, N., Evangelou, K., Da-Re, C., Huber, F., et al. (2016). Mammalian RAD52 functions in break-induced replication repair of collapsed DNA replication forks. *Mol. Cell* 64, 1127–1134. doi: 10.1016/j.molcel.2016.10.038

Sozen, B., Amadei, G., Cox, A., Wang, R., Na, E., Czukiewska, S., et al. (2018). Self-assembly of embryonic and two extra-embryonic stem cell types into gastrulating embryo-like structures. *Nat. Cell Biol.* 20, 979–989. doi: 10.1038/s41556-018-0147-7

Spies, J., Lukas, C., Somyajit, K., Rask, M. B., Lukas, J., and Neelsen, K. J. (2019). 53BP1 nuclear bodies enforce replication timing at under-replicated DNA to limit heritable DNA damage. *Nat. Cell Biol.* 21, 487–497. doi: 10.1038/s41556-019-0293-6

Stewart, G. S., Wang, B., Bignell, C. R., Taylor, A. M., and Elledge, S. J. (2003). MDC1 is a mediator of the mammalian DNA damage checkpoint. *Nature* 421, 961–966. doi: 10.1038/nature01446

Stracker, T. H., and Petrini, J. H. J. (2011). The MRE11 complex: starting from the ends. *Nat. Rev. Mol. Cell Biol.* 12, 90–103. doi: 10.1038/nrm3047

Strzalka, W., and Ziemienowicz, A. (2011). Proliferating cell nuclear antigen (PCNA): a key factor in DNA replication and cell cycle regulation. *Ann. Bot.* 107, 1127–1140. doi: 10.1093/aob/mcq243

Symington, L. S. (2016). Mechanism and regulation of DNA end resection in eukaryotes. *Crit. Rev. Biochem. Mol. Biol.* 51, 195–212. doi: 10.3109/10409238.2016.1172552

Taglialatela, A., Alvarez, S., Leuzzi, G., Sannino, V., Ranjha, L., Huang, J. W., et al. (2017). Restoration of replication fork stability in BRCA1- and BRCA2-deficient cells by inactivation of SNF2-family fork remodelers. *Mol. Cell* 68, 414–430.e8. doi: 10.1016/j.molcel.2017.09.036

Takai, H., Tominaga, K., Motoyama, N., Minamishima, Y. A., Nagahama, H., Tsukiyama, T., et al. (2000). Aberrant cell cycle checkpoint function and early embryonic death in Chk1(-/-) mice. *Genes Dev.* 14, 1439–1447.

Takeuchi, A., Iida, K., Tsubota, T., Hosokawa, M., Denawa, M., Brown, J. B., et al. (2018). Loss of Sfpq Causes Long-Gene Transcriptopathy in the Brain. *Cell Rep.* 23, 1326–1341. doi: 10.1016/j.celrep.2018.03.141

Tam, P. P. (1989). Regionalisation of the mouse embryonic ectoderm: allocation of prospective ectodermal tissues during gastrulation. *Development* 107, 55–67.

Tam, P. P., Williams, E. A., and Chan, W. Y. (1993). Gastrulation in the mouse embryo: ultrastructural and molecular aspects of germ layer morphogenesis. *Microsc. Res. Tech.* 26, 301–328. doi: 10.1002/jemt.1070260405

Tam, P. P. L., Nelson, J., and Rossant, J. (2013). *Mammalian Development*. Cold Spring Harbor, NY: Cold Spring Harbor Laboratory Press.

Tebbs, R. S., Flannery, M. L., Meneses, J. J., Hartmann, A., Tucker, J. D., Thompson, L. H., et al. (1999). Requirement for the Xrcc1 DNA base excision repair gene during early mouse development. *Dev. Biol.* 208, 513–529. doi: 10.1006/dbio.1999.9232

Ter Huurne, M., Chappell, J., Dalton, S., and Stunnenberg, H. G. (2017). Distinct cell-cycle control in two different states of mouse pluripotency. *Cell Stem Cell* 21, 449–455.e4. doi: 10.1016/j.stem.2017.09.004

Tesar, P. J., Chenoweth, J. G., Brook, F. A., Davies, T. J., Evans, E. P., Mack, D. L., et al. (2007). New cell lines from mouse epiblast share defining features with human embryonic stem cells. *Nature* 448, 196–199. doi: 10.1038/nature05972

Thangavel, S., Berti, M., Levikova, M., Pinto, C., Gomathinayagam, S., Vujanovic, M., et al. (2015). DNA2 drives processing and restart of reversed replication forks in human cells. *J. Cell Biol.* 208, 545–562. doi: 10.1083/jcb.201406100

Theunissen, J. W., Kaplan, M. I., Hunt, P. A., Williams, B. R., Ferguson, D. O., Alt, F. W., et al. (2003). Checkpoint failure and chromosomal instability without lymphomagenesis in Mre11(ATLD1/ATLD1) mice. *Mol. Cell* 12, 1511–1523. doi: 10.1016/s1097-2765(03)00455-6

Tichy, E. D., Pillai, R., Deng, L., Liang, L., Tischfield, J., Schwemberger, S. J., et al. (2010). Mouse embryonic stem cells, but not somatic cells, predominantly use homologous recombination to repair double-strand DNA breaks. *Stem Cells Dev.* 19, 1699–1711. doi: 10.1089/scd.2010.0058

Toledo, L. I., Altmeyer, M., Rask, M. B., Lukas, C., Larsen, D. H., Povlsen, L. K., et al. (2013). ATR prohibits replication catastrophe by preventing global exhaustion of RPA. *Cell* 155, 1088–1103. doi: 10.1016/j.cell.2013.10.043

Tominaga, Y., Li, C., Wang, R.-H., and Deng, C.-X. (2006). Murine Wee1 plays a critical role in cell cycle regulation and pre-implantation stages of embryonic development. *Int. J. Biol. Sci.* 2, 161–170. doi: 10.7150/ijbs.2.161

Tomoda, K., Yoneda-Kato, N., Fukumoto, A., Yamanaka, S., and Kato, J. Y. (2004). Multiple functions of Jab1 are required for early embryonic development and growth potential in mice. *J. Biol. Chem.* 279, 43013–43018. doi: 10.1074/jbc.M406559200

Tsuzuki, T., Fujii, Y., Sakumi, K., Tominaga, Y., Nakao, K., Sekiguchi, M., et al. (1996). Targeted disruption of the Rad51 gene leads to lethality in embryonic mice. *Proc. Natl. Acad. Sci. U.S.A.* 93, 6236–6240. doi: 10.1073/pnas.93.13.6236

Uchimura, A., Hidaka, Y., Hirabayashi, T., Hirabayashi, M., and Yagi, T. (2009). DNA polymerase delta is required for early mammalian embryogenesis. *PLoS One* 4:e4184. doi: 10.1371/journal.pone.0004184

Uziel, T., Lerenthal, Y., Moyal, L., Andegeko, Y., Mittelman, L., and Shiloh, Y. (2003). Requirement of the MRN complex for ATM activation by DNA damage. *EMBO J.* 22, 5612–5621. doi: 10.1093/emboj/cdg541

Vallabhaneni, H., Lynch, P. J., Chen, G., Park, K., Liu, Y., Goehe, R., et al. (2018). High basal levels of gammaH2AX in human induced pluripotent stem cells are linked to replication-associated DNA damage and repair. *Stem Cells* 36, 1501–1513. doi: 10.1002/stem.2861

Valnegri, P., Huang, J., Yamada, T., Yang, Y., Mejia, L. A., Cho, H. Y., et al. (2017). RNF8/UBC13 ubiquitin signaling suppresses synapse formation in the mammalian brain. *Nat. Commun.* 8:1271. doi: 10.1038/s41467-017-01333-6

van Harten, A. M., Buijze, M., Van Der Mast, R., Rooimans, M. A., Martens-De Kemp, S. R., Bachas, C., et al. (2019). Targeting the cell cycle in head and neck cancer by Chk1 inhibition: a novel concept of bimodal cell death. *Oncogenesis* 8:38. doi: 10.1038/s41389-019-0147-x

Van Ly, D., Low, R. R. J., Frolich, S., Bartolec, T. K., Kafer, G. R., Pickett, H. A., et al. (2018). Telomere loop dynamics in chromosome end protection. *Mol. Cell* 71, 510–525.e6. doi: 10.1016/j.molcel.2018.06.025

Wachowicz, P., Fernández-Miranda, G., Marugán, C., Escobar, B., and De Cárcer, G. (2016). Genetic depletion of Polo-like kinase 1 leads to embryonic lethality due to mitotic aberrancies. *Bioessays* 38(Suppl. 1), S96–S106. doi: 10.1002/bies.201670908

Wallace, S. S. (2014). Base excision repair: a critical player in many games. *DNA Repair* 19, 14–26. doi: 10.1016/j.dnarep.2014.03.030

Wang, X., Chang, Y., Li, Y., Zhang, X., and Goodrich, D. W. (2006). Thoc1/Hpr1/p84 is essential for early embryonic development in the mouse. *Mol. Cell. Biol.* 26, 4362–4367. doi: 10.1128/MCB.02163-05

Wang, Y., Putnam, C. D., Kane, M. F., Zhang, W., Edelmann, L., Russell, R., et al. (2005). Mutation in Rpa1 results in defective DNA double-strand break repair, chromosomal instability and cancer in mice. *Nat. Genet.* 37, 750–755. doi: 10.1038/ng1587

Wang, Z. Q., Auer, B., Stingl, L., Berghammer, H., Haidacher, D., Schweiger, M., et al. (1995). Mice lacking ADPRT and poly(ADP-ribosyl)ation develop normally but are susceptible to skin disease. *Genes Dev.* 9, 509–520. doi: 10.1101/gad.9.5.509

Ward, I. M., Minn, K., Van Deursen, J., and Chen, J. (2003). p53 Binding protein 53BP1 is required for DNA damage responses and tumor suppression in mice. *Mol. Cell. Biol.* 23, 2556–2563. doi: 10.1128/mcb.23.7.2556-2563.2003

Watanabe, N., Arai, H., Nishihara, Y., Taniguchi, M., Watanabe, N., Hunter, T., et al. (2004). M-phase kinases induce phospho-dependent ubiquitination of somatic Wee1 by SCFbeta-TrCP. *Proc. Natl. Acad. Sci. U.S.A.* 101, 4419–4424. doi: 10.1073/pnas.0307700101

Watson, C. M., and Tam, P. P. (2001). Cell lineage determination in the mouse. *Cell Struct. Funct.* 26, 123–129.

Weiss, R. S., Enoch, T., and Leder, P. (2000). Inactivation of mouse Hus1 results in genomic instability and impaired responses to genotoxic stress. *Genes Dev.* 14, 1886–1898.

Wen, B., Li, R., Cheng, K., Li, E., Zhang, S., Xiang, J., et al. (2017). Tetraploid embryonic stem cells can contribute to the development of chimeric fetuses and chimeric extraembryonic tissues. *Sci. Rep.* 7:3030. doi: 10.1038/s41598-017-02783-0

Wilhelm, T., Olziersky, A.-M., Harry, D., De Sousa, F., Vassal, H., Eskat, A., et al. (2019). Mild replication stress causes chromosome mis-segregation via premature centriole disengagement. *Nat. Commun.* 10:3585. doi: 10.1038/s41467-019-11584-0

Xanthoudakis, S., Smeyne, R. J., Wallace, J. D., and Curran, T. (1996). The redox/DNA repair protein, Ref-1, is essential for early embryonic development in mice. *Proc. Natl. Acad. Sci. U.S.A.* 93, 8919–8923. doi: 10.1073/pnas.93.17.8919

Xiao, Y., and Weaver, D. T. (1997). Conditional gene targeted deletion by Cre recombinase demonstrates the requirement for the double-strand break repair Mre11 protein in murine embryonic stem cells. *Nucleic Acids Res.* 25, 2985–2991. doi: 10.1093/nar/25.15.2985

Xiao, Z., Chen, Z., Gunasekera, A. H., Sowin, T. J., Rosenberg, S. H., Fesik, S., et al. (2003). Chk1 mediates S and G2 arrests through Cdc25A degradation in response to DNA-damaging agents. *J. Biol. Chem.* 278, 21767–21773. doi: 10.1074/jbc.M300229200

Xie, R., Medina, R., Zhang, Y., Hussain, S., Colby, J., Ghule, P., et al. (2009). The histone gene activator HINFP is a nonredundant cyclin E/CDK2 effector during early embryonic cell cycles. *Proc. Natl. Acad. Sci. U.S.A.* 106, 12359–12364. doi: 10.1073/pnas.0905651106

Xu, Y., Ashley, T., Brainerd, E. E., Bronson, R. T., Meyn, M. S., and Baltimore, D. (1996). Targeted disruption of ATM leads to growth retardation, chromosomal fragmentation during meiosis, immune defects, and thymic lymphoma. *Genes Dev.* 10, 2411–2422. doi: 10.1101/gad.10.19.2411

Yamazaki, S., Ishii, A., Kanoh, Y., Oda, M., Nishito, Y., and Masai, H. (2012). Rif1 regulates the replication timing domains on the human genome. *EMBO J.* 31, 3667–3677. doi: 10.1038/emboj.2012.180

Yang, W., Klaman, L. D., Chen, B., Araki, T., Harada, H., Thomas, S. M., et al. (2006). An Shp2/SFK/Ras/Erk signaling pathway controls trophoblast stem cell survival. *Dev. Cell* 10, 317–327. doi: 10.1016/j.devcel.2006.01.002

Yata, K., Bleuyard, J. Y., Nakato, R., Ralf, C., Katou, Y., Schwab, R. A., et al. (2014). BRCA2 coordinates the activities of cell-cycle kinases to promote genome stability. *Cell Rep.* 7, 1547–1559. doi: 10.1016/j.celrep.2014.04.023

Yonemasu, R., Minami, M., Nakatsu, Y., Takeuchi, M., Kuraoka, I., Matsuda, Y., et al. (2005). Disruption of mouse XAB2 gene involved in pre-mRNA splicing, transcription and transcription-coupled DNA repair results in preimplantation lethality. *DNA Repair* 4, 479–491. doi: 10.1016/j.dnarep.2004.12.004

Yoon, J. C., Ling, A. J., Isik, M., Lee, D. Y., Steinbaugh, M. J., Sack, L. M., et al. (2014). GLTSCR2/PICT1 links mitochondrial stress and Myc signaling. *Proc. Natl. Acad. Sci. U.S.A.* 111, 3781–3786. doi: 10.1073/pnas.1400705111

Yoshida, K., Kuo, F., George, E. L., Sharpe, A. H., and Dutta, A. (2001). Requirement of CDC45 for postimplantation mouse development. *Mol. Cell. Biol.* 21, 4598–4603. doi: 10.1128/MCB.21.14.4598-4603.2001

Zaugg, K., Su, Y. W., Reilly, P. T., Moolani, Y., Cheung, C. C., Hakem, R., et al. (2007). Cross-talk between Chk1 and Chk2 in double-mutant thymocytes. *Proc. Natl. Acad. Sci. U.S.A.* 104, 3805–3810. doi: 10.1073/pnas.0611584104

Zaveri, L., and Dhawan, J. (2018). Cycling to meet fate: connecting pluripotency to the cell cycle. *Front. Cell Dev. Biol.* 6:57. doi: 10.3389/fcell.2018.00057

Zellweger, R., Dalcher, D., Mutreja, K., Berti, M., Schmid, J. A., Herrador, R., et al. (2015). Rad51-mediated replication fork reversal is a global response to genotoxic treatments in human cells. *J. Cell Biol.* 208, 563–579. doi: 10.1083/jcb.201406099

Zeman, M. K., and Cimprich, K. A. (2014). Causes and consequences of replication stress. *Nat. Cell Biol.* 16, 2–9. doi: 10.1038/ncb2897

Zhang, Y., and Hunter, T. (2014). Roles of Chk1 in cell biology and cancer therapy. *Int. J. Cancer* 134, 1013–1023. doi: 10.1002/ijc.28226

Zhang, Y., Zolov, S. N., Chow, C. Y., Slutsky, S. G., Richardson, S. C., Piper, R. C., et al. (2007). Loss of Vac14, a regulator of the signaling lipid phosphatidylinositol 3,5-bisphosphate, results in neurodegeneration in mice. *Proc. Natl. Acad. Sci. U.S.A.* 104, 17518–17523. doi: 10.1073/pnas.0702275104

Zhao, B., Zhang, W., Cun, Y., Li, J., Liu, Y., Gao, J., et al. (2018). Mouse embryonic stem cells have increased capacity for replication fork restart driven by the specific Filia-Floped protein complex. *Cell Res.* 28, 69–89. doi: 10.1038/cr.2017.139

Zhao, B., Zhang, W. D., Duan, Y. L., Lu, Y. Q., Cun, Y. X., Li, C. H., et al. (2015). Filia Is an ESC-Specific Regulator of DNA Damage Response and Safeguards Genomic Stability. *Cell Stem Cell* 16, 684–698. doi: 10.1016/j.stem.2015.03.017

Zheng, P. (2020). Maintaining genomic stability in pluripotent stem cells. *Genome Instabil. Dis.* 1, 92–97.

Zhou, Z., Wang, L., Ge, F., Gong, P., Wang, H., Wang, F., et al. (2018). Pold3 is required for genomic stability and telomere integrity in embryonic stem cells and meiosis. *Nucleic Acids Res.* 46, 3468–3486. doi: 10.1093/nar/gky098

Zhu, J., Petersen, S., Tessarollo, L., and Nussenzweig, A. (2001). Targeted disruption of the Nijmegen breakage syndrome gene NBS1 leads to early embryonic lethality in mice. *Curr. Biol.* 11, 105–109. doi: 10.1016/s0960-9822(01)00019-7

Ziegler-Birling, C., Helmrich, A., Tora, L., and Torres-Padilla, M.-E. (2009). Distribution of p53 binding protein 1 (53BP1) and phosphorylated H2A.X during mouse preimplantation development in the absence of DNA damage. *Int. J. Dev. Biol.* 53, 1003–1011. doi: 10.1387/ijdb.082707cz

Zimmermann, M., Lottersberger, F., Buonomo, S. B., Sfeir, A., and De Lange, T. (2013). 53BP1 regulates DSB repair using Rif1 to control 5′ end resection. *Science* 339, 700–704. doi: 10.1126/science.1231573

Zong, D., Adam, S., Wang, Y., Sasanuma, H., Callen, E., Murga, M., et al. (2019). BRCA1 haploinsufficiency is masked by RNF168-mediated chromatin ubiquitylation. *Mol. Cell* 73, 1267–1281.e7. doi: 10.1016/j.molcel.2018.12.010

Conflict of Interest: The authors declare that the research was conducted in the absence of any commercial or financial relationships that could be construed as a potential conflict of interest.

frontiers in Cell and Developmental Biology

ORIGINAL RESEARCH
published: 05 June 2020
doi: 10.3389/fcell.2020.00358

Ppp2r2a Knockout Mice Reveal That Protein Phosphatase 2A Regulatory Subunit, PP2A-B55α, Is an Essential Regulator of Neuronal and Epidermal Embryonic Development

Nikita Panicker[1,2], Melody Coutman[1,2], Charley Lawlor-O'Neill[1,2], Richard G. S. Kahl[1,2], Séverine Roselli[1,2†] and Nicole M. Verrills[1,2†]*

[1] School of Biomedical Sciences and Pharmacy, Faculty of Health and Medicine, Priority Research Centre for Cancer Research, Innovation and Translation, University of Newcastle, Callaghan, NSW, Australia, [2] Hunter Cancer Research Alliance, Hunter Medical Research Institute, New Lambton, NSW, Australia

OPEN ACCESS

Edited by:
Andrew Burgess,
ANZAC Research Institute, Australia

Reviewed by:
Joshua Oaks,
Lynx Biosciences, Inc., United States
Veerle Janssens,
KU Leuven, Belgium

***Correspondence:**
Nicole M. Verrills
nikki.verrills@newcastle.edu.au

† These authors have contributed equally to this work

Specialty section:
This article was submitted to Cell Growth and Division, a section of the journal Frontiers in Cell and Developmental Biology

Received: 17 February 2020
Accepted: 22 April 2020
Published: 05 June 2020

Citation:
Panicker N, Coutman M, Lawlor-O'Neill C, Kahl RGS, Roselli S and Verrills NM (2020) Ppp2r2a Knockout Mice Reveal That Protein Phosphatase 2A Regulatory Subunit, PP2A-B55α, Is an Essential Regulator of Neuronal and Epidermal Embryonic Development. Front. Cell Dev. Biol. 8:358. doi: 10.3389/fcell.2020.00358

The serine/threonine protein phosphatase 2A (PP2A) is a master regulator of the complex cellular signaling that occurs during all stages of mammalian development. PP2A is composed of a catalytic, a structural, and regulatory subunit, for which there are multiple isoforms. The association of specific regulatory subunits determines substrate specificity and localization of phosphatase activity, however, the precise role of each regulatory subunit in development is not known. Here we report the generation of the first knockout mouse for the *Ppp2r2a* gene, encoding the PP2A-B55α regulatory subunit, using CRISPR/Cas9. Heterozygous animals developed and grew as normal, however, homozygous knockout mice were not viable. Analysis of embryos at different developmental stages found a normal Mendelian ratio of $Ppp2r2a^{-/-}$ embryos at embryonic day (E) 10.5 (25%), but reduced $Ppp2r2a^{-/-}$ embryos at E14.5 (18%), and further reduced at E18.5 (10%). No live $Ppp2r2a^{-/-}$ pups were observed at birth. $Ppp2r2a^{-/-}$ embryos were significantly smaller than wild-type or heterozygous littermates and displayed a variety of neural defects such as exencephaly, spina bifida, and cranial vault collapse, as well as syndactyly and severe epidermal defects; all processes driven by growth and differentiation of the ectoderm. $Ppp2r2a^{-/-}$ embryos had incomplete epidermal barrier acquisition, associated with thin, poorly differentiated stratified epithelium with weak attachment to the underlying dermis. The basal keratinocytes in $Ppp2r2a^{-/-}$ embryos were highly disorganized, with reduced immunolabeling of integrins and basement membrane proteins, suggesting impaired focal adhesion and hemidesmosome assembly. The spinous and granular layers were thinner in the $Ppp2r2a^{-/-}$ embryos, with aberrant expression of adherens and tight junction associated proteins. The overlying stratum corneum was either absent or incomplete. Thus PP2A-B55α is an essential regulator of epidermal stratification, and is essential for ectodermal development during embryogenesis.

Keywords: PP2A, knockout mouse, embryo, lethality, skin, epidermal barrier

INTRODUCTION

Mammalian development is a highly complex process requiring exquisite regulation of cellular growth, differentiation and morphogenesis. The signaling pathways controlling these processes are mediated, in large part, by phosphorylation cascades. Protein phosphatases control the rate and duration of these signals, yet our understanding of the functional roles of protein phosphatases in mammalian development is poor. Protein phosphatase 2A (PP2A) is a ubiquitously expressed serine-threonine phosphatase that has key roles in growth, differentiation and morphogenesis (Olsen et al., 2006; Moorhead et al., 2007). Serine and threonine residues dominate the human phosphoproteome, together representing 98% of phosphorylation sites identified. Together with protein phosphatase 1 (PP1), PP2A is responsible for over 90% of Ser/Thr de-phosphorylation in most cells (Eichhorn et al., 2009). Dysregulated PP2A activity is associated with numerous diseases, including, but not limited to, Alzheimer's disease, various cancers, diabetes, cardiac disease, asthma, inflammation and auto-immune conditions (Calin et al., 2000; Takagi et al., 2000; Suzuki and Takahashi, 2003; Neviani et al., 2005; Kowluru and Matti, 2012; Collison et al., 2013; Crispin et al., 2013; Sontag and Sontag, 2014; Lei et al., 2015; Goldsworthy et al., 2016; Ross et al., 2017; Refaey et al., 2019).

Protein phosphatase 2A is a complex family of enzymes, composed of structural (A), catalytic (C) and regulatory (B) subunits. The PP2A core dimer consists of a structural and catalytic subunit, of which there are two isoforms (α and β) expressed in mammals (Hemmings et al., 1990). The tissue and substrate specificity of PP2A activity is mediated by binding of one of the four families of regulatory B-subunits: B55, B56, B″, and B‴ (each with multiple isoforms) to the core dimers. This results in over 80 different potential PP2A configurations (Smith A.S. et al., 2011), which can target a multitude of largely mutually exclusive substrate proteins (e.g., AKT, ERK, cJun, etc.), in diverse signaling pathways, including DNA damage repair, cell cycle progression and mitosis, proliferation, apoptosis and metabolism. Most regulatory B-subunits are ubiquitously expressed, but some demonstrate tissue specificity. For example, members of the B56 family are highly expressed in almost all major organs and tissues (Reynhout and Janssens, 2019). In contrast, the B″ family generally shows low expression in most tissues, with the exception of high B″α in the heart and high B″γ in embryonic brain. The B55 family is highly expressed in the brain, with B55γ almost exclusively expressed in embryonic and adult brain, and other family members to a lower extent. The B55α subunit shows the widest expression pattern within the B55 family (Reynhout and Janssens, 2019). The specific substrates and the functional roles of each regulatory subunit in health and disease, however, have not been well studied.

In vivo studies, using knockout mouse models for genes encoding the catalytic and structural subunits, have revealed a vital role for PP2A in embryonic development [recently reviewed in Reynhout and Janssens (2019)]. Knockout of PP2A-Cα (*Ppp2ca*) causes lethality at embryonic day (E) 6.5 (Götz et al., 1998), and knockout of PP2A-Aα (*Ppp2r1a*) results in lethality before E10.5, implying no functional redundancy with the β isoforms of either the A or C subunits in embryonic development, despite high sequence similarity (Ruediger et al., 2011). Of the regulatory B-subunits, knockout of three members have been reported. In the case of B56δ, there are opposing reports, with one study finding homozygous *Ppp2r5d*$^{-/-}$ animals were viable (Louis et al., 2011), and another that mice heterozygous for a strongly hypomorphic *Ppp2r5d* gene-trap allele were viable, but no homozygotes were recovered (Kapfhamer et al., 2010). Constitutive homozygous deletion of *Ppp2r5c* (B56γ) resulted in neonatal death at post-natal (P) day 1–2 due to heart defects (Varadkar et al., 2014); and gene-trap mediated constitutive *Ppp2r5a* (B56α) knockout mice were viable, however, displayed heart and nerve defects (Little et al., 2015), skin lesions, hyperproliferation of the epidermis and hair follicles, and increased hematopoiesis (Janghorban et al., 2017). Thus, specific PP2A B56 subunits play diverse roles in mammalian development. To date, however, the role of B55 subunits in mammalian development is not known.

The PP2A-B55α subunit (encoded by the *PPP2R2A* gene) is expressed in all tissues, with highest levels observed in the embryonic central nervous system and limbs, as well as adult brain, bladder, adrenal glands, ovaries and placenta (Reynhout and Janssens, 2019). Inactivation or genetic loss of B55α has been implicated in human diseases including cancer and Alzheimer's disease (Sontag et al., 2004; Ruvolo et al., 2011; Kalev et al., 2012; Beca et al., 2015; Watt et al., 2017). Therefore understanding the functional role of B55α in normal physiology is of particular interest. In cellular models, PP2A-B55α complexes have been shown to exert positive regulation of the ERK/MAPK pathway, but negative regulation of the PI3K/AKT pathway (Smith A.M. et al., 2011). PP2A-AB55αC complexes have also been implicated in DNA damage repair pathways by dephosphorylating ATM; cell cycle regulation by dephosphorylation and activation of the retinoblastoma-related protein p107; control of mitotic exit by deactivation of Cyclin-dependent kinase B-Cdk1 and many of its target proteins (Burgess et al., 2010; Gharbi-Ayachi et al., 2010; Manchado et al., 2010; Mochida et al., 2010; Schmitz et al., 2010; Cundell et al., 2013); and cell adhesion and migration by dephosphorylation of Rac1 and AP-1 (Gilan et al., 2015; Bousquet et al., 2016). PP2A-B55α has emerged as a tumor-suppressor in many epithelial and blood cancers. The *PPP2R2A* gene is commonly deleted in human breast (Curtis et al., 2012) and prostate tumors (Cheng et al., 2011), and *PPP2R2A* knockdown in breast cancer cell lines increases tumorigenicity (Watt et al., 2017). *PPP2R2A* is also commonly down-regulated in non-small cell lung carcinomas (Kalev et al., 2012). A recent ENU-induced mutagenesis study reported a splice-site mutation in *Ppp2r2a* resulting in reduced PP2A-B55α expression. Generation of double heterozygous mice for this *Ppp2r2a* mutation and a null allele of the gene encoding the insulin receptor, resulted in a diabetic phenotype characterized by hyperglycemia, hyperinsulinemia, impaired glucose tolerance, and glycosuria (Goldsworthy et al., 2016), suggesting PP2A-B55α may play a role in metabolism and insulin signaling.

PP2A-B55α dephosphorylates β-catenin during Wnt signaling, suggesting it may play a role in development (Zhang et al., 2009). In support of this, *ex vivo* knockdown of PP2A-B55α suggested an essential role for this subunit in mouse oocyte maturation (Liang et al., 2017) and in epidermal barrier formation (O'Shaughnessy et al., 2009). To investigate the function of this subunit *in vivo*, we have generated the first constitutive *Ppp2r2a* knockout mouse using CRISPR/Cas9. Homozygous *Ppp2r2a* deletion resulted in embryonic lethality post E10.5. *Ppp2r2a*$^{-/-}$ embryos displayed neural tube defects, limb defects and impaired epidermal barrier formation. The latter was associated with aberrant polarization of basal keratinocytes and aberrant keratinocyte differentiation. Therefore PP2A-B55α has essential roles in embryonic development, in particular in epidermal barrier formation.

MATERIALS AND METHODS

Generation of *Ppp2r2a* Knockout Mice

Ppp2r2a knockout mice were generated at the Australian Phenomics Network (Monash University, Melbourne, Australia), using the CRISPR/Cas9 technology. The CRISPR Design site http://crispr.mit.edu/ was used to identify guide RNA target sites flanking exon ENSMUSE00000482200 (exon 4) of the *Ppp2r2a* gene. The following guide RNAs were used: – 5′ TACGATAAAGCAGCCTAGTT 3′ for the 5′ end of exon 4, and – 5′ TTTGCTTTCAGGTACTACAT 3′ for the 3′ end of exon 4. Complementary oligonucleotides corresponding to the RNA guide target sites were annealed and cloned into *Bbs*I (NEB) digested plasmid pX330-U6-Chimeric_BB-CBh-hSpCas9 (Addgene plasmid #42230). Single guide RNAs (sgRNA) were generated using the HiScribe^{TM} T7 Quick High Yield RNA Synthesis Kit (NEB) according to the manufacturer's instructions. The sgRNAs were purified using the RNeasy Mini Kit (Qiagen). Cas9 mRNA (30 ng/mL, Sigma) and the sgRNAs (15 ng/mL) were microinjected into the cytoplasm of C57BL/6J zygotes at the pronuclei stage. Injected zygotes were transferred into the uterus of pseudopregnant F1 (C57BL/6 × CBA) females. Forward (5′ GTGTTCCAGCCAGCTGTTTCT 3′) and reverse (5′ GACACTGCTGCCTATGTCTGCT 3′) genotyping PCR primers flanking the targeted region and amplifying a product of 819 bp from the wild-type DNA were used to characterize gene editing events in the resulting mice.

Animals and Genotyping

Animals were used in accordance with the Australian Code of Practice for the Care and Use of Animals for Scientific Purposes and all protocols were approved by the University of Newcastle Animal Care and Ethics Committee. Mice were housed in individually ventilated cages on a 12 h light/dark cycle and fed standard chow *ad libitum*. Timed matings between heterozygous breeding pairs were set up with midday the next day designated as 0.5 days post coitus (dpc), and pregnant mice identified via the presence of a vaginal plug. Mice were euthanased using CO_2 asphyxiation, and embryos harvested at 10.5 days of development (E10.5), E14.5 and E18.5. Pregnant females were monitored and the day of birth of the pups was designated P0. Euthanasia of E18.5 embryos and neonates was performed by decapitation. Genotyping was performed by PCR on DNA extracted from tail tips, using the REDExtract-N-Amp^{TM} Tissue PCR Kit (Sigma-Aldrich #XNAT) as per the manufacturer's recommendations. The same PCR primers flanking exon 4 and used to characterize the gene editing events (described above) were used.

Protein Extraction and Immunoblotting

Protein extraction was conducted by grinding whole embryos to a fine powder in liquid nitrogen, using a mortar and pestle, and proteins solubilized using RIPA lysis buffer (0.05M Hepes pH 7.4, 1% Triton X-100, 0.1% SDS, 50 mM Sodium Fluoride, 0.05M EDTA, 1 mM Sodium Orthovanadate, 2.5% Protease Inhibitor Cocktail (Sigma #P8340), 5% Sodium Deoxycholate). Protein was quantitated using a BCA assay, separated using 4–12% Bis-Tris SDS-PAGE and transferred to nitrocellulose. Immunoblotting was performed using a commercial anti-PP2A-B55α rabbit polyclonal (Cell Signaling Technology #4953); an in-house rabbit polyclonal antibody raised against the B55α peptide FSQVKGAVDDDVAE (residues 14–27) (Strack et al., 1998); a polyclonal rabbit anti-PP2A-A (Merck Millipore #07-250); a mouse monoclonal anti-PP2A-C (Merck Millipore #05-421); and anti-rabbit/mouse HRP-conjugated secondary antibodies. A HRP-conjugated anti-actin antibody (Sigma #A3854) was used as a loading control. Images were captured on a Biorad ChemiDoc^{TM} Imaging system using ECL.

RNA Isolation, cDNA Synthesis and qPCR

Total RNA was prepared from embryonic tissue using the Isolate II RNA Mini Kit (Bioline #BIO-52072) and 1 μg was used to generate cDNA using the SensiFAST^{TM} cDNA Synthesis Kit (Bioline #BIO-65053) according to manufacturer's instructions. Gene expression analysis was conducted using the SensiFAST^{TM} SYBR® Hi-ROX Kit (Bioline #BIO-92020) and detected using an Applied Biosystems 7900HT Fast Real-Time PCR system. The cycling conditions used were 95°C for 2 min, followed by 40 cycles of 95°C for 15 s and 60°C for 1 min, and a final melt curve analysis at 95°C for 15 s, 60°C for 15 s and 95°C for 15 s. Primers were used at a final concentration of 0.3 μM. The primers used were *Ppp2r1a* (forward 5′ ACTCTTCTGCATCAATGTGTT 3′, reverse 5′ ATACGAAGAACTGTGGGCA 3′), *Ppp2r1b* (forward 5′ GCTTCAGATGAACAGGACTCT 3′, reverse 5′ AGACAGT AACTGGGCAATGC 3′), *Ppp2ca* (forward 5′ CTTGTAGCTCT TAAGGTTCG 3′, reverse 5′ TCTGCTCTCATGATTCCCTC 3′), *Ppp2cb* (forward 5′ TTCTTGTAGCATTAAAGGTGCG 3′, reverse 5′ TCCATACTTCCGTAGGCAC 3′), *Ppp2r2a* (forward 5′ CCGTGGAGACATACCAGGTA 3′, reverse 5′ AACACTGT CAGACCCATTCC 3′), *Ppp2r2b* (forward 5′ GGACCTCAAC ATGGAAAATC 3′, reverse 5′ CGCTGTCTGACCCATTCCAT 3′), *Ppp2r2c* (forward 5′ AGCGGGAACCAGAGAGTAAG 3′, reverse 5′ GTAGTCAAACTCCGGCTCG 3′), *Ppp2r2d* (forward 5′ TTACGGCACTACGGGTTCCA 3′, reverse 5′ TTCGTCGT GGACTTGCTTCT 3′), *Rpl19* (forward 5′ CTCAGGAGATACC GGGAATCCAAGAAGA 3′, reverse 5′ CACATTCCCTTTGAC

CTTCAG 3′). Genes of interest were normalized to the included housekeeping gene *Rpl19*, and relative gene expression was quantified using the comparative cycle (Ct) method ($2^{-\Delta\Delta Ct}$) relative to wildtype.

Histology and Immunohistochemistry

Embryos fixed in neutral buffered formalin (NBF) at various stages (E10.5, E14.5, and E18.5) were embedded in paraffin and sectioned at 5 μm before subsequent hematoxylin and eosin (H&E) staining or immunohistochemistry (IHC). Occasionally for H&E only, embryos were fixed in Bouins (**Figure 4A** E14.5 embryos). The H&E stained sections were analyzed by a veterinary anatomical pathologist at APN for stage-specific developmental features. IHC was performed as previously described (Pundavela et al., 2015). Briefly, following deparaffinization and rehydration steps using standard procedures, heat induced epitope retrieval (HIER) was carried out in a low pH, citrate-based antigen unmasking solution (Vector Laboratories, Burlingame, CA, United States, #H-3300) using a decloaking chamber (Biocare, West Midlands, United Kingdom) at 105°C for 5 min. After quenching of endogenous peroxidases in 0.3% H_2O_2, primary antibodies were prepared in 1% BSA, 0.1% Tween-20 in phosphate-buffered saline (PBS), and applied to the sections. Primary antibodies were rabbit polyclonal anti-cleaved caspase 3 (1:200; Cell Signaling Technology #9661), rabbit monoclonal anti-Ki67 [SP6] (1:100; Abcam, ab16667) and rabbit monoclonal p-cJun (1:100; Cell Signaling Technology #2361). The ImmPRESS (Peroxidase) Polymer secondary antibody kit and ImmPACT DAB (Vector Laboratories) were used for detection of the primary antibodies as per the manufacturer's recommendations and the sections were counterstained with hematoxylin, dehydrated in a series of ethanol washes, and cleared in xylene before mounting with Ultramount No. 4 (Fronine #FNNII065C). Slides were scanned using a Leica Biosystems Aperio AT2 Scanner at 20× magnification.

Immunofluorescence

Embryos were fixed overnight in 4% paraformaldehyde and cryopreserved through a sucrose gradient (10 and 30%) before freezing in O.C.T. Compound (Tissue-Tek®; Proscitech IA018) using isopentane cooled down in dry ice. Eight μm thick frozen sections were prepared using a Leica cryostat and immunofluorescence experiments were performed at room temperature, using a slightly modified procedure to previously described (Naudin et al., 2017). Briefly, sections were thawed, air dried, rehydrated in PBS and free aldehyde groups were blocked using a solution of 0.1M glycine in PBS for 10 min. Sections were then permeabilized in 0.3% Triton X-100 in PBS, and blocked with a solution of 1% BSA, 0.1% Tween-20 and 5% donkey serum in PBS for 30 min. Incubation with the primary antibodies was carried out at room temperature for 1 h before washing with PBS and applying the secondary antibodies for 1 h. The primary antibodies used were rabbit anti-keratin1 at 1:400 (Biolegend #Poly19052), rabbit anti-keratin14 at 1:400 (Biolegend #Poly19053), rabbit anti-loricrin at 1:500 (Biolegend #Poly19051), rabbit anti-B55α at 1:100 (Cell Signaling Technology #4953), an in-house rabbit polyclonal antibody against a PP2A-C peptide [PHVTRRTPDYFL (Sim et al., 1998)] at 1:500, a rabbit anti-Collagen IV at 1:100 (Millipore #AB756P), rat anti-Laminin γ1 at 1:1000 (Chemicon #1914), rat anti-Integrin β1 at 1:500 (BD Pharmingen #553715), rat anti-Integrin β4 at 1:200 (BD Biosciences #346-11A), rabbit anti-β-Catenin at 1:250 (Abcam # ab32572), and rabbit anti-ZO-1 at 1:100 (Thermo Fisher Scientific #61-7300). Alexa fluor-488 and -594 secondary antibodies (Abcam) were used at 1:500. All antibody dilutions were made in 1% BSA, 0.1% Tween-20 in PBS. After the secondary antibody incubation, slides were washed in PBS and mounted with Prolong gold antifade mountant with DAPI (Thermo Fisher Scientific #P36941), cured for 24 h in the dark at room temperature, coverslipped and stored at 4°C. Imaging was performed on a Fluoview FV1000 confocal microscope (Olympus).

Keratinocyte Cultures

Primary keratinocyte cultures were derived as previously described by Li et al. (2017). Briefly, the skin from E18.5 embryos was collected, washed in PBS then incubated overnight at 4°C in 4 mg/mL ice cold dispase II (Merck #D4693) made up in Keratinocyte Serum Free Medium (ThermoFisher, #17005042) with added 1% Penicillin-Streptomycin antibiotic (Sigma #P4333). The next morning epidermis was isolated and incubated with the basal layer down on a 500 μL drop of 0.25% trypsin-EDTA in PBS with gentle rocking at room temperature for 20 min. Keratinocytes were mechanically detached by vigorously rubbing each epidermal sheet three times in 2 mL media. The detached keratinocyte suspensions were centrifuged at 180 × *g* for 5 min and seeded onto collagen I (Trevigen #3442-100-01) coated plates at a density of 1.67×10^5 cells/mL. After growing to confluency, keratinocyte differentiation was induced by increasing the $CaCl_2$ concentration in the media from 0.06 to 0.2 mM. Cells were imaged using a Zeiss Axiovert 200 inverted light microscope and Zeiss AxioVision software.

Epidermal Barrier Staining

Immediately upon retrieval, E18.5 embryos were washed in PBS and incubated in X-gal reaction mix (100 mM $NaPO_4$, 1.3 mM $MgCl_2$, 3 mM $K_3Fe(CN)_6$, 3 mM $K_4Fe(CN)_6$ and 1 mg/mL X-Gal (Promega #V3941) at pH 4.5, with gentle rocking at 37°C for 3–4 h, followed by overnight incubation at room temperature. The following day, embryos were imaged using a digital camera.

RESULTS

Constitutive Deletion of *Ppp2r2a* Is Lethal

We generated *Ppp2r2a* knockout mice by targeting exon 4 using CRISPR/Cas9. Genotyping PCR primers flanking the targeted region and amplifying a product of 819 bp from the wild-type allele were used to characterize gene editing events in the resulting mice (**Figure 1**). Sequence analysis of the PCR products identified two mice with the expected deletion of

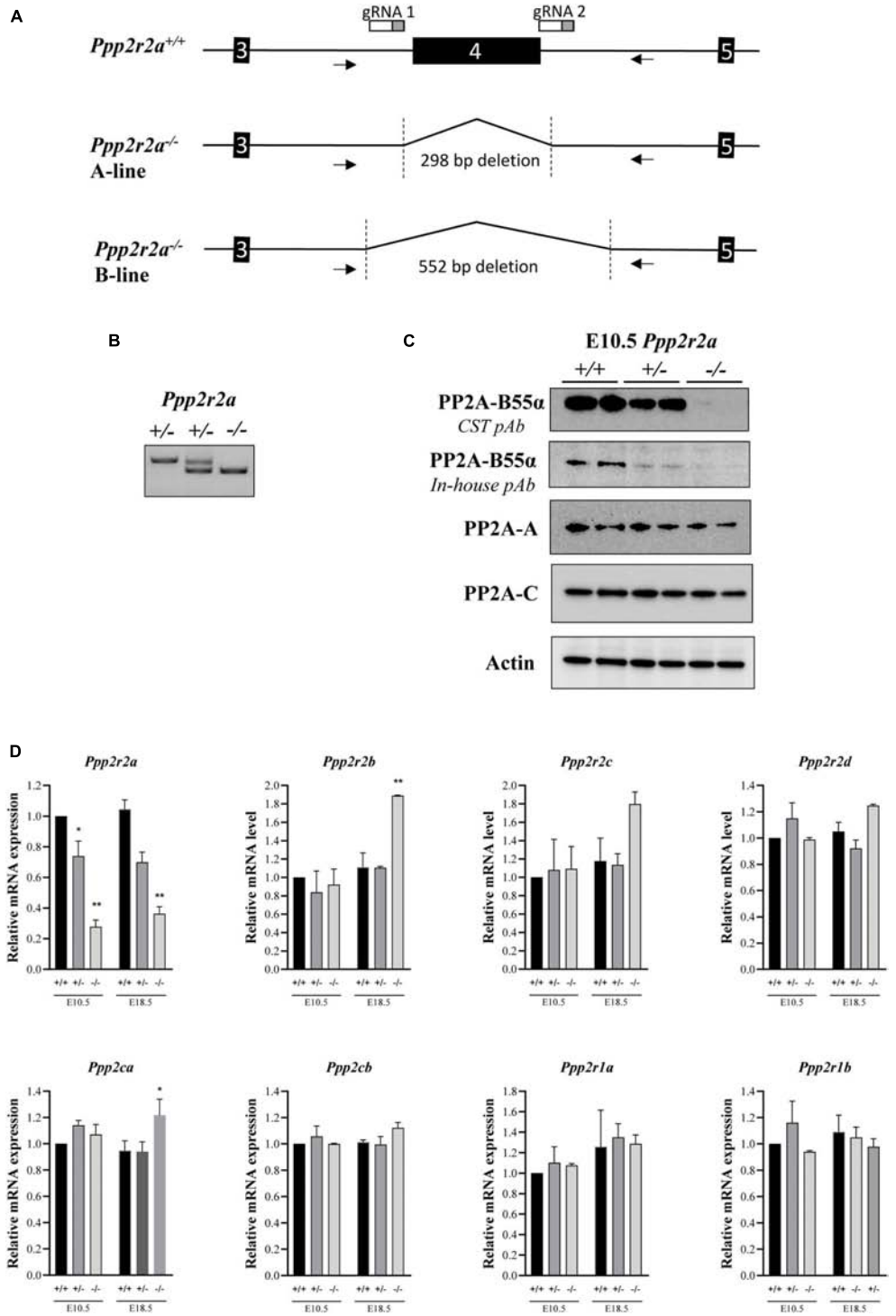

FIGURE 1 | Generation of *Ppp2r2a* null mice lacking B55α protein expression. **(A)** Schematic of *Ppp2r2a* wildtype (+/+) allele and *Ppp2r2a* knockout alleles (–/–) from the A-line and B-line, showing the extent of deletion of exon 4 and partial flanking introns. The arrows show primer binding regions. gRNA 1 and 2 show binding site of CRISPR/Cas9 guide RNAs. **(B)** DNA genotyping gel of E10.5 embryos showing *Ppp2r2a* wild-type, heterozygous and knockout progeny. **(C)** Representative immunoblot of two E10.5 embryos of each genotype, revealing complete loss of PP2A-B55α expression in *Ppp2r2a* knockout (–/–) embryos using a primary polyclonal antibody to PP2A-B55α (CST #4953) and an in-house primary polyclonal antibody to B55α as described in the methods. Representative immuno-blots of PP2A-A and –C subunits. Actin was used as a loading control. **(D)** The mRNA expression of the B55 subunit genes *(Ppp2r2a, Ppp2r2b, Ppp2r2c, Ppp2r2d*), the PP2A catalytic subunit genes (*Ppp2ca* and *Ppp2cb)* and the PP2A structural subunit genes (*Ppp2r1a* and *Ppp2r1b*) were assessed by quantitative real time PCR. Data was normalized to the housekeeping gene, *Rpl19*, which was constant between genotypes and embryonic stages, and is represented as a fold change relative to the respective wildtype embryos for each stage. $n = 2$, $^{*}p < 0.05$, $^{**}p < 0.01$, two-tailed *t*-test compared to wildtype.

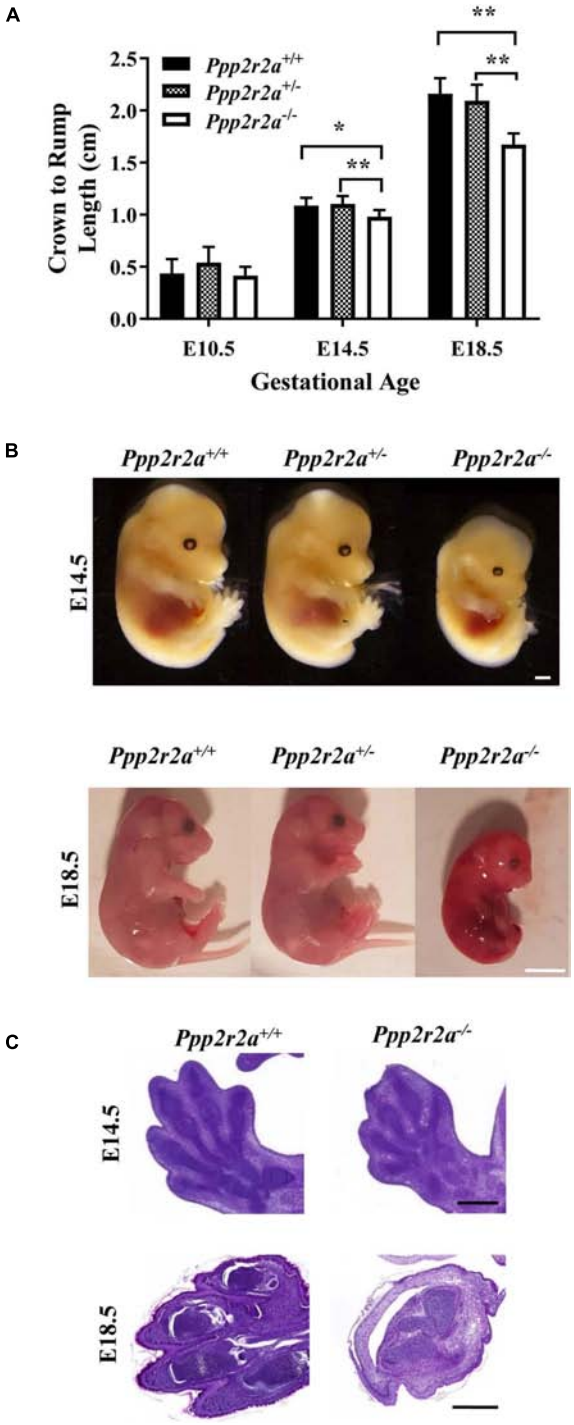

FIGURE 2 | *Ppp2r2a* knockout embryos are small with epidermal hemorrhaging and syndactyly. **(A)** Crown-to-rump measurements of embryos at three developmental stages: embryonic day 10.5 (E10.5) (n = 5 per genotype), E14.5 (n = 7) and E18.5 (n = 7). *$p < 0.05$, **$p < 0.01$, unpaired two-tailed t-test. **(B)** Representative photographs of E14.5 and E18.5 embryos. *Ppp2r2a*$^{-/-}$ embryos display reduced size, syndactyly and gross epidermal hemorrhaging (E18.5). E14.5 scale bar = 0.5 mm; E18.5 scale bar = 5 mm **(C)**. H&E staining of E14.5 and E18.5 embryo sections demonstrates syndactyly of the hind limbs in *Ppp2r2a*$^{-/-}$ embryos. Scale bars = 0.5 mm.

exon 4 plus part of the flanking introns (**Figure 1A** and **Supplementary Figure S1**). These mice were used as founders to establish two independent *Ppp2r2a* knockout mouse lines, named *Ppp2r2a*-line A and B, respectively. The genomic deletion covers 298 bp in line A and 552 bp in line B (**Supplementary Figure S1**), removing *Ppp2r2a* exon 4 and resulting in a frameshift that prevents the expression of the full-length protein.

The founders were crossed twice to C57BL/6J before setting up heterozygous breeding pairs. In line A, out of 170 pups born from heterozygous breeding pairs, 100 (36%) were *Ppp2r2a*$^{+/+}$, and 174 (64%) were *Ppp2r2a*$^{+/-}$ (**Table 1**). Similarly, in line B, out of 104 pups born from heterozygous breeding pairs, 43 (41%) were *Ppp2r2a*$^{+/+}$, and 61 (59%) were *Ppp2r2a*$^{+/-}$ (**Table 1**). No homozygous knockout pups were observed at the time of genotyping (post-natal day 14) in either line, suggesting that constitutive deletion of *Ppp2r2a* results in early lethality with complete penetrance.

Genotyping of embryos at E10.5 confirmed the presence of homozygous *Ppp2r2a*$^{-/-}$ embryos (**Figure 1B**) and immunoblot analysis using two different anti-B55α antibodies of whole E10.5 embryos revealed absence of B55α protein in *Ppp2r2a*$^{-/-}$ embryos, and reduced B55α protein in *Ppp2r2a*$^{+/-}$ embryos (**Figure 1C**). This was further corroborated by immunoblot analysis of E14.5 embryos (**Supplementary Figure S2**). There was no change in protein expression of the PP2A-C catalytic subunit, or the PP2A-A structural subunit.

Similarly, at the mRNA level, *Ppp2r2a* expression was decreased in *Ppp2r2a*$^{+/-}$ embryos and further reduced in *Ppp2r2a*$^{-/-}$ embryos compared to *Ppp2r2a*$^{+/+}$ at both E10.5 and E18.5 (**Figure 1D**). This suggests that the altered mRNA synthesized from the *Ppp2r2a* knockout allele is unstable and mostly degraded, with only a small residual amount detected in *Ppp2r2a*$^{-/-}$ animals. We next assessed the expression of genes encoding the other B55 isoforms, and the catalytic and structural PP2A subunits. A significant increase in *Ppp2r2b* (B55β) expression was observed with *Ppp2r2a* knockout at E18.5. The expression of the *Ppp2ca* (encoding the PP2A-Cα subunit) was also increased with *Ppp2r2a* knockout at E18.5. The increased *Ppp2r2b* and *Ppp2ca* may be an attempt to compensate for the lack of B55α.

Heterozygous *Ppp2r2a*$^{+/-}$ mice in both the A and B lines grew normally, appeared healthy, were fertile and females nursed their pups. There were no major differences in size between *Ppp2r2a*$^{+/+}$ and *Ppp2r2a*$^{+/-}$ mice monitored up to 24 months of age, and no obvious gross anatomical or behavioral problems were observed in *Ppp2r2a*$^{+/-}$ mice (**Supplementary Figures S3A,B**), despite a reduction in B55α protein expression observed in adult tissues (**Supplementary Figure S3C**). Further investigation into the *Ppp2r2a*$^{-/-}$ animals was focused on the A line.

Ppp2r2a Is Required for Late Embryonic Development

The absence of homozygous *Ppp2r2a*$^{-/-}$ animals at 14 days of age suggested neonatal or *in utero* lethality. At E10.5, 25% of embryos harvested were *Ppp2r2a*$^{-/-}$, consistent with

TABLE 1 | Number of mice per genotype at various embryonic and post-natal stages.

	Line A					Line B
	E10.5[a]	E14.5[b]	E18.5[c]	P0[d]	P14[e]	P14[f]
Ppp2r2a$^{+/+}$	14 (20%)	30 (29%)	30 (29%)	13 (37%)	100 (36%)	43 (41%)
Ppp2r2a$^{+/-}$	38 (55%)	55 (55%)	62 (61%)	21 (60%)	174 (64%)	61 (59%)
Ppp2r2a$^{-/-}$	17 (25%)	19 (18%)	10 (10%)	1[g] (3%)	0 (0%)	0 (0%)

a-8 litters; b-13 litters; c-17 litters; d-5 litters; e-70 litters; f-24 litters; g, this neonate was found dead the day of birth.

the expected Mendelian ratio from a heterozygous cross. The percentage of *Ppp2r2a*$^{-/-}$ embryos at E14.5, however, dropped to 18% and it decreased further at E18.5, to only 10% (**Table 1**). At birth, this percentage dropped to 3%, corresponding to only one knockout offspring found amongst a total of 35 pups from 5 litters. It must be noted, however, that this neonate was found dead while litter mates were still being born, suggesting that it was still-born or died very soon after birth, indicating perinatal lethality.

Late-Stage *Ppp2r2a*$^{-/-}$ Embryos Are Small With Neural, Cranial and Limb Abnormalities

To investigate the cause of the embryonic lethality, we first examined embryo size and gross morphology. At mid-gestation (E10.5), embryos of all three genotypes appeared macroscopically normal, and there was no difference in size, as determined by measuring the crown to rump length (**Figure 2A**). In contrast, *Ppp2r2a*$^{-/-}$ embryos at E14.5 and E18.5 were significantly smaller than *Ppp2r2a*$^{+/+}$ and *Ppp2r2a*$^{+/-}$ embryos, and displayed abnormal morphology (**Figures 2A,B** and **Supplementary Figure S4**). Notably, a lack of divergent digits (syndactyly) was a common feature in all E14.5 (n = 19) and E18.5 (n = 10) *Ppp2r2a*$^{-/-}$ embryos, and was confirmed by histopathology analysis (**Figure 2C**).

While no macroscopic abnormalities were observed in E10.5 *Ppp2r2a*$^{-/-}$ embryos, histopathology analysis revealed differences in neural development. One litter analyzed displayed inconsistent neuro-epithelium in all three *Ppp2r2a*$^{-/-}$ embryos, compared to the one wild-type litter mate. Lamination of the cerebral cortex involves organization of the neurons into six layers in mammals (Chen et al., 2017). At E10.5 the *Ppp2r2a*$^{+/+}$ embryo displays this emerging lamination (**Figure 3A**). This was not observed in the *Ppp2r2a*$^{-/-}$ embryos, but rather the neuro-epithelium displayed cellular degeneration and debris (**Figure 3A**). In contrast, in a second litter analyzed containing two *Ppp2r2a*$^{-/-}$ embryos, no histological differences were observed between the *Ppp2r2a*$^{+/+}$ and *Ppp2r2a*$^{-/-}$ embryos (data not shown), suggesting incomplete penetrance of this phenotype at E10.5.

Out of 13 *Ppp2r2a*$^{-/-}$ embryos analyzed at E14.5, gross changes in cranial and/or embryo shape were observed in five embryos. Three embryos displayed a bulbous cranium, almost translucent compared to the rest of the body (**Supplementary Figure S4A**-representative). Another had a slight bulge at the cranial apex and small raised bulge along the upper dorsal region (**Supplementary Figure S4B**). The last also had a slight bulge at the cranial apex and a raised ridge-like structure along the dorsal region (**Supplementary Figure S4C**). These features suggested possible internal defects in the neural tube, such as exencephaly and spina bifida, and were confirmed by histopathology, with three *Ppp2r2a*$^{-/-}$ embryos displaying exencephaly (**Figure 3B**). One of these embryos also had cranial bulging due to edema at the cranial apex, and a protruding and poorly contained spinal cord in the cervical dorsal region (not shown). A further embryo was found to have spina bifida (**Figure 3B**).

Out of 10 *Ppp2r2a*$^{-/-}$ pups collected at E18.5, all showed movement or reacted to touch at the time of dissection. However, the skin of all E18.5 *Ppp2r2a*$^{-/-}$ embryos was shiny and displayed significant erythroderma, with visible superficial hemorrhaging particularly at the tips of the tail and limbs (**Figure 2B**). The morphology and histopathology of E18.5 *Ppp2r2a*$^{-/-}$ placentas (n = 3) appeared normal (data not shown). The only abnormal feature noted among the wild-type or heterozygous littermates was syndactyly in 1/30 (3.33%) *Ppp2r2a*$^{+/+}$ embryos, however, this embryo was partially degenerated at the time of dissection and thus was likely a runt already undergoing the process of degradation. Histopathological analysis of four E18.5 *Ppp2r2a*$^{-/-}$ embryos found that one had cranial vault collapse (**Figure 3C**).

The one dead *Ppp2r2a*$^{-/-}$ pup observed at P0 (**Table 1**) was much smaller than *Ppp2r2a*$^{+/+}$ and *Ppp2r2a*$^{+/-}$ littermates, and was partially degraded (**Supplementary Figure S5**). While *Ppp2r2a*$^{+/+}$ and *Ppp2r2a*$^{+/-}$ pups were pale pink all over, the *Ppp2r2a*$^{-/-}$ pup was deep red in color, with the exception of a white tail, and exhibited an incomplete skin layer with large patches missing from the abdomen and a smaller patch on the lower spine, suggesting a potential epidermal barrier defect. As observed in the E18.5 embryos, the digits were also poorly defined.

We next investigated whether the cranial defects observed were associated with changes in aberrant cell proliferation or cell death. IHC staining for the proliferation marker Ki67, showed similar levels of Ki67^{+} cells in comparable brain regions of *Ppp2r2a*$^{+/+}$ and *Ppp2r2a*$^{-/-}$ embryos at E14.5 (**Supplementary Figure S6**). There were very occasional cleaved caspase 3 (CC3) positive cells in the *Ppp2r2a*$^{+/+}$ cerebellum and forebrain and none in the thalamus. In contrast, CC3^{+} cells were found in all three brain regions in the *Ppp2r2a*$^{-/-}$ brain (**Figure 3D**). This suggests the neuronal defects in *Ppp2r2a* knockout embryos are associated with increased apoptosis.

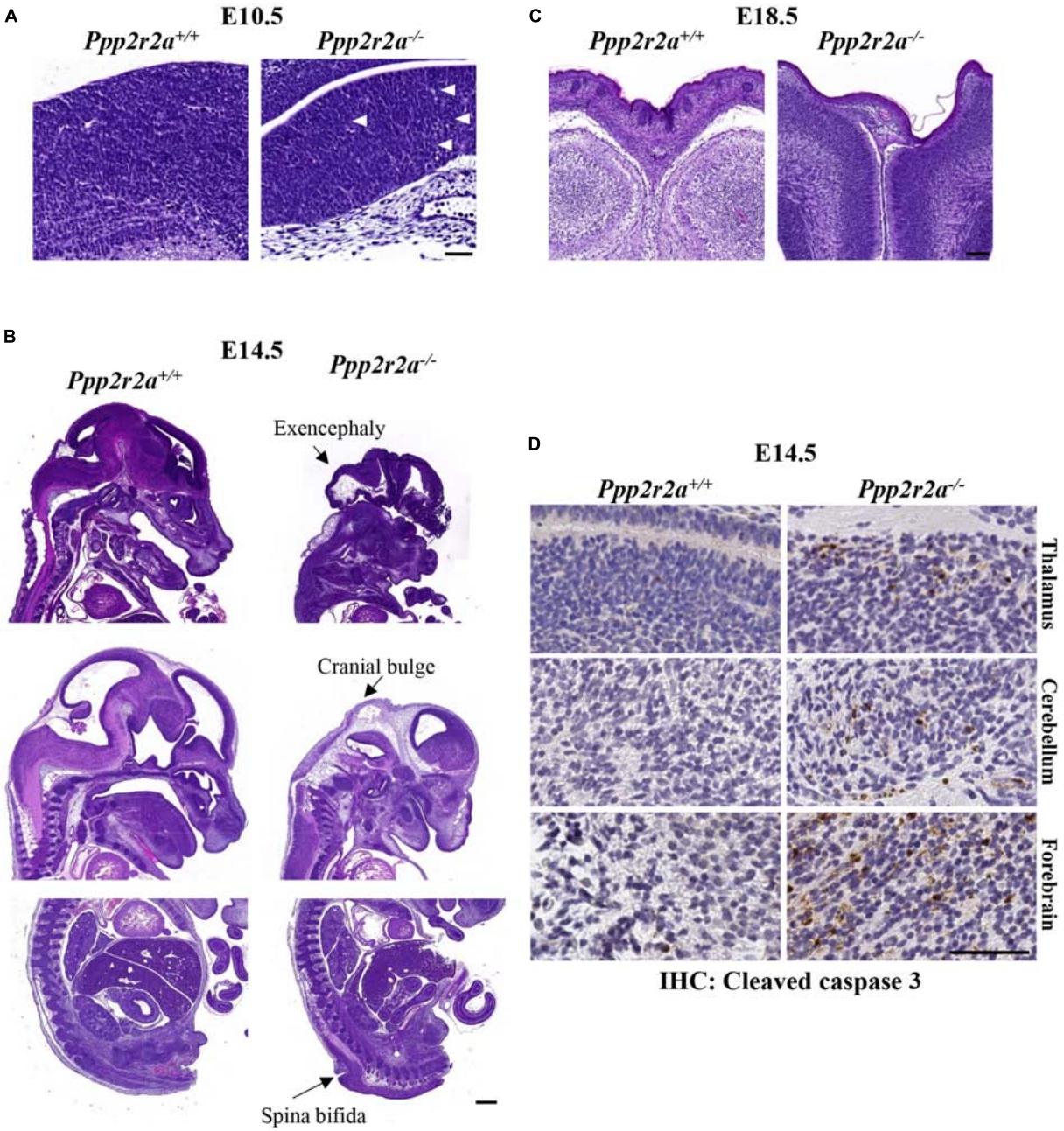

FIGURE 3 | Neural defects in *Ppp2r2a* knockout embryos. **(A–C)** H&E staining at various stages of development. **(A)** At E10.5, defects of the neuroepithelium consist of a lack of emerging lamination and cellular degeneration and debris (white arrows) in *Ppp2r2a*$^{-/-}$embryos. Scale bar = 50 μm. **(B)** At E14.5 the neural defects in *Ppp2r2a*$^{-/-}$ embryos include excencephaly, cranial bulging and spina bifida. Scale bar = 500 μm. **(C)** At E18.5, cranial vault collapse was observed in a *Ppp2r2a*$^{-/-}$ embryo. Also evident in these sections is a thinner epidermis in the *Ppp2r2a*$^{-/-}$ embryo. Scale bar = 100 μm. **(D)** IHC labeling for cleaved caspase 3 in the thalamus, cerebellum and forebrain of *Ppp2r2a*$^{+/+}$ *and Ppp2r2a*$^{-/-}$ embryos. Scale bar = 50 μm.

Ppp2r2a$^{-/-}$ Embryos Display a Thin Stratified Epidermis With a Defective Stratum Corneum

At E10.5, the epidermal committed basal layer in *Ppp2r2a*$^{-/-}$ embryos was much thinner and disrupted compared to the wild-type. In some instances, this layer was also detached from the underlying dermis (**Figure 4A**). As noted above, the skin of E18.5 *Ppp2r2a*$^{-/-}$ embryos was deep red with multiple sites of hemorrhaging. This was supported by histopathology analysis, with *Ppp2r2a*$^{-/-}$ embryos demonstrating superficial epidermal hemorrhage and edema at both E14.5 and E18.5 (**Figure 4A**). At E14.5, *Ppp2r2a*$^{-/-}$ embryos had a thinner basal epidermal layer than *Ppp2r2a*$^{+/+}$ mice, with disorganized and irregular

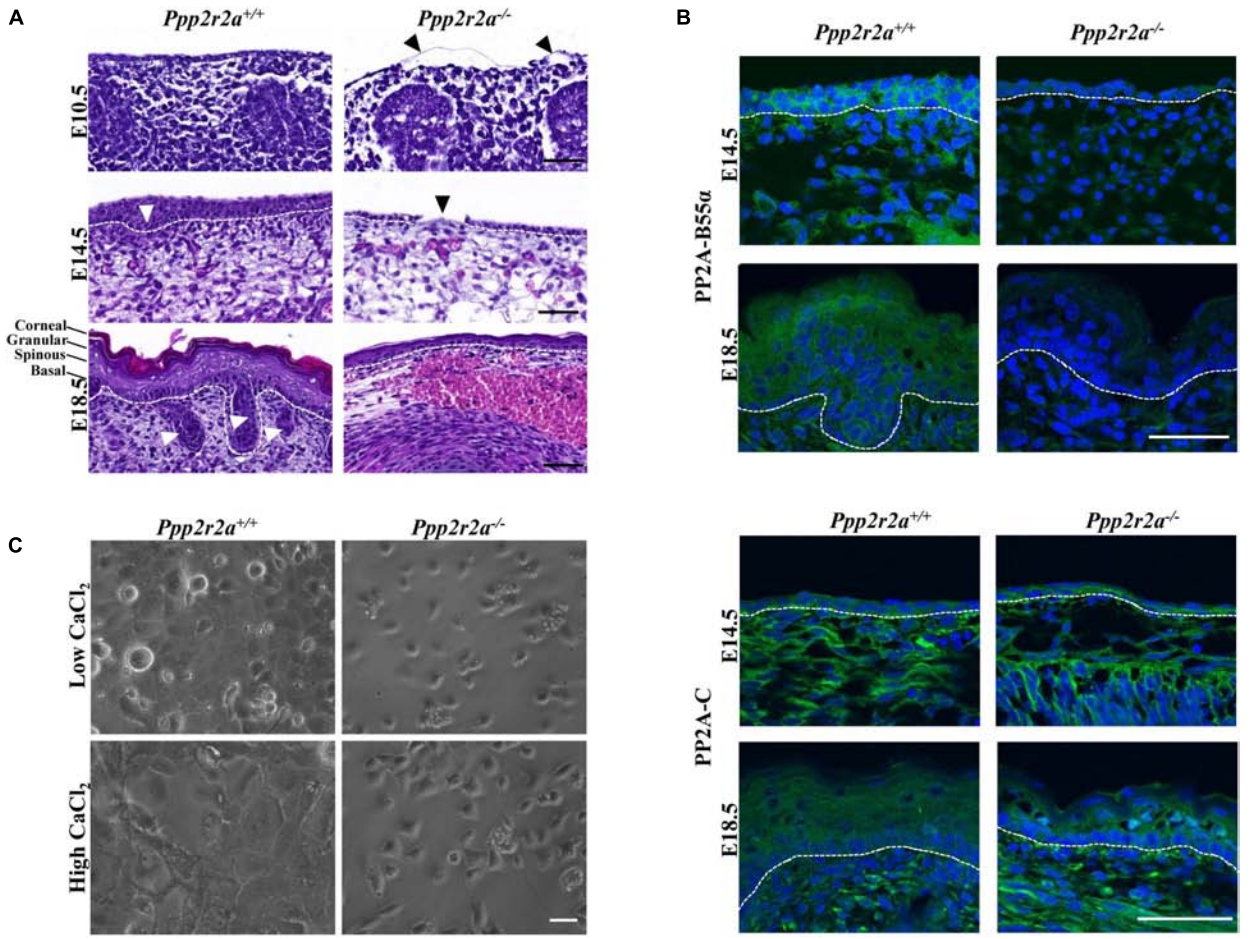

FIGURE 4 | Epidermal defect in late stage *Ppp2r2a* knockout embryos. **(A)** Representative H&E images of the epidermis of E10.5, E14.5 and E18.5 $Ppp2r2a^{+/+}$ and $Ppp2r2a^{-/-}$ mice. All three stages show thinner epidermal layers. E10.5 $Ppp2r2a^{-/-}$ embryos have regions of detached emerging epidermis (black arrowhead). Both E14.5 and E18.5 show subcutaneous hemorrhage and edema in the $Ppp2r2a^{-/-}$ embryos. $Ppp2r2a^{+/+}$ display emerging hair follicles at E14.5, and dermal appendages at E18.5 (white arrowhead), but these are absent in $Ppp2r2a^{-/-}$ embryos. At E14.5 the $Ppp2r2a^{-/-}$ embryos also showed regions of disrupted epidermis (black arrowhead). Dashed white line indicates dermal-epidermal junction. Scale bars = 50 μm. **(B)** Representative immunofluorescence of PP2A-B55α (green) and PP2A-C (green) in $Ppp2r2a^{+/+}$ and $Ppp2r2a^{-/-}$ epidermis at E14.5 and 18.5. Co-staining for DAPI is shown in blue. Dashed white line indicates the dermal-epidermal junction. Scale bars = 50 μm. **(C)** $Ppp2r2a^{+/+}$ and $Ppp2r2a^{-/-}$ keratinocytes in low calcium and high calcium (post-48 h). Scale bar = 100 μm.

cell orientation, and a complete lack of an epidermal layer in some segments (**Figure 4A**, black arrowhead). Furthermore, they showed no emerging hair follicles – a hallmark feature of normal epidermis at E14.5 (Mann, 1962; Hardy, 1992; Cheng et al., 2014).

At E18.5, the epidermis of $Ppp2r2a^{-/-}$ embryos was also much thinner than $Ppp2r2a^{+/+}$ embryos at the dorsal and caudal regions. The basal layer was often disorganized, the spinous and granular layers were thin, and the upper stratum corneum was less distinct and often missing altogether. These key phenotypic differences observed in the E14.5 and E18.5 epidermis were most prominent in the dorsal region. E18.5 $Ppp2r2a^{-/-}$ embryos also lacked dermal appendages, such as sweat glands, sebaceous glands and hair follicles, which are a normal feature of developing skin at this stage (**Figure 4A**; Hardy, 1992; Chu and Loomis, 2004; Schmidt-Ullrich and Paus, 2005).

Immunofluorescence analysis revealed PP2A-B55α expression in the basal and suprabasal layer of the epidermis, as well as dermal cells, in wild-type embryos at E14.5. At E18.5 PP2A-B55α was observed in all layers, with strongest expression in the granular layer (**Figure 4B**). The faint staining in the $Ppp2r2a^{-/-}$ embryos may be due to cross-reactivity of this antibody with the closely related B55δ subunit, however, lack of a specific B55δ antibody for immunofluorescence precludes us from confirming this. Immunofluorescence for PP2A-C showed a similar localization to PP2A-B55α at both embryonic stages (**Figure 4B**).

$Ppp2r2a^{-/-}$ Keratinocyte Cultures and Epidermis Display Impaired Differentiation

To further examine the epidermal phenotype of the $Ppp2r2a^{-/-}$ embryos, keratinocytes were isolated from the epidermis of E18.5 $Ppp2r2a^{+/+}$ and $Ppp2r2a^{-/-}$ embryos.

Interestingly, the epidermal layer separated more rapidly from the dermis of *Ppp2r2a*$^{-/-}$ than wild-type embryos, suggesting a weaker connection between the two layers. Less keratinocytes were consistently isolated from *Ppp2r2a*$^{-/-}$ skin, and these cells proliferated less than the wild-type cells (**Figure 4C**). Furthermore, the addition of high Ca^{2+} induced differentiation in the wild-type keratinocytes but not in knockouts. After 48 h in high Ca^{2+} the cytoplasm of *Ppp2r2a*$^{+/+}$ keratinocytes expanded and the cells arranged in a distinctive cobble-stone pattern with clear cell-cell adhesions (**Figure 4C**). In contrast, the shape and pattern of the *Ppp2r2a*$^{-/-}$ keratinocytes showed very little change to untreated cells (**Figure 4C**), suggesting both proliferation and differentiation of isolated keratinocytes is impaired with PP2A-B55α loss.

We next examined the epidermal proteins Keratin 14 (K14), a marker of proliferating basal cells; Keratin1 (K1), a marker of the spinous layer; and loricrin, a marker of the granular layer, by immunofluorescence labeling. At E14.5, K14 was present in both *Ppp2r2a*$^{-/-}$ and *Ppp2r2a*$^{+/+}$ epidermis (**Figure 5A**). The *Ppp2r2a*$^{+/+}$ epidermis was 1–2 cells thick, with all basal cells staining for K14, and the most prominent expression observed at the baso-lateral side of cells. In contrast, only one layer of cells was evident in the *Ppp2r2a*$^{-/-}$ epidermis, which was strongly positive for K14, with expression at both the apical and basal side, as well as the lateral junctions between cells (**Figure 5A**). Many cells in this single layer appeared flatter and irregularly positioned compared to the well-organized, regular cuboidal-type basal layer of the wild-type epidermis, indicating a potential defect in cell polarity in the *Ppp2r2a*$^{-/-}$ basal layer. In the *Ppp2r2a*$^{+/+}$ epidermis, there was also a thinner layer of K14-negative cells (the intermediate layer) emerging above the K14-positive basal layers (**Figure 5A** indicated by a white arrow head), which is absent in the knockout epidermis.

At E18.5 in wild-type embryos all four layers of the epidermis have developed: basal, spinous, granular and stratum corneum (**Figure 5B**). Both the histological and immunofluorescence analysis showed that each layer of *Ppp2r2a*$^{-/-}$ epidermis was thinner than in the *Ppp2r2a*$^{+/+}$ mice. K14 marked basal and spinous layer cells in wild-type E18.5 epidermis, however, similar to that observed at E14.5, only a single basal layer of K14^{+} cells was observed throughout most of the E18.5 *Ppp2r2a*$^{-/-}$ epidermis, and the cells were highly disorganized, further supporting a polarity defect (**Figure 5B**). K1^{+} cells were observed in spinous and granular layers of E18.5 *Ppp2r2a*$^{+/+}$ epidermis. In contrast, strong K1 immunolabelling was observed in many cells within the basal layer of *Ppp2r2a*$^{-/-}$ epidermis. The overlying spinous layer was much thinner than the wild-type, and contained very few K1^{+} cells, and the very thin granular layer was negative for K1 (**Figure 5B**). Immunostaining for loricrin confirmed a thinner granular layer in the *Ppp2r2a*$^{-/-}$ epidermis (**Figure 5B**). Given cells in the stratum corneum are anuclear, the few unstained nuclei above the granular layer in the *Ppp2r2a*$^{-/-}$ epidermis (**Figure 5B**, indicated by white arrowheads) indicate a defective and persisting periderm.

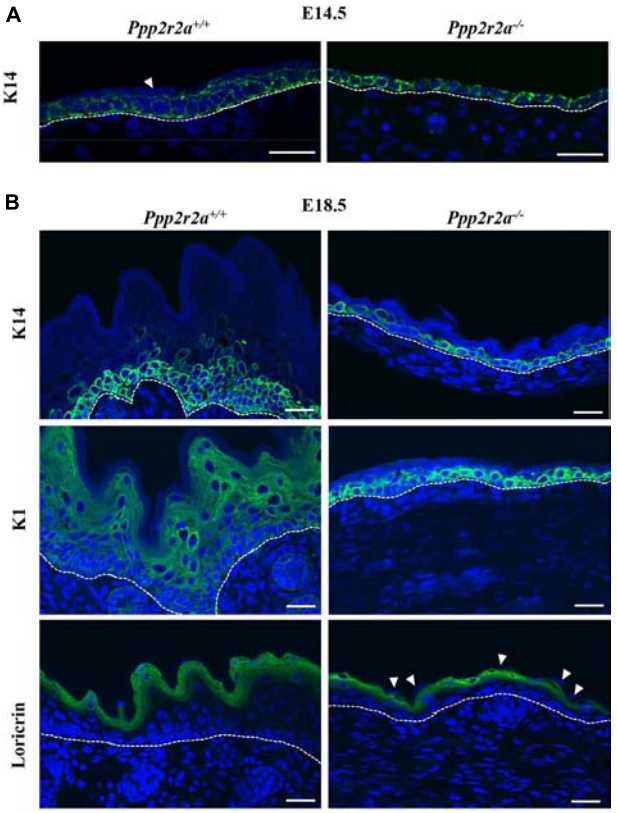

FIGURE 5 | Epidermal defects are associated with abnormal differentiation. Immunofluorescent labeling for epidermal markers Keratin 14 (K14), Keratin 1 (K1) and Loricrin (green) in E14.5 **(A)** and E18.5 **(B)** embryos, with nuclei stained by DAPI (blue). White arrowheads show the unstained superficial epidermal cell layer. Dashed white line indicates the dermal-epidermal junction. All scale bars = 25 μm.

Reduced Basement Membrane and Integrins in *Ppp2r2a*$^{-/-}$ Epidermis

Proper epithelial formation and integrity relies on formation of the basement membrane (BM), a specialized extracellular matrix (ECM) that is produced, secreted and assembled by the basal keratinocytes (Fuchs and Raghavan, 2002). The lack of mature stratified epithelium in the *Ppp2r2a* knockouts suggested there might be a defect in the BM. Immunolabelling for collagen IV and laminin γ1, two major components of the BM, was similar in both genotypes at E14.5 (**Figure 6A**), however, was markedly reduced in the *Ppp2r2a*$^{-/-}$ BM at E18.5 (**Figure 6B**).

The major cell surface receptors that recognize and assemble the BM are integrins; heterodimeric transmembrane proteins made up of an α and β subunit. Laminin binding to α3β1 integrin results in the assembly of focal adhesions, while binding to α6β4 integrin results in formation of hemidesmosomes, specialized adhesions that link the BM to the intermediate filament network (Tsuruta et al., 2008; Wickstrom et al., 2011). These integrin-mediated adhesions play critical roles in keratinocyte polarization and migration (Stepp, 1999; Rippa et al., 2013). At E14.5 β4 integrin was expressed on the basal side of the

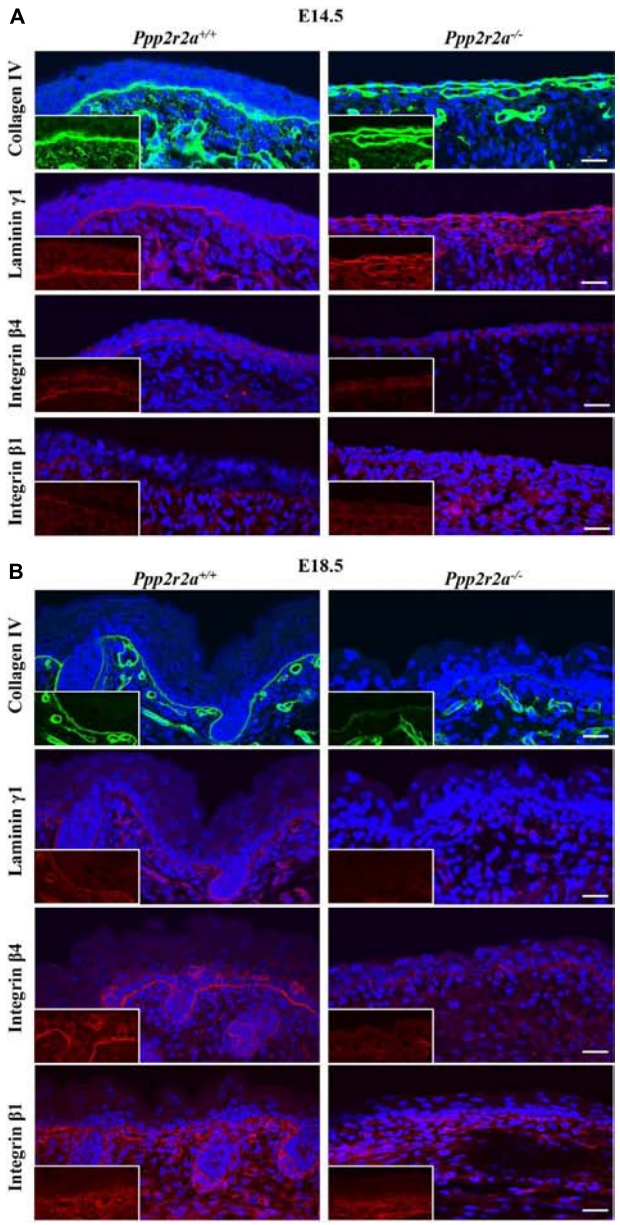

FIGURE 6 | Reduced basement membrane and integrins in *Ppp2r2a* knockout epidermis. Representative immunofluorescent pictures of Collagen IV (green), Laminin γ1 (red), Integrin β4 (red) and Integrin β1 (red) in *Ppp2r2a*$^{+/+}$ *and Ppp2r2a*$^{-/-}$ epidermis at both E14.5 **(A)** and E18.5 **(B)**. DAPI is shown in blue. Inserts show a region from each image without the DAPI to highlight the protein labeling. All scale bars = 25 μm.

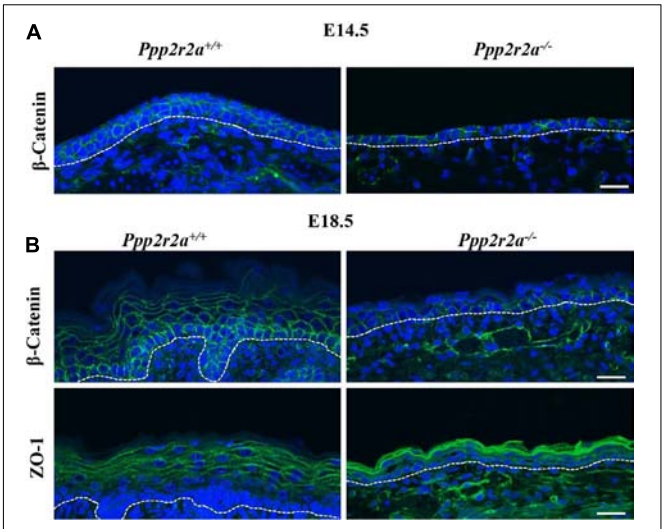

FIGURE 7 | Aberrant cell-cell junctions in the *Ppp2r2a* knockout epidermis. **(A)** Representative immunofluorescent pictures of β-Catenin (green) labeling at E14.5 in *Ppp2r2a*$^{+/+}$ *and Ppp2r2a*$^{-/-}$ epidermis. DAPI is shown in blue. **(B)** Representative immunofluorescent pictures of β-Catenin (green) and ZO-1 (green) in E18.5 *Ppp2r2a*$^{+/+}$ *and Ppp2r2a*$^{-/-}$ epidermis. DAPI is shown in blue. Dashed white line indicates the dermal-epidermal junction. All scale bars = 25 μm.

Ppp2r2a$^{+/+}$ basal and suprabasal cells, whereas in the single layer of *Ppp2r2a*$^{-/-}$ cells, β4 integrin was expressed but did not show a preferential basal orientation. At E18.5, β4 integrin immunolabelling is strongest along the basement membrane of wildtype embryos. In contrast, in the *Ppp2r2a*$^{-/-}$ epidermis staining is weak and discontinuous (**Figures 6A,B**). Similarly, β1 integrin immunolabelling along the BM is weaker in the *Ppp2r2a*$^{-/-}$ dorsal skin, most notably at E18.5 (**Figures 6A,B**). The reduced BM and integrins would likely compromise the adhesion between the epidermis and dermis, and thus contribute to the blistering and ready separation of these layers described above.

Ppp2r2a$^{-/-}$ Embryos Have Aberrant Junctions in the Epidermis

In addition to the hemidesmosomes and focal adhesions attaching the epidermis to the BM, adherens and tight junctions play a key role in cell-cell attachment and formation of the protective epidermal barrier. β-catenin links membrane bound E-cadherin to the actin cytoskeleton at adherens junctions, and is also a key effector of the canonical Wnt pathway which is important in epidermal stratification (Capaldo and Macara, 2007; Hartsock and Nelson, 2008; Zhu et al., 2014). β-catenin labeling of the E14.5 *Ppp2r2a*$^{+/+}$ epidermis is strongest along the cell-cell junctions between keratinocyte layers, and also between keratinocytes within a layer (**Figure 7A**). In contrast, β-catenin labeling in the *Ppp2r2a*$^{-/-}$ epidermis is inconsistent and patchy (**Figure 7A**). At E18.5, β-catenin is still highly expressed on the apico-lateral junctions between keratinocytes of the basal layer, and to a lesser extent in the spinous layers (**Figure 7B**). In comparison, weaker β-catenin is observed in the apico-lateral regions of the basal layer, and is absent from the thin suprabasal layers, in the *Ppp2r2a*$^{-/-}$ epidermis.

The tight junction protein, ZO-1 (Capaldo and Macara, 2007; Hartsock and Nelson, 2008) in E18.5 *Ppp2r2a*$^{+/+}$ epidermis was localized at the cell-cell junctions of keratinocytes of the upper-spinous and granular layers (**Figure 7B**). Interestingly, ZO-1 junctional labeling was much stronger in the granular/spinous

layers of *Ppp2r2a*$^{-/-}$ embryos compared to wildtypes but did not appear as well structured as seen on the wildtype (**Figure 7B**). Thus, the loss of PP2A-B55α affects the composition and/or organization of cell-ECM and cell-cell junctions in the developing skin.

Late Stage *Ppp2r2a*$^{-/-}$ Embryos Have Incomplete Epidermal Barrier Acquisition

The epidermis is essential for life as it provides a protective barrier, preventing water loss and protecting from external environmental factors (O'Shaughnessy et al., 2009). To test whether the epidermal abnormalities affected epidermal barrier function, a skin permeability assay was conducted on E18.5 embryos. In embryos with an incompletely formed epidermis the X-gal substrate will penetrate the skin, be cleaved by the endogenous β-galactosidase enzyme in the skin and form a blue precipitate in low pH conditions (Hardman et al., 1998; Guttormsen et al., 2008). In all *Ppp2r2a*$^{+/+}$ and *Ppp2r2a*$^{+/-}$ embryos, only the edges of skin where the tail and umbilical cord were cut, turned slightly blue due to experimentally interrupted barrier. In contrast *Ppp2r2a*$^{-/-}$ embryos developed patchy blue staining all over the epidermis, confirming the presence of a disrupted epidermis, resulting in defective barrier function (**Figure 8A**).

Altered Proliferation in *Ppp2r2a*$^{-/-}$ Epidermis

The primary cultures suggested that proliferation may be impaired in the epidermis of *Ppp2r2a*$^{-/-}$ embryos. Therefore we stained for the proliferation marker, Ki67, via IHC. At E14.5, as noted above, the dorsal *Ppp2r2a*$^{-/-}$ epidermis was generally 1-cell thick, with only an occasional suprabasal layer, whereas the *Ppp2r2a*$^{+/+}$ epidermis was 1–3 cells thick. However, in both genotypes the majority of epidermal cells were Ki67^{+} (**Figures 8B,C**). In E18.5 *Ppp2r2a*$^{+/+}$ embryos, Ki67^{+} cells were present in the basal layer of the epidermis and surrounding the dermal appendages, with only a few positive cells in the spinous and subsequent outer stratified layers (**Figures 8B,C**). In comparison, the *Ppp2r2a*$^{-/-}$ epidermis contained fewer Ki67^{+} in the basal layer. In the suprabasal layer, where the cells are more compact in the knockout compared to the wild-type, there were reduced total numbers of cells, however, more cells were Ki67^{+}. Therefore, homozygous *Ppp2r2a* deletion results in slightly reduced epidermal basal cell proliferation, but increased proliferation in the more apical suprabasal cells, which at this stage should be ceasing proliferation and starting to terminally differentiate.

The Epidermal Defect in *Ppp2r2a*$^{-/-}$ Mice Is Associated With Increased Phosphorylation of the PP2A Target cJun

cJun is a subunit of the transcription factor AP-1, and functions in epidermal development downstream of PP2A and AKT (Karin, 1995; Kallunki et al., 1996). We found increased phosphorylation of cJun at S63, a site which enhances cJun transcriptional activity (Pulverer et al., 1991; Smeal et al., 1991;

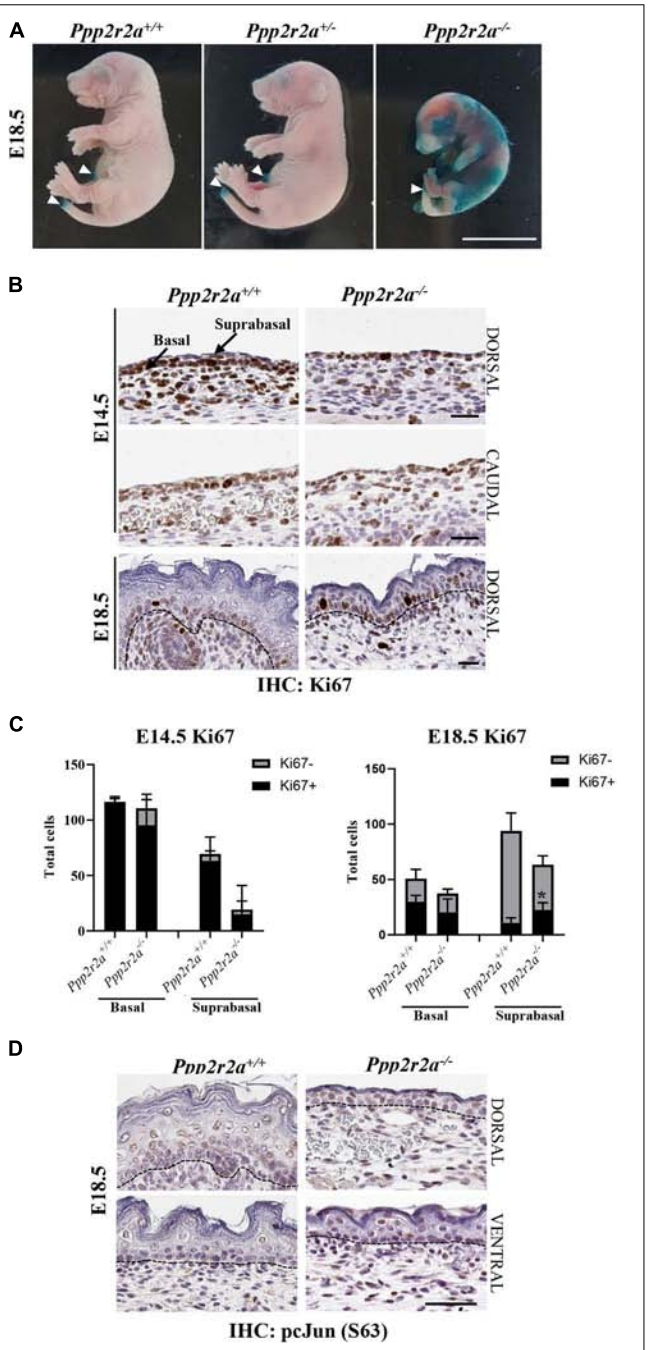

FIGURE 8 | Defective epidermal barrier in *Ppp2r2a* knockout embryos is associated with changes in proliferation, and p-cJun signaling. **(A)** X-gal substrate penetration (permeability) assay in E18.5 embryos. Areas stained blue on the *Ppp2r2a*$^{-/-}$ embryo indicates regions with an impaired epidermal barrier. White arrowheads mark regions (umbilical cord and tail) that stained blue as they were cut during dissection. Representative of $n = 3$. Scale bar = 1 cm. **(B)** *Ppp2r2a*$^{+/+}$ and *Ppp2r2a*$^{-/-}$ epidermal regions at E14.5 and E18.5 showing Ki67 (proliferation marker) staining. Dashed black line indicates the dermal-epidermal junction. **(C)** Quantitation of Ki67 positive and negative cells in E14.5 and E18.5 epidermis. Ki67^{+} cells were significantly increased in the *Ppp2r2a*$^{-/-}$ suprabasal epidermis compared to the wild-type. $^{*}p < 0.05$, unpaired two-tailed *t*-test. **(D)** IHC for p-cJun (S63) in *Ppp2r2a*$^{+/+}$ and *Ppp2r2a*$^{-/-}$ epidermal regions. Dashed black line indicates the dermal-epidermal junction. All scale bars = 50 μm.

Deng and Karin, 1994), in the basal, spinous and granular layers of dorsal and ventral *Ppp2r2a*$^{-/-}$ epidermis, compared to wild-type epidermis (**Figure 8D**), suggesting loss of PP2A-B55α leads to hyperphosphorylation and activation of cJun in the developing skin.

DISCUSSION

We have generated and characterized the first constitutive *Ppp2r2a* knockout mouse. Homozygous deletion of *Ppp2r2a* resulted in embryonic lethality between E10.5 and birth, while heterozygous mice were viable and grew normally. Late stage *Ppp2r2a* knockout embryos were significantly smaller in size than littermate controls, and displayed various abnormalities such as syndactyly, neural defects and epidermal defects. The epidermal defect was characterized by thinner basal, spinous and granular layers, and a discontinuous stratum corneum. The structural defects of the epidermis were accompanied by a lack of dermal appendages and increased epidermal hemorrhage and edema. Functionally, the morphological skin defects translated to impaired epidermal barrier integrity, which is the likely cause of *Ppp2r2a*$^{-/-}$ neonatal death.

While this is the first reported *in vivo* analysis of *Ppp2r2a* deletion in mice, a study in zebrafish embryos revealed the importance of PP2A-B55α in cytoskeletal regulation to promote stable angiogenesis (Martin et al., 2013). Similarly, a prior *ex vivo* mouse embryo study had suggested that PP2A-B55α was essential in early embryogenesis (Liang et al., 2017). Double-stranded RNA-mediated *Ppp2r2a* knockdown in fertilized mouse zygotes arrested *in vitro* embryonic development, in association with increased DNA damage and apoptosis (Liang et al., 2017). In contrast, we observed close to Mendelian ratios of all three genotypes at E10.5, showing that PP2A-B55α is not essential for early embryonic development *in vivo*. However, the percentage of *Ppp2r2a*$^{-/-}$ embryos recovered at E14.5 and E18.5 steadily declined, suggesting that some knockout mice die between E10.5 and E14.5, others between E14.5 and E18.5, and a final few between E18.5 and P0. Therefore, there is significant heterogeneity in the penetrance of the phenotypes caused by *Ppp2r2a* loss.

The lethality observed in our *Ppp2r2a* knockout mice occurred later in embryogenesis than that reported in knockout mice for the PP2A structural and catalytic subunits (Götz et al., 1998; Ruediger et al., 2011). PP2A-Aα (*Ppp2r1a*) deletion resulted in the absence of homozygous knockout embryos by E10.5, but the cause of lethality was not determined (Ruediger et al., 2011). Given our E10.5 *Ppp2r2a* knockout embryos appeared grossly normal, we can infer that PP2A-B55α is not essential for implantation or gastrulation. However, the few occurrences of neural-related defects observed between E10.5 and E18.5 suggest that neurulation (∼E7.5) may not be fully functional. Homozygous PP2A-Cα knockout (*Ppp2ca*$^{-/-}$) embryos had a developmental block at E6.5, before completing gastrulation (Götz et al., 1998). Moreover, *Ppp2ca*$^{-/-}$ embryos examined at E7.5 were found to be amorphous, smaller in size than controls and have a degenerated embryonic ectoderm (Götz et al., 1998). The early developmental block makes it difficult to compare the phenotype exactly to that of our *Ppp2r2a* knockout, however, some similarities are apparent; *Ppp2r2a* knockout embryos were also significantly smaller than wild-type littermates, and showed defects in neural and epidermal tissue, both of which derive from the ectodermal germ layer (Loebel et al., 2003). Thus, PP2A complexes containing B55α play an essential role in the development and differentiation of the ectoderm, but other PP2A regulatory subunit(s) are necessary, or are able to compensate for the loss of B55α, in the earliest stages of development.

Lamination refers to the differentiation of neurons into morphologically distinct layers in the neuroepithelium and begins around E10.0-10.5 (Chen et al., 2017). The emergence of these layers was seen in the E10.5 *Ppp2r2a*$^{+/+}$ neuroepithelium (**Figure 3A**), but was not apparent in the *Ppp2r2a* knockout embryos. At E14.5 there is a continuation of neuroepithelium stratification and differentiation in wild-type mice, while at this stage *Ppp2r2a*$^{-/-}$ embryos exhibited neural tube defects. To our knowledge, PP2A has not previously been implicated in these developmental disorders. Exencephaly and spina bifida occur due to neurulation defects, such as inadequate neural tube folding, apposition or fusion, resulting in failure of neural fold closure (Harris and Juriloff, 2007; Chen et al., 2017). These defects begin early, with neurulation starting at ∼E7.5 and neural tube folding and fusion by ∼E10.5. The physical separation of the neuroectoderm from the surface ectoderm (future skin) also begins at ∼E10.5 (Chen et al., 2017). Thus, PP2A-B55α is important for normal development of the neuroepithelium.

There is a wide variety of genetic causes of neural tube defects [reviewed in Harris and Juriloff (2007, 2010)]. Mutation or reduced expression of numerous members of Wnt, FGF, or BMP pathways, for example FGFr1 and Axin, can lead to exencephaly and spina bifida (Juriloff and Harris, 2000). Neural cells develop from the ectoderm in the absence of canonical Wnt signaling when FGF signaling predominates and inhibits BMP. Conversely, an epidermal fate is adopted when active Wnt and BMP signaling predominates and promotes β-catenin activity (Finley et al., 1999; Stern, 2005; Fuchs, 2007). PP2A is known to regulate various proteins within these pathways and thus can have direct and indirect effects on neurulation. For example, it can positively regulate Raf-1, negatively regulate Erk downstream of FGF (Abraham et al., 2000; Jaumot and Hancock, 2001; Kubicek et al., 2002; Strack, 2002; Adams et al., 2005), and can exert both positive and negative regulation on Wnt/β-catenin signaling (Götz et al., 2000; Ivaska et al., 2002; Su et al., 2008; Clevers and Nusse, 2012; Mitra et al., 2012; Stamos and Weis, 2013; Thompson and Williams, 2018). PP2A-B55α complexes in particular can dephosphorylate β-catenin, leading to its stabilization and promotion of Wnt signaling (Zhang et al., 2009). Thus PP2A-B55α loss would be predicted to reduce Wnt signaling, and hence there may be no problem in committing to a neural fate, but rather in subsequent neurulation steps.

Further neural tube folding is promoted by the Sonic hedgehog (SHH) protein, alone and interacting with Wnts/BMPs (Colas and Schoenwolf, 2001; Ybot-Gonzalez et al., 2002). Loss of function of GLI3, a key SHH effector causes embryonic exencephaly, as does ectopic SHH expression (Echelard et al.,

1993; Hui and Joyner, 1993). PP2A is also involved in SHH signaling via negative regulation of GLI3 (Krauß et al., 2008). AP-2 is a retinoic acid inducible transcription factor that is expressed by non-neuronal ectodermal cells but is also vital for neural tube closure, and AP-2 null mice develop exencephaly (Zhang et al., 1996). B55α containing PP2A complexes can dephosphorylate and decrease AP-2 activity (Ricotta et al., 2008). Similar pathways and proteins are also involved in syndactyly development, including the HOX genes (SHH and Indian hedgehog), FGFs, BMPs and Wnt, implying that PP2A-B55α regulates these pathways in multiple regions of the developing embryo (Manouvrier-Hanu et al., 1999).

The cellular degeneration and debris observed at E10.5 indicates that cell death is also occurring in *Ppp2r2a* knockouts. Whether this is due to PP2A specifically regulating cell death pathways, or is a consequence of the defective differentiation and the beginning of embryo degradation and resorption, is not clear. The neural defects observed at E14.5, were associated with increased apoptosis. Apoptosis is a normal and important part of shaping neuroepithelial development; however, it occurs in a very precise spatiotemporal manner. At later stages of gestation (E12–18), apoptosis occurs in regions that become the ventricular zone, intermediate zone, and the developing cortical plate and dorsal root ganglion of the cerebral cortex (Haydar et al., 2000; Yeo and Gautier, 2004; Chen et al., 2017). In the E14.5 *Ppp2r2a*$^{-/-}$ neuroepithelium, however, apoptosis was found in the thalamus, cerebellum and forebrain regions, which at this stage should be undergoing enlargement and differentiation (Chen et al., 2017).

Ppp2r2a deletion led to severe defects in epidermal stratification, including separation of the dermo-epidermal junction, subcutaneous hemorrhage and edema, and a thin and disorganized epidermis. Defective *Ppp2r2a*$^{-/-}$ keratinocyte differentiation was also evidenced in culture. These epithelial defects further indicate a failure of normal ectoderm differentiation with *Ppp2r2a* deletion. After neural tube fusion, the overlying epidermal ectoderm is separated from the neural tube and becomes what will be the skin at the back of the embryo (Colas and Schoenwolf, 2001). Interestingly, the most severe epidermal defects in the *Ppp2r2a* knockout occurred in the dorsal skin. Wnt/FGF/BMP signaling is important in induction of an epidermal fate and is also continually required through epidermal development and stratification (Zhu et al., 2014), providing further evidence for PP2A-B55α acting on these pathways in different regions of the developing embryo. In support of this hypothesis, B55α has been implicated in the regulation of BMP/TGF-β signaling by enhancing the TGF-β/Activin/Nodal signaling pathway (Batut et al., 2008). This pathway is essential for cell fate determination during development and for regulation of epidermal differentiation. Indeed, as mentioned previously, Wnt and BMP signaling are required for the ectoderm to develop into the epidermis, and this is further promoted by combined gradients of BMP and Nodal signaling during embryonic development which block neuroectoderm formation (Camus et al., 2006) and regulate patterning of the embryonic axes and neural and gut tubes (Arnold and Robertson, 2009; Pauklin and Vallier, 2015).

PP2A has previously been implicated in epidermal barrier formation. Mice with K14-Cre driven conditional knockout of PP2A-Cα had significant hair loss and disruption in the hair follicle regeneration cycle, as well as stunted size, melanin deposition and hyper-proliferation at the base of their claws (Fang et al., 2016). Furthermore, *ex vivo* studies have implicated the B55α subunit in epidermal development (O'Shaughnessy et al., 2009; Gerner et al., 2013; Youssef et al., 2013). Of the *Ppp2r2* family, the *Ppp2r2a* isoform is the most highly expressed during epidermal barrier acquisition in mouse embryos (O'Shaughnessy et al., 2009). Indeed, we found B55α protein to be expressed in all epidermal layers of E14.5 and E18.5 wild-type embryos. The epidermal defects observed with *Ppp2r2a* deletion now confirm an essential functional role for PP2A-B55α in epidermal development.

The formation of the epidermal barrier is a key element of late embryonic development that facilitates survival *ex-utero*, and should be completely formed by E18.5 in C57BL/6 embryos (O'Shaughnessy et al., 2009). However, the epidermal barrier in E18.5 *Ppp2r2a*$^{-/-}$ embryos was patchy and penetrable, which would inevitably result in the rapid death of pups at birth, as evidenced by the one *Ppp2r2a*$^{-/-}$ pup found dead at P0 that had visible skin defects. In the *Ppp2r2a*$^{-/-}$ epidermis the basal, spinous and granular layers were thin and poorly defined, and the stratum corneum was inconsistent or absent. The stratum corneum plays a major role in preventing water loss and protecting against the external environment (Sandilands et al., 2009). The presence of a few cells with intact nuclei in the uppermost layer of the *Ppp2r2a*$^{-/-}$ epidermis (above the loricrin stained granular layer **Figure 5B**) may indicate a persisting periderm, the transitory layer that normally disappears by ∼E17.5 (Sengel, 1976; M'Boneko and Merker, 1988; Zhang et al., 2005), and adds to the evidence of defective final cornification.

In the *Ppp2r2a*$^{-/-}$ epidermis there was also a lack of dermal appendages, which develop into hair follicles, sebaceous glands and sweat glands (Liu et al., 2013). Dermal appendages arise from interactive signaling between the epidermis and underlying dermis (mesoderm), and is mediated by similar signaling proteins and pathways as neural and epidermal development (Wnt, BMP, FGF, SHH) (Duverger and Morasso, 2009; Sennett and Rendl, 2012; Biggs and Mikkola, 2014; Ahn, 2015). Epidermal Wnt production modulates a BMP-FGF signaling cascade in the dermis and is essential for proper stratification and formation of the spinous layer, and for hair follicle initiation (Fu and Hsu, 2013; Zhu et al., 2014). This Wnt signaling cascade also promotes normal p63 expression in proliferating basal keratinocytes, and is required for the normal stratification process. When epidermal Wnt signaling is disrupted, the subsequent loss of p63 expression ablates the proliferative capacity of basal keratinocytes to properly stratify, resulting in a hypoplastic spinous layer, similar to the thin spinous layer of *Ppp2r2a* knockouts, thus further implicating aberrant Wnt signaling in lethality of these knockouts (Zhu et al., 2014).

Epidermal stratification and hair follicle formation also rely on β1-integrin mediated remodeling of the basement membrane. Epidermal specific (K14-Cre) β1-integrin knockout mice exhibit severe skin blistering and hair defects, accompanied by

massive failure of BM assembly/organization, hemidesmosome instability, and a failure of hair follicle keratinocytes to remodel BM and invaginate into the dermis (Raghavan et al., 2000). Thus, the reduced β1-integrin in our *Ppp2r2a* knockouts likely contributes to the failure of developing hair follicles to invaginate into the underlying dermis.

The interaction and signaling between the epidermis and dermis via the BM, is also essential for keratinocyte polarization, proliferation and differentiation. α6β4 integrin heterodimers form hemidesmosomes by attaching to intracellular keratin filaments and anchoring basal keratinocytes to the BM (Jones et al., 1998). The BM layer was reduced and inconsistent in the *Ppp2r2a*$^{-/-}$ skin, and the expression of β4-integrin was also markedly reduced. β4-integrin null mice have hemidesmosome loss and show defective epidermal stratification, weak attachment to the basal lamina and basal and spinous keratinocyte disorganization leading to gross skin denuding (Dowling et al., 1996). Indeed, the separation of the dermis and epidermis, or blistering, and associated hemorrhage observed in the *Ppp2r2a*$^{-/-}$ skin (**Figures 2B**, **4A**), are reminiscent of these β4-integrin knockouts. Furthermore, the stratified layers of these mice displayed mitotic basal-like keratinocytes, similar to the proliferative (Ki67^{+}) cells observed in the suprabasal layers of the *Ppp2r2a*$^{-/-}$ embryos. Correct timing of hemidesmosome internalization and detachment from the BM is vital for formation of the spinous layer (Poumay et al., 1994). The ability of B55α null and β4-integrin null keratinocytes to maintain expression of basal cell markers and undergo mitosis indicates that loss of attachment to the BM and impaired polarization leads to premature release of basal cells into the stratified layers, without appropriate signals to terminally differentiate (Stepp, 1999; Rippa et al., 2013).

Keratinocyte polarity is not only vital for the appropriate cell-BM attachment, but also for correct orientation of the mitotic spindle, which under normal conditions is oriented parallel to the BM during basal layer formation, and changes to perpendicular to the BM to form suprabasal keratinocyte layers, with distinct differentiation markers (Smart, 1970; Lechler and Fuchs, 2005; Muroyama and Lechler, 2012). PP2A-B55α is known to play a role in cytoskeletal regulation and spindle dynamics during mitosis (Martin et al., 2013; Williams et al., 2014; Wang et al., 2015, 2018; Liang et al., 2017) thus, loss of PP2A-B55α-mediated regulation of cell polarity could cause defective "asymmetric" division, leading to accumulation of immature and mitotic suprabasal keratinocytes.

In addition to the reduction of β1- and β4-integrins, the *Ppp2r2a*$^{-/-}$ basal and spinous layers displayed reduced and inconsistent membrane labeling of the adherens junction associated protein, β-catenin. In contrast, the tight-junction associated ZO-1 labeling in the thin granular layers of *Ppp2r2a*$^{-/-}$ basal keratinocytes was stronger than the wildtype. Whether this is a compensatory mechanism to adjust for reduced hemidesmosomes, focal adhesions and adherens junction attachments remains to be determined.

The expression of K1 in *Ppp2r2a*$^{-/-}$ basal keratinocytes, which is normally restricted to keratinocytes committed to terminal differentiation (Sur et al., 2006), further indicates aberrant differentiation, and is reminiscent of ΔNp63 null mice (Romano et al., 2012). ΔNp63, a transcription factor with high homology to the tumor suppressor p53, and downstream mediator of Wnt signaling, is a master regulator of epithelial development and differentiation, and its deletion results in severe developmental abnormalities including truncated forelimbs, the absence of hind limbs, and a poorly developed stratified epidermis comprising isolated clusters of disorganized epithelial cells, with premature expression of markers associated with terminal differentiation, such as K1 (Romano et al., 2012). Like the *Ppp2r2a* knockouts, ΔNp63 null mice also had dramatic reduction in collagen and laminin BM proteins. PP2A was recently reported in ΔNp63 immunoprecipitates from squamous cell carcinoma cell lines (Katoh et al., 2016), but whether B55α directly or indirectly regulates ΔNp63 activity remains to be determined.

Taken together, our data suggests that PP2A-B55α is involved in epidermal development via regulation of WNT and BMP signaling pathways, together with cell polarity and adhesion regulation. Which specific substrates are involved in mediating these functions is not fully clear. cJun is a known target of PP2A-B55α (Gilan et al., 2015), and O'Shaughnessy et al. (2009) showed that there is a pulse of p-AKT leading to transient phospho-cJun (p-cJun) dephosphorylation during barrier acquisition (∼E17.5) and proposed that this occurs via PP2A-B55α. They further found that *Ppp2r2a* knockdown in skin explant cultures resulted in increased cJun phosphorylation and epidermal barrier incompetence (O'Shaughnessy et al., 2009). The increased p-cJun in the E18.5 *Ppp2r2a* knockout epidermis supports PP2A-B55α being the effector of AKT-mediated cJun dephosphorylation, and provides the first *in vivo* evidence for *Ppp2r2a* loss leading to defective epidermal barrier acquisition through increased aberrant p-cJun signaling, thus disrupting this spatiotemporally sensitive sequence of events that must occur at this time.

During the very late stages of embryonic and epidermal development, PP2A can also regulate the conversion of profilaggrin to free filaggrin monomers, which contribute to the protein scaffold upon which the uppermost impenetrable stratum corneum will attach (Kam et al., 1993; Sandilands et al., 2009). The lack of stratum corneum and dysfunctional epidermal barrier in the *Ppp2r2a* knockouts suggests that the PP2A-B55α regulatory subunit may regulate filaggrin. However, it is unlikely that PP2A-B55α regulation of cJun or filaggrin at these late stages of epidermal stratification are the only factors leading to the epidermal defects observed, particularly given defects were observed as early as E14.5. PP2A regulation of components of the Wnt, β-catenin, BMP, FGF, and SHH signaling pathways, are more likely to be driving neural development early on, and limb and epidermal development in later stages. Integrins, keratins, catenins, and tight junction proteins such as ZO-1, are all regulated by phosphorylation, therefore hyperphosphorylation of one or more of these proteins in the absence of B55α may also contribute.

In summary, our study provides the first *in vivo* evidence for the requirement of *Ppp2r2a* in embryonic development, with *Ppp2r2a* knockout causing limb, neural and epidermal

defects. These aspects of embryonic development are for the majority controlled by key signaling pathways driving ectoderm development, such as Wnt/β-catenin, BMP, FGF and SHH. This highlights a novel role for PP2A-B55α in the control of ectodermal development. Future identification of the specific PP2A-B55α substrates mediating these effects will shed further light on the functional role of this essential protein phosphatase in normal development and disease.

DATA AVAILABILITY STATEMENT

All datasets generated for this study are included in the article/**Supplementary Material**.

ETHICS STATEMENT

The animal study was reviewed and approved by the University of Newcastle Animal Care and Ethics Committee.

AUTHOR CONTRIBUTIONS

All authors contributed to this manuscript. NP, MC, CL-O, RK, and SR performed the experiments. NP, SR, and NV wrote the manuscript. NV and SR designed the study.

FUNDING

This work was supported by grants from the Cancer Council NSW (APP1086334) and the Australian Research Council (FT170100077). NP was supported by a Research Training Program Scholarship, University of Newcastle Vice Chancellors' Scholarship, and NV by an Australian Research Council Future Fellowship. The APN was supported by the Australian Government through the National Collaborative Research Infrastructure Strategy (NCRIS) Program.

ACKNOWLEDGMENTS

The authors thank Prof. Allison Cowin, University of South Australia, and Prof. Christopher Dayas, University of Newcastle, for critical review of the manuscript. The *Ppp2r2a* mouse line were produced by the Monash University node of the Australian Phenomics Network (APN). This study also utilized the Australian Phenomics Network Histopathology and Organ Pathology Service, the University of Melbourne.

SUPPLEMENTARY MATERIAL

The Supplementary Material for this article can be found online at: https://www.frontiersin.org/articles/10.3389/fcell.2020.00358/full#supplementary-material

REFERENCES

Abraham, D., Podar, K., Pacher, M., Kubicek, M., Welzel, N., Hemmings, B. A., et al. (2000). Raf-1-associated Protein Phosphatase 2A as a positive regulator of kinase activation. *J. Biol. Chem.* 275, 22300–22304. doi: 10.1074/jbc.M003259200

Adams, D. G., Coffee, R. L., Zhang, H., Pelech, S., Strack, S., and Wadzinski, B. E. (2005). Positive regulation of Raf1-MEK1/2-ERK1/2 signaling by protein serine/threonine phosphatase 2A holoenzymes. *J. Biol. Chem.* 280, 42644–42654. doi: 10.1074/jbc.M502464200

Ahn, Y. (2015). "Chapter Thirteen–signaling in. tooth, hair, and mammary placodes," in *Current Topics in Developmental Biology*, ed. P. A. Trainor (Cambridge, MA: Academic Press), 421–459. doi: 10.1016/bs.ctdb.2014.11.013

Arnold, S. J., and Robertson, E. J. (2009). Making a commitment: cell lineage allocation and axis patterning in the early mouse embryo. *Nat. Rev. Mol. Cell Biol.* 10, 91–103. doi: 10.1038/nrm2618

Batut, J., Schmierer, B., Cao, J., Raftery, L. A., Hill, C. S., and Howell, M. (2008). Two highly related regulatory subunits of PP2A exert opposite effects on TGF-beta/Activin/Nodal signalling. *Development* 135, 2927–2937. doi: 10.1242/dev.020842

Beca, F., Pereira, M., Cameselle-Teijeiro, J. F., Martins, D., and Schmitt, F. (2015). Altered PPP2R2A and Cyclin D1 expression defines a subgroup of aggressive luminal-like breast cancer. *BMC Cancer* 15:285. doi: 10.1186/s12885-015-1266-1

Biggs, L. C., and Mikkola, M. L. (2014). Early inductive events in ectodermal appendage morphogenesis. *Semin. Cell Dev. Biol.* 25-26, 11–21. doi: 10.1016/j.semcdb.2014.01.007

Bousquet, E., Calvayrac, O., Mazieres, J., Lajoie-Mazenc, I., Boubekeur, N., Favre, G., et al. (2016). RhoB loss induces Rac1-dependent mesenchymal cell invasion in lung cells through PP2A inhibition. *Oncogene* 35, 1760–1769. doi: 10.1038/onc.2015.240

Burgess, A., Vigneron, S., Brioudes, E., Labbe, J. C., Lorca, T., and Castro, A. (2010). Loss of human Greatwall results in G2 arrest and multiple mitotic defects due to deregulation of the cyclin B-Cdc2/PP2A balance. *Proc. Natl. Acad. Sci. U.S.A.* 107, 12564–12569. doi: 10.1073/pnas.0914191107

Calin, G. A., di Iasio, M. G., Caprini, E., Vorechovsky, I., Natali, P. G., Sozzi, G., et al. (2000). Low frequency of alterations of the alpha (PPP2R1A) and beta (PPP2R1B) isoforms of the subunit A of the serine-threonine phosphatase 2A in human neoplasms. *Oncogene* 19, 1191–1195. doi: 10.1038/sj.onc.1203389

Camus, A., Perea-Gomez, A., Moreau, A., and Collignon, J. (2006). Absence of Nodal signaling promotes precocious neural differentiation in the mouse embryo. *Dev. Biol.* 295, 743–755. doi: 10.1016/j.ydbio.2006.03.047

Capaldo, C. T., and Macara, I. G. (2007). Depletion of E-cadherin disrupts establishment but not maintenance of cell junctions in Madin-Darby canine kidney epithelial cells. *Mol. Biol. Cell* 18, 189–200. doi: 10.1091/mbc.e06-05-0471

Chen, V. S., Morrison, J. P., Southwell, M. F., Foley, J. F., Bolon, B., and Elmore, S. A. (2017). Histology Atlas of the developing prenatal and postnatal mouse central nervous system, with emphasis on prenatal days E7.5 to E18.5. *Toxicol. Pathol.* 45, 705–744. doi: 10.1177/0192623317728134

Cheng, C. W., Niu, B., Warren, M., Pevny, L. H., Lovell-Badge, R., Hwa, T., et al. (2014). Predicting the spatiotemporal dynamics of hair follicle patterns in the developing mouse. *Proc. Natl. Acad. Sci. U.S.A.* 111, 2596–2601. doi: 10.1073/pnas.1313083111

Cheng, Y., Liu, W., Kim, S. T., Sun, J., Lu, L., Sun, J., et al. (2011). Evaluation of PPP2R2A as a prostate cancer susceptibility gene: a comprehensive germline and somatic study. *Cancer Genet.* 204, 375–381. doi: 10.1016/j.cancergen.2011.05.002

Chu, D. H., and Loomis, C. A. (2004). "Chapter 59–structure and development of the skin and cutaneous appendages," in *Fetal and Neonatal Physiology*, Third Edn, eds R. A. Polin, W. W. Fox, and S. H. Abman (Philadelphia, PA: W. B. Saunders), 589–596.

Clevers, H., and Nusse, R. (2012). Wnt/beta-catenin signaling and disease. *Cell* 149, 1192–1205. doi: 10.1016/j.cell.2012.05.012

Colas, J. F., and Schoenwolf, G. C. (2001). Towards a cellular and molecular understanding of neurulation. *Dev. Dyn.* 221, 117–145. doi: 10.1002/dvdy.1144

Collison, A., Hatchwell, L., Verrills, N., Wark, P. A. B., de Siqueira, A. P., Tooze, M., et al. (2013). The E3 ubiquitin ligase midline 1 promotes allergen and rhinovirus-induced asthma by inhibiting protein phosphatase 2A activity. *Nat. Med.* 19, 232–237. doi: 10.1038/nm.3049

Crispin, J. C., Hedrich, C. M., and Tsokos, G. C. (2013). Gene-function studies in systemic lupus erythematosus. *Nat. Rev. Rheumatol.* 9, 476–484. doi: 10.1038/nrrheum.2013.78

Cundell, M. J., Bastos, R. N., Zhang, T., Holder, J., Gruneberg, U., Novak, B., et al. (2013). The BEG (PP2A-B55/ENSA/Greatwall) pathway ensures cytokinesis follows chromosome separation. *Mol. Cell.* 52, 393–405. doi: 10.1016/j.molcel.2013.09.005

Curtis, C., Shah, S. P., Chin, S. F., Turashvili, G., Rueda, O. M., Dunning, M. J., et al. (2012). The genomic and transcriptomic architecture of 2,000 breast tumours reveals novel subgroups. *Nature* 486, 346–352. doi: 10.1038/nature10983

Deng, T., and Karin, M. (1994). c-Fos transcriptional activity stimulated by H-Ras-activated protein kinase distinct from JNK and ERK. *Nature* 371, 171–175. doi: 10.1038/371171a0

Dowling, J., Yu, Q. C., and Fuchs, E. (1996). Beta4 integrin is required for hemidesmosome formation, cell adhesion and cell survival. *J. Cell Biol.* 134, 559–572. doi: 10.1083/jcb.134.2.559

Duverger, O., and Morasso, M. I. (2009). Epidermal patterning and induction of different hair types during mouse embryonic development. *Birth Defects Res. C Embryo Today* 87, 263–272. doi: 10.1002/bdrc.20158

Echelard, Y., Epstein, D. J., St-Jacques, B., Shen, L., Mohler, J., McMahon, J. A., et al. (1993). Sonic hedgehog, a member of a family of putative signaling molecules, is implicated in the regulation of CNS polarity. *Cell* 75, 1417–1430. doi: 10.1016/0092-8674(93)90627-3

Eichhorn, P. J. A., Creyghton, M. P., and Bernards, R. (2009). Protein phosphatase 2A regulatory subunits and cancer. *Biochim. Biophys. Acta* 1795, 1–15. doi: 10.1016/j.bbcan.2008.05.005

Fang, C., Li, L., and Li, J. (2016). Conditional knockout in mice reveals the critical roles of Ppp2ca in epidermis development. *Int. J. Mol. Sci.* 17:756. doi: 10.3390/ijms17050756

Finley, M. F. A., Devata, S., and Huettner, J. E. (1999). BMP-4 inhibits neural differentiation of murine embryonic stem cells. *J. Neurobiol.* 40, 271–287.

Fu, J., and Hsu, W. (2013). Epidermal Wnt controls hair follicle induction by orchestrating dynamic signaling crosstalk between the epidermis and dermis. *J. Investig. Dermatol.* 133, 890–898. doi: 10.1038/jid.2012.407

Fuchs, E. (2007). Scratching the surface of skin development. *Nature* 445, 834–842.

Fuchs, E., and Raghavan, S. (2002). Getting under the skin of epidermal morphogenesis. *Nat. Rev. Genet.* 3, 199–209. doi: 10.1038/nrg758

Gerner, L., Youssef, G., and O'Shaughnessy, R. F. (2013). The protein phosphatase 2A regulatory subunit Ppp2r2a is required for Connexin-43 dephosphorlyation during epidermal barrier acquisition. *Exp. Dermatol.* 22, 754–756. doi: 10.1111/exd.12234

Gharbi-Ayachi, A., Labbe, J. C., Burgess, A., Vigneron, S., Strub, J. M., Brioudes, E., et al. (2010). The substrate of Greatwall kinase, Arpp19, controls mitosis by inhibiting protein phosphatase 2A. *Science* 330, 1673–1677. doi: 10.1126/science.1197048

Gilan, O., Diesch, J., Amalia, M., Jastrzebski, K., Chueh, A. C., Verrills, N. M., et al. (2015). PR55alpha-containing protein phosphatase 2A complexes promote cancer cell migration and invasion through regulation of AP-1 transcriptional activity. *Oncogene* 34, 1333–1339. doi: 10.1038/onc.2014.460

Goldsworthy, M., Bai, Y., Li, C.-M., Ge, H., Lamas, E., Hilton, H., et al. (2016). Haploinsufficiency of the insulin receptor in the presence of a splice-site mutation in Ppp2r2a results in a novel digenic mouse model of Type 2 diabetes. *Diabetes Metab. Res. Rev.* 65, 1434–1446. doi: 10.2337/db16-0249

Götz, J., Probst, A., Ehler, E., Hemmings, B., and Kues, W. (1998). Delayed embryonic lethality in mice lacking protein phosphatase 2A catalytic subunit Cα. *Proc. Natl. Acad. Sci. U.S.A* 95, 12370–12375. doi: 10.1073/pnas.95.21.12370

Götz, J., Probst, A., Mistl, C., Nitsch, R. M., and Ehler, E. (2000). Distinct role of protein phosphatase 2A subunit Cα in the regulation of E-cadherin and β-catenin during development. *Mech. Dev.* 93, 83–93. doi: 10.1016/s0925-4773(00)00267-7

Guttormsen, J., Koster, M. I., Stevens, J. R., Roop, D. R., Williams, T., and Winger, Q. A. (2008). Disruption of epidermal specific gene expression and delayed skin development in AP-2 gamma mutant mice. *Dev. Biol.* 317, 187–195. doi: 10.1016/j.ydbio.2008.02.017

Hardman, M. J., Sisi, P., Banbury, D. N., and Byrne, C. (1998). Patterned acquisition of skin barrier function during development. *Development* 125, 1541–1552.

Hardy, M. H. (1992). The secret life of the hair follicle. *Trends Genet.* 8, 55–61. doi: 10.1111/exd.13384

Harris, M. J., and Juriloff, D. M. (2007). Mouse mutants with neural tube closure defects and their role in understanding human neural tube defects. *Birth Defects Res. Part A Clin. Mol. Teratol.* 79, 187–210. doi: 10.1002/bdra.20333

Harris, M. J., and Juriloff, D. M. (2010). An update to the list of mouse mutants with neural tube closure defects and advances toward a complete genetic perspective of neural tube closure. *Birth Defects Res. Part A Clin. Mol. Teratol.* 88, 653–669. doi: 10.1002/bdra.20676

Hartsock, A., and Nelson, W. J. (2008). Adherens and tight junctions: structure, function and connections to the actin cytoskeleton. *Biochim. Biophys. Acta* 1778, 660–669. doi: 10.1016/j.bbamem.2007.07.012

Haydar, T. F., Nowakowski, R. S., Yarowsky, P. J., and Krueger, B. K. (2000). Role of founder cell deficit and delayed neuronogenesis in microencephaly of the trisomy 16 mouse. *J. Neurosci.* 20, 4156–4164. doi: 10.1523/JNEUROSCI.20-11-04156.2000

Hemmings, B. A., Adams-Pearson, C., Maurer, F., Muller, P., Goris, J., Merlevede, W., et al. (1990). alpha- and beta-forms of the 65-kDa subunit of protein phosphatase 2A have a similar 39 amino acid repeating structure. *Biochemistry* 29, 3166–3173. doi: 10.1021/bi00465a002

Hui, C. C., and Joyner, A. L. (1993). A mouse model of greig cephalopolysyndactyly syndrome: the extra-toesJ mutation contains an intragenic deletion of the Gli3 gene. *Nat. Genet.* 3, 241–246. doi: 10.1038/ng0393-241

Ivaska, J., Nissinen, L., Immonen, N., Eriksson, J. E., Kahari, V. M., and Heino, J. (2002). Integrin alpha 2 beta 1 promotes activation of protein phosphatase 2A and dephosphorylation of Akt and glycogen synthase kinase 3 beta. *Mol. Cell. Biol.* 22, 1352–1359. doi: 10.1128/mcb.22.5.1352-1359.2002

Janghorban, M., Langer, E. M., Wang, X., Zachman, D., Daniel, C. J., Hooper, J., et al. (2017). The tumor suppressor phosphatase PP2A-B56alpha regulates stemness and promotes the initiation of malignancies in a novel murine model. *PLoS One* 12:e0188910. doi: 10.1371/journal.pone.0188910

Jaumot, M., and Hancock, J. F. (2001). Protein phosphatases 1 and 2A promote Raf-1 activation by regulating 14-3-3 interactions. *Oncogene* 20, 3949–3958. doi: 10.1038/sj.onc.1204526

Jones, J. C., Hopkinson, S. B., and Goldfinger, L. E. (1998). Structure and assembly of hemidesmosomes. *Bioessays* 20, 488–494.

Juriloff, D. M., and Harris, M. J. (2000). Mouse models for neural tube closure defects. *Hum. Mol. Genet.* 9, 993–1000. doi: 10.1002/ajmg.a.40519

Kalev, P., Simicek, M., Vazquez, I., Munck, S., Chen, L., Soin, T., et al. (2012). Loss of PPP2R2A inhibits homologous recombination DNA repair and predicts tumor sensitivity to PARP inhibition. *Cancer Res.* 72, 6414–6424. doi: 10.1158/0008-5472.CAN-12-1667

Kallunki, T., Deng, T., Hibi, M., and Karin, M. (1996). c-Jun can recruit JNK to phosphorylate dimerization partners via specific docking interactions. *Cell* 87, 929–939. doi: 10.1016/s0092-8674(00)81999-6

Kam, E., Resing, K. A., Lim, S. K., and Dale, B. A. (1993). Identification of rat epidermal profilaggrin phosphatase as a member of the protein phosphatase 2A family. *J. Cell Sci.* 106, 219–226.

Kapfhamer, D., Berger, K. H., Hopf, F. W., Seif, T., Kharazia, V., Bonci, A., et al. (2010). Protein Phosphatase 2A and glycogen synthase Kinase 3 signaling modulate prepulse inhibition of the acoustic startle response by altering cortical M-Type potassium channel activity. *J. Neurosci.* 30, 8830–8840. doi: 10.1523/JNEUROSCI.1292-10.2010

Karin, M. (1995). The regulation of AP-1 activity by mitogen-activated protein kinases. *J. Biol. Chem.* 270, 16483–16486. doi: 10.1074/jbc.274.2.801

Katoh, I., Fukunishi, N., Fujimuro, M., Kasai, H., Moriishi, K., Hata, R.-I., et al. (2016). Repression of Wnt/β-catenin response elements by p63 (TP63). *Cell Cycle* 15, 699–710. doi: 10.1080/15384101.2016.1148837

Kowluru, A., and Matti, A. (2012). Hyperactivation of protein phosphatase 2A in models of glucolipotoxicity and diabetes: potential mechanisms and functional consequences. *Biochem. Pharmacol.* 84, 591–597. doi: 10.1016/j.bcp.2012.05.003

Krauß, S., Foerster, J., Schneider, R., and Schweiger, S. (2008). Protein phosphatase 2A and rapamycin regulate the nuclear localization and activity of the

transcription factor GLI3. *Cancer Res.* 68, 4658–4665. doi: 10.1158/0008-5472.CAN-07-6174

Kubicek, M., Pacher, M., Abraham, D., Podar, K., Eulitz, M., and Baccarini, M. (2002). Dephosphorylation of Ser-259 regulates Raf-1 membrane association. *J. Biol. Chem.stry* 277, 7913–7919. doi: 10.1074/jbc.M108733200

Lechler, T., and Fuchs, E. (2005). Asymmetric cell divisions promote stratification and differentiation of mammalian skin. *Nature* 437, 275–280. doi: 10.1038/nature03922

Lei, M., Wang, X., Ke, Y., and Solaro, R. J. (2015). Regulation of Ca2+ transient by PP2A in normal and failing heart. *Front. Physiol.gy* 6:13. doi: 10.3389/fphys.2015.00013

Li, F., Adase, C. A., and Zhang, L. J. (2017). Isolation and culture of primary mouse keratinocytes from neonatal and adult mouse skin. *J. Vis. Exp.* 125:56027. doi: 10.3791/56027

Liang, S., Guo, J., Choi, J.-W., Shin, K.-T., Wang, H.-Y., Jo, Y.-J., et al. (2017). Protein phosphatase 2A regulatory subunit B55α functions in mouse oocyte maturation and early embryonic development. *Oncotarget* 8, 26979–26991. doi: 10.18632/oncotarget.15927

Little, S. C., Curran, J., Makara, M. A., Kline, C. F., Ho, H. T., Xu, Z., et al. (2015). Protein phosphatase 2A regulatory subunit B56alpha limits phosphatase activity in the heart. *Sci. Signal.* 8:ra72. doi: 10.1126/scisignal.aaa5876

Liu, S., Zhang, H., and Duan, E. (2013). Epidermal development in mammals: key regulators, signals from beneath, and stem cells. *Int. J. Mol. Sci.* 14, 10869–10895. doi: 10.3390/ijms140610869

Loebel, D. A., Watson, C. M., De Young, R. A., and Tam, P. P. (2003). Lineage choice and differentiation in mouse embryos and embryonic stem cells. *Dev. Biol.* 264, 1–14. doi: 10.1016/s0012-1606(03)00390-7

Louis, J. V., Martens, E., Borghgraef, P., Lambrecht, C., Sents, W., Longin, S., et al. (2011). Mice lacking phosphatase PP2A subunit PR61/B'delta (Ppp2r5d) develop spatially restricted tauopathy by deregulation of CDK5 and GSK3beta. *Proc. Natl. Acad. Sci. U.S.A.* 108, 6957–6962. doi: 10.1073/pnas.1018777108

Manchado, E., Guillamot, M., de Carcer, G., Eguren, M., Trickey, M., Garcia-Higuera, I., et al. (2010). Targeting mitotic exit leads to tumor regression in vivo: modulation by Cdk1, Mastl, and the PP2A/B55alpha,delta phosphatase. *Cancer Cell* 18, 641–654. doi: 10.1016/j.ccr.2010.10.028

Mann, S. J. (1962). Prenatal formation of hair follicle types. *Anat. Rec.* 144, 135–141.

Manouvrier-Hanu, S., Holder-Espinasse, M., and Lyonnet, S. (1999). Genetics of limb anomalies in humans. *Trends Genet TIG* 15, 409–417.

Martin, M., Geudens, I., Bruyr, J., Potente, M., Bleuart, A., Lebrun, M., et al. (2013). PP2A regulatory subunit Balpha controls endothelial contractility and vessel lumen integrity via regulation of HDAC7. *EMBO J.* 32, 2491–2503. doi: 10.1038/emboj.2013.187

M'Boneko, V., and Merker, H. J. (1988). Development and morphology of the periderm of mouse embryos (days 9-12 of gestation). *Acta Anat.* 133, 325–336. doi: 10.1159/000146662

Mitra, A., Menezes, M. E., Pannell, L. K., Mulekar, M. S., Honkanen, R. E., Shevde, L. A., et al. (2012). DNAJB6 chaperones PP2A mediated dephosphorylation of GSK3β to downregulate β-catenin transcription target, osteopontin. *Oncogene* 31, 4472–4483. doi: 10.1038/onc.2011.623

Mochida, S., Maslen, S. L., Skehel, M., and Hunt, T. (2010). Greatwall phosphorylates an inhibitor of protein phosphatase 2A that is essential for mitosis. *Science* 330, 1670–1673. doi: 10.1126/science.1195689

Moorhead, G. B., Trinkle-Mulcahy, L., and Ulke-Lemee, A. (2007). Emerging roles of nuclear protein phosphatases. *Nat. Rev. Mol. Cell Biol.* 8, 234–244. doi: 10.1038/nrm2126

Muroyama, A., and Lechler, T. (2012). Polarity and stratification of the epidermis. *Semin. Cell Dev. Biol.* 23, 890–896. doi: 10.1016/j.semcdb.2012.08.008

Naudin, C., Smith, B., Bond, D. R., Dun, M. D., Scott, R. J., Ashman, L. K., et al. (2017). Characterization of the early molecular changes in the glomeruli of Cd151 (-/-) mice highlights induction of mindin and MMP-10. *Sci. Rep.* 7:15987. doi: 10.1038/s41598-017-15993-3

Neviani, P., Santhanam, R., Trotta, R., Notari, M., Blaser, B. W., Liu, S., et al. (2005). The tumor suppressor PP2A is functionally inactivated in blast crisis CML through the inhibitory activity of the BCR/ABL-regulated SET protein. *Cancer Cell* 8, 355–368. doi: 10.1016/j.ccr.2005.10.015

Olsen, J. V., Blagoev, B., Gnad, F., Macek, B., Kumar, C., Mortensen, P., et al. (2006). Global, in vivo, and site-specific phosphorylation dynamics in signaling networks. *Cell* 127, 635–648. doi: 10.1016/j.cell.2006.09.026

O'Shaughnessy, R. F., Welti, J. C., Sully, K., and Byrne, C. (2009). Akt-dependent Pp2a activity is required for epidermal barrier formation during late embryonic development. *Development* 136, 3423–3431. doi: 10.1242/dev.037010

Pauklin, S., and Vallier, L. (2015). Activin/Nodal signalling in stem cells. *Development* 142, 607–619. doi: 10.1242/dev.091769

Poumay, Y., Roland, I. H., Leclercq-Smekens, M., and Leloup, R. (1994). Basal detachment of the epidermis using dispase: tissue spatial organization and fate of integrin alpha 6 beta 4 and hemidesmosomes. *J. Invest. Dermatol.* 102, 111–117. doi: 10.1111/1523-1747.ep12371742

Pulverer, B. J., Kyriakis, J. M., Avruch, J., Nikolakaki, E., and Woodgett, J. R. (1991). Phosphorylation of c-jun mediated by MAP kinases. *Nature* 353, 670–674. doi: 10.1038/353670a0

Pundavela, J., Roselli, S., Faulkner, S., Attia, J., Scott, R. J., Thorne, R. F., et al. (2015). Nerve fibers infiltrate the tumor microenvironment and are associated with nerve growth factor production and lymph node invasion in breast cancer. *Mol. Oncol.* 9, 1626–1635. doi: 10.1016/j.molonc.2015.05.001

Raghavan, S., Bauer, C., Mundschau, G., Li, Q., and Fuchs, E. (2000). Conditional ablation of β1 integrin in skin: severe defects in epidermal proliferation, basement membrane formation, and hair follicle invagination. *J. Cell Biol.* 150, 1149–1160. doi: 10.1083/jcb.150.5.1149

Refaey, M. E., Musa, H., Murphy, N. P., Lubbers, E. R., Skaf, M., Han, M., et al. (2019). Protein phosphatase 2A regulates cardiac Na+ channels. *Circ. Res.* 124, 737–746. doi: 10.1161/CIRCRESAHA.118.314350

Reynhout, S., and Janssens, V. (2019). Physiologic functions of PP2A: lessons from genetically modified mice. *Biochim. Biophys. Acta* 1866, 31–50. doi: 10.1016/j.bbamcr.2018.07.010

Ricotta, D., Hansen, J., Preiss, C., Teichert, D., and Höning, S. (2008). Characterization of a Protein Phosphatase 2A holoenzyme that dephosphorylates the clathrin adaptors AP-1 and AP-2. *J. Biol. Chem.* 283, 5510–5517. doi: 10.1074/jbc.M707166200

Rippa, A. L., Vorotelyak, E. A., Vasiliev, A. V., and Terskikh, V. V. (2013). The role of integrins in the development and homeostasis of the epidermis and skin appendages. *Acta Nat.* 5, 22–33.

Romano, R.-A., Smalley, K., Magraw, C., Serna, V. A., Kurita, T., Raghavan, S., et al. (2012). ΔNp63 knockout mice reveal its indispensable role as a master regulator of epithelial development and differentiation. *Development* 139, 772–782. doi: 10.1242/dev.071191

Ross, E. A., Naylor, A. J., O'Neil, J. D., Crowley, T., Ridley, M. L., Crowe, J., et al. (2017). Treatment of inflammatory arthritis via targeting of tristetraprolin, a master regulator of pro-inflammatory gene expression. *Ann. Rheum. Dis.* 76, 612–619. doi: 10.1136/annrheumdis-2016-209424

Ruediger, R., Ruiz, J., and Walter, G. (2011). Human cancer-associated mutations in the Aα subunit of Protein Phosphatase 2A increase lung cancer incidence in Aα knock-in and knockout mice. *Mol. Cell. Biol.* 31, 3832–3844. doi: 10.1128/MCB.05744-11

Ruvolo, P. P., Qui, Y. H., Coombes, K. R., Zhang, N., Ruvolo, V. R., Borthakur, G., et al. (2011). Andreeff, and Kornblau, S. M., Low expression of PP2A regulatory subunit B55alpha is associated with T308 phosphorylation of AKT and shorter complete remission duration in acute myeloid leukemia patients. *Leukemia* 25, 1711–1717. doi: 10.1038/leu.2011.146

Sandilands, A., Sutherland, C., Irvine, A. D., and McLean, W. H. (2009). Filaggrin in the frontline: role in skin barrier function and disease. *J. Cell Sci.* 122, 1285–1294. doi: 10.1242/jcs.033969

Schmidt-Ullrich, R., and Paus, R. (2005). Molecular principles of hair follicle induction and morphogenesis. *Bioessays* 27, 247–261. doi: 10.1002/bies.20184

Schmitz, M. H., Held, M., Janssens, V., Hutchins, J. R., Hudecz, O., Ivanova, E., et al. (2010). Live-cell imaging RNAi screen identifies PP2A-B55alpha and importin-beta1 as key mitotic exit regulators in human cells. *Nat. Cell Biol.* 12, 886–893. doi: 10.1038/ncb2092

Sengel, P. (1976). *Morphogenesis of Skin*. Cambridge: Cambridge University Press.

Sennett, R., and Rendl, M. (2012). Mesenchymal–epithelial interactions during hair follicle morphogenesis and cycling. *Semin. Cell Dev. Biol.* 23, 917–927. doi: 10.1016/j.semcdb.2012.08.011

Sim, A. T. R., Collins, E., Mudge, L.-M., and Rostas, J. A. P. (1998). Developmental regulation of protein phosphatase Types 1 and 2A in post-hatch chicken brain. *Neurochem. Res.* 23, 487–491. doi: 10.1023/a:1022422332404

Smart, I. H. (1970). Variation in the plane of cell cleavage during the process of stratification in the mouse epidermis. *Br. J. Dermatol.* 82, 276–282. doi: 10.1111/j.1365-2133.1970.tb12437.x

Smeal, T., Binetruy, B., Mercola, D. A., Birrer, M., and Karin, M. (1991). Oncogenic and transcriptional cooperation with Ha-Ras requires phosphorylation of c-Jun on serines 63 and 73. *Nature* 354, 494–496. doi: 10.1038/354494a0

Smith, A. S., Roberts, K. G., and Verrills, N. M. (2011). "Ser/Thr Phosphatases: the new frontier for myeloid leukemia therapy?," in *Myeloid Leukemia - Basic Mechanisms of Leukemogenesis*, ed. D. S. Koschmieder (Rijeka: InTech), 2011.

Smith, A. M., Roberts, K. G., and Verrills, N. M. (2011). "Ser/Thr Phosphatases: the New Frontier for Myeloid Leukemia Therapy?," in *Myeloid Leukemia - Basic Mechanisms of Leukemogenesis*, eds S. Koschmieder and U. Krug (Rijeka: InTech), 123–148.

Sontag, E., Luangpirom, A., Hladik, C., Mudrak, I., Ogris, E., Speciale, S., et al. (2004). Altered expression levels of the Protein Phosphatase 2A ABαC enzyme are associated with Alzheimer disease pathology. *J. Neuropathol. Exp. Neurol.* 63, 287–301. doi: 10.1093/jnen/63.4.287

Sontag, J. M., and Sontag, E. (2014). Protein phosphatase 2A dysfunction in Alzheimer's disease. *Front. Mol. Neurosci.* 7:16. doi: 10.3389/fnmol.2014.00016

Stamos, J. L., and Weis, W. I. (2013). The β-catenin destruction complex. *Cold Spring Harb. Perspect. Biol.* 5:a007898. doi: 10.1101/cshperspect.a007898

Stepp, M. A. (1999). α9 and β8 integrin expression correlates with the merger of the developing mouse eyelids. *Dev. Dyn.* 214, 216–228. doi: 10.1002/(SICI)1097-0177(199903)214:3$<$216::AID-AJA5$>$3.0.CO;2-4

Stern, C. D. (2005). Neural induction: old problem, new findings, yet more questions. *Development* 132, 2007–2021. doi: 10.1242/dev.01794

Strack, S. (2002). Overexpression of the protein phosphatase 2A regulatory subunit bγ promotes neuronal differentiation by activating the MAP kinase (MAPK) cascade. *J. Biol. Chem.* 277, 41525–41532. doi: 10.1074/jbc.M203767200

Strack, S., Zaucha, J. A., Ebner, F. F., Colbran, R. J., and Wadzinski, B. E. (1998). Brain protein phosphatase 2A: developmental regulation and distinct cellular and subcellular localization by B subunits. *J. Comp. Neurol.* 392, 515–527.

Su, Y., Fu, C., Ishikawa, S., Stella, A., Kojima, M., Shitoh, K., et al. (2008). APC Is Essential for Targeting Phosphorylated beta-Catenin to the SCFbeta-TrCP Ubiquitin Ligase. *Mol. Cell.* 32, 652–661. doi: 10.1016/j.molcel.2008.10.023

Sur, I., Rozell, B., Jaks, V., Bergström, Å, and Toftgård, R. (2006). Epidermal and craniofacial defects in mice overexpressing Klf5 in the basal layer of the epidermis. *J. Cell Sci.* 119, 3593–3601. doi: 10.1242/jcs.03070

Suzuki, K., and Takahashi, K. (2003). Reduced expression of the regulatory A subunit of serine/threonine protein phosphatase 2A in human breast cancer MCF-7 cells. *Int. J. Oncol.* 23, 1263–1268.

Takagi, Y., Futamura, M., Yamaguchi, K., Aoki, S., Takahashi, T., and Saji, S. (2000). Alterations of the PPP2R1B gene located at 11q23 in human colorectal cancers. *Gut* 47, 268–271. doi: 10.1136/gut.47.2.268

Thompson, J. J., and Williams, C. S. (2018). Protein Phosphatase 2A in the regulation of Wnt signaling. *Stem Cells Cancer Genes* 9:121. doi: 10.3390/genes9030121

Tsuruta, D., Kobayashi, H., Imanishi, H., Sugawara, K., Ishii, M., and Jones, J. C. (2008). Laminin-332-integrin interaction: a target for cancer therapy? *Curr. Med. Chem.* 15, 1968–1975. doi: 10.2174/092986708785132834

Varadkar, P., Despres, D., Kraman, M., Lozier, J., Phadke, A., Nagaraju, K., et al. (2014). The protein phosphatase 2A B56gamma regulatory subunit is required for heart development. *Dev. Dyn.* 243, 778–790. doi: 10.1002/dvdy.24111

Wang, F., Zhu, S., Fisher, L. A., Wang, W., Oakley, G. G., Li, C., et al. (2018). Protein interactomes of protein phosphatase 2A B55 regulatory subunits reveal B55-mediated regulation of replication protein A under replication stress. *Sci. Rep.* 8:2683. doi: 10.1038/s41598-018-21040-6

Wang, L., Guo, Q., Fisher, L. A., Liu, D., and Peng, A. (2015). Regulation of polo-like kinase 1 by DNA damage and PP2A/B55alpha. *Cell Cycle* 14, 157–166. doi: 10.4161/15384101.2014.986392

Watt, L. F., Panicker, N., Mannan, A., Copeland, B., Kahl, R. G. S., Dun, M. D., et al. (2017). Functional importance of PP2A regulatory subunit loss in breast cancer. *Breast Cancer Res. Treat.* 166, 117–131. doi: 10.1007/s10549-017-4403-5

Wickstrom, S. A., Radovanac, K., and Fassler, R. (2011). Genetic analyses of integrin signaling. *Cold Spring Harb. Perspect. Biol.* 3:a005116. doi: 10.1101/cshperspect.a005116

Williams, B. C., Filter, J. J., Blake-Hodek, K. A., Wadzinski, B. E., Fuda, N. J., Shalloway, D., et al. (2014). Greatwall-phosphorylated Endosulfine is both an inhibitor and a substrate of PP2A-B55 heterotrimers. *eLife* 3:e01695. doi: 10.7554/eLife.01695

Ybot-Gonzalez, P., Cogram, P., Gerrelli, D., and Copp, A. J. (2002). Sonic hedgehog and the molecular regulation of mouse neural tube closure. *Development* 129, 2507–2517.

Yeo, W., and Gautier, J. (2004). Early neural cell death: dying to become neurons. *Dev. Biol.* 274, 233–244. doi: 10.1016/j.ydbio.2004.07.026

Youssef, G., Gerner, L., Naeem, A. S., Ralph, O., Ono, M., O'Neill, C. A., et al. (2013). Rab3Gap1 mediates exocytosis of Claudin-1 and tight junction formation during epidermal barrier acquisition. *Dev. Biol.* 380, 274–285. doi: 10.1016/j.ydbio.2013.04.034

Zhang, J., Hagopian-Donaldson, S., Serbedzija, G., Elsemore, J., Plehn-Dujowich, D., McMahon, A. P., et al. (1996). Neural tube, skeletal and body wall defects in mice lacking transcription factor AP-2. *Nature* 381, 238–241. doi: 10.1038/381238a0

Zhang, J., Zhi, H. Y., Ding, F., Luo, A. P., and Liu, Z. H. (2005). Transglutaminase 3 expression in C57BL/6J mouse embryo epidermis and the correlation with its differentiation. *Cell Res.* 15, 105–110. doi: 10.1038/sj.cr.7290274

Zhang, W., Yang, J., Liu, Y., Chen, X., Yu, T., Jia, J., et al. (2009). PR55α, a regulatory subunit of PP2A, specifically regulates PP2A-mediated β-Catenin dephosphorylation. *J. Biol. Chem.* 284, 22649–22656. doi: 10.1074/jbc.M109.013698

Zhu, X.-J., Liu, Y., Dai, Z.-M., Zhang, X., Yang, X., Li, Y., et al. (2014). BMP-FGF signaling axis mediates Wnt-induced epidermal stratification in developing mammalian skin. *PLoS Genet.* 10:e1004687. doi: 10.1371/journal.pgen.1004687

Conflict of Interest: The authors declare that the research was conducted in the absence of any commercial or financial relationships that could be construed as a potential conflict of interest.

frontiers in Cell and Developmental Biology

ORIGINAL RESEARCH
published: 16 June 2020
doi: 10.3389/fcell.2020.00493

Telomere Length Measurement by Molecular Combing

Vivian F. S. Kahl[1†], Joshua A. M. Allen[1†], Christopher B. Nelson[1], Alexander P. Sobinoff[1], Michael Lee[1], Tatjana Kilo[2], Raja S. Vasireddy[2] and Hilda A. Pickett[1]*

[1] Telomere Length Regulation Unit, Children's Medical Research Institute, Faculty of Medicine and Health, The University of Sydney, Sydney, NSW, Australia, [2] Department of Hematology, Children's Hospital at Westmead, Sydney Children's Hospitals Network, Sydney, NSW, Australia

Telomeres are repetitive regions of DNA bound by specialized proteins at the termini of linear chromosomes that prevent the natural chromosome ends from being recognized as DNA double strand breaks. Telomeric DNA is gradually eroded with each round of cell division, resulting in the accumulation of critically short or dysfunctional telomeres that eventually trigger cellular senescence. Consequently, telomere length is indicative of the proliferative capacity of a cell. Multiple methods exist to measure telomere length and telomere content, but a simple and reliable technique to accurately measure individual telomere lengths is currently lacking. We have developed the Telomere length Combing Assay (TCA) to measure telomere length on stretched DNA fibers. We used TCA to measure telomere erosion in primary human fibroblasts, and to detect telomere lengthening in response to activation of telomere maintenance pathways. TCA was also used to accurately measure telomere length in healthy individuals, and to identify critically short telomeres in patients with telomere biology disorders. TCA is performed on isolated DNA, negating the need for cycling cells. TCA is amenable to semi-automated image analysis, and can be fully automated using the Genomic Vision molecular combing platform. This not only precludes sampling bias, but also provides the potential for high-throughput applications and clinical development. TCA is a simple and versatile technique to measure the distribution of individual telomere lengths in a cell population, offering improved accuracy, and more detailed biological insight for telomere length measurement applications.

Keywords: telomere, telomere length, senescence, Telomere length Combing Assay, telomerase

OPEN ACCESS

Edited by:
Liz Caldon,
Garvan Institute of Medical Research, Australia

Reviewed by:
Shang Li,
Duke-NUS Medical School, Singapore
Predrag Slijepcevic,
Brunel University London, United Kingdom

****Correspondence:***
Hilda A. Pickett
hpickett@cmri.org.au

† These authors have contributed equally to this work

Specialty section:
This article was submitted to Cell Growth and Division, a section of the journal Frontiers in Cell and Developmental Biology

Received: *14 February 2020*
Accepted: *25 May 2020*
Published: *16 June 2020*

Citation:
Kahl VFS, Allen JAM, Nelson CB, Sobinoff AP, Lee M, Kilo T, Vasireddy RS and Pickett HA (2020) Telomere Length Measurement by Molecular Combing. Front. Cell Dev. Biol. 8:493. doi: 10.3389/fcell.2020.00493

INTRODUCTION

Telomeres are specialized nucleoprotein structures at the ends of linear chromosomes that function to protect the chromosome ends, thereby maintaining the stability of the genome. Telomeric DNA comprises repetitive sequences of the hexanucleotide $TTAGGG_n$ repeat unit, bound in a sequence-specific manner to the protein complex shelterin, and assembled into macromolecular structures called telomere-loops (t-loops; Griffith et al., 1999; Blackburn, 2000; Van Ly et al., 2018). In normal human somatic cells, telomeres range from 5–15 kb in length (Pickett et al., 2011), and telomere length variability exists between individual telomeres and between different cell types. Inter-individual variability is also observed across the human population, superimposed on the well-established age-associated decline in telomere length (Aubert and Lansdorp, 2008).

The negative correlation between telomere length and chronological age is attributed to terminal replication limitations, oxidative damage, and nucleolytic degradation (Harley et al., 1990; Baird, 2008a).

The telomere attrition that accompanies cellular proliferation eventually leads to an accumulation of critically short or unprotected telomeres, which signals the onset of replicative senescence (Hayflick and Moorhead, 1961; Kaul et al., 2012). Senescence provides a barrier to unlimited cellular proliferation, thereby fulfilling a potent tumor suppressive role (Reddel, 2010). In some rare cases, cells are able to bypass replicative senescence by inactivating tumor suppressor pathways, allowing cells to proceed into crisis, which is characterized by catastrophic telomere shortening and widespread genome instability (Reddel, 2010). This process provokes the emergence of cancer cells with tumorigenic advantage. However, oncogenic progression necessitates stabilization of the genome to overcome crisis, which is dependent upon activation of a telomere maintenance mechanism (TMM; Maciejewski and de Lange, 2017). Telomere maintenance is achieved by one of two defined mechanisms. First, activation of the ribonucleoprotein enzyme telomerase, which uses a template sequence embedded within the RNA component of the enzyme to reverse transcribe telomeric sequences directly onto the chromosome termini (Bryan et al., 1998; Reddel, 2014). Second, the Alternative Lengthening of Telomeres (ALT) pathway, which co-opts homology-directed repair mechanisms to drive template-mediated telomere extension (Cesare and Reddel, 2010; Reddel, 2014; Pickett and Reddel, 2015).

Telomerase is also active in the germline, during embryogenesis, and in hematopoietic, stem and rapidly renewing cells, but is suppressed to undetectable levels upon differentiation in human somatic cells. In this capacity, telomerase supports the proliferative requirements of the organism by maintaining telomere length. When telomere length cannot be adequately maintained, highly proliferative tissues become impacted. Telomere biology disorders (TBDs) are a group of diseases caused by germline mutations in genes involved in telomere maintenance and function (Bertuch, 2016). The clinical manifestations of these disorders include bone marrow failure, aplastic anemia, pulmonary fibrosis and acute myeloid leukemia, which are attributed to the premature loss of stem cell populations. TBDs are typically characterized by telomere lengths in the bottom percentile of the normal population, and telomere length measurement is used for the clinical diagnosis of patients, bone marrow donor screening, and to direct effective treatment regimens for bone marrow transplant. Milder deficiencies in telomere length have also been implicated as risk factors in several diseases, including cardiovascular disease, diabetes mellitus, obesity, liver cirrhosis, and cancer (Epel et al., 2004; Sampson and Hughes, 2006; Willeit et al., 2010; Haycock et al., 2014; Opresko and Shay, 2016).

A variety of telomere length measurement methods exist, each with its own strengths and weaknesses. Accuracy and precision are critical for the utility of telomere length measurement in clinical, epidemiological and research studies. Many current measurement techniques provide an average or relative measurement of telomere length or telomere content; however, it is well established that it is the shortest telomeres, rather than average telomere length, that trigger cellular senescence (Hemann et al., 2001; Herbig et al., 2004; Zou et al., 2004; Kaul et al., 2012). Measurement techniques that provide the distribution of telomere lengths in a cell population offer improved and more informative data regarding telomere length dynamics.

Here, we have developed the Telomere length Combing Assay (TCA) as an accurate and robust technique to measure the distribution of telomere lengths in a cell population. TCA involves stretching DNA fibers onto coated glass coverslips using a constant stretching factor (Schurra and Bensimon, 2009). Telomeric DNA is then visualized with telomere-specific PNA probes, and individual telomere lengths are measured manually or using automated software and converted to absolute telomere length measurements according to the stretching factor. We demonstrate that telomere length measurements obtained by TCA are comparable to other widely utilized methods, and that TCA can detect dynamic changes in telomere length. TCA can be used to measure telomere lengths in healthy individuals and can accurately identify TBD patients with critically short telomeres. Finally, we demonstrate that TCA is amenable to semi-automated image analysis through two open-source software platforms and fully automated image analysis using the Genomic Vision molecular combing platform, and can therefore be adapted for high-throughput applications.

MATERIALS AND METHODS

Cell Culture

The cell lines U-2 OS, HeLa, HT1080, HT1080 hTR, and IIICF/c were cultured in Dulbecco's Modified Eagle's Medium (DMEM; Gibco, Paisley, United Kingdom) with 10% fetal bovine serum (FBS) at 37°C in 10% CO_2. MRC-5 cells were cultured similarly, but in 5% CO_2. The CCRF-CEM cell line was cultured in RPMI (Thermo Scientific, Norwood, Australia) with 10% FBS. All cell lines were authenticated by 16-locus short-tandem-repeat profiling and confirmed to be free of mycoplasma contamination by CellBank Australia (Children's Medical Research Institute, Westmead, Australia).

Subjects

Peripheral blood was collected from healthy individuals and clinically referred individuals suspected of having a TBD through the Department of Hematology Telomere Length Testing Facility, Sydney Children's Hospitals Network. Informed consent was obtained from all participating individuals, and the studies were approved by the Human Research Ethics Committee of the Sydney Children's Hospitals Network.

Genomic DNA Extraction

Cells were harvested with 0.05% Trypsin-EDTA (Gibco, Grand Island, United States), washed in PBS and lysed in DNA extraction buffer [100 mM Tris–HCl pH 7.6, 100 mM NaCl, 10 mM EDTA, and 1% (w/v) N-lauroylsarcosine]. Lysates were digested with 50 μg/mL RNase A for 20 min at room

temperature and then with 100 μg/mL proteinase K at 55°C for 12–16 h. DNA was extracted using three rounds of phenol/chloroform/isoamyl alcohol (25:24:1) solution (Sigma-Aldrich, Castle Hill, Australia) in MaXtract High Density tubes (Qiagen, Maryland, United States). DNA from the aqueous phase was then precipitated with 0.1 volume of 3 M sodium acetate pH 5.2 and 2.5 volumes of cold 100% ethanol. Finally, genomic DNA was washed with 70% ethanol, air dried and dissolved in 10 mM Tris–HCl pH 8.0, 1 mM EDTA. All subsequent assays (TCA, TRF, and qPCR) were carried out on the same sample of genomic DNA extracted from U-2 OS, HT1080, HT1080 hTR, HeLa, IIICF/c, and MRC-5 cells to minimize experimental variability.

Whole blood from healthy individuals and TBD patients was collected through venipuncture. For flow-fluorescence *in situ* hybridization (FISH), peripheral mononuclear blood cells (PBMCs) were isolated from whole blood using Histopaque-1077 (Sigma-Aldrich, Castle Hills, Australia) after the blood was homogenized with Hanks Balanced Salt Solution (Sigma-Aldrich, Castle Hills, Australia) to maintain pH and osmotic balance. For qPCR procedures, DNA from the whole blood of healthy individuals and TBD patients was extracted using QIAGEN QIAamp DNA Mini Kit (Qiagen, Maryland, United States) according to the manufacturer's protocol.

Telomere Length Combing Assay (TCA)

A detailed working protocol is provided in the **Supplementary Material** and an overview of the method is shown in **Figure 1**. Briefly, cells were isolated by trypsinization, embedded in agarose plugs (Sigma-Aldrich, Castle Hills, Australia), and subjected to proteinase K (0.5 M EDTA pH 8.0, 10% (v/v) sarcosyl/0.5 M EDTA, and 20 mg/mL proteinase K) digestion at 50°C for 12–16 h. Plugs were dissolved with agarase (Thermo Scientific, Norwood, Australia) for 12–16 h. The DNA solution was then transferred to a reservoir (Genomic Vision, Paris, France). Molecular combing was performed using the FiberComb® Molecular Combing System (Genomic Vision, Paris, France) with a constant stretching factor of 2 kb/μm using vinylsilane coverslips (20 × 20 mm; Genomic Vision, Paris, France), according to the manufacturer's instructions. Quality and integrity of stretched DNA fibers were checked using the YOYO-1™ Iodide counterstain (Thermo Scientific, Norwood, Australia). Combed coverslips were incubated at 60°C for 4 h to minimize photobreaking, followed by serial ethanol dehydration (70–100%). Coverslips were hybridized with telomeric C- or G-rich PNA probe [TAMRA-OO-$(CCCTAA)_3$ or TAMRA-OO-KK$(TTAGGG)_3$] (Panagene, Daejeon, South Korea) in PNA hybridization buffer [70% (v/v) deionized formamide, 0.25% (v/v) NEN blocking reagent (PerkinElmer), 10 mM Tris–HCl (pH 7.5), 4 mM Na_2HPO_4, 0.5 mM citric acid, and 1.25 mM $MgCl_2$] at room temperature for 12–16 h. Coverslips were washed and counterstained with YOYO-1™ Iodide. Telomere fibers were detected on a Zeiss Axio Imager microscope and analyzed using ZEN v2.3 Pro software (Carl Zeiss, North Ryde, Australia).

Terminal Restriction Fragment (TRF)

Terminal restriction fragments were obtained from genomic DNA by complete digestion with the restriction enzymes *Hin*fI and *Rsa*I. TRFs were separated by pulsed-field gel electrophoresis. Gels were dried, denatured and subjected to in-gel hybridization with a γ-[^{32}P]-ATP-labeled $(CCCTAA)_4$ oligonucleotide probe. Gels were washed and the telomeric signal visualized by PhosphorImage analysis (Conomos et al., 2012). TRFs were either visually compared or processed by MultiGauge image analysis software (Fuji Pharma) to quantitate mean telomere length.

Quantitative PCR (qPCR)

Telomere qPCR was performed relative to the single copy gene 36B4 or HBG (Cawthon, 2002; Lee et al., 2014). Results were expressed relative to U-2 OS and presented as relative telomere content (arbitrary units). Experiments were carried out in a Rotor-Gene Q platform (Qiagen, Maryland, United States) and analyzed using Rotor-Gene 6000 series software (Qiagen, Maryland, United States).

Quantitative-Fluorescence *in situ* Hybridization (Q-FISH)

Cells were treated with 10 μg/mL colcemid (Gibco, Grand Island, United States) for 3 h to arrest cells in metaphase, harvested by trypsinization, and resuspended in 75 mM KCl at 37°C for 20 min. Cells were fixed in methanol:acetic acid (3:1), and chromosome spreads were obtained according to standard cytogenetic methods. Microscope slides were subjected to serial ethanol dehydration (70–100%), followed by hybridization with 0.3 μg/mL Alexa-488-OO-$(CCCTAA)_3$ telomeric PNA probe (Panagene, Daejeon, South Korea) at 80°C for 5 min, then at room temperature for 8 h. Slides were washed at 43°C for 5 min with each of the following solutions: 50% formamide in 2xSSC; 2xSSC; and 0.1% Tween-20/2xSSC. Slides were mounted using ProLong™ Gold antifade with DAPI counterstaining (Invitrogen, Norwood, Australia). One hundred and fifty metaphases from each cell line were scored using MetaSystems software (MetaSystems, North Ryde, Australia). Results were shown as mean telomere intensity (arbitrary units × 1000).

Flow-Fluorescence *in situ* Hybridization (Flow-FISH)

Equal numbers (3×10^6) of control CCRF-CEM cells were mixed with experimental cells prior to denaturation and overnight hybridization at room temperature with 0.3 nM FITC-OO-$(CCCTAA)_3$ telomeric PNA probe (Panagene, Daejeon, South Korea). Unstained duplicate tubes were run in parallel to determine autofluorescence. Cells were washed twice (70% formamide, 0.1% Tween-20), once (PBS, 0.1% Tween-20), followed by incubation at 4°C for 3 h with 500 μL of PBS containing 0.1% BSA, RNase A, and DNA binding dye LDS-751 (Santa Cruz Biotech, CA, United States). Data were acquired using FACS-Canto (BD Biosciences, NJ, United States) by acquisition of 1×10^4 cells (with and without PNA probe incubation) to calculate mean fluorescence intensity (FI). Data were analyzed using FACSDiva™ software (BD Biosciences, NJ, United States). Cells were gated to include the tetraploid CCRF-CEM cells. Relative telomere length (RTL) was calculated using the following formula: RTL = (mean FI of experimental cells

with PNA probe) – (mean FI of experimental cells without PNA probe)/(mean FI of CCRF-CEM cells with PNA probe) – (mean FI of CEM cells without PNA probe). Results were shown as RTL.

Semi-Automated Image Analysis for TCA

Two user-friendly semi-automated pipelines were developed using free, open-source platforms for quantification of TCA: CellProfiler v2.2.0 (Jones et al., 2008) and ImageJ v1.8.0 for Windows (NIH, Bethesda, MD, United States). Overall, both pipelines use a similar general approach for semi-automatic detection and size annotation of telomere fiber signals. However, some program-specific adaptations were made to improve the accuracy of telomere fiber identification.

CellProfiler Pipeline

Image manipulation (*tubeness*) was applied to smooth telomere fibers and reduce background. Telomere fibers were subjected to a maximum correlation threshold (MCT) algorithm and selected based on the following parameters: (1) ratio between major and minor axis > 2; (2) eccentricity ≥ 0.75; (3) width > 5 and < 15 pixels; (4) orientation of the major axis of the object is $\pm 15°$ of vertical relative to *X*-axis of the image. Telomere fibers that met the selection criteria were refined further by closing small gaps along the length of the fiber. Finally, telomere fiber identification was manually checked for accuracy and corrected, if necessary, using the manually edit objects function.

ImageJ Pipeline

Prior to telomere identification a separate pipeline was used to create a binary mask of the image for background detection and refinement. This involved applying a series of open shape selector indicators as disk, horizontal lines and the 45° and 145° lines, using the MorphoLibJ plugin (v1.4.1). Next, a *tubeness* processing filter was used to smooth telomere fibers and reduce background. Telomere fibers were then subjected to a user-defined threshold (chosen with a slider bar) and a binary mask was created. Finally, the background mask generated in the first pipeline was subtracted from the newly generated telomere mask image and telomere fibers were further selected by the following parameters: (1) size $> 0.250\ \mu m^2$; (2) circularity from 0 to 0.5. Telomere fibers that met the selection criteria were refined further by closing small gaps along the length of the fiber (MorphoLibJ plugin, v1.4.1).

Automated Image Analysis for TCA Using the Molecular Combing Platform

The FiberVision® scanner (Genomic Vision, Paris, France) was used to acquire multi-color images of the whole surface of combed coverslips. FiberStudio® software (Genomic Vision, Paris, France) was used to detect and measure telomere fiber signals using a custom-designed algorithm. Samples were prepared as described in the Telomere length Combing Assay (TCA) section, with minor modifications. First, coverslips were hybridized with telomeric C-rich PNA probe (Alexa647-OO-$(CCCTAA)_3$; 0.3 μg/mL; Panagene, Daejeon, South Korea). Second, for imaging and analysis purposes, coverslips were mounted in barcoded cartridges (Genomic Vision, Paris, France), and loaded onto the FiberVision® scanner. Third, images were automatically acquired at 40×, imported into FiberStudio® software, and automatically scored. FiberStudio® software allows the scoring to be reviewed, and generates a report containing the telomere length distribution for all regions of interest (ROI).

Statistics

Graphs and statistical analysis were generated using GraphPad Prism v5.04. The two-sided Student's *t*-test was performed on normally distributed data, while the two-sided Mann-Whitney test was performed on data assumed to be non-normally distributed. Linear regression was used to test the correlation between datasets. Further details of statistical analyses are provided in the figures and figure legends.

RESULTS

Molecular Combing Can Be Used to Measure Telomere Length

Molecular combing, or DNA fiber analysis, is a powerful technique used to visualize genomic loci and repetitive sequences in the genome (Parra and Windle, 1993). DNA fiber analysis involves extracting DNA from cells such that the chromatin is deproteinized leaving naked DNA, which is then stretched onto a glass microscope slide. This can be combined with FISH for the detection and measurement of specific genomic sequences (Ersfeld, 1994). More recently, DNA fiber analysis has been used to study replication dynamics by tracking the sequential incorporation of halogenated nucleotides into replicating DNA (Norio and Schildkraut, 2001). This technique has been further adapted to analyze the progression of replication forks through telomeric DNA (Sfeir et al., 2009), as well as for the measurement of telomere extension events (Sobinoff et al., 2017; Lu et al., 2019).

An underexplored application of molecular combing is the direct measurement of telomere length (Wang et al., 2013). More recently, a CRISPR-Cas9 nickase system has been used to label telomere tracts, followed by nanochannel array analysis to measure discrete telomere lengths (McCaffrey et al., 2017). We have developed the TCA to measure the distribution of individual telomere lengths in a cell population. A schematic representation of TCA is presented (**Figure 1A**), and a detailed protocol is provided (**Supplementary Material**). To preserve the integrity of the telomeric DNA and to minimize shearing, cells were embedded in agarose plugs, prior to protein digestion to release the DNA from the chromatin scaffold. The DNA was then solubilized. Vinylsilane treated glass coverslips were submerged in the solution and withdrawn mechanically, allowing the DNA molecules to be stretched at a constant stretching factor of 2 kb/μm. The utilization of a constant stretching factor that is both irrespective of sequence content and DNA fiber length, and uniform across the glass surface (Schurra and Bensimon, 2009), obviates the requirement to normalize the fiber length internally, providing that the stretching dynamics are regularly calibrated. DNA fibers were then hybridized to a telomere-specific PNA probe and subjected to DNA counterstaining. The YOYO-1 counterstain was used to provide additional

information pertaining to the terminal location of the telomere, thus minimizing the inclusion of interstitial repeat arrays or extra-chromosomal telomeric repeats (ECTRs) in the telomere length measurements. Finally, telomere fibers were detected by fluorescence microscopy (**Figure 1B**), and the length of the telomere repeat tracts measured using the associated microscope software, or by automated image analysis (**Figure 1C**). TCA was able to accurately measure telomere lengths in human cells or extracted DNA within a range of <1 kb and >80 kb. TCA is a simple and robust technique to measure the telomere lengths of individual DNA molecules, providing the distribution of telomere lengths in a cell population.

Comparison of TCA With Established Telomere Length Measurement Techniques

Established telomere length measurement techniques have various strengths and limitations (Aubert et al., 2012; Montpetit et al., 2014; Lai et al., 2018), with most techniques providing a relative or average measurement of length or telomere content. TCA overcomes this limitation by measuring individual telomeres. We measured the distribution of telomere lengths by TCA in four different cell lines (**Figure 2A**). These cell lines were selected based on their well-established differences in telomere length and TMM, with HeLa, and HT1080 having short telomeres and utilizing telomerase as the TMM, and IIICF/c and U-2 OS having longer and heterogeneous telomere lengths and utilizing the ALT pathway of telomere maintenance (**Supplementary Table S1**; Lee et al., 2014). TCA demonstrated different telomere length distribution profiles in the four different cell lines. Mean telomere length measurements were 4.55 kb for HeLa (min: 0.96 kb; max: 14.29 kb), 7.60 kb for IIICF/c (min: 0.87 kb; max: 62.09 kb), 36.11 kb for U-2 OS (min: 1.41 kb; max: 145.10 kb), and 6.95 kb for HT1080 (min: 1.82 kb; max: 16.46 kb; **Figure 2A**). Telomere length analysis by TCA further identified the presence of very long (>80 kb) as well as very short (<1 kb) telomere lengths in U-2 OS and IIICF/c cells, consistent with these cell lines utilizing the ALT mechanism of telomere maintenance (**Figure 2A**). This contrasted with the short homogeneous telomere lengths observed in the two telomerase-positive cell lines (HeLa and HT1080).

We then compared TCA to the most commonly utilized telomere length measurement techniques in the same four cell lines (**Figures 2A–E**). TRF analysis is the gold standard telomere length measurement technique employed by molecular biology labs (Kimura et al., 2010; Mender and Shay, 2015). TRF analysis was used to visualize the intensity and size distribution of TRFs (**Figure 2B**), and the mean telomere length from the contributing cell population was estimated from the size of the heterogeneous telomere smear (**Figure 2B**). Quantitative-FISH (Q-FISH) can be applied to interphase or metaphase cells to provide high resolution measurements of individual

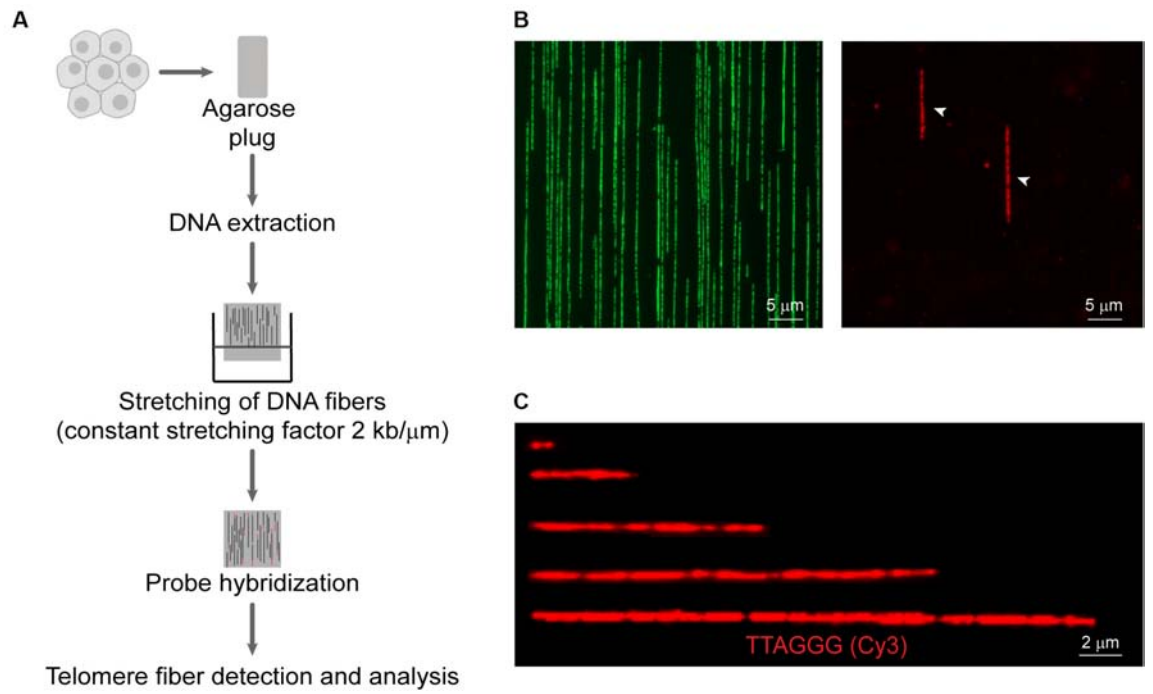

FIGURE 1 | Overview of the Telomere length Combing Assay (TCA). **(A)** Cells are embedded in agarose plugs, prior to protein digestion. High molecular weight DNA is stretched onto vinylsilane coverslips and hybridized with a telomeric PNA probe. Telomeric fibers are then detected and measured. **(B)** Representative images of DNA counterstained by YOYO-1 (left panel) and telomere fibers (right panel). Telomere fibers are indicated by white arrows. Scale bars are 5 μm. **(C)** Examples of telomere fibers. Scale bars are 2 μm.

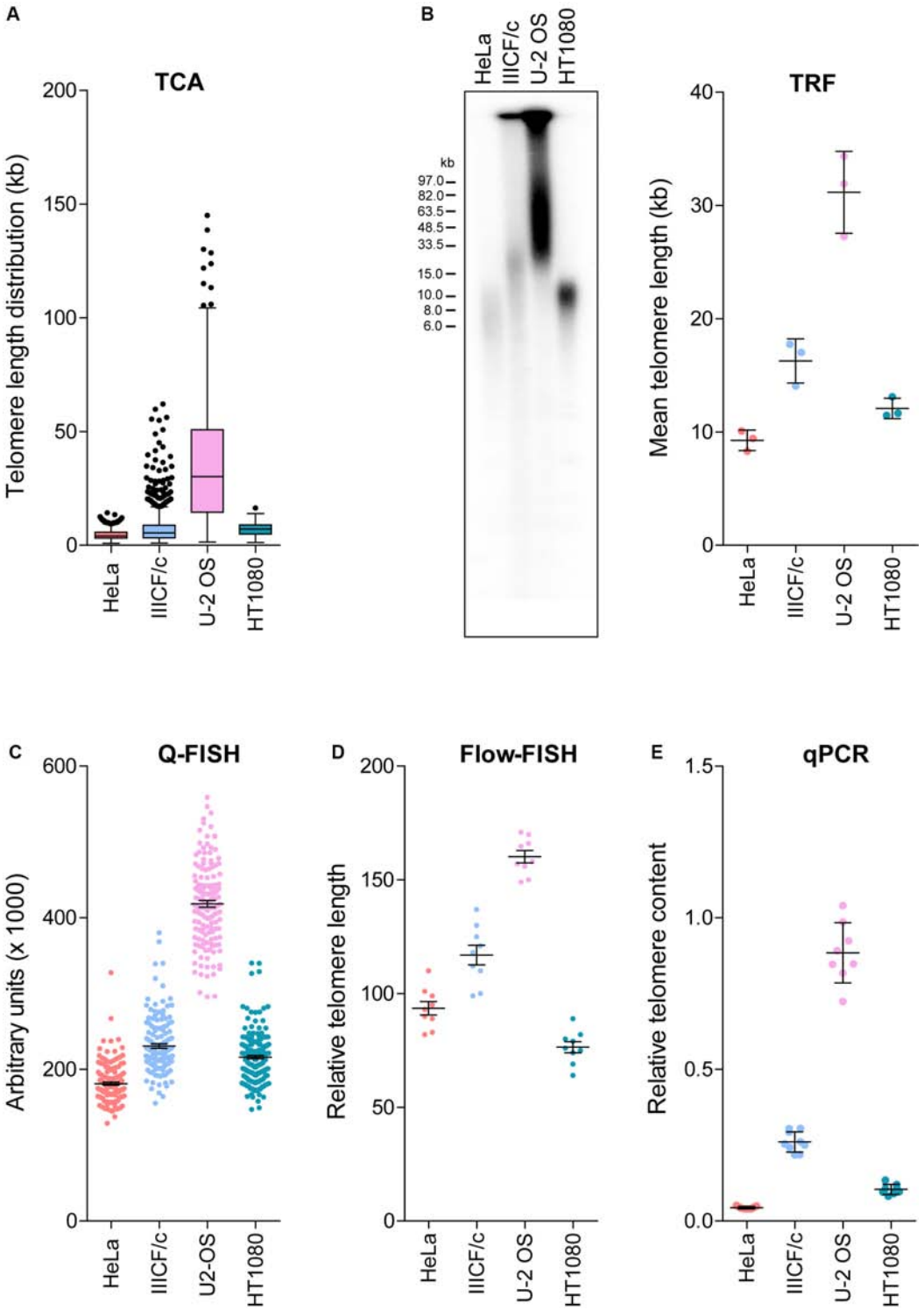

FIGURE 2 | Comparison of telomere length measurement methods. **(A)** Distribution of individual telomere lengths measured by TCA in HeLa (telomerase-positive), IIICF/c (ALT), U-2 OS (ALT) and HT1080 (telomerase-positive) cell lines. Tukey boxplots of median from >450 telomeric fibers from $n = 3$ technical replicates. **(B)** TRF analysis of telomere length (left panel) and mean telomere length quantitated using MultiGauge image analysis software (right panel). Error bars are mean ± SEM from $n = 3$ independent experiments. **(C)** Telomere length measurements by Q-FISH. Results are presented as arbitrary units (×1000). Error bars are mean ± SEM from ≥3,000 telomere signals. **(D)** Telomere length measurements by flow-FISH. Results are presented as relative telomere length (RTL). Error bars are mean ± SEM from $n = 3$ independent experiments with 3 technical replicates each. **(E)** Telomere content analyzed by qPCR relative to the single copy gene 36B4 and normalized to the U-2 OS reference sample. Error bars are mean ± SEM from $n = 3$ independent experiments with 3 technical replicates each.

telomere lengths (Lansdorp et al., 1996; Lai et al., 2018), while flow-FISH has been extensively validated for clinical diagnostic purposes and employs flow cytometry to detect telomere-bound fluorescently labeled probes in individual viable cells (Rufer et al., 1998; **Figures 2C,D**). Quantitative PCR (qPCR) has been broadly adopted for clinical and epidemiological studies, and benefits from its technical simplicity and the requirement for small amounts of DNA, but produces variable results (Cawthon, 2002; Lai et al., 2018). qPCR of amplified telomeric products was compared to a reference single copy gene, to provide a measure of relative telomere content in the four cell lines (**Figure 2E**).

Overall, we found that telomere lengths were comparable across all five techniques (**Figures 2A–E**), with the U-2 OS cell line consistently displaying the longest and most heterogeneous telomere lengths. The HeLa and HT1080 cell lines consistently displayed short telomere lengths. Some variability regarding the cell line with the shortest telomeres was observed, with flow-FISH indicating that HT1080s had the shortest telomere lengths, in contrast to all other methods, which identified HeLa as having the shortest telomeres. Variability in the RTL of the four cell lines was also observed between methods. TCA and Q-FISH were the only techniques employed here that measure individual telomere lengths. The distribution of telomere lengths measured by TCA and Q-FISH were further compared using telomere length frequency histograms, with TCA demonstrating increased resolution of very long telomeres in the two ALT cell lines compared to Q-FISH (**Supplementary Figure S1**). By directly comparing telomere lengths measured by TCA to measurements made using the other methods, the most tightly correlated techniques were TCA and qPCR (R^2 = 0.93), followed by TCA and Q-FISH (R^2 = 0.91), TCA and TRF (R^2 = 0.80), and TCA and flow-FISH (R^2 = 0.78).

We then aimed to determine the accuracy and reproducibility of TCA, and its versatility to different sample preparations. TCA is typically performed on freshly harvested cells embedded in agarose plugs and in-gel protein digestion to minimize DNA shearing, prior to stretching of DNA fibers. We compared embedded cells versus phenol-chloroform extracted DNA from U-2 OS and HeLa cell lines and from the MRC-5 mortal cell strain (**Supplementary Figure S2**). Telomere length measurements were comparable for HeLa and MRC-5 cells, which have short telomere lengths, whilst significant variability in telomere length was observed between the extracted DNA samples compared to the cell preparation samples for U-2 OS cells (**Supplementary Figure S2**). Specifically, telomere length distributions revealed an under-representation of the longest telomeres in U-2 OS cells, indicative of some level of DNA shearing. This suggests that, whilst TCA is a reproducible and versatile technique, the requirement for embedded cells is more critical when analyzing cells with very long telomeres, in contrast to shorter telomeres, which are less sensitive to DNA processing. This is unlikely to be a concern when analyzing human samples, as only ALT cells with extremely long telomeres were significantly impacted by the skewed representation. Overall, these data support the utility of TCA as an accurate and robust technique to measure the distribution of individual telomere lengths in a cell population.

TCA Can Be Used to Measure Dynamic Changes in Telomere Length

Telomere attrition and TMMs contribute to telomere length regulation, and telomere length ultimately dictates the proliferative capacity of a cell. To address whether TCA provides sufficient sensitivity to detect dynamic changes in telomere length, we used three separate cell systems. First, we used primary human fibroblasts that undergo telomere attrition at a rate of 50–150 bp per cell division (Harley et al., 1990), until telomere lengths become critically short and the cell reaches senescence. Cellular senescence is characterized by an absence of mitotic cell division and permanent disengagement from the cell cycle (Reddel, 2000). TCA was used to measure telomere lengths in the MRC-5 mortal human lung fibroblast cell strain at early, mid and late population doublings (PDs; **Figure 3A**). Telomere shortening was observed with increasing PDs. Specifically, early and mid PDs demonstrated mean telomere length measurements of 10.55 kb and 9.32 kb, respectively. The late timepoint (PD 60) corresponded with the approximate onset of cellular senescence (Kaul et al., 2012), and had a mean telomere length of 4.52 kb. This demonstrates the sensitivity of TCA to accurately determine telomere length changes of $\geq$1 kb. Absolute telomere length measurements were used to calculate a rate of attrition of approximately 70 bp/cell division, consistent with normal rates of telomere attrition in cells lacking a TMM. Importantly, TCA is not dependent on mitotic cells for the measurement of individual telomere lengths, allowing senescent cells to be measured by TCA.

Telomere length measurements by TCA were then compared to telomere lengths measured by TRF analysis and by qPCR in MRC-5 cells at early, mid and late PDs (**Figures 3B,C**). All three techniques demonstrated telomere shortening with increasing PD (**Figures 3A–C**); however, the difference in telomere length by TRF was only significant between early and late PD, indicative of the lower sensitivity of TRF analysis to detect dynamic changes in telomere length (**Figure 3B**). Interestingly, absolute telomere length measurements at early and mid-timepoints were similar for TCA and TRF analysis. These two techniques provide a measure of telomere length in kb, although TRFs include variable amounts of subtelomeric regions, dictated by the position of the terminal restriction enzyme site. At the later timepoints telomere lengths appeared shorter when measured by TCA compared to TRF analysis, supporting TCA being the more sensitive technique (**Figures 3A,B**).

Second, we used the previously described HT1080 hTR super-telomerase cell line to measure telomerase-mediated telomere lengthening (Pickett et al., 2009). HT1080 hTR cells that exogenously express hTR display elevated levels of telomerase activity and progressive telomere lengthening over 150 PDs, until telomere lengths plateau (Pickett et al., 2009). TCA identified progressive telomere lengthening in the HT1080 hTR cell line at early (mean telomere length: 11.12 kb) and late (26.59 kb) PDs compared to the parental HT1080 wild-type (5.25 kb) cell line, with the late timepoint corresponding to approximately 90 PDs post stable overexpression of hTR (**Figure 3D**). Telomere lengthening was similarly observed by TRF analysis and by

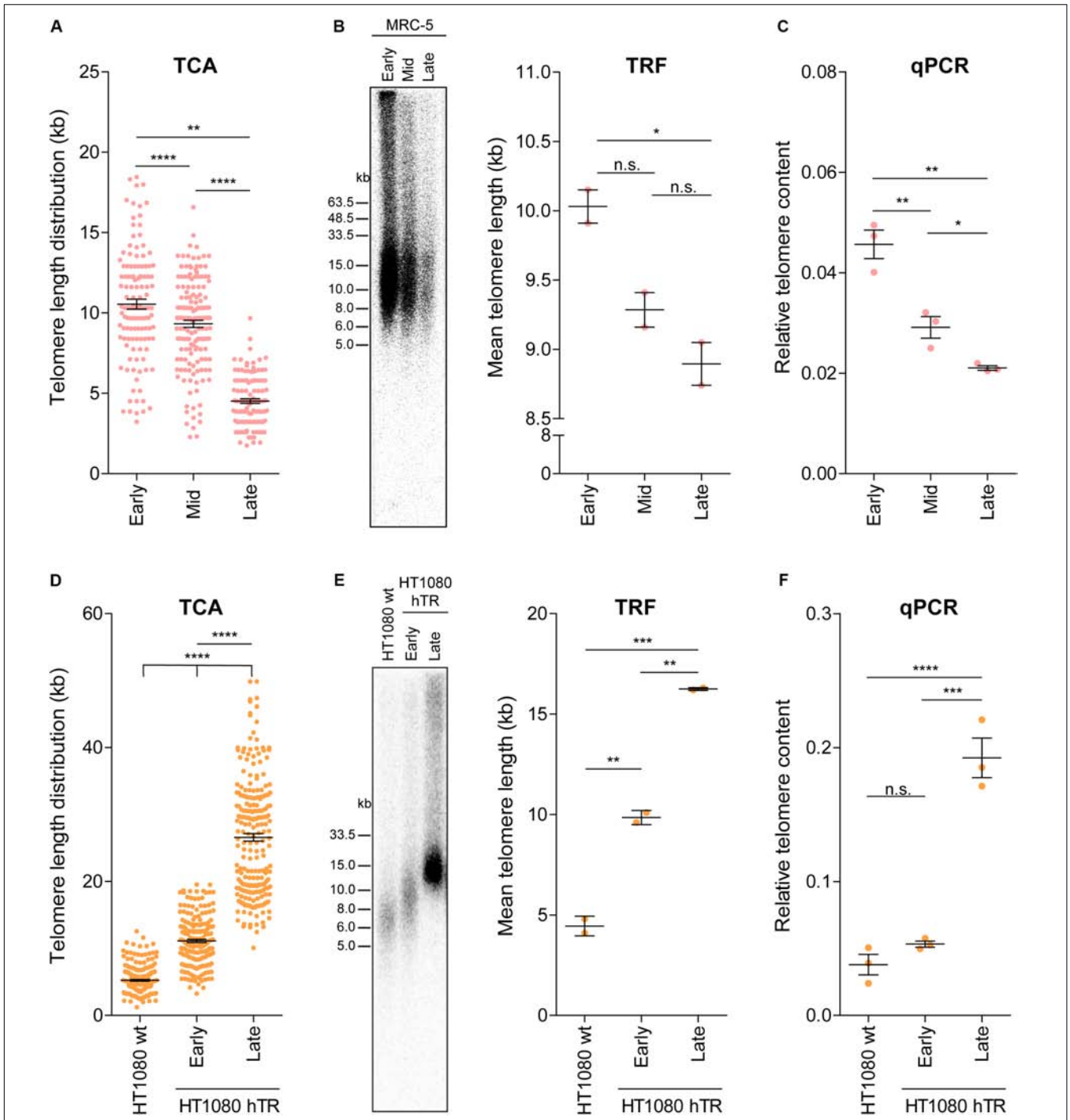

FIGURE 3 | TCA can accurately measure telomere attrition and telomerase-mediated telomere extension. **(A)** Telomere length measurements in MRC-5 fibroblasts at early (20), mid (40), and late (60) population doublings (PDs). Scatterplots showing the distribution of ≥150 individual telomere fiber lengths measured by TCA. Error bars represent the mean ± SEM from $n = 3$ technical replicates, $^{**}p < 0.01$ and $^{****}p < 0.0001$. Student's t-test. **(B)** TRF analysis (left panel) and quantitation using MultiGauge image analysis software (right panel). Error bars represent the mean ± SEM from $n = 2$ technical replicates, $^{*}p < 0.05$ and n.s. $p > 0.05$. Student's t-test. **(C)** Telomere content analyzed by qPCR relative to the single copy gene 36B4 and normalized to the U-2 OS reference sample. Error bars represent the mean ± SEM from $n = 3$ technical replicates, $^{*}p < 0.05$ and $^{**}p < 0.01$. Student's t-test. **(D)** Telomere length measurements in HT1080 wild type (wt) and HT1080 hTR at early (10) and late (90) PDs. Scatterplots showing the distribution of ≥150 individual telomeric fiber lengths measured by TCA. Error bars represent the mean ± SEM from $n = 3$ technical replicates, $^{****}p < 0.0001$. Student's t-test. **(E)** TRF analysis (left panel) and quantitation using MultiGauge image analysis software (right panel). Error bars represent the mean ± SEM from $n = 2$ technical replicates, $^{**}p < 0.01$ and $^{***}p < 0.001$. Student's t-test. **(F)** Telomere content analyzed by qPCR relative to the single copy gene 36B4 and normalized to the U-2 OS reference sample. Error bars represent the mean ± SEM from $n = 3$ technical replicates, $^{***}p < 0.001$, $^{****}p < 0.0001$, and n.s. $p > 0.05$. Student's t-test.

qPCR (**Figures 3E,F**). TCA was able to provide a more detailed distribution profile of telomere lengths than the telomere length measurements obtained by TRF and qPCR analysis. This was most striking at the later timepoints when telomere lengths were longer and more heterogeneous (**Figure 3D**).

Third, we used TCA to measure the telomere length changes that occur in ALT cells in response to manipulation of SLX4 and BLM levels (Sobinoff et al., 2017). Specifically, we used SLX4 overexpression to promote resolution of telomere recombination intermediates, thereby causing telomere shortening, and BLM overexpression to promote ALT-mediated telomere extension (Sobinoff et al., 2017). Telomere length distribution profiles obtained by TCA demonstrated telomere shortening in response to SLX4 overexpression, and telomere lengthening in response to BLM overexpression in IIICF/c (mean telomere lengths: empty vector: 14.24 kb; BLM + : 20.77; and SLX4 + : 10.92), and U-2 OS (empty vector: 22.73 kb; BLM + : 25.91; and SLX4 + : 12.30) ALT cell lines, but not in HT1080 hTR telomerase-positive cells (empty vector: 10.05 kb; BLM + : 10.92; and SLX4 + : 10.79; **Supplementary Figure S3**), consistent with previous reports (Sobinoff et al., 2017). Notably, TCA was able to provide more precise measurements of the distribution of individual telomere lengths, identifying a striking decrease in long telomeres in the SLX4 overexpressing cells, and a noticeable increase in very long telomeres in the BLM overexpressing cells (**Supplementary Figure S3**). Overall, these data demonstrate that TCA can accurately measure dynamic changes in telomere length, including normal telomere attrition in primary human cells, and both telomerase- and ALT-mediated telomere extension in cancer cells.

TCA Can Be Used to Measure Telomere Length in the Human Population

Telomere length decreases with advancing age and is considered a biomarker of chronological aging. Nevertheless, inter-individual telomere lengths at any given age are highly variable in the human population (Harley et al., 1990; Aubert and Lansdorp, 2008). To determine whether TCA can detect age-associated decline in telomere length, we accessed DNA extracted from peripheral blood mononuclear cells (PBMCs) from twelve healthy individuals spanning ages 4 to 75 years of age, collected as part of a cohort of 240 healthy individuals used to obtain normal telomere length percentiles for different ages through the Department of Hematology Telomere Length Testing Facility, Sydney Children's Hospitals Network, Australia. TCA provided a distribution of telomere lengths for each individual, demonstrating an overall decrease in telomere length with chronological age (**Figure 4A**).

Telomere biology disorders are premature aging diseases caused by abnormally short telomeres, with lengths typically falling below the bottom percentile of the normal healthy population. The clinical characteristics of TBDs are diverse, but patients frequently develop bone marrow failure and idiopathic pulmonary fibrosis (Mangaonkar and Patnaik, 2018). Telomere length analysis is used to identify individuals suspected of having TBDs, but can also provide prognostic information regarding disease onset and clinical manifestations, as well as directing treatment regimens (Alder et al., 2018). We used TCA to measure the telomere lengths of five individuals (ages 1, 1.5, 14, 45, and 48 years old) that had previously been diagnosed with TBDs, using DNA extracted from PBMCs. TCA analysis showed that these individuals all had strikingly short telomere length distribution profiles, and that their mean telomere lengths were substantially shorter than those of healthy individuals (**Figure 4A**).

We then compared telomere length measurements by TCA to telomere lengths measured by flow-FISH and qPCR for the healthy individuals and the TBD patients. Normal telomere length percentiles for the cohort of 240 healthy individuals were included for the flow-FISH and qPCR datasets (**Figures 4B,C**). Telomere lengths for the healthy individuals were somewhat variable across the three different techniques, but an overall decline in telomere length with chronological age was always observed (**Figures 4A–C**). TCA correlated well with qPCR (R^2 = 0.77), but not as well with flow-FISH (R^2 = 0.52), for this specific dataset (**Figure 4D**). This is consistent with previous reports that indicate variable correlations between different telomere length measurement methods (Khincha et al., 2017). All three techniques identified the TBD patients as having abnormally short telomeres (**Figures 4A–C**), falling below the tenth percentile of the healthy cohort. These data demonstrate that TCA can be used to measure telomere lengths in PBMCs from healthy individuals. Importantly, TCA can reliably identify patients with critically short telomere lengths, supporting a potential practical application for TCA in the diagnosis and treatment of TBDs.

Software Automation for TCA Quantification

Detection and measurement of telomere fibers was performed manually using image manipulation tools. Each technical replicate generated an average of 300 individual telomere fibers to be scored. In order to adapt TCA for high-throughput applications, we developed pipelines for the semi-automated detection and size annotation of telomere lengths using the open-source image processing platforms CellProfiler and ImageJ, and we evaluated fully automated telomere length measurement using FiberStudio® automated analysis and reporting software, in collaboration with Genomic Vision (France).

The detection and analysis pipelines for CellProfiler and ImageJ are presented (**Supplementary Figures S4A,B**). Tubeness processing allows both CellProfiler and ImageJ algorithms to close small gaps along the identified telomeric fiber. Both CellProfiler and ImageJ provide an optional step for the user to check and modify identified fibers. This was employed here to validate the pipelines. Cell Profiler and ImageJ pipelines require manual imaging of the telomere fibers through microscope tiling image manipulation tools and are, therefore, semi-automated pipelines. In contrast, the FiberVision® scanner automatically images the slide, and custom-designed FiberStudio® software detects, quantifies, and annotates the telomere fibers, providing a fully automated platform.

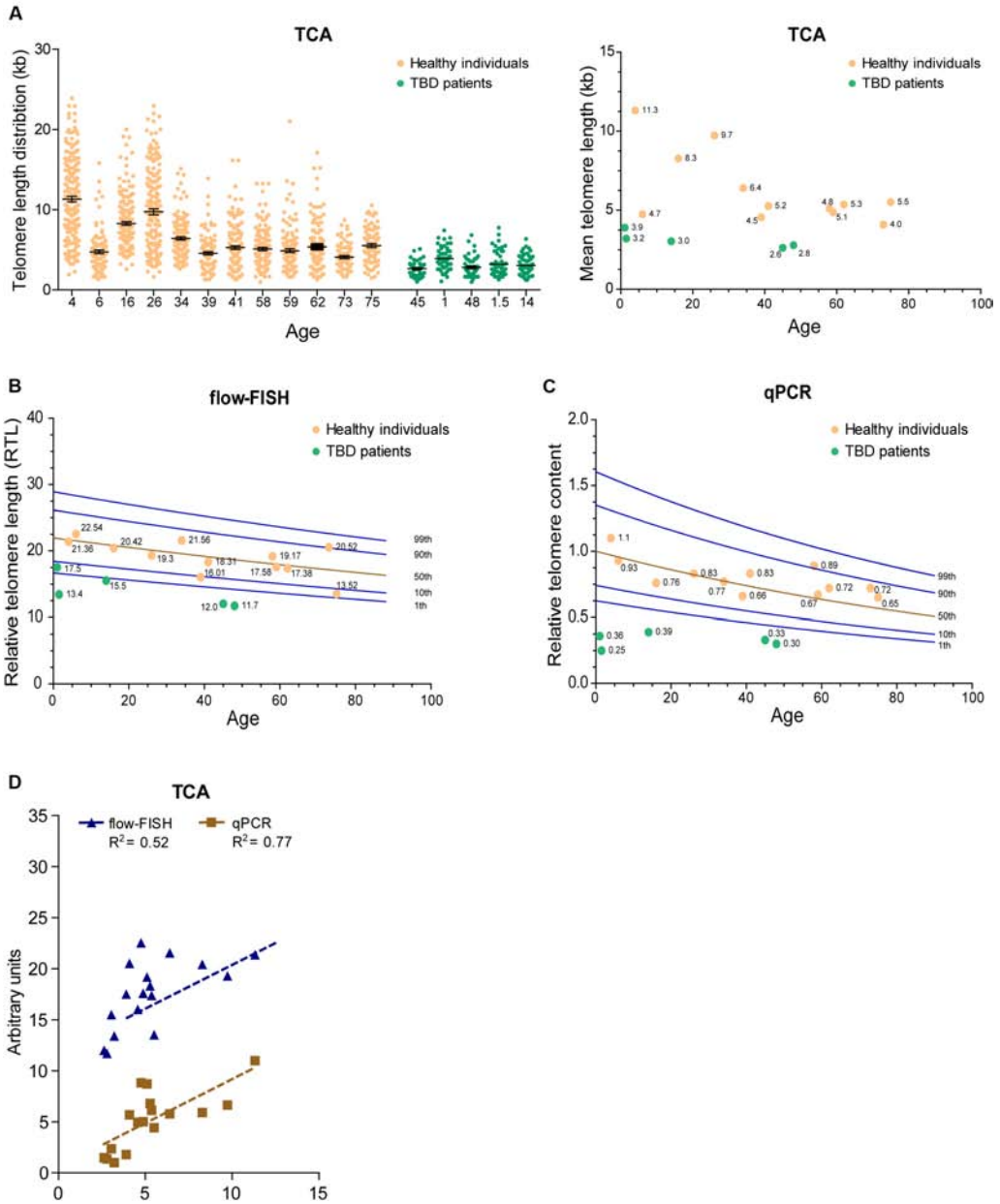

FIGURE 4 | TCA can be used to measure telomere length in the human population. **(A)** Telomere length measurements in twelve healthy individuals spanning ages 4 to 75 years and five TBD patients. Scatterplots showing the distribution of ≥150 individual telomeric fiber lengths measured by TCA. Error bars are mean ± SEM from $n = 2$ technical replicates (left panel). Mean telomere length determined by TCA plotted against age for healthy individuals and TBD patients. Annotated numbers indicate mean telomere length (kb; right panel). **(B)** RTL measured by flow-FISH plotted against age for healthy individuals and TBD patients. Lines indicate the 1st, 10th, 50th, 90th, and 99th telomere length percentiles from a cohort of 240 normal controls. **(C)** Telomere content analyzed by qPCR. Ratio between telomere content and single copy gene HBG plotted against age for healthy individuals and TBD patients. Lines indicate the 1st, 10th, 50th, 90th, and 99th telomere length percentiles from a cohort of 240 normal controls. **(D)** Linear regression of TCA against flow-FISH ($R^2 = 0.52$) and qPCR ($R^2 = 0.77$) for healthy individuals and TBD patients. Spearman correlation test.

While differences in image manipulation and telomere signal detection exist between the two semi-automated programs, both CellProfiler and ImageJ performed similarly, and produced comparable measurements of mean telomere fiber length to the measurements obtained from manual analysis in the HeLa, IIICF/c, U-2 OS, and HT1080 cell lines (**Figure 5**). FiberStudio® also demonstrated accuracy in measuring telomere lengths from HeLa, IIICF/c, U-2 OS, and HT1080 cell lines when compared to manual scoring (**Figure 5**).

To demonstrate the accuracy of TCA, we measured the same fifty fibers from HeLa cells three separate times. Measurements were made manually, and each replicate

was scored independently. Telomere length measurements demonstrated a very high level of accuracy between replicates (**Supplementary Figure S5A**).

Finally, to determine the potential utility of automated TCA analysis, we directly compared the lengths of fifty telomere fibers from HeLa cells measured manually to the lengths of the same fifty telomere fibers measured using CellProfiler, ImageJ, and FiberStudio®. The individual telomere length measurements obtained by manual assessment correlated similarly with those obtained using CellProfiler (R^2 = 0.80) and ImageJ (R^2 = 0.81), and correlated slightly better with measurements obtained using FiberStudio® (R^2 = 0.84; **Supplementary Figure S5B**). These results demonstrate that TCA is suitable for both semi-automated and fully automated image analysis. The successful application of CellProfiler, ImageJ, and FiberStudio® to the detection and accurate measurement of telomere fibers, with high correlation to manual measurements, demonstrates the utility of these programs in providing an unbiased approach for the detection and measurement of individual telomere fibers, with potential high-throughput capabilities.

DISCUSSION

We have developed TCA as a simple and accessible method to accurately measure the distribution of individual telomere lengths in a cell population. TCA involves stretching DNA fibers onto coated glass coverslips using a constant stretching factor. This achieves unbiased and uniform stretching of millions of DNA molecules, which can then be probed with telomere-specific PNA probes for the detection and measurement of individual telomere lengths. The major strengths of TCA are its simplicity, adaptability to image automation for high-throughput purposes,

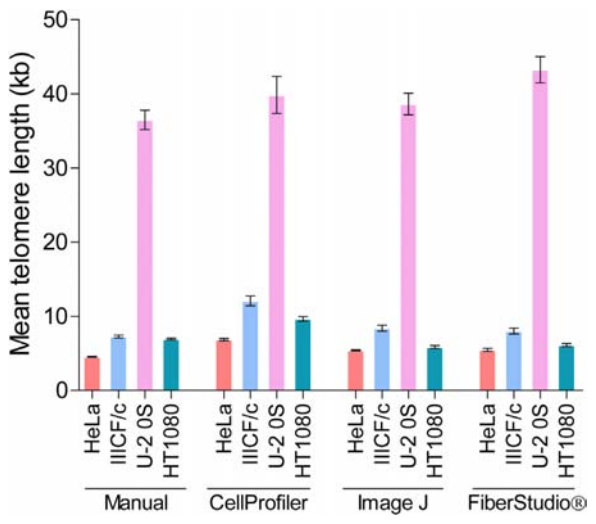

FIGURE 5 | Mean telomere length (kb) measured by TCA in HeLa, IIICF/c, U-2 OS, and HT1080 cell lines using manual measurement tools compared to the CellProfiler and ImageJ semi-automated image analysis pipelines and to FiberStudio® automated software.

lack of requirement for cycling cells, and ability to accurately detect all telomere lengths in a cell population, including very short (<1 kb), and very long (>80 kb) telomeres. The main limitations of TCA are that it is relatively time-consuming and expensive (approximately twice the cost of flow-FISH), and relies on specialized molecular combing equipment and consumables.

By directly comparing TCA to other widely utilized telomere length measurement techniques (TRF, Q-FISH, flow-FISH, and qPCR), we demonstrated that TCA is sensitive and accurate for telomere detection and length measurement. TCA provides important and relevant information regarding the distribution of individual telomere lengths in a cell population. This is not achievable using current methods, which include TRF for molecular research, flow-FISH for clinical telomere length measurement applications and the diagnosis of TBDs, and qPCR for large-scale clinical and epidemiological applications. Other techniques, including Single TElomere Length Analysis (STELA), universal STELA (U-STELA; Bendix et al., 2010), and Telomere Shortest Length Assay (TeSLA; Lai et al., 2017), are able to detect individual telomere lengths, but include a PCR step that precludes the amplification and detection of very long telomeres, and are somewhat limited by their technical complexity (Lai et al., 2017, 2018).

TCA is versatile and can be applied reliably to both freshly harvested cells and extracted DNA, although the use of agarose-embedded cells is preferable for the measurement of very long telomeres to prevent shearing through mechanical manipulation. The requirement for isolated DNA as the starting material means that telomere length measurements by TCA are not dependent on cycling cells, in contrast to flow-FISH and Q-FISH methods. This is particularly important for the analysis of cells with a low mitotic index or cells approaching or at senescence (Kaul et al., 2012). In addition, the removal of nucleosomes by protease digestion leaves the DNA naked and amenable for stretching. This means that telomere length measurements are not affected by aberrant chromatin compaction that has the propensity to influence the binding of telomere FISH probes (Bandaria et al., 2016; Timashev et al., 2017; Vancevska et al., 2017).

TCA provides absolute measurements of individual telomere lengths, rather than an estimate of RTL or content. The telomere length distribution profile is representative of the range of telomere lengths in the cell population, and absolute measurements provide precise information regarding telomere length. In this study, we were able to measure telomere lengths as short as 0.87 kb and as long as 145.1 kb. The proportion of very short or very long telomeres in a cell population is biologically relevant (Aubert and Lansdorp, 2008; Baird, 2008a,b; Muntoni et al., 2009; Stanley and Armanios, 2015), but is typically not considered in clinical, epidemiological and research-based investigations. TCA provides the means to interrogate telomere length associations in far more detail than currently achievable.

TCA is sufficiently sensitive to detect dynamic changes in telomere length. Specifically, we measured telomere attrition in primary human fibroblasts, telomere lengthening in response to increased telomere maintenance by telomerase or ALT, and telomere shortening following the inhibition of telomere maintenance by ALT. TCA provided additional biological insight

into these processes by uncovering the changes that occurred at the telomere length extremes, as well as identifying the overall shift in individual telomere length distribution profiles. The sensitivity of TCA to detect these intricacies will provide a more complete understanding of how telomere length drives replicative senescence and tumorigenic escape, as well as how inhibition of TMM pathways impacts telomere length and cell proliferation.

Telomere length measurements are increasingly being used as an indicator of lifetime health, to assess risk of many age-associated diseases, and to diagnose TBDs (Epel et al., 2004; Sampson and Hughes, 2006; Willeit et al., 2010; Haycock et al., 2014; Bertuch, 2016; Opresko and Shay, 2016; Khincha et al., 2017; Maciejewski and de Lange, 2017; Alder et al., 2018; Mangaonkar and Patnaik, 2018). We demonstrated that TCA can be used to measure age-associated telomere length in PBMCs isolated from healthy individuals spanning over 70 years and can accurately detect short telomeres in patients with TBDs. Interestingly, the telomere length distribution profiles obtained from patients with TBDs were very distinctive, showing very short and homogeneous telomere lengths. This supports the utility of TCA as an improved telomere length measurement technique for clinical testing and diagnosis.

We also demonstrated that TCA is readily amenable to automated image analysis. Specifically, we implemented two open-source software pipelines using CellProfiler and ImageJ, to semi-automatically measure the manually imaged TCA samples from HeLa, IIICF/c, U-2 OS, and HT1080 cell lines. Both pipelines were comparable to manual scoring. We then compared fully automated TCA using the FiberVision® automated scanner and accompanying custom-designed FiberStudio® software, and demonstrated an even higher correlation to manual scoring. Importantly, automation precludes bias and subjectivity, and enables rapid and accurate analysis of extensive datasets.

In summary, TCA is a simple and precise method for the measurement of telomere length. TCA has the potential to supersede currently available methods by fulfilling several advantages. First, TCA measurements provide additional relevant biological insight by measuring the distribution of individual telomere lengths, including both telomere length extremes. Second, TCA is versatile in terms of the sample preparation and starting material required. Third, TCA is adaptable to automated image analysis, which precludes bias and will facilitate high-throughput applications. TCA may be further improved by the inclusion of subtelomeric probes to enable the measurement of chromosome-specific telomeres, and the combined use of variant telomere repeat probes as an indicator of telomere directionality and integrity. Automated TCA represents an exciting and promising telomere length measurement technique for clinical and research applications.

DATA AVAILABILITY STATEMENT

All datasets generated for this study are included in the article/**Supplementary Material**.

ETHICS STATEMENT

The studies involving human participants were reviewed and approved by Human Research Ethics Committee of the Sydney Children's Hospitals Network. Written informed consent to participate in this study was provided by the participants' legal guardian/next of kin.

AUTHOR CONTRIBUTIONS

HP, JA, and VK conceived the idea and designed the experiments. VK, JA, CN, AS, ML, TK, and RV performed the experiments and analyzed the data. HP and VK wrote the manuscript. All authors contributed to the manuscript and approved the submitted version.

FUNDING

This work was supported by the National Health and Medical Research Council Australia (1162886 to HP), Cancer Australia (1160171 to VK and 1099299 to AS), and Cancer Institute of New South Wales (ECF171269 to AS).

ACKNOWLEDGMENTS

The authors would like to acknowledge their collaboration with Genomic Vision, Bagneux, France. Telomere qPCR and microscopy were performed in the ACRF Telomere Analysis Centre, supported by the Australian Cancer Research Foundation and the Ian Potter Foundation.

SUPPLEMENTARY MATERIAL

The Supplementary Material for this article can be found online at: https://www.frontiersin.org/articles/10.3389/fcell.2020.00493/full#supplementary-material

REFERENCES

Alder, J. K., Hanumanthu, V. S., Strong, M. A., DeZern, A. E., Stanley, S. E., Takemoto, C. M., et al. (2018). Diagnostic utility of telomere length testing in a hospital-based setting. *Proc. Natl. Acad. Sci. U.S.A.* 115, E2358–E2365. doi: 10.1073/pnas.1720427115

Aubert, G., Hills, M., and Lansdorp, P. M. (2012). Telomere length measurement-caveats and a critical assessment of the available technologies and tools. *Mutat. Res.* 730, 59–67. doi: 10.1016/j.mrfmmmm.2011.04.003

Aubert, G., and Lansdorp, P. M. (2008). Telomeres and aging. *Physiol. Rev.* 88, 557–579. doi: 10.1152/physrev.00026.2007

Baird, D. M. (2008a). Mechanisms of telomeric instability. *Cytogenet. Genome Res.* 122, 308–314. doi: 10.1159/000167817

Baird, D. M. (2008b). Telomere dynamics in human cells. *Biochimie* 90, 116–121. doi: 10.1016/j.biochi.2007.08.003

Bandaria, J. N., Qin, P., Berk, V., Chu, S., and Yildiz, A. (2016). Shelterin protects chromosome ends by compacting telomeric chromatin. *Cell* 164, 735–746. doi: 10.1016/j.cell.2016.01.036

Bendix, L., Horn, P. B., Jensen, U. B., Rubelj, I., and Kolvraa, S. (2010). The load of short telomeres, estimated by a new method, Universal STELA, correlates with number of senescent cells. *Aging Cell* 9, 383–397. doi: 10.1111/j.1474-9726.2010.00568.x

Bertuch, A. A. (2016). The molecular genetics of the telomere biology disorders. *RNA Biol.* 13, 696–706. doi: 10.1080/15476286.2015.1094596

Blackburn, E. H. (2000). Telomere states and cell fates. *Nature* 408, 53–56. doi: 10.1038/35040500

Bryan, T. M., Englezou, A., Dunham, M. A., and Reddel, R. R. (1998). Telomere length dynamics in telomerase-positive immortal human cell populations. *Exp. Cell Res.* 239, 370–378. doi: 10.1006/excr.1997.3907

Cawthon, R. M. (2002). Telomere measurement by quantitative PCR. *Nucleic Acids Res.* 30:e47. doi: 10.1093/nar/30.10.e47

Cesare, A. J., and Reddel, R. R. (2010). Alternative lengthening of telomeres: models, mechanisms and implications. *Nat. Rev. Genet.* 11, 319–330. doi: 10.1038/nrg2763

Conomos, D., Stutz, M. D., Hills, M., Neumann, A. A., Bryan, T. M., Reddel, R. R., et al. (2012). Variant repeats are interspersed throughout the telomeres and recruit nuclear receptors in ALT cells. *J. Cell Biol.* 199, 893–906. doi: 10.1083/jcb.201207189

Epel, E. S., Blackburn, E. H., Lin, J., Dhabhar, F. S., Adler, N. E., Morrow, J. D., et al. (2004). Accelerated telomere shortening in response to life stress. *Proc. Natl. Acad. Sci. U.S.A.* 101, 17312–17315. doi: 10.1073/pnas.0407162101

Ersfeld, K. (1994). "Fiber-FISH: fluorescence in situ hybridization on stretched DNA," in *Parasite Genomics Protocols. Methods in Molecular Biology™*, ed. S. E. Melville (Totowa, NJ: Humana Press), 395–402. doi: 10.1385/1-59259-793-9:395

Griffith, J. D., Comeau, L., Rosenfield, S., Stansel, R. M., Bianchi, A., Moss, H., et al. (1999). Mammalian telomeres end in a large duplex loop. *Cell* 97, 503–514. doi: 10.1016/s0092-8674(00)80760-6

Harley, C. B., Futcher, A. B., and Greider, C. W. (1990). Telomeres shorten during ageing of human fibroblasts. *Nature* 345, 458–460. doi: 10.1038/345458a0

Haycock, P. C., Heydon, E. E., Kaptoge, S., Butterworth, A. S., Thompson, A., and Willeit, P. (2014). Leucocyte telomere length and risk of cardiovascular disease: systematic review and meta-analysis. *BMJ* 349:g4227. doi: 10.1136/bmj.g4227

Hayflick, L., and Moorhead, P. S. (1961). The serial cultivation of human diploid cell strains. *Exp. Cell Res.* 25, 585–621. doi: 10.106/0014-4827(61)90192-6

Hemann, M. T., Strong, M. A., Hao, L. Y., and Greider, C. W. (2001). The shortest telomere, not average telomere length, is critical for cell viability and chromosome stability. *Cell* 107, 67–77. doi: 10.1016/s0092-8674(01)00504-9

Herbig, U., Jobling, W. A., Chen, B. P., Chen, D. J., and Sedivy, J. M. (2004). Telomere shortening triggers senescence of human cells through a pathway involving ATM, p53, and p21(CIP1), but Not p16INK4A. *Mol. Cell* 14, 501–513. doi: 10.1016/s1097-2765(04)00256-4

Jones, T. R., Kang, I. H., Wheeler, D. B., Lindquist, R. A., Papallo, A., Sabatini, D. M., et al. (2008). CellProfiler Analyst: data exploration and analysis software for complex image-based screens. *BMC Bioinformatics* 9:16. doi: 10.1186/1471-2105-9-482

Kaul, Z., Cesare, A. J., Huschtscha, L. I., Neumann, A. A., and Reddel, R. R. (2012). Five dysfunctional telomeres predict onset of senescence in human cells. *EMBO Rep.* 13, 52–59. doi: 10.1038/embor.2011.227

Khincha, P. P., Dagnall, C. L., Hicks, B., Jones, K., Aviv, A., Kimura, M., et al. (2017). Correlation of leukocyte telomere length measurement methods in patients with Dyskeratosis Congenita and in their unaffected relatives. *Int. J. Mol. Sci.* 18:E1765. doi: 10.3390/ijms18081765

Kimura, M., Stone, R. C., Hunt, S. C., Skurnick, J., Lu, X., Cao, X., et al. (2010). Measurement of telomere length by the Southern blot analysis of terminal restriction fragment lengths. *Nat. Protoc.* 5, 1596–1607. doi: 10.1038/nprot.2010.124

Lai, T. P., Wright, W. E., and Shay, J. W. (2018). Comparison of telomere length measurement methods. *Philos. Trans. R. Soc. Lond. B. Biol. Sci.* 373:20160451. doi: 10.1098/rstb.2016.0451

Lai, T. P., Zhang, N., Noh, J., Mender, I., Tedone, E., Huang, E., et al. (2017). A method for measuring the distribution of the shortest telomeres in cells and tissues. *Nat. Comm.* 8:1356. doi: 10.1038/s41467-017-01291-z

Lansdorp, P. M., Verwoerd, N. P., van de Rijke, F. M., Dragowska, V., Little, M. T., Dirks, R. W., et al. (1996). Heterogeneity in telomere length of human chromosomes. *Hum. Mol. Genet.* 5, 685–691. doi: 10.1093/hmg/5.5.685

Lee, M., Hills, M., Conomos, D., Stutz, M. D., Dagg, R. A., Lau, L. M., et al. (2014). Telomere extension by telomerase and ALT generates variant repeats by mechanistically distinct processes. *Nucleic Acids Res.* 42, 1733–1736. doi: 10.1093/nar/gkt1117

Lu, R., O'Rourke, J. J., Sobinoff, A. P., Allen, J. A. M., Nelson, C. B., Tomlinsom, C. G., et al. (2019). The FANCM-BLM-TOP3A-RMI complex suppresses alternative lengthening of telomeres (ALT). *Nat. Comm.* 10:2252. doi: 10.1038/s41467-019-10180-6

Maciejewski, J., and de Lange, T. (2017). Telomeres in cancer: tumour supression and genome instability. *Nat. Rev. Mol. Cell Biol.* 18, 175–186. doi: 10.1038/nrm.2016.171

Mangaonkar, A. A., and Patnaik, M. M. (2018). Short telomere syndromes in clinical practice: bridging bench and bedside. *Mayo Clin. Proc.* 93, 904–916. doi: 10.1016/j.mayocp.2018.03.020

McCaffrey, J., Young, E., Lassahn, K., Sibert, J., Pastor, S., Riethman, H., et al. (2017). High-throughput single-molecule telomere characterization. *Genome Res.* 27, 1904–1915. doi: 10.1101/gr.222422.117

Mender, I., and Shay, J. (2015). Telomere restriction fragment (TRF) analysis. *Bio Protoc.* 5:e1658. doi: 10.21769/bioprotocol.1658

Montpetit, A. J., Alhareeri, A. A., Montpetit, M., Starkweather, A. R., Elmore, L. W., Filler, K., et al. (2014). Telomere length: a review of methods for measurement. *Nurs. Res.* 63, 289–299. doi: 10.1097/NNR.0000000000000037

Muntoni, A., Neumann, A. A., Hills, M., and Reddel, R. R. (2009). Telomere elongation involves intra-molecular DNA replication in cells utilizing alternative lengthening of telomeres. *Hum. Mol. Genet.* 18, 1017–1027. doi: 10.1093/hmg/ddn436

Norio, P., and Schildkraut, C. L. (2001). Visualization of DNA replication on individual Epstein-Barr virus episomes. *Science* 294, 2361–2364. doi: 10.1126/scienc.1064603

Opresko, P. L., and Shay, J. W. (2016). Telomere-associated aging disorders. *Ageing Res. Rev.* 33, 52–66. doi: 10.1016/j.arr.2016.05.009

Parra, I., and Windle, B. (1993). High resolution visual mapping of stretched DNA by fluorescent hybridization. *Nat. Genet.* 5, 17–21. doi: 10.1038/ng0993-17

Pickett, H. A., Cesare, A. J., Johnstone, R. L., Neumann, A. A., and Reddel, R. R. (2009). Control of telomere length by a trimming mechanism that involves generation of t-circles. *EMBO J.* 28, 799–809. doi: 10.1038/emboj.2009.42

Pickett, H. A., Henson, J. D., Au, A. Y., Neumann, A. A., and Reddel, R. R. (2011). Normal mammalian cells negatively regulate telomere length by telomere trimming. *Hum. Mol. Genet.* 20, 4684–4692. doi: 10.1093/hmg/ddr402

Pickett, H. A., and Reddel, R. R. (2015). Molecular mechanisms of activity and derepression of alternative lengthening of telomeres. *Nat. Struct. Mol. Biol.* 22, 875–880. doi: 10.1038/nsmb.3106

Reddel, R. R. (2000). The role of senescence and immortalization in carcinogenesis. *Carcinogenesis* 21, 477–484. doi: 10.1093/carcin/21.3.477

Reddel, R. R. (2010). Senescence: an antiviral defense that is tumor suppressive. *Carcinogenesis* 31, 19–26. doi: 10.1093/carcin/bgp274

Reddel, R. R. (2014). Telomere maintenance mechanisms in cancer: clinical implications. *Curr. Pharm. Des.* 20, 6361–6374. doi: 10.2174/1381612820666140630101047

Rufer, N., Dragowska, W., Thornbury, G., Roosnek, E., and Lansdorp, P. M. (1998). Telomere length dynamics in human lymphocyte subpopulations measured by flow cytometry. *Nat. Biotechnol.* 16, 743–747. doi: 10.1038/nbt0898-743

Sampson, M. J., and Hughes, D. A. (2006). Chromosomal telomere attrition as a mechanism for the increased risk of epithelial cancers and senescent phenotypes in type 2 diabetes. *Diabetologia* 49, 1726–1731. doi: 10.1007/s00125-006-032-4

Schurra, C., and Bensimon, A. (2009). Combing genomic DNA for structural and functional studies. *Methods Mol. Biol.* 464, 71–90. doi: 10.1007/978-1-60327-461-6_5

Sfeir, A., Kosiyatrakul, S. T., Hockemeyer, D., MacRae, S. L., Karlseder, J., Schildkraut, C. L., et al. (2009). Mammalian telomeres resemble fragile sites and require TRF1 for efficient replication. *Cell* 138, 90–103. doi: 10.106/j.cell.2009.06.021

Sobinoff, A. P., Allen, J. A., Neumann, A. A., Yang, S. F., Walsh, M. E., Henson, J. D., et al. (2017). BLM and SLX4 play opposing roles in recombination-dependent replication at human telomeres. *EMBO J.* 36, 2907–2919. doi: 10.15252/embj.201796889

Stanley, S. E., and Armanios, M. (2015). The short and long telomere syndromes: paired paradigms for molecular medicine. *Curr. Opin. Genet. Dev.* 33, 1–9. doi: 10.1016/j.gde.2015.06.004

Timashev, L. A., Babcock, H., Zhuang, X., and de Lange, T. (2017). The DDR at telomeres lacking intact shelterin does not require substantial chromatin decompaction. *Genes Dev.* 31:11. doi: 10.1101/gad.294108.116

Van Ly, D., Low, R. R. J., Frolich, S., Bartolec, T. K., Kafer, G. R., Pickett, H. A., et al. (2018). Telomere loop dynamics in chromosome end protection. *Mol. Cell.* 71, 510.e6–525.e6. doi: 10.1016/j.molcel.2018.06.025

Vancevska, A., Douglas, K. M., Pfeiffer, V., Manley, S., and Lingner, J. (2017). The telomeric DNA damage response occurs in the absence of chromation decompaction. *Genes Dev.* 31:10. doi: 10.1101/gad.294082.116

Wang, K. Z., Zhang, W., Jiang, Y., and Zhang, T. (2013). Systematic application of DNA fiber-FISH technique in cotton. *PLoS One* 8:e75674. doi: 10.1371/journal.pone.0075674

Willeit, P., Willeit, J., Mayr, A., Weger, S., Oberhollenzer, F., Brandstatter, A., et al. (2010). Telomere length and risk of incident cancer and cancer mortality. *JAMA* 304, 69–75. doi: 10.1001/jama.2010.897

Zou, Y., Sfeir, A., Shay, J. W., and Wright, W. E. (2004). Does a sentinel or a subset of short telomeres determine replicative senescence? *Mol. Biol. Cell* 15, 3709–3718. doi: 10.1091/mbc.e04-03-0207

Conflict of Interest: The authors declare that the research was conducted in the absence of any commercial or financial relationships that could be construed as a potential conflict of interest.

frontiers in Cell and Developmental Biology

ORIGINAL RESEARCH
published: 03 July 2020
doi: 10.3389/fcell.2020.00568

rDNA Chromatin Activity Status as a Biomarker of Sensitivity to the RNA Polymerase I Transcription Inhibitor CX-5461

Jinbae Son[1,2], Katherine M. Hannan[3,4], Gretchen Poortinga[1,2,5], Nadine Hein[3], Donald P. Cameron[3], Austen R. D. Ganley[6], Karen E. Sheppard[1,2,4], Richard B. Pearson[1,2,4,7], Ross D. Hannan[1,2,3,4,7,8]† and Elaine Sanij[1,2,9]*†*

[1] Peter MacCallum Cancer Centre, Melbourne, VIC, Australia, [2] Sir Peter MacCallum Department of Oncology, The University of Melbourne, Parkville, VIC, Australia, [3] ACRF Department of Cancer Biology and Therapeutics, The John Curtin School of Medical Research, Australian National University, Canberra, ACT, Australia, [4] Department of Biochemistry and Molecular Biology, The University of Melbourne, Parkville, VIC, Australia, [5] Department of Medicine, St. Vincent's Hospital, The University of Melbourne, Parkville, VIC, Australia, [6] School of Biological Sciences, The University of Auckland, Auckland, New Zealand, [7] Department of Biochemistry and Molecular Biology, Monash University, Clayton, VIC, Australia, [8] School of Biomedical Sciences, The University of Queensland, Brisbane, QLD, Australia, [9] Department of Clinical Pathology, The University of Melbourne, Parkville, VIC, Australia

OPEN ACCESS

Edited by:
Andrew Burgess, Anzac Research Institute, Australia

Reviewed by:
Tom Moss, Laval University, Canada
Wenbing Xie, Johns Hopkins Medicine, United States
Jaclyn Elizabeth Quin, Stockholm University, Sweden

***Correspondence:**
Ross D. Hannan
ross.hannan@anu.edu.au
Elaine Sanij
elaine.sanij@petermac.org

† These authors have contributed equally to this work

Specialty section:
This article was submitted to Cell Growth and Division, a section of the journal Frontiers in Cell and Developmental Biology

Received: *16 December 2019*
Accepted: *15 June 2020*
Published: *03 July 2020*

Citation:
Son J, Hannan KM, Poortinga G, Hein N, Cameron DP, Ganley ARD, Sheppard KE, Pearson RB, Hannan RD and Sanij E (2020) rDNA Chromatin Activity Status as a Biomarker of Sensitivity to the RNA Polymerase I Transcription Inhibitor CX-5461. Front. Cell Dev. Biol. 8:568. doi: 10.3389/fcell.2020.00568

Hyperactivation of RNA polymerase I (Pol I) transcription of ribosomal RNA (rRNA) genes (rDNA) is a key determinant of growth and proliferation and a consistent feature of cancer cells. We have demonstrated that inhibition of rDNA transcription by the Pol I transcription inhibitor CX-5461 selectively kills tumor cells *in vivo*. Moreover, the first-in human trial of CX-5461 has demonstrated CX-5461 is well-tolerated in patients and has single-agent anti-tumor activity in hematologic malignancies. However, the mechanisms underlying tumor cell sensitivity to CX-5461 remain unclear. Understanding these mechanisms is crucial for the development of predictive biomarkers of response that can be utilized for stratifying patients who may benefit from CX-5461. The rDNA repeats exist in four different and dynamic chromatin states: inactive rDNA can be either methylated silent or unmethylated pseudo-silent; while active rDNA repeats are described as either transcriptionally competent but non-transcribed or actively transcribed, depending on the level of rDNA promoter methylation, loading of the essential rDNA chromatin remodeler UBF and histone marks status. In addition, the number of rDNA repeats per human cell can reach hundreds of copies. Here, we tested the hypothesis that the number and/or chromatin status of the rDNA repeats, is a critical determinant of tumor cell sensitivity to Pol I therapy. We systematically examined a panel of ovarian cancer (OVCA) cell lines to identify rDNA chromatin associated biomarkers that might predict sensitivity to CX-5461. We demonstrated that an increased proportion of active to inactive rDNA repeats, independent of rDNA copy number, determines OVCA cell line sensitivity to CX-5461. Further, using zinc finger nuclease genome editing we identified that reducing rDNA copy number leads to an increase in the proportion of active rDNA repeats and confers sensitivity to CX-5461 but also induces genome-wide instability and sensitivity to DNA damage. We propose that the proportion of active to

inactive rDNA repeats may serve as a biomarker to identify cancer patients who will benefit from CX-5461 therapy in future clinical trials. The data also reinforces the notion that rDNA instability is a threat to genomic integrity and cellular homeostasis.

Keywords: RNA polymerase I, CX-5461, ovarian cancer, DNA damage response, rDNA copy number

INTRODUCTION

Transcription of the rDNA repeats by Pol I within the nucleoli is a critical step in ribosome biogenesis and accounts for over 60% of all cellular transcription (Warner, 1999; Moss and Stefanovsky, 2002; Moss et al., 2007). The rDNA encodes the 47S pre-rRNA precursor of the 18S, 5.8S, and 28S rRNAs, which together with 5S rRNA constitute the RNA component of ribosomes. The rDNA is organized into large blocks of tandem repeats, with 400–600 repeats divided among the five pairs of acrocentric chromosomes in the human genome (Stults et al., 2009). Modulation of transcriptional rates can be achieved by regulating Pol I transcription initiation, elongation, and/or processing of the 47S rRNA precursor (Stefanovsky et al., 2001; Schneider, 2012; Goodfellow and Zomerdijk, 2013; Hung et al., 2017). Remarkably, only a fraction of the rDNA repeats are actively transcribed at any one time, providing an additional layer of regulation with transcription output being determined at two levels: the active copy number in combination with the rate of transcription per rDNA repeat (Sanij et al., 2008; Zentner et al., 2011; Hamdane et al., 2014). However, the majority of short-term regulation affects rDNA transcription rate through changing the rate of transcription from active genes, reviewed in McStay and Grummt (2008), Sanij and Hannan (2009), Goodfellow and Zomerdijk (2013). In mammalian cells, the rDNA chromatin can exist in active or inactive states (**Figure 1A**) [reviewed in Sanij and Hannan (2009), Hamperl et al. (2013), Poortinga et al. (2014), Moss et al. (2019), Potapova and Gerton (2019), Warmerdam and Wolthuis (2019)]. Active rDNA repeats are defined as open/accessible chromatin structures, bound by the upstream binding factor (UBF), which is essential for decondensing rDNA chromatin and determining the active rDNA state (Sanij et al., 2008; Hamdane et al., 2014). Active repeats can be either transcriptionally active or transcriptionally competent but non-transcribed, depending on cell cycle phase, cellular signaling, nutrient availability and/or stress stimuli (Schneider, 2012; Xie et al., 2012; Goodfellow and Zomerdijk, 2013; Zhao et al., 2016; Hung et al., 2017). Inhibition of Pol I transcription by loss of the initiation factor RRN3 or upon treatment with the selective inhibitor CX-5461 has no effect on UBF binding nor the proportion of active to inactive rDNA ratio (Quin et al., 2016; Herdman et al., 2017). Thus, UBF binding, not transcription, establishes the active rDNA fraction consistent with (Moss et al., 2019). Inactive rDNA repeats, which lack UBF binding, can be CpG methylated at the rDNA promoter and stably silenced, or non-methylated and hence be in a "pseudo-silent" state (Sanij et al., 2008; Sanij and Hannan, 2009; Hamperl et al., 2013). UBF binding/release is critical for the conversion between active/inactive rDNA repeats, termed rDNA class switching (Sanij et al., 2008; Hamdane et al., 2014; Diesch et al., 2019).

Dysregulated rDNA transcription is linked to a diverse range of human disorders including cancer (Hannan K.M. et al., 2013; Valori et al., 2020). This link is underscored by the modulation of rDNA transcription and rDNA silencing during differentiation and tumorigenesis (Conconi et al., 1989; Sanij et al., 2008; Grummt and Langst, 2013; Hamperl et al., 2013; Hayashi et al., 2014; Savic et al., 2014; Woolnough et al., 2016; Diesch et al., 2019; Prakash et al., 2019). Increased rDNA transcription is a well-known hallmark of cancer. We have shown that a high rDNA transcription rate is required for the oncogene MYC to drive transformation (Chan et al., 2011; Bywater et al., 2012). Thus, rather than being a housekeeping process, rDNA transcription is a key driver of oncogenesis (Hein et al., 2013). Interestingly, variation in the number of rDNA repeats has also been associated with cancer (Stults et al., 2009). This variation in copy number is due to the tandem arrangement of the rDNA rendering it susceptible to recombination, which can result in rDNA instability, such as the loss and gain of rDNA copies. Intriguingly, spontaneous alterations in rDNA organization were over 100-fold elevated in cells lacking Bloom Syndrome protein, a RECQ helicase involved in homologous recombination (HR) DNA repair, and 10-fold elevated in cells lacking ATM (ataxia-telangiectasia, mutated) compared with wild-type controls (Killen et al., 2009). These rDNA alteration phenotypes seem to correlate with the increased cancer predisposition reported in Bloom syndrome and ataxia-telangiectasia patients (Killen et al., 2009). These results suggest that rDNA instability may mediate the predisposition for cancer progression. It has been proposed that reduction of rDNA silencing and rDNA instability underpin global genomic instability, and that this can drive the etiology and progression of cancer (Diesch et al., 2014; Wang and Lemos, 2017; Xu B. et al., 2017; Udugama et al., 2018; Valori et al., 2019). Nevertheless, it appears that increased rRNA production can be achieved even if the rDNA copy number is reduced (Wang and Lemos, 2017), which can occur by regulating the rate of Pol I transcription per rDNA repeat and/or the number of active rDNA repeats.

Pol I transcription is a therapeutic target for small anti-cancer drugs (Bywater et al., 2012; Hein et al., 2013; Peltonen et al., 2014). The first-in-class Pol I transcription inhibitor, CX-5461 is a promising cancer therapy as a single agent and in combination therapy in pre-clinical models of lymphoma, acute myeloid leukemia, prostate and ovarian cancer (Bywater et al., 2012; Devlin et al., 2016; Rebello et al., 2016; Hein et al., 2017; Yan et al., 2019; Sanij et al., 2020). Recently, the sensitivity profile of CX-5461 was shown to closely resemble a topoisomerase II (TOP2) poison (Olivieri et al., 2019; Bruno et al., 2020). TOP2a is an essential component of the Pol I pre-initiation complex (Ray et al., 2013) and while CX-5461 demonstrates highly selective

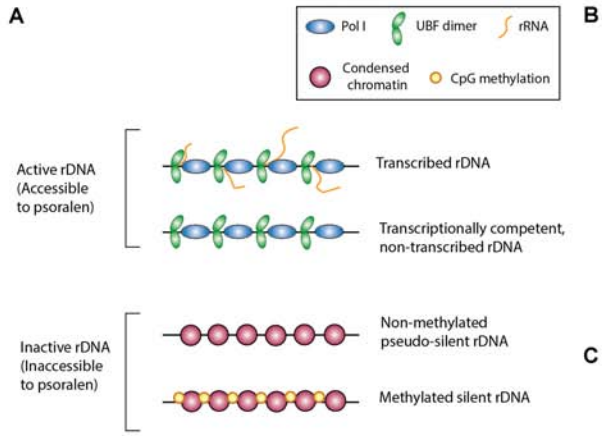

B

Term	Definition
rDNA dosage	rDNA copy number
Proportion of active rDNA	% of active rDNA repeats
Active rDNA dosage	Number of active rDNA repeats
Inactive rDNA dosage	Number of inactive rDNA repeats
Basal rDNA transcription rate (Sanij et al., 2020)	rDNA transcrption rate of exponentially growing cells
rDNA transcription rate per active rDNA	Rate of rDNA transcription normalised to active rDNA dosage
CX-5461 GI50 (Sanij et al., 2020)	CX-5461 dose that induced a 50% reduction in cell proliferation after 48h treatment

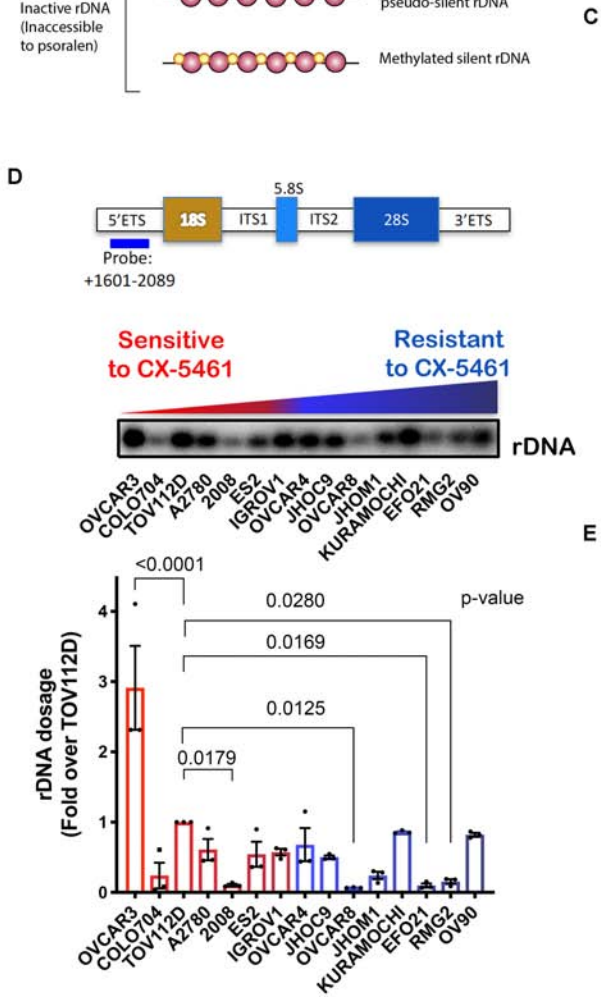

FIGURE 1 | (A) Schematic of the rDNA chromatin states. **(B)** A summary of the rDNA activity parameters assessed in this study. **(C)** Basal rDNA transcription rates of OVCA cell lines was reported in Sanij et al. (2020). We have re-used the data under the Creative Commons Attribution 4.0 International License [http://creativecommons.org/licenses/by/4.0/]. 47S rRNA levels were determined in exponentially growing OVCA cell lines by qRT-PCR analysis using the ETS2 primers (**Supplementary Table S3**) specific to the external transcribed spacer 5'ETS. Expression levels in each cell line were normalized to Vimentin mRNA and expressed as fold change relative to TOV112D cells. Each dot represents the mean value of $n = 3$ biologically independent experiments per cell line (Individual data points are provided in Sanij et al., 2020). Error bars represent mean ± SD. Statistical analysis was performed using a two-tailed unpaired *t* test. **(D)** OVCA cell lines display a range of rDNA content. Top panel, a schematic of the transcribed region of the rDNA repeat detailing the position of the probe used for Southern blotting and a representative Southern blot of gDNA from 15 OVCA cell lines, ordered by increasing GI50 values of CX-5461 as reported in Sanij et al. (2020). gDNA was isolated from 10^6 cells and Southern blotting for rDNA performed and quantitated using ImageQuant pTL software (GE Healthcare). Graph represents rDNA dosage expressed as fold over that for TOV112D; $n = 3$; mean ± SEM. CX-5461-sensitive cell lines are indicated in red and resistant cell lines are in blue. Statistical analysis was performed using two-sided one-way ANOVA Dunnett's multiple comparisons test. **(E)** Correlation analysis of rDNA dosage and sensitivity to CX-5461 (GI50) in 15 OVCA cell lines using GraphPad Prism. Error bars represent mean ± SD. Pearson's r is -0.16, NS (not significant) denotes p-value > 0.05; Spearman's rho is −0.29, NS (not significant) denotes p-value > 0.05.

inhibition of Pol I transcription initiation, it is possible that it does so, in part, by trapping TOP2a at the rDNA repeats. Importantly, our first-in-human trial of CX-5461 in patients with advanced hematological cancers established on-target efficacy in targeting Pol I transcription and demonstrated single-agent anti-tumor activity in p53 wildtype and p53-mutant hematologic malignancies (Khot et al., 2019). CX-5461 is also in Phase I clinical trial in solid tumors and has shown preliminary activity in patients with HR deficiency tumors (Xu H. et al., 2017; Hilton et al., 2020). In order to maximize the clinical impact and success of CX-5461, it is crucial to identify biomarkers of response to enable patient stratification.

CX-5461 induces the p53-dependent "nucleolar stress response" (Bywater et al., 2012; Devlin et al., 2016; Pelletier et al., 2018) and a p53-independent checkpoint induced by targeted activation of the DNA-damage response (DDR) upon the induction of chromatin defects and replication stress at the rRNA genes (Quin et al., 2016; Sanij et al., 2020). Activation of each checkpoint results in different cellular phenotypes depending on cell type and cellular context (Yan et al., 2017; Sanij et al., 2020). The nucleolar stress response results in p53-mediated G1/S arrest and apoptosis, with apoptosis being the major response in MYC-driven lymphoma. The p53-independent checkpoint results in S and G2/M phase cell cycle arrest and is the predominant phenotype of solid tumor cells (Quin et al., 2016; Sanij et al., 2020). CX-5461 has been shown to activate ATM/ATR (ataxia telangiectasia and RAD3 related) signaling and a G2/M cell cycle checkpoint in ovarian cancer (OVCA) cells with differential sensitivities observed across a panel of 32 OVCA cell lines (Sanij et al., 2020). OVCA cell lines with higher rates of Pol I transcription are more sensitive to CX-5461 (Sanij et al., 2020). Thus, rDNA copy number and rDNA chromatin status may function as biomarkers of response to inhibition of Pol I transcription.

Here we investigated whether alterations in rDNA copy number and changes in the proportion of active to inactive rDNA repeats correlate with sensitivity to CX-5461 across a panel of OVCA cell lines. We found that an increase in the proportion of active rDNA repeats correlates with increased OVCA cell sensitivity to CX-5461. Further, deleting rDNA copies led to an increase in the proportion of active rDNA repeats, which also correlated with increased sensitivity to CX-5461 and genome-wide instability. Therefore, we propose that an increased fraction of active rDNA repeats is a potential biomarker of response to CX-5461 therapy. Our data also demonstrates that deleting rDNA copies is associated with increased sensitivity to DNA damage highlighting the strong interplay between rDNA and genome-wide instability.

MATERIALS AND METHODS

Cell Culture

Individuality and the identity of OVCA cell lines (listed in **Supplementary Tables S1, S2**) were confirmed by a PCR-based short tandem repeat (STR) analysis using six STR loci. Cell lines were maintained in culture (**Supplementary Table S1**) for a maximum of 8–10 weeks. CX-5461 was purchased from Synkinase and 10 mM stocks were prepared in 50 mM NaH_2PO_4. Proliferation time course and growth curves for the OVCA cell lines were obtained by assessing cell confluency using the Incucyte ZOOM (Essen Instruments) imaging system. Doubling time for each cell line was calculated using non-linear fit of exponential growth using GraphPad prism software.

47S rRNA Expression

For 47S rRNA expression analysis, cells were lysed, RNA extracted, and first-strand cDNA synthesized using random hexamer primers and Superscript III (Invitrogen). Quantitative reverse transcription PCR (qRT-PCR) was performed in triplicate using FAST SYBR Green on the StepOnePlus real-time PCR system (Applied Biosystems, United States). Primer sequences are listed in **Supplementary Table S3**. Measurement of baseline (basal) rDNA transcription rates of exponentially growing OVCA cell lines was reported in Sanij et al. (2020), determined by qRT-PCR analysis using primers specific to the external transcribed spacer 5'ETS (ETS2). Expression levels in each cell line were normalized to Vimentin mRNA and expressed as fold change relative to TOV112D cells. The mean and standard error of the mean (SEM) values of $n = 3$ biologically independent experiments per cell line were utilized in this study.

ZFN Gene Editing

Zinc Finger Nucleases (ZFNs) induce double strand DNA breaks (DSBs) at a specific target region, recognized by a zinc finger DNA-binding domain fused with DNA-cleavage domain Gaj et al. (2013). TOV112D cells were transduced with Lentiviruses expressing empty vector or co-transduced with two ZFN targeting rDNA sequences (**Supplementary Figure S1**) followed by selection with puromycin for 5 days, then FACS to generate clonal cell lines.

Measurement of rDNA Copy Number

qPCR analysis of 100 ng of genomic DNA (gDNA) was performed in triplicate using FAST SYBR Green on the StepOnePlus real-time PCR system (Applied Biosystems, United States). Primer sequences are listed in **Supplementary Table S3**. Changes in abundance were to normalized to corresponding Vimentin levels as a single copy locus control and expressed as fold change relative to TOV112D by $2(^{-\Delta\Delta CT})$.

For quantification using Southern blotting, gDNA was isolated from 10^6 cells, digested with *Sal*I, and separated on a 0.9% agarose gel, and alkaline southern blotting was performed. rDNA was visualized using a ^{32}P (Amersham)-labeled probe (+1601-2089 base pair relative to transcription start site) within the 5'ETS (external transcribed spacer) region of rDNA and binding detected using a Phosphorimager (GE Healthcare). Signal quantitation was performed using ImageQuant (TLv2005.04; GE Healthcare).

Psoralen Cross-Linking Assay

Cells were lysed in 10 mM Tris–HCl, pH 7.4, 10 mM NaCl, 3 mM $MgCl_2$, and 0.5% NP-40, and nuclei were pelleted, resuspended

in 50 mM Tris–HCl, pH 8.3, 40% glycerol, 5 mM $MgCl_2$, and 0.1 mM EDTA, and irradiated in the presence of 4,5,8′-trimethylpsoralen (Sigma-Aldrich) with a 366 nm UV light box at a distance of 6 cm (Conconi et al., 1989). 200 μg/ml psoralen was added at 1:20 dilution every 4 min for a total irradiation time of 20 min. gDNA was isolated, digested with *Sal*I, and separated on a 0.9% agarose gel, and alkaline Southern blotting was performed. To reverse psoralen cross-linking, filters were treated with 254 nm UV at 1,875 × 100 μJ/cm^2 using a UV cross-linker (Stratalinker 2400; Agilent Technologies). The membrane was then hybridized to a purified ^{32}P (Amersham)-labeled rDNA probe (+ 1601-2089), visualized by scanning on a PhosphoImager (GE Healthcare), and quantitated using ImageQuant (TLv2005.04; GE Healthcare).

Chromatin-Immunoprecipitation (ChIP)

Chromatin-immunoprecipitation was performed as described previously (Poortinga et al., 2004; Sanij et al., 2008). Cross-linking was achieved with 0.6% formaldehyde and assays performed using 10^6 cells per IP. For all ChIPs, 8 μl of sera was used per IP. Samples were analyzed in triplicate using the FAST SYBR green dye on the StepOnePlus real- time PCR system (Applied Biosystems). To calculate the percentage of total DNA bound, unprecipitated input samples from each condition were used as a reference for all qPCR reactions. Primer sequences are listed in **Supplementary Table S3**.

Immunofluorescence (IF)

Cells were fixed in 4% paraformaldehyde (10 min at room temperature), permeabilized with 0.3% Triton X-100 in PBS for 10 min on ice, washed with PBS, and blocked with 5% goat serum and 0.3% Triton X-100 in PBS for 30 min. Cells were sequentially incubated with the primary and secondary antibody (**Supplementary Table S4**), then washed with PBS. Nuclei were counterstained with DAPI in VECTASHIELD mounting media (Vector Labs). Images were acquired on an Olympus BX-61 microscope equipped with a Spot RT camera (model 25.4), using the UPlanAPO 60X, NA 1.2 water immersion objective and Spot Advanced software (v.4.6.4.3). The gamma adjust and background subtract settings for adjusting the image after acquisition were identical for all images.

rDNA Fluorescent *in situ* Hybridization (FISH)

Following performing IF, slides were fixed in methanol:acetic acid (3:1) for 5 min at room temperature then dehydrated through a 70%–80% ethanol series. Slides were denatured in 70% formamide/2XSSC (saline-sodium citrate) or 10 min at 83°C, then dehydrated through the ethanol series and air-dried. Probes derived from the intergenic spacer of the human ribosomal gene repeat provided by Prof. Brain McStay, NUI Galway. 100 ng of denatured biotin-labeled probe were combined with 30 μg salmon sperm DNA and 18 μg Cot1 carrier DNA (Invitrogen) in 2XSSC with 50% formamide and 20% dextran sulfate and added per slide then hybridized at 37°C for 24 h in a humidified chamber. Slides were washed in 50% formamide/2XSSC at 42°C for 15 min and 0.1XSSC at 60°C for 15 min. Streptavidin-Alexa fluor 488 was added for 1 hr at 37°C and the slides then washed in 0.05% Tween-20/4XSSC for 15 min. Slides were mounted in DAPI. Images were acquired on an Olympus BX-61 microscope as described above.

COMET Assay

Cells were collected and processed as described in the manufacturer's protocol (Trevigen, Comet Assay 4250-050-K). Images were acquired on an Olympus BX-61 microscope using the Olympus UPlanAPO 203, NA 1.2 water immersion objective as described above.

Statistical Analysis

Pearson correlation coefficient, Spearman's rank correlation coefficient, one-way ANOVA multiple tests and Student's *t*-test were employed as indicated in figure legends.

RESULTS

A Higher Proportion of Active rDNA Repeats Correlates With OVCA Cell Sensitivity to CX-5461

Our aim was to characterize rDNA features (**Figure 1B**) that correlate with sensitivity to CX-5461 in order to identify possible predictive biomarkers of response to CX-5461. To do this, we employed a panel of established human OVCA cell lines from a range of histological subtypes. We previously reported that the concentration of drug that induces a 50% reduction in cell proliferation (GI50) varied profoundly between individual OVCA cell lines, and these cell lines were defined as resistant or sensitive to CX-5461 if the GI50 was above or below the geometric GI50 median of 360 nM, respectively (Sanij et al., 2020). We also reported that CX-5461 sensitivity correlates with basal rDNA transcription rate (i.e., rDNA transcription rate of exponentially growing cells) (Sanij et al., 2020) (shown here in **Figure 1C**). Specifically, we demonstrated that sensitive OVCA cell lines exhibited higher rDNA transcription rates than resistant lines. In this study we extend on the earlier work of Sanij et al. (2020) to assess whether differences in basal rDNA transcription rate were associated with rDNA copy number, and therefore whether copy number may explain OVCA cell line sensitivity to CX-5461. To test this, we measured rDNA copy number (dosage) in 15 OVCA cell lines by Southern blotting, and expressed rDNA dosage as fold change relative to the rDNA copy number of TOV112D cells. A wide range of rDNA dosage, from 0.07-fold in OVCAR8 to 3-fold in OVCAR3, were observed (**Figure 1D**). We also measured rDNA dosage using FISH in 4 OVCA cell lines and showed that the range of rDNA dosage concorded between the two assays confirming the differences in rDNA dosage between the OVCA cell lines (**Supplementary Figure S2A**). However, despite this wide range in rDNA dosage, we did not observe a correlation between rDNA dosage and CX-5461 GI50 values

(**Figure 1E**). Thus, these results do not support the hypothesis that rDNA copy number directly determines OVCA cell line sensitivity to CX-5461.

We have previously shown that CX-5461 activates nucleolar DDR by inducing chromatin defects and replication stress at the rDNA (Quin et al., 2016; Yan et al., 2019; Sanij et al., 2020). Therefore, we examined whether the number of active rDNA repeats and/or the proportion of active to inactive rDNA repeats are determining factors for CX-5461 sensitivity. To do this, we performed psoralen cross-linking followed by Southern blotting of gDNA from the 15 OVCA cell lines. Actively transcribed and open chromatin rDNA states are accessible to psoralen crosslinking, thus active repeats migrate slower than inactive repeats during agarose gel electrophoresis, allowing the proportion of active/inactive repeats to be quantified (Conconi et al., 1989; Sanij et al., 2008). The relative proportion of active to inactive rDNA repeats varied substantially across the OVCA cell lines (**Figure 2A** and **Supplementary Figure S2B**). We found that CX-5461-sensitive cell lines exhibited higher relative proportions of active rDNA repeats compared to resistant cell lines (**Figure 2B**). We considered whether this sensitivity simply reflects the absolute number of active rDNA repeats. To test this, we calculated active rDNA dosage by normalizing the proportion of active repeats to the relative rDNA dosage in **Figure 1D**. Interestingly, OVCA cell line sensitivity to CX-5461 showed a trend in correlation with the active rDNA dosage (**Figures 2C,E**) but not the inactive rDNA dosage (**Figures 2D,F**). Since sensitivity to CX-5461 correlated with higher basal rate of rDNA transcription (**Figure 1C**; Sanij et al., 2020), we examined whether this also correlated with parameters of rDNA chromatin activity (**Supplementary Figures S3A–C**). Basal rate of rDNA transcription did not correlate with rDNA dosage nor the proportion of active to inactive repeats (**Supplementary Figures S3A,B**) but did show a trend in correlation with active rDNA dosage (**Supplementary Figure S3C**). Therefore, we tested whether OVCA cell line sensitivity to CX-5461 correlates with rDNA transcription rate normalized to active rDNA dosage, but found no correlation with sensitivity to CX-5461 (**Figure 2G**). Thus, of all the rDNA activity parameters examined, only the ratio of active to inactive genes and the basal rate of rDNA transcription (Sanij et al., 2020) correlated with CX-5461 sensitivity in OVCA cell lines. However, we cannot dismiss that the technically challenging nature of the assays examined lead to variabilities that may limit our ability to detect correlations.

Recent studies proposed that variation in rDNA copy number is an adaptive response to DNA replication stress, specifically allowing cells with reduced rDNA copy number to rapidly complete replication and cell cycle progression (reviewed in Salim and Gerton, 2019). Therefore, we investigated whether rDNA dosage or the proportion of active to inactive rDNA repeats correlated with OVCA cell line doubling time (**Supplementary Table S2**). While we observed no correlation between rDNA dosage and OVCA cell line doubling time (**Figure 2H**), a trend in correlation between doubling time and the proportion of active rDNA repeats (**Figure 2I**) and sensitivity to CX-5461 (**Figure 2J**) was observed. Our data therefore suggests that OVCA cell lines with a higher proportion of active rDNA repeats proliferate faster (**Figure 2I**), and are more sensitive to CX-5461 (**Figure 2J**). As replication of active rDNA chromatin occurs in early S phase whereas the silent repeats are replicated from mid to late S-phase (Li et al., 2005), it is plausible that cells with elevated proportions of inactive rDNA require a longer S phase in order to complete DNA replication and thus exhibit a longer doubling time.

UBF has an essential role in establishing and maintaining active rDNA chromatin (Sanij et al., 2008, 2015). To test whether UBF loading on rDNA correlates with sensitivity to CX-5461, we examined UBF and Pol I loading at the rDNA in TOV112D, OVCAR4 and EFO21 cell lines. These cell lines were chosen as they exhibit differential sensitivity to CX-5461 and also vary with respect to rDNA dosage and the ratio of active to inactive rDNA repeats (**Figures 1D**, **2A**). The TOV112D cell line, which has higher rDNA dosage and proportion and of active rDNA than the other two cell lines, also showed a higher occupancy of UBF and Pol I across the transcribed region of the rDNA, while UBF and Pol I rDNA occupancy did not differ between EFO21 and OVCAR4 (**Figure 3A**). Since UBF and Pol I bind to the active, psoralen-accessible rDNA repeats, their occupancy was normalized to the proportions of active rDNA (**Figure 3B**). EFO21, which was the least sensitive to CX-5461 (Sanij et al., 2020) and had the lowest active rDNA dosage (**Figure 2C**) of the three OVCA cell lines, had the highest loading of UBF and Pol I normalized to the proportions of active rDNA (**Figure 3B**). Thus, while UBF binding defines active repeats, the amount of UBF binding per repeat can vary. Consistent with the elevated UBF and Pol I loading, this cell line also has a higher rate of Pol I transcription normalized to active rDNA dosage compared to the other cell lines tested (**Figure 3C**). Therefore, the data suggests that the level of Pol I loading and transcription rate normalized to the proportions of active rDNA do not influence sensitivity to CX-5461, but rather sensitivity to CX-5461 is determined by the proportion of active to inactive rDNA repeats and the basal rate of rDNA transcription (i.e., total rDNA transcription output).

Reducing rDNA Copy Number Increases the Proportion of Active rDNA Repeats and Is Associated With Elevated Genomic Instability

To obtain independent evidence supporting a role for the proportion of active to inactive rDNA repeats in mediating sensitivity to CX-5461, we reduced the rDNA copy number, which has been shown in yeast to mediate an increase in the activity of the remaining repeats (French et al., 2003; Ide et al., 2010). We did this by utilizing zinc-finger nuclease (ZFN) genome-editing. Two pairs of ZFNs were designed to specifically induce double strand DNA breaks (DSBs) targeting the intergenic spacer (IGS) region upstream and downstream of the transcribed unit of the rDNA repeat thus mediating a loss in rDNA copy number (**Supplementary Figure S1**). Copy number was measured by qPCR in eight empty vector

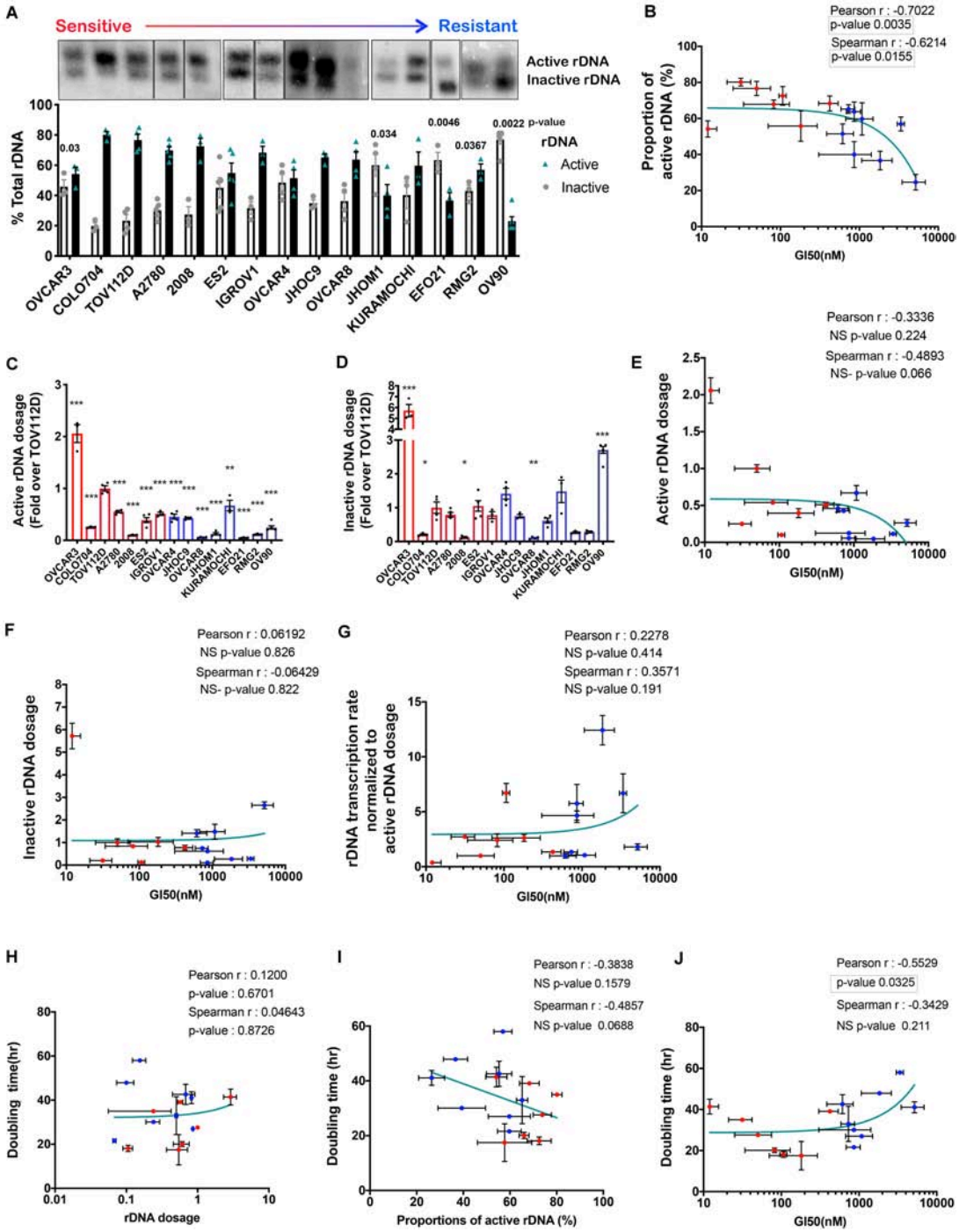

FIGURE 2 | The proportion of active to inactive rDNA chromatin correlates with sensitivity to GI50 by CX-5461 in 15 OVCA cell lines. **(A)** A representative psoralen cross-linking Southern blot analysis of 15 OVCA cell lines. The proportion of active versus inactive rDNA was quantified as a % total rDNA; $n = 3$–4; mean ± SEM. Statistical test of change relative to TOV112D was performed using unpaired *t*-test, *p*-values are indicated. **(B)** Correlation analysis of OVCA cell lines proportion of active rDNA and sensitivity to CX-5461 (GI50). The sensitive cell lines are marked as red dots while the resistant cell lines are blue. Error bars represent mean ± SD. **(C)** The active rDNA dosage and **(D)** inactive rDNA dosage were calculated by multiplying the mean rDNA dosage (**Figure 1D**) with the mean proportion of active or inactive rDNA, respectively and expressed as fold over TOV112D; $n = 3$, mean ± SEM. Statistical analysis was performed using two-sided one-way ANOVA Dunnett's multiple comparisons test. **p*-value < 0.05, ***p*-value < 0.01, ****p*-value < 0.001, compared to TOV112D. Correlation analysis of OVCA cells sensitivity to CX-5461 (GI50) and: **(E)** active rDNA dosage; **(F)** Inactive rDNA dosage. **(G)** A correlation analysis of OVCA cells sensitivity to CX-5461 (GI50) with rDNA transcription rate normalized to active rDNA dosage [calculated by dividing the basal rate of rDNA transcription in **Figure 1C** (Sanij et al., 2020) by active rDNA dosage from **(C)**]. **(H)** Correlation analysis of OVCA cell doubling time (**Supplementary Table S2**) with rDNA dosage, **(I)** the proportions of active rDNA repeats and **(J)** OVCA cells sensitivity to CX-5461 (GI50). Error bars on all correlation graphs represent mean ± SD. Significant *p*-values $p < 0.05$ are highlighted by the rectangles.

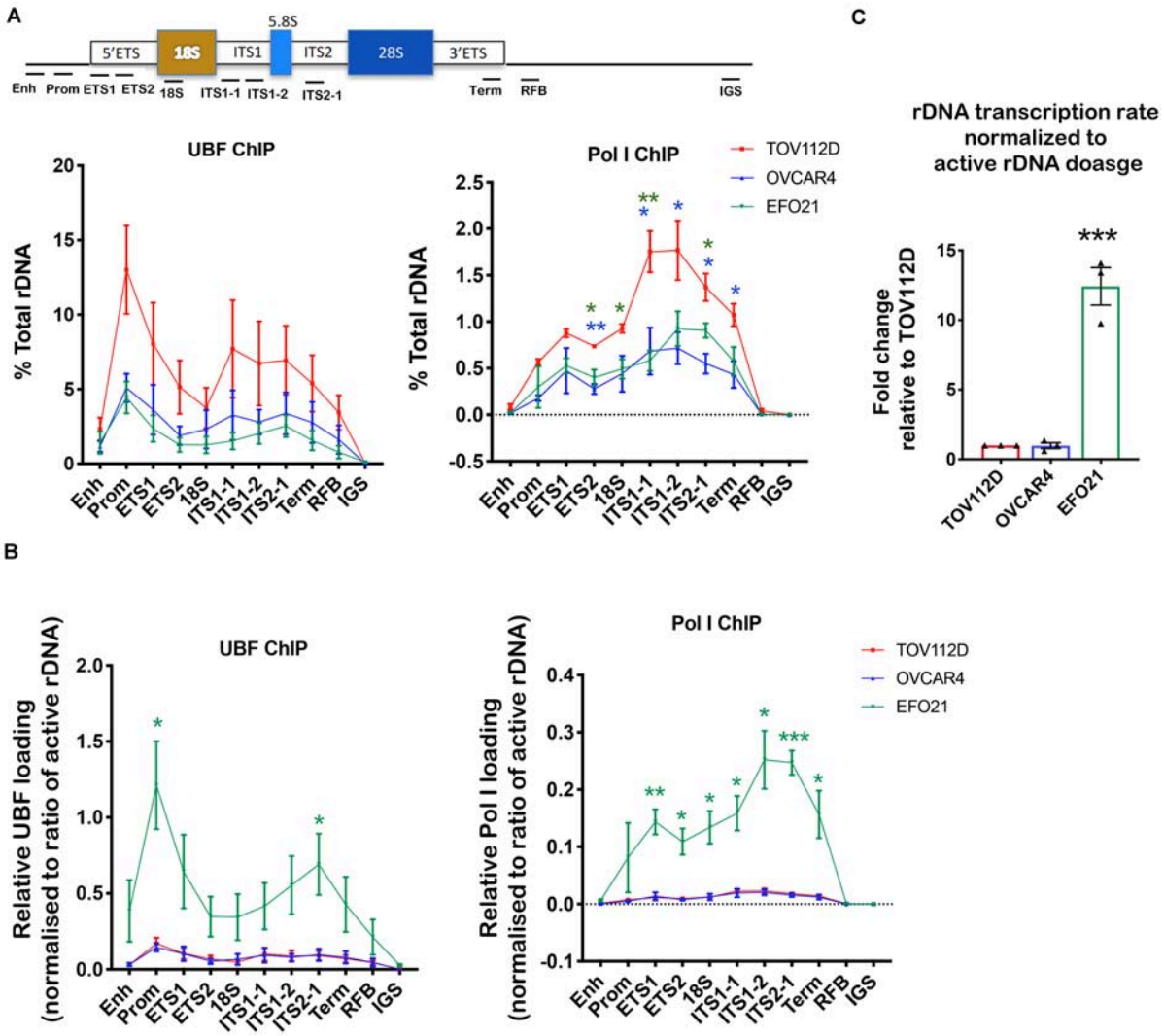

FIGURE 3 | Determining UBF and Pol I occupancy on the rDNA in OVCA cell lines with differential rDNA dosage. **(A)** Quantitative ChIP analysis of UBF and Pol I (POLR1A subunit) loading across the rDNA repeat. The % of total rDNA immunoprecipitated (IP) with the UBF or POLR1A antibodies relative to input control after subtracting background (DNA IP with rabbit sera); Error bars represents mean ± SEM, $n = 3$. Statistical analysis was performed using two-sided unpaired *t*-test. **p*-value < 0.05, ***p*-value < 0.01, OVCAR4 (blue) and EFO21 (green) compared to corresponding TOV112D (red) values. **(B)** UBF and Pol I loading were normalized to the mean proportion of active rDNA as determined by psoralen cross-linking in **Figure 2A**. Error bars represent mean of $n = 3$ ± SEM. Statistical analysis was performed using two-sided unpaired *t*-test. **p*-value < 0.05, EFO21 compared to corresponding TOV112D values. **(C)** The basal rDNA transcription rate normalized to active rDNA dosage was calculated by multiplying the basal rate of rDNA transcription from **Figure 1C** (Sanij et al., 2020) with the mean values of active rDNA dosage (**Figure 2C**) and presented as a relative fold change to that for TOV112D. Error bars represent mean ± SEM, $n = 3$, statistical analysis was performed using two-sided unpaired *t*-test,****p*-value < 0.001 compared to TOV112D.

(EV) transduced TOV112D cell lines and ten ZFN clonal TOV112D cell lines, then expressed as fold change relative to the first EV cell line (EV1). A robust decrease in rDNA copy number (∼20–50%) was observed in the ZFN expressing cell lines compared to EV controls (**Figure 4A**). We measured the effect of reducing the rDNA copy number on cell proliferation using the IncuCyte (**Figures 4B,C**). Overall, the ZFN cell lines exhibited reduced proliferation and longer doubling times (25.6 to 196.8 h) compared to the EV clones (21.9 to 34.9 h), suggesting that the ZFN-mediated reduction in rDNA copy number leads to defects in proliferation. However, it is also plausible that the ZFNs induced multi-DSBs within the rDNA loci leading to activation of a DNA damage response and growth inhibition.

We next evaluated a ZFN clone (Z38) that exhibited a ∼68% reduction in rDNA copy number compared to the EV cell line (**Figure 4D**). Quantitation of rDNA copy number performed using Southern blotting (**Figure 4D**) and rDNA-FISH combined with IF for UBF (**Figure 4E**) confirmed the reduced rDNA dosage in Z38 cells compared to EV cells. Psoralen cross-linking assays demonstrated a higher proportion of active rDNA in Z38 cells compared to EV cells (76%

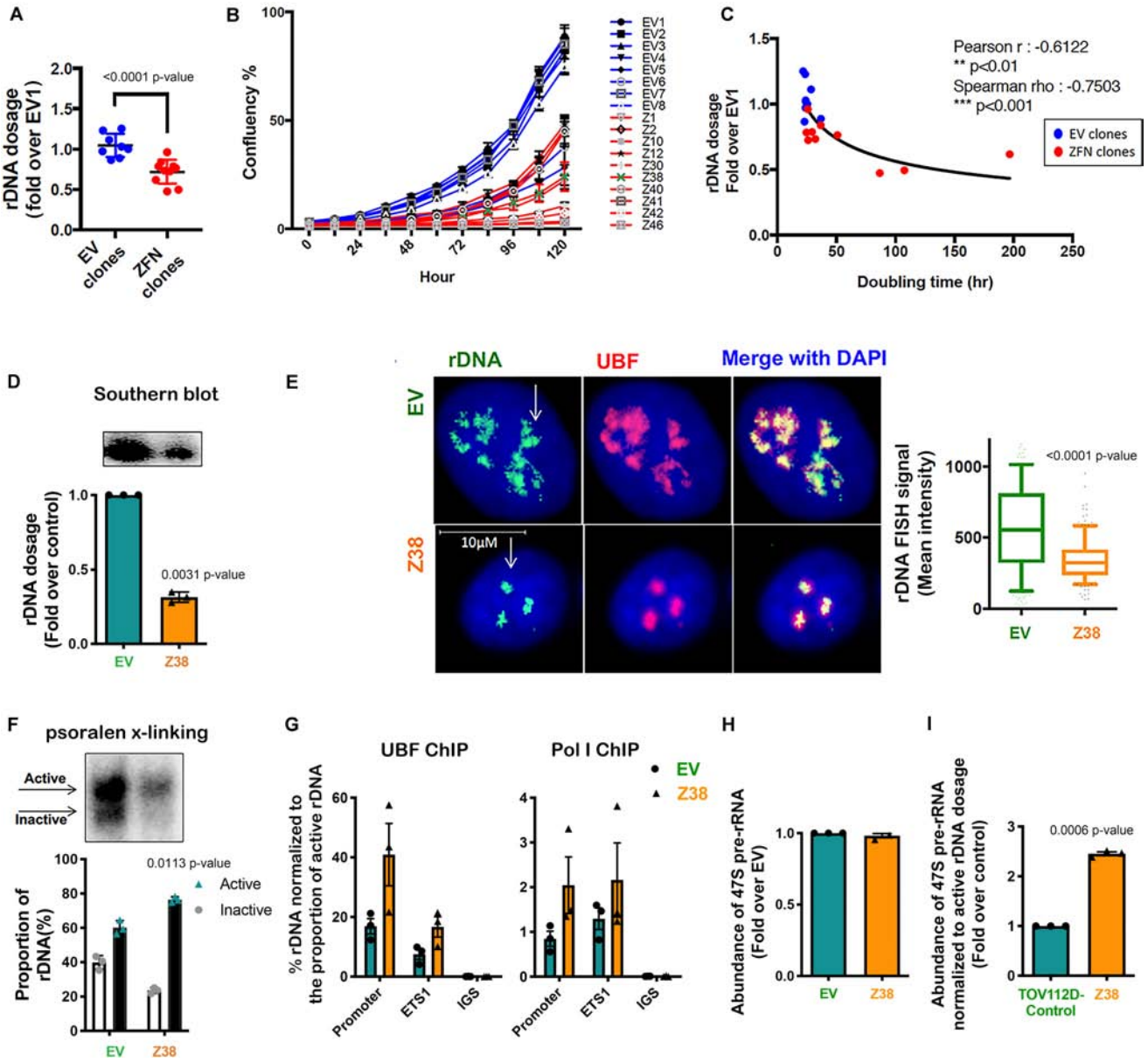

FIGURE 4 | Reducing rDNA copy number is associated with an increased proportion of active to inactive rDNA chromatin and rate of rDNA transcription in the remaining rDNA pool. **(A)** TOV112D cells were infected with Lentivirus expressing empty vector (EV) or 2 ZFNs targeting rDNA sequencing and clonal cell lines generated by puromycin selection. gDNA was extracted from 8 EV and 10 ZFNs exponentially growing clones and rDNA dosage measured by qPCR using the 5'ETS (ETS2) primers, then normalized to Vimentin as a single copy locus control (**Supplementary Table S3**). Data is represented as fold change over EV1; *** indicates $p < 0.001$ according to unpaired *t*-test. **(B)** The proliferation rate of EV and ZFN clonal cell lines was monitored and the % of cell confluency determined using the IncuCyte; $n = 3$ of technical replicates, mean ± SD. **(C)** Doubling time of cell lines was determined using the IncuCyte measurements and analyzed using GraphPad prism. Correlation analysis of rDNA dosage **(A)** and doubling time for the EV and ZFN clones was performed; Pearson's r is -0.61, ** indicates $p < 0.01$; Spearman's rho is -0.75, ***$p < 0.001$. **(D)** A representative rDNA Southern blot from EV and Z38 cells (upper panel) with quantitation expressed as fold over control (EV); mean ± SEM of $n = 3$ (lower panel). Paired *t* test analysis was performed. **(E)** IF-FISH analysis of rDNA (green: white arrows) and UBF (pink) and DAPI (blue) stained EV and Z38 cells. The intensity of rDNA FISH signal was quantitated using Definiens Tissue Software (Definiens) and graphed as mean ± SD of $n = 150$ cells analyzed over 3 biological replicates, *** indicates $p < 0.001$ according to two-sided Mann-Whitney *t*-test. **(F)** A representative of psoralen cross-linking (x-linking) analysis of EV and Z38 cells (upper panel) and quantitation of $n = 3$; mean ± SEM (lower panel). Paired *t* test analysis was performed. **(G)** qChIP analysis of UBF and Pol I (POLR1A subunit) loading on the rDNA. UBF and Pol I enrichment was calculated as described in **Figure 3A** and normalized to the mean proportion of active rDNA as determined by psoralen cross-linking in **(F)**, mean ± SEM of $n = 3$. **(H)** The abundance of the 47S pre-rRNA was measured by qRT-PCR and expressed as fold change over control (EV); mean ± SEM of $n = 3$. Paired *t* test analysis was performed. **(I)** The basal rate of rDNA transcription normalized to active rDNA dosage in EV and Z38 cells was calculated by multiplying the rate of rDNA transcription in **(H)** with the mean active rDNA dosage from **(D,F)** and expressed as fold over control (EV); mean ± SEM of $n = 3$. Paired *t* test analysis was performed.

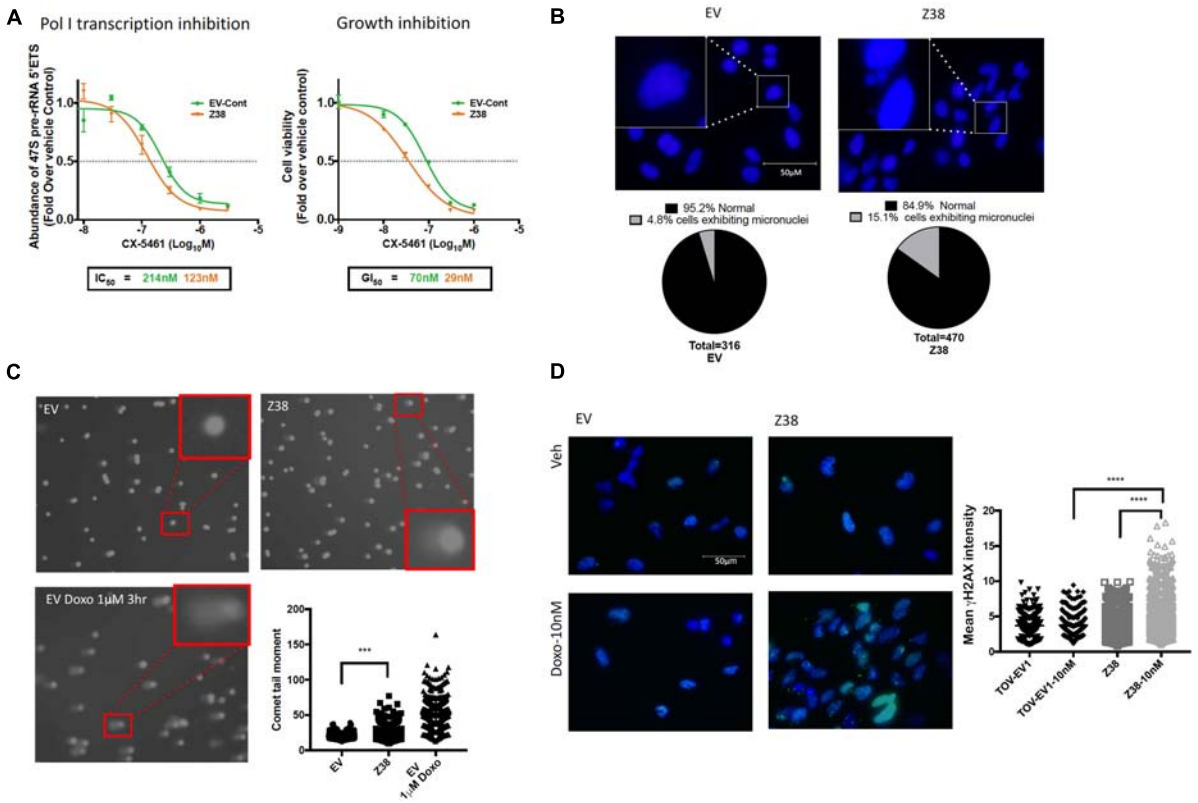

FIGURE 5 | Z38 cells with reduced rDNA copy number exhibit a higher sensitivity to CX-5461 and doxorubicin compared to EV control cells. **(A)** analysis of Pol I transcription inhibition by CX-5461 in EV control (EV-Cont) and Z38 cell lines (left panel). Cells were treated with increasing concentrations of CX-5461 for 1 h and the abundance of 47S pre-rRNA determined by qRT-PCR. IC50 of Pol I transcription inhibition for each cell lines was determined using GraphPad prism; $n = 3$; mean ± SEM. Analysis of growth inhibition by CX-5461 in EV and Z38 cell lines (right panel). Cells were treated with increasing concentrations of CX-5461 for 48 h and the cell viability (PI staining) was measured using IncuCyte; $n = 3$; mean ± SEM. **(B)** Z38 cells exhibit higher basal level of micronuclei formation. Representative images and quantitation of % of cells with micronuclei, $n = 1$. **(C)** Representative images of alkaline comet assay in EV and Z38 cell lines for detecting basal DNA damage levels. EV cells were treated with 1 μM Doxorubicin for 3 h as a positive control for DNA damage. Quantitation of comet tail moment was performed using OpenComet v.1.3 software; $n = 3$, mean ± SEM, statistical significance determined using one-way ANOVA, ** indicates $p < 0.01$. **(D)** IF analysis of γH2AX foci as a marker of DSBs in EV and Z38 cells treated with vehicle (Veh) or Doxorubicin (Doxo-10nM) for 3 h. Quantitation of the mean signal intensity was determined using Definiens of $n = 245$ cells analyzed over two biologically independent experiments, mean ± SD. Statistical analysis was performed using one-way ANOVA multiple comparisons, **** indicates $p < 0.0001$.

compared to 60%; **Figure 4F**), which was associated with an increase in UBF and Pol I occupancy normalized to the proportion of active rDNA (**Figure 4G**). However, the EV and Z38 cells displayed similar rates of basal rDNA transcription (**Figure 4H**). Together, the data suggest that as a consequence of reducing rDNA copy number, the proportion of active rDNA repeats increases, concomitant with an increase in Pol I transcription rate normalized to active rDNA dosage (**Figure 4I**), to maintain total rDNA transcriptional output (**Figure 4H**).

We next determined the sensitivity of Z38 cells to CX-5461. Exponentially growing cells were treated with increasing concentrations of CX-5461 for one hour followed by determination of 47S rRNA abundance. Interestingly, CX-5461 IC50 values for Pol I transcription inhibition by CX-5461 decreased by 50% in the Z38 clone (123 nM) compared to EV (214 nM) (**Figure 5A**). Thus, Z38 cells are more sensitive to Pol I transcription inhibition by CX-5461 than the control cells (EV). We also determined the rate of proliferation 48 h after treatment. Similarly, GI50 for CX-5461 in Z38 cells (29 nM) was reduced by 60% compared to EV cells (70 nM) (**Figure 5A**). Thus, the increase in the proportion of active rDNA repeats in Z38 cells is associated with increased sensitivity to CX-5461. This is consistent with the correlation between the ratio of active to inactive rDNA repeats and sensitivity to CX-5461 (**Figures 2A,B**).

Several studies suggest a strong correlation between rDNA chromatin activity status and genome integrity (reviewed in Diesch et al., 2014). In mouse cells, loss of rDNA silencing results in destabilization of the perinucleolar heterochromatin, which is crucial for ensuring genome stability (Guetg et al., 2010). In addition, yeast with low-copy strains have impaired DNA damage repair during S-phase and consequently higher sensitivity to DNA damaging agents such as ultraviolet radiation and methyl methanesulfonate (Ide et al., 2010). Hence, variation in rDNA chromatin states may predispose cells to genomic

instability and influence cellular responses to DNA damage. To investigate this possibility, we assessed micronuclei formation, a marker of genome instability, and used the alkaline comet assay to measure single strand DNA breaks, DSBs and other DNA lesions at a single cell level in Z38 cells. The Z38 cells exhibited a higher abundance of micronuclei formation (**Figure 5B**) and significantly brighter and longer comet tails (**Figure 5C**) compared to the EV cells, suggesting a higher degree of basal DNA damage although at a lower level compared to EV cells treated with doxorubicin. Furthermore, while the basal level of phosphorylated histone variant (γH2AX), a marker of DNA damage, was similar in the Z38 and EV cells, low dose doxorubicin (Doxo, 10 nM) treatment for 3 h mediated a significant increase in γH2AX foci staining specifically in the Z38 cells (**Figure 5D**). Thus, Z38 cells with a higher proportion of active rDNA repeats exhibit greater sensitivity to DNA damage mediated by doxorubicin. Altogether, these results suggest that a reduction in rDNA copy number by ZFNs mediates an increase in the ratio of active to inactive rDNA repeats and enhances the cells sensitivity to CX-5461 and DNA damage.

DISCUSSION

In this report, we utilized a panel of human OVCA cell lines to identify potential predictive biomarker(s) of therapeutic response to CX-5461. Our data revealed that sensitivity to CX-5461 significantly correlates with the basal rDNA transcription rate (total rDNA transcriptional output), the proportion of active to inactive rDNA repeats and doubling time. Our analyses also showed a correlation trend for sensitivity to CX-5461 with active rDNA dosage, but there was no correlation between CX-5461 sensitivity and rDNA dosage (copy number), inactive rDNA dosage or rDNA transcription rate normalized to active rDNA dosage. However, we cannot exclude that the high variation in rDNA copy number and proportion of active rDNA repeats measurements may limit our ability to detected significant correlations. Such correlations may be revealed in time should methods that more precisely measure these parameters be developed.

The strong association of higher proportions of active rDNA with sensitivity to growth inhibition by CX-5461 is consistent with CX-5461's mode of action in triggering defects associated with open chromatin and replication stress at the rDNA (Quin et al., 2016; Yan et al., 2019; Sanij et al., 2020), including potentially acting as a TOP 2 poison (Bruno et al., 2020) selectively at the rDNA and/or across the genome. We have demonstrated that CX-5461 activates nucleolar ATM and ATR leading to activation of cell cycle checkpoints and global replication-mediated DNA damage (Quin et al., 2016; Yan et al., 2019; Sanij et al., 2020). Our data therefore suggests that cells with a higher ratio of active rDNA are more sensitive to CX-5461-mediated nucleolar DDR and activation of cell cycle checkpoints, with faster proliferating cells being more responsive to cell cycle arrest.

We found that the proportion of active rDNA repeats does correlate with OVCA cell doubling time. This finding is important in the context of recent bioinformatic analyses of whole genome sequencing data demonstrating that rDNA repeats tend to be lost in cancers (Wang and Lemos, 2017; Xu H. et al., 2017). These results are consistent if we assume that the lower rDNA copy number reported for these cancers has resulted in an increased proportion of active rDNA repeats. However, we also found that rDNA copy number did not correlate with doubling time (**Figure 2H**), suggesting that the relationship between copy number and proliferation time is more complex, which might reflect the multiple ways cells can achieve a certain level of rDNA transcription. Consistent with this, we also showed that the baseline rate of rDNA transcription does not correlate with the proportion of active rDNA repeats or rDNA dosage, although there is a trend in correlation with active rDNA dosage (**Supplementary Figure S3**), possibly due to the rDNA transcription rate being dependent on both the number of active rDNA repeats and the density of Pol I loading/transcription elongation at these active repeats (Conconi et al., 1989; French et al., 2003; Schneider, 2012; Hung et al., 2017). In this case, the increased rate of rDNA transcription observed in cancer cells (Drygin et al., 2010; Hannan R.D. et al., 2013) could be mediated independently of rDNA copy number. We therefore propose that an increase in the proportion of active rDNA repeats is likely to be a more consistent phenotype of proliferative cancers than a reduction in rDNA copy number.

We demonstrated that rDNA copy number can be reduced using dual ZNF targeting. Whether this occurred via precise deletion of whole rDNA repeats, thus by homologous recombination-mediated repair of DSBs, or by non-homologous end joining of the break sites remains unclear. Distinguishing between these two possibilities requires sequencing of the ZNF clones, but the interpretation is likely to be complicated by reports suggesting there are pre-existing incomplete units in the human rDNA (Caburet et al., 2005). The reduced rDNA copy number in the ZFN-targeted TOV112D cells is associated with an increased proportion of active rDNA repeats, in agreement with previous reports in yeast showing altering rDNA copy number modulated rDNA chromatin states (Ide et al., 2010). The increased proportion of active rDNA repeats may result from rDNA class switching, specifically the reduced pool of rDNA repeats promotes UBF binding to any inactive repeats thus converting them to active repeats (Diesch et al., 2019). Alternatively, ZNF deletion may selectively target inactive rDNA repeats. However, CRISPR Cas9-mediated DSBs preferentially occurs in euchromatic regions in the genome, suggesting gene editing is more efficient in euchromatin than in heterochromatin (Jensen et al., 2017). Furthermore, dynamic switching between active and inactive repeats was reported upon ATRX depletion, which resulted in reduced rDNA silencing, specific loss of the inactive rDNA repeats and increased proportions of active rDNA repeats (Udugama et al., 2018) thus making the distinction in genome editing bias toward active or inactive rDNA repeats largely void. Importantly, our data demonstrates that the reduction in rDNA copy number observed in Z38 cells induced genome-wide

instability, as illustrated by increased micronuclei formation and other markers of DNA damage (**Figure 5**). Furthermore, Z38 was more sensitive to doxorubicin-induced DNA damage, consistent with results in yeast showing reduced rDNA copy number increases sensitivity to DNA damaging agents (Ide et al., 2010). Whether this increased genomic instability is mediated by the reduced rDNA copy number, the increased proportion of active rDNA repeats, or another feature due to ZNF treatment remains to be determined.

Taken together, this study demonstrates a significant correlation between OVCA sensitivity to CX-5461 and the proportion of active to inactive rDNA repeats. These data suggest that rDNA chromatin states may be a useful biomarker for sensitivity to targeted Pol I transcription therapies. Validation of this parameter as a predictive biomarker of response to CX-5461 in patient samples in future clinical trials will be important to translate these findings to the clinic. A potential barrier to the effectiveness of rDNA chromatin status as a biomarker is the lack of precision with which the proportion of active rDNA repeats can currently be determined, however our results suggest there is value in developing improved methods for measuring rDNA activity state *in situ*.

AUTHOR CONTRIBUTIONS

ES, RH, and AG conceptualized and designed the study. ES, KH, GP, NH, DC, and KS developed the methodology. JS and ES acquired the data. JS, ES, KH, RH, AG, and RP analyzed and interpreted the data. ES, RH, RP, and AG supervised the study. All authors wrote, reviewed, and/or revised the manuscript.

FUNDING

This work was supported by the National Health and Medical Research Council (NHMRC) of Australia project grants (#1100654 and #1162052). RH and RP were supported by NHMRC fellowships. AG was supported by the New Zealand Marsden Fund (14-MAU-053).

SUPPLEMENTARY MATERIAL

The Supplementary Material for this article can be found online at: https://www.frontiersin.org/articles/10.3389/fcell.2020.00568/full#supplementary-material

REFERENCES

Bruno, P. M., Lu, M., Dennis, K. A., Inam, H., Moore, C. J., Sheehe, J., et al. (2020). The primary mechanism of cytotoxicity of the chemotherapeutic agent CX-5461 is topoisomerase II poisoning. *Proc. Natl. Acad. Sci. U.S.A.* 117, 4053–4060. doi: 10.1073/pnas.1921649117

Bywater, M. J., Poortinga, G., Sanij, E., Hein, N., Peck, A., Cullinane, C., et al. (2012). Inhibition of RNA polymerase I as a therapeutic strategy to promote cancer-specific activation of p53. *Cancer Cell* 22, 51–65. doi: 10.1016/j.ccr.2012.05.019

Caburet, S., Conti, C., Schurra, C., Lebofsky, R., Edelstein, S. J., and Bensimon, A. (2005). Human ribosomal RNA gene arrays display a broad range of palindromic structures. *Genome Res.* 15, 1079–1085. doi: 10.1101/gr.3970105

Chan, J. C., Hannan, K. M., Riddell, K., Ng, P. Y., Peck, A., Lee, R. S., et al. (2011). AKT promotes rRNA synthesis and cooperates with c-MYC to stimulate ribosome biogenesis in cancer. *Sci. Signal.* 4;ra56. doi: 10.1126/scisignal.2001754

Conconi, A., Widmer, R. M., Koller, T., and Sogo, J. M. (1989). Two different chromatin structures coexist in ribosomal RNA genes throughout the cell cycle. *Cell* 57, 753–761. doi: 10.1016/0092-8674(89)90790-3

Devlin, J. R., Hannan, K. M., Hein, N., Cullinane, C., Kusnadi, E., Ng, P. Y., et al. (2016). Combination therapy targeting ribosome biogenesis and mRNA translation synergistically extends survival in MYC-Driven lymphoma. *Cancer Discov.* 6, 59–70. doi: 10.1158/2159-8290.CD-14-0673

Diesch, J., Bywater, M. J., Sanij, E., Cameron, D. P., Schierding, W., Brajanovski, N., et al. (2019). Changes in long-range rDNA-genomic interactions associate with altered RNA polymerase II gene programs during malignant transformation. *Commun. Biol.* 2:39. doi: 10.1038/s42003-019-0284-y

Diesch, J., Hannan, R. D., and Sanij, E. (2014). Perturbations at the ribosomal genes loci are at the centre of cellular dysfunction and human disease. *Cell Biosci.* 4:43. doi: 10.1186/2045-3701-4-43

Drygin, D., Rice, W. G., and Grummt, I. (2010). The RNA polymerase I transcription machinery: an emerging target for the treatment of cancer. *Annu. Rev. Pharmacol. Toxicol.* 50, 131–156. doi: 10.1146/annurev.pharmtox.010909.105844

French, S. L., Osheim, Y. N., Cioci, F., Nomura, M., and Beyer, A. L. (2003). In exponentially growing Saccharomyces cerevisiae cells, rRNA synthesis is determined by the summed RNA polymerase I loading rate rather than by the number of active genes. *Mol. Cell. Biol.* 23, 1558–1568. doi: 10.1128/mcb.23.5.1558-1568.2003

Gaj, T., Gersbach, C. A., and Barbas, C. F. III (2013). ZFN, TALEN, and CRISPR/Cas-based methods for genome engineering. *Trends Biotechnol.* 31, 397–405. doi: 10.1016/j.tibtech.2013.04.004

Goodfellow, S. J., and Zomerdijk, J. C. (2013). Basic mechanisms in RNA polymerase I transcription of the ribosomal RNA genes. *Subcell. Biochem.* 61, 211–236. doi: 10.1007/978-94-007-4525-4_10

Grummt, I., and Langst, G. (2013). Epigenetic control of RNA polymerase I transcription in mammalian cells. *Biochim. Biophys. Acta* 1829, 393–404. doi: 10.1016/j.bbagrm.2012.10.004

Guetg, C., Lienemann, P., Sirri, V., Grummt, I., Hernandez-Verdun, D., Hottiger, M. O., et al. (2010). The NoRC complex mediates the heterochromatin formation and stability of silent rRNA genes and centromeric repeats. *EMBO J.* 29, 2135–2146. doi: 10.1038/emboj.2010.17

Hamdane, N., Stefanovsky, V. Y., Tremblay, M. G., Nemeth, A., Paquet, E., Lessard, F., et al. (2014). Conditional inactivation of Upstream Binding Factor reveals its epigenetic functions and the existence of a somatic nucleolar precursor body. *PLoS Genet.* 10:e1004505. doi: 10.1371/journal.pgen.1004505

Hamperl, S., Wittner, M., Babl, V., Perez-Fernandez, J., Tschochner, H., and Griesenbeck, J. (2013). Chromatin states at ribosomal DNA loci. *Biochim. Biophys. Acta* 1829, 405–417. doi: 10.1016/j.bbagrm.2012.12.007

Hannan, K. M., Sanij, E., Rothblum, L. I., Hannan, R. D., and Pearson, R. B. (2013). Dysregulation of RNA polymerase I transcription during disease. *Biochim. Biophys. Acta* 1829, 342–360. doi: 10.1016/j.bbagrm.2012.10.014

Hannan, R. D., Drygin, D., and Pearson, R. B. (2013). Targeting RNA polymerase I transcription and the nucleolus for cancer therapy. *Expert Opin. Ther. Targets* 17, 873–878. doi: 10.1517/14728222.2013.818658

Hayashi, Y., Kuroda, T., Kishimoto, H., Wang, C., Iwama, A., and Kimura, K. (2014). Downregulation of rRNA transcription triggers cell differentiation. *PLoS One* 9:e98586. doi: 10.1371/journal.pone.0098586

Hein, N., Cameron, D. P., Hannan, K. M., Nguyen, N. N., Fong, C. Y., Sornkom, J., et al. (2017). Inhibition of Pol I transcription treats murine and human AML by targeting the leukemia-initiating cell population. *Blood* 129, 2882–2895. doi: 10.1182/blood-2016-05-718171

Hein, N., Hannan, K. M., George, A. J., Sanij, E., and Hannan, R. D. (2013). The nucleolus: an emerging target for cancer therapy. *Trends Mol. Med.* 19, 643–654. doi: 10.1016/j.molmed.2013.07.005

Herdman, C., Mars, J. C., Stefanovsky, V. Y., Tremblay, M. G., Sabourin-Felix, M., Lindsay, H., et al. (2017). A unique enhancer boundary complex on the mouse ribosomal RNA genes persists after loss of Rrn3 or UBF and the inactivation of RNA polymerase I transcription. *PLoS Genet.* 13:e1006899. doi: 10.1371/journal.pgen.1006899

Hilton, J., Gelmon, K., Cescon, D., Tinker, A., Jonker, D., Goodwin, R., et al. (2020). "Abstract PD4-02: Canadian cancer trials group trial IND.231: a phase 1 trial evaluating CX-5461, a novel first-in-class G-quadruplex stabilizer in patients with advanced solid tumors enriched for DNA-repair deficiencies," in *Proceedings of the Cancer Research Abstracts: 2019 San Antonio Breast Cancer Symposium; December 10-14, 2019*, San Antonio, TX.

Hung, S. S., Lesmana, A., Peck, A., Lee, R., Tchoubrieva, E., Hannan, K. M., et al. (2017). Cell cycle and growth stimuli regulate different steps of RNA polymerase I transcription. *Gene* 612, 36–48. doi: 10.1016/j.gene.2016.12.015

Ide, S., Miyazaki, T., Maki, H., and Kobayashi, T. (2010). Abundance of ribosomal RNA gene copies maintains genome integrity. *Science* 327, 693–696. doi: 10.1126/science.1179044

Jensen, K. T., Floe, L., Petersen, T. S., Huang, J., Xu, F., Bolund, L., et al. (2017). Chromatin accessibility and guide sequence secondary structure affect CRISPR-Cas9 gene editing efficiency. *FEBS Lett.* 591, 1892–1901. doi: 10.1002/1873-3468.12707

Khot, A., Brajanovski, N., Cameron, D. P., Hein, N., Maclachlan, K. H., Sanij, E., et al. (2019). First-in-human RNA polymerase I transcription inhibitor CX-5461 in patients with advanced hematological cancers: results of a phase I dose escalation study. *Cancer Discov.* 9, 1036–1049. doi: 10.1158/2159-8290.CD-18-1455

Killen, M. W., Stults, D. M., Adachi, N., Hanakahi, L., and Pierce, A. J. (2009). Loss of Bloom syndrome protein destabilizes human gene cluster architecture. *Hum. Mol. Genet.* 18, 3417–3428. doi: 10.1093/hmg/ddp282

Li, J., Santoro, R., Koberna, K., and Grummt, I. (2005). The chromatin remodeling complex NoRC controls replication timing of rRNA genes. *EMBO J.* 24, 120–127. doi: 10.1038/sj.emboj.7600492

McStay, B., and Grummt, I. (2008). The epigenetics of rRNA genes: from molecular to chromosome biology. *Annu. Rev. Cell Dev. Biol.* 24, 131–157. doi: 10.1146/annurev.cellbio.24.110707.175259

Moss, T., Langlois, F., Gagnon-Kugler, T., and Stefanovsky, V. (2007). A housekeeper with power of attorney: the rRNA genes in ribosome biogenesis. *Cell Mol. Life. Sci.* 64, 29–49. doi: 10.1007/s00018-006-6278-1

Moss, T., Mars, J. C., Tremblay, M. G., and Sabourin-Felix, M. (2019). The chromatin landscape of the ribosomal RNA genes in mouse and human. *Chromosome Res.* 27, 31–40. doi: 10.1007/s10577-018-09603-9

Moss, T., and Stefanovsky, V. Y. (2002). At the center of eukaryotic life. *Cell* 109, 545–548. doi: 10.1016/s0092-8674(02)00761-4

Olivieri, M., Cho, T., Álvarez-Quilón, A., Li, K., Schellenberg, M. J., Zimmermann, M., et al. (2019). A genetic map of the response to DNA damage in human cells. *bioRxiv* [preprint]. doi: 10.1101/845446

Pelletier, J., Thomas, G., and Volarevic, S. (2018). Ribosome biogenesis in cancer: new players and therapeutic avenues. *Nat. Rev. Cancer* 18, 51–63. doi: 10.1038/nrc.2017.104

Peltonen, K., Colis, L., Liu, H., Trivedi, R., Moubarek, M. S., Moore, H. M., et al. (2014). A targeting modality for destruction of RNA polymerase I that possesses anticancer activity. *Cancer Cell* 25, 77–90. doi: 10.1016/j.ccr.2013.12.009

Poortinga, G., Hannan, K. M., Snelling, H., Walkley, C. R., Jenkins, A., Sharkey, K., et al. (2004). MAD1 and c-MYC regulate UBF and rDNA transcription during granulocyte differentiation. *EMBO J.* 23, 3325–3335. doi: 10.1038/sj.emboj.7600335

Poortinga, G., Quinn, L. M., and Hannan, R. D. (2014). Targeting RNA polymerase I to treat MYC-driven cancer. *Oncogene* 34, 403–412. doi: 10.1038/onc.2014.13

Potapova, T. A., and Gerton, J. L. (2019). Ribosomal DNA and the nucleolus in the context of genome organization. *Chromosome Res.* 27, 109–127. doi: 10.1007/s10577-018-9600-5

Prakash, V., Carson, B. B., Feenstra, J. M., Dass, R. A., Sekyrova, P., Hoshino, A., et al. (2019). Ribosome biogenesis during cell cycle arrest fuels EMT in development and disease. *Nat. Commun.* 10:2110. doi: 10.1038/s41467-019-10100-8

Quin, J., Chan, K. T., Devlin, J. R., Cameron, D. P., Diesch, J., Cullinane, C., et al. (2016). Inhibition of RNA polymerase I transcription initiation by CX-5461 activates non-canonical ATM/ATR signaling. *Oncotarget* 7, 49800–49818. doi: 10.18632/oncotarget.10452

Ray, S., Panova, T., Miller, G., Volkov, A., Porter, A. C., Russell, J., et al. (2013). Topoisomerase IIalpha promotes activation of RNA polymerase I transcription by facilitating pre-initiation complex formation. *Nat. Commun.* 4:1598. doi: 10.1038/ncomms2599

Rebello, R. J., Kusnadi, E., Cameron, D. P., Pearson, H. B., Lesmana, A., Devlin, J. R., et al. (2016). The dual inhibition of RNA Pol I transcription and PIM kinase as a new therapeutic approach to treat advanced prostate cancer. *Clin. Cancer Res.* 22, 5539–5552. doi: 10.1158/1078-0432.CCR-16-0124

Salim, D., and Gerton, J. L. (2019). Ribosomal DNA instability and genome adaptability. *Chromosome Res.* 27, 73–87. doi: 10.1007/s10577-018-9599-7

Sanij, E., Diesch, J., Lesmana, A., Poortinga, G., Hein, N., Lidgerwood, G., et al. (2015). A novel role for the Pol I transcription factor UBTF in maintaining genome stability through the regulation of highly transcribed Pol II genes. *Genome Res.* 25, 201–212. doi: 10.1101/gr.176115.114

Sanij, E., Hannan, K. M., Yan, S., Xuan, J., and Ahern, J. (2020). CX-5461 activates the DNA damage response and demonstrate therapeutic efficacy in high-grade serous ovarian cancer. *Nat. Commun.* 11:2641.doi: 10.1101/621623

Sanij, E., and Hannan, R. D. (2009). The role of UBF in regulating the structure and dynamics of transcriptionally active rDNA chromatin. *Epigenetics* 4, 374–382. doi: 10.4161/epi.4.6.9449

Sanij, E., Poortinga, G., Sharkey, K., Hung, S., Holloway, T. P., Quin, J., et al. (2008). UBF levels determine the number of active ribosomal RNA genes in mammals. *J. Cell Biol.* 183, 1259–1274. doi: 10.1083/jcb.200805146

Savic, N., Bar, D., Leone, S., Frommel, S. C., Weber, F. A., Vollenweider, E., et al. (2014). lncRNA maturation to initiate heterochromatin formation in the nucleolus is required for exit from pluripotency in ESCs. *Cell Stem Cell* 15, 720–734. doi: 10.1016/j.stem.2014.10.005

Schneider, D. A. (2012). RNA polymerase I activity is regulated at multiple steps in the transcription cycle: recent insights into factors that influence transcription elongation. *Gene* 493, 176–184. doi: 10.1016/j.gene.2011.08.006

Stefanovsky, V. Y., Pelletier, G., Hannan, R., Gagnon-Kugler, T., Rothblum, L. I., and Moss, T. (2001). An immediate response of ribosomal transcription to growth factor stimulation in mammals is mediated by ERK phosphorylation of UBF. *Mol. Cell.* 8, 1063–1073. doi: 10.1016/s1097-2765(01)00384-7

Stults, D. M., Killen, M. W., Williamson, E. P., Hourigan, J. S., Vargas, H. D., Arnold, S. M., et al. (2009). Human rRNA gene clusters are recombinational hotspots in cancer. *Cancer Res.* 69, 9096–9104. doi: 10.1158/0008-5472.CAN-09-2680

Udugama, M., Sanij, E., Voon, H. P. J., Son, J., Hii, L., Henson, J. D., et al. (2018). Ribosomal DNA copy loss and repeat instability in ATRX-mutated cancers. *Proc. Natl. Acad. Sci. U.S.A.* 115, 4737–4742. doi: 10.1073/pnas.1720391115

Valori, V., Tus, K., Laukaitis, C., Harris, D. T., LeBeau, L., and Maggert, K. A. (2019). Human rDNA copy number is unstable in metastatic breast cancers. *Epigenetics* 15, 85–106. doi: 10.1080/15592294.2019.1649930

Valori, V., Tus, K., Laukaitis, C., Harris, D. T., LeBeau, L., and Maggert, K. A. (2020). Human rDNA copy number is unstable in metastatic breast cancers. *Epigenetics* 15, 85–106.

Wang, M., and Lemos, B. (2017). Ribosomal DNA copy number amplification and loss in human cancers is linked to tumor genetic context, nucleolus activity, and proliferation. *PLoS Genet.* 13:e1006994. doi: 10.1371/journal.pgen.1006994

Warmerdam, D. O., and Wolthuis, R. M. F. (2019). Keeping ribosomal DNA intact: a repeating challenge. *Chromosome Res.* 27, 57–72. doi: 10.1007/s10577-018-9594-z

Warner, J. R. (1999). The economics of ribosome biosynthesis in yeast. *Trends Biochem. Sci.* 24, 437–440. doi: 10.1016/s0968-0004(99)01460-7

Woolnough, J. L., Atwood, B. L., Liu, Z., Zhao, R., and Giles, K. E. (2016). The regulation of rRNA gene transcription during directed differentiation of human embryonic stem cells. *PLoS One* 11:e0157276. doi: 10.1371/journal.pone.0157276

Xie, W., Ling, T., Zhou, Y., Feng, W., Zhu, Q., Stunnenberg, H. G., et al. (2012). The chromatin remodeling complex NuRD establishes the poised state of rRNA genes characterized by bivalent histone modifications and altered nucleosome positions. *Proc. Natl. Acad. Sci. U.S.A.* 109, 8161–8166. doi: 10.1073/pnas.1201262109

Xu, B., Li, H., Perry, J. M., Singh, V. P., Unruh, J., Yu, Z., et al. (2017). Ribosomal DNA copy number loss and sequence variation in cancer. *PLoS Genet.* 13:e1006771. doi: 10.1371/journal.pgen.1006771

Xu, H., Di Antonio, M., McKinney, S., Mathew, V., Ho, B., O'Neil, N. J., et al. (2017). CX-5461 is a DNA G-quadruplex stabilizer with selective lethality in BRCA1/2 deficient tumours. *Nat. Commun.* 8:14432. doi: 10.1038/ncomms14432

Yan, S., Frank, D., Son, J., Hannan, K. M., Hannan, R. D., Chan, K. T., et al. (2017). The potential of targeting ribosome biogenesis in high-grade serous ovarian cancer. *Int. J. Mol. Sci.* 18:210. doi: 10.3390/ijms18010210

Yan, S., Madhamshettiwar, P. B., Simpson, K. J., Ellis, S., Kang, J., Cullinane, C., et al. (2019). Targeting RNA Polymerase I transcription synergises with TOP1 inhibition in potentiating the DNA damage response in high-grade serous ovarian cancer. *bioRxiv* [Preprint]. doi: 10.1101/849307

Zentner, G. E., Saiakhova, A., Manaenkov, P., Adams, M. D., and Scacheri, P. C. (2011). Integrative genomic analysis of human ribosomal DNA. *Nucleic Acids Res.* 39, 4949–4960. doi: 10.1093/nar/gkq1326

Zhao, Z., Dammert, M. A., Grummt, I., and Bierhoff, H. (2016). lncRNA-induced nucleosome repositioning reinforces transcriptional repression of rRNA genes upon hypotonic stress. *Cell Rep.* 14, 1876–1882. doi: 10.1016/j.celrep.2016.01.073

Conflict of Interest: RH is a Chief Scientific Advisor to Pimera Inc.

The remaining authors declare that the research was conducted in the absence of any commercial or financial relationships that could be construed as a potential conflict of interest.

Advantages of publishing in Frontiers

OPEN ACCESS
Articles are free to read for greatest visibility and readership

FAST PUBLICATION
Around 90 days from submission to decision

HIGH QUALITY PEER-REVIEW
Rigorous, collaborative, and constructive peer-review

TRANSPARENT PEER-REVIEW
Editors and reviewers acknowledged by name on published articles

Frontiers
Avenue du Tribunal-Fédéral 34
1005 Lausanne | Switzerland

Visit us: www.frontiersin.org
Contact us: info@frontiersin.org | +41 21 510 17 00

REPRODUCIBILITY OF RESEARCH
Support open data and methods to enhance research reproducibility

DIGITAL PUBLISHING
Articles designed for optimal readership across devices

FOLLOW US
@frontiersin

IMPACT METRICS
Advanced article metrics track visibility across digital media

EXTENSIVE PROMOTION
Marketing and promotion of impactful research

LOOP RESEARCH NETWORK
Our network increases your article's readership